FEASIBILITY STUDIES TO IMPROVE PLANT AVAILABILITY AND REDUCE TOTAL INSTALLED COST IN IGCC PLANTS

Final Technical Report

Reporting Period
Beginning October 1, 2011
Ending December 31, 2014

Principal Authors:
Kevin Sullivan, William Anasti, Yichuan Fang, Karthik Subramanyan, Tom Leininger, Christine Zemsky

March 30, 2015

DE-FE0007859

Submitted By:
GE Energy (USA), LLC
1333 West Loop South
Houston, TX 77027

DISCLAIMER

ABSTRACT

The main purpose of this project is to look at technologies and philosophies that would help reduce the costs of an Integrated Gasification Combined Cycle (IGCC) plant, increase its availability or do both. GE's approach to this problem is to consider options in three different areas: 1) technology evaluations and development; 2) constructability approaches; and 3) design and operation methodologies. Five separate tasks were identified that fall under the three areas: Task 2 – Integrated Operations Philosophy; Task 3 – Slip Forming of IGCC Components; Task 4 – Modularization of IGCC Components; Task 5 – Fouling Removal; and Task 6 – Improved Slag Handling.

Overall, this project produced results on many fronts. Some of the ideas could be utilized immediately by those seeking to build an IGCC plant in the near future. These include the considerations from the Integrated Operations Philosophy task and the different construction techniques of Slip Forming and Modularization (especially if the proposed site is in a remote location or has a lack of a skilled workforce). Other results include ideas for promising technologies that require further development and testing to realize their full potential and be available for commercial operation. In both areas GE considers this project to be a success in identifying areas outside the core IGCC plant systems that are ripe for cost reduction and availability improvement opportunities.

TABLE OF CONTENT

DISCLAIMER **2**

ABSTRACT **3**

EXECUTIVE SUMMARY **5**

REPORT DETAILS **7**

1.0 Overall Project Scope and Goals 7

2.0 Task 2 – Integrated Operations Philosophy 9

2.1 Experimental Methods 9
2.2 Results and Discussions 11
2.3 Conclusion 23

3.0 - Task 3 and 4 – Slip Form/Modularization Gasification/IGCC Components 25

3.1 Experimental Methods 25
3.2 Results and Discussions 25
3.3 Conclusion 31

5.0 Task 5 – Radiant Syngas Cooler (RSC) Fouling Removal System 33

5.1 Understanding Fouling Mechanisms 33
5.2 Feasibility of Online Fouling Removal 44
5.3 Down Select Fouling Removal Concepts 73
5.4 Develop PDE Fouling Removal Subscale Testing 92
5.5 RSC Fouling Coupon Preparation 109
5.6 Fouling Removal Subscale Testing (PDE) 157
5.7 Conclusions and Recommendations 170

6.0 Task 6 – Continuous Blowdown System for Slag Handling 172

6.1 Introduction 172
6.2 Technology Selection 173
6.3 Design of the CSRP 195
6.4 Analysis and Discussion of the CSRP 203
6.5 Conclusions 235
6.6 Recommendations 236

7.0 Overall Program Conclusions/Recommendations 236

Acknowledgment 239

APPENDIX A ***240***

GRAPHICAL MATERIALS LISTS **240**

REFERENCES **248**

LIST OF ACRONYMS AND ABBREVIATIONS **253**

APPENDIX B ***255***

Copy of Kiewit Final Report **255**

EXECUTIVE SUMMARY

The main purpose of this project is to look at technologies and philosophies that would help reduce the costs of an Integrated Gasification Combined Cycle (IGCC) plant, increase its availability or do both. GE's approach to this problem is to consider options in three different areas: 1) technology evaluations and development; 2) constructability approaches; and 3) design and operation methodologies. Five separate tasks were identified that fall under the three areas:

Task 2 – Integrated Operations Philosophy
Task 3 – Slip Forming of IGCC Components
Task 4 – Modularization of IGCC Components
Task 5 – Fouling Removal
Task 6 – Improved Slag Handling

Task 2 focused on cost and availability improvements that could be gleaned by looking into and aligning operations and maintenance processes. To improve upon a standard reference design, a focus team took up the task of reviewing lessons learned from the operation of the current design and brainstorming new ideas to improve operability, maintainability, and the bottom line on economics. The culminating result included some operational improvements in the areas of sparing philosophies, maintainability ideas in terms of spare usages, and differing approaches of both for improving the cost of the plant.

From this brainstorming 47 improvement ideas were identified as being successful candidates for further, more detailed analysis. From these 47 ideas the project saved $2.45MM from the original design per train or $4.9MM for a two-train plant. In those same 47 ideas, an improvement in RAM of nearly a quarter percent exists (~$1.2MM/year revenue savings), and at least one idea provides a method to increase the gasifier run length significantly.

Tasks 3 and 4 were combined during execution of the project and yielded rather unexpected results. In an Integrated Gasification Combined Cycle (IGCC) system, the traditional means of constructing many of the plant subsystems is through a "stick-built" approach which consists of individually lifting into final position structural steel columns, beams, and braces one "stick" or piece at a time. GE worked with Kiewit Power Engineers on this project as they bring real-world experience and success in designing with such techniques. The tasks considered multiple proposed concepts and their likelihood of resulting in significant reduces costs and/or schedule.

The Gasification Process Structure had the most alteration in terms of construction techniques studied – as it combined both slip forming as well as modularization. For this solution the walls of the structure are made using the slip forming method and the floors were constructed as modules either off-site or elsewhere on the site. This change yielded an improvement in schedule (6.5%) and cost (less than 1%) which was an unexpectedly modest improvement.

Although the study did not show a significant reduction in cost, schedule and constructability for a currently configured IGCC plant on the Gulf Coast at current prevailing conditions, the slip form and modularization technique should not be eliminated as potential cost and schedule saving construction techniques for IGCC plants in the future. The following items could have a definite on the magnitude of savings when utilizing these construction techniques as compared to the stick building option (or combination thereof): Improvements in the gasification island design; site geological and geographical conditions; site labor rates; site labor availability and

skills; steel and concrete costs; and production revenue (increase of initial revenue by being able to start earlier).

The objective of Task 5 is to develop a system which will remove fouling deposits on the heat exchanger tubes in the syngas cooler. The removal of fouling deposits will effectively improve steam production and availability for the IGCC plant, and increase plant efficiency. Consequently, this will lower the plant Cost of Electricity (COE, $/kWhr) and expand the coal operability range. In order to effectively identify and evaluate a viable RSC fouling removal system, it is important to first understand ash deposit formation and distribution as well as mechanical and thermal properties.

Following a detailed survey of the fouling mechanisms and state-of-the-art fouling removal techniques a pulse detonation engine was down selected from the overall list as the technology of choice to be lab tested at the University of Texas at Arlington for feasibility. The experiments demonstrated the feasibility of fouling removal from repeated detonations based on subscale testing. Recommendations are proposed to transition the concept to a commercial product.

The concern of Task 6 is to develop a preliminary design for an improved blow down system for slag handling for IGCC applications that meets the availability/cost goals of the program. The improved blowdown system for slag handling that has been developed in this project falls mainly into the latter category: decreasing cost without sacrificing reliability when compared with the conventional slag handling system. In carrying out this task, GE decided to replace the lockhopper-based batch system with an improved continuous blowdown process. Based on a detailed technology evaluation, a slag-water letdown turbine, which is based on running a rotating parallel disc pump in reverse, was identified as the best option. The slag-water letdown turbine assembly will consist of a Discflo® pump head, an eddy current brake, a friction brake, a clutch and a variable speed electric motor - all connected via a common rotating shaft.

The improved system is 62% less expensive ($15.6M) than the lockhopper system on a total installed cost basis. 81% of the savings in total direct field costs is attributable to the fact that the CSRP is a much more compact system that allows three decks (50 ft.) to be removed from the gasifier support structure. 10% of the cost savings in total direct field costs is attributable to the lower cost of the CSRP major equipment compared with the cost of the lockhopper system major equipment. A detailed test plan required to move to a commercial produce is included.

REPORT DETAILS

1.0 Overall Project Scope and Goals

In early 2011, the U.S. Department of Energy (DOE) released Funding Opportunity Announcement (FOA) number DE-FOA0000496 titled *Advanced Gasification: Novel CO_2 Utilization Systems, Low Rank Coal IGCC Optimization, and Improvements in Gasification Systems Availability and Costs*. The FOA solicited responses in three topic areas, as indicated by the title. All three topic areas support DOE's goal of fostering the development of lower cost Integrated Gasification Combined Cycle (IGCC) power generation technology with carbon capture, while maintaining the highest environmental standards. The availability of lower cost IGCC power plants fueled by America's abundant coal reserves will help provide a clean, stable, secure and affordable energy supply to meet the nation's growing energy demands. The General Electric Company (GE) was awarded funding support for a project in the third topic area (TA-3) – Gasification Plant Availability and Cost Improvements – under DOE contract number DE-FE-0007589.

Integrated Gasification Combined Cycle is a technology that generates electrical power from fossil fuels, such as coal, by first converting the coal into a gas in a high temperature, high pressure gasification process. The coal gas is then cleaned to remove contaminants such as particulates, sulfur, oxides of nitrogen and mercury before being burned in a gas turbine (the Brayton Cycle) to generate power. Heat recovered from the exhaust of the gas turbine, as well as from elsewhere in the gasification plant, is used to raise superheated steam, which is expanded in a steam turbine (the Rankine Cycle) to generate additional power. The combination of the two thermodynamic power producing cycles integrated with a gasification process is what is known as Integrated Gasification Combined Cycle technology, or IGCC. Combining these two systems increases the complexity of the plant and, thus the possibility of a less available and more costly plant.

The main purpose of this project is to look at technologies and philosophies that would help reduce the costs of an IGCC plant, increase its availability or do both. GE's approach to this problem is to consider options in three different areas: 1) technology evaluations and development; 2) constructability approaches; and 3) design and operation methodologies. Five separate tasks were identified that fall under the three areas:

Task 2 – Integrated Operations Philosophy
Task 3 – Slip Forming of IGCC Components
Task 4 – Modularization of IGCC Components
Task 5 – Fouling Removal
Task 6 – Improved Slag Handling

For each task techno-economic studies were completed that concentrated on either cost or availability criterion or both, where applicable. The scope of work included the identification of system and component level requirements for each task and subtask, the development of designs and materials as required for technical evaluation of concepts, validation, and testing of components/sub-systems, the development of appropriate operating methodologies, simulations and controls philosophies, where applicable.

It is important to note that under this DOE solicitation it was clearly stated that certain portions of the IGCC plant (gasifier, air separation units, syngas acid gas and trace

contaminant cleanup systems, carbon-dioxide/hydrogen separation technologies and the turbines) were not to be included in the current study as the DOE already supports substantial research in these areas under separate programs.

2.0 Task 2 – Integrated Operations Philosophy

A plant operational philosophy is a general term that could be defined differently depending on the project goals. The goals of this program are to make Integrated Gasification Combined Cycle (IGCC) plants more affordable by reducing cost and / or improving plant availability. The discussion below provides details on the approach used to narrow focus down to detailed philosophies that can be utilized in the plant design phase and during operation to make IGCC plants more affordable.

2.1 Experimental Methods

As GE considered the scope of an integrated operations philosophy, a broader perspective came into focus. Certainly, the mere consideration of an integrated plant spanning gasification and power production was obvious but the aspect of integrating the operations to the maintenance – and vice versa - seemed equally important. Hand-in-hand with operations goes maintenance and so goes maintenance with operations. Differing methodologies and opinions exist to describe the relationship between operations and maintenance, yet both are required to achieve a successful facility. The team concentrated on making an IGCC facility highly operable, easily maintained, and considered economic impact during those phases.

GE spent a considerable amount of time and resources during the original design work of the current two-train IGCC facility. This included a very detailed and methodical approaches to the heat balance across the plant, integration of syngas cleanup, integrated control schemes to best manage syngas loads, and flexibilities in the slurry preparation area. The resulting design contained many lessons learned from experience over a 30-year period of chemical and power plant operations. This positioned the newly designed facility with an expectation of a high reliability, suitable operability and maintenance, and an approachable cost.

To improve upon this design, a focus team took up the task of scouring additional lessons learned from the operation of the current design and brainstorming new ideas to improve operability, maintainability, and the bottom line on economics. The culminating result included some operational improvements in the areas of sparing philosophies, maintainability ideas in terms of spare usages, and differing approaches of both for improving the cost of the plant.

> GE Lessons Learned Instruction
> "This procedure covers the Lessons Learned within Gasification. Lessons Learned apply to any activity or process that may positively affect the quality and/or continuous improvement of the business. In general, Lessons Learned may be initiated by anyone. Lessons Learned opportunities shall be reviewed and documented as an integral part of the technical and commercial development, review, and improvement processes."

During the original design work for the then current design, a series of reliability, availability, and maintainability (RAM) analyses were performed. In this initial analysis, GE relied on experiences from a few key gasification customers. Those experiences laid groundwork for understanding the intricacies of the interlacing of operations and maintenance with respect to how to operate a piece of equipment and when to perform maintenance on that piece of equipment.

After establishing the baseline data for the RAM of a typical IGCC plant, the team set out using established methodologies for defining if and how each of the selected improvement ideas would impact the reliability of the plant.

The RAM model uses distributions to describe the randomness associated with equipment failure and repair cycles. Each piece of equipment, marked by one Reliability Block Diagram (RBD), is assigned failure and repair distributions with appropriate parameters (e.g. MTBF – Mean Time between Failure and MTTR – Mean Time to Repair). The model uses the Monte Carlo technique to randomly generate a number between 0 and 1. Next, the most common method is to use the inverse cumulative distribution function to convert the random number to a number from the assigned distribution for time to failure or time to repair. Those times are tracked over the simulation period and are used to calculate reliability and availability.

One of the aspects of RAM modeling not fully engaged concerns reliability centered maintenance (RCM). To fully vet an RCM program, an owner uses years of historical maintenance records and operability data to determine when best to perform certain types of maintenance on equipment. GE leveraged the experience of its internal experts as well as the experts at customer sites to quickly identify the maintenance items within the IGCC facility and how they align to others.

Apparent from research was the trend that certain pieces of equipment require a periodicity of maintenance that “shadows” others to the point they not need be counted. We labeled this as synchronous maintenance. Further, we identified this as remaining true until there is a technological advancement in the most frequent piece of equipment that shadows others. GE encourages the makers of this equipment to achieve the advancements and owners to be on the lookout for them, both as ways to improve the RAM and economics of an IGCC facility. Using these methods produced the RAM improvement for the selected improvement ideas collectively.

To wrap all of the selected improvement ideas neatly into a quantitative measure, GE utilized simple estimation tools. Estimations were prepared for the base cost and the cost of the proposed change. From these we established the overall differential for the improvement ideas monetarily.

As an example of the process, consider item 02-009 from Table 1 which discusses converting an installed spare to a warehouse spare for the Recycle Solids pump. The Recycle Solids pump is common to both gasifier trains and will lead to shutdown of the grinding systems if the pump were to fail. However, the slurry run tanks provide several hours of storage capacity of slurry. Recycle Solids pump failure would not lead directly to a gasification train trip unless the issue was not resolved within a timely manner.

Removal of the installed spare would reduce the amount of piping and space requirements in the coal grinding area. The cost and availability impacts are listed below.

Net Removal of:

~70 feet of 8” diameter Carbon steel piping
Thirteen (13) Carbon steel valves
Estimated Cost Impact = reduction of < 1-2% of total plant cost (actual calculated value in Table 1)
Estimated Availability Impact = negligible

The trade-off between capital expenditure (CAPEX) and availability is best presented in terms of dollars. The results shown in this paper are presented as the change in availability due to the proposed improvement. The availability change is also equated to dollars, or revenue impact, using the following formula:

$$\mathrm{Rev}[\$MM/yr] = 0.0544[\$MM/hr] \times \frac{\Delta Avail[\%]}{100\%} \times 8760[hrs/yr]$$

Equation 1 - Total Plant Revenue

Where,
Rev = total plant revenue gained or lost per year

ΔAvail = the percent change in Availability due to the proposed improvement

The factor of 0.0544 $MM/hr is the assumed plant revenue per hour of operation at rated capacity. This factor depends on current price of electricity, plant capacity, and plant operating load (i.e. some plants reduce load during non-peak hours). For the purposes of this report it is assumed that the plant operates at full capacity when online. Electricity generation data was obtained for year 2011 from the U.S. Energy Information Administration. The "Revenue from Retail Sales of Electricity" for 2011 was ~$372 billion and the "Net Generation for All Sectors" for 2011 was ~4105 million megawatt-hours (U.S. Energy Information Administration, "Revenue…" 2012 and U.S. Energy Information Administration, "Net Generation…", 2012). The ratio of Revenue to Net Generation provides the average revenue per megawatt-hour of power generation for all power generation stations in the United States in 2011. This ratio is then multiplied by the assumed capacity of the plant to obtain 0.0544 $MM/hr as shown in Equation 1, above.

2.2 Results and Discussions

In the early phase of the project, GE subject matter experts (SME) generated 100 improvement ideas. These ranged from a simple isolation philosophy to more complex controls schemes. And, as the plant is integrated, so the improvement ideas were integrated. More specifically, the ideas covered slurry preparation through the steam and condensate systems across the plant.

Consideration for generating the ideas came from experience in operations, operability, maintenance, maintainability, maintenance planning, equipment sparing, and general simplification. Some automation was removed and some was added. Additionally, in locations the SMEs thought there might be benefit dual trains of equipment were combined (heat exchangers, pumps). Discussions were focused on ideas that met the following sub-goals:

Improvements shall positively impact one aspect of affordability (CAPEX or availability/OPEX) and have little to no negative impact to the other. In general, any cost reductions will have negative effects on plant availability, and any availability improvements typically require additional equipment and therefore larger capital investment.
Philosophies shall be broadly applicable to different IGCC configurations and technologies.
Quantitative examples of implementation of the philosophy shall be evaluated using existing tools (RAM model, Class III cost analysis).

With the above sub-goals in mind, the team brainstormed and down-selected different improvement areas that could be evaluated during review of GE Gasification's IGCC Reference Plant design.

Isolation Philosophy: There are several areas of an IGCC plant that require isolation for normal plant operation, startup / shutdown activities, and online and offline maintenance. The main and

most important purpose for isolation is safety; however, this effort will focus on evaluation of other factors such as cost and operational efficiency.

Common Equipment Sparing Philosophy: A multiple-train system offers opportunities to utilize common installed spares between trains to remove redundant equipment within the system while maintaining desired availability. The sparing philosophy for this paper will be mainly focused on process pumps.

Multiple Service Sparing Philosophy: Several services within the IGCC system operate under similar conditions and process fluid that similar frame types and sizes of equipment can be used for multiple services. Utilizing similar frame sizes and types of equipment can help reduce warehouse inventory and space requirements while maintaining appropriate equipment spares and parts. The sparing philosophy for this paper will be mainly focused on process pumps.

Reliability Centered Maintenance / Synchronized Maintenance Philosophy: For some services within the IGCC system, non-critical equipment can be operated to failure to extend maintenance intervals and increase availability; however, a “run to fail” philosophy must be balanced and synchronized with critical equipment maintenance seeking to optimize plant availability (i.e. non-critical equipment must be restored to normal service during major plant outages addressing critical equipment).

Personnel Investment: Personnel investment refers to operator training, management philosophy, and performance incentives. Personnel investment ultimately factors in to a plant’s time-to-maturity and is therefore a trade-off between capital investment and availability in the first years of plant operation. A plant operator may choose to invest heavily in training personnel prior to plant commissioning and startup versus an on the job training approach.

During generation, ideas were not evaluated. Instead, GE used a brainstorming technique so as not to prematurely eliminate any ideas. Once the 100 ideas were generated, the panel of subject matter experts engaged principal engineers to evaluate the ideas. Some were found to be not worthy of pursuing. The remaining ideas were evaluated both from a RAM perspective and a change-cost perspective.

The ideas that were not further evaluated number 52. The reasons for not further assessing these ideas vary from no perceived benefit to a negative benefit. This could be from any of the criteria areas listed in the second paragraph of this section. The following descriptions identify some specific reasons for removing some of the 52 ideas.

- Vendor package data is not available to GE in detail enough to evaluate economically. Combining two smaller systems into one will result in the same quantity of equipment with a new configuration
- The idea does not consider the elevation placement of the equipment and, therefore, would not be feasible. An extensive amount of piping re-routing/addition would likely be necessary to effectively employ this idea.
- Removal of equipment (simplification) would create an emissions compliance challenge for the customer.

It is important to note that GE made a best effort attempt to use RAM modeling during the development of the current IGCC two-train design. This work involved scouring historical data, surveying subject matter experts, and surveying customers. Each piece of data took the typical approach used in RAM modeling: mean time between failures, mean time to repair, types of

failure, and repair or replacement to return to service. This helped to drive some of the decisions in the design of the current IGCC plant and revealed some interesting discoveries.

Along the course of surveying customers, GE discovered a few keys factors. In at least one case, a customer had executed a full-blown reliability centered maintenance (RCM) program. This was an extensive and time consuming process that took maintenance practices to a level of detail that became cumbersome in and of itself. As required maintenance patterns emerged, another discovery was made: synchronous maintenance.

How do you schedule maintenance across an IGCC plant with varying types of equipment with varying types of maintenance requirements? Synchronous maintenance answered that question well. It became the norm for planning and guiding maintenance in the IGCC plant design. It is also how the focus team approached improvement ideas in this project.

Using synchronous maintenance as a guide, the RAM team was better equipped to rapidly evaluate the focus team's improvement ideas. With an understanding of how frequently each piece of equipment required maintenance the teams were better equipped to identify which pieces of equipment had matching maintenance activities. Specifically speaking, an idea that was not further pursued due to the "shadow" of maintenance and no expected operational benefit: reduce the number of operating slurry additive pumps from one per train to one for both trains. Maintenance required on the slurry additive pumps falls on frequency that aligns with maintenance on the slurry charge pump, which falls in line with the GE feed injector life. At the end of life of the feed injector, a gasifier is shutdown, the slurry charge pump is maintained, and periodically (every third or fourth occurrence) the additive pumps are maintained as well.

Other, more prominent pieces of equipment throughout the plant fall in this pattern of synchronous maintenance. A gas turbine requires a hot gas path inspection every three years. Likewise, gasifier refractory can be managed to a life of three or more years. Aligning these two major (25-35 days) maintenance items allows an IGCC facility to minimize the number of outages required to perform maintenance and minimize the duration of all outages in general. And as each facility has specialized equipment to handle and process raw materials into the specific products due to the customers – power in the case of IGCC – each owner will need to determine how to align each of these maintenance requirements accordingly.

Another improvement idea came from a current facility operating in conjunction with material providers to more efficiently handle replacement parts. Moreover, the customer, knowing the operational life of a particular pump and its versatility, replaced several pumps across multiple similar process streams for the one style, minimized the on hand warehouse spares, and coordinated with their vendor for inventory control. The vendor would maintain some quantity of replacement pump on hand, the customer would maintain a warehouse inventory lessor than could be, and that inventory could be used across the facility. This allowed the staggering and aligning of maintenance of this style pump in similar fashion as aforementioned refractory/gas turbine maintenance.

Sparing philosophies vary – usually by the end user's experience and budget. By joining forces with a vendor, understanding the versatility of the equipment, and paying particular attention to the mean time between failures (MTBF) and mean time to repair (MTTR), a facility can improve operability, maintainability, and reduce costs. These ideas are not just in similar style pumps but can also be found in determining whether to install spares or use warehouse spares. Depending on the service severity, need of rapid spare utility, and ease of repair, we found certain applications for each.

For this project, the focus team concentrated on ideas that could save capital expenditures (CAPEX) and reduce the operating expenditures (OPEX). One purpose was to improve operability. An improvement idea along these lines occurred in the separation of a process stream into two streams from a vessel through two pumps. The idea combined the two pumps into a single pump and utilized control valves to separate the streams.

This was a common theme through the project: many seemingly good ideas to make improvements in one area did not necessarily pan out a savings in CAPEX or OPEX or improve operability to a degree worthy of the spending. In order to move from the list of original ideas to a list of ideas that made sense, additional evaluation was essential. A cost estimation of the original equipment was placed alongside the estimation for the change ideas.

On paper the idea above seemed great in providing an online spare pump and simplifying the process to improve operability. However, while taking the CAPEX into consideration, the evaluation of this idea deemed it a detriment to the project and was thusly removed from the list of improvement ideas in that it increased CAPEX by nearly $1.5MM. Our intuition doesn't always make the grade.

Stated another way, we found 48 ideas measuring standards to evaluate economically. Once we completed that evaluation, it became clear only 47 of those ideas were worthy of meeting our criteria. Hence, from 47 improvement ideas, the project saved $2.45MM from the original design per train or $4.9MM for a two-train plant. In those same 47 ideas, an improvement in RAM of nearly a quarter percent exists (~$1.2MM/year revenue savings), and at least one idea provides a method to increase the gasifier run length significantly.

Table 1, below, includes the listing of the ideas, a brief description, the proposed change and the estimated savings (Class 3/4).

The discussion may twist from the original problem in this manner: while there are some very dedicated methods to employ in improving RAM, each facility must utilize tools in ways that are specific to that facility and at an appetite/tolerance level of the leadership to reach desired results.

Table 1. Summary of Ideas and Estimated Savings

Item	Item Name	Description	Proposed Change	Net Savings
02-001	Coal bunkers	Base design has two coalbunkers; reference plant originally had one bunker. Both designs have dedicated feed systems to each train from the coalbunkers.	Approach optimization of the size and configuration of the coalbunkers in terms of CAPEX and OPEX.	$692,950
02-004	Grind Mill Discharge Duct Fan	Base design has dedicated duct fans for each train.	Consider utilizing a common duct fan for multiple trains. Evaluate what would be the most trains that could be supported by one fan.	$115,472

02-005	Mill Discharge Pumps	Base design has installed spares for the mill discharge pumps.	Due to the ease of exchanging mill discharge pumps, consider changing the installed spare to a warehouse spare to save plot space and piping.	$141,318
02-006	Slurry vibrating screens	Current design uses slurry vibrating screens to filter out large particles prior to making it to the charge pump.	Evaluate the cost impact of removing the vibrating screen, and lengthening the trommel screen at the grind mill to increase the residence time for large particle removal.	$62,788
02-007	Slurry Charge Pump	Charge pump dedicated to each train.	Consider adding a common spare (a 3rd pump) to allow the plant to be restarted after a significant failure of a charge pump.	$(442,189)
Item	**Item Name**	**Description**	**Proposed Change**	**Net Savings**
02-008	Recycle Solids Pumps	Recycle Solids Pumps, settler bottoms pumps, and LP Grey Water pumps experience similar service conditions.	Recycle Solids Pumps, settler bottoms pumps, and LP Grey Water pumps experience similar services conditions. Consider using the same size/style of pump for Recycle Solids and LP Grey Water to reduce the number of spares required.	Discussed in narrative. No dollar amount assigned.
02-009	Recycle Solids Pumps	Base design has installed spare for recycle solids pump.	Due to the ease of exchanging the Recycle Solids Pumps, consider changing to a warehouse spare. If this change is made, consider connecting a makeup water line to the inlet of the grind mill as backup in case the recycle solid pump trips.	$98,730
02-010	Grinding Area Sump Pumps	Base design has installed spare for Grinding Area Sump Pumps.	Due to the ease of exchanging Grinding Area Sump Pumps, consider changing the installed spare to a warehouse spare.	$17,790
03-001	NIH to RSC Quench Swing El	Positive isolation between 1200 PSIG NIH and 650 PSIG RSC Quench Section. Current design is for this connection to be swung out before light off after startup purging.	Remove Swing El. Rely on manual isolation valves and an automatic block valve for isolation since the NIH will remain higher pressure when isolated.	$1,214
03-002	RSC HP Circ Pump Common Spare	Both trains have A and B pumps. In base design, the spare pump may be required to support New and Clean RSC cases.	Make a common spare that supports both trains, and remove one pump from the design. The main pump would have to be increased in size to account for a New and Clean Case RSC.	$303,139

03-003	RSC Quench Pump	Current design uses a Scrubber RSC Quench pump and Nozzle Scrubber pump. The Nozzle scrubber pump is a backup to the RSC Quench pump on loss of quench flow.	Feed the RSC Quench Ring and Nozzle Scrubber from the same pump, and use the other as a spare. **Not used in calculation for total savings. Removed due to high cost.	$(1,446,847)
03-004	NIH Nitrogen connections	Used for purges	Consider changing all Swing Elbows to speed up startup/shutdown activities	$1,158
Item	**Item Name**	**Description**	**Proposed Change**	**Net Savings**
03-007	Slurry line flushes	Several manual utility water flushes on slurry line.	Consider automation around slurry line flushing connections to speed up startup / shutdown operations and reduce the risk of plugging.	$(977)
03-011	FICW System	Current design has dedicated FICW drums, pumps, and exchanger for each train.	Consider a common drum, pumps, and/or exchanger for multiple trains, with dedicated return systems that can detect syngas leakage. Could also use a common spared pump. Also evaluate exchangers.	$270,520
03-012	Startup Aspirator Spec Blind	Current design requires the Spec Blind to be closed after Startup Purging and before gasifier light off. Currently the startup timeline accounts for 60mins to close the spec blind.	Remove or Change Spec Blind to automated isolation to save time during startup. Control aspiration through moderating the steam instead of controlling air flow. Add a manual bleed to flare that is lined up to flare during normal operation to account for leaks.	$(23,322)
03-015	SG Scrubber Pump drives	Current design is variable speed pumps.	Consider changing to a fixed speed pump, with flow control valves. The type of service may require variable speed pumps with block valves due to plugging.	$119,942
03-017	Syngas Cooler Blow down Drum	Dedicated blow down drum for each train.	Consider using common drum blow down drum for the syngas cooler HP steam drums.	$173,858
04-001	LH Flush Drum	Dedicated LH Flush Drums per train.	Consider making the LH Flush drum common to multiple trains. The LH flush drum will need to be sized appropriately in order to handle flushes for both Lockhopper trains.	$152,971

04-002	LH Flush Drum	Multiple train LH's can sequence such that the "dump" step occurs at the same time, as long as they are not in shared slag sump mode.	Current design accounts for both Lockhoppers being able to dump simultaneously (double capacity). Consider implementing an operational philosophy that requires that the LH's cannot execute a "dump" step at the same time.	Logic modification – no dollar amount assigned
04-005	LH Circulation Valves	Current design uses two automatic isolation valves to isolate the LH during dump modes.	Current design uses two automatic isolation valves to isolate the LH during dump modes. Evaluate the removal of one isolation valve. Current standard only uses one.	$51,499
Item	**Item Name**	**Description**	**Proposed Change**	**Net Savings**
04-006	LH Circulation Pump	Base design uses a variable speed pump.	Consider changing to a fixed speed pump.	$(30,031)
04-010	Overflow Slag Sump	Base design has a dedicated Over Flow Slag Sump per train.	Consider changing to a common Overflow Slag Sump for multiple trains. Both Slag Drag conveyors can overflow to one sump.	$254,362
04-011	Slag Drag Conveyor / Slag Pad	Base design uses a Slag Drag Conveyor	Evaluate the economic and operational benefits of using a Slag Pad vs. a Slag Drag conveyor. Also consider a combination of the two to eliminate one Slag Drag Conveyor.	$(349,754)
04-012	Slag Sump Pumps	Base has dedicated Slag Sump Pumps for each train, with installed spares.	Consider removing one installed spare, and making the installed spare common to both trains.	$164,041

04-013	Slag Sump Pumps / Preheat	Base design has Slag Sump pumps that also function as Quench preheat pumps.	Compare using dedicated Slag Sump Pumps and Gasifier Preheat pumps to the case where the Slag Sump Pumps are used during Gasifier Preheat. This would reduce cost by making the Slag Sump Pumps dual purpose.	$52,048
04-014	Slag Area Sump Pumps	Base design has an installed spare.	Evaluate cost / RAM impact of switching to a warehouse spare.	$2,027
04-015	Slag Transport Sump Pumps	Base design has an installed spare.	Evaluate cost / RAM impact of switching to a warehouse spare.	$882
Item	**Item Name**	**Description**	**Proposed Change**	**Net Savings**
05-001	Spec break on Preheat water to overflow slag sump circuit	Currently, the design has a spec blind upstream & downstream of the automatic valve to the overflow slag sump. There is a spec break on the downstream side of this valve & its manual bypass. Suggest relocating the manual block valve immediately upstream of the automatic valve, closer to the first manual block valve. This would allow a single spec blind to be installed	Current design only contains one block & one bleed further upstream, close to the tie-in point on the RSC blow down line. Suggest relocating the manual block valve immediately upstream of the automatic valve, closer to the first manual block valve. This would allow a single spec blind to be installed. By moving the location of the spec blind, it will allow the piping to be rated for a lower pressure to reduce cost. Instead of having two spec blinds (upstream & downstream of the overflow sump), only one spec blind could be installed.	$1,571
05-003	LP Flash OH Exchanger	There is currently one common exchanger for both trains. This exchanger may be subject to fouling.	This exchanger is subject to fouling. Suggest adding a second or spare exchanger.	$(249,372)

05-004	Angle valves on the black water from LP Flash Drums to the Vacuum Flash Drum	The Base design currently has two angle valves on the black water to the Vacuum Flash Drum. These valves are very expensive & are typically used in high dp & abrasive services. The large pressure drop occurred upstream of the LP Flash Drum.	Consider the possibility of switching to a different, less expensive valve. The supply pressure should be fairly low (between 40 - 60 psi), so there may not be a need for these expensive valves designed for high dp. Consider installing less expensive valves with internals designed for corrosive or abrasive service.	Estimated new valve at equal cost.
05-005	Inertia breakers on the black water from LP Flash Drums to the Vacuum Flash Drum	Base design has inertia breakers on the black water to the Vacuum Flash Drum. These inertia breakers may not be needed, since the press drop was taken upstream of the LP Flash Drum.	May be able to remove the inertia pots/breakers totally, due to the relatively low dp.	$25,581
Item	**Item Name**	**Description**	**Proposed Change**	**Net Savings**
05-006	Automatic valves on the suction & discharge of the Settler Feed pumps	Automatic valves are not needed on the suction & discharge of the Settler Feed pumps. This configuration is not offered in our PDP packages & it should slightly increase RAM, because the automatic valves are failed close.	Suggest switching these automatic valves to manual valves. This will eliminate the cost of all of the associated instrumentation. If this service is not time-critical and the backup pump can be lined up manually, the update will not significantly affect reliability.	$173,889
05-010	VF Condensate Pumps	Base design has an installed spare.	Consider changing to a warehouse spare since the criticality of the pumps is low.	$37,532
06-002	Settler Bottoms Pumps	Base design has installed spares for each train.	Consider removing one pump.	$78,320
06-003	Settler Bottoms Pumps	The pumps are variable speed.	Consider updating to a fixed speed pump, with a control valve.	$(34,624)
06-004	Settler Bottoms Pumps and Vacuum Flash Condensate Pumps.	The Settler Bottoms Pumps are similar in size to the Vacuum Flash Condensate Pumps.	Consider making them the same style pump, and using common warehouse spares.	$134,319
06-005	Settler Bottoms	Base design has automatic block valves on	Consider changing the automatic block valves to manual.	$27,741

	Pumps	the pump discharge.		
06-006	HP GW Pumps	HP GW Pumps are variable speed.	Consider changing to fixed speed pumps.	$(32,216)
07-002	NH3 Stripper OH Press Control	Base has Stripper OH pressure control located right at the stripper, as well as pressure control downstream at the SRU.	Consider removing pressure control at the stripper OH and allow pressure control strictly at the SRU.	$38,397
08-001	COS Reactor Preheat	NIH exchanging heat with steam is passed through the COS reactor and vented to flare to preheat the COS catalyst.	Add a recirculation line to use a fixed amount of N2 during preheat.	$(47,993)
08-005	Condensate return pumps	Condensate return pumps have 2x100% per train.	Consider adding a common spare for both trains and removing one pump.	$88,157
08-006	Trim Cooler KO Pumps	KO pumps have 2x100% per train.	Consider adding a common spare for both trains and removing one pump.	$81,897
Item	**Item Name**	**Description**	**Proposed Change**	**Net Savings**
26-001	Diluent N2/Extraction Air Exchanger	Base design has a dedicated exchanger for each train.	Consider making the exchanger common to both trains.	$(90,077)
29-001	IP Feedwater System	Currently, there are two automatic control valves on the IP feedwater to the common header (IP to Process Block - Letdown the pressure from ~ 1100 to 905 psi (2 per train). There are also downstream flow control valves for each train. There is also a pressure control valve downstream of the tie-in point where both trains connect. The downstream pressure control valve controls the header pressure of the common header.	Propose that the automatic letdown valves downstream of the HP/IP pumps & the downstream flow control valves (upstream of the tie-in point of both trains) be obsoleted from future IGCC designs (Six valves total).	$63,224
58-001	HP Steam Purge KO Drum	Current design utilizes the HP Steam Purge KO drum to supply the slurry line purge during Gasifier shutdowns. The drum is sized for 1.5 adequate single train purges. It was	Remove HP Steam Purge KO drum, and supply the slurry steam purge via piping.	$163,183

		found that makeup to the drum would always be needed during a purge.		
58-002	RSC Intermittent Blowdown	The RSC HP Steam drum has 3 blowdowns: startup, intermittent, and continuous.	Consider removing the intermittent blowdown to Area 58 blowdown drum.	$10,689
58-003	RSC HP Steam Letdown to MP Steam Drum	There are bypasses around the RSC HP Steam to MP steam drum flow control valves. There are also double block and bleeds upstream of the valve.	Evaluate isolation philosophy of these control valves. Consider removing the bypass around the control valves and eliminating one of the manual block valves.	$20,891
Item	**Item Name**	**Description**	**Proposed Change**	**Net Savings**
58-006	Process Stm Condensate Pumps	Current design utilizes condensate pumps and pumps in the polisher package.	Evaluate eliminating the pump redundancy between the LLP Steam Condensate KO drum and the Condensate Polisher.	$130,403
			Total savings per train	$2,451,948
			Total expenditure (included in $2.45MM calc)	$(1,300,555)

A Note on Personnel Investment

Time-to-maturity is the length of time it takes a new plant to reach its availability entitlement. For example: a plant may be designed to be available 95% of the time, but it may take 5 years for the plant performance to reach that availability target. The following factors play a role in a plant's time-to-maturity.

- Out-of-the-box Availability: Due to infant mortality rates of some equipment, a portion of a plant's initial cause for downtime is repair of equipment that fails much sooner than the projected life. Unforeseen process design / system integration issues may also play a role in out-of-the-box availability.

- System complexity: A complex system is obviously harder to operate than a less-complex system. For example, a multi-train unit with several common supply or product headers is a much more difficult system to operate than a single-train unit with dedicated supply or product headers. Another example is a system that significantly relies on manual operation versus a system that is highly-automated.

- Learning parameter: The learning parameter is a factor that depends on the plant personnel expertise and the ability to successfully operate the system. For example, a highly experienced and knowledgeable staff will be able to move through initial startup and reach its entitled availability more quickly than a less experienced staff.

The above factors are significant in a plant's availability in the first years of operation. As time progresses infant mortality is no longer a factor, and operators get more familiar with how to operate the system successfully.

Personnel investment directly impacts the learning parameter. Initial investment in hiring experienced personnel or pre-training less qualified personnel creates an expert team of operators who can respond appropriately to plant issues that arise throughout the first years of operation. An "on-the-job" training approach may be more cost effective early in the project; however, it will most certainly lead to significant plant downtime in the first several years of operation as the personnel gain adequate knowledge and expertise in responding to planned and unplanned events.

The following section offers some guidance on obtaining a well-trained, well-equipped staff.

- Create a structured training program for each employee, relative to their position (e.g. plant operators, production technicians, mechanics, I&E technicians). Training programs should consist of classroom training (theory) and On-The-Job training to ensure the maximum opportunity for success. Test the employee during pre-determined milestones and at the end of their training program for competency.

- Develop good operating procedures early in the project. It is often helpful to involve the future operators in the procedure development if available.

- Provide the necessary resources and ensure they are readily available for employees (e.g. drawings, procedures, supervision, and maintenance tools).

- Establish a Management of Change process. Tracking and managing plant changes is critical to ensure operators are trained on the latest information and procedures are up-to-date.

- Schedule periodic "Refresher training" sessions every three years to keep the operations workforce trained and aware of the latest changes to the plant and/or the operating philosophy.

- Cross-train workforce. This will create flexibility and enable the workforce to operate and/or work on various systems or equipment. Having a flexible and cross-trained workforce allows the plant to continue to function efficiently, during various plant and personnel changes throughout the lifecycle of the plant.

- If possible, use an Operator Training Simulator to train operators on how to perform various functions in the plant (e.g. dynamically simulated plant startup, shutdown, and malfunction scenarios). This will greatly assist employees in understanding the process dynamics, control system responses, and interface with the plant HMI screens.

This is only a qualitative discussion on how personnel investment plays a role in the availability of an IGCC plant. Any future work should involve deeper investigation into the impact of personnel investment on initial plant costs and improvements in availability.

2.3 Conclusion

Given all of the information presented thus far for improving operability and reducing CAPEX and OPEX, what should a design group do to create the best fit for a new IGCC complex? While the numbers speak a great deal from a simple perspective of nipping here and tucking there, an underlying story exists that is more compelling. It lies in an often untold or little spoken of aspect of industrial plant design, construction, and operation.

From the material presented, one can deduce that, given a designed IGCC facility, many methods exist for reducing the CAPEX or OPEX. Some may take shape in early, decisive engineering decisions based on equipment reliabilities, costs, and targets set by the customer. Others, being a little less apparent and visible, emerge through the course of the operation of the facility whereby reliability is learned (beyond manufacturer guarantees and predictions) and operating costs are realized over an entire complex versus an individual piece of equipment. RAM modeling, RCM practices, and equipment cost estimations, all play a huge part in the design of the IGCC facility. However, the project still lacks something.

The something lacking is vision from conception to plant maturity and the journey between the two. This project attempted to garner the overall experience from that journey and present it in meaning data: taking an existing design/facility and nipping and tucking it into a more economically and operable presentation to drive to success. A technology provider's engineering team, a detailed-designer's team, and a forward design team of the customer may not hold enough knowledge to complete a design that matches our goal. Bottom line: a little more resources spent in the front end with customer end-users and technology provider engineers experienced in real-world applications can enhance the process of detailing the design to cater it to the end user's needs.

Clear critical to quality/operability specifications should be set early. They should be concise and targeted on the goals of the end user. In our research, we found an improvement idea that cost nearly $450K but would allow an increase in operability from a 60-day cycle to one closer to six months. And another idea costing $23K more than the original design would allow operators to eliminate 1.5 hours of activity at each startup and shutdown event and do so more safely by eliminating the maneuvering of a spectacle blind flange. So, converse to the idea of saving costs, the project found some forward thinking that improved operability as well. This is a key for the front-end designers.

Another manner to state this principle is to apply original technology provider intent for systems and equipment and consider any specializations or customizations carefully. Likewise, the technology provider should execute deeper research in market trends and necessities in order to customize the original design to meet the market needs more appropriately. Numerous improvement ideas corrected one or the other of these statements. While no designer has a crystal ball by which to design an IGCC facility, especially given the durational nature of such projects, re-work and corrective engineering can be minimized.

Finally, the focus group executing the integrated operations philosophy portion of the study exemplifies a needed portion of IGCC facility design. A focus team often is capable of identifying more quickly and more appropriately areas from which to trim the fat or question intent as well as align to end user requirements for operability, reliability, and maintainability. A focus group comprised of personnel from the two aforementioned design teams and the end user group

could meet periodically through the design phase to help keep the project on track without becoming mired in the expansive details of it.

3.0 - Task 3 and 4 – Slip Form/Modularization Gasification/IGCC Components

In an Integrated Gasification Combined Cycle (IGCC) system, the traditional means of constructing many of the plant subsystems is through a “stick-built” approach which consists of individually lifting into final position structural steel columns, beams, and braces one “stick” or piece at a time. Tasks 3 and 4 of this project investigate considering alternate construction methods, namely concrete slip forming and modularization, respectively, for specific portions of the plant for the purpose of reducing cost and/or schedule. GE worked with Kiewit Power Engineers on this project as they bring real-world experience and success in designing with such techniques. The tasks considered multiple proposed concepts and their likelihood of resulting in significant reduces costs and/or schedule. During execution of the tasks it became clear that there was a solution that combined the two methods, thus the results of these tasks will be reported on together. Concentrating on combining a concrete slip form with modular floors for the gasification island is the primary concept and recommendation as well as investigating concrete slip form for coal silos and modularization for select piping racks.

3.1 Experimental Methods

Some ways that costs can potentially be reduced without any process and/or machinery changes is to consider improvements in lay-out and construction method. The study would need to include not only a look at the construction/start-up phase but also any effects improvements in this phase affected the design phase. The methodology followed was:

1. Select a representative plant design and comparison site.

2. Select an engineering, procurement and construction (EPC) firm that is an expert with different construction methods and design experience of industrial processes as GE’s areas of expertise lie more in the areas of power generation, gasification equipment, and related auxiliaries and not in power plant design.

3. Investigate representative site with the selected EPC.

4. Determine potential areas that may benefit from the different construction methodologies.

    - Outlining the potential areas
    - Initial sketches of the areas

5. Compare the results (cost and schedule) between the traditional construction methods utilized and new construction methods

    - Provide more detail drawings
    - Provide cost/schedule estimate for current construction methods in the selected areas.
    - Provide cost, schedule and constructability estimate for the proposed construction methods on the selected areas.
    - Use the US Gulf Coast as the standard for the estimates for each method.

3.2 Results and Discussions

The results can be broken down into two phases:

1. Conceptual Design – Identification of candidate structures/systems
2. Preliminary Design – Class 3/4 costs estimates of identified structures/systems

Conceptual Design

The plant that was selected for investigation was the IGCC facility for Duke Energy in Edwardsport, Indiana. The site was chosen because it best represented the current IGCC design for the US. Schematics and photographs of the plant may be found at the following link: http://www.duke-energy.com/about-us/igcc.asp

The region that was selected as the basis for the comparison was the US Gulf Coast.

GE selected Kiewit as the EPC for the study. Kiewit is an expert at updated construction methods that can impact cost and schedule.

After a site visit and review of related documents Kiewit provided an assessment detailing the areas investigated and a listing of which areas provided the highest potential for cost/schedule savings based upon construction methods. The most significant structures in the IGCC plant were noted as:

- Air Separation
- Coal Handling
- Gasification Island
- Pipe Racks
- Gas Turbine
- Steam Turbine
- Byproduct Removal
- Water Treatment
- Cooling Towers
- Electrical Substation

Recall that the gas turbine, steam turbine, air separation unit, gasifier, syngas acid gas and trace contaminant cleanup systems, and carbon dioxide/hydrogen separation technologies were excluded from consideration for this project as the Department of Energy already supports substantial research for these systems.

After removing the systems listed above and considering systems that had already been optimized over the years the Gasification Island was indicated as having the most potential for a cost/schedule savings based upon construction methods.

Traditional Construction Methods Used:

- Stick Building – structure is composed of columns and beams that are individually lifted into place by cranes, one piece or “stick” at a time.
- Jump Forming – structure is poured by concrete in stages. For example, concrete is poured in a form up to 4 to 6 feet in height and allowed to dry. The next day the forms are set up at the top of the dried section and another 4 to 6 feet of concrete are poured. This process takes place, day after day, until the final height of the structure is achieved.

New Construction Methods (not typically applied to Gasification Islands)

- Modularization

    - This is where piping and equipment for the structure is preassembled off-site in a fabrication yard and then shipped to site. This technique is popular in the oil and gas industry for offshore oil platforms.
- Slip forming
    - This is a technique of a “continuous” pour of cement while moving the “form” up. In the case of structures it can replace steel.

More specific breakdown is as follows:

Gasification Area	Slip forming	Modularization
Gasifier Process Structure	X	X
Coal Silos	X	
Pipe Racks		X

For more detail please refer to the Kiewit Position Paper in the appendix (Appendix H of Tasks 3 and 4 Final Report). There was an initial assessment of the areas with the more detail than just the site visit – and then the areas that showed promise were investigated further.

Preliminary Design

In the next phase Kiewit provided a Final Report detailing the study. The following are a summary of the findings of the report (for all the details please refer to the Final Report in the appendix). For each comparison for cost and schedule the new construction method was compared to the most appropriate traditional construction method.

Gasifier Process Structure

The gasification structure used for comparison in this study was based on a structure similar to that found at the Duke Edwardsport site. The structure is approximately 292 feet tall and has dimensions of 135 feet by 150 feet at the base and 65 feet by 150 feet for the upper 13 floors.

Figure 1 shows an isometric view of a stick built gasifier structure similar to the gasifier process structure at the Duke Edwardsport plant.

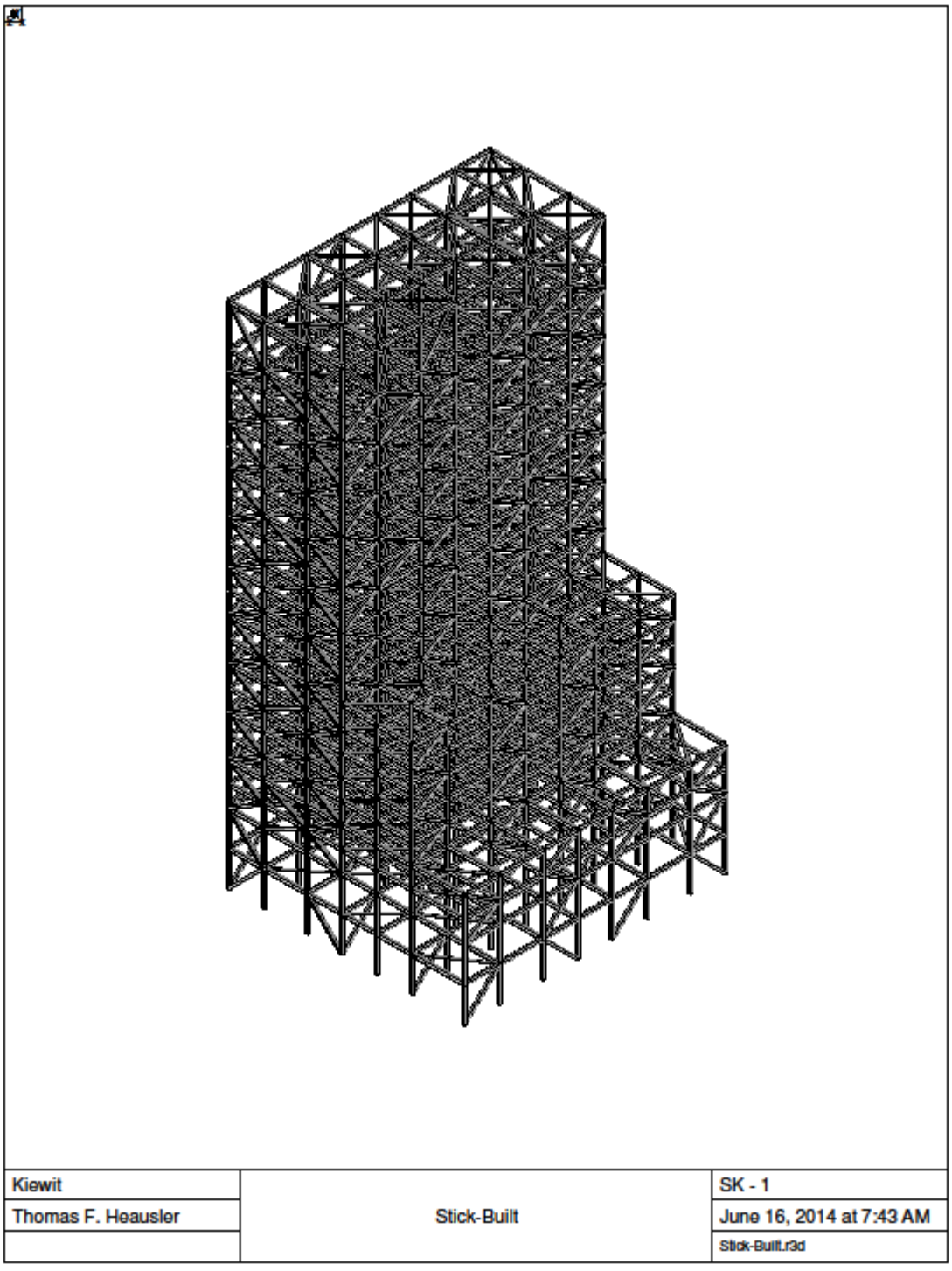

Figure 1. Isometric of Stick-Built Structure

The Gasification Process Structure had the most alteration in terms of construction techniques studied – as it combined both slip forming as well as modularization. For this solution the walls of the structure are made using the slip forming method and the floors were constructed as modules either off-site or elsewhere on the site. Figure 2 shows a concept of the general arrangement for the gasifier island structure from a slip form perspective.

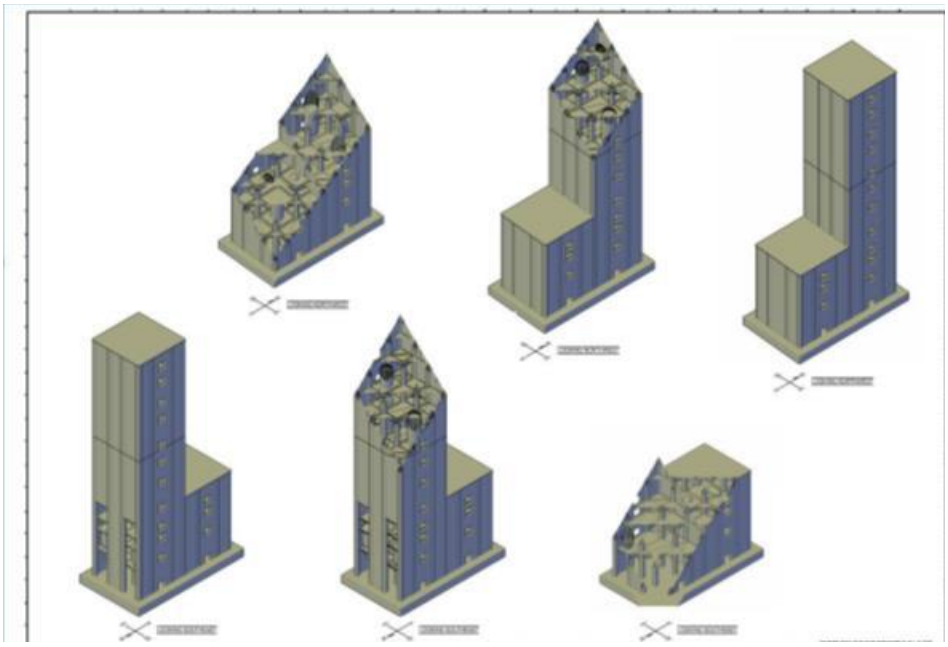

Figure 2. Concrete Slip form for Gasification Island Structure

Example of Slip form Scheme and General Arrangement

Table 2. Gasifier Island cost and schedule for traditional vs. slip form/modularization

Technique	Total Installed Cost	Total Design/Install Schedule
Slip form/Modularization	$319,000,000	43 Months
Stick Build	$321,000,000	46 Months

The results in Table 2 show an improvement in schedule (6.5%) and cost (less than 1%), but it is well within the margin of error for a Class 3/4 estimate. For this project a Class 3 estimate is defined as -10% to -20%/+10% - +30% and Class 4 is defined as -15% to -30%/+20% to +50%. This is much less than initially anticipated or previously thought. However, as the detail was looked into on constructability, the cost/schedule advantage of the slip form is muted by the equipment that spans multiple modules.

The use of slip forming/modularization at this point for the Gasifier Structure should be investigated on a project-by-project basis.

Pipe Rack Modularization

Upon investigating the actual amount of piping/equipment contained in the pipe racks and as modularizing the pipe racks does not provide any significant effect on the overall cost and schedule of the project for the US Gulf Coast region a more detailed comparison was deemed unnecessary. The use of pipe rack modules would be more beneficial in a remote site location with a high labor risk than it would on the chosen site of the US Gulf Coast. Figure 3 contains an example of a Kiewit project using modularization for the pipe rack.

Figure 3. Example of Kiewit project using modularization for a pipe rack type structure

The use of pipe rack modularization should be investigated on a project-by-project basis and has the following advantages and disadvantages:

Advantages

- Reduce/minimize on-site labor.
- Labor cost reduction based on fabrication location. The labor cost decrease can be substantial based on union vs. non-union and remote site construction.
- Reduction of on-site safety risk by moving work to an offsite fabrication yard.

- Reduction of construction schedule through parallel activities (i.e. foundation concrete and module fabrication occurring concurrently).
- Majority of steel/mechanical installation occurs in a controlled yard environment. This can increase productivity and reduce weather related delays.
- Typically reduces quality risks due to fabrication in a controlled environment.

Disadvantages

- Increased cost for transportation. A completed module can weigh in excess of 100 tons.
- Additional bracing is typically required for transportation loads.
- All piping and equipment must be secure prior to transportation which can add labor and materials.
- On-site module installation generally requires larger equipment, lift and set pipe racks modules.

Coal Silo

Due to the large size of the Coal Silos they appeared to be a good candidate for utilization of the slip forming technique versus the traditional jump forming technique.

Table 3. Coal Silo cost and schedule for slip form vs. jump form

Technique	Total Installed Cost	Total Design/Install Schedule
Slip form	$4,500,000	4 ½ Months
Jump Form	$3,000,000	5 ½ Months

Although there is a time saving for the slip forming technique – it comes at an increased cost, as shown in Table 3.

The use of slip forming the coal silo should be investigated on a project-by-project basis.

3.3 Conclusion

Although the study did not show a significant reduction in cost, schedule and constructability for a currently configured IGCC plant on the Gulf Coast at current prevailing conditions, the slip form and modularization technique should not be eliminated as potential cost and schedule saving construction techniques for IGCC plants in the future. The following items could have a definite on the magnitude of savings when utilizing these construction techniques as compared to the Stick Building option (or combination thereof):

- Improvements in the Gasification Island design
- Site geological and geographical conditions
- Site labor rates
- Site labor availability and skills
- Steel and Concrete costs
- Production Revenue (increase of initial revenue by being able to start earlier)

5.0 Task 5 – Radiant Syngas Cooler (RSC) Fouling Removal System

5.1 Understanding Fouling Mechanisms

5.1.1 Introduction

A typical configuration of syngas cooler with a gasifier used for gasifying coal feedstock in the Integrated Gasification Combined Cycle (IGCC) process is shown in Figure 4. Coal is pulverized and mixed with a fluid carrier to create slurry, which is then injected into the gasifier. The coal reacts in the gasifier to form syngas, which is used to fuel the gas turbine portion of the plant. This conversion of the coal results in a reducing atmosphere, with CO and H_2 being the dominant syngas species from the organic portion of the coal. After the high temperature syngas leaves the gasifier, it passes through the radiant syngas cooler (RSC) containing a series of heat exchanger tubes. Here, the syngas is cooled against boiler feed water to produce steam, which is combined with steam generated from the exhaust of the gas turbine and elsewhere in the power plant to produce power in a steam turbine. The production of syngas to fuel the gas turbine and the generation of steam for use in the steam turbine is what defines the "combined cycle" portion of the IGCC process. This combined cycle operation maximizes the amount of energy that can be extracted from the coal fuel source.

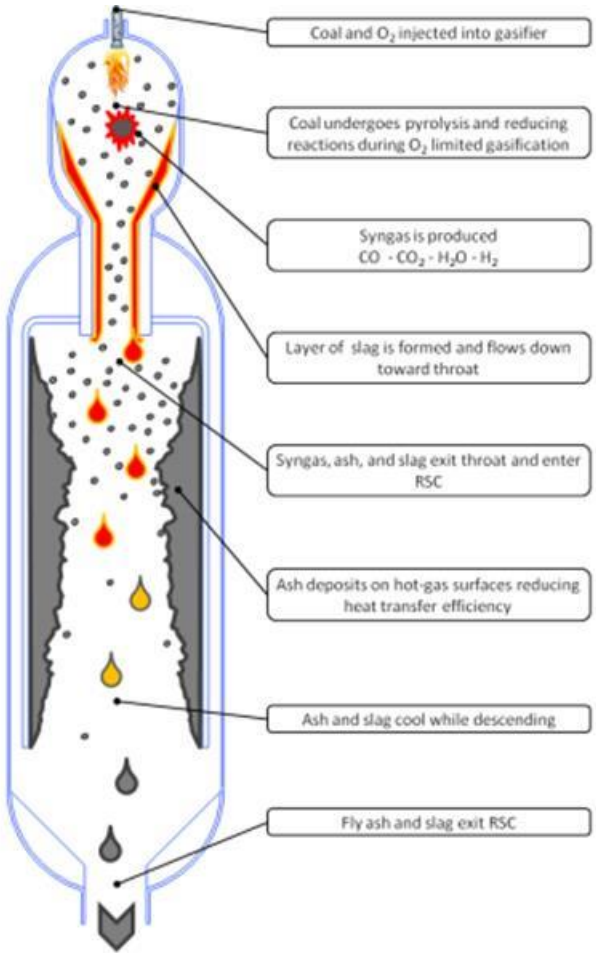

Figure 4. Schematic illustration of coal gasifier and RSC with ash deposits of an IGCC Power Plant

A byproduct of the coal gasification process is the generation of ash through volatilization of the carbon material and other organic matter. A portion of this ash byproduct accumulates on the heat exchanger surfaces of the RSC creating an insulating layer or fouling layer (as shown in Figure 4) that inhibits heat recovery from the hot syngas stream. This results in reduced efficiency and higher operating costs by decreasing the steam, and hence power generation capacity. Periodic shutdowns may be required to remove RSC fouling deposits and further increase plant operating costs.

The objective of the task is to develop a system which will remove fouling deposits on the heat exchanger tubes in the syngas cooler. The removal of fouling deposits will effectively improve steam production and availability for the IGCC plant, and increase plant efficiency. Consequently, this should lower the plant Cost of Electricity (COE, $/kWhr) and expand the coal operability range. In order to effectively identify and evaluate a viable RSC fouling removal system, it is important to first understand ash deposit formation and distribution as well as mechanical and thermal properties.

5.1.2 Ash Formation and Deposition

As show in Figure 5, the coal gasification produces ash and volatile inorganics which are formed from the coal mineral matter. Most of the ash is captured as a molten layer of slag on the gasifier refractory wall. Slag droplets are formed at the gasifier exit and fall through the RSC. The majority of the volatile inorganics, such as sodium, potassium, chlorine, fluorine, and sulfur, pass through the gasifier in the vapor phase with the syngas. The mineral matter that does not impact on the gasifier wall either becomes entrained in the syngas (if the particle or droplet size is small), or passes through the RSC together with the larger slag droplets. Inside the RSC, the vapor pressures of the volatile inorganics drop due to the cooling of syngas and/or contact with cooled water wall. If the vapor pressure becomes lower than saturation pressure, the aggregated state changes to liquid or solid phases and fine particles are formed in the gas phase. The fine particles may then condense against the metal surfaces forming ash deposits when the vapor pressure on the wall is lower than the boundary layer pressure. Other ash particles may then hit and stick on the deposit, causing the deposit to grow.

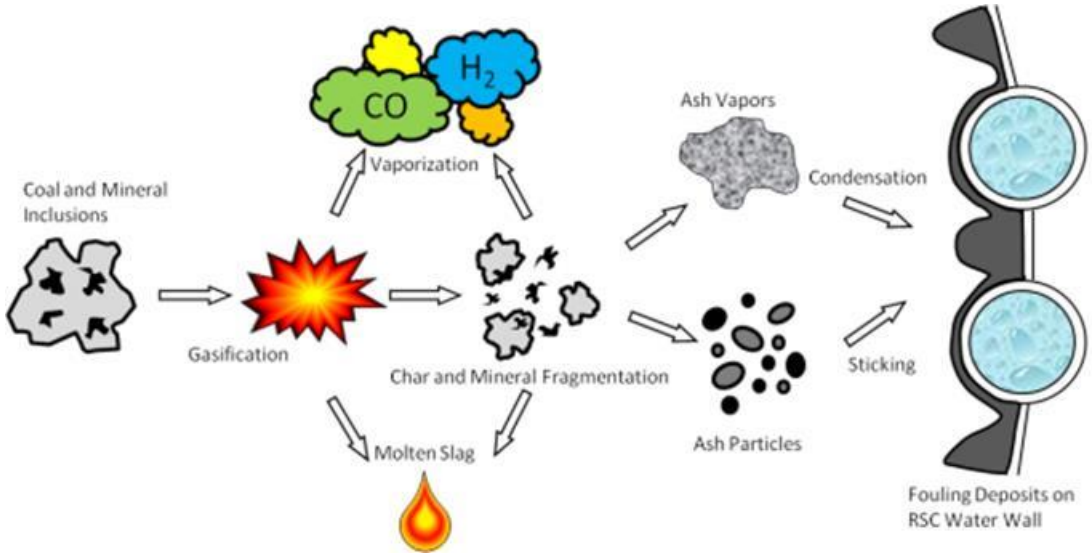

Figure 5. Ash deposition process in coal gasification

A wide variety of parameters affect the fouling process; fouling mechanisms are driven by the type of coal used, the combustion environment, and RSC internal geometry for example. The extent of ash formation depends upon the quantity and association of inorganic constituents in the fuel and upon gasification conditions. The fuels utilized in entrained flow gasification systems typically consist of high rank bituminous coals and petroleum coke, but may include subbituminous and lignite coals. The inorganic constituents in coal are in several forms, including organically associated inorganic elements and discrete minerals. The types of inorganic components present depend upon the rank of the coal and the environment in which the coal was formed. The inorganic components in high rank coals are mainly mineral grains that include clay minerals (kaolinite, illite, and montmorillonite), carbonates, sulfides, oxides, and quartz. Lower-rank sub bituminous and lignitic coals contain higher levels of organically associated cations such as sodium, calcium, magnesium, potassium, strontium, and barium in addition to the mineral grains that are found in bituminous coals. The inorganic components in petroleum coke include metals that are organically associated at levels that total less than 1% (nickel, iron, vanadium, copper, arsenic), salts that total less than 1% (sodium chloride, potassium chloride, magnesium chloride, calcium chloride), and relatively high levels of sulfur.

During coal gasification, minerals and other inorganic components associated with the coal and other carbonaceous fuels undergo a complex series of transformations that result in the formation of inorganic vapors, liquids, and solids in the flame. The inorganic vapors, liquids, and solids, referred to as “intermediates”, are cooled when transported with the bulk gas flow through the body of the gasifier and gas cooling and cleaning systems. The cooling process causes the vapor-phase inorganic components to condense and the liquid-phase components to solidify. The major transformation pathways during coal gasification are shown in Figure 6. Some trace elements can accumulate in the system and contribute to the accumulation of ash in various parts of the gasification system.

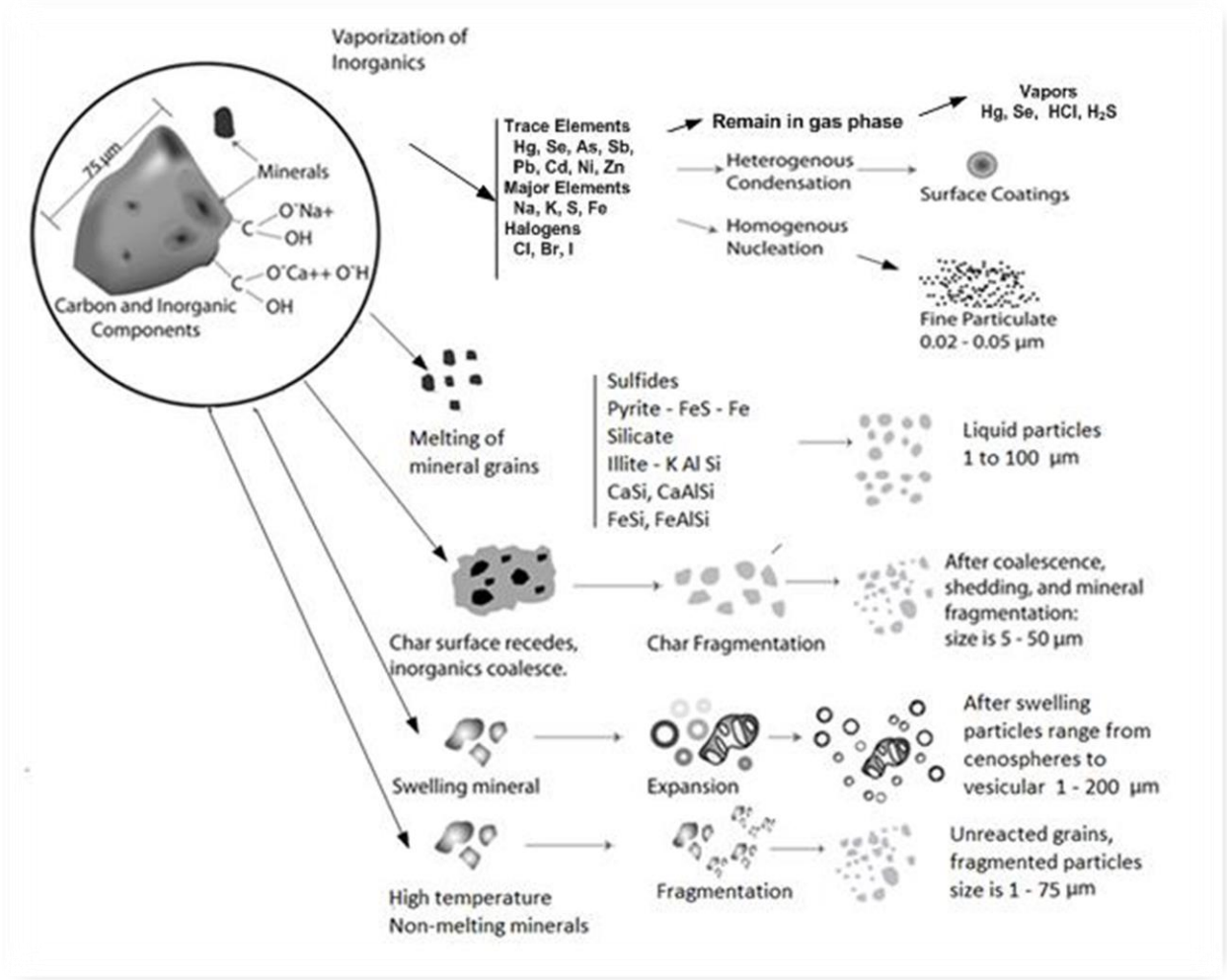

Figure 6. Major physical transformations of ash components during gasification (modified based on Benson and Laumb, 2007)

The physical and chemical characteristics of the intermediate materials that are being transported through the gasifier and RSC dictate their ability to produce a deposit that will flow from the system and form ash deposits. Ash deposition occurs when the intermediate ash species are transported to internal surfaces within the system, and then accumulate, sinter, and develop strength. The particle size of the deposited materials is important in the formation of strong deposits. Small particles will sinter and develop strength faster than larger particles. Major transport mechanisms are inertial impaction, thermophoresis, and turbulent eddy impaction, as illustrated in Figure 7. The ash deposit formation is further facilitated by condensation and chemical reaction.

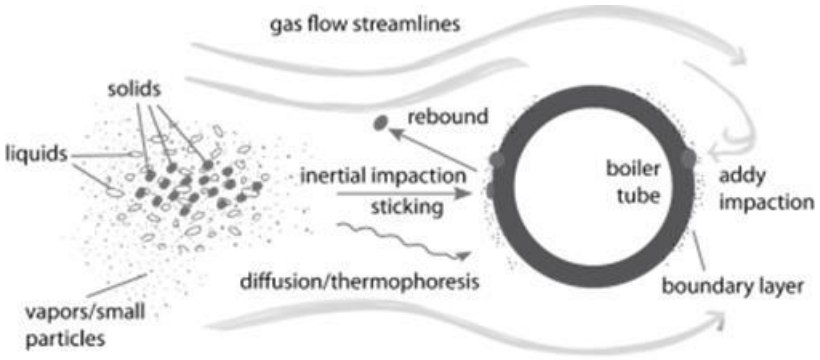

Figure 7. Major mass transport mechanisms of ash components to heat transfer surfaces (Benson and Laumb, 2007)

Inertial impaction is most often the process by which the bulk of the ash deposit is transported to the heat exchanger surface. The rate of inertial impaction depends predominately on target geometry, particle size and density, and gas flow properties. This process is most important for large particles (10 μm or larger) and results in a coarse grained deposit. The impaction rates are highest at the cylinder stagnation point, decreasing rather rapidly with angular position along the surface as measured from this stagnation point. At angular displacements larger than about 50° (as measured from the forward stagnation point), the rate of inertial impaction drops to essentially zero under conditions typical of combustor operation. Figure 8 illustrates this mechanism. Shown in Figure 8 is a particle being captured on the tube surface as well as a particle rebounding as a result of the impaction angle (Baxter, 2000).

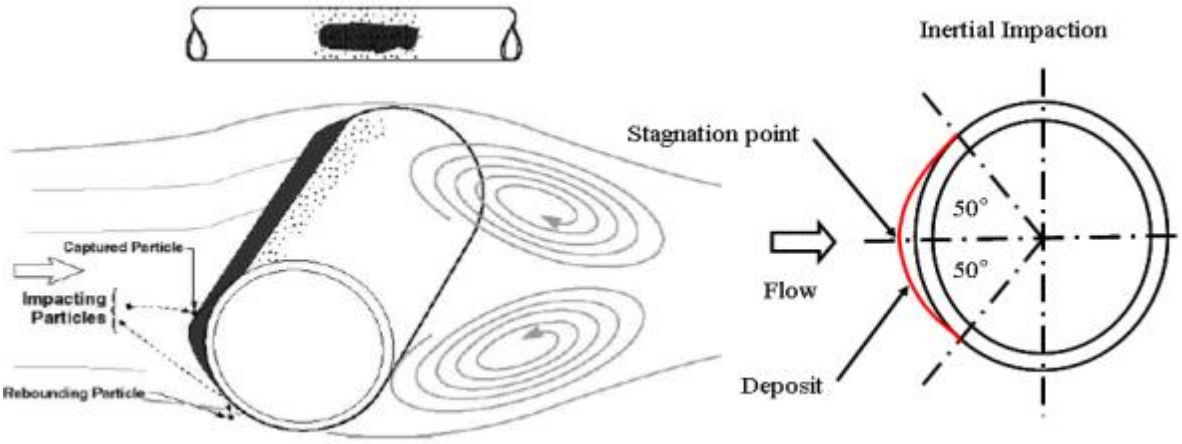

(a) (b)

Figure 8. Inertial impaction for ash deposition. (a) Inertial impaction with sticking and rebounding particles; (b) Deposit is coarse grained, with max thickness occurring at stagnation point tapering to zero beyond 50°. (modified based on Baxter, 2000)

Thermophoresis is a process of particle transport in a gas due to local temperature gradients. As shown in Figure 9, ash deposits are fine grained and evenly distributed on the surface. The origin of thermophoretic forces on a particle can be appreciated from the following, overly simplified argument: A particle suspended in a fluid with a strong temperature gradient interacts with molecules that have higher average kinetic energies on the side with the hot fluid than on the side with the cold fluid. The energetic collisions of the high energy molecules on the hot side of the particle create a stronger force than those of the low energy molecules on the cold side. The resulting imbalance gives rise to a net force on the particle. In general, these forces act in the direction opposite to that of the temperature gradient, although they can act in the direction of the gradient under certain conditions of particle surface temperature. With increasing deposit accumulation on the tube surface, there is a decrease in the temperature gradient in the thermal boundary layer, decreasing the rate of thermophoresis (Baxter, 2000).

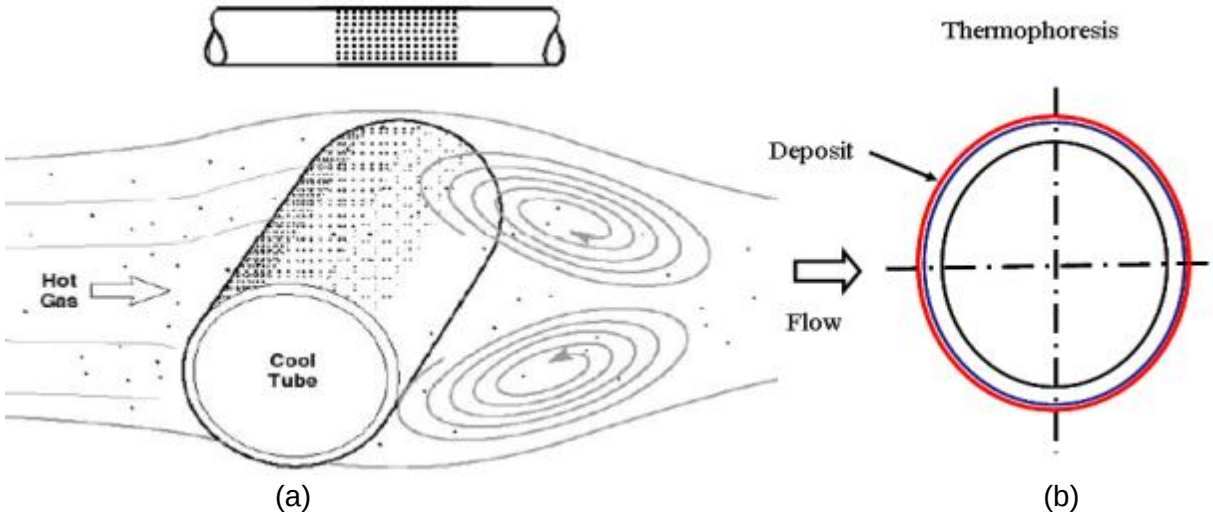

Figure 9. Thermophoresis impaction for ash deposition. (a) Thermophoretic deposition on a tube in a cross flow; (b) Deposit is finer grained with an evenly distributed buildup around the tube. (modified based on Baxter, 2000)

Eddy impaction is a process by which particles too small or light to inertially impact arrive at surfaces. They are deposited by the actions of turbulent eddies within or near the boundary layer rather than solely by their inertia as in inertial impaction. Consequently, eddy impaction influences only relatively small particles.

Condensation is the mechanism by which vapors are collected on surfaces cooler than the local gas. All vapors that enter the thermal boundary layer around a cool surface and subsequently are deposited on the surface can be thought of as condensate. The amount of condensate in a deposit depends strongly on the mode of occurrence of the inorganic material in the coal. Low rank (sub bituminous) coals have the potential of producing large quantities of condensable material. Condensate can increase the contacting area between an otherwise granular deposit and a surface by several orders of magnitude. This increases by the difficulty of removing the deposit from the surface by a similar amount. Condensate can also increase the contacting area between particles by many orders of magnitude, having profound influences in

the bulk strength, thermal conductivity, mass diffusivity, etc. of the deposit. Condensation is a relatively minor contributor to the development of deposits and their properties for most high-rank coals. However, in lower grade coals condensation becomes a significant contributor. The transportation of the vapors is highly temperature dependent. (Baxter, 2000).

Vaporization and condensation of inorganic elements contribute to the formation of fine particulates when the vapors condense homogeneously. In addition, these vapors can condense on surfaces of entrained ash particles and ash deposits, producing low-melting-point phases. In the gasification process, the coal and char particles are exposed to very high temperatures in a combustion/gasification process, where the process occurs in an overall reducing environment.

Chemical reactions involve the heterogeneous reactions of gases with materials in the deposit or, less commonly, with the deposition surface itself. Some of the chemical species found in deposits are not stable at gas temperatures, alkali sulfates being typical examples. The sole source of these species is heterogeneous reactions between gas phase constituents and constituents of the lower temperature deposits. Among the most important chemical reactions with respect to ash deposition during coal combustion are: (1) sulfidation, and (2) alkali absorption. The principal sulfating species of concern are compounds containing the alkali metals, sodium and potassium. Sodium and potassium in the forms of condensed hydroxides and possibly chlorides are susceptible to sulfidation. Silica absorbs alkali material to form silicates. Silicates are less rigid and melt at lower temperatures than silica. The transformations of silica to silicates in deposits can induce sintering and significant changes in deposit properties. These reactions are relatively slow compared to sulfidation. Generally chemical reactions have strong temperature dependence and give rise to spatial variation in ash deposit composition. (Baxter, 2000).

5.1.3 Ash Deposit Bonding Strength

The bonding of ash and slag deposits for coal combustion systems has been investigated extensively. Raask (1985) provided a review of the bonding mechanisms for combustion systems. Benson (1987) and Moza and Austin (1982) have studied ash sticking to heat transfer surfaces under combustion conditions. Tangsathitkulchai and Austin (1986) investigated sticking of ash materials to steel surfaces under gasification atmospheres. Ash and slag deposits can be mechanically bonded to the surface. The roughness of the steel surface will increase the degree of mechanical bonding. The steel surfaces are usually rough due to interaction of ash species with the surface. Mechanical bonding is typically weak. Chemical bonding of ash particles or slag materials to steel surfaces is very strong and occurs if oxygen or sulfur species are available on the steel surface to react with the ash particles or slag materials. In combustion systems, the steel surfaces have layers that consist of corrosion products that are rich in oxygen and sulfur. Carbon steels have significant layers of oxidation and corrosion products, while stainless steels are more resistant to oxidation and corrosion. Under the reducing environments present in gasification systems, initial layers on steel are enriched in sulfides (Tangsathitkulchai and Austin, 1986; and Benson and Laumb, 2007). The formation of strong bonds between steel surfaces and ash particles or slag materials depends on the following:

1) Surface tension or wetting ability of the deposited material
2) Temperature of the steel surface and the deposit
3) Type of steel/alloy

4) Characteristics of the steel surface or ability to form chemical bonds with deposited material
5) Similarity in thermal expansion coefficient between the deposit and steel surface

5.1.4 Mechanisms of RSC Deposit Formation

Coal ash deposition and agglomeration in a gasification environment occurs primarily by the combined action of primary particle liquid phase formation and liquid condensed phases derived from volatile species. The primary particle liquid phases are largely silicate and aluminosilicate based. The viscosity of the silicate base liquid phases can be used to describe the sticking behavior. The vapor phase can condense and react on coal ash surfaces to form a range of compounds. For example, alkali-iron sulfide eutectics are chemically stable in a gasification environment below about 750°C (400°F), but decompose or vaporize above that temperature. CaS is stable at higher temperatures up to about 900°C (1650°F) and may form CaS-FeS solid solutions at lower temperatures where FeS is stable. Eutectics formed from Na_2S, FeS, Na_2O, and SiO_2 are believed to be the principal cause of sintering at temperatures below 700°C (1290°F). Figure 10 shows the surface of a silicate particle coated with iron sulfide. Table 4 summarizes analysis of deposits, slag, and coal ash materials. The deposits have an elevated level of sulfur. Above 750°C (400°F), sulfided silicates may cause sintering. Gas transport processes that move volatile species from higher-temperature regions to lower-temperature zones promote sintering below about 700°C (1290°F). Water vapor absorbed into fused silicate glass below 720°C (1328°F) may also contribute to mass transport in the liquid phase by reducing the viscosity of eutectic melts (Uchins and others, 1991). Above 1000 °C (1832°F) silicates and aluminosilicates containing alkali and alkaline earth elements and iron contribute to deposition, clinkering and slag formation.

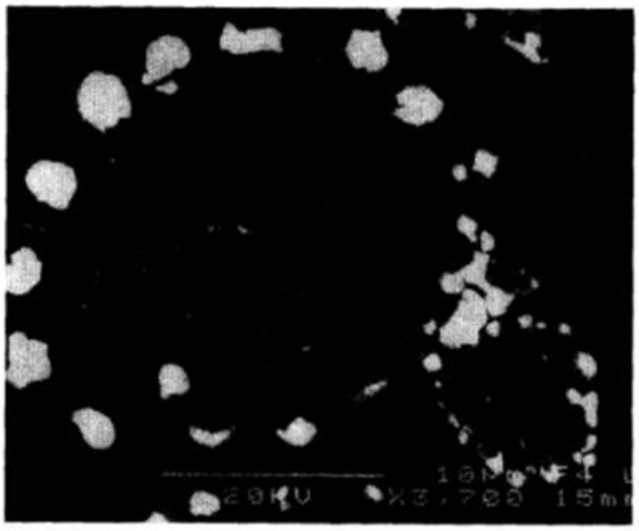

Figure 10. Iron sulfide phase coating the surface of particles produced in an entrained flow gasifier (Brooker and Oh, 1995).

Table 4. Analysis of deposits, slags, and coal ash from Cool-Water syngas cooler (elemental wt. %).

	Na	Mg	Al	Si	P	S	K	Ca	Fe
Bulk									
Gas side	1.4	2.4	17.7	34.1	0.4	10.9	3.1	8.3	20.1
Interior	1.5	2.0	17.2	31.0	0.7	11.0	2.4	8.7	24.6
Clarifier	2.5	2.1	18.6	31.2	0.3	3.2	2.8	7.9	27.9
Slag	2.1	1.8	20.6	35.8	0.4	2.3	2.1	6.0	29.7
Pittsburgh No. 8-ash	1.1	1.1	21.7	39.5	0.4	0.2	3.0	7.6	22.1
Average of 15 particles									
Deposit–outside	1.6	1.7	19.8	41.0	1.0	4.3	2.8	7.0	19.7
Deposit–middle	1.5	1.5	19.6	48.1	0.7	1.8	5.0	13.0	7.4
Clarifier	1.8	2.2	22.4	40.5	0.3	1.1	3.1	7.2	21.6

Analysis was made using some fouling deposit samples from a RSC, with results summarized in Table 5 and Table 6. The results show that the deposits consist mainly of zinc, iron, and sulfur. The results presented in Table 6 are carbon free and normalized to 100%. This allows for easy comparison to the components in the ash. The higher levels of zinc accumulated in the deposits is likely due to recycling the fine ash. Vanadium was also found in the deposit suggesting that the system was co-fired with petroleum coke. These deposits were dominated by sulfide-based phases.

Table 5. RSC deposit analysis (elemental wt. %)

	C	O	Na	Mg	Al	Si	P	S	K	Ca	Ti	V	Fe	Ni	Zn	Total
Sample 13																
Surface Layer	16.42	20.88			3.06	4.8		18.7	0.42	0.95	0.21	0.39	11.95		22.22	100
Above Stripe	6.82	25.9			4.79	8.9		15.64	1.08	1.11	0.5		5.75		29.51	100
Stripe	11.95	22.42		0.41	3.32	6.84		14.62	0.36	1.52		2.38	5.1	0.46	30.61	99.99
Metal Interface	23.13	24.01		0.36	3.13	8.13		8.59	1.49	0.54		2.78	2.64	0.65	24.55	100
Sample 19																
Surface Layer	15.79	40.61	1.98	0.26	5.92	9.87	0.31	6.51	0.65	2.62	0.52	3.21	0.83	0.94	2.51	92.53
White layer	2.67	48.67	3.72	0.44	9.45	18.75		3.31	1.71	3.24	1.26	0.39	6.41			100.02
Dark Stripe	13.3	22.23			3.18	6.46		17.53	0.8	0.8		0.41	25.27	0.65	9.38	100.01
Thin Stripe	32.27	29.94			3.09	7.26		6.44	0.68	1.6			5.8		12.91	99.99
Middle	17.11	19.84			2.98	6.37		15.54	0.82	0.95		1.1	5.43		29.86	100
Metal Interface	29.64	20.84			2.76	5.58		10.15	0.88	0.63		2.02	2.71	0.59	24.21	100.01
Sample 20																
Surface Layer	18.59	34.82		0.49	5.09	9.93		8.38	1.71	1.11	0.66		5.5		13.72	100
Middle	18.34	33.78			4.69	9.77	0.26	8.64	1.9	1.24	0.51		4.06		16.8	99.99
Metal Interface	16.04	32.26			4.98	12.03		7.79	2.32	1.7	0.69		8.41		13.79	100.01

Table 6. RSC deposit analysis on a carbon-free equivalent oxide basis, normalized to 100%.

	Na_2O	MgO	Al_2O_3	SiO_2	P_2O_5	SO_3	K2O	CaO	TiO2	V_2O_5	Fe_2O_3	NiO	ZnO	total
Sample 13														
Surface Layer	0.00	0.00	5.32	9.30	0.00	42.27	0.46	1.20	0.32	0.63	15.47	0.00	25.04	100.00
Above Stripe	0.00	0.00	7.93	16.43	0.00	33.69	1.12	1.34	0.72	0.00	7.09	0.00	31.68	100.00
Stripe	0.00	0.61	5.74	13.19	0.00	32.89	0.39	1.92	0.00	3.83	6.57	0.53	34.33	100.00
Metal Interface	0.00	0.68	6.82	19.74	0.00	24.34	2.04	0.86	0.00	5.63	4.28	0.94	34.68	100.00
Sample 19														
Surface Layer	3.86	0.62	16.45	30.56	1.03	23.52	1.13	5.31	1.26	8.29	1.72	1.73	4.52	100.00
White layer	5.52	0.80	19.98	44.17	0.00	9.10	2.27	4.99	2.31	0.77	10.09	0.00	0.00	100.00
Dark Stripe	0.00	0.00	5.30	12.00	0.00	38.01	0.84	0.97	0.00	0.64	31.38	0.72	10.14	100.00
Thin Stripe	0.00	0.00	9.13	23.91	0.00	24.75	1.26	3.45	0.00	0.00	12.77	0.00	24.74	100.00
Middle	0.00	0.00	5.33	12.69	0.00	36.14	0.92	1.24	0.00	1.83	7.23	0.00	34.62	100.00
Metal Interface	0.00	0.00	6.39	14.40	0.00	30.58	1.28	1.06	0.00	4.35	4.67	0.91	36.36	100.00
Sample 20														
Surface Layer	0.00	0.99	11.86	25.78	0.00	25.39	2.50	1.88	1.34	0.00	9.54	0.00	20.72	100.00
Middle	0.00	0.00	10.76	24.98	0.71	25.78	2.74	2.07	1.02	0.00	6.94	0.00	24.99	100.00
Metal Interface	0.00	0.00	10.59	28.51	0.00	21.55	3.10	2.64	1.28	0.00	13.32	0.00	19.02	100.00

The mechanisms of RSC deposit formation are shown in Figure 11. The curve is based on the thermodynamic stability of sulfide and aluminosilicate based phases. The ash intermediates that consist of inorganic gases, liquids, and solids interact during gas cooling and are transported to the heat transfer surface by inertial impaction, diffusion, and thermophoresis. The ability of the depositing materials to stick to the heat transfer surface is dependent upon the properties of the heat transfer surface. In gasification systems, the heat transfer surface is exposed to reducing atmospheres that contain H_2S. The H_2S reacts with the heat transfer surface producing a sulfur-rich layer on the steel. The ash materials being transported to the surface interact with the sulfide layer producing bonds. The ash materials that contain elements such as iron, zinc, nickel, and other metals react with the H_2S to produce sulfides. The sulfide materials are the primary bonding components at lower temperatures near the surface. At higher temperatures the sulfides are no longer stable and the silicate and aluminosilicate phases react and combine with elements such as sodium, calcium, iron, and potassium. The silicate and aluminosilicate phases combine with alkali, alkaline earth, and metal oxides (iron) resulting in the formation of viscoelastic liquid phases. The melting and flow behavior of the silicate and aluminosilicates can be described by viscosity. The temperature range of the phases is shown in Figure 12.

The definition of the five regimes:

- Regime I. Dry sticking – no glue – according to Raask (1985) this regime is associated with small particles held in place due to van der Waals and electrostatic forces.
- Regime II. Vapor phase or thermophoretically deposited glue – vapor solid reactions and thermophoresis is a transport phenomenon of very small particles (<1 micrometer) associated with a temperature gradient and is defined by Raask (1985).
- Regime III. Heterogeneous chemical reactions as vapor ash interface – bonding associated with sulfur species are no longer stable because of increasing temperature. Heterogeneous reactions are occurring between silicate and aluminosilicate particle that are causing the bonding to occur.
- Regime IV. Ash particle softening – based on the viscoelastic behavior of ash particles that are defined by viscosity temperature relationship. Sticking temperature is based on the viscosity of the particles.
- Regime V. Wet Limit – surface of the deposit become molten and ash particle based on the viscosity of the surface. The sticking coefficient approaches unity where all ash particles stick.

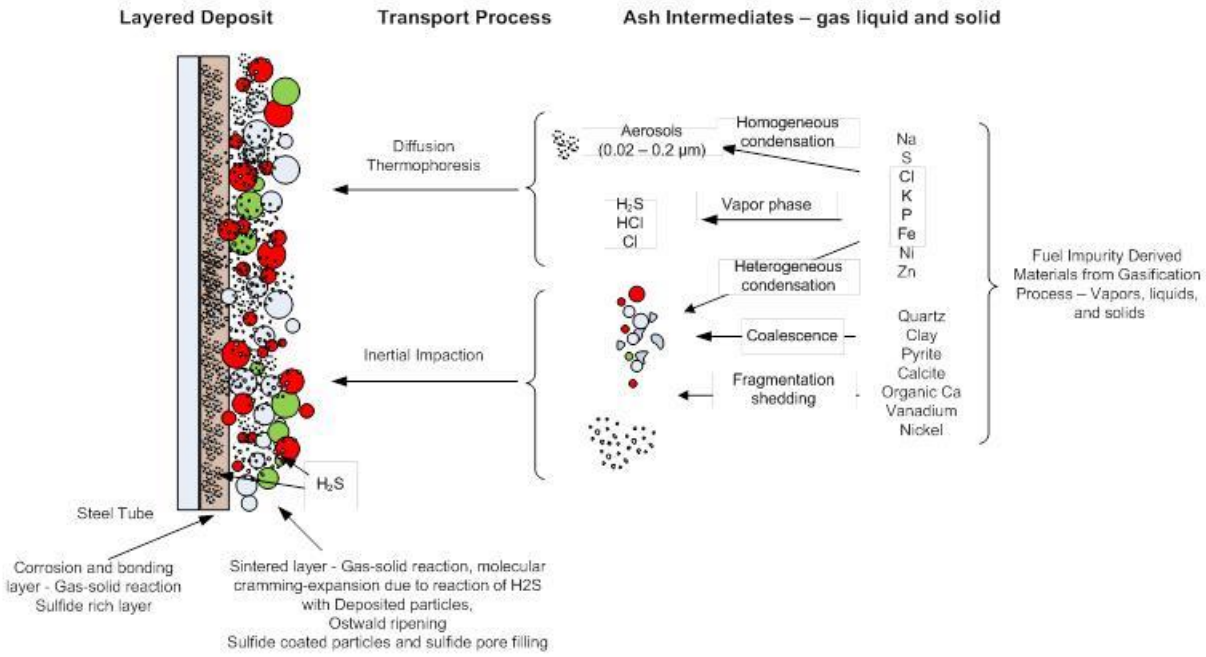

Figure 11. Transport and bonding mechanisms of ash components to heat transfer surfaces in syngas cooling systems.

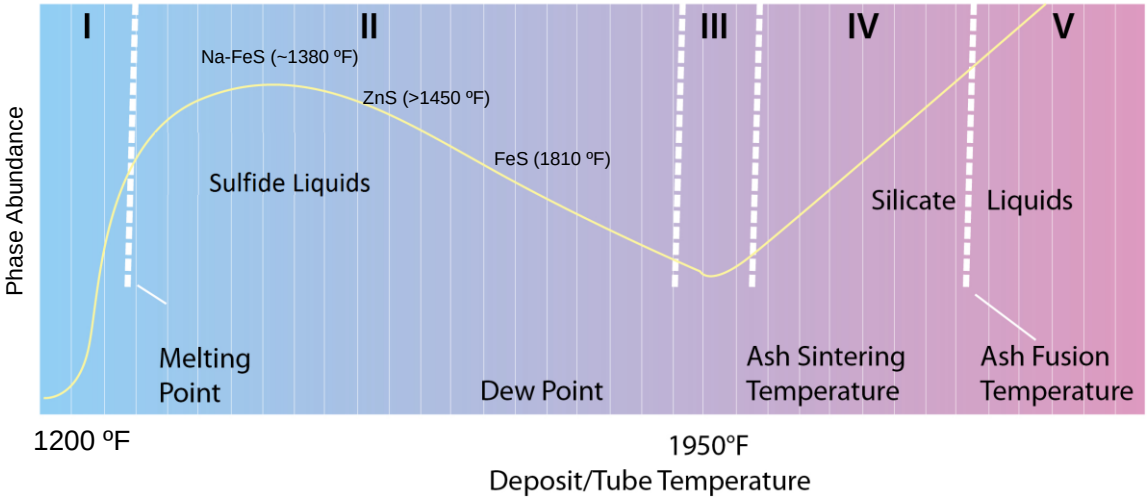

Deposition Regimes:

1. Dry-sticking regime: no glue
2. Vapor or thermophertically deposited liquid glue
3. Glue produced by heterogenous chemical reactions at vapor-ash interface
4. Ash particle softening on impact
5. Wet limit (sticking coefficient nearly unity)

Figure 12. Temperature impacts on bonding phase formation.

Phase diagrams for the sulfide systems were examined in an effort to better understand the melting behavior of the sulfides of concern. The lowest melting point eutectic for the Fe-S system is about 988ºC (1810ºF). The ZnS system appears to be the most stable with melting points above 800ºC (1450 ºF).

5.2 Feasibility of Online Fouling Removal

5.2.1 Fouling Removal Mechanisms

A US patent search was conducted investigating fouling prevention and fouling removal methods for IGCC gasification systems. The focus was on the heat exchanger surfaces in the RSC section. Some patents dealing with the gasifier and the gasifier/RSC connection were explored because of their effect on the conditions on the RSC.

The patents have been summarized in Table 7 and fall into six different groups: rapper devices, ceramic coatings or plating, cooled liners, process control, geometry change, and cleaning devices. The rapper group contains eight patents. Seven are mechanical types which would require access through the pressure vessel. One is a rapping device that isn't mechanical (has no moving parts) that uses water/steam to generate vibrational energy to knock off the fouling/slag. This concept has the potential to vary the frequency and location of the shock (water hammer). The ceramic coatings or plating group has two patents. One patent has been issued and the other applied for. The ceramic coatings are proposed on the basis that they may prevent fouling or slag buildup and would only need to be applied in the high temperature area where sticking occurs. The cooled liner group has two patents. The presumed intent of these is to cool the connecting section between the gasifier and the RSC. The process control group has four patents. Two of the non-GE patents are in the gasifier area. The GE patent is a method of achieving the fouling reversal experienced during shut down/restarts. The other patent thermally cycles the heat exchanger causing the deposits to fall off. The geometry and design change group has three patents. One patent is for two gasifiers, one is for the quench system, and the other is for a special arrangement of heat exchanger surfaces (platens). The cleaning device group has one patent, awarded to an individual. This is a temporary cleaning device to be used during shut down.

Table 7. Results for Fouling Removal Patent Search

Patent/Application Number	***Title***	***Patent Owner***
Rapper Device Group		
20,100,132,142	Rapper Device	Shell
5,429,077	Water Hammer Rapper Method and Apparatus	Babcock and Wilcox
7,823,627	Device for Generating Acoustic and/or Vibration Energy for Heat Exchanger Tubes	ExxonMobil
5,238,055	Field Adjustable Rapper Tie Bar	Babcock and Wilcox
6,460,628	Rapper Assembly	Kennecott Utah Copper Corporation
3,605,915	Pneumatic Rapper for Electrostatic Precipitators	Koppers Company

4,693,732	Piston Vibrator	Martin Engineering Company
5,639,359	Electrostatic Precipitator Discharge Rapper Anvil	Babcock and Wilcox
Ceramic Coatings or Plating Group		
7,914,904	Component in a combustion system. and process for preventing, and slag, ash, and char buildup	GE
20090202717	Anti-fouling coatings for combustion system components exposed to slag, ash and/or char	GE
Cooled Liner Group		
4,874,037	Apparatus for Cooling a Hot Product Gas	Korf Engineering GmbH
5,443,654	Method of Removing Deposits from the Walls of a Gas Cooler Inlet Duct, and a Gas Cooler Inlet Duct Having a Cooled Elastic Metal Structure	A. Ahlstrom Corporation
Process Control Groups		
4,461,629	Heat Recovery Process in Coal Gasification	Babcock and Wilcox
5,672,246/GB 2140144A	Increasing the Capacity of a Recovery Boiler by withdrawing some of the Exhaust Gases from the Furnace Section	A. Ahlstrom Corporation
20,110,036,096	Integrated Gasification Combined Cycle (IGCC) Power Plant Steam Recovery System	GE
20,070,274,886	Removal and Recovery of Deposits from Coal Gasification System	Microbeam Technologies, Inc.
Geometry and Design Change Group		
7587995	Radiant Syngas Cooler	Babcock and Wilcox
7534276	In-situ Gasification of Soot Contained in Exothermically Generated Syngas Stream	National Institute for Strategic Technology Acquisition and Commercialization
Cleaning Device Group		
4,428,417	Heat Exchanger Cleaner	No Assignee Specified

5.2.1 Fouling Removal

Four general mechanisms can be defined for online fouling removal: mechanical, thermal, thermal-mechanical and chemical. Examples of “mechanical” mechanisms include pulse detonation wave, soot blowers, water lances, acoustic horns and rappers. Examples of “thermal-mechanical” mechanisms include fouling reversal and water / steam hammer. An example of a “thermal” mechanism would be a technique to cause expansion and contraction of the heat exchanger tubes; this is essentially to create “fouling reversal” via the use of a thermal system. And finally, examples of “chemical” mechanisms include ceramic coatings / plating, heat exchanger material selection, fuel additives and feed stock selection.

5.2.1.1 Mechanical Fouling Removal Methods

1. Soot blowers

Soot blowers use high velocity gas (compressed air or steam) to blow the deposits off from the radiant water walls and convective pass tubes in utility boilers. In gasification units, the soot blowing gas may either be nitrogen, recycle syngas or even superheated steam. Typically, soot blowers are able to break the bonds between the deposit and the heat transfer surface, resulting in removing the deposit. This high velocity gas is about forty times higher than the normal flue-gas impact velocity, and over time has the tendency to erode the heat transfer surfaces it impacts. Soot blowers are not able to clean the complete heat exchanger surface because some areas cannot be reached. Usually, each soot blower cleans a region that ranges from 4 to12 feet in diameter. The high velocity gas gives only line of sight cleaning from the nozzles, and soot blowing is ineffective at removing sintered deposits. Thus, offline cleaning is typically still required. Therefore, soot blowers are typically considered to be better at preventing rather than removing established deposits.

TECO had a number of issues using soot blowers. This included issues with the seals that led to a 55 day outage in mid-2001. In addition, (1) the flanged connections were prone to leak at both the cooling steam/water connections and syngas/nitrogen connections; (2) despite a continual purge flow, soot and syngas migrated up the lances, causing deposits, condensate pockets, and severe internal corrosion of the lines; and (3) the seals where the lances penetrated the waterwall posed a threat of leakage resulting in hot gas impingement on the shell and shell overheating (Tampa Electric Company 2002). Figure 13 shows a soot blower installed at the TECO facility.

Figure 13. Soot blowers at TECO (Tampa Electric Company 2002).

2. Pulse Detonation Engine

Pulse detonation is an alternative to conventional soot blowing technologies. This is typically done using a Pulse Detonation Engine (PDE) that creates a controlled gaseous explosion in a confined combustor, external to the heat exchanger. Detonation consists of injecting a mixture of fuel and oxidizer into a combustion chamber, igniting this mixture, transitioning

the resulting combustion wave to a detonation wave. This is followed by a purge step to prepare for the next cycle. The detonation wave travels at supersonic speeds within the PDE combustion chamber and quickly decays to a sonic blast wave once it leaves the PDE combustion chamber and propagates in open space (or within a large structure, such as an RSC). The blast wave, also known as a pressure wave, a pressure pulse or simply an impulse has the energy required to remove sintered and unsintered ash on the heat transfer surfaces. The blast wave expands in all directions, even around obstructions, even reaching areas that are not in line-of-sight of the combustor. The blast wave itself is of short duration and accelerates entrained ash particles to relatively low velocity.

PDEs are typically used while a unit is up and running. PDEs are also expected to reduce heat exchanger tube wear relative to conventional soot blowing technology.

Podimov (1979) examined the use of pulse detonation methods to remove deposits. The method examined used a valve-less pulse-jet to provide a repetitive pressure wave. The PDE technology was successful in several industrial boiler applications in Russia. Pulse detonation with controlled pressure waves was tested using a laboratory model and in two full-scale, 300 MWe utility boilers in Bosnia (Hanijalić and Smajević, 1991; 1993; 1994a; and 1994b). The pulsed devices were used to clean tubes in the convective pass and economizer regions of the boilers. The results showed good cleaning performance, with no adverse effects on boiler tubes after 18 months of operation. Pulse detonation has also been tested for cleaning rotary air pre-heater surfaces in several full-scale utility boilers in China (Fan and others, 2002; Yu and others, 2001).

Based on past work, pulse detonation cleaning has the potential to remove hard deposits as well as loose ash. Additionally, a pulsed detonation device may be able to clean large areas and areas inaccessible to conventional soot blowing devices. A concern with pulse detonation is the possibility of tube damage due to the detonation pressure wave.

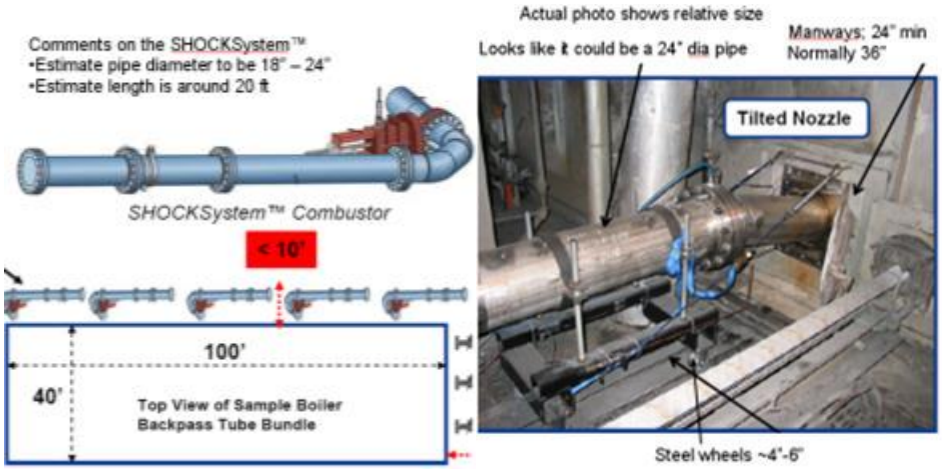

Figure 14. A typical PDE for fouling removal (McCormick, 2006). (a) Basic shape and size of PDE; (b) Installed PDE device.

Figure 14 shows the size and shape of the SHOCKSystem™ pulse detonation system, which is a commercial PDE system developed by Pratt & Whitney. Included in Figure 14 is an actual photo of an installed detonation system which in this case was done

through a manhole of a low pressure boiler. The PDE shown is likely larger than what would be needed for an RSC.

The system is further depicted in Figure 15(a) which shows how the nozzle is just inside the wall (similar to an RSC water wall). Figure 15(b) is the computational fluid dynamics (CFD) simulation of the blast wave propagation into a chamber of tube bundles (typically an RSC would have heat exchanging tubes running in a different direction, but the same theory applies).

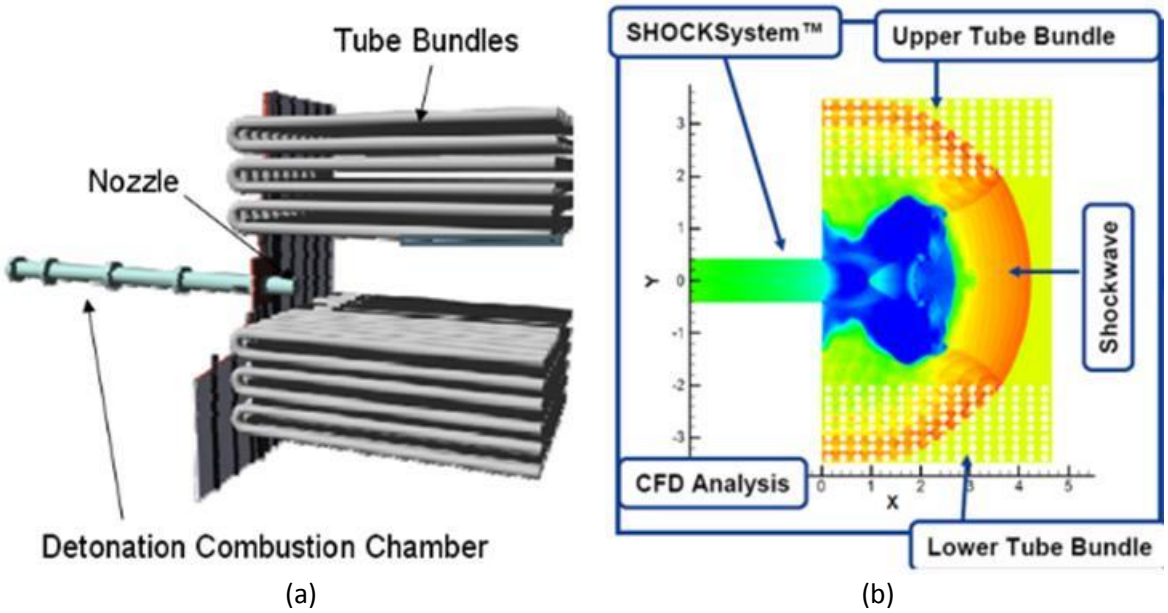

(a) (b)

Figure 15. Application of PDE wave for fouling removal (McCormick, 2006). (a) PDE nozzle with tube bundles; (b) CFD analysis of PDE wave interaction with tube bundles.

3. Acoustic Horns

Acoustic horn cleaning offered the promise of omnidirectional cleaning ability without the negative tube erosion effects of traditional air and steam soot blowers. However, research indicates that the results from acoustic horns have been moderate at best. Acoustic horns are intended to create sound waves, at various frequencies, to dislodge unsintered ash in the lower temperature regions of the heat exchanger. It has been reported that in certain applications sonic horns are required to run much more often than originally envisioned in an effort to improve their performance. Acoustic cleaning is used primarily in a continuous-maintenance mode and is reported to be inadequate to remove ash that's been allowed to accumulate and sinter (McCormick, 2007).

4. Water Lances

Water lances are typically used in the most aggressive situations, such as removing slag or cement-like deposits. A typical water lance is shown in Figure 16 with a cut out of the heat exchanger wall. The penetration hole through the heat exchanger would likely need to be sealed when not in use. But this technology has not been found in the application of RSC.

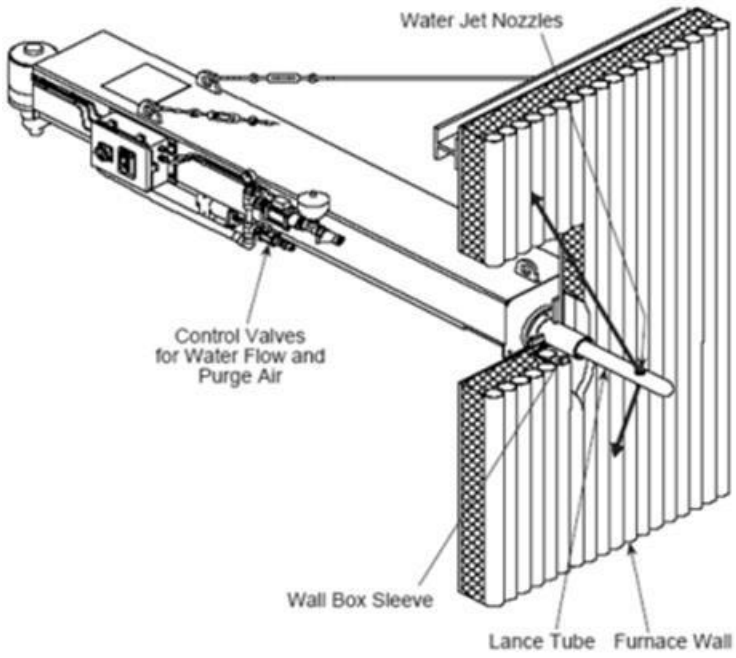

Figure 16. Water lance penetrates through heat exchanger wall.

5. Rapper Devices

Rapper devices are usually mounted outside the pressure vessel, as shown in Figure 17. A striker rod penetrates through the pressure vessel wall and strikes a portion of the heat transfer surface (such as the water wall in an RSC) through a special anvil plate. The force from this impact vibrates the surfaces, knocking off the deposits. Analysis would be required to determine the structural effect of the impact. Rapper devices were used at the Puertollano facility in Spain. The rapping devices had limited functions due to blockages inside the housing.

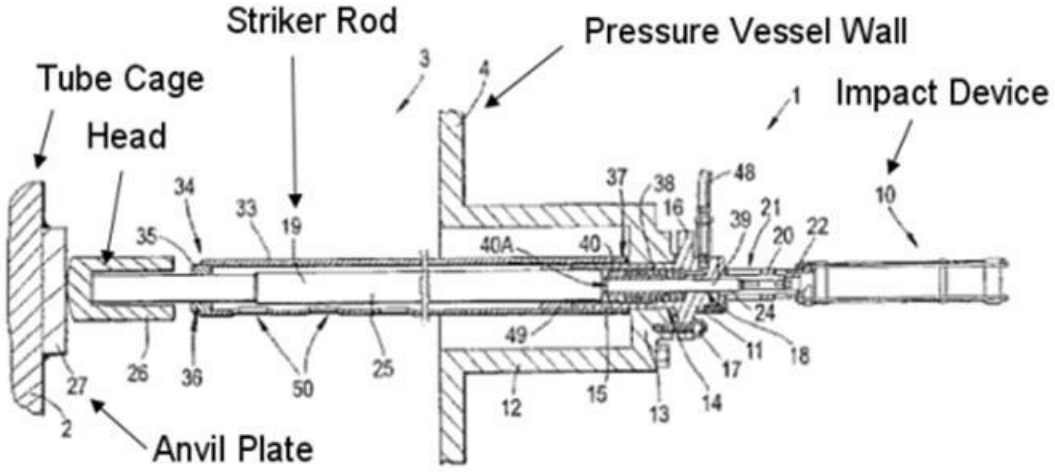

Figure 17. Typical rapper device.

6. Heat Exchanger Geometry

The aerothermal hot-gas path can be improved to control the flue gas temperature and velocities in a desirable range. This in turn can reduce fouling and may even help with fouling attrition.

5.2.1.2 Thermal Fouling Removal Methods

A technique to thermally expand and contract the heat exchanger tubes could conceivably be developed that may result in spallation of the deposits. For example, one downcomer at a time could be fed colder water for a given amount of time, causing contraction of that tube. If this contraction was appreciably different than the contraction of the deposit on the tube, spallation of the deposit could potentially occur. The loss in steam efficiency resulting from this technique would need to be evaluated, along with the long term structural effects of thermally cycling the heat exchanger components.

5.2.1.3 Mechanical Thermal Fouling Methods

1. Fouling Reversal

Fouling reversal is an interesting phenomenon that has been found where upon shut down / startup, some fouling falls off of the heat exchanger surfaces. This phenomenon has been termed “fouling reversal” and a patent has been applied for (reference patent application US 20,110,036,096). It is assumed in this case that fouling reversal can restore significant portion of the lost heat transfer capability as a result of such transients.

2. Water/Steam Hammer

A water/steam hammer effect may be created in the heat exchangers tubes by causing a local disturbance. Utilization of a technique like this could conceivably be an online cleaning method. However, there would likely be a loss in steam efficiency associated with the use of this technique.

5.2.1.4 Chemical Fouling Removal Methods

1. Ceramic Coating and Plating

It is helpful in preventing fouling to coat or plate the heat exchanger surfaces with ceramic in the area where fouling is expected. There are many different types of ceramics coatings and plating that offer potential solutions. The cost needs to be investigated to better understand the trade-offs between the costs of the coating/plating, impact on the coating/plating on heat transfer and fouling reduction, as well as the durability and maintainability of the coating/plating.

2. Heat Exchanger Material

Different heat exchanger material provides different bonding strength with fouling/deposit. It may be possible in some cases to reduce fouling deposits by selecting a proper material for the heat exchangers for a given fuel and operating conditions. Further research and testing would need to be conducted to determine cases where this technique may offer promise.

3. Fuel Additives

Chemicals and/or other additives could potentially be added to the fuel supply to change the fouling characteristics and reduce the fouling deposit. However, depending on how used, these could increase operating costs because of the cost of the additives, as well as increased solids disposal costs.

5.2.2 Engineering Physics of Fouling Removal

5.2.2.1 Thermal Mechanical Properties of Fouling Deposits

The thermal and mechanical properties of slags have significant impacts on the ability to remove deposits with various cleaning devices such as soot blowers. Deposits (water walls and convective pass) consist of complex materials that contain pores, unreacted ash particles, amorphous glassy phases, and crystalline phases. The characteristics of the deposited materials will depend upon the fuel composition, plant operating conditions, and location within the boiler. Wain and others (1992) examined the compressive strength, elastic modulus, thermal conductivity, and coefficient of expansion for slag deposits, and made relationships to slag deposit composition, crystallinity, and porosity. Their efforts were focused on developing a tool that could provide an indication of soot blower effectiveness.

Soot blowing relies on using a combination of thermal and mechanical shock to fracture the deposit. Crack propagation in slag is dependent upon a rapid change in temperature. In Wain's model, deposits are assumed to be brittle materials consisting of glass and crystalline material below the glass transition temperature, and the thermal stress generated in deposits can be defined by the thermal shock parameter:

$$\sigma = \frac{E \cdot \alpha \cdot \Delta T}{(1-\upsilon)}$$

where σ is the fracture stress, E is the elastic modulus, ΔT is the temperature change and υ is Poisson's ratio.

The equation can be re-written to find the temperature change ΔT or energy change required to reach the fracture stress σ in the form of two additional thermal shock parameters, R and R'. These in turn can be used to rank the susceptibility of various ceramic/glass materials to stress and crack propagation based on the measurement of thermal and mechanical properties of slag that vary with slag composition, crystallinity, and porosity.

$$R = \frac{\sigma \cdot (1-\upsilon)}{E \cdot \alpha} \quad \text{and} \quad R' = \frac{\sigma \cdot (1-\upsilon) \cdot k}{E \cdot \alpha}$$

where k is the thermal conductivity of the slag.

Wain and others (1992) measured the thermal and mechanical properties of ten slag samples from selected pulverized coal-fired boilers. They found that the thermal conductivity of the slags

was related primarily to its porosity, and the slag composition and crystallinity had little impact. The relationship between slag thermal conductivity and porosity is shown in Figure 18. They were not able to identify relationships between chemical composition, crystallinity, or porosity and thermal expansion, but found that slag compressive strength could be related to the porosity by the relationship:

$$\sigma = \sigma_0 \exp^{-nP}$$

where σ_0 is the compressive strength of the material with zero porosity, σ is the strength at porosity level P, and n is a curve fitting parameter.

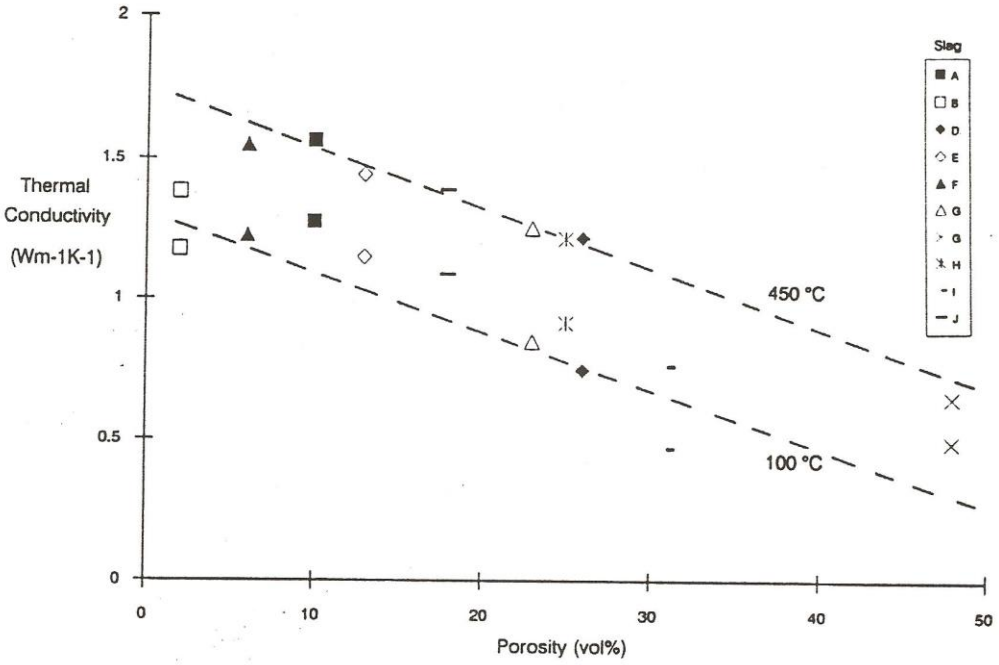

Figure 18. Relationship between slag thermal conductivity (k) and porosity. (Wain, 1992)

Rezaei and others (2000) compared measurements of thermal conductivity to show that the physical structure of deposits has a significant impact on thermal conductivity. Figure 19 illustrates the variation of thermal conductivity and ash porosity at temperatures between 350 and 800°C (662 and 1472ºF). Thermal conductivity decreases with an increase in the porosity, and increases with increasing temperature.

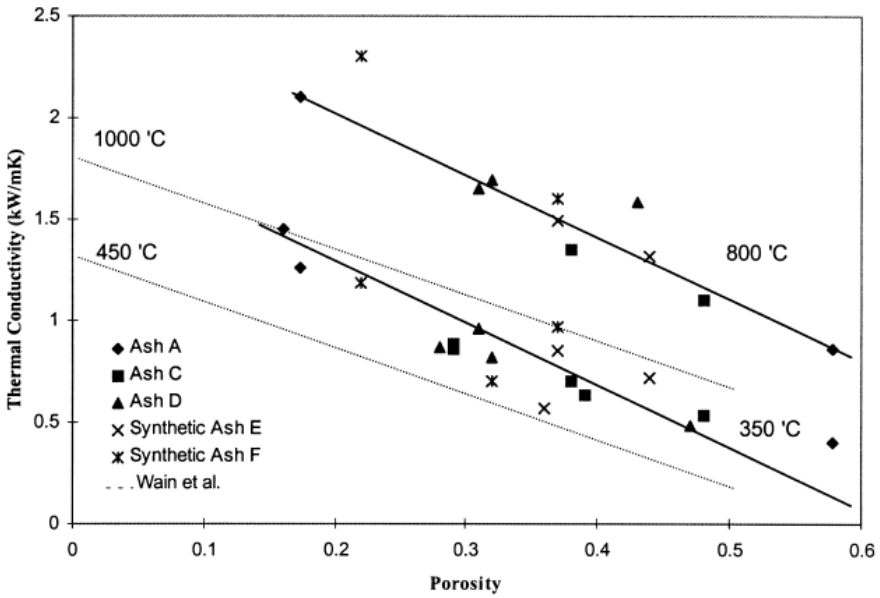

Figure 19. Thermal conductivity and porosity based on work conducted by Rezaei and others (2000).

Thermal shock parameters, R and R' were calculated from a combination of thermal and mechanical properties (Wain and others, 1992). The thermal shock resistance (R and R') as a function of porosity is illustrated in Figure 20. Based on the work by Wain and others, crack propagation would be easier in highly porous, glassy slag deposits. A lower porosity and higher-crystalline-content slag deposit would be more resistant to fracture. The resistance to fracture was found to decrease significantly for slags having a porosity of less than 25%.

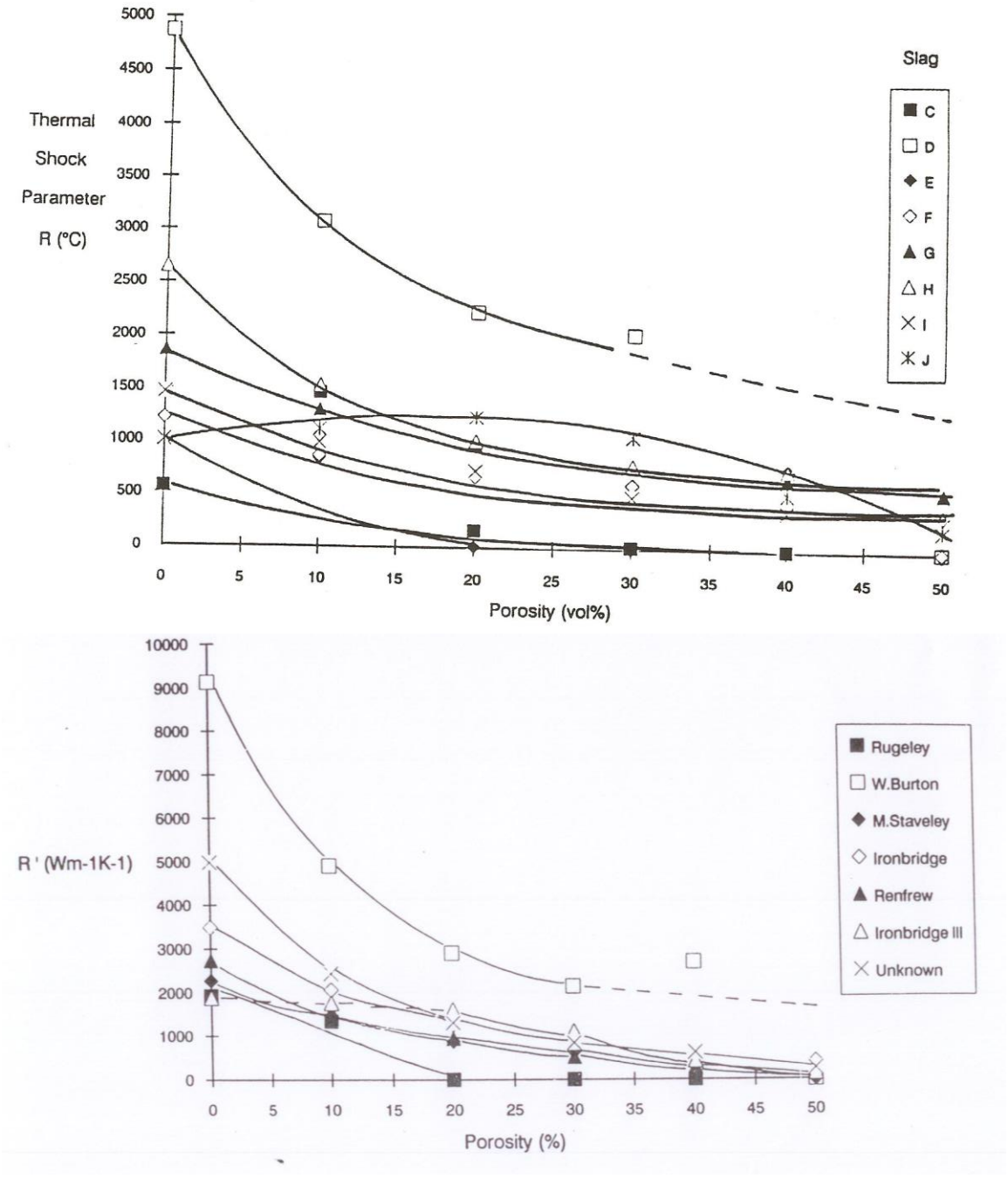

Figure 20. Relationship between shock parameters (R and R') and slag porosity (Wain and others, 1992).

5.2.2.2 Deposit Removal Force

Soot blower

The ability of a soot blower to remove deposits is related to the force of the soot blowing medium on the deposit. The measure of soot blower effectiveness is the peak impact pressure

(PIP). This is the stagnation pressure along the nozzle centerline at a given distance from the outlet of the soot blower nozzle (Kashitani and others, 1998). The PIP decreases with distance from the nozzle.

Several researchers have performed detailed numerical modeling of soot blower nozzle jets to determine PIP at a selected distance from the nozzle. Kaliazine and others (1997) developed relationships to calculate the PIP, as follows:

$$V/V_{ex} = 1 - \exp\{-1/[k_v(\rho_4/: \rho_{ex})^{½} \cdot \chi/R_{ex}-0.7]\}$$

and

$$(H_x - H_{ex})/(H_o - H_{ex}) = 1 - \exp\{-1k_H(\rho_4/:\rho_{ex})^{½} \cdot \chi/R_{ex}-0.7]\}$$

where χ is the distance from nozzle exit, V_{ex} is the jet velocity at the nozzle exit, H_{ex} is the stagnation enthalpy at the nozzle exit, H_o is the enthalpy of the surrounding medium, R_{ex} is the nozzle exit radius, ρ_4 is the ambient gas density, ρ_{ex} is the nozzle exit gas density, M_{ex} is equal to $V_{ex}/V\gamma RT_{ex}$, and is the Mach number at the nozzle exit, and γ is equal to c_p/c_v, or the ratio of specific heat capacities for the jet gas.

The main mechanical factor that influences the removal of the deposit is the stagnation pressure due to the deceleration of the jet when it slows by hitting the deposit surface (Kaliazine and others, 1999). The stagnation pressure at the jet axis is called the peak impact pressure, P. Using these equations, the peak impact pressure can be calculated at any distance from the nozzle for a fully expanded jet:

$$P/P_{ex} = [1 + M^2(\gamma - 1)/2]^{\gamma/\gamma - 1}$$

$$P/P_{ex} = [(\gamma+1)/2]^{(\gamma+1)/(\gamma-1)} M^2[\gamma-(\gamma-1)/2M^2]^{-\gamma/(\gamma-1)}$$

where P_4 is the ambient pressure.

Figure 21 shows the relative performance of a conventional high-PIP nozzle to that of a fully-expanded nozzle on PIP, as a function of distance (Jameel and others, 1994). Based on experimental work, a theoretical fully-expanded nozzle would have a higher PIP at a greater distance than an experimental high-PIP conventional nozzle.

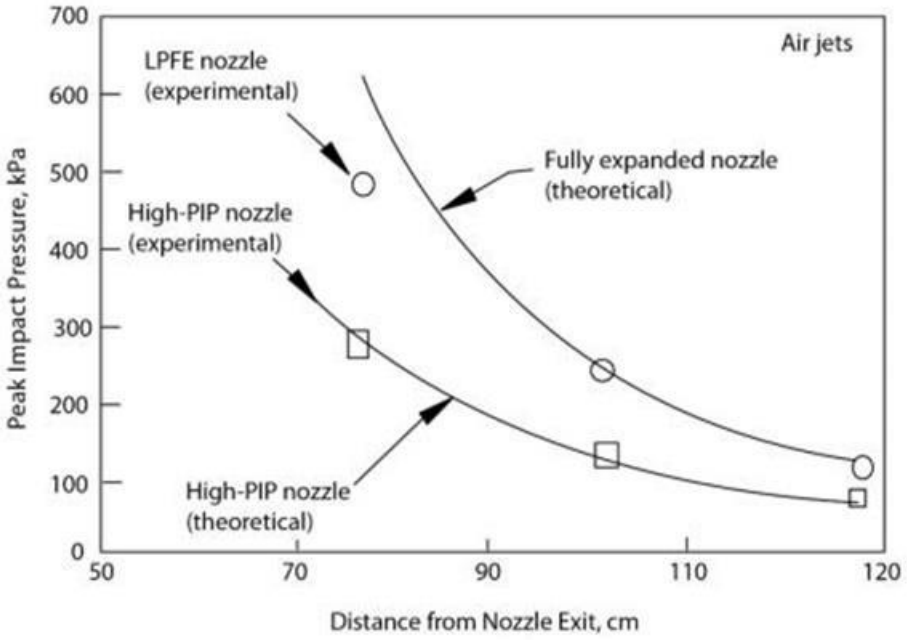

Figure 21. PIP as a function of distance from nozzle exit (Jameel and others, 1994).

The PIP decreases with distance from the soot blower nozzle, as shown in Figure 22 and Figure 23. The presence of heat-exchange surfaces impacts the PIP, as shown in Figure 24 where the PIP for a free jet and for a jet confined between simulated platens are compared (Kermani and others, 2001). In this experiment, the PIP of the confined jet was approximately fifty percent higher than that of the free jet, at distances greater than 29.5 inches (0.75 meters) from the nozzle.

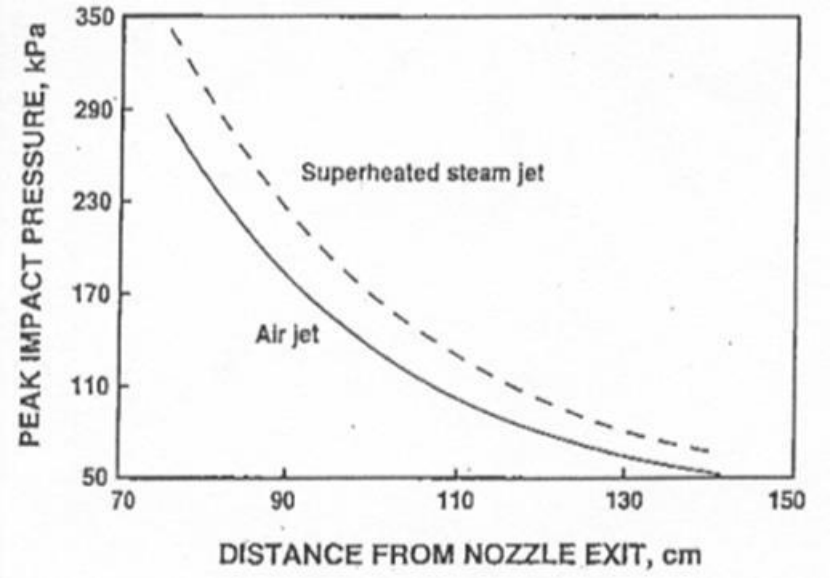

Figure 22. PIP as a function distance from the nozzle for air and steam (Jameel and others, 1994).

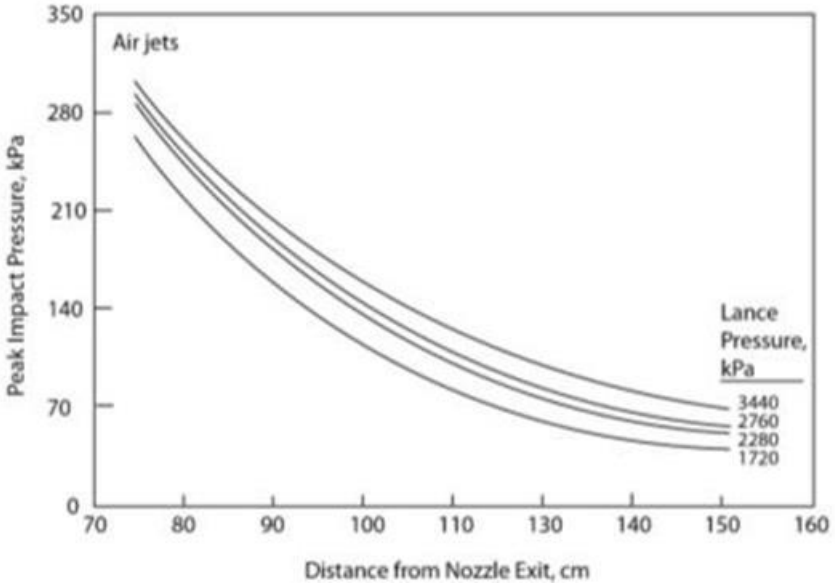

Figure 23. **P**IP as a function distance from nozzle exit for various lance pressures (Jameel and others, 1994).

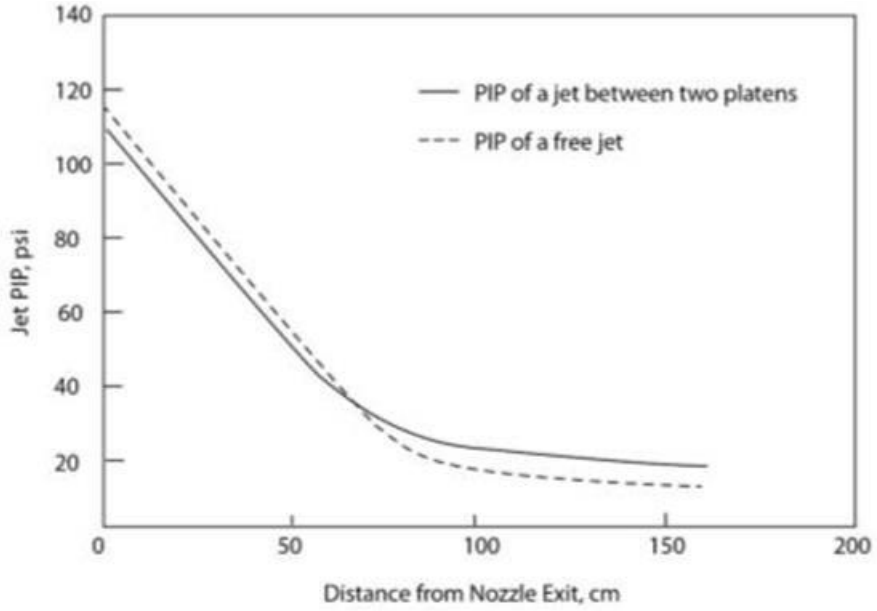

Figure 24. PIP profiles for a free jet and between platens (Kermani and others, 2001).

Ash deposit removal by soot blowers is related to the PIP that is delivered to the deposit, the deposit tensile strength, and the angle of impaction of the jet. Kaliazine and others (1997) utilized a criterion for deposit removal, in which the PIP needs to be greater than twice that of the deposit tensile strength, in order for impaction normal to the deposit to occur:

$$P > 2\,S_t$$

where P is the PIP, and St is the deposit tensile strength.

Using a series of model deposits of known tensile strength, Kaliazine has formulated an approximate expression that accounts for jets impacting at an oblique angle (Kaliazine and others (1997) :

$$P > 2\ S_t / \cos^2(a)$$

where a is the angle of the jet, relative to the deposit surface.

The influence of deposit tensile strength on the pressure (or distance) from the jet required to fracture the simulated deposit is illustrated in Figure 25. As tensile strength of the deposit increases, the pressure required to fracture the deposit also increases. The angle of incidence required to remove a simulated deposit, as a function of the deposit tensile strength, is shown in Figure 26 (Kaliazine and others, 1997).

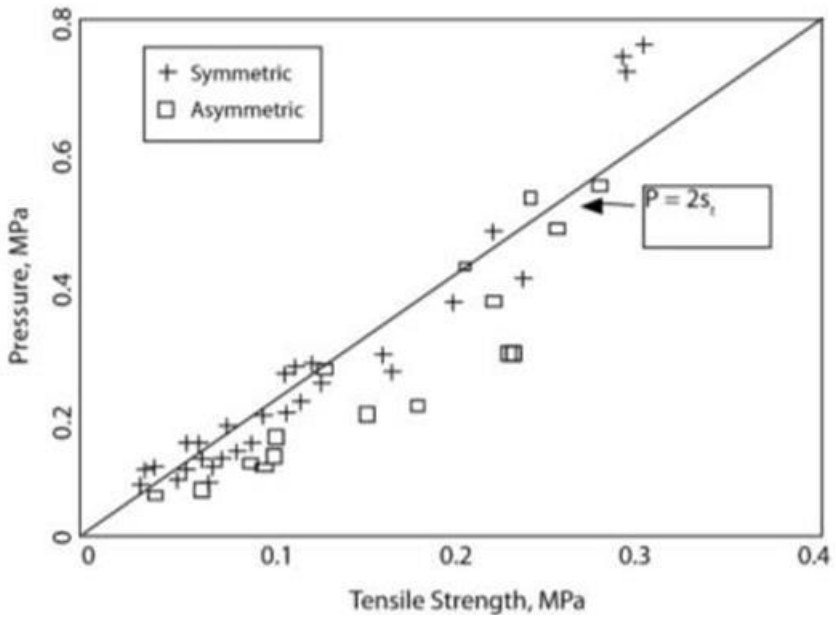

Figure 25. PIP versus tensile strength required to break simulated deposit (Kaliazine and others, 1997).

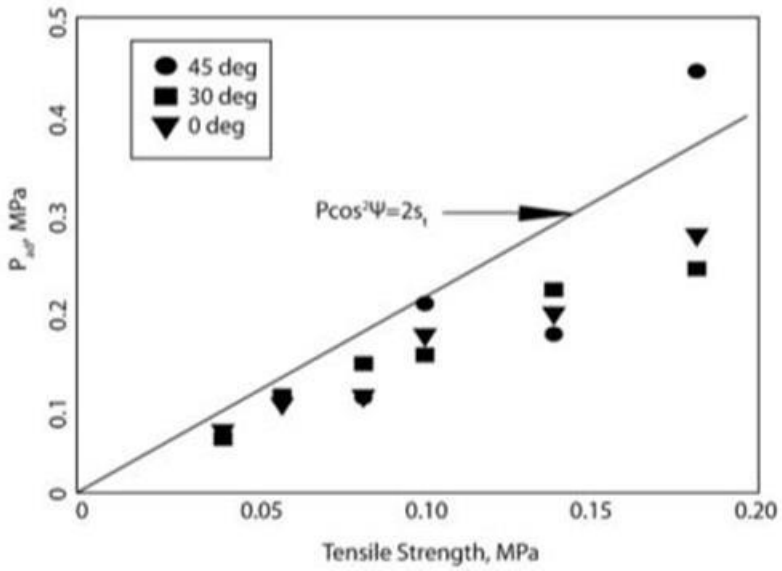

Figure 26. PIP required to remove the deposit versus tensile strength for different attack angles (Kaliazine and others, 1997).

Kermani and others (2001) developed a numerical model based on concurrent laboratory measurements. The model relates the drag force on the deposit (from the soot blower jet) to the stress induced in a deposit:

$$s = F/A$$

where s is the deposit adhesion strength, F is the drag force imposed on the deposit by a soot blower jet, and A is the contact area of the deposit with the underlying tube surface. Deposit removal will occur if the stress exerted within the deposit is greater than the adhesion strength of the deposit. In this case, the size of the deposit is important – the drag force increases with the deposit size. The influence of deposit height and distance from nozzle on drag force was also examined, as illustrated in Figure 27.

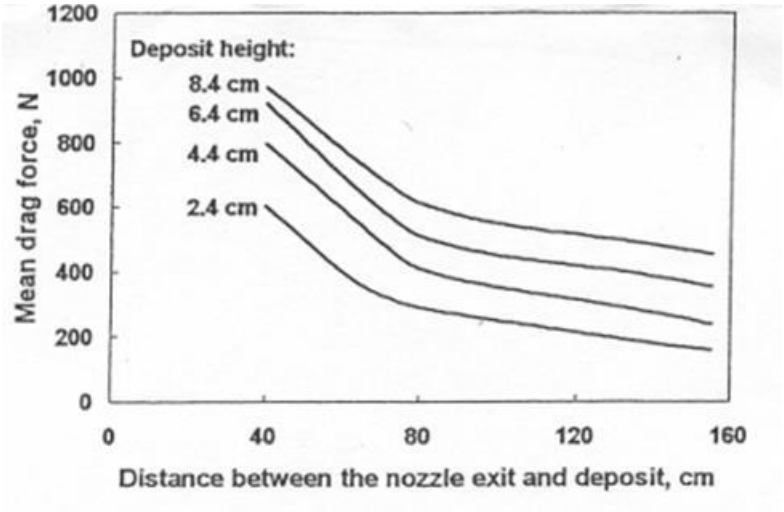

Figure 27. Drag force as a function of distance between nozzle and deposits of different heights (Kermani and others, 2001).

The force required for deposit removal can be estimated from the soot blower PIP, distance from the nozzle, the typical effective cleaning radius, and deposit tensile strength. The minimum cleaning radius for long retractable soot blowers is 4 feet (about 120 cm). At that minimum cleaning radius, indicative of deposits most difficult to remove, typical PIP values (estimated from Figures 27, 28, and 30) ranged from 10 to 22 psi.

Sonic Horns

Sonic horns, or acoustic soot-blowers, operate with a sound pressure of approximately 150 dB, equivalent to only 0.09 psi. This pressure is significantly less than measured values of deposit tensile and adhesion strengths. Because of the lower pressure, acoustic soot-blowing can only remove loosely-bonded or powdery ash material, and is not effective on materials that have developed any strength.

Water Cannons

Water cannons utilize a high-pressure water jet in which the pressure is estimated to be two to three orders of magnitude higher than the pressure of a steam jet at the same velocity. The higher pressure is due to the greater density of water in its liquid form, and, as a result of this higher pressure, water cannons are capable of removing water wall slag and high-temperature fouling deposits on platens.

Pulse Detonation

Pulse detonation is an emerging technology that has the potential to remove deposits by sending high pressure waves at the deposit. Experiments in a test furnace have indicated that the pressure wave produced is between 14.5 at 43.5 psi (Hanijalić and Smajević, 1993, 1994). This pressure appears to be significantly higher than a steam or air soot-blower jet at a comparable distance.

5.2.2.3 Comparison of Fouling Removal Methods

Normal flue gas velocity in the convective pass is generally limited by design in pulverized coal fired boilers to 50-60 ft/sec (15-18 m/sec) in order to keep tube metal removal rate associated with fly ash erosion within acceptable limits of nominally 3 to 4 millionths of an inch per hour (75 to 100 nm/h) (Parish, 2006).

The expanding jet from a soot blower lance mixes with approximately an equal volume of flue gas for every distance of the jet diameter it travels. Thus by the time the jet reaches the tubes, it consists largely of ash-laden flue gas. Although there are variations in nozzle geometry, soot blowing media, source pressure, and range from the nozzle, the jet diffusion model estimates the jet impact velocity at the tube surface to be about 1400-2900 ft/sec (430 to 880 m/sec) with jet impact dwell time of tens of milliseconds on a given heat exchanger tube. This is on average *forty times* the normal flue-gas-imparted impact velocity (Parish, 2006).

Heat exchanger surface erosion, and potentially subsequent corrosion, can result from fly-ash particles being accelerated and impacting these surfaces. The velocity imparted to fly ash by the SHOCKSystem™ blast wave depends upon the SHOCKSystem™ configuration, boiler temperature, and range from the nozzle. Nevertheless, gas dynamic theory and field testing estimate the peak gas velocity following the blast wave to be 170 to 900 ft/sec (50 to 275

m/sec), with an effective dwell time of about 1.5 milliseconds on a given boiler tube. These representative velocity and dwell time estimates of the SHOCKSystem™ vs. conventional soot blowing are summarized in Table 8.

Table 8. Relative flow velocity and dwell time of flue gas, gas accelerated by SHOCKSystem blast wave, and the conventional soot blower jet (Parish, 2006)

Erosion Mechanism	Velocity	Time Duration
Fly ash erosion	50 – 60 ft/sec	Continuous
Gas accelerated by SHOCKSystem blast wave	170 – 900 ft/sec	.0015 Seconds/Cycle
Conventional Sootblower Jet	1400 - 2900 ft/sec	~ 0.020 Seconds/Cycle

Considering the strong influence that velocity has on erosion of heat exchanger surfaces, the reduction of particle impact velocity associated with the SHOCKSystem™ suggests that a dramatic reduction in tube erosion (and associated tube leaks) can be expected with the implementation of the SHOCKSystem™ versus conventional soot blowing. (Parish 2006)

Detonation cleaning provides a cleaning blast wave that is omnidirectional, propagating through the entire tube assembly whereas soot blowing technology is restricted to line-of-sight cleaning. Each detonation impulse is equivalent to multiple 6-minute soot blowing cycles and one combustor can replace up to four soot blowers, depending on the boiler configuration. A standard detonation cleaning schedule calls for 10 pulses repeated every 12 hours per combustor (20 cycles per day) and soot blowers can require one cycle every four hours per soot blower (six cycles per day). Detonation cleaning is successful in continuous-maintenance mode and remedial cleaning mode removing established deposits upon initial installation. (McCormick, 2007)

When comparing a detonation device and an acoustic horn, they both create a pressure wave. A blast wave is a discrete pressure discontinuity, which is fundamentally different from the cyclic waves of acoustic horns. The pressure amplitude is orders of magnitude higher for a blast wave compared to an acoustic horn sound wave. Detonation cleaning is successful in continuous-maintenance mode and remedial cleaning mode where established deposits must be removed. Acoustic cleaning is used primarily in a continuous-maintenance mode and is inadequate to remove ash that's been allowed to accumulate and sinter. (McCormick, 2007)

Fracture mechanics suggests that one strong blast is much more effective than many small waves to fracture brittle deposits. For example, for an assumed exponent where m = 10, then 1020 cycles at 130 dB (.01psi) produce the same effect as 1 cycle at 170 dB (1psi). This means that one blast wave from a detonation combustor delivers more cleaning energy than an acoustic horn running continuously at 75 Hz for far longer than the life of the boiler. Figure 28 shows the pressure profiles for both systems. (McCormick 2007)

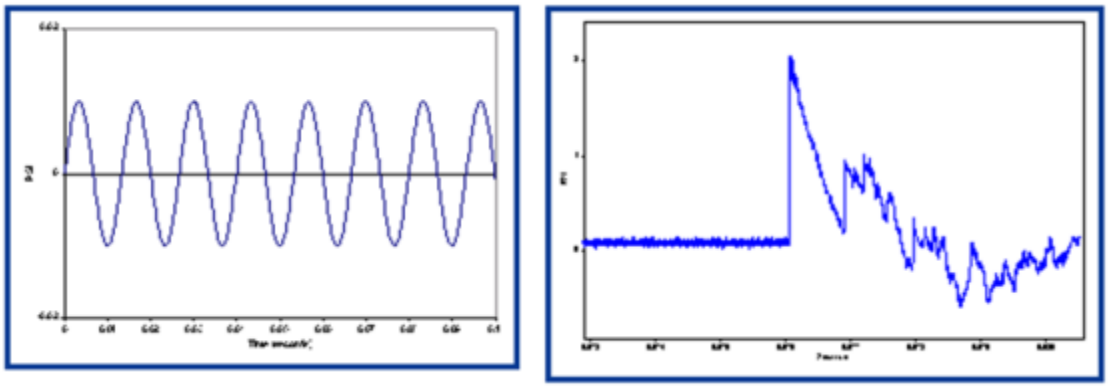

(a) (b)

Figure 28. Comparison of pressure profile between acoustic horn and PDE. (a) acoustic horn; (b) PDE (McCormick, 2007).

The first documented full-scale daily operation of the detonation wave technique for on-load removal of ash deposit found during the course of this research began in 1982 in the thermal power plant “Kakanj” in Bosnia. It was claimed that the effects of this application were immediately visible. The previous fouling and ash agglomeration, despite the regular use of 28 steam soot blowers, substantially diminished and boiler steam production and general performance improved. Then, in 1986 the technique was installed into another boiler of the same capacity and similar configuration. No negative effects were noticed over the years in any of the boilers, despite regular use of detonation waves two or three times per day. Since then, the detonation-wave technique has been in continuous use (except for a two years interruption during the war 1993-95) and has become the standard cleaning technique in the plant. (Hanjalic, K. and Smajevic 2003)

As of now, it appears pulse detonation devices have not been used in RSC applications. It is expected that sealing problems would be similar to the soot blower. The detonation combustion chamber and nozzle would likely be fixed to the pressure vessel while the water wall will thermally grow radially and axially. Structural analyses of the heat exchanger components would need to be conducted to understand the long term effects.

5.2.3 Fouling Removal System Attributes

The attributes factors listed in Table 9 are considered important to achieving a feasible, effective, and reliable RSC fouling removal system.

Table 9. Key attributes for RSC fouling removal system.

No.	Importance Ranking	Attribute	Definition
1	5	Fouling removal effectiveness	
2	5	No syngas leakage to atmosphere	
3	5	Online Cleaning Capability	
4	5	Minimal Risk of Damage to RSC	Potential for syngas leakage to annular space, corrosion, cycle fatigue, impact stress / fracture, etc.
5	5	Technology compatibility to RSC	Likelihood that this technology will work in an RSC environment
6	4	Installation cost	

7	5	Service Life	Fouling removal system life
8	4	O&M cost	Includes utility consumption (N2, air, steam, fuel, etc.)
9	4	Time to develop	
10	3	Impact on syngas quality (LHV)	
11	3	Operation complexity of device	Includes operator knowledge, control system logic, etc.
12	3	Other EHS compatibility	Includes noise, electrical shock
13	3	Parasitic load (long term)	On a per unit time basis (including activation interval)
14	3	Thermal mass of device (warm-up)	Cycle time for warm-up or cool down
15	2	Ability to remove fouling online and offline	
16	2	Design complexity	Moving parts, activation time, activation interval, installation complexity, etc.
17	2	Operability (tune-ability in removal effectiveness)	Tune force, amplitude, frequency, location, etc.
18	2	Purge requirements of device	
19	2	Retrofit-ability	Ability to install in existing facility
20	1	Minimize operational impacts on steam quality	

5.2.4 Fouling Removal System Rankings

A study was conducted to rank the fouling removal mechanisms identified to date relative to how well they meet the identified RSC fouling removal system attributes. The results favor mechanical pressure pulse as the top fouling removal method, as shown in Figure 29.

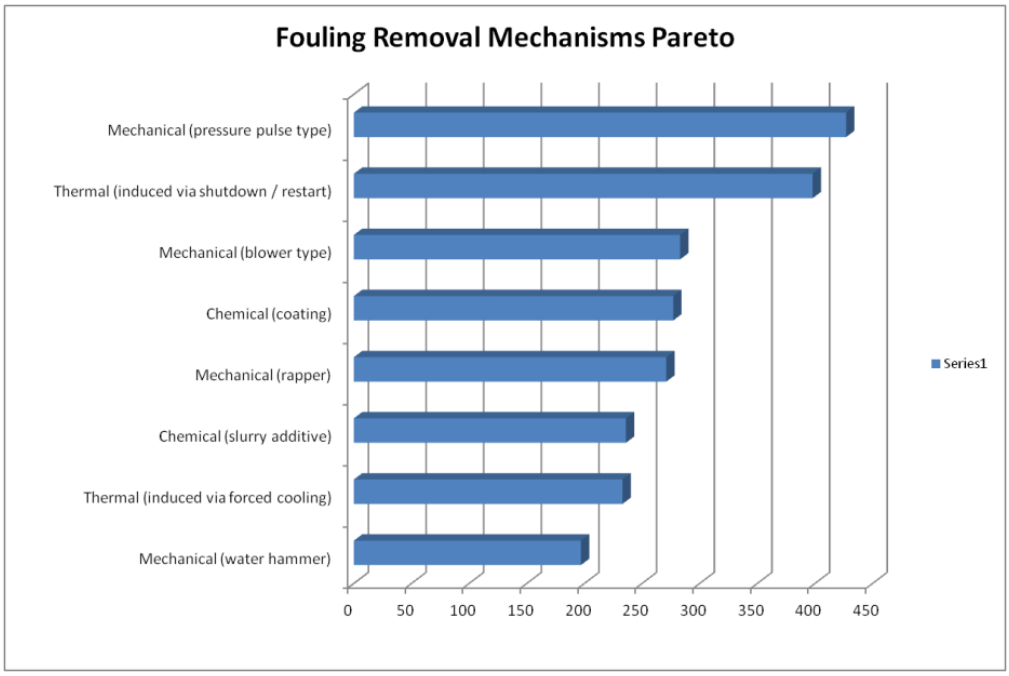

Figure 29. Fouling Removal Mechanisms Pareto Chart.

5.2.5 Feasibility of PDE Fouling Removal

5.2.5.1 Brief Background on PDE Detonation

Detonation is a supersonic combustion process involving a reacting shock wave where reactants are converted into products accompanied by a rapid energy release. Since the detonation is supersonic, the reactants ahead are not disturbed prior to shock arrival and remain in their initial state. As this strong shock wave passes, it compresses, heats and ignites the reactants resulting in a combustion zone propagating with the velocity of the shock. The shock wave and the combustion zone following it can be regarded as a single surface of discontinuity separating the burned and unburned gases. Such an approach was independently developed by Chapman and Jouguet, resulting in the Chapman–Jouguet (CJ) theory. This discontinuity is called the detonation wave. Across the detonation wave, thermodynamic properties such as pressure, temperature, etc. increase sharply. Detonations are a rare class of combustion.

On the other hand, deflagrations represent the common class of combustion. It is also referred to as slow combustion since the flame propagates with a velocity of less than O(10) m/s. Simultaneous heat conduction and diffusion of radicals ensure that the combustion speed is low and this slow reaction allows for the pressure to remain nearly constant during the process. Table 10 shows the qualitative differences between detonations and deflagrations. The subscript 1 for the parameters represents the initial state of the reactants and subscript 2 represents the final state of the products. Specifically, the table shows the large increase in pressure, temperature and density downstream of the detonation wave.

Table 10. Qualitative differences between detonations and deflagrations in gases.

Parameter	Detonation	Deflagration
u_1/c_1	5–10	0.0001–0.03
u_2/u_1	0.4–0.7	4–16
p_2/p_1	13–55	0.98–0.976
T_2/T_1	8–21	4–16
ρ_2/ρ_1	1.4–2.6	0.06–0.25

Detonations can be initiated by various methods. The simplest is direct initiation but this requires that an exorbitant amount of energy be deposited in a small volume. On the other hand, a detonation can be initiated naturally in a long tube closed at one end and filled with a detonable mixture in the presence of a prominent ignition source. In such a scenario, the flame that travels along the tube towards the open end will have products expanding behind it. This expansion of products emits disturbances in the form of compression waves propagating at the local sound speed. The trailing compression wave catches up with the leading waves due to the higher sound speed of the former, thereby coalescing to form a shock wave. This shock wave is supported by the rapid heat release with the complex known as a detonation wave.

The above description is of a deflagration-to-detonation transition (DDT). While much effort in detonation has focused on safety which aims to suppress DDT, there is also recent interest in applying detonations where the focus is to reduce DDT without introducing an exorbitant ignition source. These efforts have generally utilized DDT enhancement devices such as a Schelling spiral, grooves, dimples, etc. The actual DDT mechanism is still subject to debate and so is the

role of DDT enhancement devices. The general consensus is that turbulence is involved. The turbulence improves the mixing of fuel and oxidizer, thereby allowing the flame to propagate rapidly. The penalty paid for this is the friction from the process. Nonetheless, DDT enhancement devices are simple to implement and have been effective in reducing the DDT length. The tradeoff between a short DDT length and the drag appears acceptable.

The stages of a PDE cycle are shown schematically in Figure 30. The detonation chamber is initially at quiescent, ambient conditions (1). It is then filled with a fuel/oxidizer mixture (2), which in the figure is shown as end-wall injection. At some time (3), the mixture is ignited, ideally such that the detonation wave meets the mixture front at the exit of the detonation chamber (4, 5). The detonation chamber is then scavenged by a blowdown or exhaust stage (6) after which the cycle repeats itself.

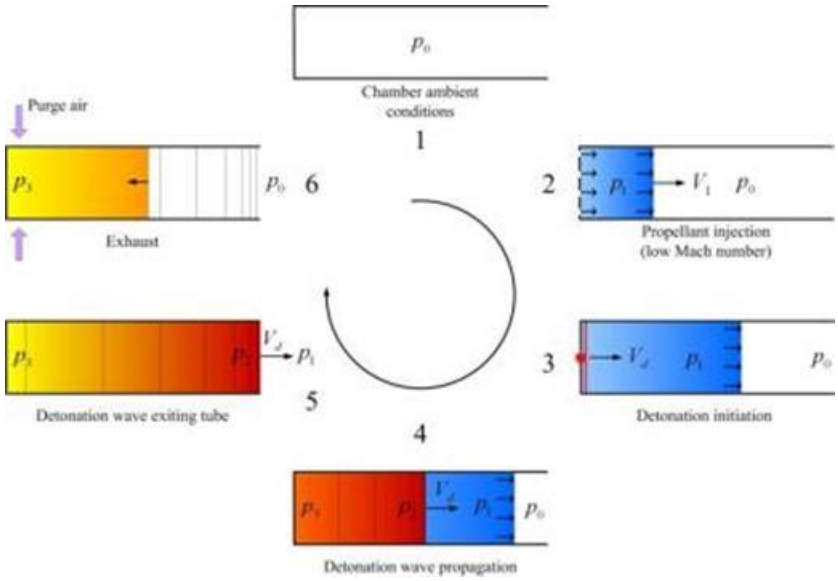

Figure 30. Stages in a PDE cycle.

5.2.5.2 PDE Fouling Removal Concept

A conceptual PFD (process flow diagram) for a pulse detonation cleaning device that could be applied to an RSC is given in Figure 31. It is inspired by the GE Powerwave^{+} system and will require additional refinement to adapt current impulse cleaning technology to the RSC application. Auxiliary systems are also pictured, including a nitrogen purge system. In the purge system, RSC environment requires a dry, inert gas to help prevent oxidation. Unlike a conventional PDE applied to a boiler application, it is assumed that the fuel will be injected into the combustion chamber first, followed by the oxidizer. This is due to concerns that high temperature syngas in the combustion chamber (present because of PDE exposure to the RSC environment) when mixed with oxidizer might cause premature combustion.

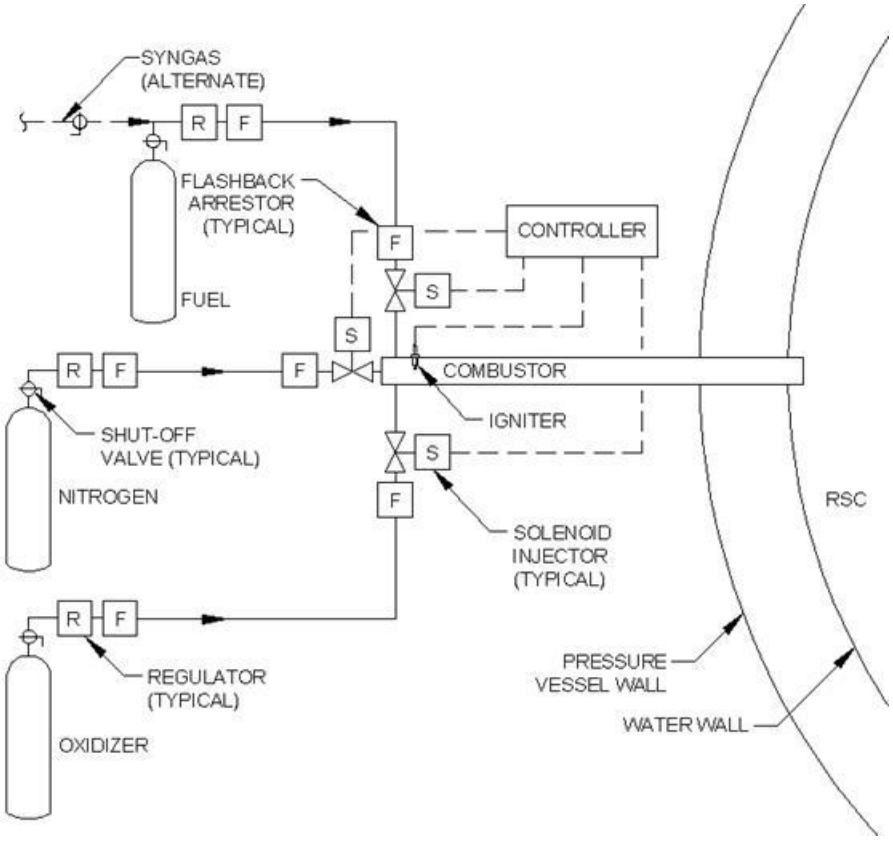

Figure 31. Preliminary PFD for PDE fouling removal system for RSC Applications.

5.2.5.3 Feasibility of PDE in RSC Application

PDE is a mature technology, which has been widely applied in atmospheric and dilute conditions. There are challenges in applying PDE in high pressure and fuel rich environment of RSC. Therefore, CFD simulations have been made to explore the feasibility of applying PDE technology to fouling removal in the RSC. Feasibility will be assessed by the following criteria questions:

1) Does a pressure wave exit the PDE cannon at the high pressure conditions associated with the RSC environment?
2) What is the magnitude of the force on the RSC platens due to the PDE pressure wave?
3) Is there risk of Oxygen intrusion into the RSC when PDE fails?

1. CFD Model Setup

A CFD model was developed to simulate the use of PDE technology in the RSC. The model was a two-dimensional, planar, unsteady-state simulation, based on the proposed geometry, initial conditions, and the chemical combustion reactions assumed would occur in the detonation wave.

A typical RSC is a vertical, symmetrical, cylindrical vessel with heat exchanger tubes grouped into platens in a radial arrangement, as show in Figure 32(a). Application of PDE technology to

the RSC for the purpose of fouling removal would likely require locating multiple PDEs around the RSC perimeter and at different heights. For the requirements of our task, only a portion of the RSC horizontal cross-section was considered in the simulation. This model of the RSC vessel region included two platens symmetrical about the PDE/RSC interface, representing only a portion of the complete RSC horizontal cross-section. In addition, the sizing of RSC diameter (tube cage) and platens were made similar to those used in real application today.

The PDE is essentially a horizontal cylinder that extends into the RSC and spans the annular space between the tube cage and the outer pressure vessel, as shown in Figure 32(b). In the model, the annular space is not essential to the simulation so was omitted. The ignition region is where the spark occurs and initiates combustion. This reaction then travels through the combustion region to the PDE exit. As part of the analysis, the diameter of the PDE and lengths for the ignition and combustion regions were varied.

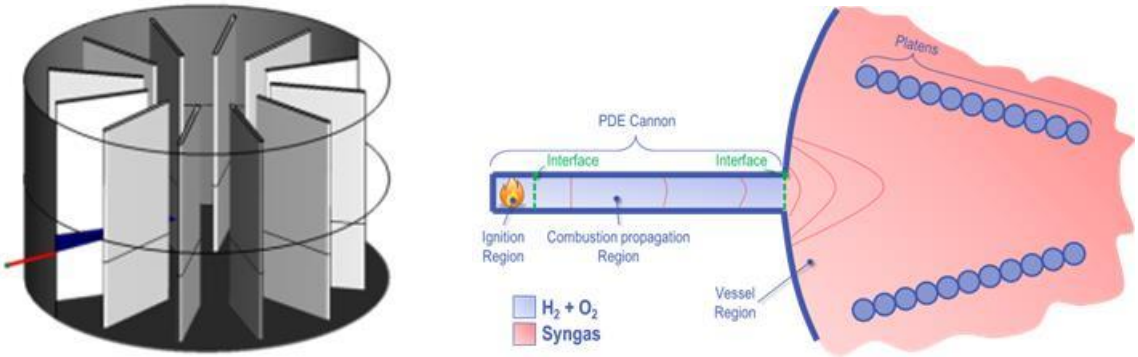

(a) (b)

Figure 32. Diagram of RSC heat transfer surface, and CFD model. (a) RSC platen orientation and attached PDE; (b) CFD model for PDE regions, species present, and interfaces.

Figure 33 shows the CFD model geometry which is broken up into four regions: ignition, combustion, vessel, and extension region. The ignition and combustion regions make up the PDE, the vessel and extension region are components of RSC. These regions were created in order to separate the various fluids and initial conditions involved in the CFD analysis. The model was a simplified, 2 dimensional (2D), planar representation of a PDE system used for fouling removal in the RSC. The extension region of the RSC was incorporated to monitor the pressure flux at the exit of the vessel region. This was done to yield more realistic and useful pressure data since in reality, the pressure wave would continue onward throughout the RSC. The extension region also minimized the effects of the PDE pressure wave reflecting off the rear of the vessel region, that otherwise might produce higher than expected forces on the platens. Consequently, with the addition of the extension region, the pressure waves are believed to have behaved in a more realistic manner, making the estimated forces on the platens more credible.

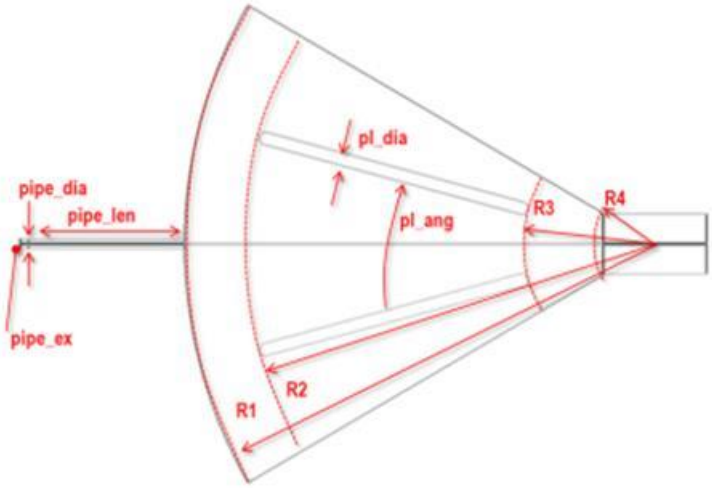

Figure 33. CFD model geometry.

2. Initial Conditions

In the ignition and combustion regions, hydrogen gas is used as fuel and oxygen is used as the oxidizer. These gases combust in the ignition region when the spark is initiated, then the reaction continues into the combustion region. This reaction, when occurring at a rapid rate, is the driving force for the creation of a pressure wave in the PDE. The balanced chemical equation that describes this reaction is:

$$2H_2 + O_2 \rightarrow 2H_2O$$

Based on the equation, the mass fraction of H2 was set at 11% and the mass fraction of O2 is 89%. In addition, the initial temperature was set to 71°F (22°C) for both regions.

The vessel and extension regions of the RSC were assumed to have an initial temperature of 1700°F (927°C) and contain syngas. Syngas is composed primarily of hydrogen, carbon monoxide, carbon dioxide and water, where the mass fractions of these species were assumed to be as follows:

$H_2 = 30\%$
$CO = 30\%$
$CO_2 = 16\%$
$H_2O = 24\%$

Another important reaction that the CFD analysis took into account in the vessel and extension regions was the following:

$$2CO + O_2 \leftarrow\rightarrow 2CO_2$$

This reaction is one of the reactions crucial to monitoring the oxygen levels in the RSC regions. It is important that the oxygen injected into the PDE is consumed by the PDE fuel and does not enter the RSC in large quantities, where it could react with the syngas species. Oxygen in the RSC is undesirable since it reacts with carbon monoxide (carbon monoxide and hydrogen are the main components of syngas) to produce carbon dioxide. As a result, this would cause a decrease syngas quality. The reverse reaction is also considered and involves carbon dioxide

decaying to oxygen and carbon monoxide. Refer to Figure 32(b) for fluid species breakup by region.

The model is 2D, planar, transient (unsteady) simulation with turbulent flow defined by the k-epsilon model with standard wall functions. The combustion model applied is the species transport model with combustion turbulence modeled by the eddy-dissipation concept. The specific heats of the fluid species were modeled by the mixing law so that they increased with the rise in temperature to increase the accuracy of the simulation.

3. CFD Modeling Results

In order to answer the feasibility criteria questions, a CFD analysis was completed for five different cases listed here:

A. PDE with **base** diameter @ **14.7 psia** condition
B. PDE with **base** diameter @ **650 psig** condition
C. PDE with **2 x base** diameter @ **14.7 psia** condition
D. PDE with **2 x base** diameter @ **400 psig** condition
E. PDE with **2 x base** diameter @ **650 psig** condition

The 400 psig and 650 psig pressures represent common normal operating pressures for an RSC. The atmospheric pressure condition of 14.7 psia was also considered, as this reflects downtime conditions, including pre-startup or post-shutdown conditions. These pressure conditions were applied to all model regions. Both the PDE diameter and combustion region length dimensions were also varied by a factor of two in order to explore the relationship of PDE geometry to the feasibility criteria.

The CFD model monitored the interfaces between each region for pressure, temperature and species mass composition, as shown in Figure 32(b). Interface 1 refers to the border between the ignition and combustion region. Interface 2 is defined as the boundary between the combustion and vessel regions, and Interface 3 is between the vessel and extension regions. The pressure on the platen surface was also monitored and used to obtain normal force, normal stress and shear stress data. Figure 34 through Figure 37 below refer to Case D (PDE with 2 x base diameter @ 400 psig condition), although the data trends are consistent across the cases.

As Figure 34 shows, for both Interfaces 1 and 2, hydrogen and oxygen are quickly consumed and their concentrations approach 0% while the concentration of water vapor rapidly increases to 100%.

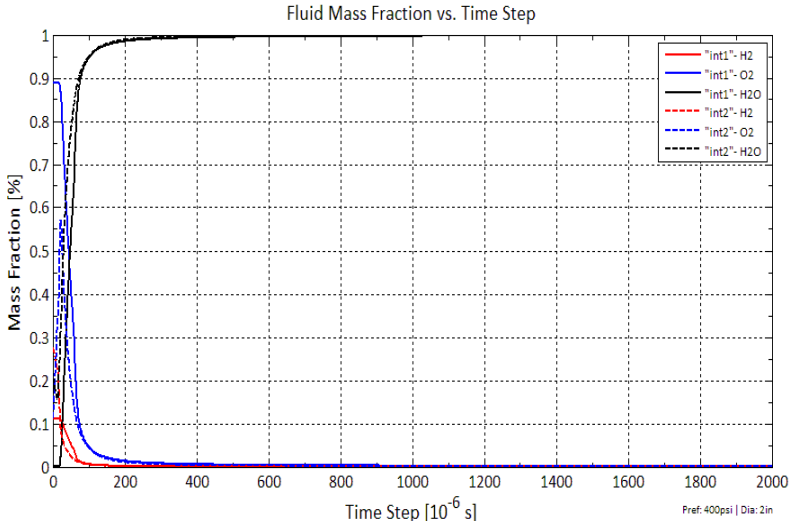

Figure 34. Gas species mass fractions vs. time for Case D.

Figure 35(a) and (b) show the platen load variation with time from a single PDE pulse wave, with Figure 35(a) for the bulk force and Figure 35(b) for the maximum pressure on the platen. The maximum pressure imparted to the platens is around 650 psig in a two-dimensional, planar configuration, which can be characterized as significant. Figure 35(a) is a useful tool for estimating the effect of adding a height dimension to the 2D CFD model making it a 3 dimensional (3D) representation of the problem. The bulk force per unit height (inch) on the platens for Case D is about 6,500 lbs. Case D considers the 2 x base diameter PDE which would coincide with a 13,000 lb load on the platens.

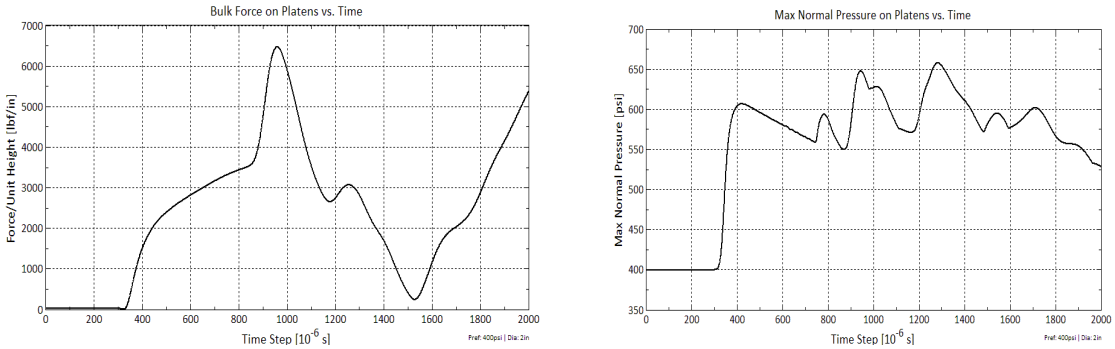

(a) (b)

Figure 35. Platen load variation with time from a single PDE pulse wave for Case D. (a) Bulk force; (b) Max pressure.

Figure 36 gives the snapshot of pressure contours around the platen from a single PDE pulse wave for Case D. It clearly shows pressure waves exiting the PDE, propagating in the open space of the RSC and impacting the platens.

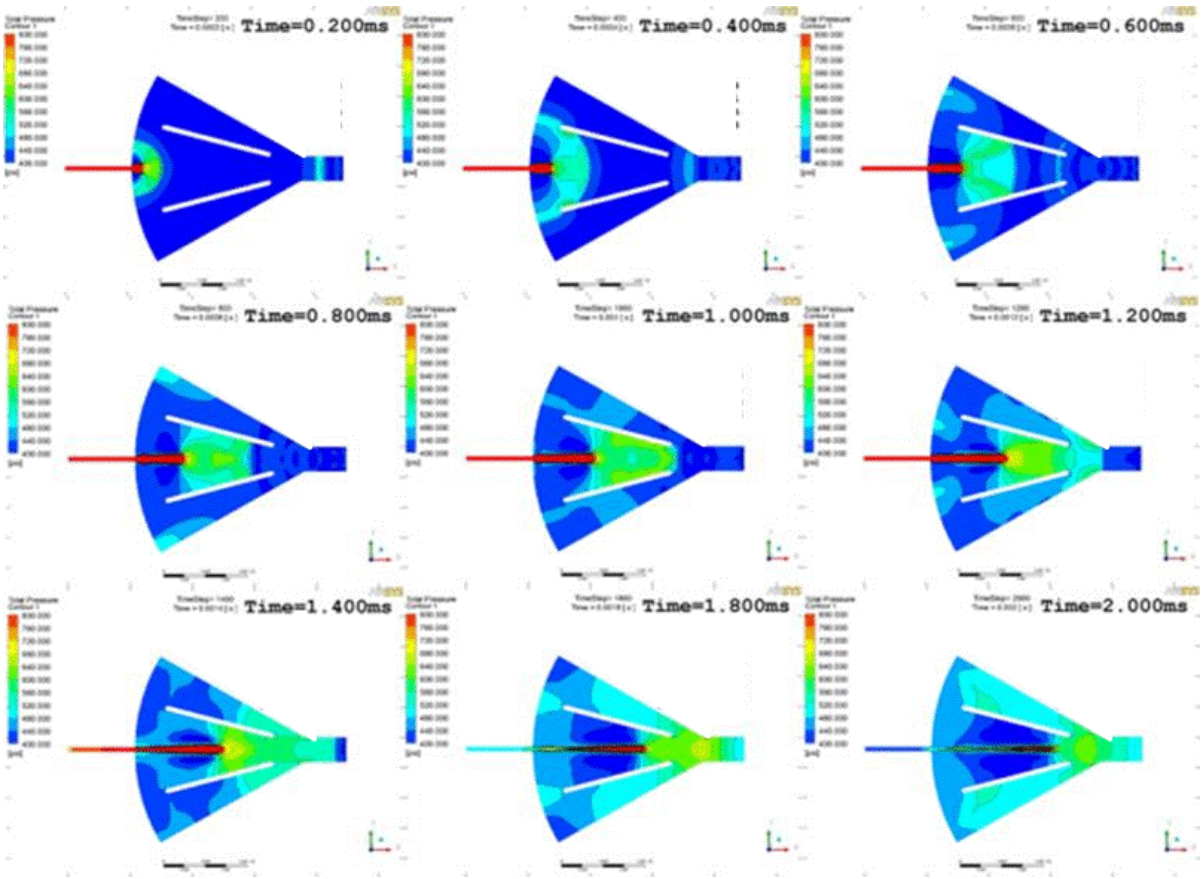

Figure 36. Snapshot of PDE wave pressure contour for Case D.

Figure 37(a) gives the total pressure force, and force components in the PDE direction (or x-coordinate) and the vertical direction (or y-coordinate), in variation with time. Figure 37(b-i) shows the evolution of the pressure distribution on the platen surface induced by a single PDE pulse wave in Case D. In the plot, the black arrow length represents the magnitude of pressure, and the single red arrow represents the total force on the platen. This analysis gives us an insight of the PDE wave impact on the platen and how to remove the fouling deposit on the platen by this PDE-induced mechanical load.

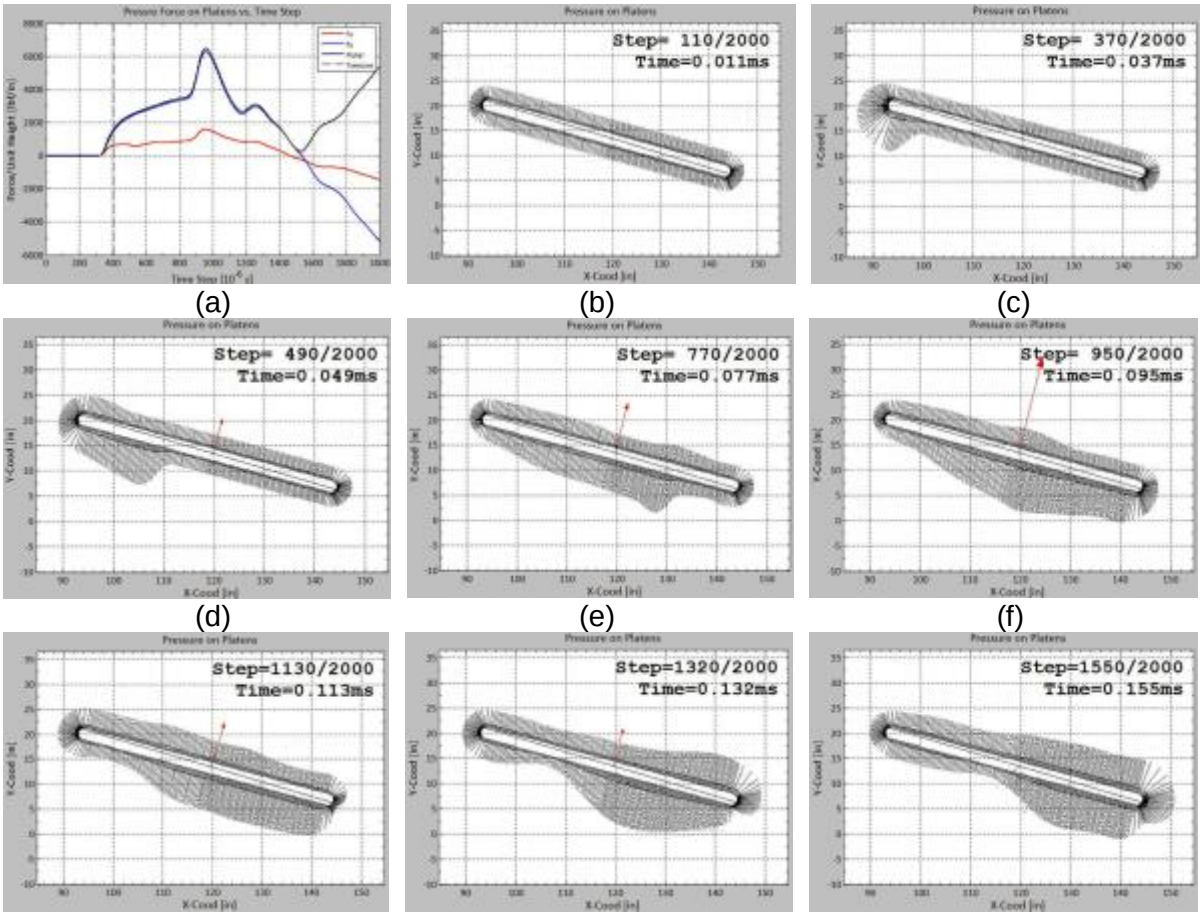

Figure 37. Snapshot of PDE wave pressure distribution on platen for Case D. (a) total pressure force and force components in PDE direction and vertical direction; (b-i) evolution of pressure distribution on platen surface induced by a single PDE pulse wave.

Table 11 summarizes the maximum loads on the RSC platen induced by a single PDE pulse wave for all simulated cases. For the atmospheric and 650 psig pressure cases, increasing the PDE diameter from base to 2 x base resulted in an increase in load on the platens by a factor of 4. It can also be seen that the load on the platens increased significantly as pressure was increased.

Table 11. Platen maximum loads for each configuration.

Pressure Condition	Pressure Factor	Load from Base PDE	Load from 2 x Base PDE	Load increase due to pressure	Load increase from Base to 2 x Base PDE
14.7 psia	1x	150 lbs	600 lbs	--	4x
400 psig	27x	--	13,000 lbs	22x	--

650 psig	44x	5,000 lbs	20,000 lbs	33x	4X

In concluding from all simulations, the CFD results showed:

- Combustion waves propagated out of the PDE into the vessel even in high pressure conditions.
- Pressure wave imparted forces on the RSC platen.
- All oxygen was burned in the initial PDE combustion wave and did not exit into the vessel.

These results address the criteria laid out in the objectives and present a strong case for the feasibility of using PDE technology for fouling removal in the RSC.

5.3 Down Select Fouling Removal Concepts

5.3.1 Introduction

The PDE technology has been introduced as a fouling removal concept, with its feasibility approved preliminarily using 2D computational fluid dynamics (CFD) models in previous chapter. In this work, more accurate 3D CFD analysis is required to predict the pressure load on RSC platen with impact of PDE wave in different operating conditions, such as normal operating condition, ignition failure condition, as well as oxygen lean conditions. Also, finite element analysis (FEA) is required to predict the RSC platen structure dynamic response to the PDE waves. Through these analyses, some insight can be obtained on the effectiveness of PDE fouling removal.

5.3.2 CFD Modeling of PDE Fouling Removal Concepts

A simplified 2D CFD feasibility study was conducted to better understand the flow physics associated with a PDE in an RSC environment (high-pressure and fuel rich). The intended use of the PDE is to induce a pressure wave that will travel through the RSC and potentially remove ash deposits from the platens thereby increasing RSC heat transfer efficiency. The previous study predicted the magnitude of the force on the platens due to the pressure wave, but was rather limited in predicting the distribution of the force. A 3D CFD analysis is more ideal for predicting the distribution and magnitude of the load because it gives a more complete picture of the PDE pressure wave behavior.

Consequently, the main objective of this investigation was to use a 3D model to evaluate the force and pressure imparted on the platens due to the PDE pulse waves in different operating conditions, such as normal operating condition, ignition failure condition, as well as oxygen lean (50% O2 reduction) conditions.

1. 3D CFD Model Setup

The geometry, initial conditions and reactions were established to realistically simulate the use of a PDE fouling removal system in the RSC, and many of the same assumptions and initial conditions were used as in the 2D model. Some of the key differences include the deletion of the extension region and the addition of the diffuser region. Also, for the 3D model, a height dimension was added to the PDE and RSC regions. Furthermore, the PDE diameter and length

were held constant at the 2 x base diameter and at the base combustor length. In addition, the initial pressure was fixed in this work at 400 psig.

The model geometry was broken up into four regions; the ignition region, combustion region, diffuser region and vessel region. The ignition and combustion region make up the PDE. The vessel region contained the components of the RSC and the diffuser region was the transition between the PDE and RSC. These regions were created in order to separate the various fluids and initial conditions involved in the CFD analysis.

The model was a simplified, 3D, transient representation of a PDE system used for fouling removal in the RSC. The dimensions used for the 3D model were equal to 2 x base for the diameter and equal to the base for the ignition and combustion regions.

A typical RSC is a vertical, symmetrical, cylindrical vessel with heat exchanger tubes grouped into platens in a radial arrangement. Application of PDE technology to the RSC for the purpose of fouling removal would likely require multiple PDEs around the RSC perimeter and at different heights. For the requirements of our task, only a portion of the RSC horizontal cross-section is simulated as given in Figure 38. The RSC vessel region assumed two platens symmetrically aligned about the PDE/RSC interface that included a 60° sweep of the complete RSC horizontal cross-section. And as with the 2D model, the sizes of RSC diameter and platens were made similar to those used in real application today.

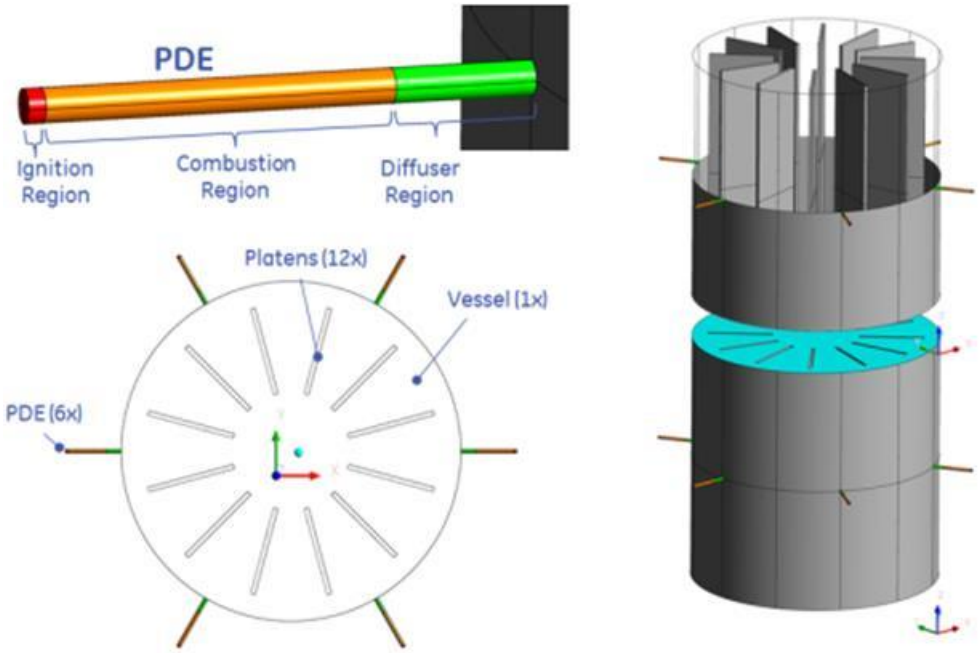

Figure 38. Simplified PDE/RSC layout for analytical model.

Figure 39 shows the CFD model geometry. In the previous 2D CFD analysis, an extension region was added at the rear of the vessel region and in line with the PDE. This region was incorporated to minimize the effects of the PDE pressure wave reflecting off the rear of the vessel region and producing higher than expected forces on the platens. For the 3D CFD

analysis, it was decided that the extension region was unnecessary and it was removed. That is because the PDE pressure wave is able to propagate into the 3D volume rather than into a small 2D plane of the vessel. This has the advantage of allowing the pressure wave to disperse more readily into the space. As a result, the reflections of the wave off the rear of the vessel were assumed to provide a truer picture of the loads induced on the platens.

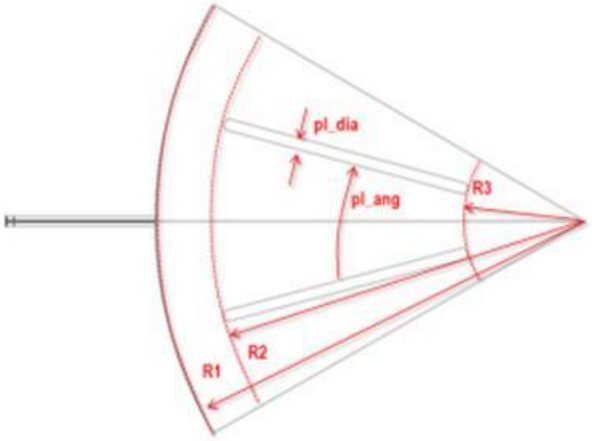

Figure 39. Top view of 3D CFD model geometry.

2. Initial Conditions

Figure 40 shows the CFD model geometry which was broken up into four regions: ignition, combustion, vessel, and diffuser region for transition from combustion to vessel region. The same initial conditions were used as with the 2D model, but with an assumed initial pressure of 400 psig for all conditions.

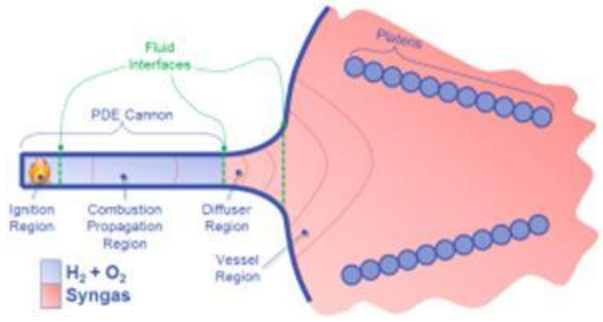

Figure 40. Diagram of 3D CFD model top view showing regions, species present, and interfaces.

The model is 3D, transient (unsteady) simulation with turbulent flow defined by the k-epsilon model with standard wall functions. The combustion model applied is the species transport model with combustion turbulence modeled by the eddy-dissipation concept. The specific heats

of the fluid species were modeled by the mixing law so that they increased with the rise in temperature to increase the accuracy of the simulation.

3. CFD Modeling Results

CFD analysis was completed for the following different conditions listed here:

- Configuration (**000**) - **Baseline**
  - ✓ Flow composition : Normal operating conditions
- Configuration (**001**) - **Low Oxygen**
  - ✓ Flow composition : 50 % reduction in oxygen content in PDE
- Configuration (**002**) - **Vessel Ignition**
  - ✓ Flow composition : PDE failure with ignition source moved into vessel

In the baseline case, the PDE volume was filled with a fuel mixture at stoichiometric ratio. This case was used as the standard to compare the magnitude of the load on the platen due to the PDE pressure wave. The maximum load on the platen experienced for the baseline case was approximately 13,900 lbs., which is similar to the 13,000 lbs. load seen in the previous 2D CFD analysis.

Next, the low oxygen configuration differed from the baseline case only in the mass fractions of oxygen and hydrogen. Adding hydrogen to the mixture without increasing the oxygen content decreased the mass fraction of oxygen and increased the mass fraction of hydrogen. Adding more hydrogen to the PDE volume resulted in an excess of hydrogen molecules that were not able to react because of their overabundance compared to oxygen. These unreacted hydrogen molecules reduced the flame front velocity and inhibited detonation leading to a weaker pressure wave and a reduction in the load experienced at the platen. For the low oxygen case, the maximum load on the platen was approximately 5,350 lbs.

The 3D CFD research also looked at what happened if the PDE system were to fail. The failure condition was defined as the fuel mixture leaking into the RSC and igniting in the vessel region as opposed to the PDE. This was meant to simulate the failure of the ignition system in the PDE and the high temperatures of the RSC causing auto-ignition of the fuel mixture in the vessel. The maximum load on the platen for this failure scenario was approximately 27,000 lb.

Figure 41 shows the evolutions of platen load induced by a single PDE pulse for these three operating conditions, with table of maximum platen load values.

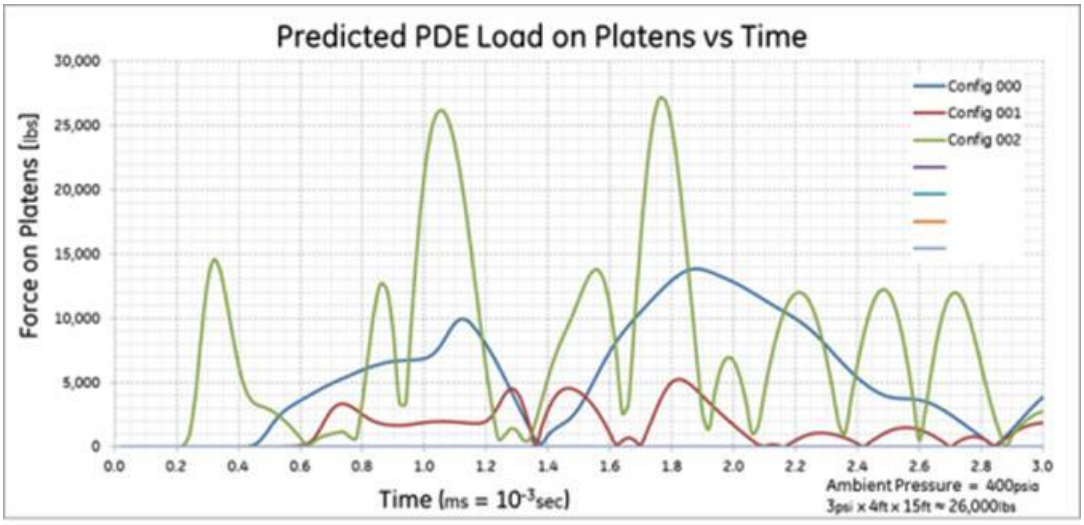

Case	ID	Description	PDE Fuel Composition	Area Ratio	Ellipse Ratio	Maximum Force on Platens (lbs)
Baseline	config000	Stoich Fuel Ratio	$2H_2+O_2$	1	1	13,855
1	config001	Reduced O2 Fuel Ratio	$20H_2+O_2$	1	1	5,247
2	config002	Fuel Ignited in Vessel	$2H_2+O_2$	1	1	27,112

Figure 41. Graph of predicted PDE load on platen vs time and table of maximum platen load values.

Figure 42 shows the calculated pressure load contours on the RSC platen front surface (facing the PDE wave) and back surface at 1 ms after a single PDE pulse for the normal operating condition, 50% oxygen reduction condition, and PDE failure condition. In comparison, the oxygen lean condition produces weaker PDE wave with less intensity and smaller swiping area on the platen; while the PDE failure case does not generate a detonation wave.

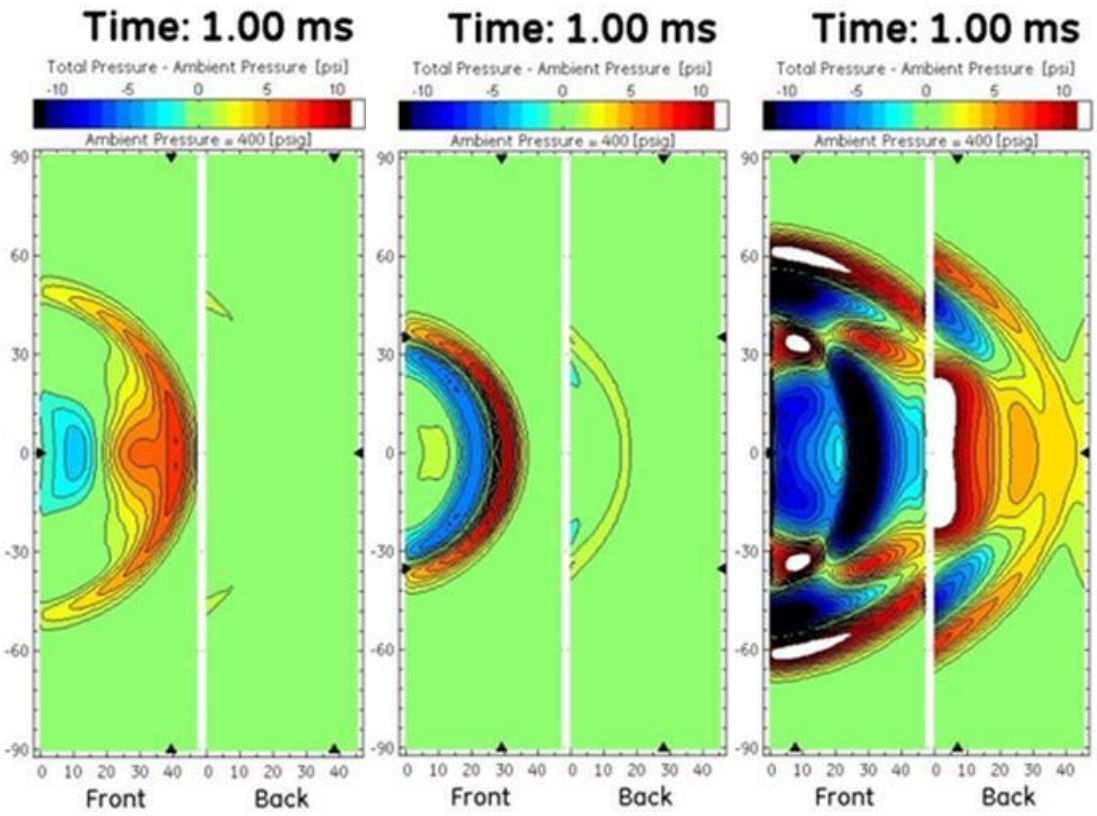

(a) (b) (c)

Figure 42. Platen pressure load induced by a single PDE pulse wave at 1ms time. (a) Normal operating condition; (b) 50% oxygen reduction condition; (c) PDE failure condition.

For the normal operating conditions (baseline) of PDE, Figure 43 gives the propagation of PDE pressure wave contours around RSC platens from the top-down view. Figure 44 shows the evolution of PDE pressure wave contours between RSC platens from the PDE centerline side view. Figure 45 represents the evolution of platen pressure load induced by a single PDE pulse, in which contours show the snapshot of pressure load on the front (facing the PDE wave) and back surface of platen; and plots the maximum, minimum pressure, and pressure variation (maximum-minimum) with reference to operating pressure. Similarly, Figure 46 through Figure 48 gives the results for the 50% oxygen reduction condition, and Figure 49 through Figure 51 shows the results for the PDE failure condition.

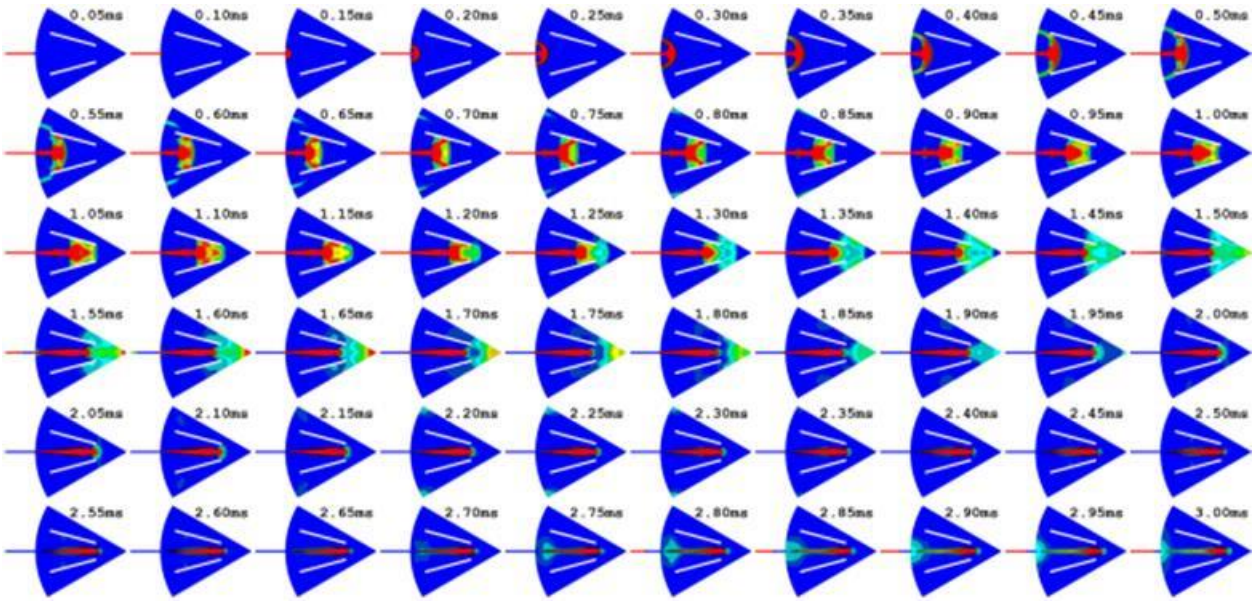

Figure 43. Propagation of PDE pressure wave contours around RSC platens from the top-down view in normal operating conditions (baseline).

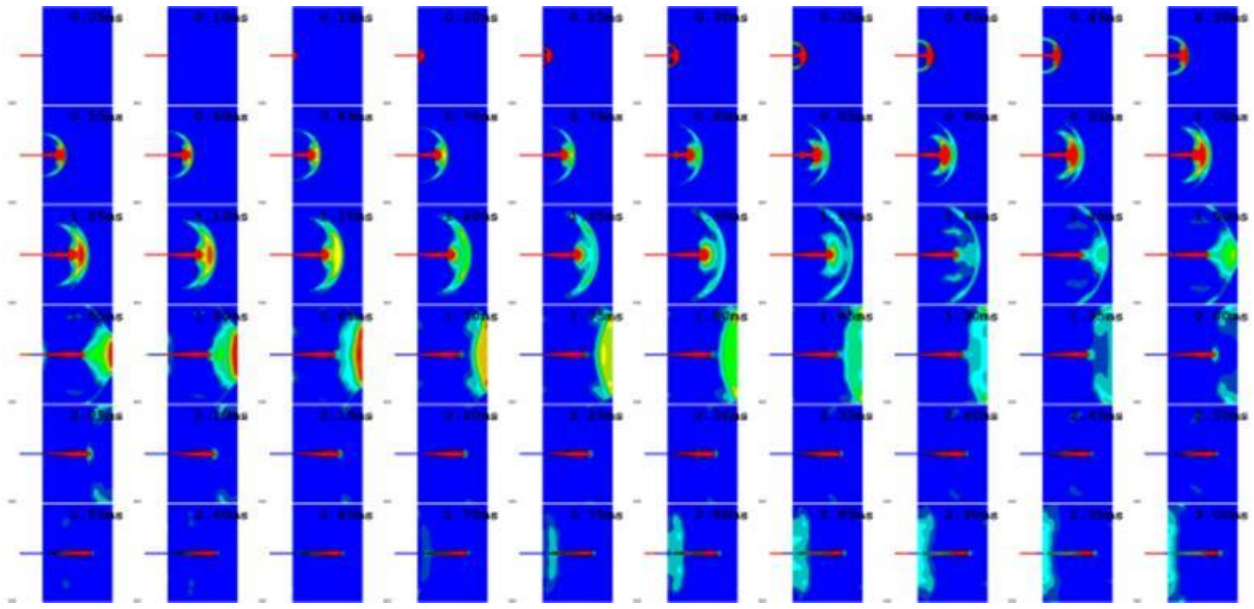

Figure 44. Propagation of PDE pressure wave contours between RSC platens from the PDE centerline side view in normal operating conditions (baseline).

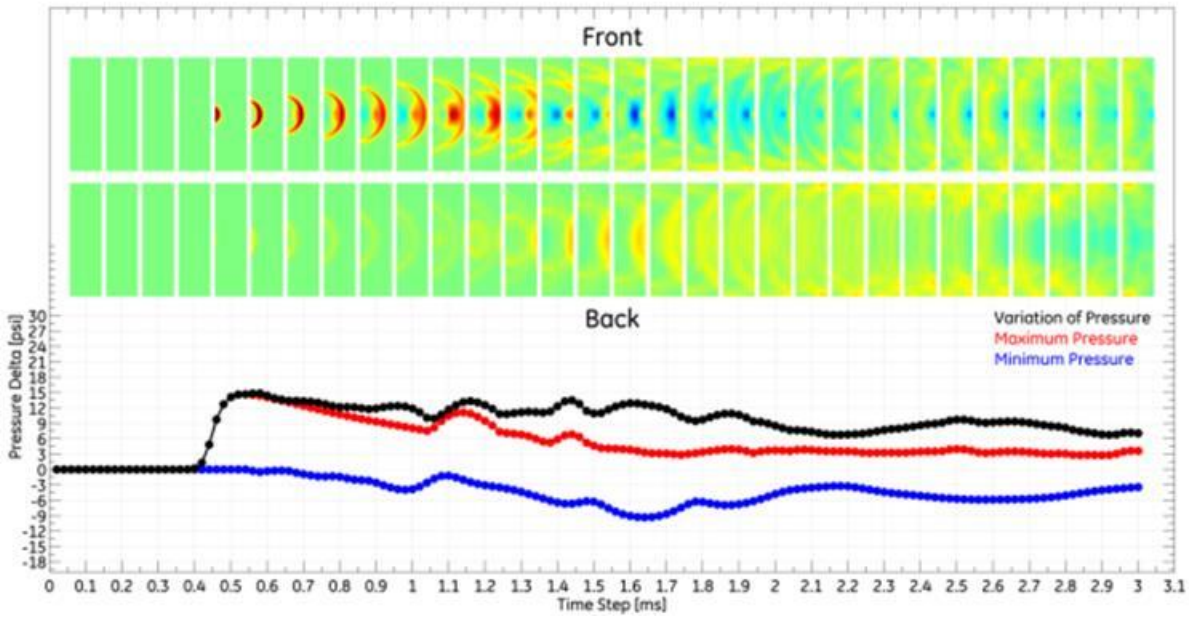

Figure 45. Evolution of platen pressure load induced by a single PDE pulse wave in the normal operating condition.

Contours show the snapshot of pressure load on the front (facing the PDE wave) and back surface of platen; plots giving the maximum, minimum pressure, and pressure variation (maximum-minimum) with reference to operating pressure.

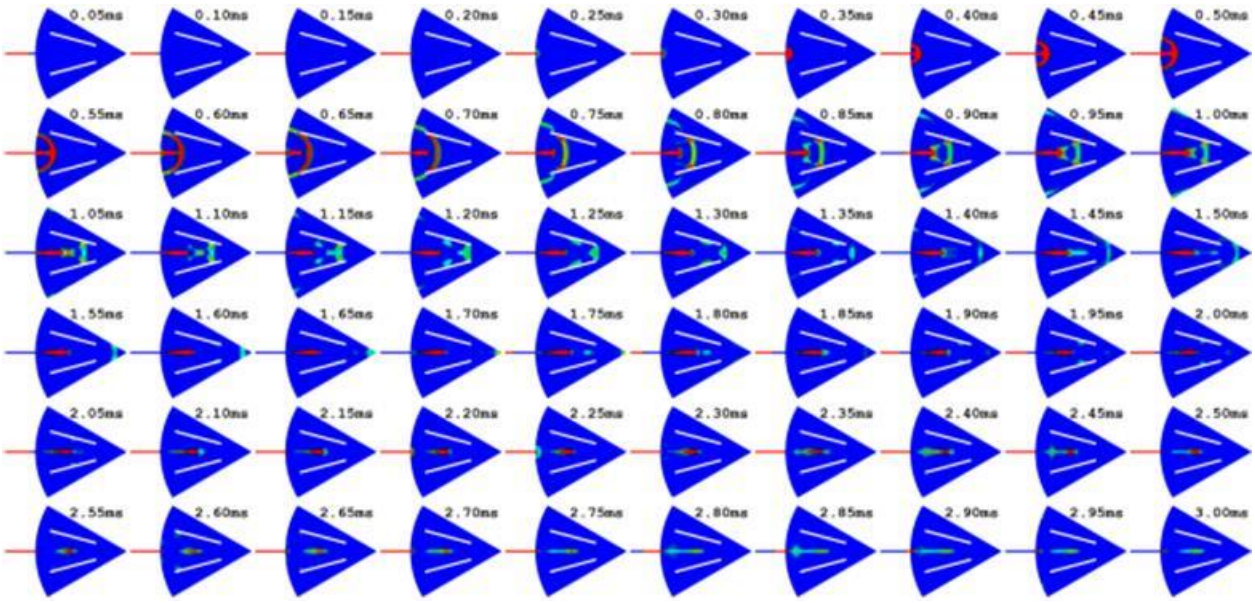

Figure 46. Propagation of PDE pressure wave contours around RSC platens from the top-down view in the low oxygen case.

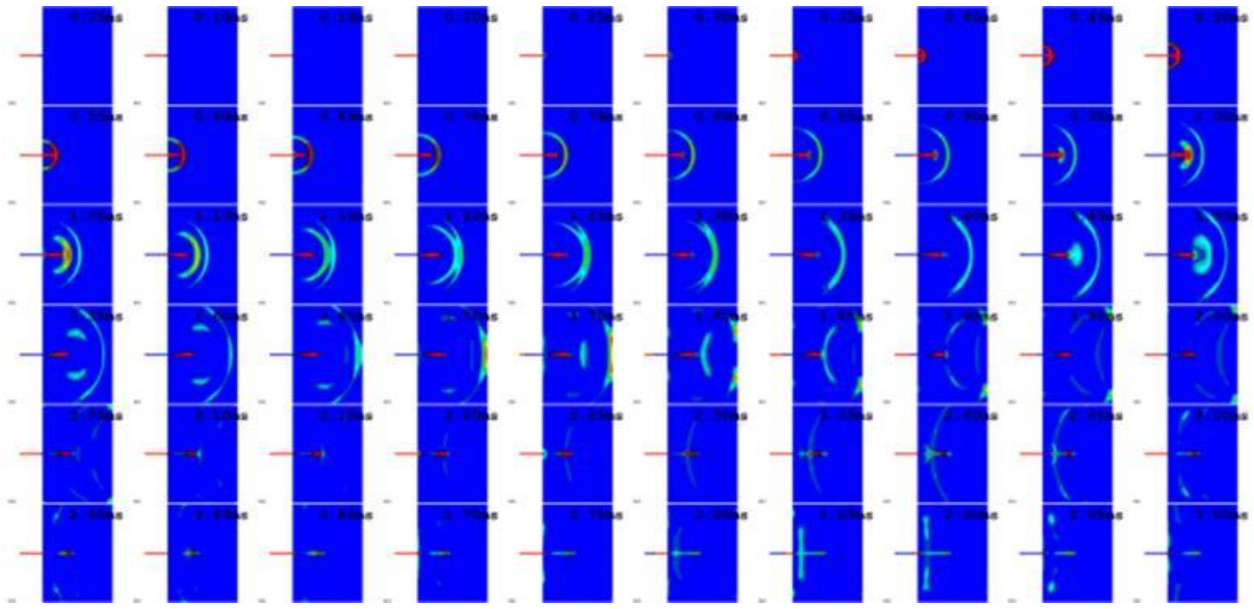

Figure 47. Propagation of PDE pressure wave contours between RSC platens from the PDE centerline side view in low oxygen case.

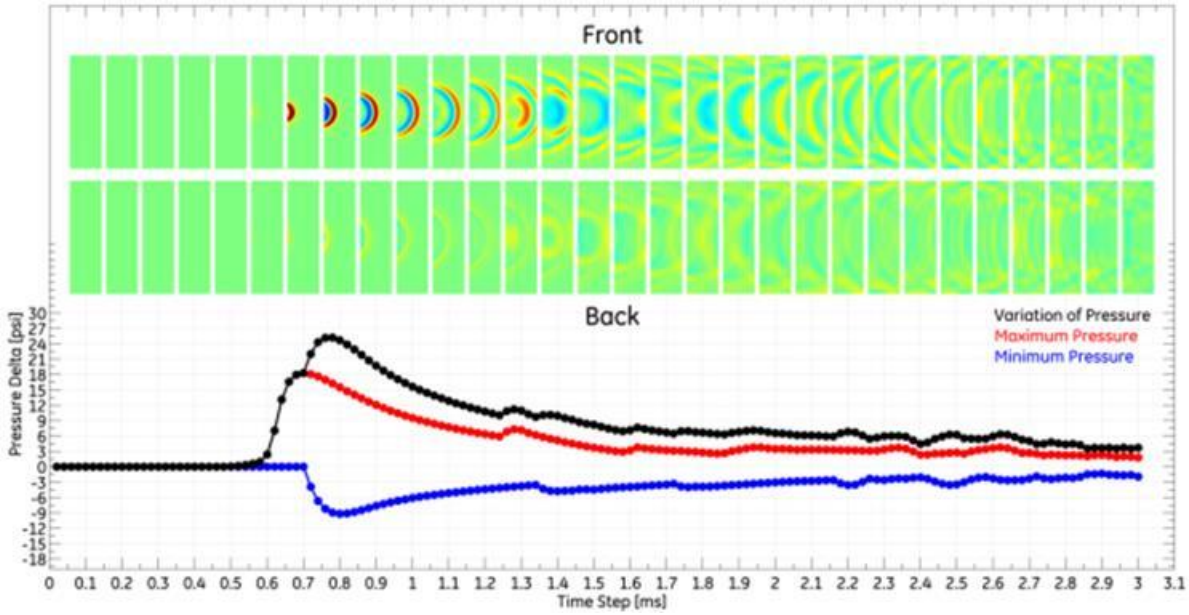

Figure 48. Evolution of platen pressure load induced by a single PDE pulse wave, in the low oxygen case.

Contours show the snapshot of pressure load on the front (facing the PDE wave) and back surface of platen; plots giving the maximum, minimum pressure, and pressure variation (maximum-minimum) with reference to operating pressure.

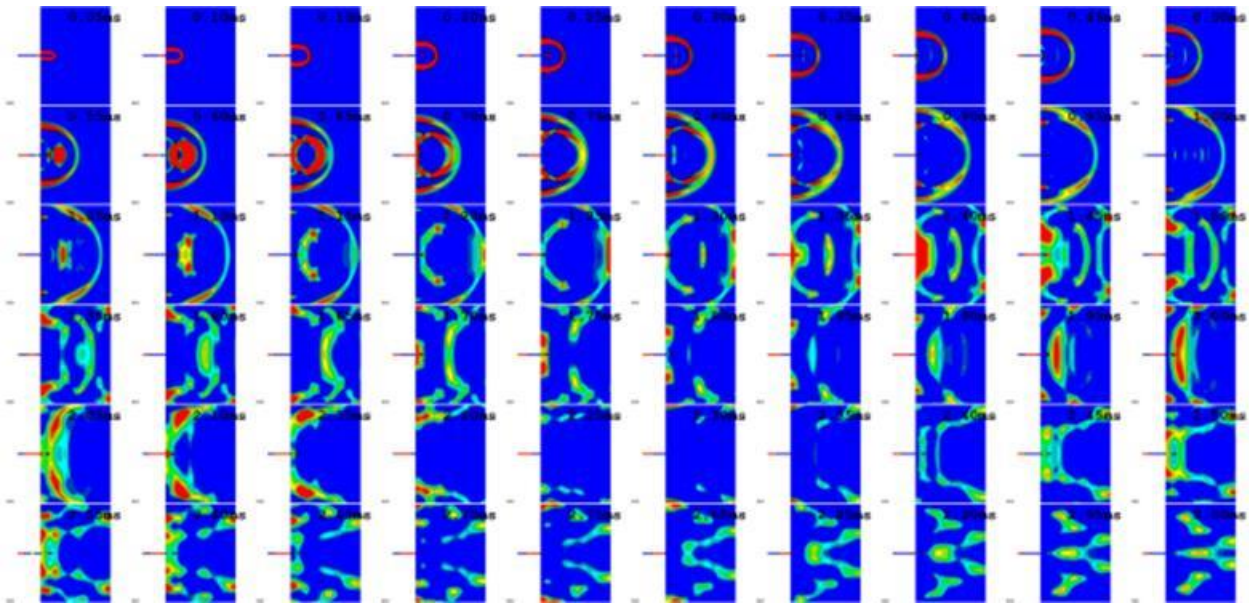

Figure 49. Propagation of PDE pressure wave contours around RSC platens from the top-down view in the PDE failure case.

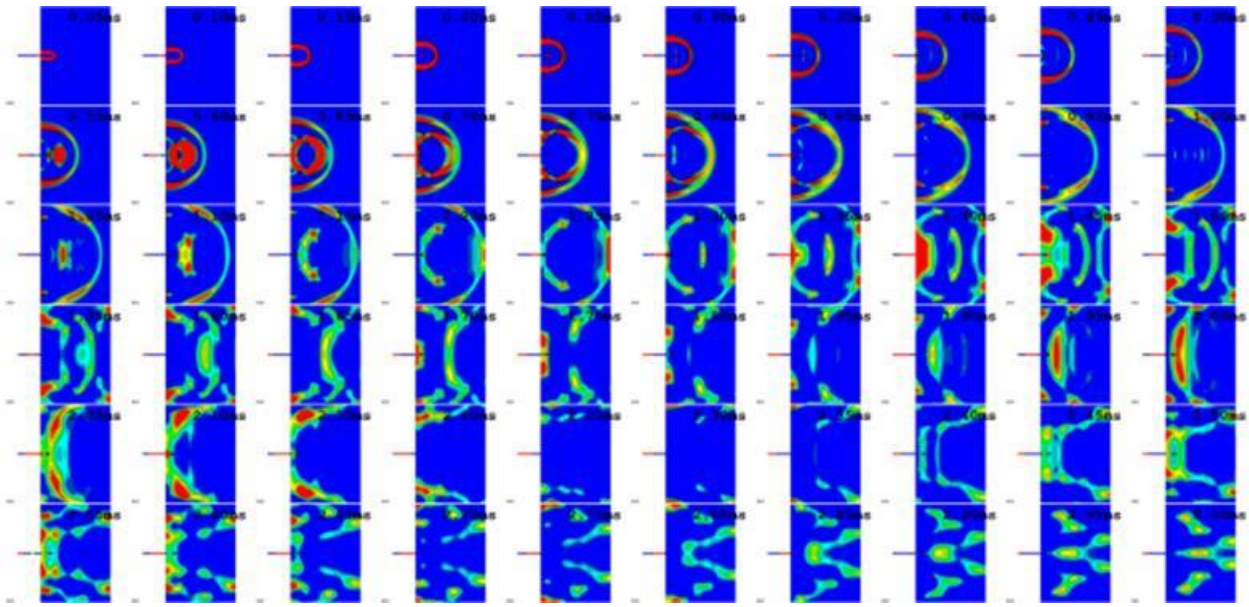

Figure 50. Propagation of PDE pressure wave contours between RSC platens from the PDE centerline side view in the PDE failure case.

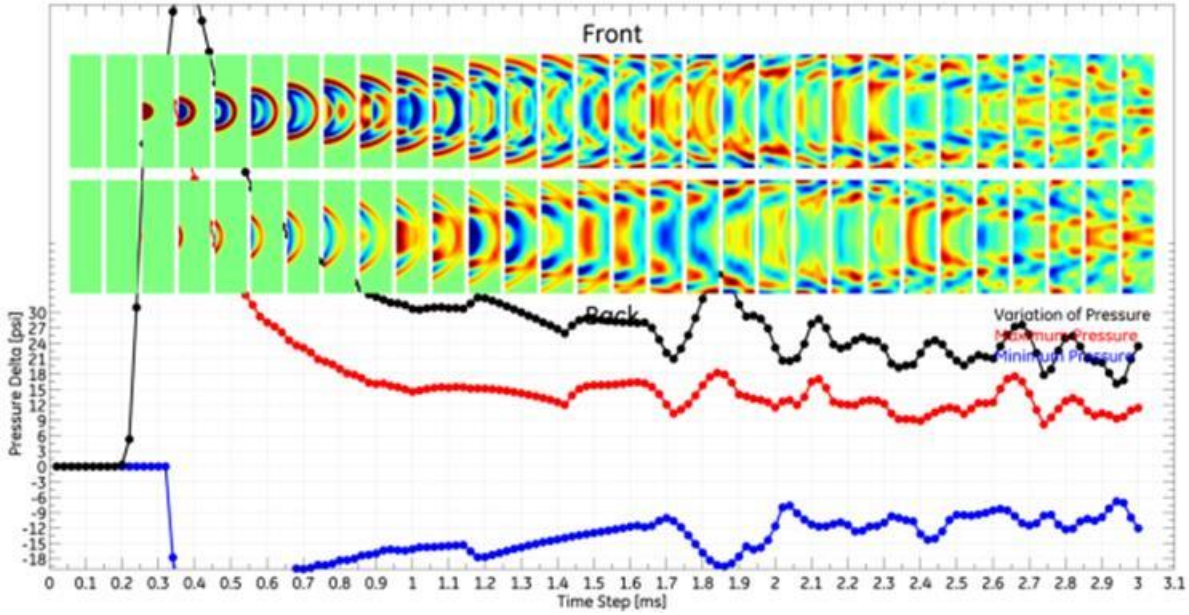

Figure 51. Evolution of platen pressure load induced by a single PDE pulse wave, in the PDE failure case.

Contours show the snapshot of pressure load on the front (facing the PDE wave) and back surface of platen; plots giving the maximum, minimum pressure, and pressure variation (maximum-minimum) with reference to operating pressure.

5.3.3 Effectiveness of PDE Fouling Removal

5.3.3.1 Introduction

In an effort to evaluate fouling removal effectiveness of the pulse detonation engine (PDE) system in the integrated gasification combined cycle (IGCC) radiant syngas cooler (RSC) environment, the 3D CFD analysis presented in the previous section was completed to simulate the effect of a PDE wave load on individual RSC platens. The results generated pressure maps of the pulse over a small area of the platen as it propagated through the vessel for a 0.003 second time period. The resulting pressure maps and applicable boundary conditions from the 3D CFD study were then applied to an FEA model to simulate the effect of a PDE pressure pulse on a simplified RSC platen model. This was done to investigate the effectiveness to fouling removal using the baseline PDE configuration CFD results.

5.3.3.2 Stress Analysis Model Setup

A simplified flat plate was modeled in ANSYS to mimic the RSC platen geometry assumed in CFD analyses. The geometry, material properties, and boundary conditions were applied to estimate the shear stress effects on the fouling/platen interface due to the simulated PDE pressure wave.

The stress analysis procedure included static, modal, and transient dynamic analyses based on the following assumptions:

- Platen geometry is simplified into a cantilevered flat plate elongated to length of RSC platen.
- Two layers of ash deposit were used on the front and the back of the plate.
- Effects of a single pressure pulse are simulated using the baseline CFD analyses (0.003 second pulse).
  - Baseline CFD configuration implements an ambient pressure of 400 psi as an initial condition.
  - For structural analysis, ambient pressure is considered to be equalized and is ignored for analysis.
  - PDE pressure distribution is taken to be a variance from ambient conditions ($p = \Delta p$) applied mid-span.
- Platen tube material properties were altered to capture the mass of the platen geometry filled with water and stiffness of the platen.
- Fouling material properties were compiled from various test samples and are considered accurate for this analysis.
- Gravity and damping effects are negligible.
- The shear strength of the ash deposit is 1 psi.
  - If resultant shear stress > allowable shear strength, fouling is removed.

1. Geometry

The RSC, in this study, was composed of 12 radial platens comprised of tube bundles. Each platen is connected to the steam circuit by an upper and lower straight header as illustrated by Figure 52. Due to the detail of the platen geometry, the FEA model was simplified to reduce analysis time while still capturing the physics of the problem. To further simplify the problem, a

cantilevered flat plate was created to mimic the platen/header profile based on the assumption that the upper header is considered to act as a fixed constraint and the lower header is considered to be free to move.

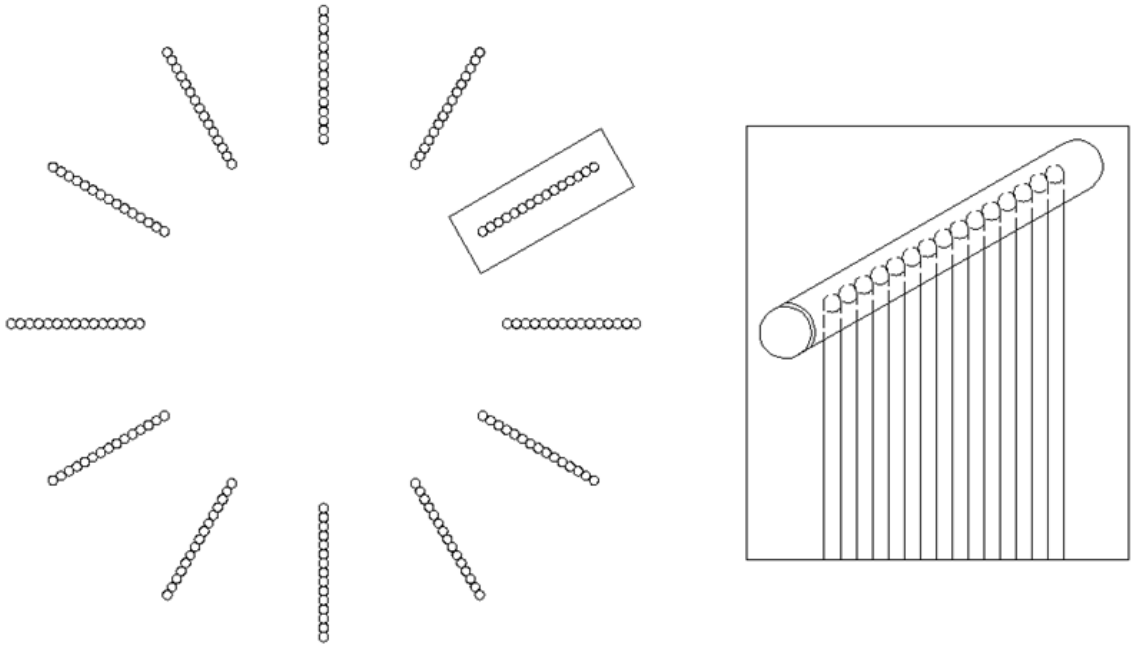

Figure 52. A typical RSC platen geometry.

The simplified geometry was created to encompass the model used for the CFD analyses, with a length reasonable to represent an industrial application. The cantilevered flat plate was modeled to calculate the shear stresses induced by the PDE acting at the center of the platen.

To more accurately reflect the mass and stiffness of the platen as a simplified plate, the density and modulus of elasticity were altered to count the water inside the tube. The fouling material was assumed to have the following properties:

Density, lb/in3……0.111
Modulus of Elasticity, ksi……166
Poisson's Ration……..0.20

2. Boundary Conditions and Mesh

The analytical model was meshed to be consistent with the CFD model in order to map the pressure wave obtained from the CFD analyses. The mesh density was composed of 264,600 elements defined by a 630 x 70 x 6 element grid of Solid 45 (8 noded brick) elements. With the cantilevered plate six elements thick, each fouling layer had a one element thickness.

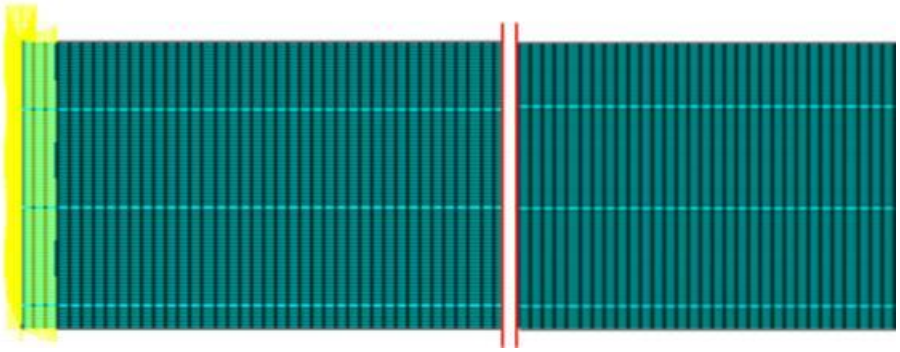

Figure 53. Mesh density of the cantilevered plate with fixed Constraint.

Illustrated in Figure 53, the top end face of the plate was fixed in all degrees of freedom (DOF). It was assumed that the platen metal temperature was equal to the temperature of the steam (637°F, 336°C). It was assumed that the platen had an equalized ambient pressure of 400 psi, and the PDE pressure wave was applied as a variance in pressure consisting of 150 load steps at 20 µsec intervals; where, each load step represented the pressure wave measured on the platens over a 3 ms period as graphed in Figure 45.

3. Analysis Methodology

Since the PDE pressure impact is a short time duration dynamic event, a full transient dynamic analysis using ANSYS was conducted for this study. To validate the model setup and correct application of boundary conditions, a static analysis was also performed.

Once the model setup was validated, a modal analysis was conducted to predict the natural frequencies and mode shapes of the structure. In theory, the impulse force applied will excite the natural frequencies of the structure, where the response will characterize its mode shapes. Since this study was transient, the time domain was resolved so that the analysis captured the highest mode of interest which required a minimum of 20 discrete time steps per period.

Once the model setup was validated and the structural behavior under natural vibration was evaluated, we proceeded to a full transient dynamic analysis. This analysis was performed to predict shear stresses and deflections induced by the PDE pressure pulse. The model was exposed to a pulse event (3 msec) and then allowed to respond for the remainder of the analysis (1.3 sec). The resulting shear stresses at the bonding layer were post-processed to predict the fouling removal effectiveness with respect to the assumed bond strength.

4. Analysis Results

Deflection Results

The modal analysis results were used to identify the natural vibration of the cantilevered flat plate. As shown in Figure 54, the first 4 mode shapes had frequencies less than 1 Hz. In order to capture any of these natural frequencies in the transient dynamic analysis, the minimum time interval needed to be resolved by t_i = 1/20f. Since the pressure load was applied mid-span of the plate, we would expect to see the structure excited in the 2nd mode at f = 0.243 Hz, where the minimum time step is t_i = 0.2058 seconds. As shown in Figure 55 and Figure 56, the deflection response from the dynamic analysis illustrates that the PDE pressure pulse excited

the 2nd mode. To better capture a full cycle of this event, the analysis would need to be recalculated to t = 4 seconds.

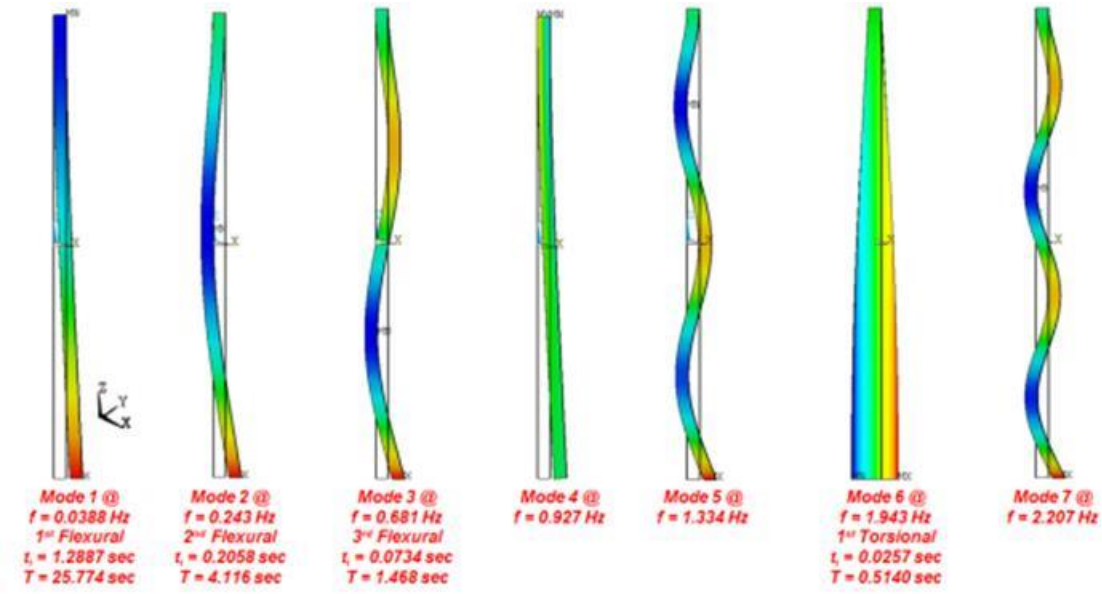

Figure 54. First 7 Mode Shapes.

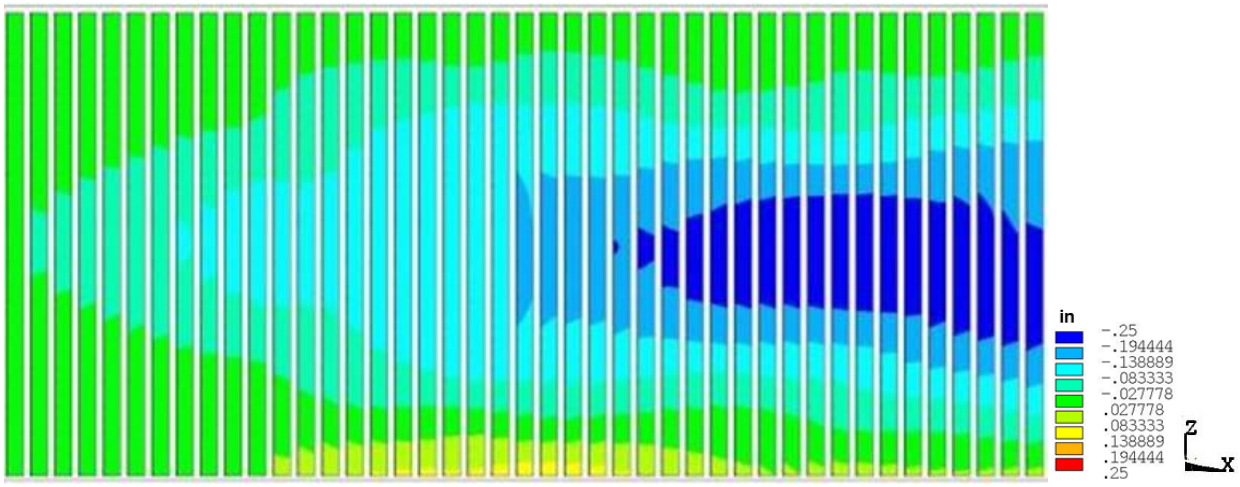

Figure 55. Deflection (UY) vs. time (to t = 1.3 seconds) [Front].

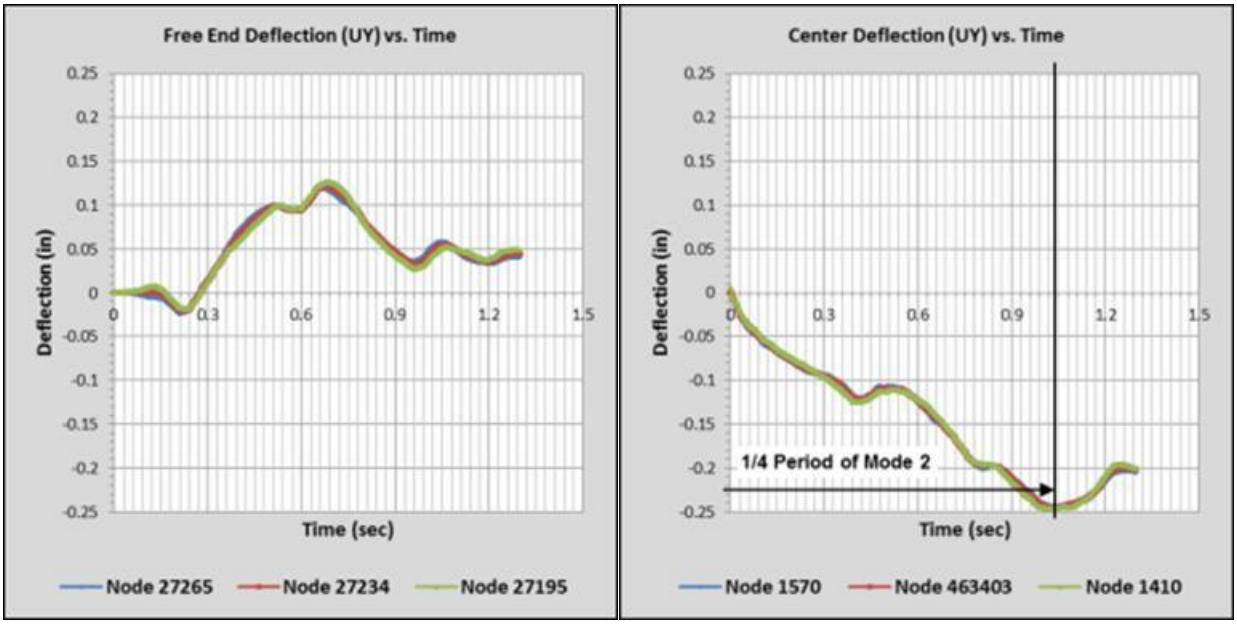

Figure 56. Deflection (UY) vs. time (Left: deflection at the center of the plate, Right: deflection at the free end).

Stress Results

Two structural behaviors occurred during this analysis: (1) stress due to the impact load when p = Δp, and (2) stress due to free vibration when p = 0. Due to this structural response, the shear stresses were identified after t = 0.003 seconds (the last time point of the PDE pressure pulse) and at t = 1.3 seconds (the last time point of the analysis) as illustrated in Figure 57.

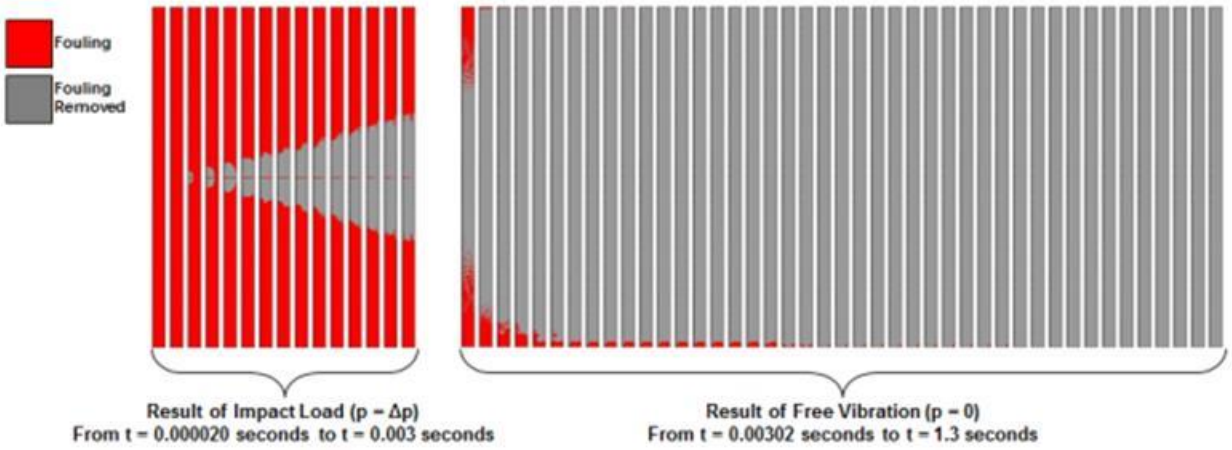

Figure 57. Result of fouling removal over time.

There were also two assumptions that drove this analysis when investigating the feasibility to predict fouling removal capability: (1) the allowable shear stress of the fouling material was 1

psi, and (2) if the resultant shear stress was greater than the assumed allowable, fouling was considered to be removed. Based on these assumptions, 36% of the area has fouling removal at t = 0.003 seconds and 100% of the area has fouling removal at t = 1.3 seconds.

Due to the uncertainty of the fouling shear strength of 1 psi, the percentage of fouling removed is plotted versus the fouling bond strength as a factor of the assumed allowable in Figure 58 to estimate the amount of predicted fouling removal for higher shear strengths.

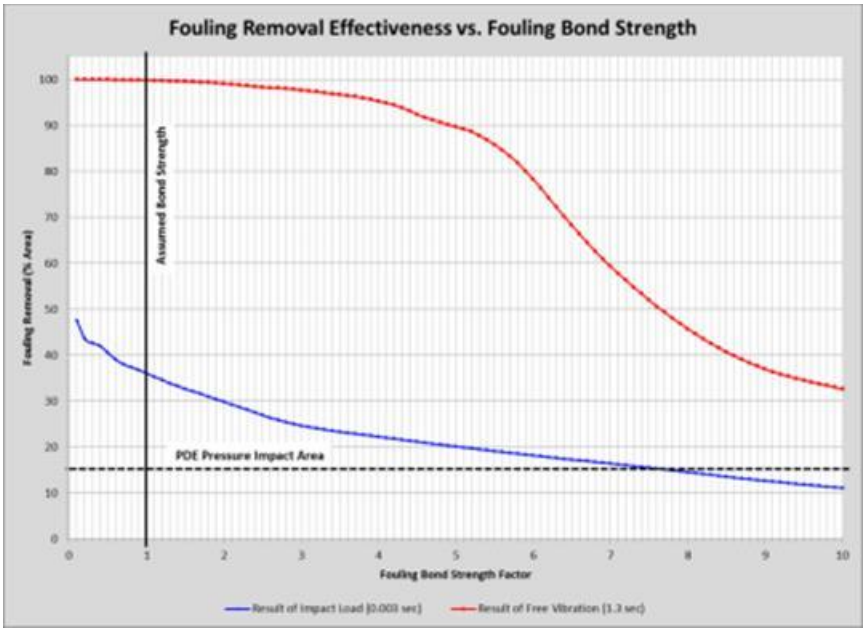

Figure 58. Percent shear stress above allowable vs. time.

The actual impact area of the cantilever plate is only 15% of the total area being analyzed. Within the impact load after 0.003 seconds, 100% of the PDE pressure impact area was predicted to have fouling removal up to 7.5x times the bond strength. After 1.3 seconds, it was expected that at least 90% of the fouling could still be removed up to 5x the bond strength of the fouling material.

Conclusions

The initial layer of ash deposits in the RSC are composed of a thin layer of condensed inorganic material at the platen surface. It is hypothesized that by inducing shear stresses greater than the allowable strength of the bonding layer, ash deposit will be removed from the platen.

The previous 3D CFD baseline configuration results generated contour maps depicting the pressures experienced on the RSC platens as a result of the PDE shockwave. By utilizing that information, the FEA approach yielded results supporting the conclusion that the analytical prediction of fouling removal is indeed feasible and effective based on the following findings:

- Pressure wave induces shear stress in the fouling bond layer and excites platen natural frequencies when applied mid-span.
- Wave induced vibratory deflections produce additional shear stress.

- Predicted shear stresses were above the assumed fouling layer bond strength; this result indicated that fouling removal should occur.

  Based on the analysis inputs and the simplified geometry, it was predicted that there was
  1) 36% fouling removal due to PDE Pressure Pulse
  2) 64% fouling removal due to Wave Induced Vibration

Two very important assumptions were made when investigating the feasibility to predict fouling removal capability: (1) the allowable shear stress of the fouling material was assumed to be 1 psi, and (2) if the resultant shear stress is greater than the assumed allowable, fouling was considered to be removed. To move forward with this analysis, it is highly recommended to comprehensively assess the material properties of the ash deposit to realistically correlate the shear strength of the bonding layer to actual fouling removal. The following are recommendations for further analyses:

- Conduct assessment of the structural impact to RSC internals
- Further investigation of existing model to evaluate reaction loads at the support
- Increase model fidelity
- Detailed model geometry to evaluate stress impacts to RSC internals and more accurately model the system stiffness

5.4 Develop PDE Fouling Removal Subscale Testing

5.4.1 Process Flow Diagram of Subscale Testing Rig

The Pratt & Whitney SHOCKSystem and the GE Powerwave+ are pulse detonation cleaning devices that have been used successfully to remove fouling from heat exchangers in coal fired boilers. They have also been used for various particulate removal tasks in other industrial applications. In addition, a substantial amount of research has been done at the University of Texas at Arlington (UTA) to investigate the use of pulse detonation engines as a means of propulsion. This work drew on both areas of experience to develop a subscale testing rig for the purpose of evaluating the fouling removal effectiveness of a PDE system in a simulated IGCC RSC environment, which was done using a PDE system built and operated by UTA, taking into consideration future adaptations for a full scale production model PDE fouling removal system that could be used in RSCs.

A simplified piping and instrumentation diagram (PID) of the PDE used for the testing is shown in Figure 59. It incorporates some modifications to the simplified PID shown in Figure 31.

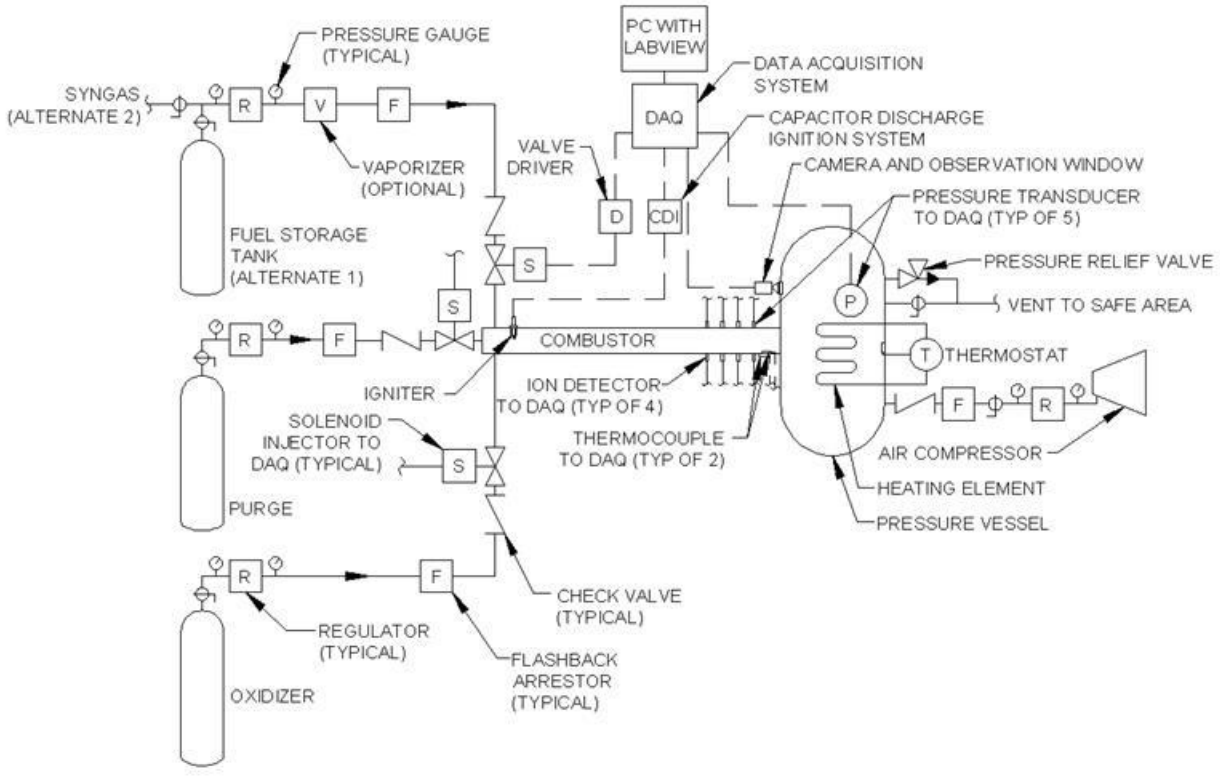

Figure 59. Simplifies PID for PDE fouling removal subscale testing.

As shown, the PDE system included a hydrogen (fuel) supply system, an oxygen supply system, and a purge gas supply system. Controls were included to regulate the flows of each into the PDE and regulate the pulse detonation and purging processes. The system also included a pressure vessel with simulated platens for measuring effect of the PDE on the

platens, including on fouling removal using special coupons and other specialized instrumentation.

1. Fuel, oxidizer and purge systems

A fuel storage tank was required for a PDE sub-scale testing rig. The tanks are usually stored outside to avoid buildup of flammable or hazardous vapors that pose a health risk to researchers. It is also beneficial for fuel storage tanks to be easily accessible for the purpose of refilling. Storage tanks for oxidizer and purge gases were also required.

Syngas is being considered as a possible fuel source for a production model PDE system. If syngas were used as fuel for such a system, a fuel storage tank might not be required. Syngas could be piped from downstream of the RSC where it has cooled significantly so as to prevent premature ignition (because of the high temperatures associated with the RSC) when it is mixed with oxidizer in the PDE. For the purposes of the PID, a syngas connection is shown as an alternate. For the purposes of testing, syngas could be used in the PDE and supplied from a storage tank.

As the fuel, oxidizer and purge gases are injected into the PDE throughout the cycle, the system line pressures begin to drop. When this occurs, the fuel to oxidizer ratio of gases injected into the PDE will change and system performance will be reduced. The gases must be injected into the PDE at stoichiometric conditions. This is due to the fact that at stoichiometric conditions, all of the fuel and oxidizer will be consumed and the reaction can occur quickly and transition to detonation. The stoichiometric ratio of fuel to oxidizer is calculated from the chemical equation of the combustion reaction. Adding a pressure regulator to the system will maintain operating pressure and decrease the effect of high frequency PDE use on line pressures and fuel to oxidizer ratio. The use of supply lines of smaller diameter (lower volume) will also help alleviate these problems. Even if the PDE system is used at low frequency and pressure drop is not a concern, the regulator pressure should be tuned to account for the flow capabilities of the supply lines and injectors to deliver the correct mixture of fuel and oxidizer. The purge system would also require a pressure regulator to ensure that the design volume of purge gas is injected resulting in the full expulsion of exhaust gases from the PDE and sufficient cooling of the combustor after each detonation. (Panicker, 2008)

A pressure gauge should be installed downstream of the regulators to observe system pressure for the purpose of experimental adjustment. Including a second pressure gauge upstream of the regulator allows researchers to make sure the pressure regulator is working properly and to monitor the amount of gas remaining in the storage tanks.

When gases are stored as liquids under pressure, they must be converted to vapor in order to be used in the PDE. Natural vaporization occurs when heat is transferred from the outside environment to the storage tank and in turn to the liquid fuel. If the PDE system is used at high frequency, natural vaporization will be unable to keep up with the system demand and a vaporizer may be necessary. A vaporizer uses indirect heat to change liquid to gas in order to keep up with system fuel requirements. It also eliminates re-condensation of vapor in the supply lines that can create a hazardous situation. The Pratt & Whitney SHOCKSystem uses a vaporizer for its propane system but it may not be necessary for all PDE systems. The decision to include it in our system will depend on fuel selection and demand. (McCormick, 2006)

Flow meters in the fuel, oxidizer and purge lines could prove useful for the purpose of experimental monitoring and adjustment. However, UTA research demonstrated that venturi

and orifice flow meters are not effective for pulsed flow applications. They would be more effective for a system with multiple PDEs at a point upstream of the individual PDE branches. Some UTA PDE prototypes also incorporated sonic nozzle flow meters, but they were found to create flow choke points and prohibit the system from delivering the required fuel to the combustor. Since the subject of this document is an individual PDE, the PI&D does not include a flow meter. (Panicker, 2008)

Safety is a key factor in the operation of a PDE system. A PDE functions by igniting a fuel/oxidizer mixture to initiate combustion, transition to detonation and create a subsequent shockwave. This is potentially an inherently dangerous process and requires proper control and safety measures. Accidental fires and explosions can cause loss of life, injury and equipment damage. There are three factors needed for a fire or explosion to occur: fuel, oxygen and ignition. Isolation of these three factors is paramount to avoiding dangerous, uncontrolled explosions and fires.

Gauges, regulators and other equipment should be oil-free because of the high flammability of oils. An oil-filled regulator or gauge on an oxidizer line meets two of the three requirements needed for combustion.

Some research on the use of PDEs for propulsion involves pre-mixing fuel and oxidizer in a staging chamber before injecting it into the combustion chamber. This is done to ensure detonation is achieved and at the high frequency required for PDE propulsion applications. For the use of PDEs as a fouling removal mechanism, high frequency operation is not as vital and the added risk of pre-mixing fuel and oxidizer in a vessel not designed to house combustion is unwarranted. An explosion could occur due to an ignition source such as heat of recompression if an oxygen or fuel valve is opened too quickly. Also, this arrangement would likely add cost, complexity, and a larger footprint to the design.

Flashback is another danger associated with the combustion of fuel and oxidizer that can be mitigated by the use of a check valve. Flashback is when a flame moves upstream into plumbing or equipment, against the normal flow path of the fuel or oxidizer. Flashback is usually the result of the reverse flow of fuel or oxidizer caused by a malfunctioning check valve, improper startup/shutdown procedures or by allowing cylinder pressures to become too low. Check valves are required on oxy-fuel welding and cutting systems to prevent backflow of fuel into the oxygen cylinder and vice-versa. They are usually integrated into the torch for oxy-fuel welding/cutting. A PDE fouling removal system would likely require check valves just upstream of the fuel/oxidizer injectors. If they were positioned further upstream and flashback occurred, the combustion may have the run-up distance needed to transition to detonation and cause significantly more damage. (Harris Products Group, 2012)

Check valves are designed primarily to stop reverse flow and not to stop a combustion or detonation wave. This is where a flashback arrestor can be useful for an extra degree of safety. Flashback arrestors can not only stop reverse flow, but they also have the ability to stop a flame from progressing upstream. These can be used in place of or in conjunction with check valves. Flashback arrestors and/or check valves should also be installed at the outlet of the fuel and oxidizer regulators to protect the cylinders and regulators. (Harris Products Group, 2012)

The final leg of the gas system supply lines should be constructed of reinforced steel braided flexible hose. This is done to avoid damage to rigid fittings due to the vibrations caused by operation of the PDE system.

Once the specific design parameters for the PDE system are chosen, more specific system components and safety measures will likely be added to the PID. For instance, if hydrogen were used as fuel for the PDE system, hydrogen detectors may be required. Also, NFPA 70 (National Fire Protection Association code) requires all metal components of a hydrogen system to be grounded to avoid buildup of static electricity that could cause a fire. All applicable safety standards and codes should be consulted during the design phase for a more complete and safe system.

The GE Powerwave+ system uses solenoid valves to control the flow of gases into the combustor. The research team at UTA has experimented with solenoid injection and rotary valve systems for their PDE tests. Rotary valves have fewer obstructions than the poppet valve arrangement in a solenoid injector. This means higher flow rates with lower loss of pressure are possible with rotary valves. On the other hand, rotary valves require a sensor to measure the position and velocity of the valve. Also, they are incapable of modulating the valve open time since it is dependent on the rotational frequency and area of the valve opening. Solenoid injectors offer a higher degree of tunability compared to rotary valves because the valve open time for any injector can be easily adjusted without affecting the timing of another. The solenoid injectors for the gas and oxidizer systems can be arranged to impinge on each other to maximize diffusion and increase the ability of the mixture to reach detonation. (Panicker, 2008)

2. Ignition system

During the course of the PDE research carried out at UTA, several ignition systems were tested. After multiple evolutions of the PDE ignition system evaluation, the researchers determined that high energy (HE) ignition systems reduced ignition delay time and produced rapid detonation of various fuel/oxidizer mixtures. Some notable drawbacks to HE systems are that they require larger, heavier power supplies and their igniter plugs are less durable than those associated with low energy (LE) ignition systems when exposed to the harsh conditions of the PDE environment. LE ignition systems were ultimately preferred by the UTA researchers because of the fact that their shortcomings in producing detonation can be overcome by providing the right fuel and oxidizer (and in the proper proportions), promoting mixing and carefully designing combustor geometry. The GE Powerwave+ employs a capacitor discharge ignition system which is a high voltage low energy ignition system commonly used in the internal combustion engines of automobiles. This type of system works by increasing the voltage by means of a transformer. This current then charges a high voltage capacitor. The charging circuit also contains a rectifier that prohibits the capacitor from discharging until the ignition system is triggered. When ignition is triggered, the capacitor discharges through the ignition coil windings, which increases the voltage further before creating a spark at the igniter plug. (Panicker, 2008)

3. Measurement and control system

Since the objective of our research is to create a subscale testing rig, it differs from a production model PDE system because it will employ an array of sensors for experimental measurements. However, the control elements for both systems will be similar. The experimental setup will require fast acting sensors capable of high sampling frequencies in order to fully characterize the detonation reaction which is capable of travelling up to 2500 m/s.

Piezoelectric dynamic pressure transducers near the end of the combustor are used to detect the pressure wave speed and magnitude. This will allow us to determine whether the reaction has reached detonation. The wave speed is determined by performing simple time of flight

calculations using the known distance between the two transducers and the time between pressure peaks of each sensor. These sensors are extremely vulnerable to the high pressures and temperatures of the PDE and do not last long under prolonged exposure. In the UTA studies, they were recessed in ports in the combustor and encased in water cooled jackets. The response time and sensitivity of the transducers were reduced as a result but this effect can be accounted for with some experimental calibration against flush mounted transducers. The cooling water was supplied at the available domestic water pressure of the building and the outgoing cooling water was discarded to a catch tray under the PDE and run to a drain. Solenoid injectors and ion detectors were also outfitted with water cooled jackets to protect them from damage in many of the UTA PDE research trials as shown in Figure 60. (Panicker, 2008)

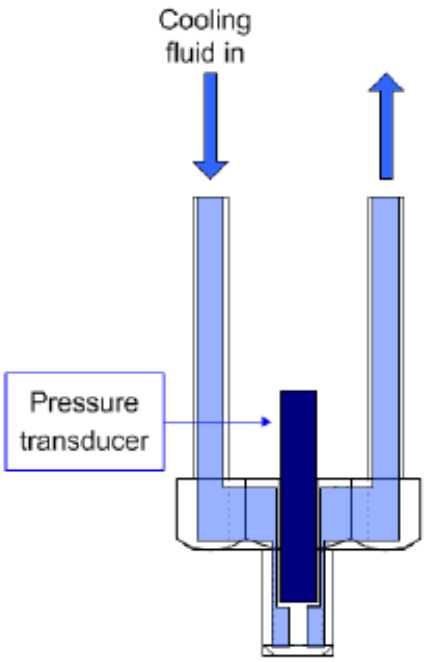

Figure 60. Pressure transducer with water cooled jacket.

Ion detectors were used in the UTA experiments to measure the speed of the flame front in order to determine if the reaction reached detonation. They can also be used to measure the speed of the pressure wave but it was found that a combination of pressure transducers and ion detectors worked best for determining detonation properties. An ion detector is essentially a circuit with a power source, resistor, ammeter and an electrode. The electrode is exposed in the combustor and insulated from the PDE tube. The tube is electrically grounded in the circuit. When the flame front arrives at the detector, it bridges the gap between the electrode and tube wall. This will cause a current to flow through the circuit as a result of the movement of electrons and ions in the flame. The ammeter then sends the current reading to the measurement and control system. Refer to Figure 61. The speed of the flame front is calculated using the same time of flight method as the pressure transducers. Ion detectors were shown to be more durable than pressure transducers within the PDE environment. As mentioned previously, ion detectors can also be encased in a water cooled jacket if needed. (Panicker, 2008)

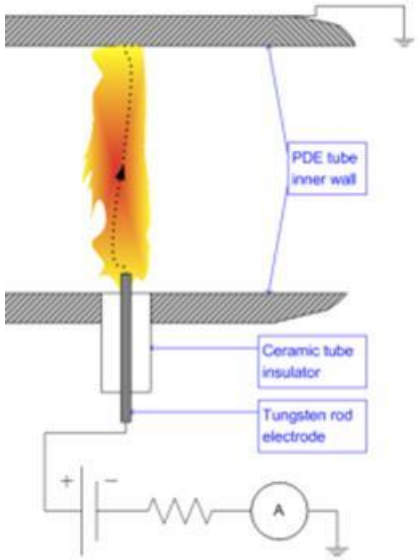

Figure 61. Ion detector diagram.

Thermocouples can be used to measure the temperature of the PDE tube exterior and the exhaust gases near the combustor exit. This is important to establish the maximum pulse frequency that the combustor can withstand. It also gives insight into the effect of temperature on the area of application beyond the PDE. Thermocouples are inexpensive, reliable and can be built to withstand the demanding environment of the PDE.

The digital acquisition system (DAQ) will be the heart of the measurement and control system for our sub-scale testing rig. All signals from sensors (pressure transducers, thermocouples, ion detectors, etc.) and all command signals to system control elements (solenoid injectors, igniter, etc.) will pass through the DAQ. The DAQ system serves three main purposes: signal conditioning, analog to digital conversion and communicating measurement and control signals between the computer, sensors, valves and ignition system. All of the sensors discussed previously, convert a physical phenomenon into an electrical output signal. Some of these signals require some type of signal conditioning which may involve amplifying, isolating, filtering or compensating the signal in some way so that it can be handled safely and accurately by the DAQ system. Analog samples from the system sensors must then be converted to a digital representation before it can be sent to the computer. Computer software such as LabVIEW reconstructs the signal and facilities the recording and post-processing of the sensor data to spreadsheets, graphs and other useful forms. Counters in LabVIEW can be used to precisely time the ignition and valve sequence of the PDE system. This is accomplished when the computer instructs the DAQ to send transistor-transistor logic (TTL) signals to a valve or ignition driver which in turn actuates the injectors or fires the ignition circuit at time intervals established by the software. (National Instruments, 2013)

In a production model PDE, the design parameters of the system would already be determined by means of experimentation and most of the sensors present in our preliminary version would not be needed. Removing these sensors from the PDE all together would yield a lower cost, more robust system. However, these end-product PDE fouling removal systems will likely be operated remotely and a method for monitoring and ensuring proper system function would still be required. The GE Powerwave+ uses an accelerometer externally mounted on the combustor. This feedback sensor measures the vibration resulting from a pulse and reports it to the

controller. The controller compares it to experimental values input by the user to determine if the system is working properly.

4. Simulating RSC

In order to evaluate the feasibility of the PDE system to remove fouling in the RSC environment, a pressure vessel (receiver tank) capable of regulating pressure will be used as a simulated RSC. The vessel itself should be designed according to ASME Boiler and Pressure Vessel Code to ensure the safety of researchers and avoid damage to system components. The design should be able to withstand the pressure pulse produced by the PDE system in addition to the static pressure in the vessel. The vessel will contain platen-like structures outfitted with a simulated fouling layer.

The simulated RSC should be capable of producing a pressurized environment up to 4 atm. This will be accomplished by incorporating an air compressor and a supply line fitted with an adjustable regulator. Similar to the fuel, oxidizer and purge systems, the compressed air piping should be outfitted with pressure gauges, a flashback arrestor, a check valve and a flexible connection to the vessel. A vent line with a manual isolation valve should be connected to the vessel to relieve the pressure and expel the exhaust gases after the PDE is fired. It can also be used to evacuate the pressure vessel of fuel and oxidizer in the event of a failure to detonate. This vent should be directed to a safe exhaust location. Once the manual valve on the vent line is open and the gases begin to exit, the pressure regulator on the compressed air supply line should begin to allow fresh air into the vessel and eventually force the unwanted gases out. A pressure relief valve should also be installed on the vessel and piped to the vent downstream of the isolation valve. The valve should be set so that if the maximum design pressure of the vessel is reached, the relief valve will open and preserve the structural integrity of the vessel.

In addition to pressure, the temperature of the simulated RSC should also be regulated. This system will be similar to that of a typical oven with electronic thermostat. When the desired temperature is set on the control interface, current will be run through the heating element. The resistance in the heating element will cause some of the current to be transferred to heat energy which will then heat the contents of the vessel. A thermocouple in the vessel will sense when the desired temperature has been reached and shut off the current to the heating element.

In order to determine the fouling removal effectiveness of the PDE system, a high speed camera might be useful to visually determine whether the fouling layer on the simulated platens is removed. High speed footage of the event may also help to reveal the physical mechanism by which the fouling is removed. The camera would remain outside of the simulated RSC and record through a small observation window in the vessel exterior. One or more pressure transducers should be positioned in the vessel in key areas adjacent to the simulated fouling layer. These sensors will be wired to the measurement and control system to record the pressures experienced by the fouling as it is acted upon by the PDE pressure pulse.

5.4.2 PDE Fouling Removal Subscale Testing Rig

The laboratory-scale testing rig used in this work was designed by and installed at the Aerodynamics Research Center (ARC) located at the southeast side of the University of Texas at Arlington. This section describes the major features of this rig and the experimental procedures.

1. Subscale Testing Rig

As shown in Figure 62, the major components of the test facility were:

- Receiver tank rated to 5 atm
- Pulse detonation engine capable of operating up to 1 Hz into an ambient pressure of up to 4 atm
- A pair of platens
- Thrust stand
- Gas supply and venting system
- Data acquisition and control system

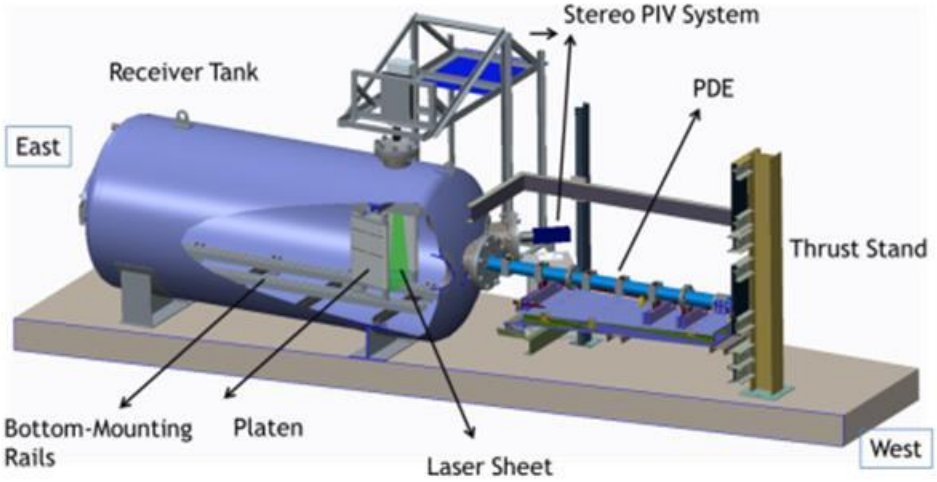

Figure 62. Side cutaway CAD rendition of the testing rig.

Figure 62 shows a computer aided design (CAD) rendition of the testing rig. The figure shows the receiver tank to the left. Attached to it on the right is a pulse detonation engine mounted on a thrust stand. A stereo particle image velocimetry (SPIV) system is also shown with one of the cameras removed. It turned out that due to difficulties with the SPIV technique that it was not used. Instead a light-scattering visualization method was used to provide qualitative understanding of the unsteady PDE exhaust jet. The cutaway reveals a pair of platens, one of which can be heated to 850°F (454°C) and holds up to four flyash coupons, two on each surface. These two are arranged so that one is in the middle of the platen and the other to the top. The other platen is unheated and is instrumented with a number of high-frequency, piezoelectric pressure transducers. Not shown in this figure are the gas supply and venting system, and the data acquisition and control system.

The receiver tank was fabricated to have an internal diameter of 42 inches (1.1 m) and an overall length of 80 inches (2 m) by Prentex, Inc., 3108, Sylvan Avenue, Dallas, TX 75212 (prentex.com). Prentex provided the structural design with input by UTA and GE. The receiver tank was rated for 5 atm with a maximum allowable working pressure of 150 psig at 366°F (186°C) per ASME Pressure Vessel Code. The receiver tank incorporated the following features:

- Flanged connection to the PDE along its axis at one end.

- Operator access into the tank from the opposite end.
- Ports for charging and discharging the tank. In the final design, these were combined into one port.
- Mounting feet.
- Optical access for stereo particle image velocimetry and for Schlieren imaging.
- Ports for instrumentation and power.
- Support lugs for internal rails for mounting platens.

A schematic diagram of the detonation tube used for testing is shown in Figure 63, which included an injection section and a detonation section. Various other subsystems were included to convert the detonation tube into a PDE. The main ones were (i) the hydrogen, oxygen and air supply, (ii) the igniter, (iii) the control and (iv) the data acquisition system. These are shown schematically in Figure 59. The operation of these subsystems will be described later.

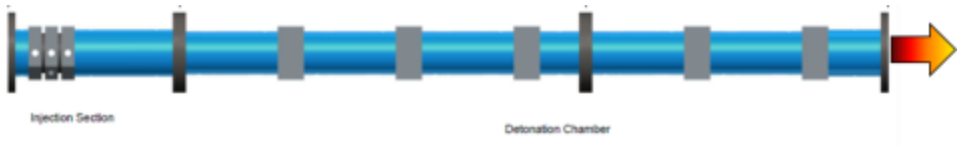

Figure 63. Schematic diagram of PDE

Two platens, Platen #1 and Platen #2, were installed in the receiver tank at an angle of 15^{o} with the axis as shown in Figure 64. The platens were sized to be 16 inches high by 12 inches wide and 2 inches thick (0.4 m high by 0.3 m wide and 50.8 mm thick). Platen #1 was used to house fly-ash coupons in the front and the back, secured by dovetail inserts. Figure 65(a) is a CAD drawing depicting one of two identical sides of Platen #1. The use of dovetail inserts provided a means to attach the fly-ash coupons that resulted in the least disturbance to the fly ash. Figure 65(b) is a cutaway view showing the locations of ring heaters located directly behind the coupon locations. These heaters made it possible to heat Platen #1 to 850^{o} F (454°C) in less than one hour. Platen #2 housed three pressure transducers on the exposed side and one on the hidden side. Figure 66 shows CAD drawings of Platen #2. The platens were impacted by detonation waves at 1 Hz frequency.

Figure 67 presents photographs of the facility. Figure 67(a) shows the view looking downstream from the PDE. The PDE is attached to the receiver tank at the head end by a flange. Clearly visible are the water-cooling lines for the pressure transducers and the PDE. One of the stereo cameras for the particle image velocimetry (PIV) system is visible to the left. The other is installed to the right. Partly visible to the left is the PIV laser that is mounted on a frame. Figure 67(b) shows the PDE attached on the left to the receiver tank and to the right onto a thrust stand. The ignition system is below the thrust stand and by the far wall is the gas supply cart that delivers hydrogen, oxygen and air.

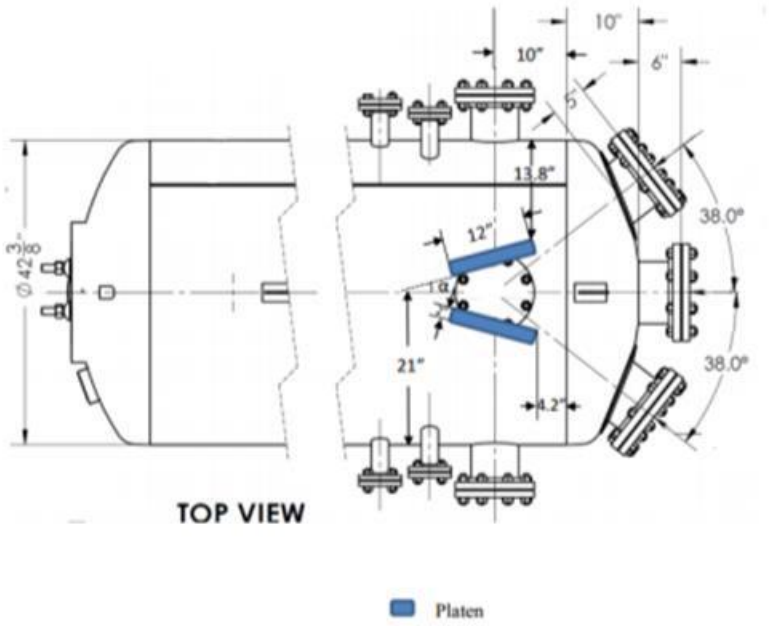

Figure 64. Schematic diagram of platens installed in the receiver tank.

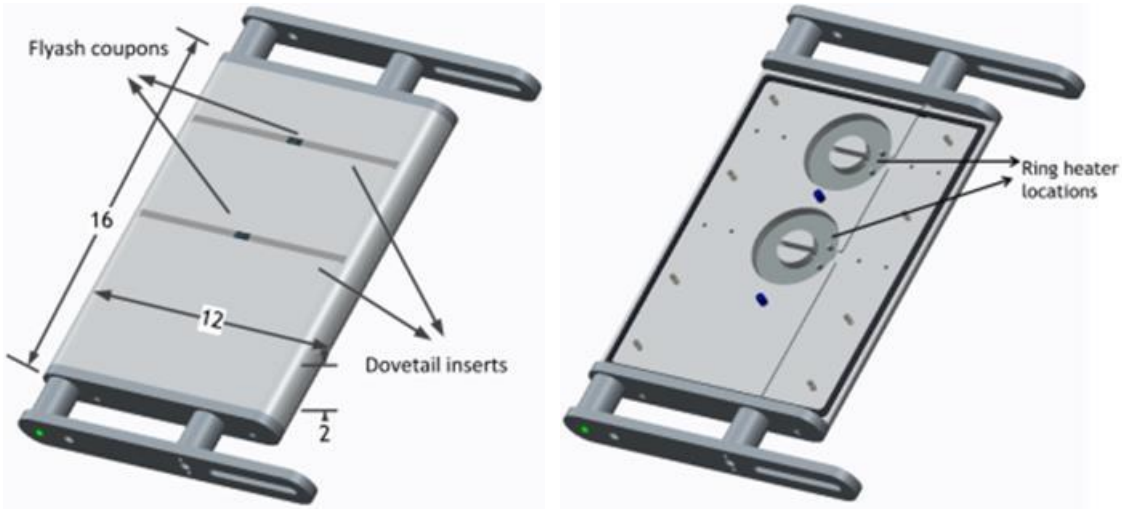

(a) (b)

Figure 65. CAD drawings of Platen #1 - fly-ash platen. (a) External view; (b) Cutaway view showing ring heater locations.

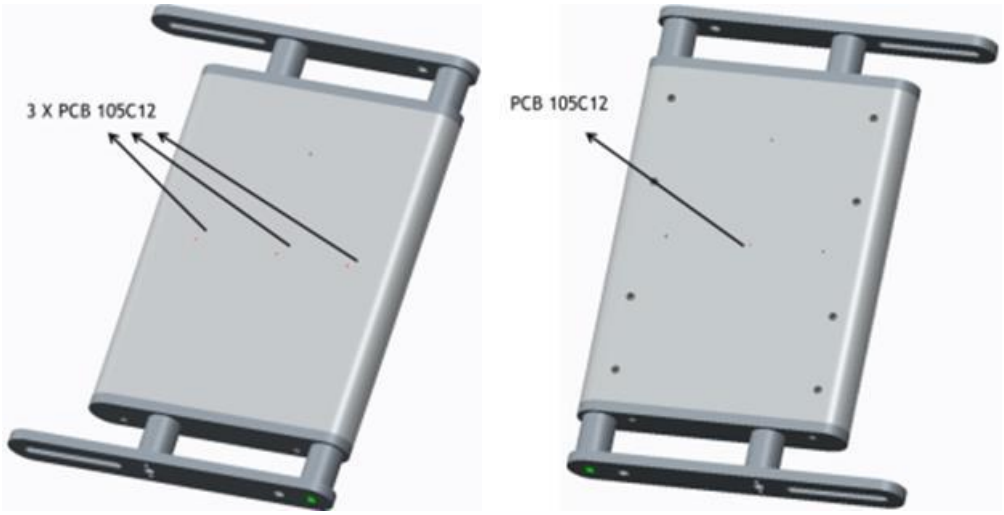

(a) (b)

Figure 66. CAD drawing of Platen #2 - instrumented platen. (a) External view; (b) External view for other surface.

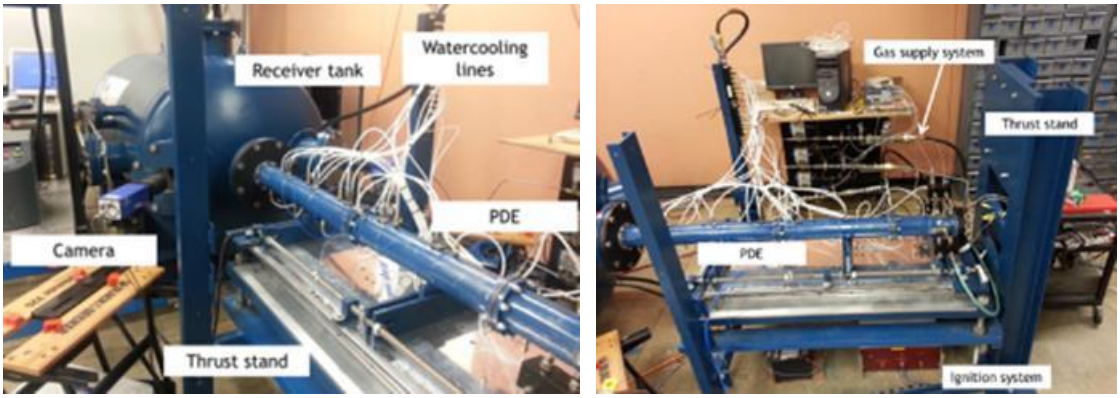

(a) (b)

Figure 67. Photographs of test facility. (a) View downstream; (b) PDE.

2. Experimental Techniques

The experimental techniques used were primarily high-frequency, simultaneous sample-and-hold pressure measurements. The pressure measurements were made at different locations on the detonation tube and in the instrumented platen. Vibration measurements were also performed with an accelerometer. Finally, high-speed flow visualizations were performed using a laser light-scattering technique. These techniques are described below.

High-Frequency Pressure Measurements

The detonation tube and the instrumented platen (Platen #2) housed Model 105C12 subminiature, piezoelectric pressure transducers from PCB Piezotronics, Inc., Depew, New

York.[1] Piezoelectric transducers have large pressure ranges and broad bandwidth. The Model 105C12 has a sensing diameter of only 0.099 inches (2.51 mm). For this particular model, the pressure range is 1000 psi which is above the pressure range expected. The resonant frequency is larger than 250 kHz. It can be noted that in practice the pressure spike of a detonation wave cannot be resolved by existing instrumentation. However, the bandwidth of piezoelectric transducers is sufficiently high to capture practically the entire detonation wave when used with a high-speed data acquisition system. For the present experiments, the DAQ was operated at 2 million samples/second, simultaneous sample and hold. Due to the heating in the detonation tube, the pressure transducers that were housed in the detonation tube were encased in water-cooled jackets. The transducers that were housed in Platen #2 were not cooled. The same type of pressure transducer was used in a pitot probe that was used to survey different exit planes of the detonation wave. To obtain the highest bandwidth and to avoid Helmholtz resonance, the transducers were all flush mounted.

Vibration Measurements

A PCB 350B04 accelerometer was mounted on the backside of the instrumentation platen in order to study the vibrations induced due to the impact of the detonation waves on the platens. The signals were acquired at 400,000 samples per second for 4 seconds. The measured acceleration signals included high frequency noise due to high sampling rate. Before analysis, the signals were passed through a Butterworth filter at 5–150,000 Hz.

Figure 68 shows the accelerometer signal upon the impact from a single pulse. The vibrations show very high frequency oscillations. The figure shows high-frequency oscillations that are due to the propagation and reflection of the initiated stress waves within the platen structure. The magnitude spectrum of the acceleration, as shown in Figure 69, shows that the lower modes have significantly less power than the higher modes. Hence, the lower modes which are usually the structural vibration modes were insignificant and damped because the platens were rigidly attached. The higher pertaining modes are the results of high-frequency, stress wave propagation and reflection.

[1] http://www.pcb.com/Products.aspx?m=105C12

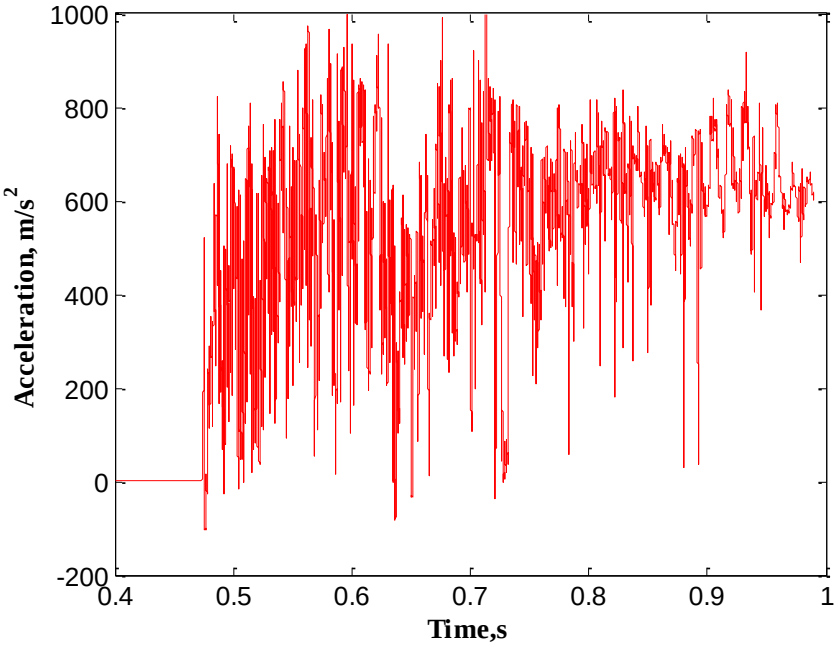

Figure 68. Signal from an accelerometer mounted on a platen.

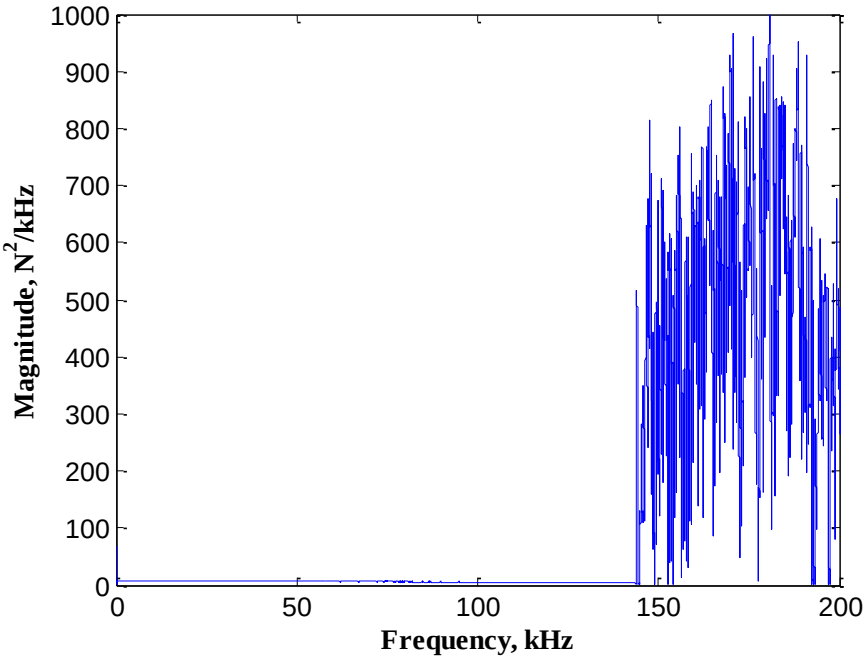

Figure 69. Spectral content of the acceleration.

In addition to the experimental study, a finite element, modal analysis of the platen vibration was also performed. The modal analysis was performed to study their vibration characteristics and to

determine the corresponding mode shapes. The modal analysis was done to provide insight on the effect of vibrations on the attached flyash coupon. The modal analysis was performed on the sub-scale platen as described earlier. ANSYS Workbench 13.0 was used for analysis. A medium quality mesh using tetrahedral elements was used to mesh the three-dimensional model of the platen. The meshed model consisted of 27679 nodes and 103494 elements. The mid-side nodes for the elements were dropped for to speed up the solution time. In addition, the mode superposition method was used to solve the eigenvalue problem to determine the modes of vibrations and corresponding mode shapes. The top and bottom surface of the platen holder were assigned as the fixed supports. The first twelve modes were retained and the corresponding natural vibration frequencies are provided below in Table 12.

Table 12. Results of modal analysis on platen vibrations

Mode	Frequency (Hz)
1	514.43
2	826.51
3	1011.8
4	1402.9
5	1962.6
6	1976.7
7	2302.2
8	2603.9
9	3158.5
10	3617.2
11	3973.1
12	4021.4

Hence, upon comparison of the experimental and numerical results, it can be concluded that the structural modes with lower frequencies are damped out due to the rigid support and therefore would have minimal effect on the removal of flyash.

High-Speed, Laser Lightsheet Visualization

The receiver tank was fabricated for stereo particle image velocimetry (SPIV). However, initial results were not satisfactory and in the interest of time the technique was not considered further. The primary reason for the difficulties was the high speed of the transient, pulsed jet and the low repetition rate of the illuminating laser of 5 Hz.

Instead of SPIV, high-speed visualization of Mie scattering from 100-nm titanium dioxide particles was applied. Such titanium dioxide particles are small enough to follow the supersonic flow except through shock waves. Titanium dioxide is also suitable for the temperature range of interest as it will not decompose.

The main oxygen supply line was split into two paths. One of the paths flowed through a container filled with titanium dioxide nanoparticles. The particle-laden oxygen line was then teed back to the other line. The combined particle-laden oxygen then flowed into the PDE through the same solenoid valve as in the same manner as filling with pure oxygen. Only a

small amount of titanium dioxide nanoparticles per charge was used to ensure that it would not affect the flow.

The particles were illuminated from the light provided by the combustion. The images were captured by a Shimadzu HPV-X high-speed camera.[2] The camera is capable of acquiring up to 256 images at framing rates of up to 2 MHz and exposure times of as short as 50 ns. The images produced were 10-bit monochrome with a resolution of 400 × 250 pixels. The synchronization between the PDE and the camera was accomplished by external triggering with the camera's software and LabVIEW. The trigger was a 5V TTL signal used for PDE ignition. The typical frame rate and exposure time were 500 kHz and 1000 ns, respectively. This helped mitigate the potential for particle streaking and under exposed images.

3. Experimental Procedures

Details of the experimental procedures are available upon request and only a brief description is provided here. The receiver tank, PDE and all the support subsystems were installed indoor in the Aerodynamics Research Center (ARC), a test center operated by the University of Texas at Arlington. The ARC has extensive experience in the development and testing of different types of detonation engines. The operation and control follows a standard operating procedure (SOP) to ensure safe operation and reliable control of the facility. This process includes filling of the receiver tank to vary the ambient operating pressure and the operation of the PDE.

Tank Fill and Discharge Procedures

Figure 59 shows a 175 psig compressor delivering dried, high-pressure air to the receiver tank. A manual valve is opened to fill the tank. The pressure of the tank is monitored in two ways: one using a pressure gauge mounted on the tank and other using a pressure transducer connected to the tank. Once the desired pressure level is reached the manual open valve is closed. The chosen operating ambient pressure conditions available are 1, 2, 3 and 4 atm. The pressure in the receiver tank can be regulated by three different ways: (1) a separate manual valve can be used to discharge the tank; (2) a solenoid valve may be connected which can be actuated by the user in the control room to discharge the tank; and (3) a pop-off valve connected to the tank may be used that is activated when the pressure in the tank is higher than 45 psig. This pop-off valve also serves as an added safety feature. The air pressure and temperature in the tank are monitored and recorded during filling and testing.

PDE Operating Procedures

The PDE utilizes gaseous hydrogen and oxygen as fuel and oxidizer respectively. Per project requirements, the PDE was operated either fuel rich (3:1 hydrogen/oxygen molar ratio) or stoichiometric (2:1 molar ratio).

The hydrogen and oxygen from 2200 psi gas cylinders were regulated for use. Figure 59 shows three nearly identical feed systems for hydrogen, oxygen and air. Regulators were used in all three lines, followed by solenoid valves that allowed remote shutoff as a safety feature. These were followed by one-way check valves for safety and by critical flow nozzles for monitoring the flow rates. (A more elaborate methodology to estimate the intermittent mass flow rates of gases

[2] http://www.shimadzu.com/an/test/hpv/hpv-x_1.html

has been developed previously and is available upon request.) The hydrogen and oxygen lines included flash arrestors (SIMAX EN-730) further downstream to prevent any potential backward traveling combustion waves from entering the hydrogen or oxygen tanks as an added safety feature. A pressure transducer (Omega PX-313-200G5V) and a thermocouple (Omega Type T) were installed in the hydrogen and oxygen lines to measure the supply pressure and temperature. Finally, all three lines discharge their respective gases into the PDE through flow control valves.

For this project, solenoid valves manufactured by AFS (Calgary, Canada) were chosen because of their superior performance.[3] The AFS injectors offered a higher mass flow rate for the same supply pressure. A schematic of the AFS solenoid valve assembly is shown in Figure 70. AFS injectors are compatible with gaseous hydrocarbon fuels, dry air and gaseous hydrogen. A TTL signal from the control program, a buffer current amplifier circuit and AFS control modules were used in coordination to properly time the cycle and operate the PDE.

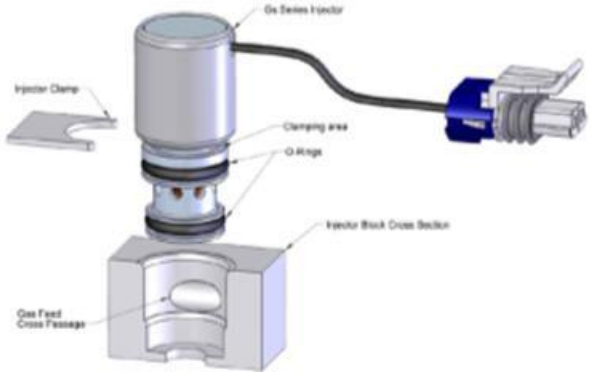

Figure 70. AFS solenoid valve assembly.

The operation of a PDE depends on the exact timing of its valves and the firing of the igniter. A typical PDE cycle has four phases as shown in Figure 71. The first phase is purging. Purging is followed by filling which incorporates gas recharge or filling of the PDE with a detonable mixture. The third phase is the combustion of the mixture by utilizing an igniter. The combustion phase is followed by a blow down phase resulting in the exhaust of the burned gases. After blow down, the purge phase restarts which involves injection of an inert buffer gas preventing the pre-ignition of the detonable mixture by separating the blow down and filling phases.

[3] http://www.afsglobal.com/

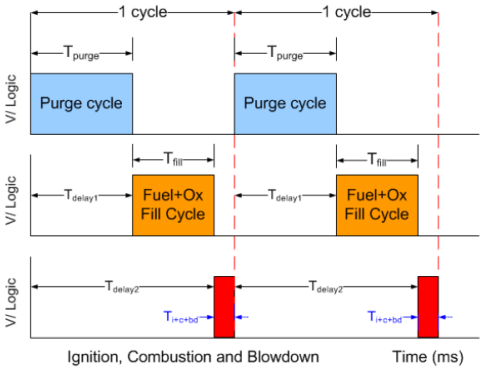

Figure 71. Phases of a PDE operation cycle.

The different phases of the PDE cycle were achieved by the timed opening of the solenoid valves and the firing of the igniter. The timing of the phases was controlled using TTL signals from a LabVIEW™-based control program. A separate DAQ and a different control program were employed to control the operation of the PDE. For safety reasons, the TTL signal for the purge phase was made the master and TTL signals for the filling and ignition phases were made slaves with proper time delays, these delays being based on the frequency of operation.

The control program commanded the DAQ to generate 5VDC TTL signals which is first digitally emitted through the NI-PXI 6722 I/O module and later converted to an analog signal by the BNC-2110 module so that they are recognized by the intended device. These TTL signals drive the solenoid valves used for the purge, fuel and oxidizer lines. In addition, a TTL signal from the control program drove the ignition spark plug.

In addition to this, a TTL signal emitted by the control program was sent to the ignition driver system which further magnifies the voltage and drives the Bosch Platinum 4 automotive spark plug. The spark plug ignited the detonable mixture causing it to deflagrate. The combustion front transitioned into a detonation wave as it traveled along the tube, aided in this process by the Shchelkin spiral.

Data was gathered by a simultaneous sample-and-hold system at 400 kHz/channel for 4 s using an NI model PXIe 8130 controller and an NI PXI 6133 DAQ card. A LabVIEW-based program was used for controlling the data acquisition system. The front-end interface allows the user to change the sampling rate and the number of samples.

RSC Fouling Coupon Data

The RSC fouling coupons were prepared from another site which will be described later, and were first inspected visually when being received from shipping. Each coupon was carefully taken out of the transportation and pictures were taken for records. All the pictures of the coupons as received are archived. The weights of the coupons were also recorded.

5.5 RSC Fouling Coupon Preparation

This section has a description of the characterization and advanced analysis of the fuel, ash, and any deposits available; the development of a standard pre-treatment procedure for the fouling coupons that was used in sticking tests and for lab scale fouling removal testing; the performance of sticking tests; and the evaluation of the effects of thermal cycling of the pre-treated coupons on the bonding strength of the slag used in the sticking tests.

5.5.1 Fouling Deposit Growth and Testing System

Equipment used in analyzing and evaluating deposit characteristics is described below. This included Microbeam Technology, Inc.'s Syngas Fouling Simulator (SFS), Ash/Slag Adhesion Test System, and advanced ash analysis equipment.

Syngas Fouling Simulator (SFS)

Benson and Laumb (2007) conducted testing on the growth and sticking behavior of ash related materials on simulated heat transfer surfaces. Simplified and schematic diagrams of the syngas fouling simulator (SFS) reactor system are shown in Figure 72 and Figure 73. The system was designed to simulate the temperature and pressure conditions in a syngas cooler. The system has been used to determine the impact of pressure (up to 400 psi) and temperature on the formation of deposits due to the condensation of vapor species. This is a major challenge associated with the formation of fouling deposits in syngas coolers. Certain species cause ash deposition and work was conducted to determine the growth of the deposition as a function of gas temperature and steel temperature. An example of the results obtained is summarized in Figure 74 and Figure 75 The SFS tests were performed using three-component blends of carbon dioxide (CO_2), carbon monoxide (CO), and hydrogen (H_2) gases. Sulfur species were formed within the system in order to simulate sulfide formation.

Ash/Slag Adhesion Test System

An Ash/Slag Adhesion Test System developed to allow for the determination of the critical substrate temperature for adhesion is shown in Figure 76. The system design is similar to the test conducted by Moza and Austin (1982). A pellet of ash or slag is formed on a platinum wire and suspended above the coupon. Propane torches are then used to melt the pellet which is dropped onto the alloy coupon held at a constant temperature. The metal ram pushes the droplet from the surface. The value indicated by the pressure transducer was recorded, and the pressure required to remove the droplet used to calculate the adhesive strength of the droplet to the steel surface. This test was used to measure adhesive strength as a function of substrate temperature and substrate composition (surface/bulk). An example of sticking tests conducted for a selected ash sample is illustrated in Figure 77. The top of the ash slag adhesion test can be fitted with a cover to assist in controlling the atmosphere.

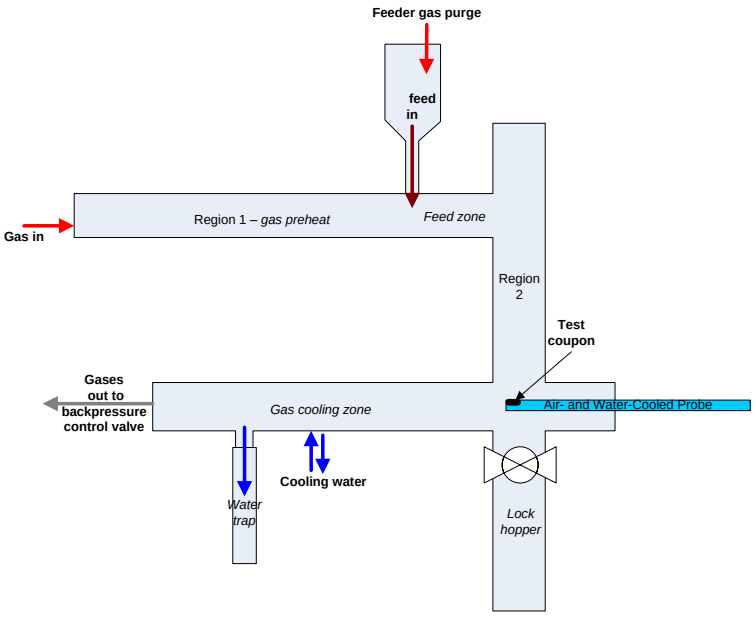

Figure 72. Simplified diagram of syngas fouling simulator (SFS) reactor system including water injection/steam.

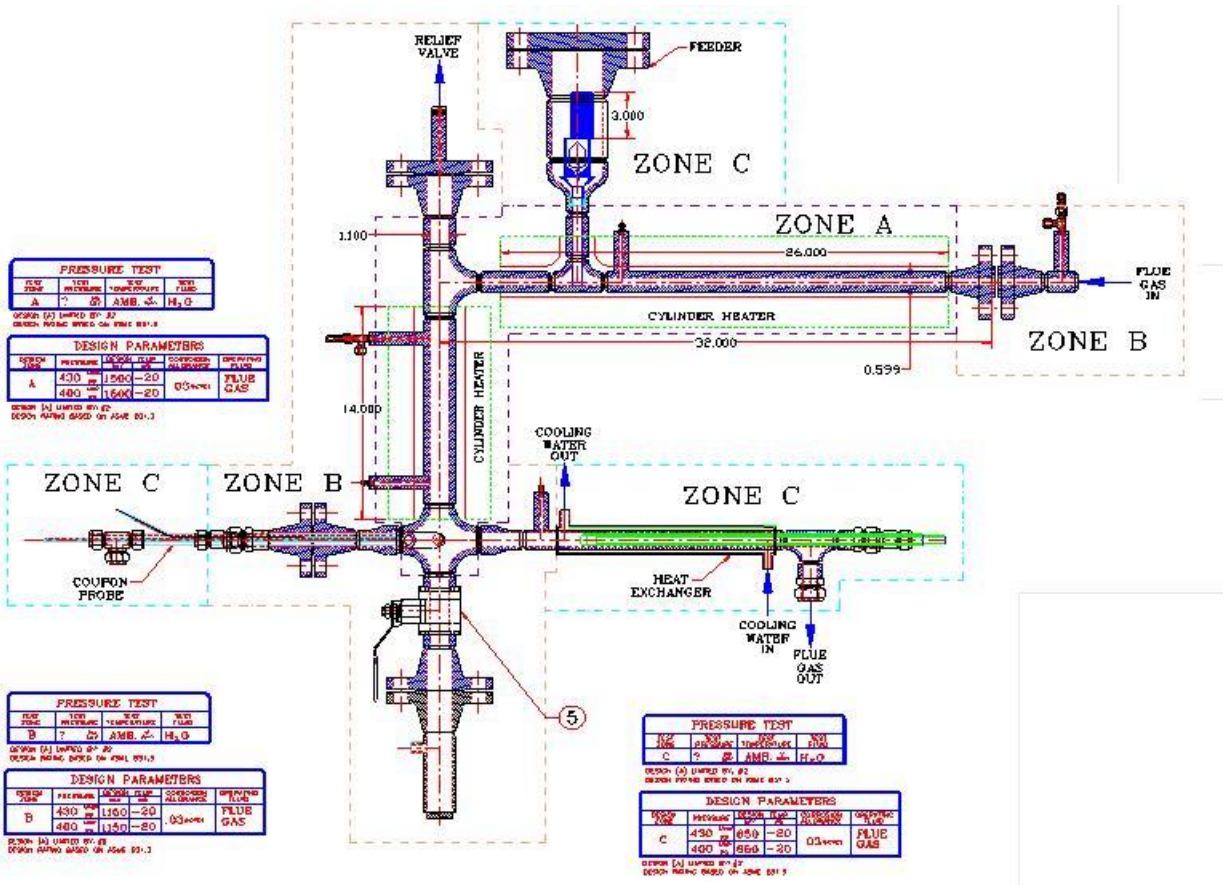

Figure 73. Schematic diagram of syngas fouling simulator (SFS) reactor system including water injection/steam.

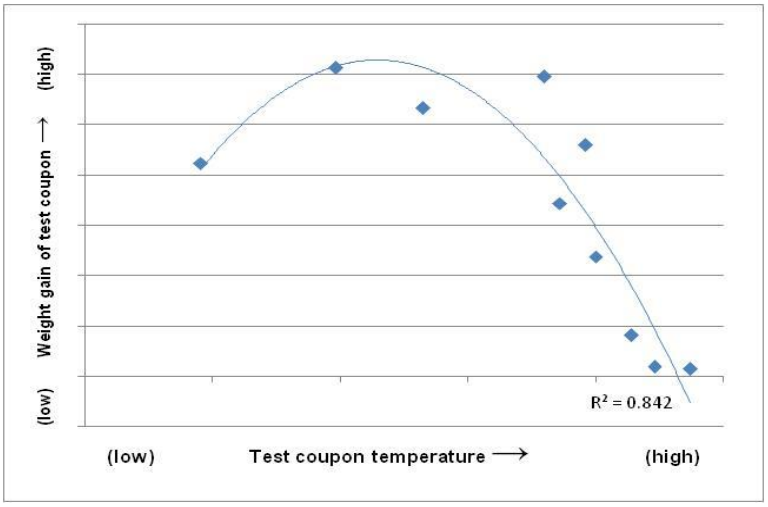

Figure 74. SFS reactor system ash deposition testing.

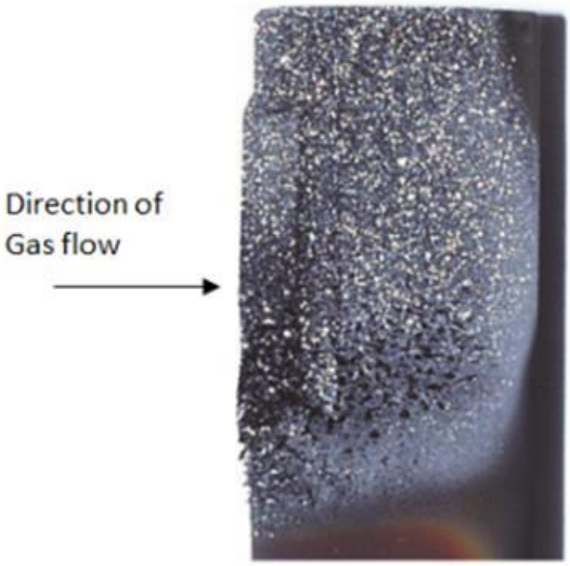

Figure 75. Ash accumulation on a simulated heat transfer surface produced in the SFS.

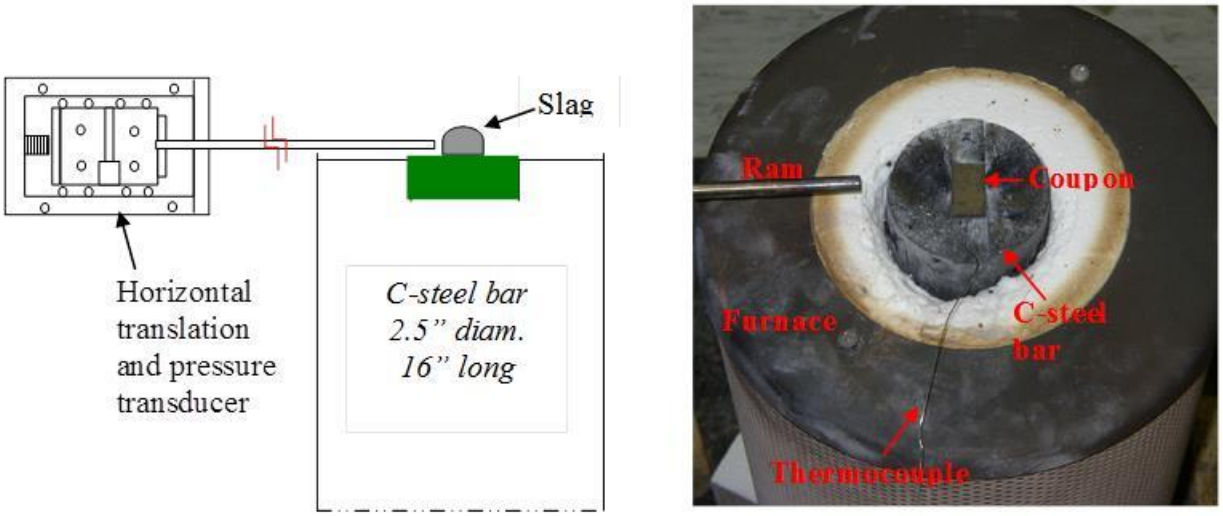

Figure 76. Ash/Slag Adhesion Test System.

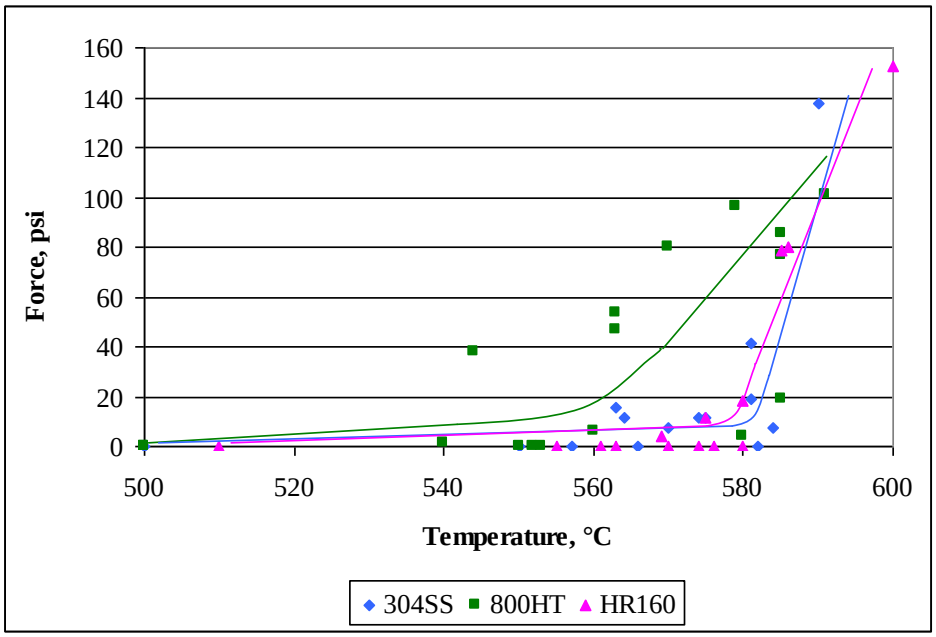

Figure 77. Example of ash adhesion testing for a selected ash material for three metals (temperature is the steel temperature).

5.5.2 Advanced Ash Analysis

Computer-controlled scanning electron microscopy (CCSEM) analysis was used to determine size, composition, and abundance of mineral grains in the samples. The polished samples are placed in the electron microscope equipped with an x-ray microanalysis and image analysis system. CCSEM utilizes backscattered electron imaging combined with automated particle recognition and chemical analysis to determine the composition, size, and abundance of particle types in coal. The CCSEM method is automated, allowing up to 3,000 mineral or ash particle grains or ash particles to be characterized. The compositional data is used to type the particles based on composition. The particle typing is based on standard mineral or ash particles.

5.5.2 Characterization and Advanced Analysis of Fine Ash Materials

The first task of fouling coupon preparation was aimed at characterizing the fuel and fine ash materials that were used in the subsequent fouling deposit growth and sticking processes. The fuel designated for the project was Indiana #5, which is the feedstock type used in the Duke Edwardsport, IN IGCC Plant.

Fine Ash Samples

Obtaining samples of fine ash for testing was found to be challenging. A sample of fine ash sample was taken from the Duke Edwardsport IGCC Plant. However, the quantity of fine ash materials in the sample was not sufficient to conduct all of the required testing. As a result, other options were identified to obtain fine ash materials from other gasification systems.

Microbeam was able to obtain a sample of fine ash from the Coffeyville, KS gasification system. However, the fine ash had high calcium content because the slag is fluxed using sub bituminous coal from the Powder River Region.

Efforts were aimed at obtaining a sample of fine ash from the gasification systems at Tampa Electric Company (TECO) that gasifies bituminous coal. A sample of fine ash was received from TECO. The analysis of the TECO ash materials obtained found that it contained mainly carbon and had an ash content of 11.61%. The proximate and ultimate analysis of the TECO ash is shown in Table 13. The ash derived from this material was analyzed by scanning electron microscopy (SEM) morphology and the results are shown in Figure 78 and Table 14. This TECO ash was rich in vanadium and the use of this material would not work for testing.

Efforts were also made to find a suitable ash material from the Illinois basin. Four ash materials were investigated. These include ash derived from the Knight Hawk and Galatia mines, both in the Illinois basin. The analysis of the Knight Hawk coal and Galatia coal are presented in Table 15 and Table 16.

Table 13. Proximate and ultimate analysis of TECO ash (MTI 14-219).

Description	**TECO Ash**	
Sample ID	MTI 14-219	
Proximate	*As-rec'd*	*Dry Basis*
Total moisture	8.14	------
Ash	11.61	12.64
Volatile matter	2.28	2.48
Fixed carbon	77.97	84.88
Heating value (BTU/lb)	11295	12295
Ultimate	*As-rec'd*	*Dry Basis*
Total moisture	8.14	------
Ash	11.61	12.64
Carbon	78.64	85.61
Hydrogen	1.18	<0.5
Nitrogen	0.83	0.90
Total sulfur	2.96	3.22
Oxygen by difference	4.78	<0.01

Table 14. SEM morphological analysis of TECO ash sample (MTI 14-219), results expressed as equivalent oxide, normalized to 100%.

	Na_2O	MgO	Al_2O_3	SiO_2	P_2O_5	SO_3	K_2O	CaO	TiO_2	V_2O_5	Fe_2O_3	NiO
14-219 Ash	11.2	1.9	15.9	25.3	2.5	0.7	2.5	2.4	0.7	21.4	11.6	3.9

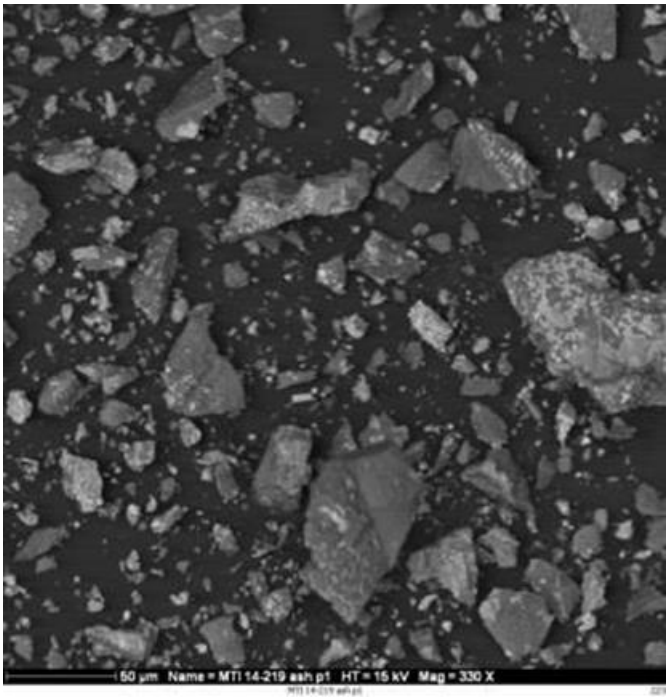

Figure 78. Backscattered scanning electron image of TECO ash MTI 14-219.

Table 15. Analysis summary of Knight Hawk and Galatia coal samples

Description	Galatia pile coal		Knight Hawk pile coal	
Proximate	*As-rec'd*	*Dry basis*	*As-rec'd*	*Dry basis*
Total moisture	7.51	-	11.31	-
Ash	8.07	8.73	10.03	11.31
Volatile matter	31.9	34.49	34.2	38.56
Fixed carbon	52.52	56.78	44.46	50.13
Heating value (BTU/lb)	12289	13286	11115	12532
Ultimate	*As-rec'd*	*Dry basis*	*As-rec'd*	*Dry basis*
Total moisture	7.51	-	11.31	-
Ash	8.07	8.73	10.03	11.31
Carbon	70.5	76.22	63.55	71.65
Hydrogen	5.51	5.05	5.74	5.04
Nitrogen	1.48	1.6	1.25	1.41
Total sulfur	2.56	2.77	3.01	3.39
Oxygen by difference	11.88	5.63	16.42	7.19
Ash composition	*Dry basis*		*Dry basis*	
SiO2	53.70		50.17	
Al2O3	19.25		19.10	
TiO2	1.00		0.92	
Fe2O3	14.40		15.57	
CaO	2.38		3.80	
MgO	1.16		1.11	
K2O	2.89		2.43	
Na2O	1.65		1.20	
SO3	2.60		3.42	

P2O5	0.14	0.24
SrO	0.03	0.03
BaO	0.04	0.05
MnO2	0.03	0.04

Table 16 compares the ash composition of the Knight Hawk and Galatia coal ash to that of the TECO and Duke fine ash materials.

Table 16. Ash composition summary comparing Knight Hawk and Galatia coal ash to that of TECO and Duke fine ash.

	TECO	Duke	Knight Hawk	Galatia
SiO_2	55.15	40.96	53.70	50.17
Al_2O_3	18.21	17.56	19.25	19.10
TiO_2	0.88	1.12	1.00	0.92
Fe_2O_3	10.58	24.13	14.40	15.57
CaO	2.25	1.81	2.38	3.80
MgO	1.73	0.73	1.16	1.11
K_2O	2.26	2.65	2.89	2.43
Na_2O	2.56	3.04	1.65	1.20
SO_3	0.00	0.00	2.60	3.42
P_2O_5	0.36	0.28	0.14	0.24
Cl	0.00	0.00		
ZnO	0.00	3.94		
total	93.96	96.22	99.17	97.96

Figure 79 shows the calculated temperature-viscosity relationships of the Knight Hawk and Galatia coals compared to that of the Duke and TECO coals. The results show that the viscosity temperature curves for the Knight Hawk and Galatia are between the Duke and TECO coals. The ash fusion results are shown for the two coals in Table 17.

Two samples of fly ash from the Wabash River combustion system, in Indiana, were obtained from an ash marketing firm. The first Wabash ash had high levels of aluminum that resulted in a fluid temperature that was higher than the fluid temperature of TECO or Duke fine ash (Figure 80). The second sample has higher calcium content and lower aluminum. The composition of the Wabash fly ash samples are compared to the Duke and TECO ash in Table 18. The calculated viscosity-temperature relationship that matches fine ash materials from Duke is shown in Figure 81. The ash fusion temperature is summarized in Table 19.

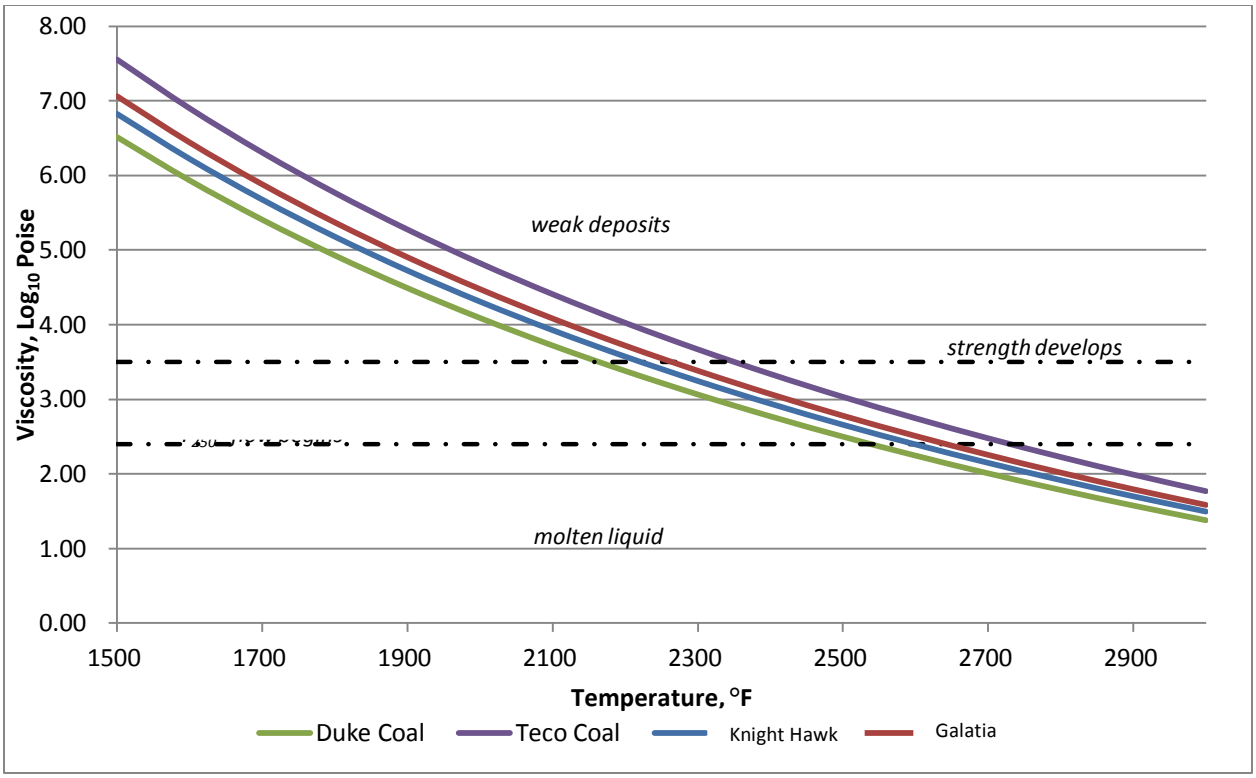

Figure 79. Viscosity-temperature relationships of the Knight Hawk, Galatia, Duke, and TECO coal ash.

Table 17. Ash fusion temperature (F) analysis for Knight Hawk and Galatia coals.

MTI #		DT	ST	HT	FT
14-218	Galatia	1841	2059	2238	2386
14-217	Knight Hawk	1901	2062	2252	2380

Table 18. Comparison of the Wabash Fly Ash samples to the Duke and TECO ash.

	TECO Fine Ash	TECO Coal	Duke Fine Ash	Duke Coal	Wabash Fly ash 1	Wabash Fly Ash 2
SiO_2	55.15	50.28	40.96	52.01	38.1	45.22
Al_2O_3	18.21	20.32	17.56	18.31	27.1	18.68
TiO_2	0.88	0.93	1.12	0.97	0.6	1.08
FE_2O_3	10.58	11.48	24.13	22.9	9.3	17.67
CaO	2.25	3.08	1.81	2.42	0.8	0.75
MgO	1.73	0.84	0.73	0.8	1.9	5.28
K_2O	2.26	1.86	2.65	2.37	3.1	6.74
Na_2O	2.56	1.06	3.04	0.64	3.4	1.77
SO_3	0.00		0.00		8.2	2.09
P_2O_5	0.36		0.28		6.9	
Cl	0.00		0.00			
ZnO	0.00		3.94			
total	93.96		96.22		99.26	100.00

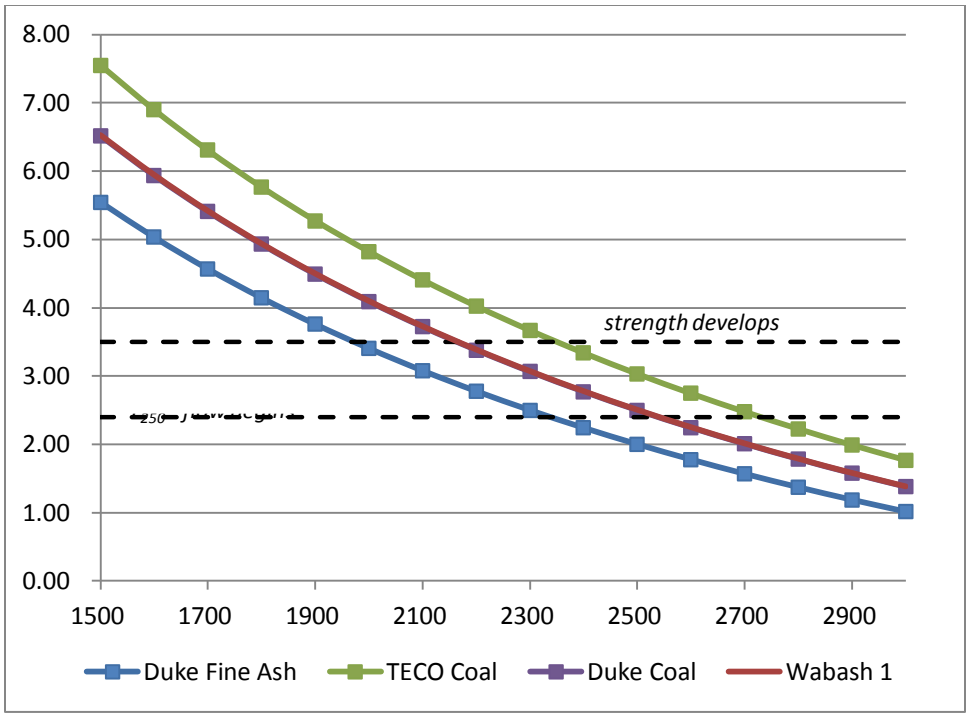

Figure 80. Viscosity-temperature relationships of the first Wabash fly ash compared to that of the TECO and Duke ash materials.

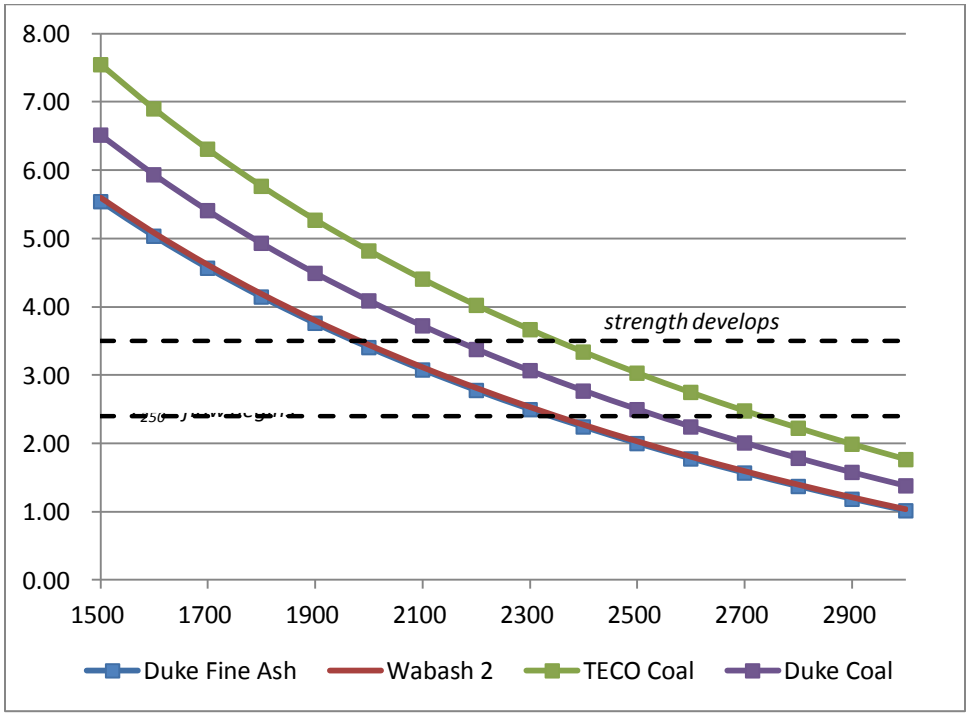

Figure 81. Viscosity-temperature relationships of the second Wabash fly ash compared to that of the TECO and Duke ash materials.

Table 19. Ash fusion temperature (F) analysis of Wabash fly ash.

	DT	ST	HT	FT
14-328	2138	2284	2447	2504

Coal analysis and Ash Behavior Index Calculations

Two coal CCSEM analyses were available in the project to calculate the ash behavior indices. The CCSEM analyses along with the ASTM analyses summarized in Table 15 were used to calculate the indices. The CCSEM analysis results for the Galatia coal are summarized in Table 20. The results show that the most abundant minerals include quartz, kaolinite, K-Al-silicate (Illite), and pyrite. The Knight Hawk coal minerals consist of quartz, kaolinite, illite, pyrite, and montmorillonite as summarized in Table 21.

Table 20. CCSEM Results for Galatia coal.

WEIGHT PERCENT ON A MINERAL BASIS							
	Particle size, microns						
	1 TO 2.2	2.2 TO 4.6	4.6 TO 10	10 TO 22	22 TO 46	46 TO 400	TOTALS
QUARTZ	0.7	2.2	5.9	5.5	1.9	0.8	16.8
IRON OXIDE	0	0.2	0	0.7	0.2	0	1.1
PERICLASE	0	0	0	0	0	0	0
RUTILE	0	0	0	0	0	0.1	0.1
ALUMINA	0	0	0	0	0	0	0
CALCITE	0	0.1	0.3	0.9	0.3	0.4	2.1
DOLOMITE	0	0	0	0	0	0.1	0.1
ANKERITE	0	0	0	0.2	0	0	0.2
KAOLINITE	0.5	2.5	3.7	2.1	1.7	0.6	11.2
MONTMORILLONITE	0.1	0.3	1.6	0.4	1	0.2	3.7
K AL-SILICATE	0.4	0.9	3.4	4.1	2	0.6	11.5
FE AL-SILICATE	0	0	0.2	0.8	0	0.1	1.2
CA AL-SILICATE	0	0	0.1	0	0	0	0.1
NA AL-SILICATE	0	0.1	0.2	0.1	0.1	0.1	0.5
ALUMINOSILICATE	0.1	0	0.6	1	0.6	0.3	2.6
MIXED AL-SILICATE	0	0.1	0.1	0.3	0.1	0.1	0.7
FE SILICATE	0	0	0	0	0	0	0
CA SILICATE	0	0	0	0	0	0	0
CA ALUMINATE	0	0	0	0	0	0	0
PYRITE	0.5	1.9	4.6	7.8	6.1	2.6	23.4
PYRRHOTITE	0.1	0.8	0.2	0.1	0.1	0.3	1.6
OXIDIZED PYRRHOTITE	0.1	0.4	0.2	0	0.2	0	0.9
GYPSUM	0	0.3	0.8	1	1.4	0.7	4.3
BARITE	0	0	0	0	0	0	0
APATITE	0	0	0	0	0	0	0.1
CA AL-P	0	0	0	0	0	0	0
KCL	0	0	0	0	0	0	0
GYPSUM/BARITE	0	0	0	0	0	0	0
GYPSUM/AL-SILICATE	0	0	0.1	0	0	0	0.2
SI-RICH	0.1	0.2	1.5	2.4	0.9	0.7	5.9
CA-RICH	0	0.1	0	0.2	0.1	0	0.4

CA-SI RICH	0	0	0	0	0	0	0
UNCLASSIFIED	0.8	1.3	4.3	2.7	1.7	0.4	11.3
TOTALS	**3.5**	**11.3**	**27.9**	**30.5**	**18.7**	**8.1**	**100**

Table 21. CCSEM Results for Knight Hawk coal.

WEIGHT PERCENT ON A MINERAL BASIS							
	Particle size, microns						
	1 TO 2.2	**2.2 TO 4.6**	**4.6 TO 10**	**10 TO 22**	**22 TO 46**	**46 TO 400**	**TOTALS**
QUARTZ	2.4	5.6	4.2	5.5	1	0.7	19.4
IRON OXIDE	0	0.4	0.1	0	0	0.5	1.1
PERICLASE	0	0	0	0	0	0	0
RUTILE	0	0	0.1	0.1	0	0	0.2
ALUMINA	0	0	0	0	0	0	0
CALCITE	0	0.7	0.4	0.4	0.3	0.8	2.7
DOLOMITE	0	0.1	0.1	0.2	0	0	0.4
ANKERITE	0	0	0	0	0	0	0
KAOLINITE	1.2	3.8	3.3	2.9	1.4	0.7	13.3
MONTMORILLONITE	0.6	2.3	1.1	0.9	0.7	0.7	6.2
K AL-SILICATE	0.9	3.2	1.9	0.4	1.2	0.4	7.9
FE AL-SILICATE	0	0	0.1	0.3	0	0	0.5
CA AL-SILICATE	0	0	0.2	0.1	0	0	0.3
NA AL-SILICATE	0.1	0	0.1	0.1	0	0	0.4
ALUMINOSILICATE	0.2	0.5	0.6	0.5	0.5	0.6	2.9
MIXED AL-SILICATE	0	0	0.1	0	0.1	0	0.2
FE SILICATE	0	0	0	0	0	0	0
CA SILICATE	0	0	0	0.1	0	0	0.2
CA ALUMINATE	0	0	0	0	0	0	0
PYRITE	0.9	2	4.6	7.2	5.7	4.7	25.1
PYRRHOTITE	0	0.1	0.1	0.5	0.1	0	0.8
OXIDIZED PYRRHOTITE	0	0.1	0.1	0	0.1	0.2	0.5
GYPSUM	0.1	0.4	0.3	0.5	0.5	0.3	2.2
BARITE	0	0	0	0	0	0	0
APATITE	0	0	0	0	0	0.1	0.1
CA AL-P	0	0	0	0	0	0	0
KCL	0	0	0	0	0	0	0
GYPSUM/BARITE	0	0	0	0	0	0	0
GYPSUM/AL-SILICATE	0	0.1	0.1	0	0	0	0.3
SI-RICH	0.5	1	0.5	0.8	0.4	0.3	3.5
CA-RICH	0	0.1	0	0	0	0.1	0.2
CA-SI RICH	0	0	0	0	0	0	0
UNCLASSIFIED	2.2	4.6	2.2	1.6	0.8	0.4	11.8
TOTALS	**9.2**	**25.1**	**20.1**	**22.2**	**12.9**	**10.5**	**100**

Fuel performance indices are shown in Figure 82. The behavior of the ash is estimated in high temperature deposition, moderate temperature deposition, low temperature deposition, abrasion and erosion wear, as follows:

- Deposit Strength Index: This index predicts the strength of deposited material. It is used in combination with the high and moderate deposition indices to assess deposit characteristics (i.e. high value for strength and a low value to deposition index indicate a strong thin deposit). Index values of less than 0.25 indicate weak deposits. Values of 0.25 to 0.34 denote low to moderate strength, values of 0.34 to 0.41 indicate strong deposits, and values above 0.41 the deposits will be plastic to molten.

- High Temperature Deposition Index (HTD): Indicates the propensity of deposits to accumulate on the radiant regions, from 2000 to 3000°F (1093 to 1649°C). The HTD index is based on mineral size (especially illite, quartz, and pyrite), association of calcium (calcite can contribute to slagging), and sticking fraction. This index is used in combination with the strength index to assess slag deposit characteristics. Values range from 1- low to 100 - severe.

- Moderate Temperature Deposition (MTD): Indicates the propensity of deposits to form from 1400 to 2000°F (760 to 1093°F). This index is related to the formation of high-temperature fouling deposits in which silicates are the primary accumulating materials and the primary bonding component. Information used to derive the index includes the size of minerals such as quartz and clay, availability of alkali and alkaline earth elements, and sticking fraction. This index is used in combination with the strength index. Values range from 1-low to 100-severe.

- Low Temperature Deposition (LTD): Indicates the propensity of low-temperature fouling deposits to form in the lower temperature regions of a gasification unit from 600 to 1400°F (316 to 760°F). This index is based on the availability of alkali (Na and K) along with iron, zinc, and nickel elements to react and bond with other available small particles as well as react with H_2S to form sulfides. Index values range from 1-low to 100-severe.

- Wear Indices

  Abrasion Index: This index indicates the potential for wear of fuel preparation and handling equipment, as related to the hardness of minerals in the coal. The primary minerals of concern are quartz and pyrite. Values range from 0.1-low to 10-severe.

  $AI = Qc + 0.5Pc + 0.2Ac$

  where Qc is the quartz content, Pc is the pyrite content, and Ac is the ash content of the coal (Raask, 1985).

  Erosion Index: This index indicates the potential for wear of heat transfer surfaces due to the impaction of fly ash particles, particularly those containing hard minerals such as quartz. The erosion index is dependent upon particle size and velocity (Raask, 1985). Values range from 0.1-low to 1.0-severe.

  $I_A = (X_1+0.5)I_G + (X_1q_1 + 0.5X_2q_2)I_Q$

  - I_A, I_G, I_Q is the erosion index of ash, glass spheres (0.4), and quartz particles (1), respectively
  - X_1 = ash fraction of >45 µm
  - X_2 = ash fraction of 5-45 µm
  - q_1 = quartz content of > 45 µm
  - q_2 = quartz content of 5-45 µm

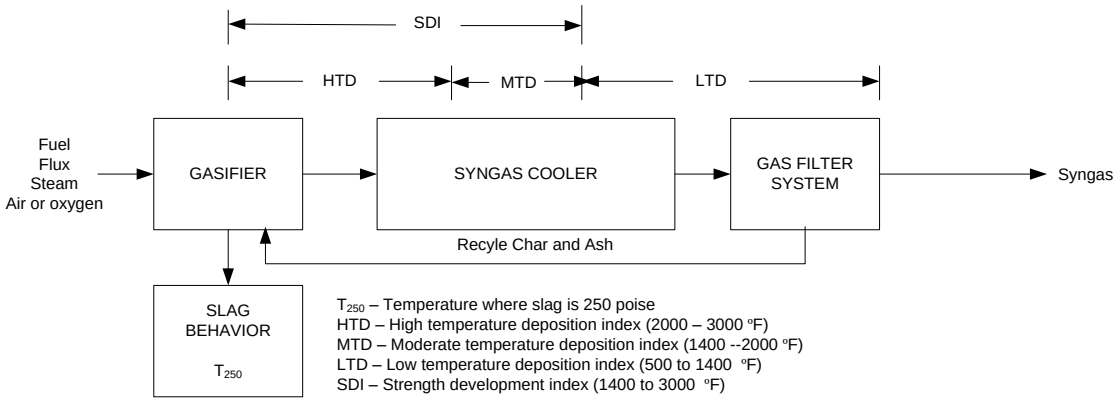

Figure 82. Overview of ash behavior indices for gasification systems.

The calculated indices are summarized in Table 22. The calculations were made with consideration for recycle of char and ash. The results show that the coals are prone to produce deposits in the moderate temperature regions. The high rates were due to the large quartz particles, illite, and pyrite components. The LTD index was low for both coals and was due to low alkali and available iron and zinc. The LTD index will increase with recycle due to increases and build-up of volatile elements such as sodium in the system. In order to simulate recycle in the system the composition of the sodium in the ash materials was increased up to 8 % and zinc was increased up to 10%.

Table 22. Calculated performance indices for Galatia and Knight Hawk coals.

Galatia	Strength	LTD	MTD	HTD	Abrasion	Erosion
Baseline (no recycle)	0.27	4.6	70.5	45.5	3.7	0.2
4% Na2O	0.27	4.6	75.6	62.3	3.7	0.2
6% Na2O	0.28	4.6	81.7	70.7	3.7	0.2
8% Na2O	0.28	4.7	87.5	77.1	3.7	0.2
3% ZnO	0.27	4.6	70.5	44.8	3.7	0.2
6% ZnO	0.27	4.6	70.4	44.1	3.7	0.2
10% ZnO	0.27	4.6	70.4	43.4	3.7	0.2
4% Na2O+3% ZnO	0.27	4.7	73.8	59.0	3.7	0.2
6% Na2O+6% ZnO	0.28	6.2	78.0	66.1	3.7	0.2
8% Na2O+10% ZnO	0.28	16.8	81.7	70.7	3.7	0.2

Knight Hawk	Strength	LTD	MTD	HTD	Abrasion	Erosion
Baseline (no recycle)	0.27	4.6	71.0	45.7	5.8	0.2
4% Na2O	0.27	4.6	77.6	64.6	5.8	0.2
6% Na2O	0.28	4.6	84.6	72.5	5.8	0.2
8% Na2O	0.28	4.8	90.7	78.6	5.8	0.2
3% ZnO	0.27	4.6	70.9	45.2	5.8	0.2
6% ZnO	0.27	4.6	70.9	44.7	5.8	0.2

10% ZnO	0.27	4.6	70.9	44.1	5.8	0.2
4% Na2O+3% ZnO	0.27	4.9	75.5	61.5	5.8	0.2
6% Na2O+6% ZnO	0.27	5.2	75.0	60.6	5.8	0.2
8% Na2O+10% ZnO	0.27	5.7	74.4	59.5	5.8	0.2

5.5.4 Development of Fouling Coupon Pre-Treatment Procedures

1. Coupon Preparation

Incoloy 800 HT was selected as the alloy for use in testing in this project. Based on past testing at Microbeam, the 800 HT showed the lowest propensity for sticking of ash materials derived from coal gasification. Slag droplets did not stick until the steel reached temperatures of over 1076 ºF (580 ºC) as illustrated in Figure 77 in the background section of this report. Incoloy 800 HT consists of Cr (19 – 23%), Ni (30 – 35%), and Fe (minimum of 39.5%).

Coupons of the Incoloy 800 HT were prepared from a plate of Incoloy 800HT in the dimension shown in Figure 83. The coupons were prepared by Precision Waterjet Concepts in Pequot Lakes, Minnesota with the following dimensions.

- Length – 0.875” +0.000”, -0.005”
- Width – 0.484”, ±0.005”
- Angle - 45° +0°, -minimum achievable

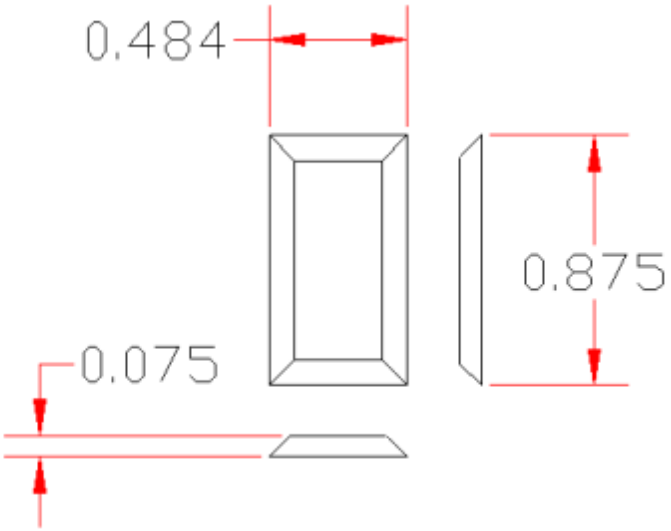

Figure 83. Coupon dimensions (inches).

The syngas fouling simulator (SFS) is shown in Figure 72. The pre-treatment of coupons in the SFS was performed to produce a sulfide layer on the surface of the coupons. This pre-treatment was done in the upper horizontal section or gas pre-heater section (Region 1) of the SFS. A shuttle was constructed to hold six coupons that would slide into the pre-heat section of the SFS. Weighed coupons were placed on the shuttle and inserted into the pre-heat section of the SFS and were treated at the desired temperatures under a flowing stream of syngas at 400 psi.

The composition of the syngas was formulated based on a typical RSC operating data summarized in in Table 23.

Table 23. Syngas composition used in the study.

Syngas composition	
Carbon monoxide	40%
Carbon dioxide	18.5 %
Hydrogen	37%
Nitrogen	1.7%
Hydrogen sulfide	1.6%
Methane	0.05%
Argon	1.15%

The probe used to hold the coupons while depositing the ash layer was redesigned to hold two coupons in order to simulate both upstream and downstream deposition on the surface as shown in Figure 84(a) and (b). A new probe was constructed with slots on the top and underside of the probe enabling coupons to be placed in both an upstream and downstream orientation.

(a)

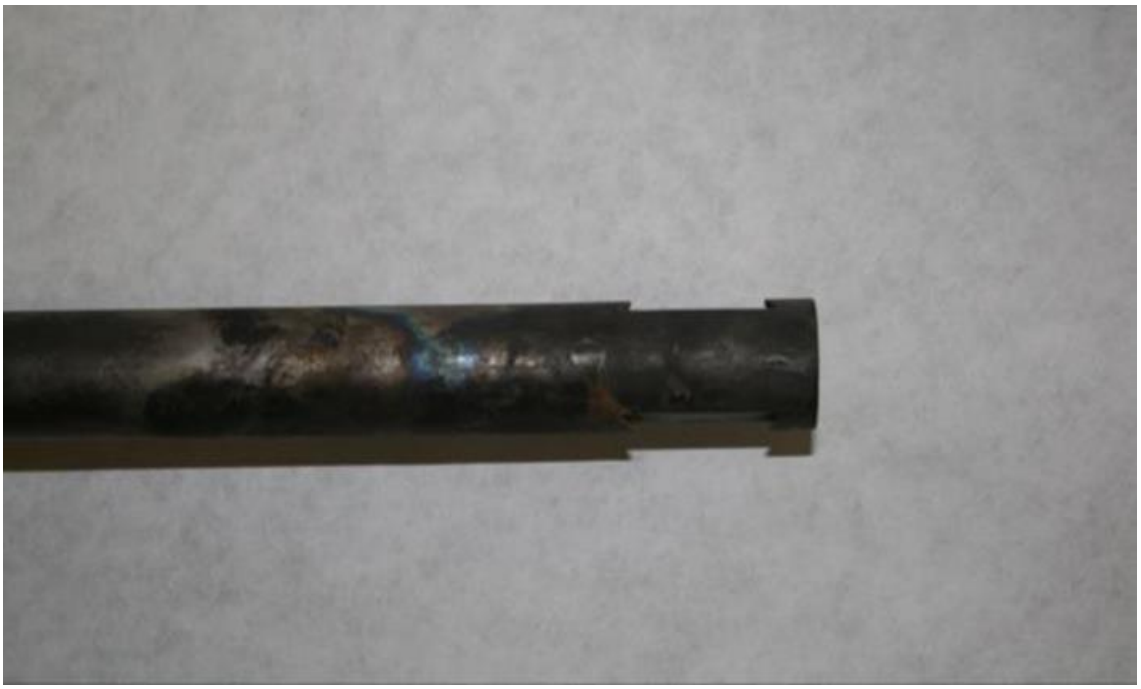

(b)

Figure 84. New probe constructed to accommodate coupons in both upstream and downstream orientations. (a): Overall view; (b): Probe tip showing slots for the coupons.

Pre-treatment tests were run at 600, 700, and 850°F (316, 371, and 454°C) where six coupons were treated for 8 hours under a flow of syngas containing H_2S. The results of the pre-treatment tests are shown in Table 24 thru Table 26. Pretreating the coupons at 600°F (316°C) yields an average weight gain of 0.0029 grams while the weight gain at 700°F (371°C) averaged 0.0043 grams and at 850°F (454°C) the coupons gained an average of 0.0046 grams. All coupons pre-treated for all subsequent testing were pre-treated at 850°F (454°C).

Table 24. Pre-treatment of coupons at 600 °F (316° C) for 8 hours.

Coupon	Wt. Before	Wt. After	Wt. gain
1 (MTI 14-220)	3.4111	3.4144	0.0033
2 (MTI 14-221)	3.3886	3.3922	0.0036
3 (MTI 14-222)	3.3124	3.3150	0.0026
4 (MTI 14-223)	3.3256	3.3286	0.0030
5 (MTI 14-224)	3.4196	3.4222	0.0026
6 (MTI 14-225)	3.3066	3.3088	0.0022
Average			0.0029

Table 25. Pre-treatment of coupons at 700 °F for 8 hours.

Coupon	Wt. Before	Wt. After	Wt. gain
7 (MTI 14-226)	3.3319	3.3361	0.0042
8 (MTI 14-227)	3.4211	3.4256	0.0045
9 (MTI 14-228)	3.4408	3.4456	0.0048
10 (MTI 14-229)	3.3589	3.3633	0.0044

11 (MTI 14-230)	3.3251	3.3294	0.0043
12 (MTI 14-231)	3.3612	3.3650	0.0038
Average			0.0043

Table 26. Pre-treatment of coupons at 850 °F for 8 hours.

Coupon	Wt. Before	Wt. After	Wt. gain
13(MTI 14-232)	3.3015	3.3060	0.0045
14 (MTI 14-233)	3.3204	3.3252	0.0048
15 (MTI 14-234)	3.4201	3.4249	0.0048
16 (MTI 14-235)	3.3927	3.3975	0.0048
17 (MTI 14-236)	3.3117	3.3157	0.0040
18 (MTI 14-237)	3.3922	3.3970	0.0048
Average			0.0046

The surface of a pre-treated coupon was analyzed by SEM/EDS (energy dispersive spectrometer) area analysis with the results presented in

Table 27. The surface analysis shows sulfur enrichment on the surface of the coupon. Figure 85 shows a photograph of the pre-treated coupons.

Detailed fundamental studies of factors that influence the sticking of coal ash slags to heat-transfer surfaces were conducted by Austin and others (Moza and Austin, 1982; Moza and others, 1980; Abbott and others, 1985; Moza and Austin, 1981; Abbott and Austin, 1982; Abbott and others, 1981; Tangsathitkulchai and Austin, 1985), who developed a simplified apparatus to produce molten droplets of slag that would fall on, and stick to a boiler steel coupon that was held at a controlled temperature. The information generated with this apparatus led to an understanding of the factors that influence the sticking behavior of slag droplets on boiler steel surfaces. The factors influencing sticking behavior included: slag droplet composition, droplet temperature, nature of the steel surface, and steel temperature. With increasing steel substrate (or “coupon”) temperature, the contact angle of the droplet decreased, causing increased wetting of the surface and increased adhesion strength. The strength of adhesion was found to increase exponentially with increasing substrate temperature; mild steels exhibited an interaction of the glass or slag droplet with the oxide layer on the steel, resulting in a strong bond. Ash droplet interaction with stainless steels exhibited poor wetting and low adhesion strengths up to 590°C (1094°F). Limited chemical reaction occurred, and initial layers that had high levels of Na_2SO_4 or NaCl decreased the sticking temperature. The adhesion force decreased as a result of decreasing substrate temperature and thermal cycling of the substrate temperature.

Bakker (2004) examined the formation of corrosion layers on steel surfaces in gasification systems. He found that without HCl in the system the corrosion losses were related to the levels of hydrogen sulfide and oxygen in the system. The corrosion rates were very low due to the formation of a protective $FeCr_2S_4$ layer on the surface of the steel. If HCl was present in the system, the protective layer was diminished allowing for more corrosion.

Table 27. SEM analysis of pre-treatment layer of coupon (elemental wt. %).

Coupon, Temp (ºF)	*Al*	*Si*	*S*	*Cr*	*Fe*	*Ni*	*O*
850	*0.3*	*1.1*	*27.1*	*12.6*	*34.8*	*21.3*	*2.9*
700	*0.6*	*2.2*	*21.7*	*10.8*	*42.1*	*20.5*	*2.2*
600	*0.7*	*0.4*	*22.3*	*14.2*	*41.1*	*20.7*	*0.6*

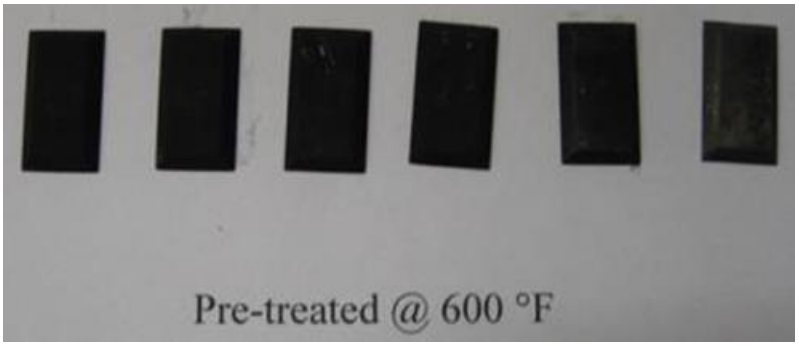

Figure 85. Pre-treated coupons produced at 600 ºF.

2. Coupon Exposure to Wabash Ash

Coupons were exposed to Wabash 2 ash material in the Syngas Fouling Simulator (SFS) according to the test matrix summarized in Table 28. Coupons with ash materials on the surface were express mailed to the University of Texas at Arlington (UTA) for testing in a pulse detonation system to remove the deposit. The ash materials were accumulated on the upstream and downstream surface and were exposed to the syngas for 4 hours. The results of the testing are summarized in Table 29. The temperature of the coupon or sintering temperature was varied from 700 to 850ºF (371 to 454°C) with the pressure of the system maintained at 400 psig and the gas temperature 1550ºF (843°C).

Table 28. Test matrix for fouling deposit coupon preparation.

SFS Tests	SFS pressure	SFS Temp.	Metal Temp.	H_2S Pretreatment Temp.	Coupons	
	psig	°F	°F	°F	Upstream	Downstream
FT-01	400	1550	700	850	CU-1	CD-1
FT-02	400	1550	700	850	CU-2	CD-2
FT-03	400	1550	775	850	CU-3	CD-3
FT-04	400	1550	775	850	CU-4	CD-4
FT-05	400	1550	850	850	CU-5	CD-5
FT-06	400	1550	850	850	CU-6	CD-6
FT-07	400	1550	700	850	CU-7	CD-7
FT-08	400	1550	700	850	CU-8	CD-8
FT-09	400	1550	775	850	CU-9	CD-9
FT-10	400	1550	775	850	CU-10	CD-10
FT-11	400	1550	850	850	CU-11	CD-11
FT-12	400	1550	850	850	CU-12	CD-12
FT-13	400	1550	700	850	CU-13	CD-13
FT-14	400	1550	700	850	CU-14	CD-14
FT-15	400	1550	775	850	CU-15	CD-15
FT-16	400	1550	775	850	CU-16	CD-16
FT-17	400	1550	850	850	CU-17	CD-17
FT-18	400	1550	850	850	CU-18	CD-18
FT-19	400	1550	700	850	CU-19	CD-19
FT-20	400	1550	700	850	CU-20	CD-20
FT-21	400	1550	775	850	CU-21	CD-21
FT-22	400	1550	775	850	CU-22	CD-22
FT-23	400	1550	850	850	CU-23	CD-23
FT-24	400	1550	850	850	CU-24	CD-24

Table 29. Tests Results for fouling coupon preparation.

Coupon	Up/Down	coupon wt.	Pretreatment wt.	Pretreatment layer	Sintered wt.	Ash layer	Sintering temp	SFS Test	Coupon
MTI 14-264	upstream	3.3493	3.3508	0.0015	3.4902	0.1394	700 F	FT-01	CU-1
MTI 14-265	downstream	3.1793	3.1805	0.0012	3.2050	0.0145	700 F	FT-01	CD-1
MTI 14-266	upstream	3.4335	3.4357	0.0022	3.5380	0.1023	700 F	FT-02	CU-2
MTI 14-267	downstream	3.3816	3.3823	0.0007	3.4050	0.0197	700 F	FT-02	CD-2
MTI 14-268	upstream	3.3155	3.3162	0.0007	3.3765	0.0603	775 F	FT-03	CU-3
MTI 14-269	downstream	3.4309	3.4325	0.0016	3.4433	0.0108	775 F	FT-03	CD-3
MTI 14-270	upstream	3.2996	3.3013	0.0017	3.3907	0.0894	775 F	FT-04	CU-4
MTI 14-271	downstream	3.3543	3.3564	0.0021	3.3623	0.0059	775 F	FT-04	CD-4
MTI 14-272	upstream	3.3232	3.3246	0.0014	3.4830	0.1584	850 F	FT-05	CU-5
MTI 14-273	downstream	3.3335	3.3351	0.0016	3.3489	0.0138	850 F	FT-05	CD-5
MTI 14-274	upstream	3.4089	3.4101	0.0012	3.5344	0.1243	850 F	FT-06	CU-6
MTI 14-275	downstream	3.4127	3.4139	0.0012	3.4272	0.0133	850 F	FT-06	CD-6
MTI 14-276	upstream	3.2849	3.2863	0.0014	3.4276	0.1413	700 F	FT-07	CU-7
MTI 14-277	downstream	3.3949	3.3964	0.0015	3.4061	0.0097	700 F	FT-07	CD-7
MTI 14-278	upstream	3.4015	3.4040	0.0025	3.5042	0.1002	700 F	FT-08	CU-8
MTI 14-279	downstream	3.3555	3.3575	0.0020	3.3615	0.0040	700 F	FT-08	CD-8
MTI 14-280	upstream	3.3537	3.3551	0.0014	3.4729	0.1178	775 F	FT-09	CU-9
MTI 14-281	downstream	3.3220	3.3238	0.0018	3.3445	0.0207	775 F	FT-09	CD-9
MTI 14-282	upstream	3.3609	3.3630	0.0021	3.4393	0.0763	775 F	FT-10	CU-10
MTI 14-283	downstream	3.3507	3.3523	0.0016	3.3637	0.0114	775 F	FT-10	CD-10
MTI 14-284	upstream	3.3784	3.3804	0.0020	3.5021	0.1217	850 F	FT-11	CU-11
MTI 14-285	downstream	3.3410	3.3415	0.0005	3.3699	0.0284	850 F	FT-11	CD-11
MTI 14-286	upstream	3.2451	3.2458	0.0007	3.3639	0.1181	850 F	FT-12	CU-12

MTI 14-287	downstream	3.3898	3.3911	0.0013	3.3994	0.0083	850 F	FT-12	CD-12
MTI 14-288	upstream	3.4277	3.4289	0.0012	3.5487	0.1198	700 F	FT-13	CU-13
MTI 14-289	downstream	3.3242	3.3262	0.0020	3.3612	0.0350	700 F	FT-13	CD-13
MTI 14-290	upstream	3.3469	3.3489	0.0020	3.4833	0.1344	700 F	FT-14	CU-14
MTI 14-291	downstream	3.2597	3.2622	0.0025	3.2789	0.0167	700 F	FT-14	CD-14
MTI 14-292	upstream	3.3154	3.3163	0.0009	3.4004	0.0841	775 F	FT-15	CU-15
MTI 14-293	downstream	3.2998	3.3012	0.0014	3.3116	0.0104	775 F	FT-15	CD-15
MTI 14-294	upstream	3.3036	3.3051	0.0015	3.3953	0.0902	775 F	FT-16	CU-16
MTI 14-295	downstream	3.3156	3.3175	0.0019	3.3310	0.0135	775 F	FT-16	CD-16
MTI 14-296	upstream	3.3771	3.3798	0.0027	3.4508	0.0710	850 F	FT-17	CU-17
MTI 14-297	downstream	3.2744	3.2763	0.0019	3.2789	0.0026	850 F	FT-17	CD-17
MTI 14-298	upstream	3.3326	3.3347	0.0021	3.3450	0.0103	850 F	FT-18	CU-18
MTI 14-299	downstream	3.3346	3.3367	0.0021	3.3462	0.0095	850 F	FT-18	CD-18
MTI 14-300	upstream	3.3802	3.3821	0.0019	3.3880	0.0059	700 F	FT-19	CU-19
MTI 14-301	downstream	3.2918	3.2943	0.0025	3.3022	0.0079	700 F	FT-19	CD-19
MTI 14-302	upstream	3.4495	3.4512	0.0017	3.5012	0.0500	700 F	FT-20	CU-20
MTI 14-303	downstream	3.2866	3.2885	0.0019	3.2928	0.0043	700 F	FT-20	CD-20
MTI 14-306	upstream	3.385	3.3879	0.0029	3.4535	0.0656	775 F	FT-21	CU-21
MTI 14-307	downstream	3.4187	3.4198	0.0011	3.4464	0.0266	775 F	FT-21	CD-21
MTI 14-308	upstream	3.3171	3.3185	0.0014	3.4004	0.0819	775 F	FT-22	CU-22
MTI 14-309	downstream	3.3593	3.3594	0.0001	3.3640	0.0046	775 F	FT-22	CD-22
MTI 14-310	upstream	3.3824	3.384	0.0016	3.4581	0.0741	850 F	FT-23	CU-23
MTI 14-311	downstream	3.4064	3.4076	0.0012	3.4241	0.0165	850 F	FT-23	CD-23
MTI 14-312	upstream	3.3074	3.3081	0.0007	3.3802	0.0721	850 F	FT-24	CU-24
MTI 14-313	downstream	3.4468	3.4481	0.0013	3.4547	0.0066	850 F	FT-24	CD-24

The coupons were removed from the SFS and a qualitative assessment was made on whether the ash layer stuck to the surface or flaked-off. The results are summarized in Table 30. The bonding between the deposited materials would break as a result of cooling the deposit and substrate. The weak bonds were broken due to differences in the thermal expansion characteristics of the coupon and the ash materials. The coupons and deposited materials were express mailed to UTA for testing. Pictures of these coupons are given in Table 31.

Table 30. Coupon preparation tests results indicating which ash stuck or flaked off.

Coupon	Up/Down	Sintering temp	SFS Test	Coupon	Ash Layer Results
MTI 14-264	upstream	700 F	FT-01	CU-1	Sticking
MTI 14-265	downstream	700 F	FT-01	CD-1	Sticking
MTI 14-266	upstream	700 F	FT-02	CU-2	Sticking
MTI 14-267	downstream	700 F	FT-02	CD-2	Sticking
MTI 14-268	upstream	775 F	FT-03	CU-3	Flaked Off
MTI 14-269	downstream	775 F	FT-03	CD-3	Sticking
MTI 14-270	upstream	775 F	FT-04	CU-4	Flaked Off
MTI 14-271	downstream	775 F	FT-04	CD-4	Sticking
MTI 14-272	upstream	850 F	FT-05	CU-5	Sticking
MTI 14-273	downstream	850 F	FT-05	CD-5	Sticking
MTI 14-274	upstream	850 F	FT-06	CU-6	Flaked Off
MTI 14-275	downstream	850 F	FT-06	CD-6	Sticking
MTI 14-276	upstream	700 F	FT-07	CU-7	Sticking
MTI 14-277	downstream	700 F	FT-07	CD-7	Sticking
MTI 14-278	upstream	700 F	FT-08	CU-8	Sticking
MTI 14-279	downstream	700 F	FT-08	CD-8	Sticking
MTI 14-280	upstream	775 F	FT-09	CU-9	Flaked Off
MTI 14-281	downstream	775 F	FT-09	CD-9	Flaked Off
MTI 14-282	upstream	775 F	FT-10	CU-10	Flaked Off
MTI 14-283	downstream	775 F	FT-10	CD-10	Sticking
MTI 14-284	upstream	850 F	FT-11	CU-11	Flaked Off

MTI 14-285	downstream	850 F	FT-11	CD-11	Sticking
MTI 14-286	upstream	850 F	FT-12	CU-12	Flaked Off
MTI 14-287	downstream	850 F	FT-12	CD-12	Sticking
MTI 14-288	upstream	700 F	FT-13	CU-13	Dropped - flaked
MTI 14-289	downstream	700 F	FT-13	CD-13	Sticking
MTI 14-290	upstream	700 F	FT-14	CU-14	Flaked Off - chunk
MTI 14-291	downstream	700 F	FT-14	CD-14	Sticking
MTI 14-292	upstream	775 F	FT-15	CU-15	Flaked off
MTI 14-293	downstream	775 F	FT-15	CD-15	Sticking
MTI 14-294	upstream	775 F	FT-16	CU-16	Sticking
MTI 14-295	downstream	775 F	FT-16	CD-16	Sticking
MTI 14-296	upstream	850 F	FT-17	CU-17	flaked off
MTI 14-297	downstream	850 F	FT-17	CD-17	Sticking
MTI 14-298	upstream	850 F	FT-18	CU-18	flaked off
MTI 14-299	downstream	850 F	FT-18	CD-18	some flaked off
MTI 14-300	upstream	700 F	FT-19	CU-19	Dropped - flaked off
MTI 14-301	downstream	700 F	FT-19	CD-19	Sticking
MTI 14-302	upstream	700 F	FT-20	CU-20	Flaked off in bottle
MTI 14-303	downstream	700 F	FT-20	CD-20	Sticking
MTI 14-306	upstream	775 F	FT-21	CU-21	Flaked Off
MTI 14-307	downstream	775 F	FT-21	CD-21	Flaked Off
MTI 14-308	upstream	775 F	FT-22	CU-22	Flaked Off
MTI 14-309	downstream	775 F	FT-22	CD-22	Sticking
MTI 14-310	upstream	850 F	FT-23	CU-23	Flaked off
MTI 14-311	downstream	850 F	FT-23	CD-23	Sticking
MTI 14-312	upstream	850 F	FT-24	CU-24	Flaked off
MTI 14-313	downstream	850 F	FT-24	CD-24	Sticking

Table 31. Pictures for fouling coupons prepared in syngas fouling simulator.

SFS Tests	Metal T	Upstream Coupons			Downsteam Coupons		
-	F	CPN#	Quality	Photo	CPN#	Quality	Photo
FT-01	700	14-264	Sticking		14-265	Sticking	
FT-02	700	14-266	Sticking		14-267	Sticking	
FT-03	775	14-268	Flaked off		14-269	Sticking	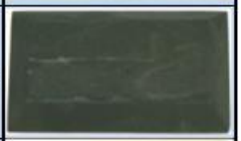
FT-04	775	14-270	Flaked off		14-271	Sticking	
FT-05	850	14-272	Sticking		14-273	Sticking	
FT-06	850	14-274	Flaked off		14-275	Sticking	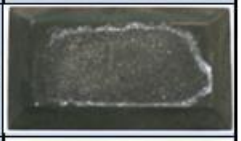
FT-07	700	14-276	Sticking		14-277	Sticking	
FT-08	700	14-278	Sticking		14-279	Sticking	
FT-09	775	14-280	Flaked off		14-281	Flaked off	
FT-10	775	14-282	Some flaked off		14-283	Sticking	
FT-11	850	14-284	Flaked off		14-285	Sticking	
FT-12	850	14-286	Flaked off		14-287	Sticking	

SFS Tests	Metal T	Upstream Coupons			Downsteam Coupons		
-	F	CPN#	Quality	Photo	CPN#	Quality	Photo
FT-13	700	14-288	Flaked off		14-289	Sticking	
FT-14	700	14-290	Flaked off		14-291	Sticking	
FT-15	775	14-292	Flaked off		14-293	Sticking	
FT-16	775	14-294	Sticking		14-295	Sticking	
FT-17	850	14-296	Flaked off		14-297	Sticking	
FT-18	850	14-298	Flaked off		14-299	Some flaked off	
FT-19	700	14-300	Flaked off		14-301	Sticking	
FT-20	700	14-302	Flaked off		14-303	Sticking	
FT-21	775	14-306	Flaked off		14-307	Flaked off	
FT-22	775	14-308	Flaked off		14-309	Sticking	
FT-23	850	14-310	Flaked off		14-311	Sticking	
FT-24	850	14-312	Flaked off		14-313	Sticking	

3. Microstructure of Deposit and Deposit Steel Interface

The morphological analysis procedure using Microbeam's scanning electron microscope (SEM) was used to obtain images and chemical composition of the deposited materials on the coupon surfaces. Cross-sections of coupons with deposits on the surface were prepared by mounting them in epoxy resin. The hardened epoxy resin plug containing the deposit and steel were cross sectioned using a diamond saw and the exposed surface was polished and placed in the SEM for analysis.

Coupon and Deposit (MTI 14-268):

Cross section analysis results of coupon 14-268 are shown in Table 32 with corresponding backscattered electron images in Figure 86 and Figure 87. This coupon is the upstream coupon from SFS Test FT-03 produced at 775°F (413°C) where the ash layer on the coupon did not adhere. The steel surface contains mainly Cr, Fe, and Ni. The surface of the steel that reacted with the syngas showed a significant increase in sulfur and depletion in the level of Cr. The thickness of the corrosion layer was 3 to 5 µm thick. The particles being captured on the surface were mainly iron rich particles with some aluminosilicate particles. Some of the particles showed evidence of reaction with H_2S.

Table 32. Morphology analysis results of Coupon CU-3 (MTI 14-268), with elemental results expressed as weight percent, normalized to 100%.

Fig.	Point	Description	Mg	Al	Si	S	K	Ca	Ti	Cr	Fe	Ni	O
Figure 86	1	Coupon	0.0	0.5	1.0	0.0	0.1	0.5	0.3	15.0	42.7	39.2	0.7
	2	Coupon coating	0.1	0.0	48.4	12.4	0.3	0.1	0.0	1.4	22.2	13.2	2.1
	3	Dark particle	1.2	11.1	41.8	0.2	3.6	0.1	0.1	0.1	2.9	0.2	38.8
	4	Bright particle	0.1	0.3	1.3	9.7	0.3	0.2	0.0	0.1	84.8	2.3	1.0
	5	Bright particle	0.0	0.3	0.6	34.1	0.1	0.2	0.0	0.2	64.0	0.5	0.0
	6	Particle coating	0.3	0.8	4.7	16.9	0.3	0.5	0.2	0.2	73.1	1.9	1.2
	7	Medium particle	0.0	1.5	2.1	7.3	0.0	0.2	0.4	0.0	86.9	1.3	0.4
	8	Dark particle	0.2	7.1	41.0	0.0	5.6	0.2	0.7	0.3	23.4	0.0	21.6
	9	Dark particle	0.5	8.0	33.1	0.3	4.4	0.0	0.7	0.0	52.0	0.2	0.7
	10	Particle coating	0.0	0.2	1.0	38.2	0.2	0.0	0.7	0.0	54.5	1.2	3.9
	11	Medium particle	0.1	0.1	1.0	0.2	0.1	0.2	0.0	0.3	95.4	2.4	0.3
Figure 87	1	Coupon	0.0	1.4	1.1	0.0	0.1	0.2	0.3	14.3	42.5	40.0	0.0
	2	Coupon coating	0.0	0.1	0.4	22.8	0.0	0.3	0.1	4.5	38.5	31.8	1.5
	3	Bright particle	0.0	0.2	0.5	32.8	0.0	0.1	0.0	0.1	50.7	13.3	2.3
	4	Medium particle	0.2	3.0	9.3	0.3	0.0	79.9	0.3	0.1	2.8	0.0	4.2
	5	Medium particle	0.5	9.8	22.7	0.2	0.9	0.1	1.2	0.2	64.0	0.2	0.4
	6	Bright particle	0.0	0.8	0.6	40.7	0.0	0.0	0.1	0.0	56.2	1.7	0.0
	7	Dark particle	0.1	0.3	41.3	0.0	0.0	0.0	0.0	0.0	0.3	0.0	58.1
Averages		**All points**	**0.2**	**2.5**	**14.0**	**12.0**	**0.9**	**4.6**	**0.3**	**2.0**	**47.6**	**8.3**	**7.6**
		Ash particles	**0.2**	**3.5**	**16.3**	**10.5**	**1.3**	**6.8**	**0.3**	**0.1**	**48.6**	**1.8**	**10.6**

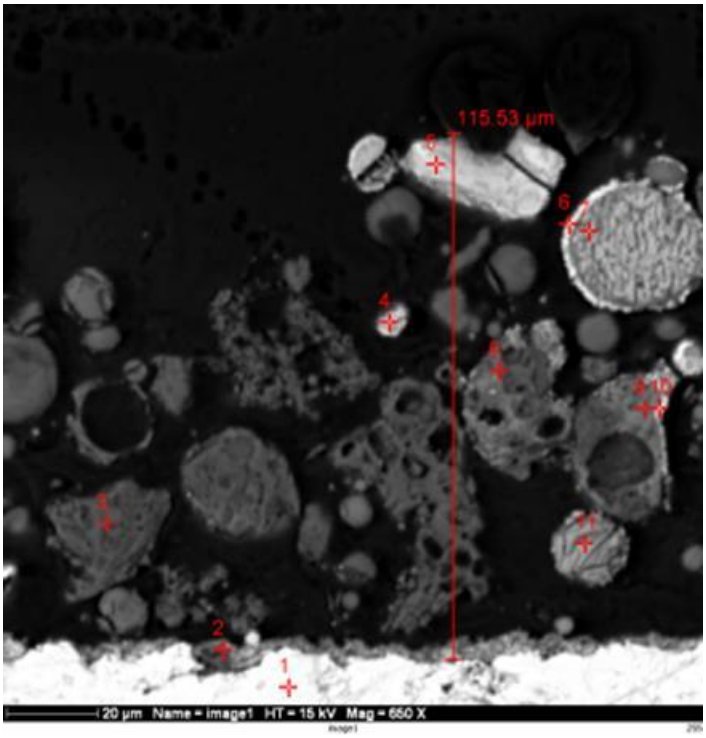

Figure 86. Backscattered electron image of coupon cross-section (MTI 14-268) showing analysis points 1-11.

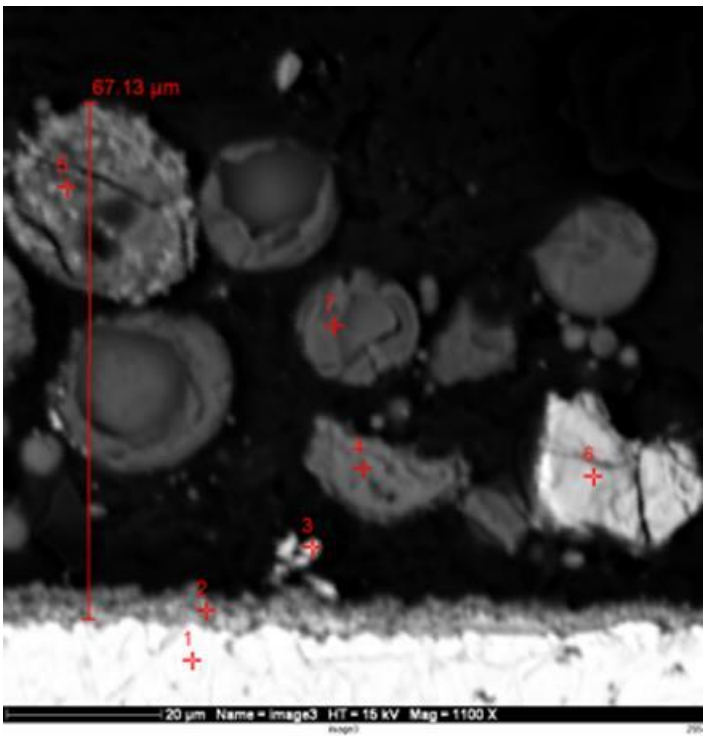

Figure 87. Backscattered electron image of coupon cross-section (MTI 14-268) showing analysis points 1-7.

Coupon and Deposit (MTI 14-274):

The morphological analysis of the cross section of coupon 14-274 is shown in Table 33 with corresponding backscattered electron images in Figure 88 and Figure 89. This coupon is the upstream coupon from SFS Test FT-06 produced at 850°F (454°C) where the ash layer on the coupon did not adhere. The initial corrosion layer next to the steel surface has very high levels of sulfur. As compared to the coupon composition, the levels of Cr and Ni were significantly reduced in the first area examined. The second area analyzed in Figure 89 showed reaction of sulfur with the steel surface. The thickness of the layer is about 5 µm. Reactions of sulfur with the surfaces of iron rich particles is evident as shown in Figure 88 analysis 4 and 6 and analysis 10 and 11 in Table 33.

Table 33. Morphology analysis results of Coupon CU-6 (MTI 14-274), with elemental results expressed as weight percent, normalized to 100%.

Fig.	Point	Description	Na	Mg	Al	Si	S	K	Ca	Ti	Cr	Fe	Ni	O
Figure 88	1	Coupon	0.0	0.2	0.9	1.5	0.0	0.0	0.2	0.5	14.2	41.6	40.8	0.0
	2	Coupon coating	0.0	0.0	0.6	0.7	40.5	0.1	0.0	0.0	2.6	49.3	6.2	0.0
	3	Bright particle	0.7	0.2	2.3	2.6	33.6	0.2	0.0	0.0	0.2	48.8	4.8	6.7
	4	Medium particle	0.9	0.4	1.0	3.5	27.7	0.2	0.0	0.1	0.0	55.3	0.7	10.4
	5	Particle coating	0.1	0.1	0.8	1.4	39.1	0.2	0.0	0.0	0.0	57.4	0.9	0.0
	6	Dark particle	2.7	0.1	8.7	32.5	0.1	6.3	0.0	0.1	0.1	0.5	0.4	48.6
	7	Bright particle	0.1	0.0	0.2	0.8	34.1	0.1	0.0	0.0	0.3	63.5	0.6	0.5
	8	Particle coating	0.6	0.1	0.7	2.2	0.1	1.3	1.5	0.9	0.0	90.1	2.0	0.6
	9	Dark particle	0.7	0.8	10.8	25.1	0.0	2.0	1.2	0.6	0.0	13.2	0.1	45.5
	10	Particle coating	0.1	0.0	0.8	1.8	34.5	0.1	0.2	0.1	0.0	59.6	0.7	2.1
	11	Bright particle	0.3	0.2	1.2	1.9	13.0	0.2	0.2	0.0	0.2	63.5	0.5	18.8
	12	Dark particle	0.7	0.7	6.7	41.0	0.0	2.8	0.6	1.0	0.0	1.4	0.3	44.9
	13	Medium particle	0.4	0.7	8.1	16.7	0.1	1.2	0.2	2.8	0.1	20.7	0.1	48.9
	14	Particle coating	0.0	0.2	1.0	2.8	17.2	0.4	0.4	0.0	0.4	71.7	5.0	1.0
	15	Medium particle	0.0	0.3	1.4	6.6	3.3	7.1	2.1	1.4	0.4	67.8	1.1	8.4
Figure 89	1	Coupon	0.0	0.1	0.6	0.7	0.0	0.0	0.2	0.2	14.8	44.1	38.3	0.9
	2	Coupon coating	0.0	0.0	0.4	0.7	24.3	0.0	0.1	0.1	9.9	30.9	30.1	3.5
	3	Bright particle	0.1	0.0	0.2	0.5	33.9	0.1	0.1	0.0	0.1	57.8	7.3	0.0
	4	Dark particle	0.4	0.8	9.9	21.6	0.2	2.5	0.0	0.8	0.1	27.2	0.3	36.3
	5	Bright particle	0.8	0.0	1.2	2.4	36.5	0.1	0.1	0.0	0.0	58.3	0.6	0.0
	6	Dark particle	0.3	0.9	14.0	27.2	0.0	2.2	0.3	3.2	0.1	4.2	0.0	47.6
	7	Medium particle	0.9	0.9	10.7	25.2	0.0	2.2	1.6	0.6	0.0	10.5	0.1	47.3
Averages		**All points**	**0.4**	**0.3**	**3.7**	**10.0**	**15.4**	**1.3**	**0.4**	**0.6**	**2.0**	**42.6**	**6.4**	**16.9**
		Ash particles	**0.6**	**0.4**	**5.5**	**14.8**	**13.0**	**1.9**	**0.5**	**0.8**	**0.1**	**35.2**	**1.2**	**26.0**

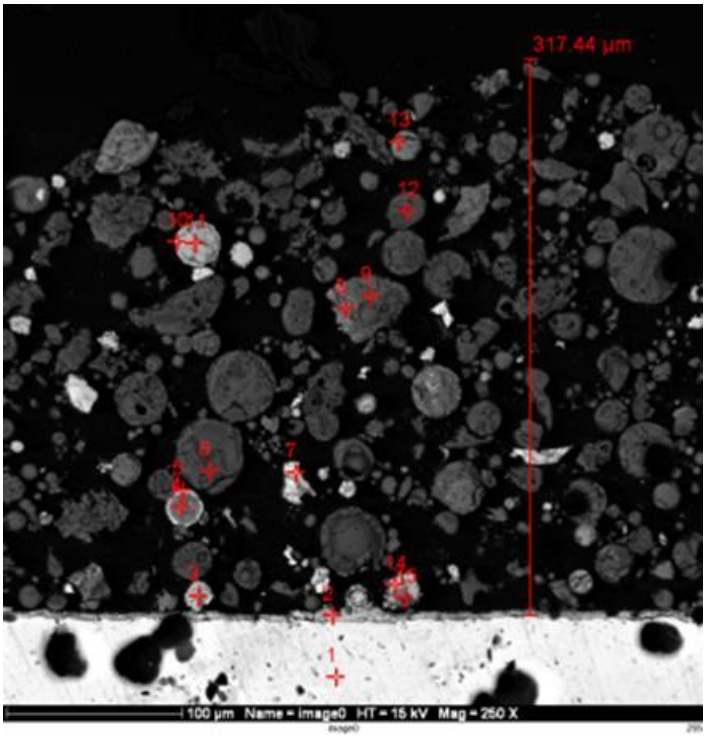

Figure 88. Backscattered electron image of coupon cross-section (MTI 14-274) showing analysis points 1-15.

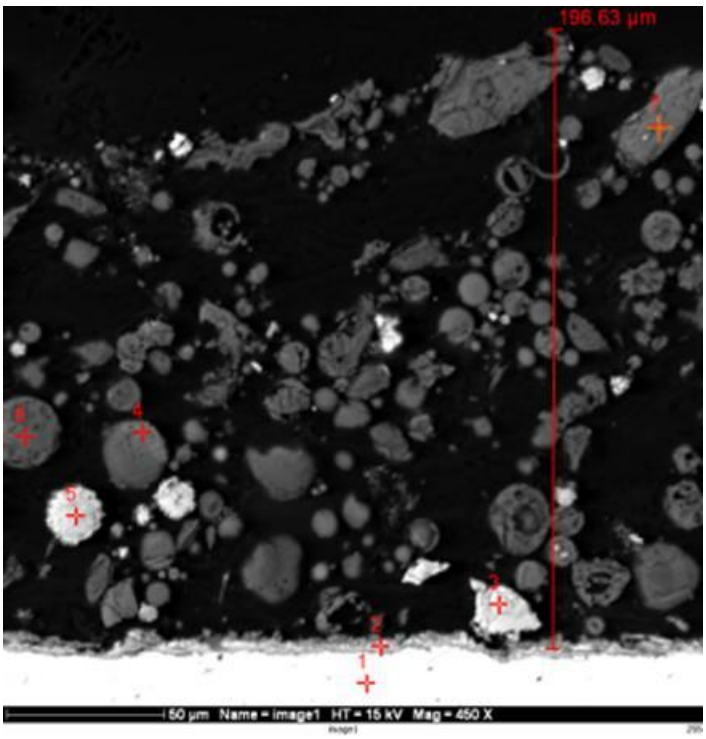

Figure 89. Backscattered electron image of coupon cross-section (MTI 14-274) showing analysis points 1-7.

Coupon and Deposit (MTI 14-288):

The morphological analysis of the cross section of coupon 14-288 is shown in Table 34 with corresponding backscattered electron images in Figure 90 and Figure 91. This coupon is the upstream coupon from SFS Test FT-13 produced at 700°F (371°C) where the ash layer on the coupon did not adhere. The corrosion layer was examined in detail. The layer was about 2.9 µm thick and about half as thick as the layers found in coupons exposed to higher temperatures. The levels of sulfur in the layer ranged from 9.6 to 37.1 % S.

Table 34. Morphology analysis results of Coupon CU-13 (MTI 14-288), with elemental results expressed as weight percent, normalized to 100%.

Fig.	Point	Description	Al	Si	S	Ti	Cr	Fe	Ni	O
Figure 90	1	Coupon	1.2	0.7	0.4	0.4	15.3	42.2	39.9	0.0
	2	Dark deposit material	1.7	6.7	27.0	0.5	22.1	16.4	6.2	19.5
	3	Light deposit material	0.3	1.1	27.7	0.3	12.6	32.4	22.3	3.3
	4	Medium deposit material	0.4	3.3	33.0	1.6	17.1	25.9	13.7	5.1
	5	Medium deposit material	0.6	0.8	32.7	0.7	24.6	26.4	8.0	6.2
Figure 91	1	Coupon	0.8	0.9	0.5	0.4	15.4	43.8	38.0	0.3
	2	Light deposit material	0.6	0.8	37.1	0.0	11.0	24.1	21.2	5.2
	3	Dark deposit material	0.3	1.0	13.7	0.4	26.5	36.7	19.6	2.0
	4	Medium deposit material	0.1	0.8	11.3	0.1	2.7	33.7	50.2	1.1
	5	Medium deposit material	0.6	1.1	18.0	0.0	32.6	32.2	13.6	2.1
	6	Light deposit material	0.5	0.7	9.6	0.0	0.9	34.3	53.5	0.6
	7	Light deposit material	0.2	0.5	26.8	0.0	6.4	28.1	35.4	2.6
	8	Medium deposit material	0.9	1.1	26.7	4.5	27.7	28.4	8.0	2.7
Averages		**All points**	**0.6**	**1.5**	**20.3**	**0.7**	**16.5**	**31.1**	**25.3**	**3.9**
		Ash particles	**0.6**	**1.6**	**24.0**	**0.7**	**16.7**	**29.0**	**22.9**	**4.6**

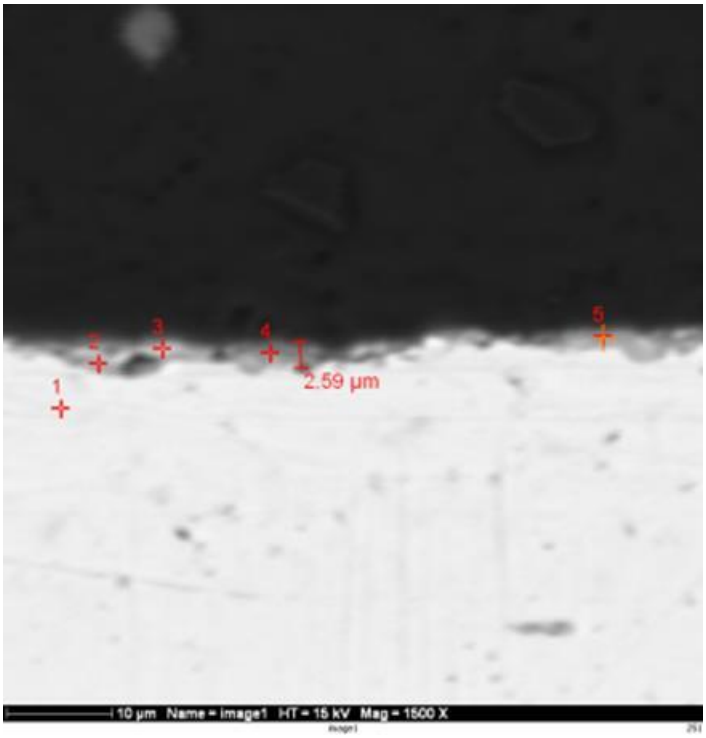

Figure 90. Backscattered electron image of coupon cross-section (MTI 14-288) showing analysis points 1-5.

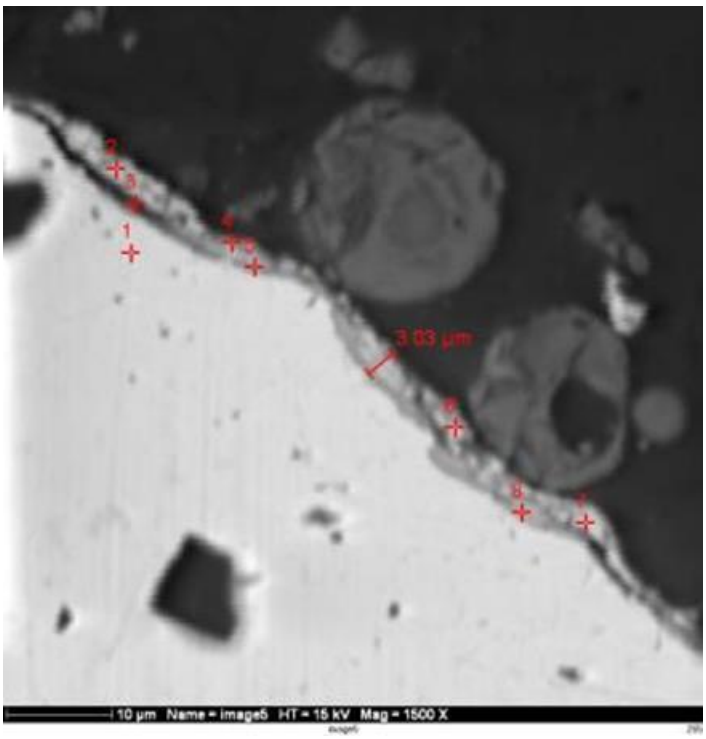

Figure 91. Backscattered electron image of coupon cross-section (MTI 14-288) showing analysis points 1-7.

Coupon and Deposit (MTI 14-290):
The morphological analysis of the cross section of coupon 14-290 is shown in Table 35 with corresponding backscattered electron images in Figure 92 and Figure 93. This coupon is the upstream coupon from SFS Test FT-14 produced at 700°F (371°C) where the ash layer on the coupon did not adhere. The coupon coating or corrosion layer had elevated levels of sulfur. The materials deposited consisted of aluminosilicate particles and iron-rich particles. Coatings on the surfaces of particles were not evident.

Table 35. Morphology analysis results of Coupon CU-14 (MTI 14-290), with elemental results expressed as weight percent, normalized to 100%.

Fig.	Point	Description	Na	Mg	Al	Si	S	K	Ti	Cr	Fe	Ni	O
Figure 92	1	Coupon coating	0.0	0.1	0.0	0.9	6.6	0.0	0.0	4.6	42.6	44.3	0.8
	2	Bright particle	0.9	0.5	1.1	1.0	41.6	0.2	0.0	0.1	54.0	0.6	0.0
	3	Medium particle	0.0	0.3	0.8	2.1	0.0	0.0	0.0	0.0	71.3	0.4	25.2
	4	Bright particle	0.2	0.2	0.2	0.5	24.8	0.2	0.2	0.0	70.6	1.4	1.8
	5	Dark particle	1.3	1.2	15.6	29.7	0.0	3.1	0.6	0.1	4.6	0.0	43.9
	6	Dark particle	1.0	1.0	13.9	26.5	0.0	2.5	3.1	0.1	2.5	0.1	49.5
Figure 93	1	Coupon coating	0.4	0.0	0.6	2.6	19.9	0.2	0.5	8.9	36.1	27.7	3.0
	2	Bright particle	0.3	0.0	1.1	2.6	28.2	0.0	0.0	0.1	58.9	4.2	4.7
	3	Bright particle	0.4	0.1	0.2	0.3	14.7	0.0	0.0	0.1	80.3	3.1	0.8
	4	Dark particle	0.2	1.0	16.8	40.3	0.1	4.3	1.1	0.0	8.3	0.0	27.9
	5	Bright particle	1.1	0.0	1.1	1.3	0.8	0.1	0.0	0.2	65.8	1.1	28.6
Averages		**All points**	**0.5**	**0.4**	**4.7**	**9.8**	**12.4**	**0.9**	**0.5**	**1.3**	**45.0**	**7.5**	**16.9**
		Ash particles	**0.6**	**0.5**	**5.6**	**11.6**	**12.2**	**1.1**	**0.6**	**0.1**	**26.2**	**1.2**	**20.2**

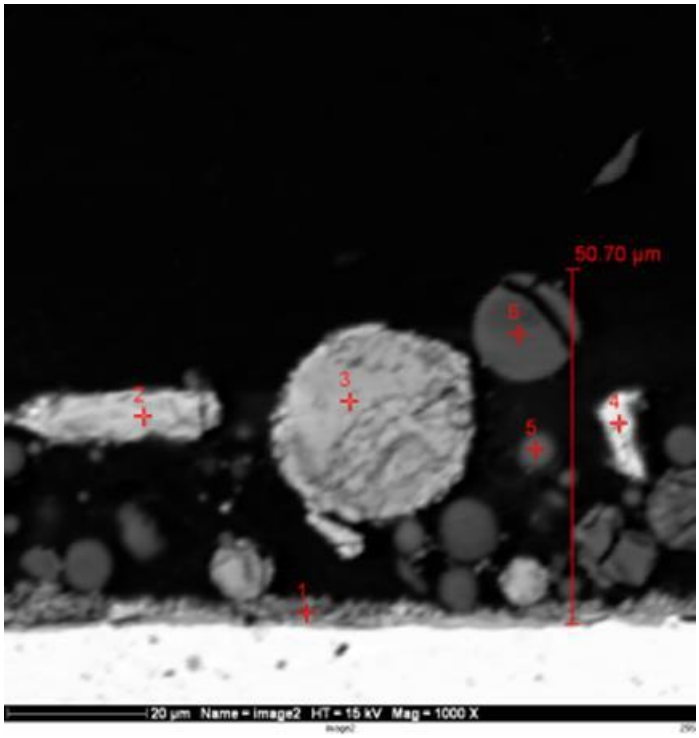

Figure 92. Backscattered electron image of coupon cross-section (MTI 14-290) showing analysis points 1-6.

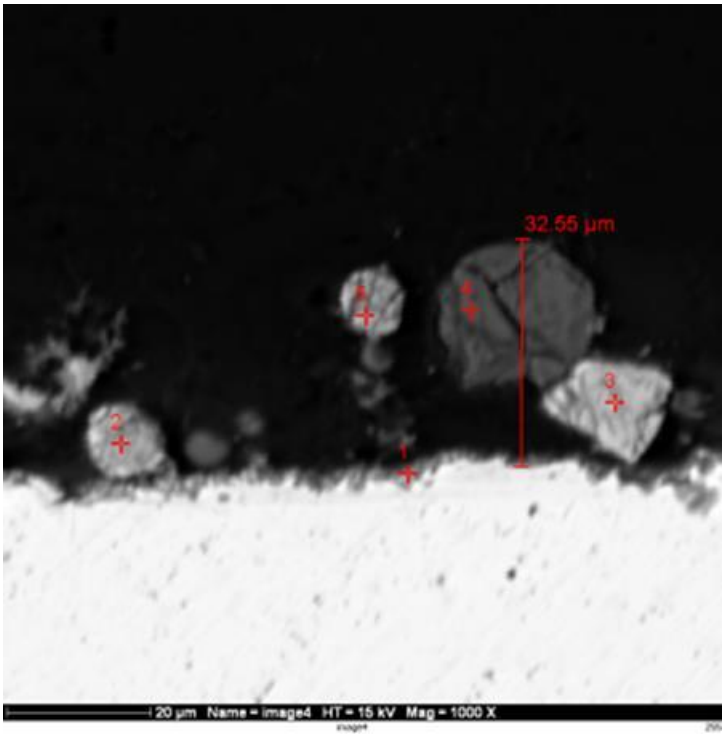

Figure 93. Backscattered electron image of coupon cross-section (MTI 14-290) showing analysis points 1-5.

Coupon and Deposit (MTI 14-292):
The morphological analysis of the cross section of coupon 14-292 is shown in Table 36 with corresponding backscattered electron images in Figure 94 and Figure 95. This coupon is the upstream coupon from SFS Test FT-15 produced at 775°F (413°C) where the ash layer on the coupon did not adhere. The coating on the steel surface showed less reaction of sulfur on the surface. Minor coatings on the surface of particles were found.

Table 36. Morphology analysis results of Coupon CU-15 (MTI 14-292), with elemental results expressed as weight percent, normalized to 100%.

Fig.	Point	Description	Na	Mg	Al	Si	S	K	Ca	Cr	Fe	Ni	O
Figure 94	1	Coupon coating	0.0	0.6	0.7	2.6	1.5	0.0	0.2	21.4	48.5	18.9	5.6
	2	Dark particle	0.8	0.5	13.7	25.2	0.2	1.9	0.2	0.0	2.8	0.0	54.8
	3	Bright particle	0.1	0.3	0.9	1.2	40.9	0.2	0.0	0.0	56.0	0.5	0.0
	4	Dark particle	0.7	0.9	12.5	21.9	0.0	1.7	0.2	0.0	1.4	0.4	60.2
	5	Medium particle	0.8	0.4	4.3	8.7	8.6	0.3	0.2	0.3	64.4	0.5	11.4
	6	Medium particle	0.0	0.0	1.5	5.4	1.1	1.0	0.2	0.0	89.7	0.7	0.5
Figure 95	1	Coupon coating	0.0	0.0	1.4	1.4	0.4	0.0	0.0	2.5	64.7	27.2	2.4
	2	Bright particle	0.3	0.0	2.0	5.4	20.1	0.2	0.5	0.4	56.8	3.9	10.5
	3	Dark particle	0.1	0.3	6.5	63.9	1.0	5.6	2.8	0.0	5.5	0.0	14.4
	4	Dark particle	0.7	0.8	8.3	29.9	0.0	1.7	0.3	0.1	14.1	0.0	44.3
	5	Bright particle	0.2	0.3	1.6	2.4	10.4	0.0	0.4	0.0	65.4	1.8	17.5
	6	Dark particle	1.2	0.9	12.5	22.8	0.1	1.8	0.1	0.1	2.4	0.0	58.1
Averages		**All points**	**0.4**	**0.4**	**5.5**	**15.9**	**7.0**	**1.2**	**0.4**	**2.1**	**39.3**	**4.5**	**23.3**
		Ash particles	**0.5**	**0.4**	**6.4**	**18.7**	**8.2**	**1.4**	**0.5**	**0.1**	**35.8**	**0.8**	**27.2**

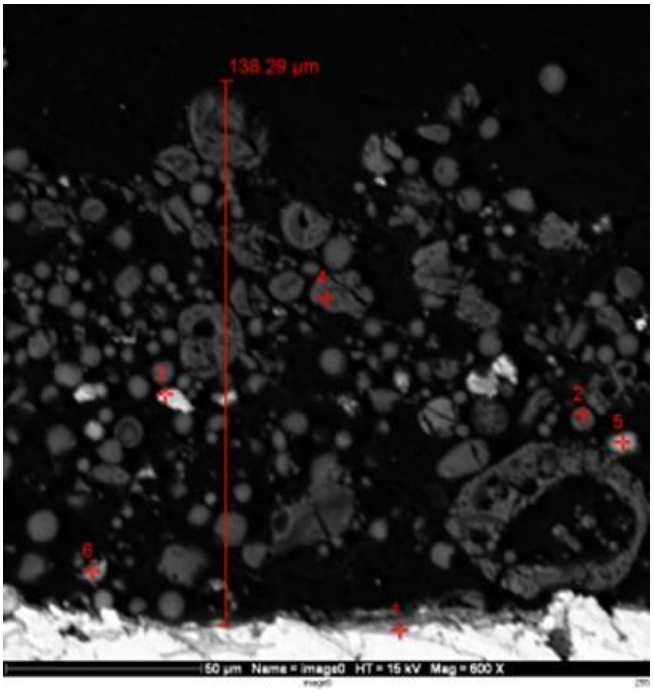

Figure 94. Backscattered electron image of coupon cross-section (MTI 14-292) showing analysis points 1-6.

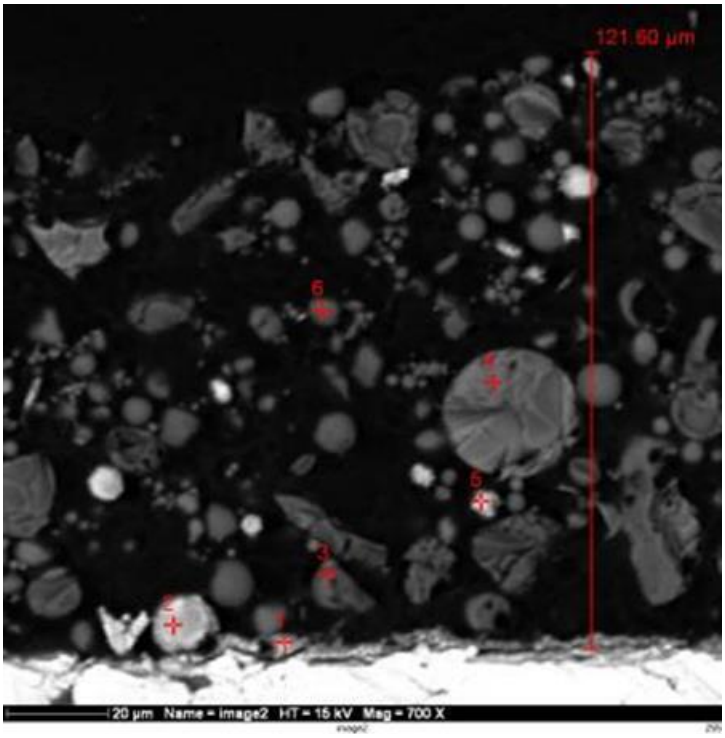

Figure 95. Backscattered electron image of coupon cross-section (MTI 14-292) showing analysis points 1-6.

Coupon and Deposit (MTI 14-296):

The morphological analysis of the cross section of coupon 14-296 is shown in Table 37 with corresponding backscattered electron images in Figure 96 and Figure 97. This coupon is the upstream coupon from SFS Test FT-17 produced at 850°F (454°C) where the ash layer on the coupon did not adhere. The initial corrosion layer had high levels of sulfur. Some particles showed evidence of bonding to the surface of the coupon as shown in Figure 97. The materials participating in bonding are rich in sulfur as illustrated by bonding materials (medium bonding material).

Table 37. Morphology analysis results of Coupon CU-17 (MTI 14-296), with elemental results expressed as weight percent, normalized to 100%.

Fig.	Point	Description	Mg	Al	Si	S	K	Ca	Ti	Cr	Fe	Ni	O
Figure 96	1	Coupon coating	0.2	0.7	1.8	29.9	0.0	0.0	0.9	26.7	28.3	4.1	7.6
	2	Medium particle	0.6	8.0	12.7	2.7	0.7	1.3	0.8	0.2	18.8	1.0	53.2
	3	Dark particle	0.8	16.0	40.1	0.4	3.7	0.1	1.0	0.2	3.5	0.0	34.3
	4	Medium particle	0.4	10.0	13.3	0.1	0.8	0.2	0.0	0.1	32.2	1.4	41.6
	5	Bright particle	0.1	1.4	1.3	34.9	0.0	0.5	0.0	0.1	53.1	8.7	0.0
	6	Medium particle	0.7	0.7	1.4	34.2	0.1	0.2	0.2	0.6	21.0	29.1	11.8
Figure 97	1	Coupon coating	0.0	1.4	2.5	23.7	0.3	0.3	3.1	28.6	23.6	7.6	9.0
	2	Dark particle	1.3	13.2	43.6	0.0	2.8	0.1	0.3	0.1	9.8	0.0	28.8
	3	Medium particle	0.0	1.3	25.2	0.2	0.7	0.1	0.4	0.1	26.5	0.8	44.8
	4	Medium bonding material	0.0	0.1	0.6	23.3	0.0	0.5	0.0	0.5	32.9	41.2	1.0
	5	Medium bonding material	0.0	0.5	0.9	31.5	0.4	0.8	0.2	0.5	30.0	33.7	1.6
	6	Medium bonding material	0.4	0.7	0.9	28.3	0.3	0.0	0.0	3.5	33.2	28.5	4.3
Averages		**All points**	**0.4**	**4.5**	**12.0**	**17.4**	**0.8**	**0.3**	**0.6**	**5.1**	**26.1**	**13.0**	**19.8**
		Ash particles	**0.4**	**5.2**	**14.0**	**15.6**	**0.9**	**0.4**	**0.3**	**0.6**	**26.1**	**14.4**	**22.1**

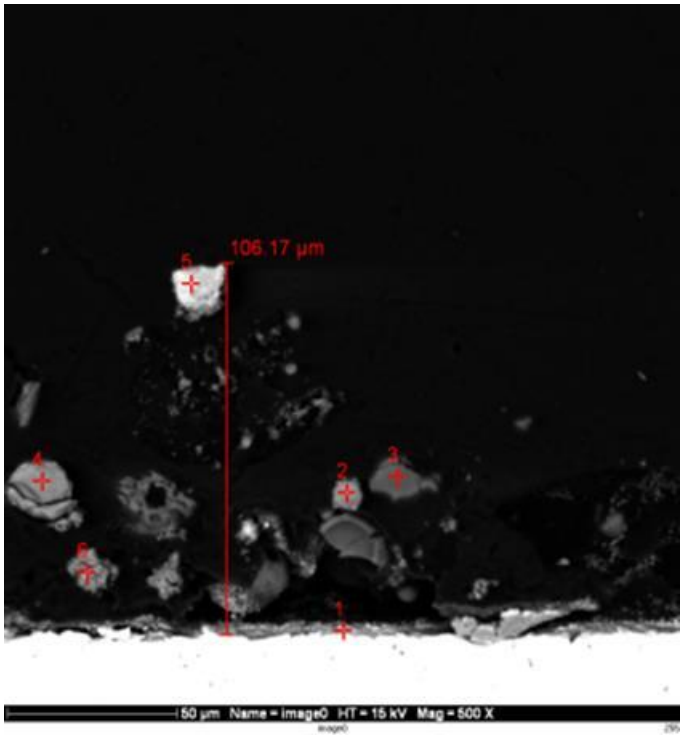

Figure 96. Backscattered electron image of coupon cross-section (MTI 14-296) showing analysis points 1-6.

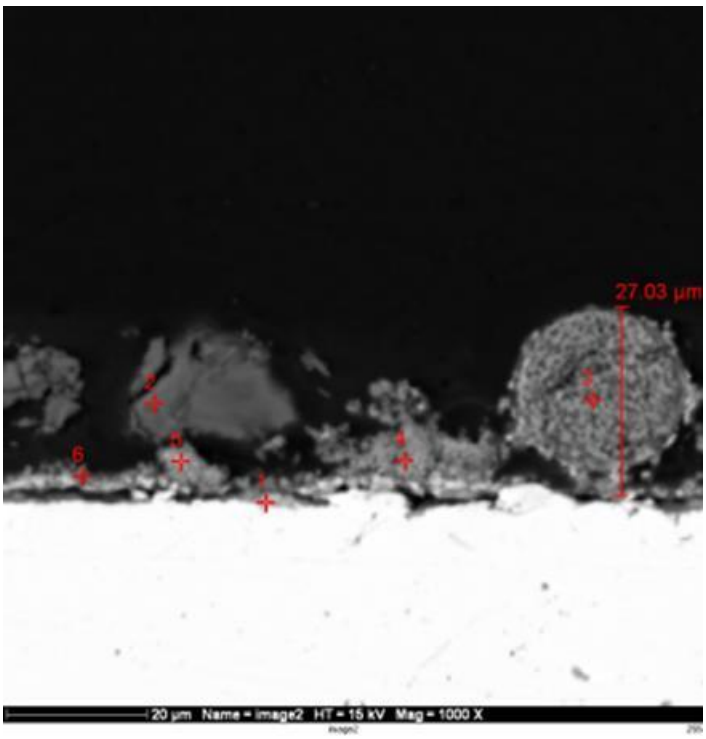

Figure 97. Backscattered electron image of coupon cross-section (MTI 14-296) showing analysis points 1-6.

A qualitative measure of the deposit thickness was performed for the deposits examined using the morphological analysis. Figure 98 shows that the thickness of the layers is suggested to be a function of temperature. The thicker layers retained were at higher temperatures.

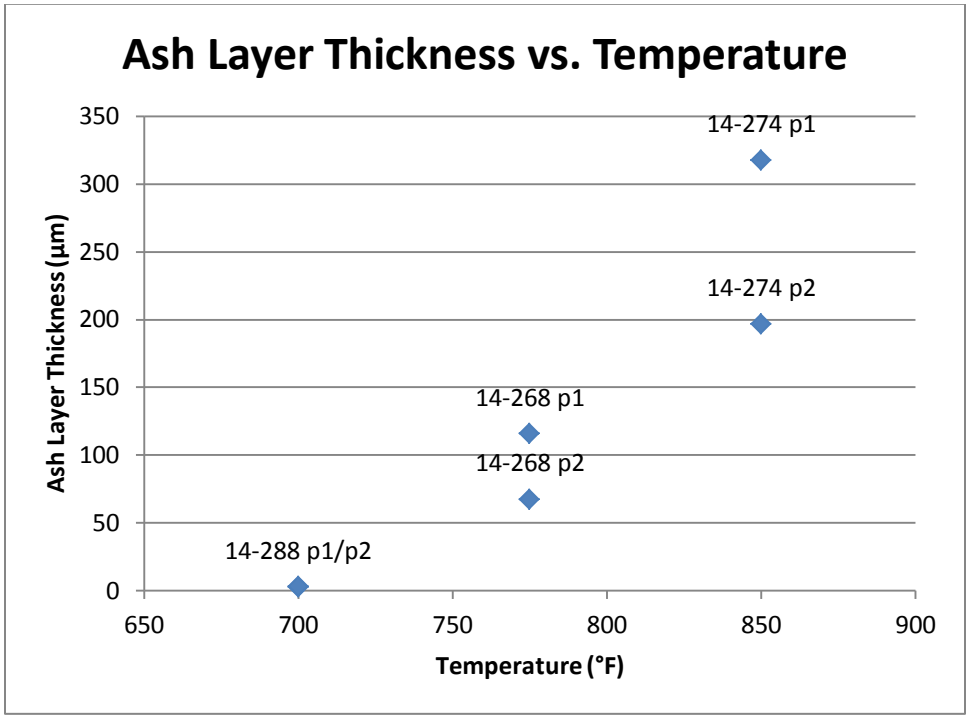

Figure 98. Thickness of the layer retained on coupon where most of the ash materials flaked off.

4. Coupon Exposure to Extreme Composition

The main challenge in the testing was to obtain strongly bonded layers to the steel surfaces. Based on the analysis of deposit samples taken from a plant RSC, the results showed high levels of sulfur, iron, and zinc. In some cases the levels of sodium were also increased in the deposits. The levels of zinc increased due to recycling the fine ash and carbon back into the gasifier to increase carbon conversion efficiency. These deposits were exposed to longer periods of time in syngas containing H_2S. In order to simulate real RSC deposits, testing with extreme compositions was conducted. The extreme compositions consisted of Wabash ash with additives of ZnS, FeS, and NaCl.

Bonded deposits with extreme compositions were produced by first applying a sodium chloride layer, sulfide layers (iron and/or zinc sulfides) to the coupons and a layer of the Wabash ash. The coupons were then sintered at 700°F (371°C) for a period of 5 hours in a muffle furnace. The extreme testing conditions are summarized in Table 38. The ash layer adhered to the all coupons in these tests.

An additional set of tests were conducted by applying upstream deposit layers of sodium and/or potassium chloride, zinc sulfide and/or iron sulfide, and Wabash ash to substrates in the syngas cooler simulator as summarized in Table 39. The coupons were exposed to reducing gas (CO/CO_2) under pressure for 4 hours. The ash materials bonded well to the coupons. The coupons were removed from the SFS and the adhesive force was measured.

Table 38. Extreme condition testing.

Coupon	Applied layers	Layer wt.	Testing
14-234	NaCl+FeS+Wabash ash	0.0824	Sent to UTA
14-235	NaCl+ZnS+Wabash ash	0.0653	Sent to UTA
14-236	NaCl+FeS+ZnS+Wabash ash	0.1531	Sent to UTA
14-242	NaCl+FeS+ZnS+Wabash ash	0.1150	Sent to UTA
14-244	NaCl+FeS+ZnS+Wabash ash	0.0986	Sent to UTA
14-245	NaCl+FeS+ZnS+Wabash ash	0.1855	Sent to UTA
14-246	NaCl+FeS+ZnS+Wabash ash	0.1166	Adhesive strength
14-247	NaCl+FeS+ZnS+Wabash ash	0.1338	Adhesive strength
14-248	NaCl+FeS+ZnS+Wabash ash	0.1341	SEM morphology

Table 39. Extreme condition testing in syngas cooler simulator.

		Wt., Grams			
Coupon	Deposit layers	Blank Coupon	Pretreated	Deposit +Coupon	Deposit Layer
14-300	NaCl+FeS+ZnS+Wabash ash	3.3802	3.3807	3.5531	0.1724
14-302	NaCl+FeS+Wabash ash	3.4495	3.4521	3.6614	0.2093
14-306	NaCl+ZnS+ Wabash ash	3.3850	3.3875	3.5885	0.2010
14-307	NaCl+KCl+FeS+ZnS+Wabash ash	3.4187	3.4192	3.6178	0.1986
14-308	Kcl+FeS+ZnS+ Wabash ash	3.3171	3.3178	3.5099	0.1921

Coupon and Deposit (MTI 14-248):

Morphological analysis of the coupon and deposit with materials having extreme compositions is summarized in Table 40 and Figure 99 and Figure 100. During sample preparation the deposited layer lifted and separated from the coupon surface as shown in Figure 99 and Figure 100. The dark region between the steel and the deposited material is the resin used to mount the sample. The initial layer (corrosion layer) was depleted in sulfur likely due to the presence of chlorine introduced in the first layer. The second layer of iron sulfide and zinc sulfide showed evidence of bonding shown in Figure 100. The subsequent layer of Wabash ash was found to be bonded to the iron sulfide/zinc sulfide layers.

Table 40. Morphological analysis of coupon cross-section 14-248 produced with extreme deposit compositions.

Fig.	Point	Description	Na	Mg	Al	Si	S	K	Ca	Cr	Fe	Ni	Cu	Zn	O
Figure 99	1	Coupon surface	0.0	0.1	0.4	2.1	0.7	0.0	0.1	5.7	41.8	47.4	0.0	1.7	0.0
	2	Bright layer - medium particle	0.0	0.0	0.1	0.3	6.5	0.0	0.0	0.1	88.8	2.0	0.8	0.5	0.8
	3	Bright layer - dark particle	1.3	3.7	8.3	25.8	0.1	1.3	3.2	0.0	5.9	0.0	0.1	0.3	50.0
	4	Bright layer - bright particle	0.0	0.2	0.3	0.7	42.6	0.2	0.3	0.0	48.9	0.0	6.5	0.4	0.0
	5	Bright layer - bright particle	0.4	0.0	0.2	0.5	23.8	0.0	0.0	0.2	69.0	1.6	1.8	0.2	2.4
	6	Dark layer - medium particle	0.1	0.7	8.7	23.5	0.0	1.5	0.2	0.0	21.9	0.0	0.0	0.1	43.3
	7	Dark layer - dark particle	1.7	0.5	7.2	31.2	0.1	2.6	0.2	0.1	1.7	0.0	0.0	0.1	54.7
	8	Dark layer - dark particle	0.4	0.6	7.3	18.6	0.1	1.2	0.3	0.0	30.1	0.1	0.0	0.0	41.4
	9	Dark layer - bright particle	0.6	0.6	1.1	1.7	0.0	0.0	0.0	0.0	66.0	0.4	0.0	0.0	29.8
Figure 100	1	Coupon surface	0.0	0.3	0.9	1.0	1.1	0.0	0.2	9.2	42.8	43.3	0.0	1.2	0.0
	2	Bright layer - bright particle	0.0	0.0	0.7	0.6	45.2	0.0	0.0	0.0	49.4	0.5	3.7	0.0	0.0
	3	Bright layer – neck	0.0	0.1	0.0	0.4	2.8	0.6	0.0	0.1	78.1	1.2	0.7	5.5	10.7
	4	Dark layer - medium particle	0.7	0.8	5.7	16.0	0.0	0.9	0.3	0.1	38.0	0.8	0.0	0.2	36.7
	5	Dark layer - bright particle	0.7	0.0	0.6	0.8	0.0	0.0	0.1	0.1	65.4	0.6	1.1	0.0	30.7
	6	Dark layer - medium particle	0.4	0.2	10.9	13.2	0.0	0.5	0.0	0.0	34.0	0.9	0.1	0.4	39.4
	7	Dark layer - bright particle	0.0	8.2	0.6	1.5	29.5	0.5	0.2	0.0	1.6	0.0	1.0	47.5	9.4
	8	Dark layer - dark particle	1.1	1.8	10.2	29.5	0.0	3.1	0.0	0.0	10.9	0.1	0.0	0.6	42.7
	9	Dark layer – neck	0.0	7.4	0.4	1.7	26.4	0.8	0.1	0.0	4.1	0.0	0.0	46.2	13.0
	Average	**All points**	**0.4**	**1.4**	**3.5**	**9.4**	**9.9**	**0.7**	**0.3**	**0.9**	**38.8**	**5.5**	**0.9**	**5.8**	**22.5**

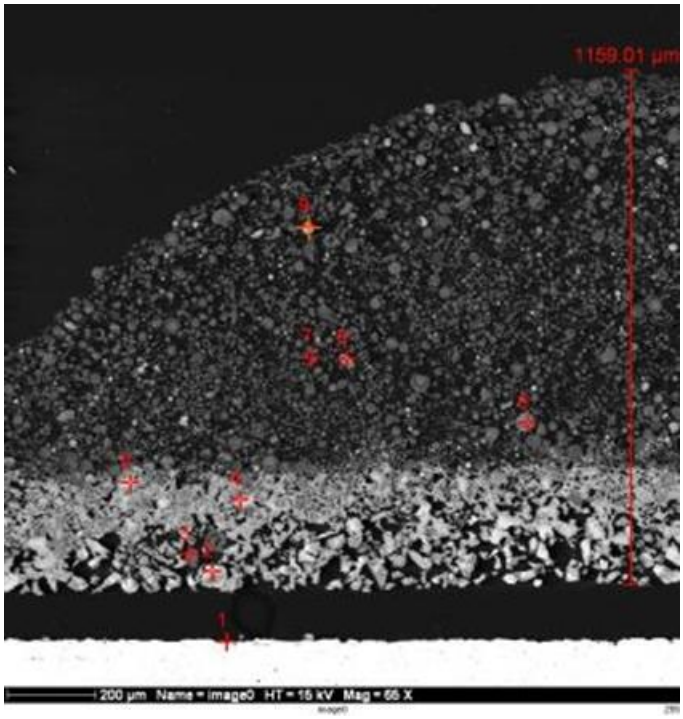

Figure 99. Backscattered electron image of coupon cross-section (MTI 14-248) showing analysis points 1-9.

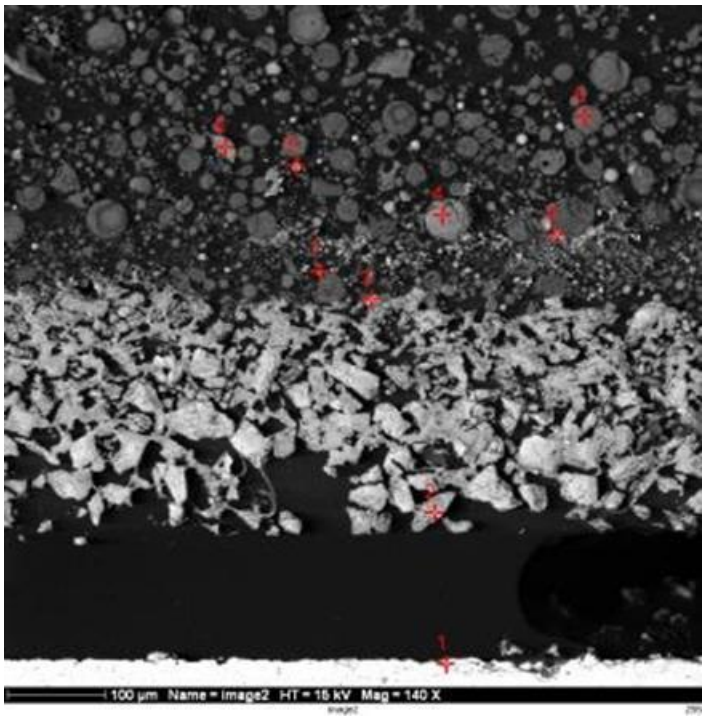

Figure 100. Backscattered electron image of coupon cross-section (MTI 14-248) showing analysis points 1-9.

Additional morphological analyses for coupon 14-248 are shown in Table 41 and Figure 101 and Figure 102 to further examine the bonding material between the Wabash ash and the ZnS/FeS layer. The results show that an iron-zinc-sulfide appears to have formed a bonding material between the Wabash ash and the sulfide layers.

Table 41. Morphological analysis of coupon cross-section 14-248 produced under the extreme conditions.

Fig.	Point	Description	Mg	Al	Si	S	Cl	K	Ca	Cr	Fe	Ni	Zn	O
46	1	Bright material	6.0	1.2	1.8	28.1	0.5	0.2	0.1	0.0	2.3	0.0	54.9	4.9
	2	Bonding material	0.8	0.5	0.7	9.2	0.0	0.3	1.2	0.0	51.1	0.6	5.7	29.9
	3	Bonding material	0.9	0.6	3.2	9.1	0.6	0.7	0.5	0.0	56.5	0.6	4.6	22.8
	4	Bonding material	0.1	0.0	0.6	1.8	0.7	0.4	0.2	0.1	74.5	1.5	6.4	13.8
	5	Bonding material	0.9	11.3	16.9	2.7	1.9	1.6	0.9	0.0	25.6	0.2	7.4	30.8
	6	Bonding material	0.9	14.8	23.1	0.2	0.1	2.6	0.2	0.1	6.6	0.0	0.7	50.6
	7	Bright particle	3.1	0.2	1.0	19.0	0.8	0.2	0.0	0.4	2.3	0.2	67.1	5.9
	8	Iron rich layer	0.0	0.1	0.5	37.9	0.0	0.0	0.0	0.3	57.7	0.8	0.6	2.1
	9	Iron rich layer	0.0	0.1	0.5	35.3	0.0	0.0	0.2	0.1	59.6	0.6	0.4	3.3
47	1	Sulfided layer	0.2	0.3	0.6	17.9	0.0	0.1	0.1	34.9	31.6	3.8	4.0	6.5
	2	Sulfided layer	0.1	0.3	0.7	32.7	0.0	0.0	0.1	18.5	31.1	3.6	0.2	12.7
	3	Sulfided layer	0.1	0.2	0.6	10.3	0.6	0.0	0.0	40.4	35.6	4.2	5.9	2.2
	Average	**All points**	**1.1**	**2.5**	**4.2**	**17.0**	**0.4**	**0.5**	**0.3**	**7.9**	**36.2**	**1.3**	**13.1**	**15.4**

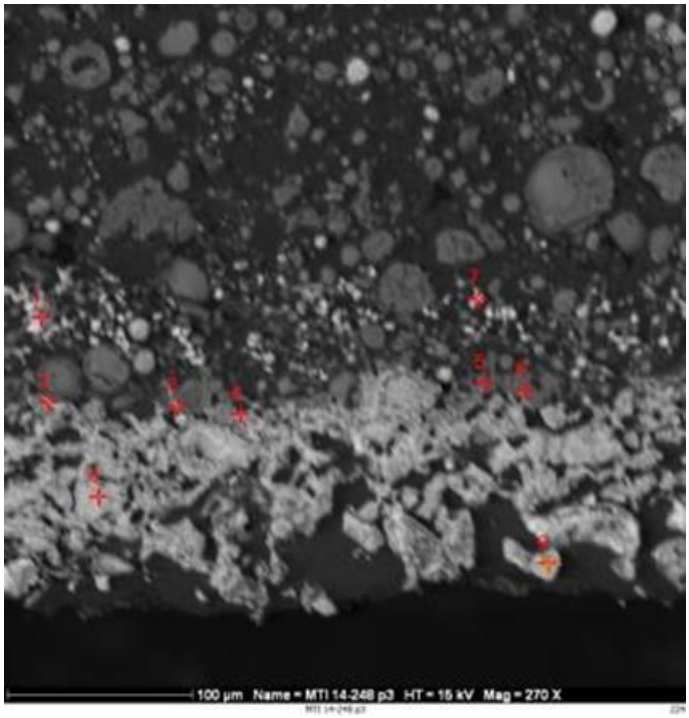

Figure 101. Backscattered electron image of coupon cross-section (MTI 14-248) showing analysis points 1-9.

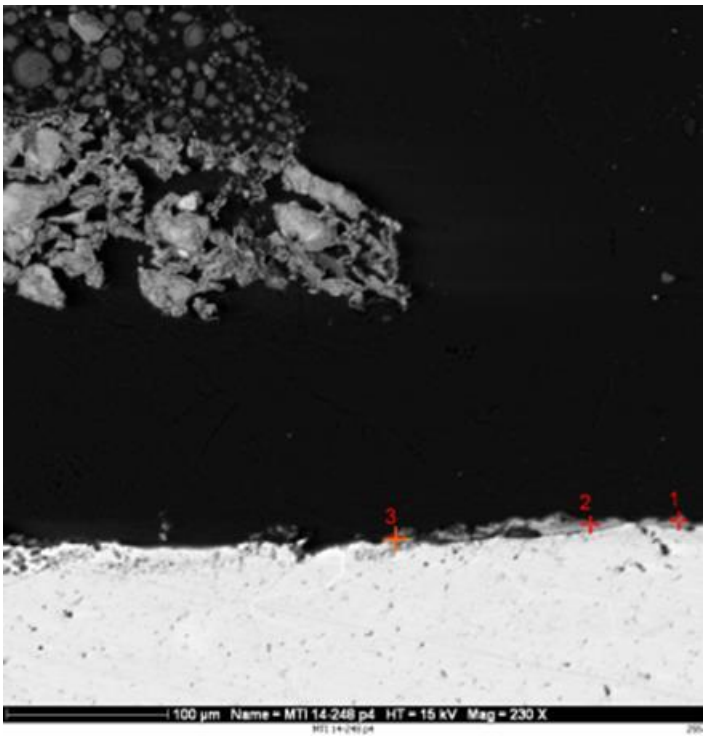

Figure 102. Backscattered electron image of coupon cross-section (MTI 14-248) showing analysis points 1-9.

Coupon and Deposit (MTI 14-246):
The SEM surface analysis of the coupon produced under extreme conditions (MTI 246) where the ash layer fell off while handling is shown in Table 42 with corresponding backscattered electron images in Figure 103 through Figure 106. The surface analysis shows the residual ash adhering to the surface along with the iron and zinc sulfide.

Coupons 14-234, 14-235, 14-236, 14-242, 14-244, and 14-245 were sent to UTA for testing using pulse detonation to remove the ash layer. Coupon 14-246 and 14-247 received testing to measure the adhesive strength of the ash on the coupon surface. Coupon 14-248 received SEM morphological analysis of the cross-section.

Table 42. SEM surface analysis of Coupon 14-246.

Fig.	Point	Description	Mg	Al	Si	S	Cl	K	Ca	Ti	Cr	Mn	Fe	Ni	Zn
Figure 103	1	Entire Frame	1.0	1.6	2.5	7.3	0.8	0.2	0.1	0.1	0.1	0.5	41.3	0.7	5.2
Figure 104	1	Area clear of ash resid	1.0	2.6	4.4	8.0	0.0	0.4	0.1	0.1	0.0	0.6	33.0	0.5	6.8
	2	Area with ash resid	0.7	6.6	16.8	1.9	0.0	1.2	0.3	0.2	0.1	0.0	23.6	0.2	9.2
	3	Area with ash resid	0.8	3.7	7.0	3.7	0.4	0.5	0.4	0.3	10.3	2.4	25.3	1.1	17.8
Figure 105	1	Area with ash resid	0.9	2.9	4.7	6.1	0.5	0.3	0.3	0.2	12.4	2.5	23.5	2.1	13.6
	2	Area clear of ash resid	0.7	2.6	2.9	7.7	1.6	0.3	0.5	0.1	0.1	0.2	34.2	0.6	2.4
Figure 106	1	Area clear of ash resid	0.3	2.9	2.6	7.3	0.1	0.2	0.2	2.5	25.4	2.8	12.8	5.6	5.1
	2	Area clear of ash resid	0.3	2.3	2.9	5.1	0.3	0.2	0.3	1.7	20.9	3.0	25.7	4.0	5.4
	3	Area with ash resid	0.8	6.8	11.1	3.5	0.1	0.9	0.4	0.2	5.0	1.3	22.9	1.3	12.2
	Average	**All points**	**0.7**	**3.6**	**6.1**	**5.6**	**0.4**	**0.5**	**0.3**	**0.6**	**8.3**	**1.5**	**26.9**	**1.8**	**8.6**

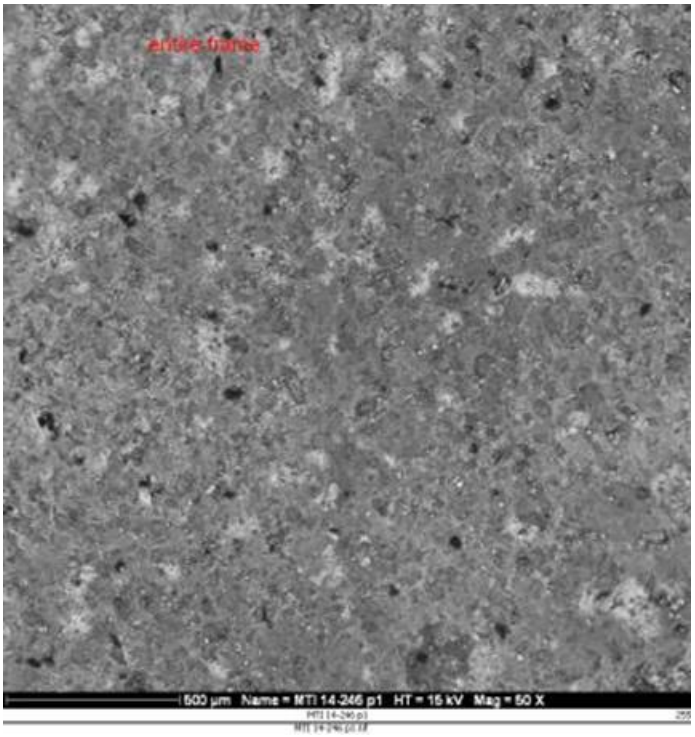

Figure 103. Backscattered electron image of coupon surface (MTI 14-246).

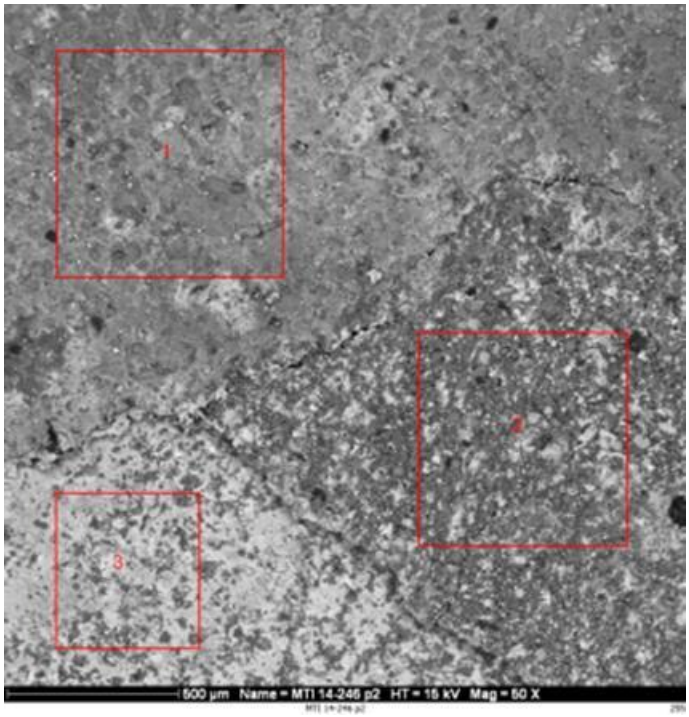

Figure 104. Backscattered electron image of coupon surface (MTI 14-246) showing analysis areas 1 - 3.

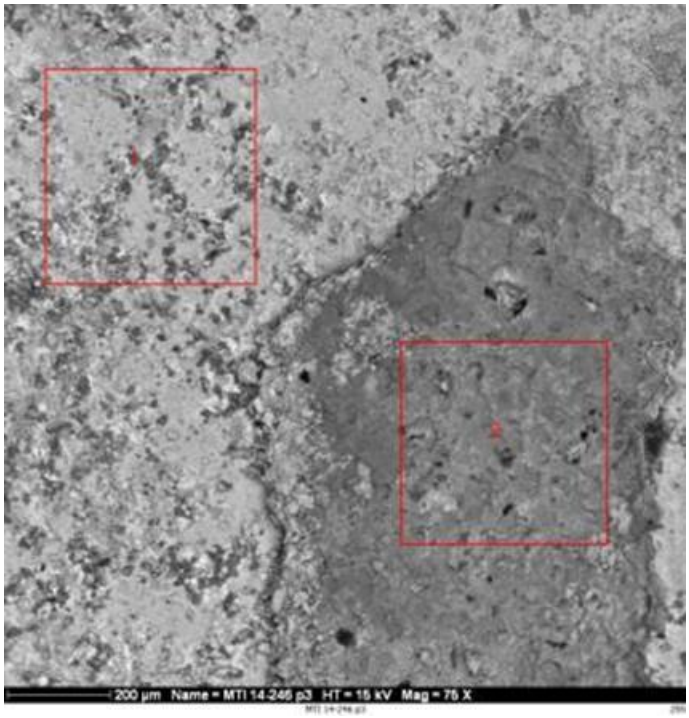

Figure 105. Backscattered electron image of coupon surface (MTI 14-246) showing analysis areas 1 - 2.

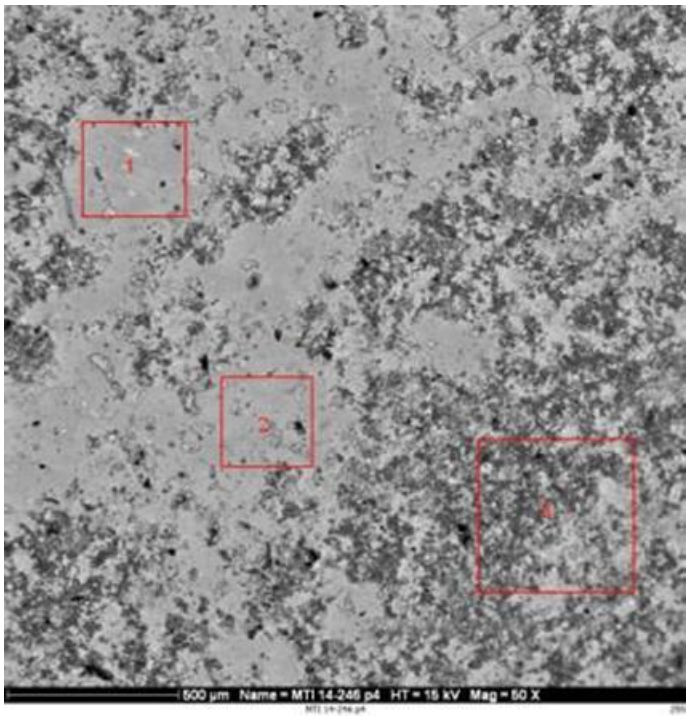

Figure 106. Backscattered electron image of coupon surface (MTI 14-246) showing analysis areas 1 - 3.

5.5.5 Fouling Deposit Sticking Tests

The adhesive strength measurements were performed using MTI sticking test apparatus, as shown in Figure 107. To measure the adhesive strength of the ash layer on the coupons, the burner assembly was lifted off the apparatus and not used. The coupon was placed on the heated plate and allowed to equilibrate to the test temperature. The push rod was used to push or scrape the ash layer from the coupon. The force required to do this was recorded from the pressure transducer readings. The measured force was converted to psi by dividing the measured force by the area of ash removed.

Adhesive strength measurements were attempted for the deposits that adhered to coupons produced in the test matrix summarized in Table 28. The force required to shear the deposits was very small and could not be detected by the pressure transducers.

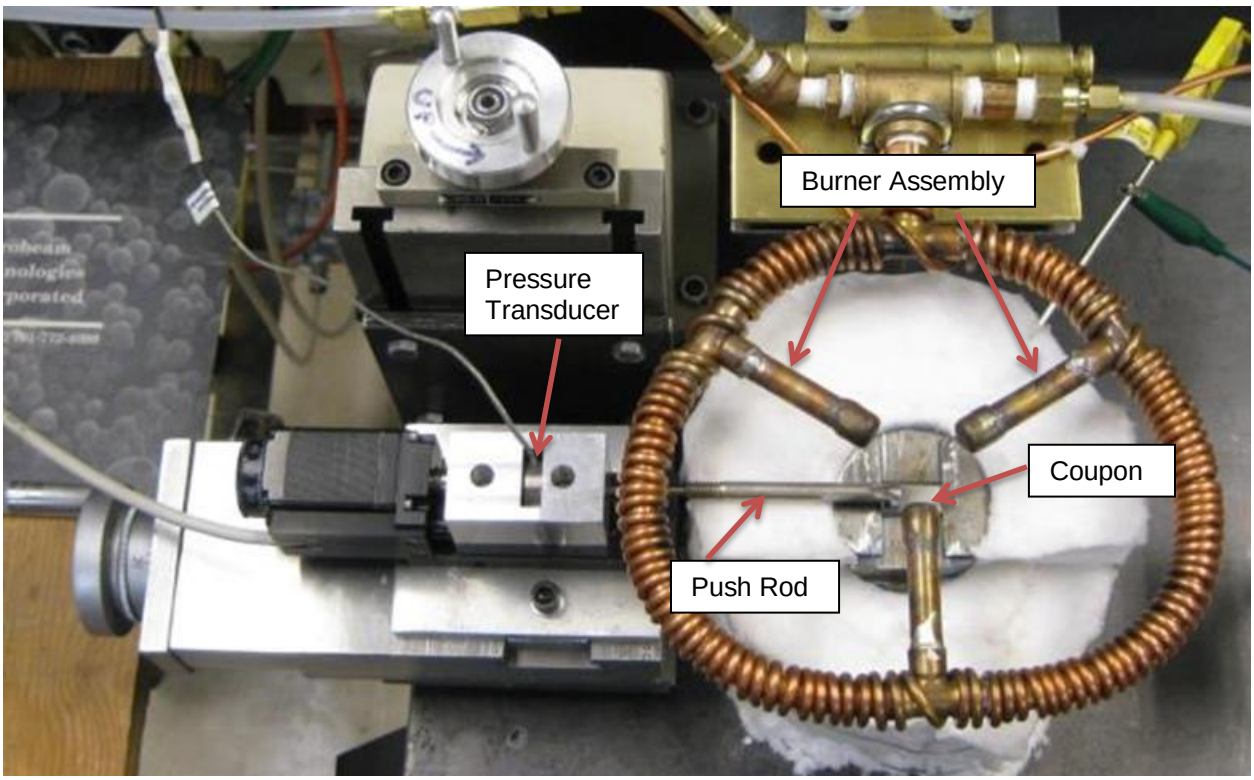

Figure 107. Sticking test apparatus.

The adhesive strength tests for the extreme testing described in Table 38 and Table 39 were conducted at temperatures of 700ºF, 800ºF and 900ºF (371, 427, and 482°C) for the extreme compositions exposed in a muffle furnace. The results are shown in Table 43 for sample 14-247. The ash layer on coupon 14-246 was damaged by handling before the adhesive strength test was performed. As a result, the layer separated from the coupon with little or no force. The adhesive strength was measured first at 700ºF (371°C) by pushing or scraping part of the ash layer from the coupon. The temperature of the coupon was raised to 800ºF (427°C) and the adhesive strength was measured by pushing or scraping off another portion of the ash layer. This was followed by a repeat of the process at 900ºF (482°C).

The process was repeated for the coupons described in Table 39 that were produced in the SFS. The adhesive strength versus temperature is illustrated in Figure 108 for these coupons. The adhesive strength was found to be the highest at 700ºF (371°C) for the coupon with the deposit produced in layers including KCl+FeS+ZnS+Wabash ash. This combination resulted in a strongly bonded deposit to the steel surface. The combination of the potassium along with FeS and ZnS plus Wabash ash produced liquid bonding phases that created bonds with the steel surface. The next strongest adhesive strength was for the combination of NaCl with FeS and Wabash ash. The sodium combined with FeS is known to cause bonding. The bonding strength in most cases decreased with increasing temperature. This is likely due to the increasing instability of sulfides with increasing temperature.

Table 43. Adhesive strength of ash layer on extreme composition coupon 14-247 exposed in a muffle furnace.

Temperature	Strength/S_{700}
700 ºF	1
800 ºF	1.01
900 ºF	1.09

Note: Reference strength S_{700} is set as adhesive strength for coupon 14-247 measured at 700ºF.

Table 44. Adhesive strength of ash layer on extreme composition coupons exposed in the syngas cooler simulator.

		Adhesion Strength / S_{700}		
		700 ºF	800 ºF	900 ºF
Coupon	**Deposit Layers**	-	-	-
14-300	NaCl+FeS+ZnS+Wabash ash	6.79	6.38	5.11
14-302	NaCl+FeS+Wabash ash	9.20	8.21	5.14
14-306	NaCl+ZnS+ Wabash ash	4.79	5.58	3.38
14-307	NaCl+KCl+FeS+ZnS+Wabash ash	4.17	5.56	7.73
14-308	KCl+FeS+ZnS+Wabash ash	15.58	7.54	7.95

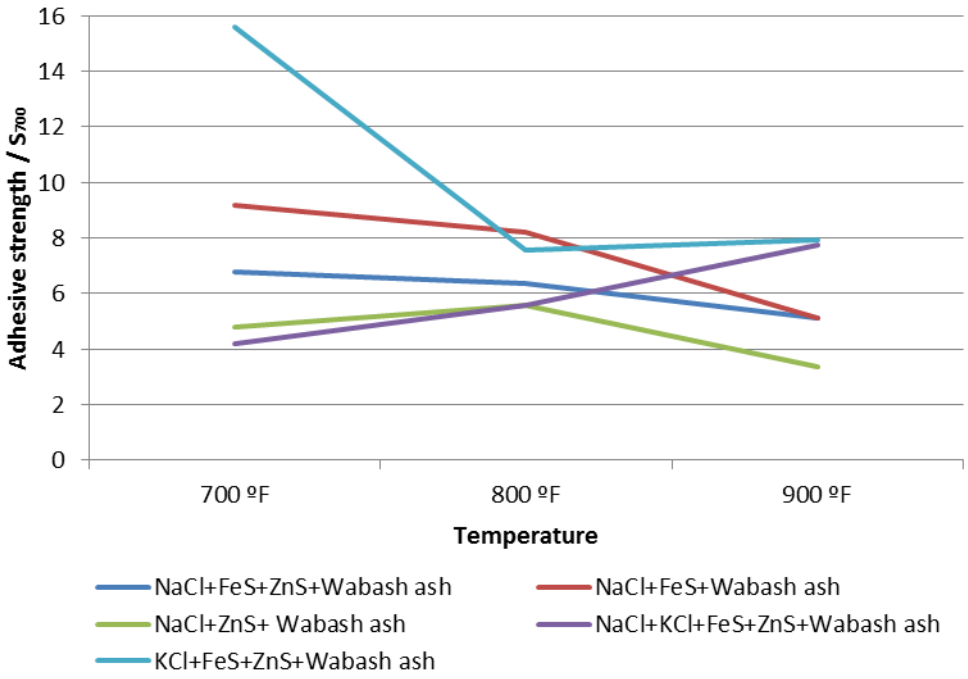

Figure 108. Adhesive strength of ash layer on extreme composition coupons exposed in the syngas cooler simulator as a function of temperature.

5.6 Fouling Removal Subscale Testing (PDE)

5.6.1 Shakedown Results

The shakedown tests included checking the facility for leaks in the supply lines, connections and flanges; and characterization of the PDE for the two lengths and different fuel-oxidizer ratios. After the installation of the entire facility, all the lines and the receiver tank were pressurized and leak detection was performed using leak detector fluid. A detailed check of the all connections for the supply lines and the flanges was carried out to ensure that the facility was leak proof. Once this step was completed the characterization of the PDE started.

The characterization of the PDE included estimating the pressure gain on the platen surface due to the propagating blast wave. This step included the operation of PDE with the two lengths (base and extended) and different fuel-oxidizer ratios. The chosen fuel-oxidizer ratios were 2:1 and 3:1, i.e., stoichiometric and fuel-rich conditions for oxyhydrogen detonations.

To facilitate the analysis, the pressure recorded by the transducer at the platen center is considered. This transducer was used to measure the pressure gain due to the propagating blast wave. Figure 109 shows the pressure gain at the platen center due to the propagating blast wave emitted using the base length PDE and Figure 110 shows the pressure gain due to using the extended length PDE. Both figures show results for stoichiometric and fuel-rich operation. In these figures, the ordinate is the peak pressure recorded by the transducer at the actual ambient tank pressure normalized by the peak pressure for the tank at 1 atm. Such a presentation is suitable for extrapolation to higher ambient pressure.

Figure 109 and Figure 110 show a general linear rise in normalized pressure with ambient pressure. This linear gain can present a serious problem if extrapolated to ambient conditions of 65 – 100 atm. The corresponding blast wave will emit extremely large pressure gain that will likely be destructive.

Since what is needed is adequate overpressure to scour the platen surface, all that is needed is an approach to deliver this overpressure regardless of the ambient. This overpressure turned out from subsequent testing to be about 100 psi.

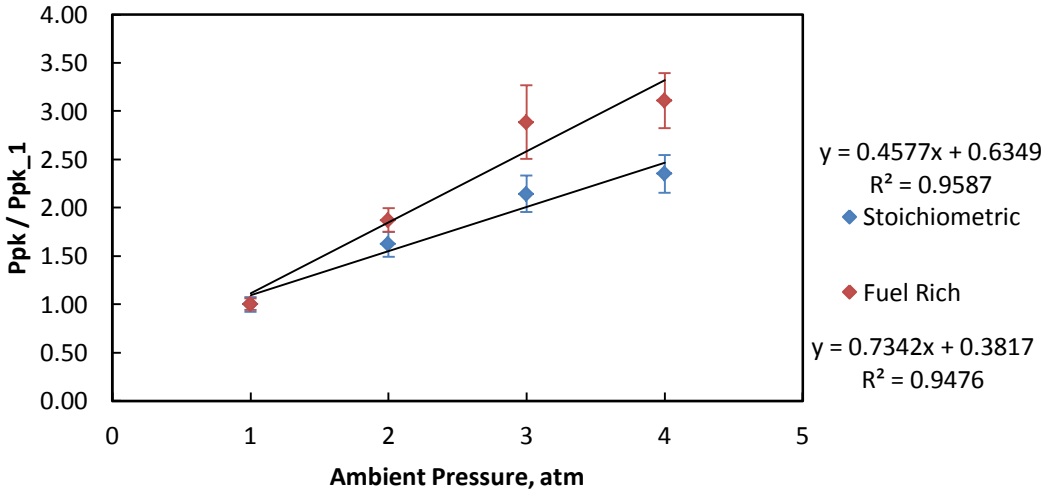

Figure 109. Pressure at the platen center base length PDE.

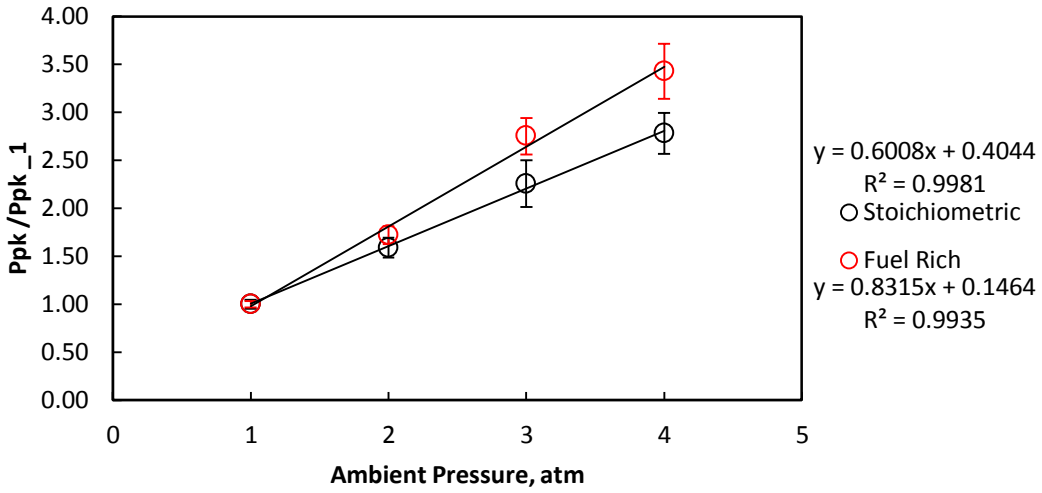

Figure 110. Pressure at platen center for extended length PDE.

5.6.2 Pitot Results

Pitot tests were performed to characterize the pressure distribution in the flow field starting from the exit of the PDE to the trailing edge of the platens. The idea was to use a pitot probe to obtain total pressure measurements at different locations between the PDE exit and trailing edge of the platen. The initial approach was to use a blunt nose cone pitot probe installed with a dynamic pressure transducer (PCB 111A24) was used. The blunt nose cone pitot probe is shown in Figure 111 mounted in the UTA Hypersonic Shock Tunnel Facility.

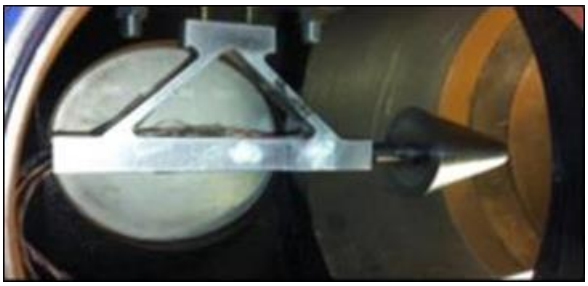

Figure 111. Instrumented blunt nose cone pitot used for total pressure measurement.

Unfortunately, this blunt cone probe caused the transducer to heat up quickly and hardened the sensing diaphragm. The reliability of the data was questionable. Therefore, an existing three-probe rake was used to obtain total pressure measurements of the blast wave. Figure 112 shows the instrumented pitot rake installed in the receiver tank used in this set of experiments. A flush mounted dynamic pressure transducer (PCB 111A23) was mounted to each probe.

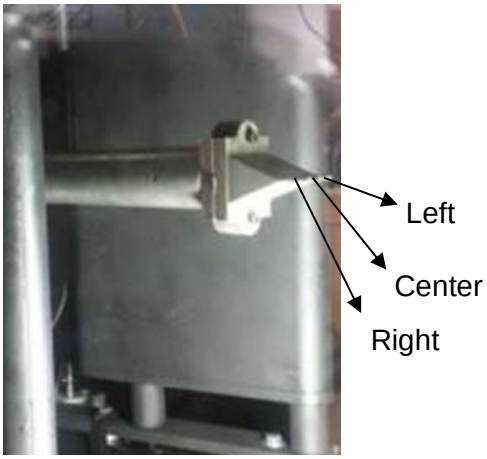

Figure 112. Pitot probe arrangement in the tank.

The blast wave scaling law, originally developed by G. I. Taylor, predicts the location and strength of a propagating shock following an explosion. The radius and pressure immediately behind the shock front are given by the following relations:

$$r = C(\gamma)\left(\frac{Et^2}{\rho_1}\right)^{1/5} \tag{13}$$

$$p_2 = C(\gamma)\left(\frac{E^2\rho_1^3}{t^6}\right)^{1/5} \tag{14}$$

where E is the total explosion energy, ρ_1 the initial ambient air density, t the time following the explosion, and C equal to 1.033 for γ = 1.4. Note that the above relations imply the property of self-similarity. The total pressure behind the shock front can be estimated by using normal shock and isentropic flow relations at the leading edge of the propagating blast wave. The blast wave Mach number with respect to the ambient gas is given by,

$$M_1^2 = \left(\frac{p_2}{p_1} - 1\right)\frac{\gamma + 1}{2\gamma} + 1 \tag{15}$$

Hence, the Mach number and total pressure just behind the shock front is given by,

$$M_2^2 = \frac{1 + \frac{\gamma - 1}{2}M_1^2}{\gamma M_1^2 - \frac{(\gamma - 1)}{2}} \tag{16}$$

$$p_0 = p_2\left(1 + \frac{\gamma - 1}{2}M_2^2\right)^{\frac{\gamma}{\gamma - 1}} \tag{17}$$

Taking E as the amount of energy released by chemical reactions for H_2/O_2 detonation from the amount fuel used to fill the PDE tube, these relations are shown in Figure 113 below. The horizontal axis is scaled by the PDE diameter while the vertical axis is scaled by the ambient pressure which is 1 atm.

Figure 113 shows the validity of the scaling law for $r/D \gtrsim 2.5$. The line through the farfield data is based on Equations (13) – (17). For simplicity, the farfield data can be fitted by an inverse square law,

$$\left(\frac{p_{pit}}{p_o}\right) = 5.87\left(\frac{r}{D}\right)^{-1/2} \tag{18}$$

with a correlation coefficient of $r^2 = 0.935$. The curvefit provides convincing validation of the theoretical analysis. Since the pressure has been normalized, the figure also allows scaling with elevated ambient pressure. For example, at $r/D = 5$, Equation (18) yields the normalized pressure $p_{pit}/p_o = 3.7$. Therefore, if the ambient pressure is 2 atm, the pitot pressure is $p_{pit} = 7.4$ atm.

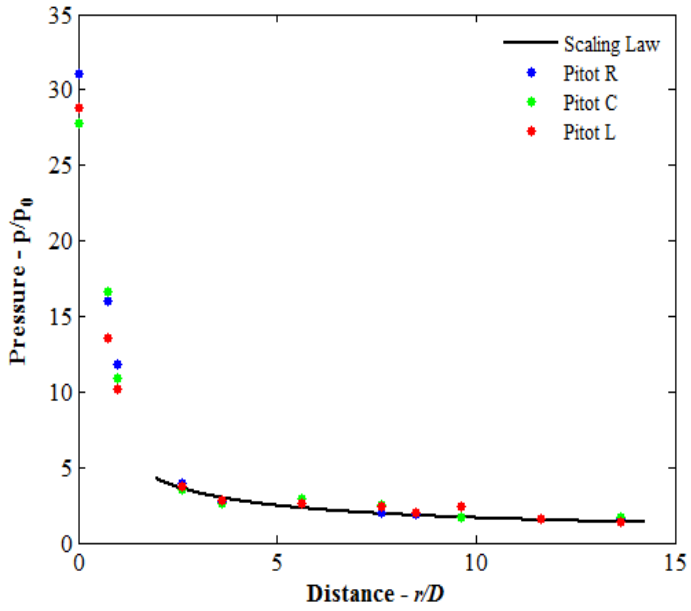

Figure 113. Pressure decay of the blast wave.

Moreover, the pitot rake was swept from up and down and from left to right to map out a region 17 in. (0.4m) from the PDE exit. This location was chosen to be the location of the flyash coupons. The results from the pressure plane survey are shown in Figure 114. The information in Figure 114 portrays that the pressure is highest in between the platens and decreases rapidly on either side. The results confirm that the PDE exhaust is dominated by the impulsive jet, not the blast wave.

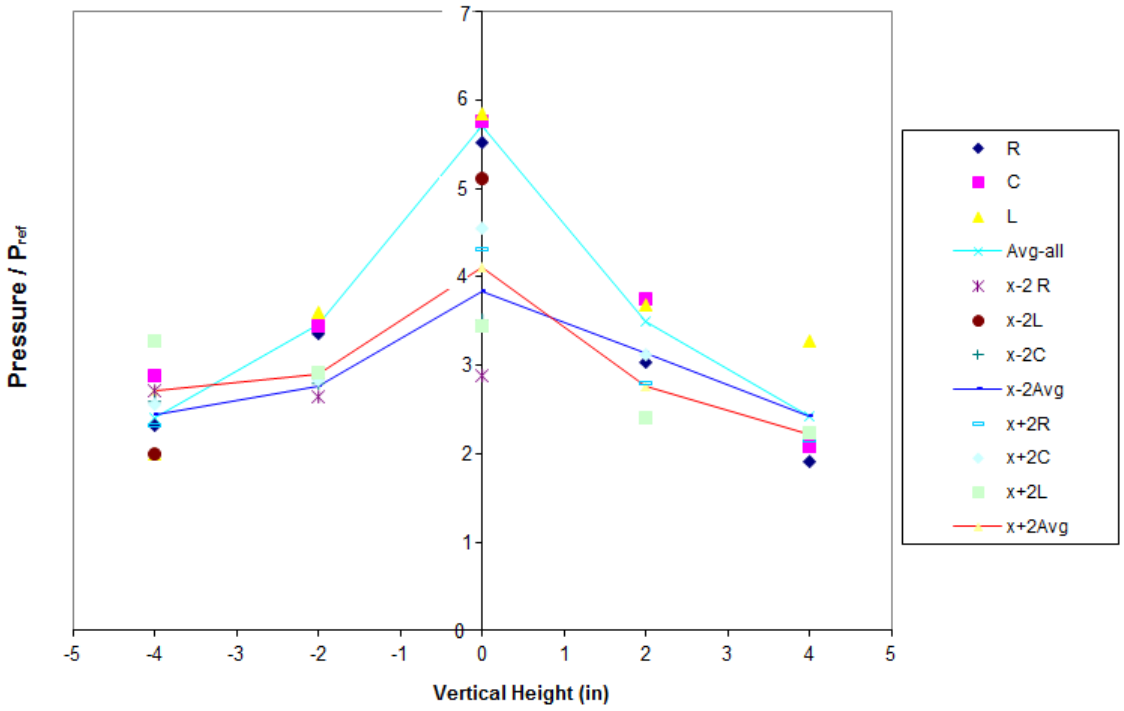

Figure 114. Wave Characterization at the PIV Plane (17in from PDE exit).
Note: P_{ref} is a reference pressure to normalize the pressure value.

5.6.3 PIV and Mie Scattering

Figure 62 shows the SPIV system used for the project where the two cameras were aligned on either side of the PDE axis. Difficulties were encountered with synchronizing between the PDE operating at 1 Hz and the PIV laser operating at 5 Hz. These difficulties meant that images were captured at random which made it extremely problematic if not impossible to obtain quantitative data. Compounding this difficulty is the transient flow. By consensus, mean velocity fields require processing of at least 300 images and turbulence fields even more. A single-shot of the exhaust jet as it arrives at the right platen, imaged by the left camera is shown in Figure 115. A similar image from the right camera is omitted for brevity. The image is uncorrected for parallax. The vortex ring is the main feature of the exhaust jet from the PDE. It appears to be coherent even after traveling 14 inches (0.4 m) from the PDE exit plane. Further discussion of the exhaust jet will be provided next.

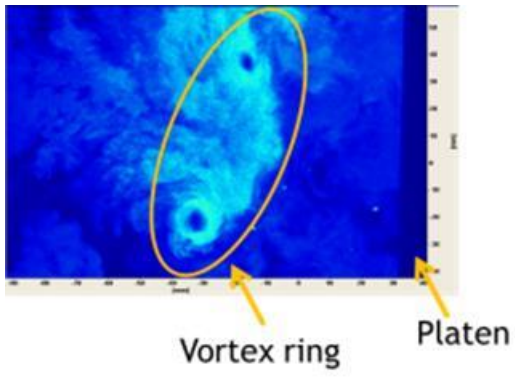

Figure 115. A single-shot image of the exhaust jet approaching the left platen.

Due to the difficulty of obtaining quantitative data, a qualitative visualization was performed. In this approach, the natural glow from the detonation process was used to illuminate the TiO_2 nanoparticles entrained into the flow from a small container attached to the PDE. A high-speed video camera was mounted perpendicular to the jet axis, thereby drastically reducing parallax. A large number of video clips were obtained for under filled, perfectly filled and overfilled cases. A sequence of images of the exhaust jet from an overfilled PDE is shown in Figure 116. The images were captured at a speed 500,000 frames/s with an exposure of 1μs. The frames are shown at 10 μs intervals. The Mie scattering technique is unable to capture the blast wave that precedes the jet. To keep the project on schedule, a Schlieren or Shadowgraphy system that was available was not implemented.

Figure 116 shows the exhaust jet leaving the PDE tube in the first few frames. Only the near field is captured. A vortex ring is developed. Due to the supersonic nature of the flow, a complex triple-shock structure forms downstream of the vortex ring. A shear layer develops from the triple-shock intersection. This shear layer is internal to the jet boundary. The entire vortex ring and triple-shock complex propagates to the right due to the continued exhaust of combustion products. The later frames show the breakdown of the jet. However, the vortex ring propagates with good coherence to impact the platen, as shown in in Figure 115. These visualizations show that the impinging vortex ring may also play a role in flyash removal, in addition to the impinging shock.

Moreover, these visualizations support the pitot probe results in showing an impulsive jet propagating axially. The rapid propagation of the blast wave was not captured in this visualization technique. It is safe to say that the duration of blast is extremely short compared to the exhaust of the jet and the persistence of the starting vortex ring.

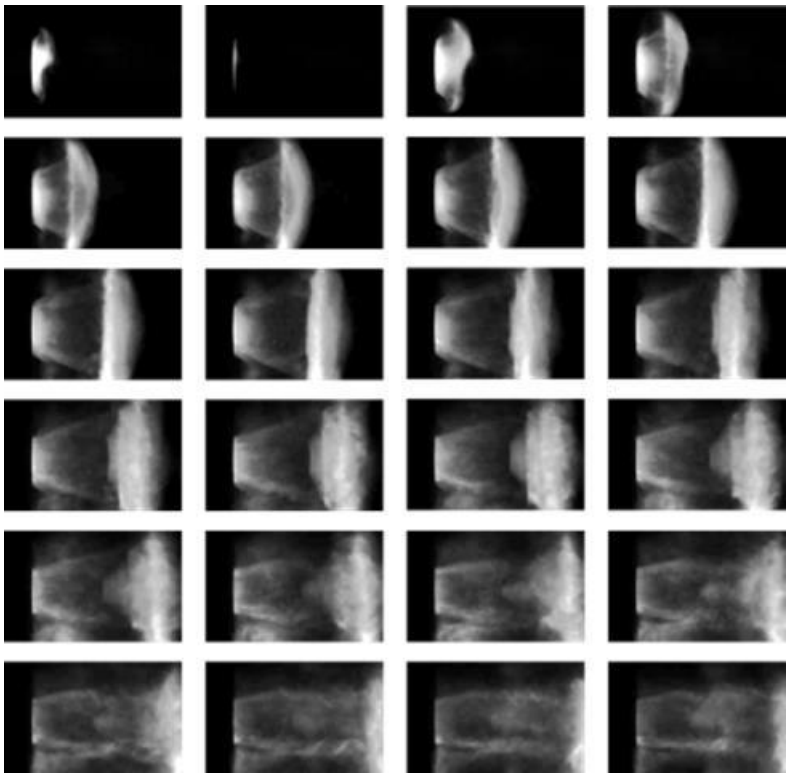

Figure 116. Images of the exhaust jet from an overfilled PDE; sequence from left to right and top to bottom.

5.6.4 Fouling Removal Testing

The fouling coupons received were installed on the platens in the dovetail grooves as shown in Figure 65(a). The installed coupons were first heated to 850ºF (454°C) before they were exposed to the blast waves emitted by the PDE. The coupons were placed at the front center and back center of the platen. A few were placed at the back top as well to evaluate the effectiveness of the PDE on cleaning the deposit at the back. The detailed results are presented in Table 48. The results indicate that the coupons placed at the front center had a higher percentage of removal as compared to the ones placed in the back. A few coupons that were installed on back top were repositioned in front center and retested. The high percentage of ash removed shows the reliability of the process to remove the deposit. Table 45, Table 46, and Table 47 show comparisons of coupons before and after fouling removal testing.

Table 48 shows ash removal of as much as 95% but typically in the 40-60% range after PDE shots.

Table 45. Photographic comparison of coupons before and after fouling removal testing.

Coupon #	PDE Operation	Location	Before Test	PDE Shots	After Test	Removal Rate
14-265	H_2:O_2 = 3:1 Length: 72in filling: 90% Pressure: 51psia	BC		60		82.4%
14-273	H_2:O_2 = 3:1 Length: 72in filling: 90% Pressure: 51psia	BT	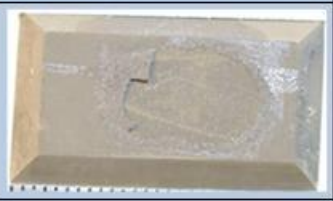	60	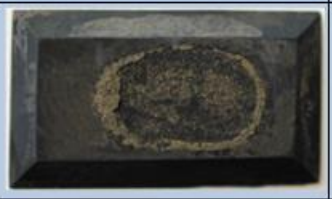	52.6%
14-294	H_2:O_2 = 3:1 Length: 72in filling: 90% Pressure: 51psia	FC		60		78.7%
14-267	H_2:O_2 = 3:1 Length: 72in filling: 90% Pressure: 51psia	FC		15		95.2%
14-282	H_2:O_2 = 3:1 Length: 72in filling: 90% Pressure: 51psia	BC	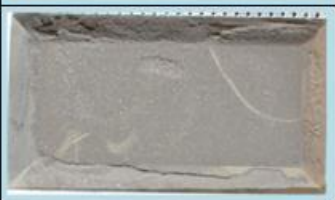	15		73.3%
14-295	H_2:O_2 = 3:1 Length: 72in filling: 90% Pressure: 51psia	BT		15		22.2%
14-271	H_2:O_2 = 3:1 Length: 72in filling: 90% Pressure: 51psia	FC		50		76.9%
14-297	H_2:O_2 = 3:1 Length: 72in filling: 90% Pressure: 51psia	BC		50		58.8%

Coupon #	PDE Operation	Location	Before Test	PDE Shots	After Test	Removal Rate
14-272	H_2:O_2= 3:1 Length: 72in filling: 90% Pressure: 51psia	BC		75		31.9%
14-275	H_2:O_2= 3:1 Length: 72in filling: 90% Pressure: 51psia	FC		75		49.2%
14-276	H_2:O_2= 3:1 Length: 72in filling: 90% Pressure: 51psia	FC		56	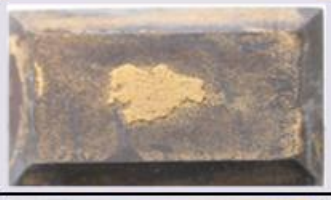	94.1%
14-278	H_2:O_2= 3:1 Length: 72in filling: 90% Pressure: 51psia	BC		56	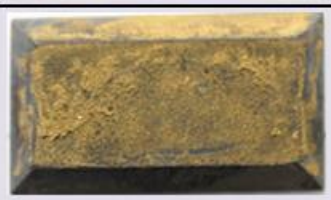	81.5%
14-279	H_2:O_2= 3:1 Length: 72in filling: 90% Pressure: 51psia	FC		60		57.1%
14-269	H_2:O_2= 3:1 Length: 72in filling: 90% Pressure: 51psia	BC		60		47.1%
14-289	H_2:O_2= 3:1 Length: 72in filling: 90% Pressure: 51psia	FC		30		94.3%
14-264	H_2:O_2= 3:1 Length: 72in filling: 90% Pressure: 51psia	BC		30	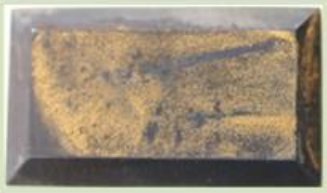	94.6%

Coupon #	PDE Operation	Location	Before Test	PDE Shots	After Test	Removal Rate
14-291	H_2:O_2 = 3:1 Length: 72in filling: 90% Pressure: 51psia	FC		30	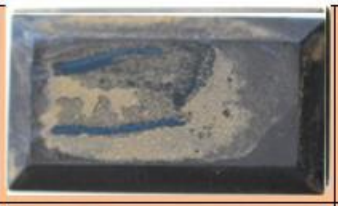	70.3%
14-311	H_2:O_2 = 3:1 Length: 72in filling: 90% Pressure: 51psia	BC	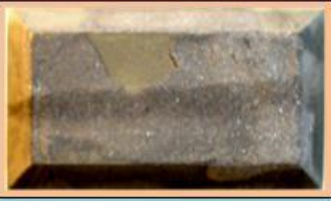	30		52.2%
14-293	H_2:O_2 = 3:1 Length: 72in filling: 90% Pressure: 51psia	FC		60	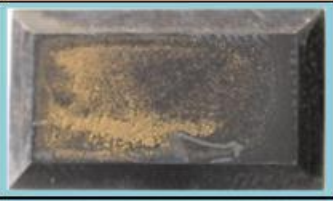	64.1%
14-277	H_2:O_2 = 3:1 Length: 72in filling: 90% Pressure: 51psia	BC		60	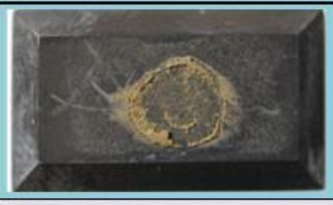	65.8%
14-299	H_2:O_2 = 3:1 Length: 72in filling: 90% Pressure: 51psia	FC		60		94.3%
14-287	H_2:O_2 = 3:1 Length: 72in filling: 90% Pressure: 51psia	BC		60		81.6%
14-301	H_2:O_2 = 3:1 Length: 72in filling: 90% Pressure: 51psia	FC		105		52.6%
14-313	H_2:O_2 = 3:1 Length: 72in filling: 90% Pressure: 51psia	BC		105		50.8%

Coupon #	PDE Operation	Location	Before Test	PDE Shots	After Test	Removal Rate
14-308	H_2:O_2 = 3:1 Length: 72in filling: 90% Pressure: 51psia	FC		60		66.7%
14-309	H_2:O_2 = 3:1 Length: 72in filling: 90% Pressure: 51psia	BC		60	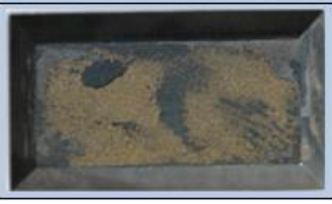	62.5%

Table 46. Photographic comparison of coupons before and after fouling removal testing for extreme condition cases.

Coupon #	PDE Operation	Location	Before Test	PDE Shots	After Test	Removal Rate
14-236	H_2:O_2 = 3:1 Length: 72in filling: 90% Pressure: 51psia	FC		15		3.4%
14-242	H_2:O_2 = 3:1 Length: 72in filling: 90% Pressure: 51psia	FC		51		38.0%
14-244	H_2:O_2 = 3:1 Length: 72in filling: 90% Pressure: 51psia	BC		51		65.4%
14-245	H_2:O_2 = 3:1 Length: 72in filling: 90% Pressure: 51psia	FC		60		49.3%

Table 47. Photographic comparison of coupons for before, after, and after retesting of fouling removal testing.

Coupon #	PDE Operation	Location	Before Test	PDE Shots	After Test	Removal Rate	PDE Shots	After Re-test	Removal Rate
14-285	H_2:O_2= 3:1 Length: 72in filling: 90% Pressure: 51psia	FC	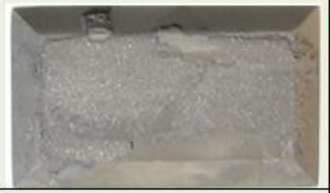	30		48.5%	30		54.5%
14-266	H_2:O_2= 3:1 Length: 72in filling: 90% Pressure: 51psia	BC		56		55.8%	30		85.9%
14-295	H_2:O_2= 3:1 Length: 72in filling: 90% Pressure: 51psia	FC		10		22.2%	10		51.9%
14-283	H_2:O_2= 3:1 Length: 72in filling: 90% Pressure: 51psia	BC		30		20.6%	10		51.6%

Table 48. Fouling coupon removal testing results

MTI ID#	Date Prepped	Coupon Pretreatment	Pretreatment Temp (F)	Ash Description	Sintering Temp (F)	Metal Temp (F)	Blank coupon weight (grams)	Column1	Initial Coupon Weight after Pre-treatment (grams)	Coupon Weight as shipped (grams)	Coupon Weight as Received (grams)	Ash Deposit Weight (grams)	Ash Received Weight (grams)	Ash Transport Weight loss (grams)	Ash Transport % Loss	Ash % Received	Tested - if yes: position in platen	**After test weight**	**Remaining Ash weight**	**Ash % removed**	**Comments**	Weight after Retest	Ash Weight after Retest	% removed after retest
MTI 14-264	9/17/2014	yes	850	Wabash A	700	700	3.3493	3.351	3.3508	3.4902	3.3730	0.1394	0.0222	0.1172	0.8407	0.1593	BC	3.3520	0.0012	94.59				
MTI 14-266	9/17/2014	yes	850	Wabash A	700	700	3.4335	3.436	3.4357	3.5380	3.4590	0.1023	0.0233	0.0790	0.7722	0.2278	BT	3.4460	0.0103	55.79	BC-retest	3.4390	0.0033	85.84
MTI 14-276	10/15/2014	yes	850	Wabash A	700	700	3.2849	3.286	3.2863	3.4276	3.3150	0.1413	0.0287	0.1126	0.7969	0.2031	FC	3.2880	0.0017	94.08				
MTI 14-278	10/15/2014	yes	850	Wabash A	700	700	3.4015	3.404	3.4040	3.5042	3.4310	0.1002	0.0270	0.0732	0.7305	0.2695	BC	3.4090	0.0050	81.48				
MTI 14-267	9/17/2014	yes	850	Wabash A	700	700	3.3816	3.382	3.3823	3.4020	3.3970	0.0197	0.0147	0.0050	0.2538	0.7462	FC	3.3830	0.0007	95.24				
MTI 14-282	10/16/2014	yes	850	Wabash A	775	775	3.3609	3.363	3.3630	3.4393	3.3780	0.0763	0.0150	0.0613	0.8034	0.1966	BC	3.3670	0.0040	73.33				
MTI 14-285	10/17/2014	yes	850	Wabash A	850	850	3.3410	3.342	3.3415	3.3699	3.3580	0.0284	0.0165	0.0119	0.4190	0.5810	BT	3.3500	0.0085	48.48	FC-retest	3.3490	0.0075	54.55
MTI 14-295	10/17/2014	yes	850	Wabash A	775	775	3.3156	3.318	3.3175	3.3310	3.3310	0.0135	0.0135	0.0000	0.0000	1.0000	BT	3.3280	0.0105	22.22	FC-retest	3.3240	0.0065	51.85
MTI 14-283	10/16/2014	yes	850	Wabash A	775	775	3.3507	3.352	3.3523	3.3637	3.3620	0.0114	0.0097	0.0017	0.1491	0.8509	BT	3.3600	0.0077	20.62	BC-retest	3.3570	0.0047	51.55
MTI 14-291	10/15/2014	yes	850	Wabash A	700	700	3.2597	3.262	3.2622	3.2789	3.2750	0.0167	0.0128	0.0039	0.2335	0.7665	FC	3.2660	0.0038	70.31				
MTI 14-311	10/28/2014	yes	850	Wabash A	850	850	3.4064	3.408	3.4076	3.4241	3.4210	0.0165	0.0134	0.0031	0.1879	0.8121	BC	3.4140	0.0064	52.24				
MTI 14-265	9/17/2014	yes	850	Wabash A	700	700	3.1793	3.181	3.1805	3.4096	3.1890	0.2291	0.0085	0.2206	0.9629	0.0371	BC	3.1820	0.0015	82.35				
MTI 14-269	10/9/2014	yes	850	Wabash A	775	775	3.4309	3.433	3.4325	3.4433	3.4410	0.0108	0.0085	0.0023	0.2130	0.7870	BC	3.4370	0.0045	47.06				
MTI 14-272	10/10/2014	yes	850	Wabash A	850	850	3.3232	3.325	3.3246	3.3483	3.3340	0.0237	0.0094	0.0143	0.6034	0.3966	BC	3.3310	0.0064	31.91				
MTI 14-277	10/15/2014	yes	850	Wabash A	700	700	3.3949	3.396	3.3964	3.4061	3.4040	0.0097	0.0076	0.0021	0.2165	0.7835	BC	3.3990	0.0026	65.79				
MTI 14-275	10/10/2014	yes	850	Wabash A	850	850	3.4127	3.414	3.4139	3.4272	3.4200	0.0133	0.0061	0.0072	0.5414	0.4586	FC	3.4170	0.0031	49.18				
MTI 14-287	10/17/2014	yes	850	Wabash A	850	850	3.3898	3.391	3.3911	3.3994	3.3960	0.0083	0.0049	0.0034	0.4096	0.5904	BC	3.3920	0.0009	81.63				
MTI 14-299	10/20/2014	yes	850	Wabash A	850	850	3.3346	3.337	3.3367	3.3462	3.3420	0.0095	0.0053	0.0042	0.4421	0.5579	FC	3.3370	0.0003	94.34				
MTI 14-301	10/24/2014	yes	850	Wabash A	700	700	3.2918	3.294	3.2943	3.3022	3.3000	0.0079	0.0057	0.0022	0.2785	0.7215	FC	3.2970	0.0027	52.63				
MTI 14-271	10/9/2014	yes	850	Wabash A	775	775	3.3543	3.356	3.3564	3.3627	3.3590	0.0063	0.0026	0.0037	0.5873	0.4127	FC	3.3570	0.0006	76.92				
MTI 14-273	10/10/2014	yes	850	Wabash A	850	850	3.3335	3.335	3.3351	3.3489	3.3370	0.0138	0.0019	0.0119	0.8623	0.1377	BT	3.3360	0.0009	52.63				
MTI 14-279	10/15/2014	yes	850	Wabash A	700	700	3.3555	3.358	3.3575	3.3615	3.3610	0.0040	0.0035	0.0005	0.1250	0.8750	FC	3.3590	0.0015	57.14				
MTI 14-297	10/17/2014	yes	850	Wabash A	850	850	3.2744	3.276	3.2763	3.2789	3.2780	0.0026	0.0017	0.0009	0.3462	0.6538	BC	3.2770	0.0007	58.82				
MTI 14-303	10/24/2014	yes	850	Wabash A	700	700	3.2866	3.289	3.2885	3.2928	3.2900	0.0043	0.0015	0.0028	0.6512	0.3488	FC	3.2890	0.0005	66.67				
MTI 14-309	10/27/2014	yes	850	Wabash A	775	755	3.3593	3.359	3.3594	3.3640	3.3610	0.0046	0.0016	0.0030	0.6522	0.3478	BC	3.3600	0.0006	62.50				
MTI 14-293	10/16/2014	yes	850	Wabash A	775	775	3.2998	3.301	3.3012	3.3116	3.3090	0.0104	0.0078	0.0026	0.2500	0.7500	FC	3.3040	0.0028	64.10				
MTI 14-294	10/16/2014	yes	850	Wabash A	775	775	3.3036	3.305	3.3051	3.3953	3.3140	0.0902	0.0089	0.0813	0.9013	0.0987	FC	3.3070	0.0019	78.65				
MTI 14-313	10/28/2014	yes	850	Wabash A	850	850	3.4468	3.448	3.4481	3.4547	3.4540	0.0066	0.0059	0.0007	0.1061	0.8939	BC	3.4510	0.0029	50.85				
MTI 14-289	10/20/2014	yes	850	Wabash A	700	700	3.3242	3.3262	3.3262	3.3612	3.3580	0.0350	0.0318	0.0032	0.0914	0.9086	FC	3.3270	0.0008	97.48				
MTI 14-234	10/31/2014	yes	850	NaCl + FeS	700	700	n/a	3.4096	3.4096	3.4920	3.4720	0.0824	0.0624	0.0200	0.2427	0.7573	FC	3.4570	0.0474	24.04				
MTI 14-235	10/31/2014	yes	850	NaCl+Zns-	700	700	n/a	3.3790	3.3790	3.4443	3.4300	0.0653	0.0510	0.0143	0.2190	0.7810	BC	3.4100	0.0310	39.22				
MTI 14-236	10/31/2014	yes	850	NaCl+FeS-	700	700	n/a	3.3117	3.3117	3.4679	3.4000	0.1562	0.0883	0.0679	0.4347	0.5653	FC	3.3970	0.0853	3.40				
MTI 14-242	11/6/2014	yes	850	NaCl+FeS-	700	700	n/a	3.4227	3.4227	3.5377	3.5260	0.1150	0.1030	0.0120	0.1020	0.8980	FC	3.4620	0.0393	38.00				
MTI 14-244	11/6/2014	yes	850	NaCl+FeS-	700	700	n/a	3.3008	3.3008	3.3994	3.3730	0.0986	0.0720	0.0260	0.2680	0.7320	BC	3.3480	0.0472	65.40				
MTI 14-245	11/7/2014	yes	850	NaCl+FeS-	700	700	n/a	3.3787	3.3787	3.5642	3.4010	0.1855	0.0223	0.1632	0.8798	0.1202	FC	3.3900	0.0113	49.33				

5.7 Conclusions and Recommendations

A pulse detonation engine (PDE) test facility was developed for subscale testing of fouling removal and installed in the premises of the Aerodynamics Research Center at UTA. The facility allowed testing PDEs with different geometries, including both a base length and an extended length detonation tubes that exhausted into a receiver tank. The PDE, which was cooled with ordinary tap water, operated with hydrogen and oxygen at frequencies of up to 1 Hz. The receiver tank was equipped with rails for mounting platens which in turn mounted fouling coupons on the front and back. These platens were placed at an angle to the direction of the PDE exhaust jet at distances that allowed the data to be extrapolated to full scale. The platens were equipped with ring heaters that provided localized heating of the fouling coupons to about 850^{o}F (454°C). The receiver tank contained a number of ports for optical and instrumentation access. The hydrogen fuel, oxygen and purge air were supplied through a "gas cart." The hydrogen and oxygen were delivered from bottles while the purge air and the air for pressurizing the receiver tank were delivered from a 175 psi compressor. The gas cart provided control valves, flow rate meters and flash arrestors. The control valves allowed the mixture ratio and amount of fill to be prescribed. A number of data acquisition systems were connected to the PDE and to the platen. The DAQ was used to control the operation remotely. During tests, all personnel were evacuated to a strengthened control room. Monitors in the control room displayed up-to-date conditions of the facility.

Typical tests require less than 60 shots. The receiver tank has an internal diameter of 42-inch (1.1 m) and an overall length of 80 inch (2 m) and was designed to operate at a maximum pressure of 5 atm. The tank was sized with the PDE and platens to ensure that waves reflected from the tank walls will have a minimal effect on the platens. The tank volume together with manual and automatic valves was able to maintain a nominal constant pressure during a test. The tank was equipped with a relief valve and can also be vented remotely by a solenoid or manual valve.

After assembly, a shakedown procedure was undertaken to ensure safe operation. A test campaign without fouling coupons allowed the facility to be characterized. The facility operated as designed, achieving the rated pressure safely. Complications with particle image velocimetry prevented quantitative data to be obtained. This was replaced by a qualitative Mie scattering visualization that showed an impulsive jet with a prominent vortex ring exiting the PDE. A pitot survey showed that the peak pressure at some distance from the PDE exit exhibit a scaled, far field behavior. Another scaling behavior of the peak platen impact pressure at elevated ambient tank pressure and tank pressure at 1 atm was obtained.

The test campaign with fouling coupons showed that repeated detonation waves with the fouling coupons located 8.5 diameters downstream of the PDE were able to remove the flyash. Ash removal of as much as 95% but typically in the 40-60% range after 60 shots could be achieved.

The experiments demonstrated the feasibility of fouling removal from repeated detonations based on subscale testing. Recommendations are proposed to transition the concept to a commercial product. These recommendations will require the construction of a test facility rated at or near full pressure and include:

1) Further validate the scaling law through a larger and higher pressure facility
2) Develop surrogate fouling coupons with well-defined properties to allow for a systematic quantification of material removal

3) Perform systematic repeated detonations on surrogate fouling coupons to quantify the removal rate of both coupons mounted in front and at the back of the platen versus the number of detonation pulses.

6.0 Task 6 – Continuous Blowdown System for Slag Handling

6.1 Introduction

In an IGCC system, high pressure slag-water slurry is a gasifier by-product stream which must be removed from the gasifier, depressurized and dewatered prior to sale or disposal. The current slag handling system in an IGCC plant is a lockhopper-based batch process where the lockhopper vessel is located beneath the gasifier quench chamber (or radiant syngas cooler slag sump) and the slag crusher. During operation, the lockhopper system alternates between collection and dump modes. In the collection mode, the lockhopper is at full gasification pressure and the inlet valves (top valve and emergency backup valve) are open, allowing the slag to pass out of the quench chamber or radiant syngas cooler (RSC) sump, through the slag crusher and lockhopper inlet valves, and into the lockhopper. In the dump mode, the lockhopper is isolated from the quench chamber or RSC sump by closing both inlet valves. The recirculation loop, which assists the flow of slag into the lockhopper by establishing a downwards flow of water through the lockhopper, is also stopped. The lockhopper is then depressured by momentarily opening a valve in a small line connected to the gasification plant's black water handling system. After depressurization, the outlet valve on the flush drum is opened, followed by the lockhopper outlet valve (the bottom valve). Water from the elevated flush drum flows by gravity through the lockhopper and flushes the slag down into the slag drag conveyor/sump system where the coarse slag is separated from the fines. The coarse slag is then discharged off-site while the fines are sent to the fines handling system to be ultimately recycled back to the gasifier. Following slag discharge, the bottom lockhopper valve is closed, the lockhopper vessel is repressured, the top lockhopper valves are opened and the cycle is restarted.

This process includes several vessels and pumps designed to periodically flush solids out of the large lockhopper vessel. In order to function properly, all of this equipment is vertically aligned within the gasifier support structure in order to take advantage of gravitational flow. This requirement adds cost to the gasification plant. Additionally, three large, expensive block valves keep the vessel alternately in line with (solids collection mode) and isolated from (solids dump mode) the high pressure gasifier quench chamber. Both the cost of the overall system and the potential reliability issues associated with the three constantly switching lockhopper valves suggest that there may be a less expensive, more reliable way of moving slag from a gasifier quench chamber or RSC sump. Therefore, the aim of DOE's Feasibility Studies to Improve Plant Availability and Reduce Total Installed Cost in IGCC Plants Task 6 is to develop a preliminary design for an improved blow down system for slag handling for IGCC applications that meets the availability/cost goals of the program. The overall program goal is to develop technologies to contribute significantly to the Gasification Program's cost reduction goals and according to the DOE FOA, the proposed process must "either increase availability of a reference plant while maintaining current costs, or maintain the availability at decreased costs or both". The improved blowdown system for slag handling that has been developed in this project falls mainly into the latter category: decreasing cost without sacrificing reliability when compared with the conventional slag handling system. In carrying out this task, GE decided to replace the lockhopper-based batch system with an improved continuous blowdown process because of the following advantages of a continuous process:

1. Being able to locate the gasifier closer to grade, thereby improving accessibility and reducing structure cost
2. Being able to use smaller and less severe service isolation valves that are less expensive and longer lasting
3. Reduced water requirements for flushing
4. Have less complex control sequence

5. Potential applicability to other industries: a continuous pressure letdown process for solids-water slurries with dissolved gas may have a wide range of applications including mining and offshore drilling. Just as in IGCC Gasification, these other industries value technology that conserves water, improves reliability, and reduces cost.

GE took the following approach in developing a new, robust pressure letdown system for slag-water slurry:

- *Survey of Options* – A survey was conducted across several industries to identify a number of potential processes for continuously depressuring slag-water slurry. Based on a set of criteria, the three most promising technologies were down selected.

- *Evaluation of Top Three Candidates* – Conceptual designs and cost estimates were developed for each of these three leading candidates, which were then compared based on process performance and cost. Based on this techno-economic comparison, the continuous process based on a slag-water letdown turbine was selected as the final choice for further analysis and development. This process was thereafter referred to as the Continuous Slag Removal Process (CSRP).

- *Evaluation and Development of Final Choice* – A preliminary process design and cost estimate were developed for the CSRP. This allowed the conventional lockhopper system and the CSRP to be compared based on performance, cost and reliability. Aspen models were developed and executed in order to identify optimization areas for the CSRP, including a sensitivity analysis on critical parameters. The continuous flow of slag and water through the quench chamber reduces the quench blowdown to the Black Water Flash (BWF) system; therefore the sizing and cost impact to the BWF system was also analyzed. Finally, prompted by feedback from a May 2014 DOE Peer Review Session, a hybrid CSRP system that combines the functions of both the slag handling and the BWF units was developed. A gasification plant using this hybrid CSRP-BWF system was compared with a gasification plant using standalone CSRP and BWF systems in an effort to explore opportunities for additional cost savings.

6.2 Technology Selection

6.2.1 GE's Current Lockhopper System

Most of the ash present in ash-containing feedstocks is removed from the Gasification Unit as solid, glass-like slag through the lockhopper system (Figure 117). The lockhopper is a batch process that follows a specific collect/depressure/dump/repressure sequence to handle the slag/ash/char from the gasification quench chamber or RSC sump. The lockhopper vessel is located beneath the gasifier quench chamber or RSC slag sump (depending upon the design of the gasifier heat recovery system) and the slag crusher. During operations, the lockhopper system alternates between collection and dump modes. In the collection mode, the lockhopper is at full gasification pressure, the outlet (bottom valve) is closed and the inlet valves (the top lockhopper valve and the emergency backup valve) are open. This allows the slag to pass out of the quench chamber or RSC sump, through the slag crusher and lockhopper inlet valves, and into the lockhopper. The typical collection portion of the cycle lasts 15-30 minutes. Although the density and size of the slag causes it to settle very rapidly, the net transport of slag into the lockhopper is facilitated by the lockhopper recirculation loop, which pumps relatively solids-free water from behind a sleeve in the top of the lockhopper into the quench or RSC sump. This in turn causes a similar volumetric flow rate of higher slag and fines containing water from the quench chamber or RSC sump into the Lockhopper. In the dump mode, the lockhopper is isolated from the quench chamber or RSC sump by closing the inlet valves. The recirculation loop is also stopped. And

the lockhopper is depressured by opening a valve on a small line that allows the pressure to be relieved to a safe location in the gasification plant BWF system. After it has been depressured, the outlet valve on the flush drum is opened, followed by the lockhopper outlet valve (the bottom valve), which is opened for a short period of time (up to 1 minute). Water from the elevated flush drum flows by gravity through the lockhopper and flushes the slag from the lockhopper downwards into a slag drag conveyor/sump system.

The bottom outlet valve of the lockhopper is timed to close so that the lockhopper is left full of water from the flush drum after the bottom outlet valve has fully closed. Once the bottom lockhopper valve has completely closed, then the flush water outlet valve is also closed. The lockhopper is then repressured with high pressure process water. By ensuring the lockhopper is completely full at the end of the dump cycle, the amount of high pressure water used and the time it takes to repressure the lockhopper is minimized. The time elapsed between the collection of the slag and the flushing of the lockhopper until the collection of solids begins again is called the cycle time.

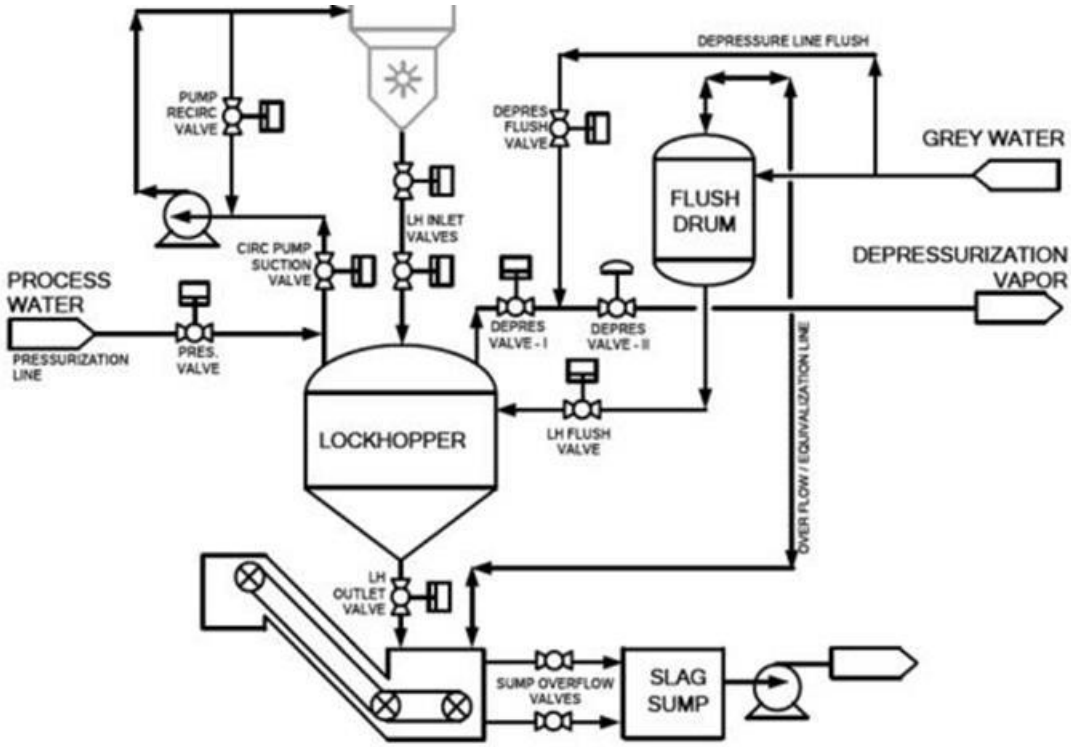

Figure 117. Lockhopper System Schematic

The aim of DOE's Feasibility Studies to Improve Plant Availability and Reduce Total Installed Cost in IGCC Plants Task 6 is to develop a preliminary design for an improved blow down system for slag handling that will replace the lockhopper system, thereby saving plant cost without sacrificing plant availability. For the improved slag handling system without a lockhopper, the IGCC layout can be modified to place the gasifier closer to grade, simplifying access for operations and maintenance personnel. The Continuous Slag Removal Process (CSRP) that was ultimately developed is much more compact than the lockhopper system, which requires that all the key pieces of equipment – the slag

crusher, the two inlet valves, the lockhopper vessel, the outlet valve and the slag drag conveyor/sump system – be stacked one on top of the other in order to facilitate gravity-driven flow of slag and water. With the elimination of the batch sequence of operations that cycle the vessel contents between high pressure and low pressure, the isolation valve service is less severe, leading to a longer lasting and less costly design. Isolation valve sizes are also smaller. Use of the CSRP also reduces operating cost by reducing the flushing water demand which, in turn, reduces water requirements for IGCC plant. Control of the CSRP is also simpler and less expensive as it does not require the complicated set of batch sequence controls required by the lockhopper system. Finally, a continuous pressure letdown process for slag-water slurries with dissolved gas can be applied to a wide range of other industries, such as mining and offshore oil drilling that must depressure and handle solids-water slurries.

The steps used in developing a replacement process for the lockhopper system were: 1) survey existing technologies; 2) develop a shortlist of the three most promising technologies for further analysis; and 3) identify, evaluate and enhance the most promising replacement technology.

6.2.2 Survey of Existing Technologies

In surveying potential existing technologies to use in developing an improved slag handling system, we made use of a number of different sources. The first section summarizes information that was gleaned from publically available texts. The next section lists patented concepts. And the final section under this heading lists summary performance information from several commercial gasification plants that use lockhopper systems for slag removal.

6.2.2.1 Public Scientific Literature

Batch operated lockhoppers are used to transport solids slurries between high and low pressure locations and vice versa. Their semi-continuous counterparts involve cyclic batching of two or more vessels that operate in parallel (Figure 118, Streat). The idea is to have one vessel valved into the gasifier quench chamber in high pressure, collection mode while the other is dumping to the low pressure, slag drag conveyor/sump system. As vessel one reaches its capacity and vessel two is empty, they switch roles. Here, a third vessel is needed to get the empty vessel up to pressure using pumped recycle water. Figure 119 (Szivak, et all) uses essentially the same approach except that three legs of isolatable piping are used in place of the large volume vessels. Although these semi-continuous alternatives could replace the current IGCC lockhopper operation, there would be no economic incentive to do so because of the increased equipment count. Similarly, although the size of the lockhoppers may be slightly reduced, the gasifier would still need to be located within the gasifier support structure at approximately the same elevation above grade compared with GE's conventional lockhopper system.

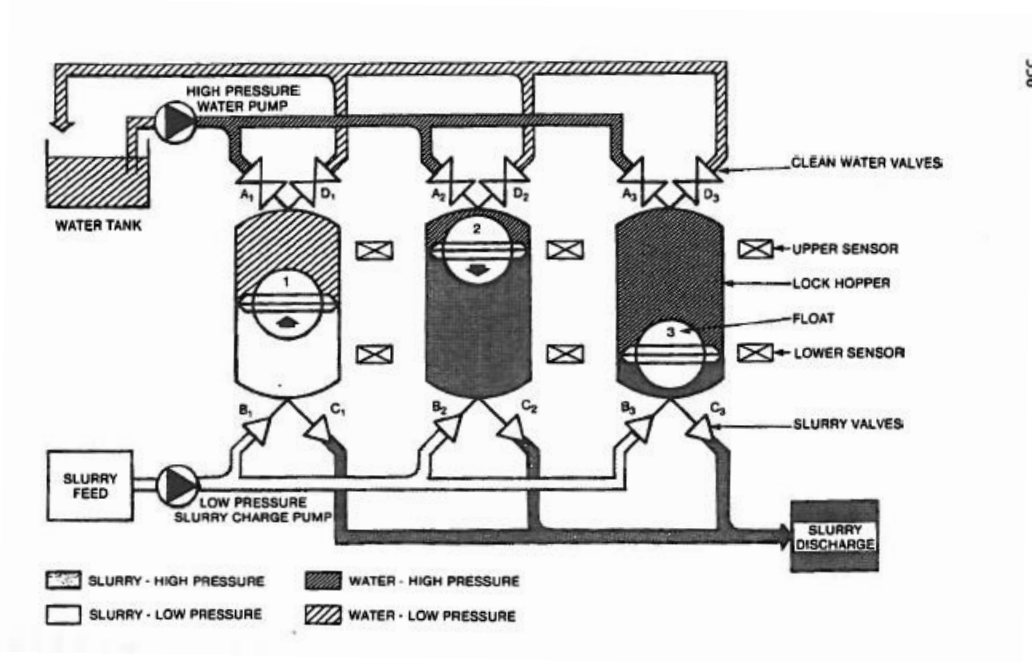

Figure 118. Continuous Solids Transport by Successive Batching of Parallel Vessels **Taken from Streat, M., "Lockhoppers and Pipe Feeders" in *Slurry Handling, Design of Solid-Liquid Systems.***

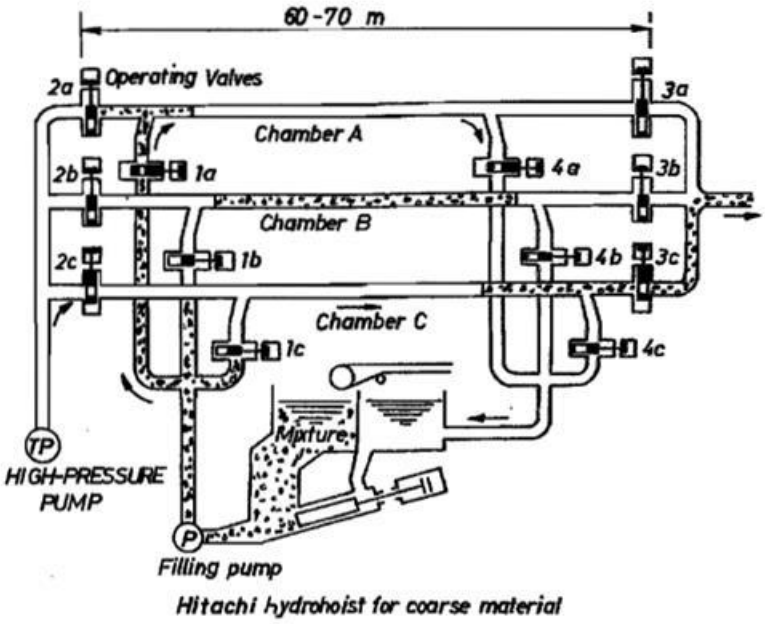

Figure 119. Continuous Solids Transport by Successive Batching of Parallel Piping **Taken from Szivak, A., Illes, K. and L. Varga, "Up-to-Date Hydraulic Transport Systems for the Delivery of Industrial Wastes". *Fifth International Conference on the Hydraulic Transport of Solids in Pipes.* May, 1978.**

Another approach employs a Kamyr Chamber Feeder (Figure 120, Streat). This rotary feeder is divided into four sections: two that are oriented in vertical configuration (slurry feeding and water

recovery) and two that are oriented perpendicular to these (flush water and slurry discharge). As the feeder rotates, low pressure solids fall into the vertical position, and high pressure water is introduced. A screen prevents additional solids from leaving the feeder through the bottom port so that the solids can be flushed out in the horizontal direction. Water that passes through the screen is recycled as makeup feed water. Despite the fact that the reference is over thirty years old, we found no evidence that the idea has been used in commercial practice.

A third idea is called a Lockhopper Pump (Figure 121, Abulnaga, 2002). It involves a pipe containing slag-water slurry separated from clean water by a "free-rolling rubber spherical piston". As slag is discharged from the gasifier quench chamber, the slurry side of the pipe fills with slag and water. Once the sphere is at its "slurry-filled" pipe position, high pressure water pushes against the piston's opposite face, reversing the direction of flow and, in turn, discharging the slurry into the slurry pipeline. After the full pipe volume has been displaced, the water injection ends and the next batch of slurry enters. Inlet and outlet check valves on both slurry and water sides of the piston control the direction of flow of slurry and water based on the movement of the spherical piston. Because of the filling and discharging cycle involved in this process, it can be classified as a semi-continuous process at best.

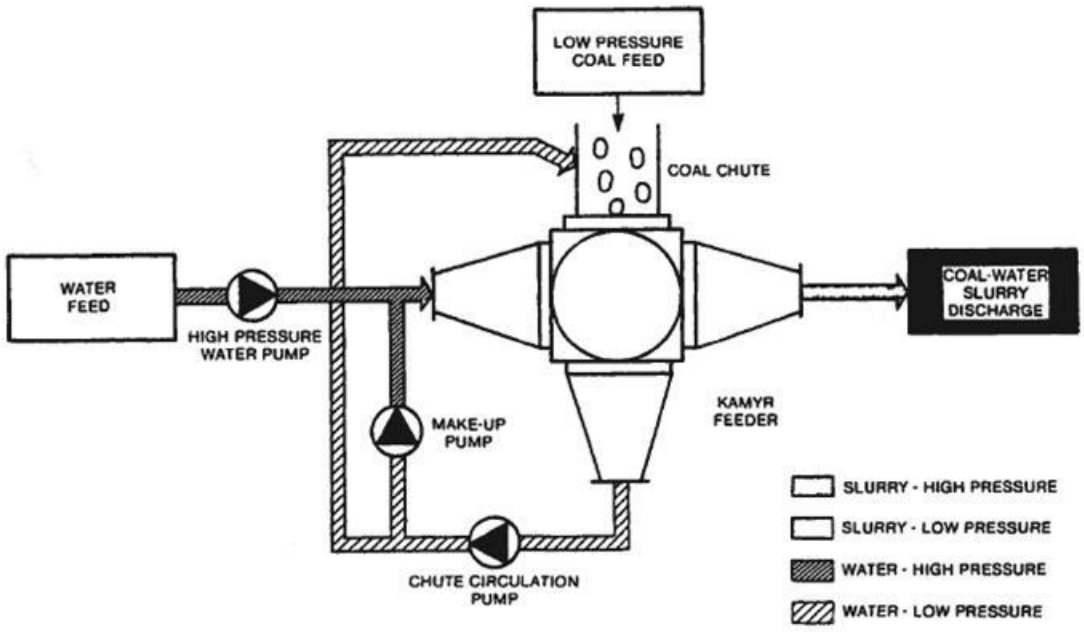

Figure 120. Kamyr Chamber Feeder for Continuous Solids Transport **Taken from Streat, M., "Lockhoppers and Pipe Feeders" in *Slurry Handling, Design of Solid-Liquid Systems.***

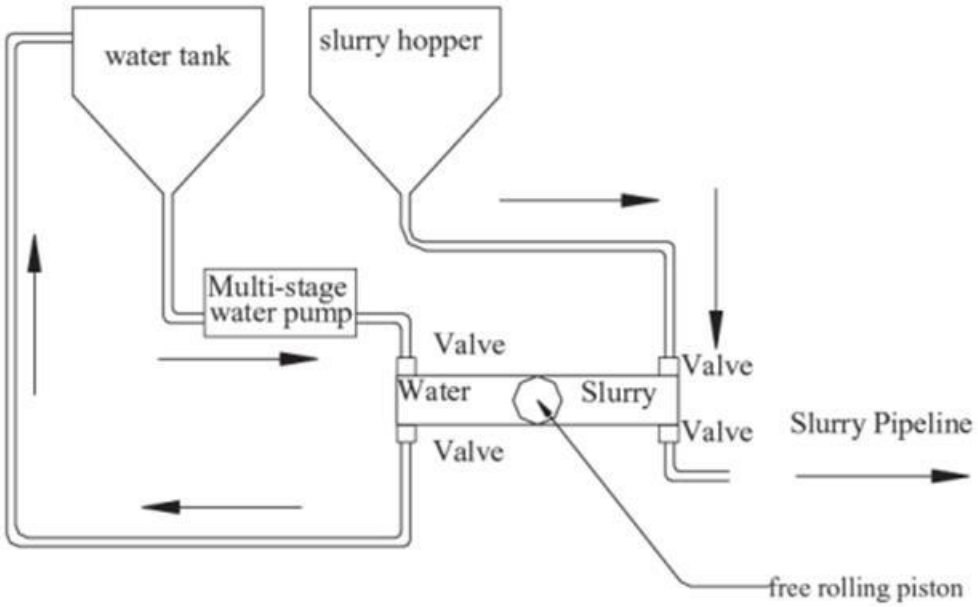

Figure 121. Continuous Solids Transport by Lockhopper Pump **Taken from Abulnaga, B. E., *Slurry Systems Handbook.* McGraw-Hill, 2002.**

6.2.2.2 IGCC Plants

Table 49 lists on-stream time and key operating issues for plants that operate lockhopper systems. Not included in the tables is the Wabash River Facility which uses the Chicago Bridge & Ironworks (CBI) proprietary gasification process. The slag letdown system for the CBI gasification process is based on a "special let-down arrangement not involving a lockhopper or the use of any valves." Their troubleshooting experience is discussed in Wabash, 2000. They modified piping systems to eliminate high velocity impact zones and added screens to protect other metal surfaces. Downstream of the crusher was especially prone to scaling. A scale inhibitor was added to the water to solve this problem.

Table 49. Summary of slag handling experience at gasification plants with lockhopper systems

Plant, Location	On-Stream Time	Reported experience
Buggenum	71.3% in 2004	No crusher; erosion, corrosion noted in slag discharge piping. These were replaced with duplex steel.
Tampa Electric	79.5-83%	Downtime not related to slag handling. Radiant syngas cooler collects slag in an RSC slag sump. Slag crusher seal cause of downtime.
Elcogas, Puertollano	51-62%	High velocities lead to significant erosion of components. Replacements made of abrasion

		resistant materials.
Valero, Delaware City	92.3%	Lockhoppers and Slag pad operated as designed.
Eastman Chemicals	98%	Slag crushers and lockhoppers operated as designed.
Coffeyville Ammonia Plant	>98%	Slag crushers and lockhoppers operated as designed.

6.2.2.3 Patent Literature

The patent literature was searched, and the following patents were identified as containing potentially useful ideas for development as a continuous slag removal process.

US 7,731,783 is a continuous pressure letdown scheme for a gas-solid stream. Here, a high pressure hopper accumulates solids which are subsequently discharged into a "cascade nozzle assembly". Claim 8 describes this assembly in terms of a series of orifice plates. From one orifice to the next, the pressure decreases. After the last orifice, enough head is available to go through an atmospheric filter system before venting. This process makes use of an inert gas to keep the solid particles suspended in the gas phase and even out variations in flow from the upstream process.

EP 0,256,186 B1 is essentially the same system as **US 7,731,783** except that solids-water streams are depressured with restriction elements rather than orifice plates. Water addition boosts the total flow rate such that the velocities are high enough to achieve the necessary pressure drop across a restriction element manifold. This patent forms the basis for the restriction element process (Option 1) that is evaluated further in the "Top Three Technologies" section.

US 4,292,991 describes an erosion resistant valve for severe throttling service. In contrast to **EP 0,256,186 B1** and **US 7,731,783**, this patent performs pressure letdown in one step through the use of a novel valve trim that incorporates an abrasion-resistant throttling plug. The plug is designed to be expendable over a long period of time. The life of the worn plug can be extended by advancing some of the additional length which is built into the plug (just like a tube of lipstick or a mechanical pencil). This activity is quick and can be performed during regular maintenance. This patent forms the basis for the coal slurry letdown valve process (Option 2) that is evaluated further in the "Top Three Technologies" section.

US 4,472,171 provides a way to depressure slag-water slurry from a gasifier using a branched line that feeds either side of a "floating piston" chamber. Slag-water slurry from a slag crusher attached to the bottom of the gasifier quench chamber alternately fills the right- and the left-hand side of the floating piston chamber. For example, when a batch of high pressure slag-water slurry has filled the left-hand side of the chamber and driven the floating piston all the way to the right, valves are used to isolate the left-hand side from the gasifier and to connect it to low pressure slag-water slurry receiving and handling equipment. Then, a second set of valves connects the right-hand side of the chamber to the gasifier so that a second batch can begin to fill the right-hand side of the chamber. As this happens, the floating piston is driven to the left-hand side of the chamber, thereby pushing the first batch of slurry out of the chamber and into the low pressure slag-water slurry receiving and handling equipment. This concept uses the pressure of the gasifier to drive the floating piston. The chamber, the floating piston and the two sets of inlet and outlet valves essentially constitute a large positive displacement pump that is driven in reverse by the pressure in the gasifier quench chamber.

6.2.3 Top Three Technologies

A team of multi-functional experts from GE Gasification and GE Oil & Gas evaluated the surveyed technology options summarized above with respect to equipment and component reliability, overall system cost, system compactness (layout, footprint) and ease of operation. As a result, three technologies that were judged to be the most promising were selected for further evaluation. There three technologies included:

Option 1 – A series of wear-resistant restriction orifices in a slag-water slurry blow down line. This concept is based on the ideas shown it European patent EP 0,256,186 B1, described above.
Option 2 – A severe slurry service pressure reducing valve with wear resistant trim that can be mechanically advanced to quickly replace worn trim material. This concept is based on the ideas shown in US patent US 4,292,991.
Option 3 – A centrifugal pump operating in the reverse direction and functioning as a slag-water letdown turbine.

Once the top three alternative technologies were chosen, equipment lists, equipment data sheets, operability evaluations, and cost estimates were developed for each option (and presented in the following sections). In order to have a common basis for comparison, the 2010 NETL Comparative IGCC Technology Evaluation (Hasselbeck, et al, 2010) was used as a source of flow rates and process conditions which were used for evaluating and comparing the lockhopper base case and the top three alternative technology options. Table 50, below, documents the design basis taken from this DOE document.

Table 50. Design Basis for Continuous Slag Removal Process Development

Parameter	GE Configuration: Continuous Slag Handling	Notes
Slag-water Slurry Pressure	615 psia	An 1800 ft^3, 600 psig gasifier corresponds to an F-class gas turbine. Case 1, (Haselbeck, et al, 2010) uses 815 psia.
Slag-water Slurry Temperature	480 °F (249°C) (syngas bubble pt. for 600 psig)	Based on Quench Gasifier. Case 1, (Haselbeck, et al, 2010) uses Radiant Syngas Cooler.
Coal	Illinois No. 6	Herrin Seam @ 11% ash, (Coal Conversion Systems Technical Data Book, 1978) Composition
Slag Rate, dry	25,190 lb/hr	Normal Operating Condition, 1 train
Solids Concentration	14% by volume, 40% by weight	Sufficiently dilute for water-like viscosities and Newtonian transport.
Particle Size	Top size 200 Mesh	Normal Operating Condition

The three most promising technology options, which were down selected from the larger group of alternative technologies what were surveyed, are described in more detail in the next three sections.

6.2.3.1 Conceptual Design Option 1: Restriction Element Option

Process Description – Option 1

Option 1 relies on a series of restriction orifices, similar to the scheme described in EP 0,256,186 B1. These orifices require a particle size smaller than 1/6 the orifice opening in order to minimize the chance of plugging. For a 4 inch (102 mm) line and **β** equal to 0.3125, the result is a slag crusher outlet spec of 0.2 inch (5 mm), which is an aggressive goal for a single stage in-line slag crusher. (**β** is the ratio of the restriction orifice bore size to the inner diameter of the pipe.) Given that the slag solids entering the system can occasionally include slag stalactites and chunks of refractory, more than one stage of crushing will likely be required. Two stages are shown in Figure 122.

Just as in the referenced patent, the slag-water stream from the quench chamber is supplemented by process water from P-100 in order to increase the pressure drop achievable through a single orifice without having to make the orifice too small. This additional flow increases the stream velocity. With this increased head, a 4 inch (102 mm) line and β equal to 0.3125, three restriction elements are required to achieve 555 psi of pressure drop. The additional water also decreases the bubble point so that the gases stay in solution for the full range of process pressures. Note, however, that because the 0.2 inch (5 mm) maximum slag particle size coming out of the second stage slag crusher is very aggressive for current slag crusher technology, in practice it may be necessary to use larger restriction orifice sizes, larger line sizes and higher supplemental water flow rates in order to avoid having to add a third stage of slag crushing.

A double-pipe exchanger, E-100, reduces the process temperature to 140°F (60°C) to keep the piping and downstream instrumentation at temperatures where stainless steel (316L) metallurgy can be used.

A Vacuum Belt Feeder, X-100 is used to remove moisture from the solids before conveyance to offsite transport. The filtrate water is pumped by P-102 to the vacuum flash drum in the black water flash (BWF) system within the gasification plant.

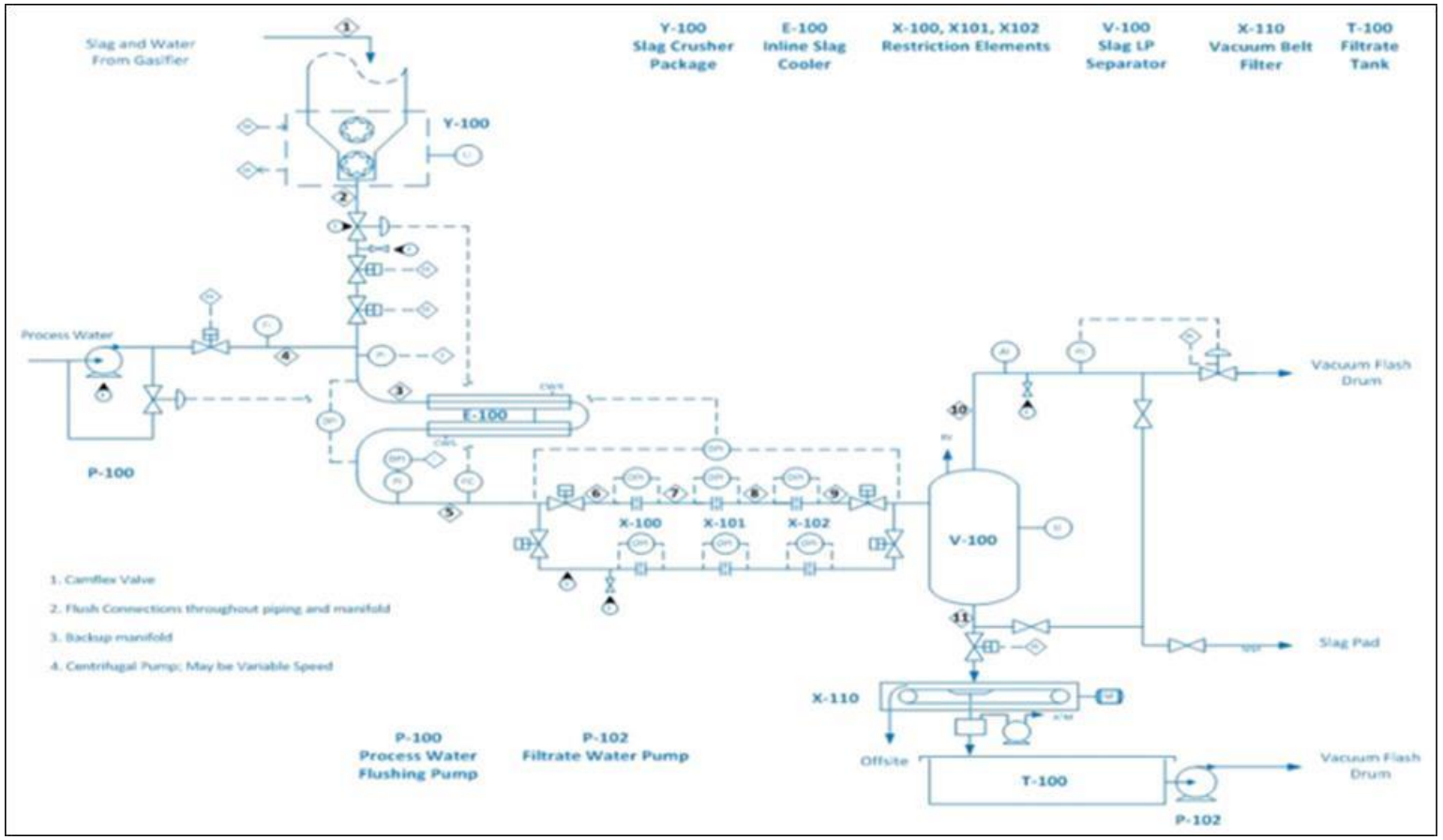

Figure 122. Restriction Elements – Option 1

Material Balance – Option 1

The following table (Table 51) presents the results of material balance calculations for Option 1. The data in each column correspond to the stream numbers shown in Figure 122.

Table 51. Material Balance – Restriction Element – Option 1

			Stream 5	Stream 8	Stream 7	Stream 8	Stream 9	Stream 10	Stream 11	Stream 12	Stream 13	Stream 15
			Design Basis	Cooler Out	Process Water	After Camflex	Re1 In	Re2 In	Re3 In	Out of RE3	SepBtms	SepOvhd
Temperature	All	Deg F	480	140	85	97	97	97	97	97	97	97
Pressure	All	psia	615	605	630	615	605	429	243	57	57	42
Density	Aqueous	lb/ft3	51.0423	61.7636	62.245	62.164	62.1623	62.1324	62.1013	62.071	62.072	62.065
Heat Capacity	Aqueous	Btu/lb/Deg F	NR	0.98726	0.982	0.983523	0.98366	0.986	0.989	0.993	0.993	0.993
Viscosity	Aqueous	cP	0.109	0.470944	0.808	0.434	0.703225	0.703	0.703	0.703	0.703	1.002
pH	Aqueous	dimensionless	8.845	11.183	6.918	11.027	11.325	11.320	11.314	11.309	11.315	11.343
Water	Aqueous	lb/hr	72796.800	69272.600	283000.000	352236.000	352236.000	352247.000	352257.000	352268.000	346932.000	4989.7
Dissolved Gases	Aqueoue	lb/hr	8.264	8.255	0.000	8.254	8.254	8.254	8.254	8.254	8.247	0.000
Dissolved Solids	Aqueous	lb/hr	859.760	412.086	0.000	404.400	404.146	399.699	395.080	**390.540**	389.772	5.271
Total	**Aqueous**	**lb/hr**	**73673.089**	**69701.196**	**283000.000**	**352656.909**	**352656.655**	**352663.208**	**352668.588**	**352675.049**	**347338.265**	**4994.971**
Density	Solid	lb/ft3	222.7790	175.174	No Solids	175.32	175.321	175.345	175.371	175.396	163.001	175.362
Heat Capacity	Solid	lb/hr	NR	0.218308	No Solids	0.208614	0.208611	0.208563	0.208514	0.208465	0.191954	0.208512
Ash	**Solid**	**lb/hr**	**50,781.300**	54753.2	**0.000**	**54797.8**	**54797.5**	**54791.7**	**54785.6**	**54718.7**	**0.287**	**54784.7**
Density	Vapor	lb/ft3	No Vapor	No Vapor	No Vapor	No Vapor	No Vapor	No Vapor	No Vapor	No Vapor	No Vapor	No Vapor
Heat Capacity	Vapor	Btu/Deg F/lb	No Vapor	No Vapor	No Vapor	No Vapor	No Vapor	No Vapor	No Vapor	No Vapor	No Vapor	No Vapor
Viscosity	Vapor	cP	No Vapor	No Vapor	No Vapor	No Vapor	No Vapor	No Vapor	No Vapor	No Vapor	No Vapor	No Vapor
Water	Vapor	lb/hr	No Vapor	No Vapor	No Vapor	No Vapor	No Vapor	No Vapor	No Vapor	No Vapor	No Vapor	No Vapor
Dissolved Gases	Vapor	lb/hr	No Vapor	No Vapor	No Vapor	No Vapor	No Vapor	No Vapor	No Vapor	No Vapor	No Vapor	No Vapor
Total	**Vapor**	**lb/hr**	**0**	**0**	**0**	**0**	**0**	**0**	**0.000**	**0.000**	**0.000**	**0.000**
Overall Density			74.465	86.362	62.245	68.073	68.071	68.040	68.007	173.156	62.100	175.331

Sized Equipment List – Option 1

The following table (Table 52) contains a list of key equipment for Option 1 along with several key sizing parameters.

Table 52. Sized Equipment List – Restriction Element – Option 1

	Label	Prating	Trating	Material	Flowrate	Solids wt%	Other
Slag Crusher Pkg.	Y-100	700 psi	450 F	316L	62.2 kpph	41	5 mm topsize
Inline Slag Cooler	E-100	700 psi	450 F	316L	373 gpm	41	Double Pipe, 2-Pass, CW on Shell, Tout = 140F
Liquid-Gas Separator	V-100	50 psi	140F	316L	373 gpm	41	Solids to bottom with minimum amt moisture
Vacuum Belt Filter	X-110		140F	PP	373 gpm	41	Vacuum Box, Filter frame, filter cloth
Filtrate Tank	T-100	Atm	140F	316L	595 gpm	1	1200 gallons
Orifices	X-100,1,2	700 psi	140F	316L	373 gpm	41	1.25"
Process water flush pump	P-101	100 psi	140F	316L	300 gpm	0	Multi-stage centrifugal, NEMA 4 Motor, 600 dP
Filtrate Water Pump	P-102	50 psi	140F	316L	595 gpm	1	Pout 10 psi

Process Operation – Option 1

Slag-water slurry (~20-30% by volume) flows at a rate that is controlled by a Camflex® valve, just downstream of the two-stage Y-100 slag crusher package. This valve is well suited to control the flow for slurry service due to its streamlined design in the flow-to-close direction coupled with abrasion-resistant trim materials. Based on the reading of a non-intrusive flow meter, the Camflex® valve opens or closes as a function of where the measured value is relative to the target flow. The slurry

temperature is reduced to 140°F (60°C) in the E-100, inline slag-water slurry cooler. Process water is added via pump P-100 in order to increase pressure drop through the restriction elements (pressure drop is proportional to velocity). Stream 10 then feeds V-100, a vapor-liquid separator, where dissolved syngas is routed overhead to the vacuum flash drum in the BWF system. The underflow from V-100 goes to the filter package which does the final dewatering of the slag. The dewatered slag is sent off-site and the low pressure filtrate water is sent to the BWF system through the P-101 slurry pump. Table 53 shows the operating conditions for Option 1.

Table 53. Operating conditions for Option 1

Normal Flow rates:		
Slag	26,000	lb/hr
Water	36,000	lb/hr
Added process water	140,000	lb/hr
Pressure:		
At PI on line 2	650	psia
At PI on line 4	615	psia
At Line 11	10	psia
Restriction Orifice Profile:		
Line 7	427	psia
Line 8	240	psia
Line 9	53	psia
Temperature:		
Upstream of E-200	480	°F
Downstream of E-200	140	°F

6.2.3.2 Conceptual Design 2: Coal Slurry Letdown Valve Option

Process Description –Coal Slurry Letdown Valve – Option 2

Option 2 relies on a valve concept suggested by GE Oil & Gas, Measurement and Controls. This valve had been demonstrated in a prior Department of Energy (DOE) project in a service that was more demanding than the one corresponding to this study (Krishnan, 1984 and Topacio, 2012). In the prior DOE work, the Coal Slurry Letdown Valve, also known as the "Lipstick" Valve, achieved extended trim life while technology from other manufacturers experienced immediate wear that required trim replacement every few days. It exhibited no body erosion, no significant trim erosion and no erosion of the inlet spool – performing better than all other control valves in that benchmarking test.

Figure 124 illustrates features of the Lipstick Valve that make it is a good candidate for the Continuous Slag Removal Process. Of these, the expendable plug is most important. Given the abrasive service and potential for flashing, the plug is simply advanced (like a mechanical pencil or a lipstick dispenser)

as wear occurs. The orientation of this drawing is opposite to X-200 in Figure 123, the process flow diagram (PFD). In the latter, the plug adjustment knob is located beneath the plug guide such that the process inlet occurs from the top and the depressurized stream exits to the right.

The crusher, Y-200, serves to reduce the particle size such that slag particles do not bridge between the plug and the throttling tube. Given that the clearances inside the valve are on the order of ¼ inch (6.4 mm), slag particles need to be ground to a diameter of 1/6th this value, or 0.04 inches (1 mm). This is an even more aggressive slag crusher outlet specification than what is required by Option 1 involving the series of restriction orifices. Given that slag solids entering the slag removal system can include stalactite-like pieces of slag, as well as pieces of refractory brick, more than one stage of crushing will be required. Two stages are shown in Figure 123, although it is likely that at least three stages will be required to meet the very aggressive slag crushing specification.

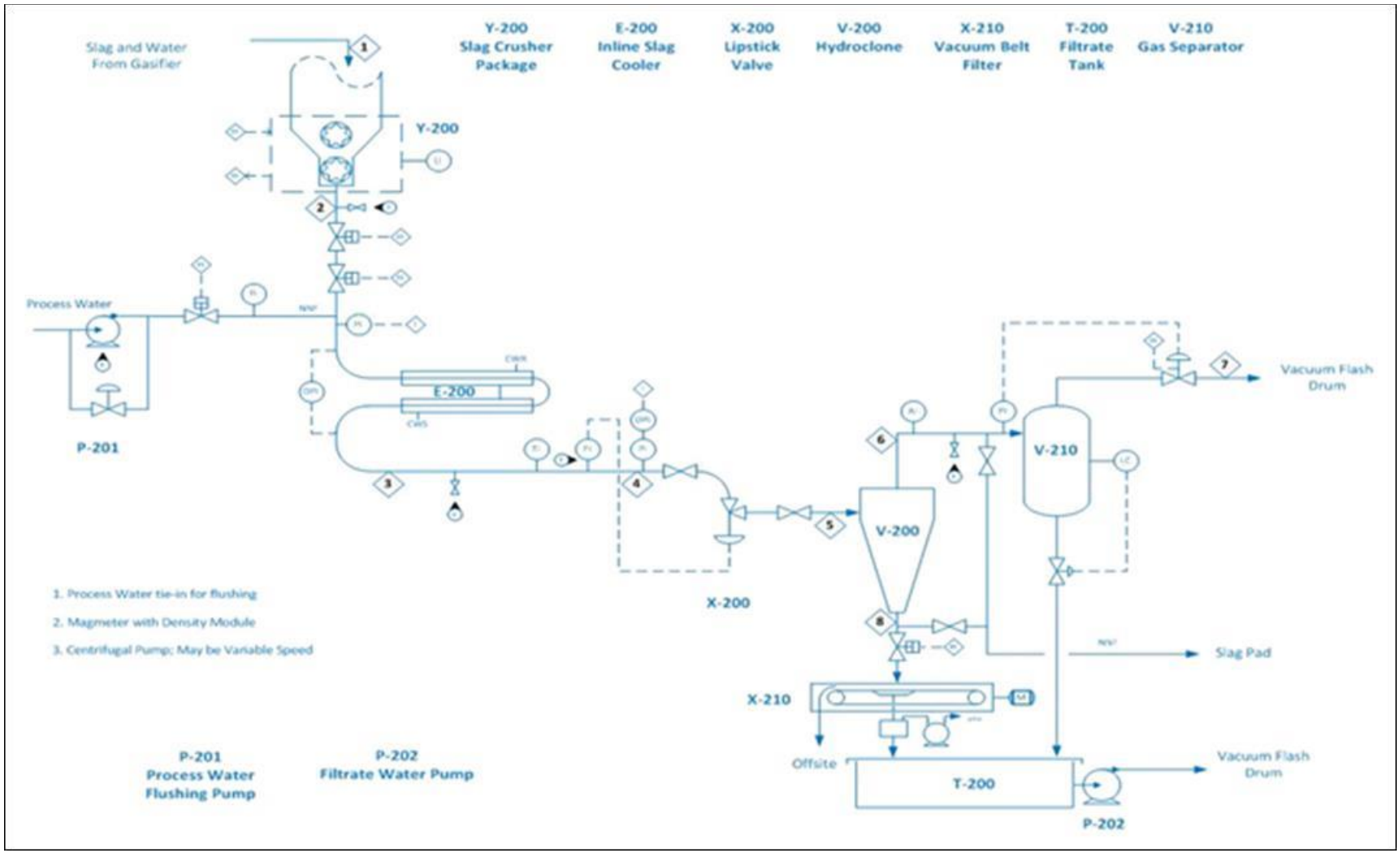

Figure 123. Lipstick Valve PFD – Option 2

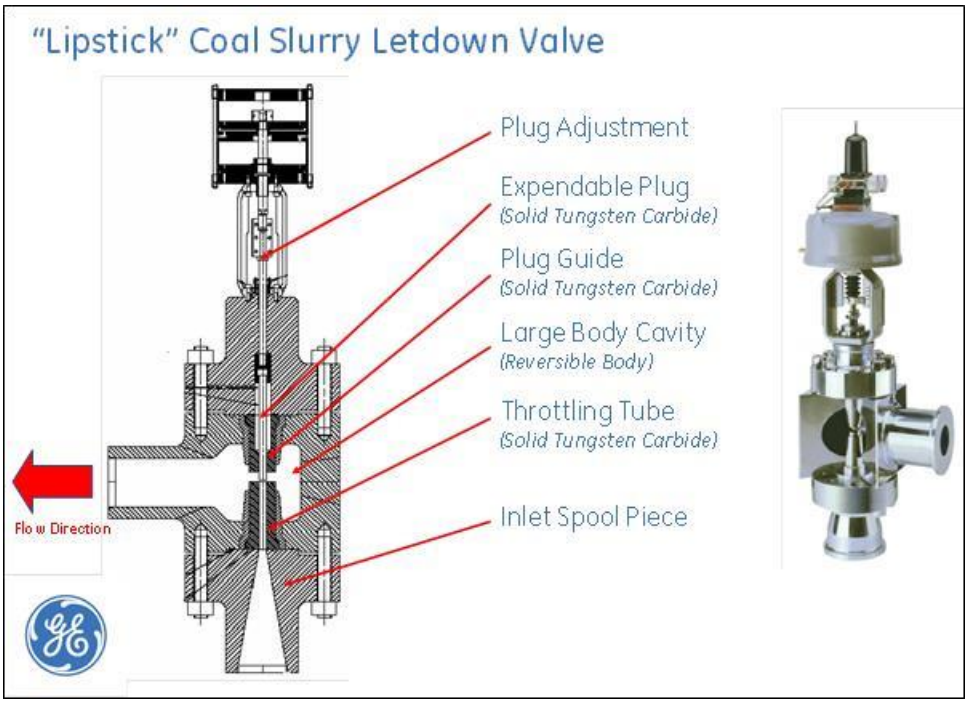

Figure 124. Coal Slurry Letdown Valve (a.k.a. "Lipstick" Valve)

E200, a two pass double-pipe exchanger reduces the slag-water slurry temperature below the bubble point for the Lipstick Valve exit pressure of 50 psia. The lower temperature also allows for more cost-effective metallurgy in the high velocity portions of the valve.

The back-end solids recovery section consists of a hydrocyclone, V-200, to separate the solids bottom stream from the overhead water phase. The dissolved syngas comes out of the water phase in the gas separator, V-210. The gas is routed to the vacuum flash drum in the BWF system while the water is combined with the water that is pulled off of the hydrocyclone bottoms in the vacuum belt filter, X-210. This combined water stream is pumped to the BWF system, while the solids are accumulated for offsite sale or disposal.

Material Balance – Option 2

The following table presents the results of material balance calculations for Option 2. The data in each column correspond to the stream numbers shown in Figure 123.

Table 54. Material Balance – Lipstick Valve – Option 2

			Stream 1	Stream 2	Stream 3	Stream 4	Stream 5	Stream 6	Stream 7	Stream 8
			Slag&Water	Crusher Out	Cooler In	Cooler Out	Cyclone In	Cyclone Ovhd	To Vac Flash	Cylone Btms
Temperature	All	Deg F	480	480	480	140	140	140	140	140
Pressure	All	psia	615	615	615	605	65	50	35	50
Density	Aqueous	lb/ft3	51.0423	51.042	51.0423	61.764	61.659	61.6567	61.6567	61.657
Heat Capacity	Aqueous	Btu/lb/Deg F	NR	NR	NR	0.987	0.992	0.991997	0.991997	0.992
Viscosity	Aqueous	cP	0.109	0.109	0.109	0.471	0.471	0.470	0.470	0.470
pH	Aqueous	none	8.845	8.845	8.845	11.183	11.182	11.183	11.183	11.183
Water	Aqueous	lb/hr	36,398.400	36,398.400	36,398.400	34636.300	34,636.000	20572.771	20572.771	14,063.229
Dissolved Gases	Aqueous	lb/hr	4.132	4.132	4.132	4.132	4.132	4.132	4.132	4.132
Dissolved Solids	Aqueous	lb/hr	429.880	429.880	429.880	206.043	207.406	123.208	0.000	0.000
Total	**Aqueous**	**lb/hr**	**36,836.544**	**36,836.544**	**36,836.544**	**34850.603**	**34,849.568**	**20,701.138**	**0.000**	**14,068.364**
Density	Solid	lb/ft3	222.779	222.779	222.7790	175.174	175.16	175.2	175.2	175.159
Heat Capacity	Solid	lb/hr	NR	NR	NR	0.218	0.218307	0.218	0.218	0.218307
Ash	**Solid**	**lb/hr**	**25,390.650**	**25,390.650**	**25,390.650**	27376.600	27375.45	**1,073.900**	**1,073.900**	**26,301.550**
Density	Vapor	lb/ft3	No Vapor	No Vapor	No Vapor	No Vapor	0.085	0.085	0.085	0.092
Heat Capacity	Vapor	Btu/Deg F/lb	No Vapor	No Vapor	No Vapor	No Vapor	0.435	0.436	0.218	0.438
Viscosity	Vapor	cP	No Vapor	No Vapor	No Vapor	No Vapor	0.017	0.017	0.009	0.017
Water	Vapor	lb/hr	No Vapor	No Vapor	No Vapor	No Vapor	0.106	0.144	0.144	0.044
Dissolved Gases	Vapor	lb/hr	No Vapor	No Vapor	No Vapor	No Vapor	2.742	3.081	2.855	1.075
Total	**Vapor**	**lb/hr**	**0**	0	**0**	**0**	**2.204**	2.543	2.543	0.529
Overall Density			74.465	74.465	74.465	86.362	83.270	58.596	29.980	105.112

Sized Equipment List – Option 2

The following table (Table 56) contains a list of key equipment for Option 2 along with several key sizing parameters.

Table 55. Sized Equipment List – Lipstick Valve – Option 2

	Label	Prating	Trating	Material	Flowrate	Solids wt%	Other
Slag Crusher Pkg.	Y-200	700 psi	450 F	316L	62.2 kpph	41	3-4 mm topsize
Inline Slag Cooler	E-200	700 psi	450 F	316L	62.2 kpph	41	Double Pipe, 2-Pass, CW on Shell, Tout = 140F
Hydrocyclone	V-200	50 psi	140F	SiCarbide	62.2 kpph	41	Solids to bottom with minimum amt moisture
Vacuum Belt Filter	X-210		140F	PP	30.0 kpph	99	Vacuum Box, Filter frame, filter cloth
Filtrate Tank	T-200	Atm	140F	316L	32.2 kpph	1	100 gallons
Gas Separator	V-210	50 psi	140F	316L	32.2 kpph	1	2' x 13'
Lipstick Valve	X-200	700 psi	140F	316L	62.2 kpph	41	Pout 50 psi, Diff Pressure 540 psi
Process water flush pump	P-201	100 psi	140F	316L	106 gpm	0	Diff Pressure 60 psi, NEMA 4 Motor
Filtrate Water Pump	P-202	50 psi	140F	316L	32.2 kpph	1	Pout 10 psi

Process Operation – Option 2

Slag-water slurry (~20-30% by volume) is crushed in Y-200 down to a maximum particle size of 0.04 inches (1 mm). It flows at a rate that is controlled downstream by the Coal Slurry Letdown Valve. The depressurized slurry then goes to V-200, an atmospheric hydrocyclone, which produces a bottoms stream of concentrated slag-water slurry and an overhead stream of water and dissolved gases. The concentrated slag-water slurry stream is fed to a vacuum belt filter, which sends the filtered solids to offsite transport. Water accumulates in T-200 and is pumped to the vacuum flash drum in the BWF

system for subsequent routing to water treatment. Table 56 describes operating conditions for Option 2.

Table 56. Operating Conditions for Option 2

Normal Flow rates:		
Slag	26,000	lb/hr
Water	36,000	lb/hr
Pressure:		
At PI on line 2	650	psia
At PI on line 4	615	psia
At Line 5	50	psia
At Line 8	14.7	psia
At Line 7 (upstream of PCV)	14.7	psia
Temperature:		
Upstream of E-200	480	°F
Downstream of E-200	140	°F

6.2.3.3 Conceptual Design 3: Slag-Water Letdown Turbine Option

Process Description – Slag-Water Letdown Turbine – Option 3

Option 3 relies on a centrifugal pump (P-300) running in reverse as a pressure letdown turbine, Figure 125. This kind of installation is typically used to recover power from high pressure liquid streams (Krassik, et al, 2001 and Heinz and Burdis, 2010). In this application, the energy recovered from the depressuring slag-water slurry is recovered as rotational energy of the pump shaft. Although a small amount of useful power may be available at the shaft, this feature is not exploited in this conceptual design. Instead, the recovered energy is dissipated as heat in a brake that retards the rotation of the shaft.

In this option, the two-stage slag crusher (Y-300) outlet particle size specification depends upon the type of centrifugal pump that is considered. For conventional centrifugal pumps, the recommended maximum slag particle size is about ¼ inch (6.4 mm). However, for the rotating parallel disc pump, described below, the maximum allowable slag particle size is about ¾ inch (19 mm). This is a considerably less aggressive slag crushing spec requirement compared to the Option 1 (0.2 inch (5 mm)) and Option 2 (0.4 inch (10 mm)) requirements. The ¾ inch (19 mm) specification can be comfortably met by a first stage slag crusher that produces a maximum particle size of 2 inches (51 mm) (typical for currently operating gasification plants) followed by a second stage that produces a maximum particle size of ¾ inch (19 mm).

The cooler's function is to reduce the temperature of the slag-water stream below the bubble point at the letdown turbine's exit pressure of 50 psia. As in the other cases, a two-pass double pipe heat exchanger (E-300) is used. The back-end solids recovery section consists of a hydrocyclone (V-300) to

separate a concentrated slag-water slurry stream (bottom stream) from water and dissolved gases (overhead stream). The dissolved gases come out of the water phase in the vapor-liquid separator (V-310). The dissolved gases are sent to the vacuum flash drum in the gasification plant's BWF system, while the water from the bottom of the separator is combined with the filtrate water recovered from the hydrocyclone bottoms using a vacuum belt filter (X-310). This combined water stream is pumped to the BWF system, while the filtered solids are accumulated for offsite sale or disposal.

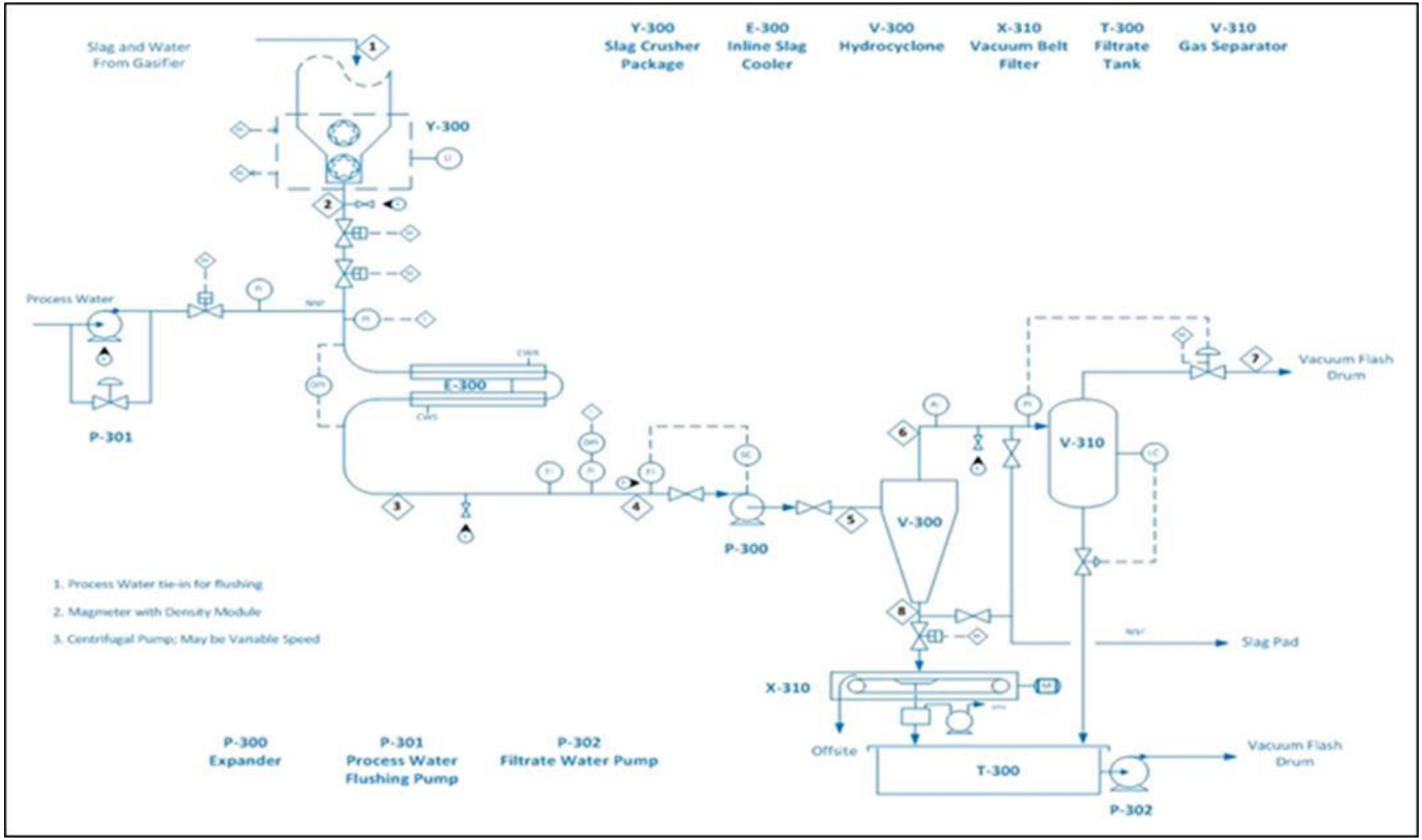

Figure 125. Slag-Water Letdown Turbine PFD – Option 3

Material Balance – Option 3

The following table (Table 57) presents the results of material balance calculations for Option 3. The data in each column correspond to the stream numbers shown in Figure 125.

Table 57. Material Balance - Slag-Water Letdown Turbine – Option 3

			Stream 5	Stream 6	Stream 7	Stream 8	Stream 10
			Cooler In	Cooler Out	Cyclone In	cyclone Ovhd	cylone Btms
Temperature	All	Deg F	480	140	140	140	140
Pressure	All	psia	615	605	65	50	50
Density	Aqueous	lb/ft3	51.0423	61.7636	61.6585	No Aqueous	61.656
Heat Capacity	Aqueous	Btu/lb/Deg F	NR	0.98726	0.991914	No Aqueous	0.992
Viscosity	Aqueous	cP	0.109	0.470944	0.47091	No Aqueous	0.471
pH	Aqueous	dimensionless	8.845	11.183	11.1823	No Aqueous	11.182
Water	Aqueous	lb/hr	36,398.400	34636.300	34,636.000	No Aqueous	34635.950
Dissolved Gases	Aqueous	lb/hr	4.132	4.128	2.030	0.000	1.578
Dissolved Solids	Aqueous	lb/hr	429.880	206.043	207.406	No Aqueous	207.444
Total	**Aqueous**	**lb/hr**	**36,836.544**	**34850.598**	**34,847.465**	**0.000**	**34,846.551**
Density	Solid	lb/ft3	222.7790	175.174	175.16	No Solid	175.16
Heat Capacity	Solid	lb/hr	NR	0.218	0.218307	No Solid	0.218307
Ash	**Solid**	**lb/hr**	**25,390.650**	27376.600	27375.45	**0.000**	27375.4
Density	Vapor	lb/ft3	No Vapor	No Vapor	0.085	0.066	No Vapor
Heat Capacity	Vapor	Btu/Deg F/lb	No Vapor	No Vapor	0.218	0.218	No Vapor
Viscosity	Vapor	cP	No Vapor	No Vapor	0.009	0.009	No Vapor
Water	Vapor	lb/hr	No Vapor	No Vapor	0.106	0.170	No Vapor
Dissolved Gases	Vapor	lb/hr	No Vapor	No Vapor	2.098	2.549	No Vapor
Total	**Vapor**	**lb/hr**	**0**	**0**	**2.204**	2.719	0
Overall Density			74.465	86.362	83.271	0.066	86.244

Sized Equipment List – Option 3

The following table (Table 58) contains a list of key equipment for Option 3 along with several key sizing parameters.

Table 58. Sized Equipment List – Slag-Water Letdown Turbine – Option 3

Equipment Name	Label	Prating	Trating	Material	Flowrate	Solids wt%	Other
Slag Crusher Pkg.	Y-300	700 psi	450 F	316L	62.2 kpph	41	6 mm topsize
Inline Slag Cooler	E-300	700 psi	450 F	316L	62.2 kpph	41	Double Pipe, 2-Pass, CW on Shell, Tout = 140F
Hydrocyclone	V-300	50 psi	140F	SiCarbide	62.2 kpph	41	Solids to bottom with minimum amt moisture
Vacuum Belt Filter	X-310		140F	PP	30.0 kpph	99	Vacuum Box, Filter frame, filter cloth
Filtrate Tank	T-300	Atm	140F	316L	32.2 kpph	1	100 gallons
Gas Separator	V-310	50 psi	140F	316L	32.2 kpph	1	2' x 13'
Expander	P-300	700 psi	140F	316L	62.2 kpph	41	Pout 50 psi, Diff Pressure 540 psi
Process water flush pump	P-301	100 psi	140F	316L	106 gpm	0	Diff Pressure 60 psi, NEMA 4 Motor
Filtrate Water Pump	P-302	50 psi	140F	316L	32.2 kpph	1	Pout 10 psi

Process Operation – Option 3

Slag-water slurry (~40% by volume) is crushed in a two-stage slag crusher (Y-300). It flows at a rate that is controlled by the slag-water letdown turbine (P-300). Downstream of the turbine, a hydrocyclone running at about 50 psi takes the water and vapor phase overhead to an overhead separator (V-300). This separator is maintained at a constant liquid level by a flow control valve on the discharge line. A concentrated stream of slag-water slurry exits the bottom of the hydrocyclone and is fed to a vacuum belt filter (X-310), which sends the filtered solids offsite. Water from both the filter and the separator is pumped to the vacuum flash drum in the BWF system for eventual routing to water treatment. Operating conditions are shown in Table 59.

Table 59. Operating Conditions – Slag-Water Letdown Turbine – Option 3

Normal Flow rates:		
Slag	26,000	lb/hr
Water	36,000	lb/hr
Pressure:		
At PI on line 2	650	psia
At PI on line 4	615	psia
At Line 5	50	psia
At Line 8	14.7	psia
At Line 7 (upstream of PCV)	14.7	psia
Temperature:		
Upstream of E-200	480	°F
Downstream of E-200	140	°F

6.2.4 Final Selection of Most Promising Technology

Table 60, below, reports Total Installed Cost (TIC) for each continuous slag handling option. Compared with the initial estimate of $10M for the major equipment in the base case lockhopper process, all three options deliver savings. With much in common, the main cost differences come down to the multi-stage slag crusher and the depressurization equipment. These Class 4 cost estimates include contingency along with installation costs based on Midwest labor rates.

The slag crusher cost is directly related to the particle size specification needed for depressurization. Many vendors have not been willing to quote the different cases, and no one has off-the-shelf machines for this service. However, several conversations were conducted with Knighthawk Industries (Conversations, 2012), a company that designs and fabricates slag crushers. They provided a scoping estimate for a custom two-stage crusher for the slag-water letdown turbine case (3/4 inch (19 mm) outlet particle size). The data from this scoping estimate was, in turn, scaled by outlet particle size specifications in order to obtain rough slag crusher cost estimates for the Options 1 and 2. It is quite possible that the actual slag crushing costs for these two options may be higher, particularly if three or more crushing stages end up being required.

The restriction elements option flush pump is different from the one used for the Lipstick Valve and letdown turbine processes. In the former, the unit runs continuously at roughly 300 gpm to generate a high enough pressure drop through each of the three restriction orifices. The other options only use flush water during startup, shutdown, and maintenance procedures.

The restriction elements were taken as special purpose fittings that were factored into the contingency for Option 1. A quote for the Lipstick Valve was provided by GE Oil & Gas – Measurement and Controls. The cost of the letdown turbine was taken from the Aspen Kbase Program based on its sizing specifications. (Note that, later on in the program we obtained a quote for the letdown turbine from a vendor and the cost was considerably more than what is shown in Table 2.1.2. Nevertheless, the value shown in the table was the best that we had at the time that we down selected to Option 3 as the final choice for further development.) Although the valve is certainly the most elegant approach to depressurization, it represents a more costly approach given its metallurgy, fabrication, and special purpose features. The centrifugal pump running in reverse as a letdown turbine appears to be more of an off-the-shelf item than the other depressurization equipment.

Table 60. Comparison of Total Installed Cost for Options 1, 2 and 3

Equipment / Costs	Option 1 Restriction Elements (1000$)	Option 2 Lipstick Valve (1000$)	Option 3 Letdown Turbine (1000$)
Slag Crusher	1,783	2,589	1,140
Flush Pump	39	35	35
Depressurization Equipment			
- Restriction Elements	21		
- Lipstick Valve		316	
- Letdown Turbine			27
Vacuum Belt Filter	684	684	684
Other (exchangers, vessels)	304	317	320
Total Equipment Cost	2,792	3,905	2,171
Installation Cost	2,171	1,971	1,941
Indirect Cost	2,739	3,019	2,605
Total Installed Cost	7,702	8,841	6,718

Option 3 (slag-water letdown turbine) was chosen as the final, winning process based on its lowest Total Installed Cost and on its significantly less aggressive requirement for slag crushing. Despite the fact that a much higher quote was obtained from a vendor for a slag-water letdown turbine at a later time, that did not prompt a reconsideration of the final technology decision. The differences in slag crushing requirements are significant. Without the availability of a commercial two-stage slag crusher that can attain extremely small maximum outlet particle sizes, the need to crush to 0.2 inches (5 mm) (Option 1) and 0.04 inch (1 mm) (Option 2) means that, ultimately, those two options are highly impractical..

One caveat regarding the foregoing technology evaluation is that one of the main goals of the project is to identify technology that also increases IGCC availability This criterion was difficult to assess in the conceptual design stage without process data for all three options. Of the three options, only the Lipstick Valve has published, demonstrated continuous on-stream time in slurry service (5000 hours in liquid depressurization service; Krishnan, 1984). Finally, Option 1 (restriction elements) was eliminated based on the high water pumping requirements that penalizes it when compared with the others.

To summarize, three conceptual process designs were developed for continuous alternatives to the current lockhopper system for handling coal gasifier slag. These processes all include steps for crushing the slag, cooling the slag-water slurry, and depressurization prior to solids separation and slag sale/disposal. They differ mainly in the extent of crushing required prior to the depressurization step as well as in the equipment used for the slag-water slurry depressurization. The most cost-effective design was the slag-water letdown turbine option, which is based on running a centrifugal pump in reverse. As a result of the down selection process, calculations showed that an approximate reduction in Total Installed Cost of about 33% could be expected relative to the current design. In the next phase of this project, which focused on the development and optimization of the winning letdown turbine concept, our intent was to look for additional cost savings through the development of an actual process layout and a more detailed comparison of the equipment and support structure costs between the base case lockhopper system and the continuous slag removal process (CSRP) based on the slag-water letdown turbine.

6.3 Design of the CSRP

Following the initial effort to screen slag depressuring technologies and to down select the most promising concept, the team began to focus on refining and optimizing the winning Continuous Slag Removal Process (CSRP) based on the letdown turbine. One of the first issues dealt with was our concern about the reliability of the double pipe heat exchanger used to cool the slag-water slurry between the gasifier and the letdown turbine. The slag-water slurry entering the CSRP needs to be cooled in order to minimize flashing in the slag-water letdown turbine. To that end, two different slag-water cooling design configurations were developed and evaluated. Configuration 1 uses the slag-water slurry cooler that was used as part of the letdown turbine option during the down selection process (Option 3). Configuration 2 uses direct injection of recycled and cooled process water into the slag-water immediately upstream of the letdown turbine. The choice of actual equipment to use for the slag-water letdown turbine is the key to the success of the CSRP system.

6.3.1 CSRP Process Overview

6.3.1.1 Configuration 1 – CSRP with Slag-Water Slurry Cooler

Figure 126 shows a process flow diagram for the version of the Continuous Slag Removal Process (CSRP) that uses a slag-water cooler to control water temperatures throughout the system. Slag-water slurry containing approximately 40 wt.% solids from the bottom of the gasifier quench chamber are passed through a two-stage slag crusher to ensure that all particles are ≤ ¾ inch, as required by the slag-water letdown turbine. The slag water then passes through two emergency shut-off valves (primary and backup), which are used only in an emergency in cases where the CSRP mush be isolated from the gasifier.

It should be noted that these two valves are significantly different from the four large valves required in the conventional lockhopper system (lockhopper inlet valve, back-up lockhopper inlet valve, lockhopper outlet valve, flush water valve). In a 300 MW gasifier operating train, these valves will typically be 18-inch valves. They are high pressure and they cycle several times each hour. In contrast, the two CSRP emergency shutoff valves are 4- or 6-inch valves that stay open all the time and only close in the event of an emergency. So, it's clear that by replacing a batch-operating lockhopper system with a continuously operating CSRP, a significant amount of capital cost and plant unreliability can be eliminated.

After passing through the two emergency shut-off valves, the crushed slag-water slurry passes through a two-pass double-pipe heat exchanger (E-400) that cools the slag-water slurry from about 480°F to 140°F (249°C to 60°C) against plant cooling water. The slag-water slurry is cooled in order to minimize the flashing of dissolved gases as the slurry depressures through the slag-water letdown turbine since the vendor claims a 40% upper operating limit on the vapor fraction. By cooling the slurry, most of the gas flashing is made to occur in downstream equipment (V-410) that is designed for that purpose. After the double pipe cooler, the slag-water slurry is depressured through a slag-water letdown turbine (PT-400) turning against the resistance of an eddy current brake from 600 psig to 50 psig. The depressurized slag-water slurry then passes through a hydrocyclone (V-400) that concentrates the slag-water slurry before feeding it to a vacuum belt filter for final dewatering. According to a vendor quote for the hydrocyclone, 99.85 wt. % of the incoming solids go to the underflow, with the remainder going to the overhead. 71 wt. % of the incoming water goes to the underflow, with the remainder going to the overhead. The underflow from the hydrocyclone goes to a vacuum belt filter for final dewatering of the slag before disposal or sale. The overhead from the hydrocyclone goes to a flash tank (V-410) operating at atmospheric pressure where dissolved gases are removed and sent to the gasification plant's black water flash (BWF) system for further processing. The degassed water from the flash tank and the filtrate from the vacuum belt filter are recycled to a separate location in the gasification plant's BWF system where the combined stream is degassed prior to reuse.

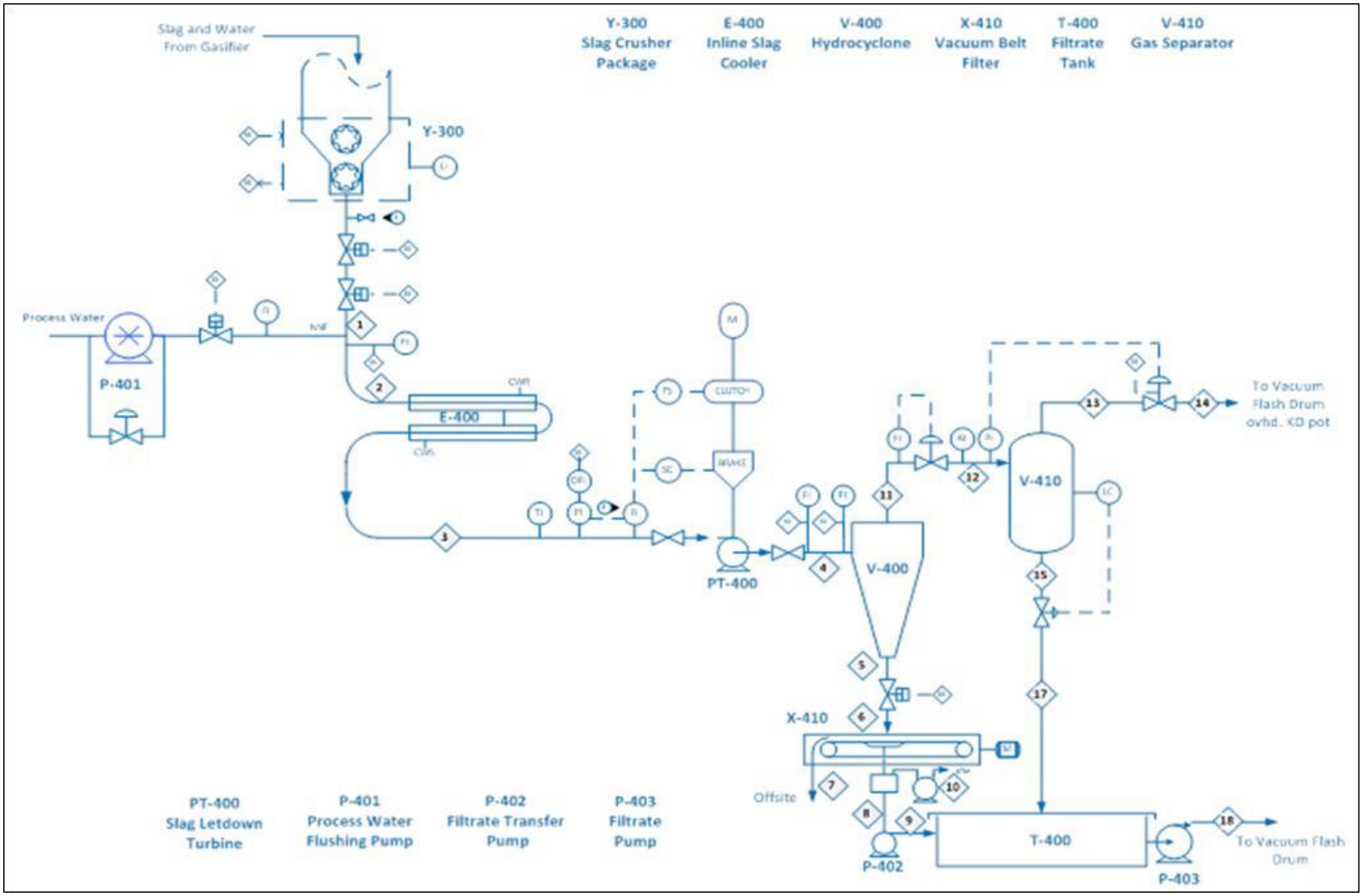

Figure 126. Slag-Water Slurry Cooler (Configuration 1)

6.3.1.2 Configuration 2 – CSRP with Direct Injection of Cooling Water

This is the same as Configuration 1, except that the slag-water slurry cooler has been removed and replaced by a mixing tee. This case was evaluated because of concerns about the reliability of the slag-water slurry cooler. Relatively particle-free water recovered from the vacuum belt filter system and the flash tank is pumped by a direct contact cooling water recycle pump through a shell and tube heat exchanger where the recycled water is cooled against plant cooling water. The cooled recycle water is then injected directly into the slag-water slurry via the mixing tee in order to lower the temperature of the mixed stream to a point where flashing is minimized in the slag-water letdown turbine. Although this increases the flow rate of water through the letdown turbine and increases the size of the turbine, it eliminates the possibility that the slag-water cooler might plug during operation. The rest of Configuration 2 is the same as Configuration 1. See Figure 127.

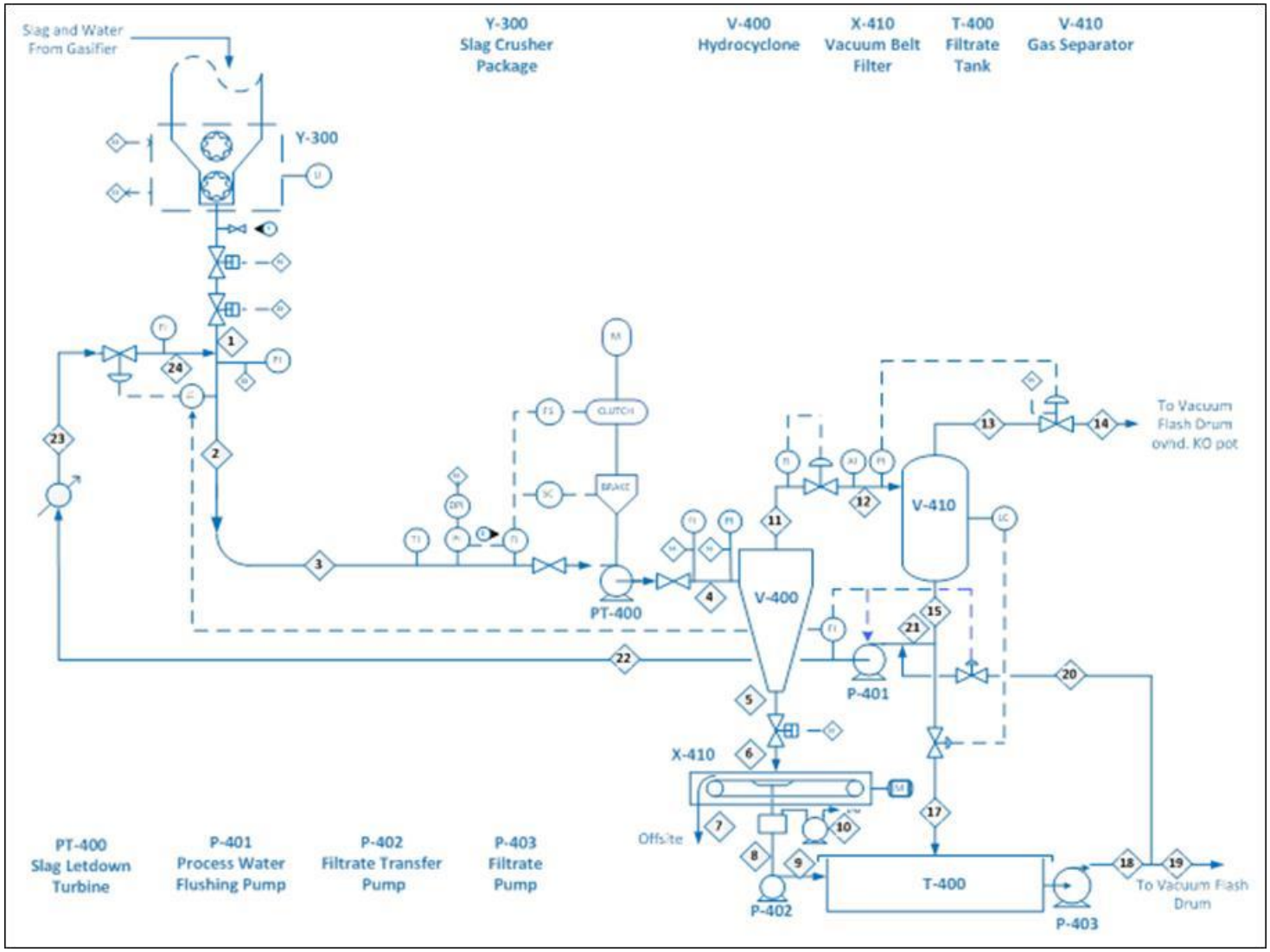

Figure 127. Direct Injection of Cooling Water (Configuration 2)

6.3.2 **Slag-Water Letdown Turbine**

The complete slag-water letdown turbine (PT-400) assembly will consist of a centrifugal pump head configured to rotate in a direction opposite to its normal rotation, an eddy current brake, a friction brake, a clutch and a variable speed electric motor all connected via a common rotating shaft, as shown in Figure 128. The plan is to assemble it from components available from several vendors. The motor, the clutch and the two brakes are all relatively common equipment that is available from various vendors. However, in searching for a suitable centrifugal pump head that could serve as a letdown turbine for roughly 40 wt.% slag-water slurry, it became apparent that, while capable in principle of doing the job, conventional centrifugal pump heads were likely to suffer significant erosion damage. This is because of the continuous impingement of slag-water slurry on the vanes of the centrifugal pump impellers. However, a persistent search of commercially available slurry pumps yielded a vendor that made what looked like a centrifugal pump, but that had an impeller with no vanes. Manufactured by the Discflo Corporation (www.discflo.com) of Santee, California, the Discflo pump is capable of pumping corrosive and non-corrosive fluids with viscosities ranging from below 1 centipoise to thousands of centipoise and containing significant quantities of suspended and erosive solids. The head of a Discflo pump, shown in Figure 129 with shaft rotating in the normal direction used for pumping, looks very much like a conventional centrifugal pump. But instead of using an impeller with vanes, the Discflo pump uses a rotor consisting of a set of parallel rotating discs. In a conventional centrifugal pump, fluid is accelerated through the pump by the vanes pushing on the fluid. But in a Discflo pump, the rotating discs impart motion to the fluid via viscous drag alone.

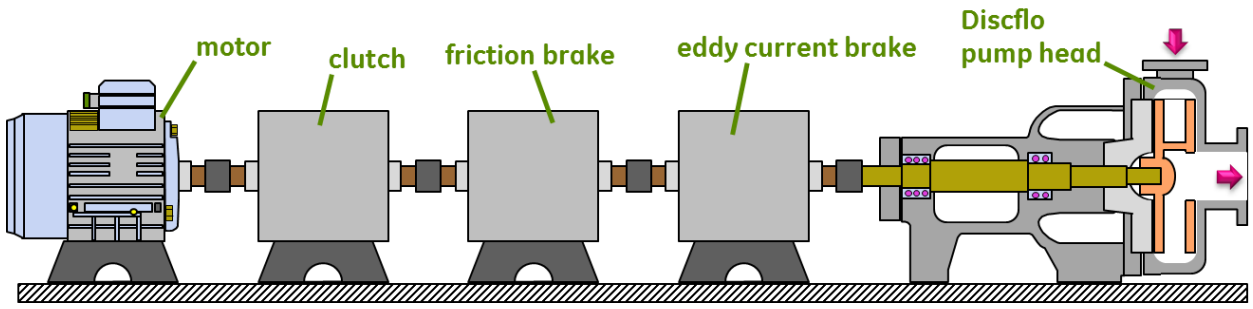

Figure 128. Slag letdown turbine equipment assembly

The rotor (also called a discpac by Discflo Corp.) inside the head of a Discflo pump consists of two parallel circular discs – a drive disc and an inflow disc – that are held together by three or more spacers (only one shown in Figure 129). As the shaft rotates the two discs, the fluid in direct contact with the inner surface of each of the two discs remains attached to the surface of the disc (no slip condition). However, moving away from the surfaces of the discs, successive layers of fluid are free to move against each other. The rotating discs transfer momentum to the fluid via viscous drag; and a centrifugal force is generated that moves the fluid radially outward between the two rotating discs. As fluid moves radially outward between the two discs, additional fluid is drawn in through the opening at the center of the inflow disc to replace it. Fluid that reaches the perimeter of the discs has been accelerated to a rotational speed that approaches the speed of the discs. As the fluid leaves the space between the two discs, the pump casing converts the fluid velocity to fluid pressure at the tangential and upward facing discharge nozzle. Different discpac designs are used in order to accommodate fluids with different properties (viscosity, solids content, particle size). One

of the advantages of using a Discflo pump rather than a conventional centrifugal pump, in which the impeller contains vanes, is that the Discflo pump is much less susceptible to damage by erosion. Whereas an impeller with vanes may rapidly deteriorate in slurry service, the velocity profile between the discs of a Discflo pump rotor is such that the solids tend to travel along the centerline between the two discs and to minimize contact with the disc surfaces. Because of this phenomenon, Discflo has sold many pumps for slurry service which experience relatively little wear over extended periods of time. Admittedly, using a Discflo pump head in the reverse direction as a letdown turbine is a non-conventional application. However, in conversations with the vendor, they agreed that such an application would be possible.

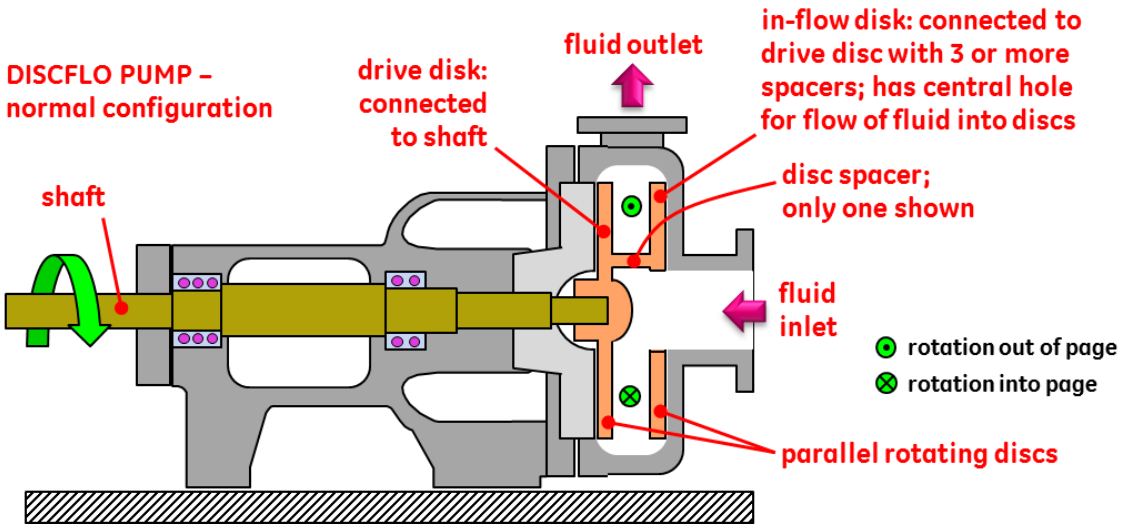

Figure 129. Discflo pump – Normal configuration

As shown in the slag-water letdown turbine assembly drawing in Figure 128, above, the Discflo pump head is connected to two brakes, a clutch and a motor. The motor and clutch are used only during startup to start the rotor turning. Once the discpac is turning on its own n the proper direction by the slag-water slurry, the clutch is disengaged and the motor turned off. From then on, the slag-water slurry turns the discpac against the electromagnetic resistance of the eddy current brake. The energy extracted from the depressurizing slag-water slurry is electromagnetically converted to heat inside the frictionless eddy current brake (which is water cooled). The back-up conventional friction brake is engaged only in the rare (and not expected) failure of the frictionless eddy current brake. Given the above description of how the assembly operates, it is probably only necessary to consider the eddy current brake and the Discflo pump head when evaluating the reliability and availability of the assembly during normal, steady state operation.

6.3.3 CSRP Process Operation and Control

For the following discussion how the CSRP operates, please refer to the PFDs shown in Figure 126 and Figure 127

Slag-water slurry containing approximately 40 wt.% solids passes from the gasifier quench chamber (or RSC sump) through a two-stage slag crusher (Y-300). This is the first piece of equipment in the slag handling system. The first stage reduces oversize material to less than 2 inches (51 mm). The second stage produces a top size of ¾ inch (19 mm). Emergency shutoff valves (one primary and one backup) are located immediately downstream of the slag crusher. These valves are normally open. They close only in the case where the control system detects a situation that requires the CSRP to be isolated from the gasifier (or RSC). The ¾ inch (19 mm) top size slag-water slurry from the slag crusher passes through a double pipe heat exchanger where the slurry temperature is cooled from approximately 480°F to approximately 140°F (249°C to 60°C). The slurry is cooled prior to pressure letdown in order to minimize the amount of dissolved gas flashing that occurs within the slag-water letdown turbine PT-400. According to Discflo®, their pump can handle 40 vol% gas and still work. For Configuration 2, the flow rate and temperature of recycle cooling stream 24 is controlled to achieve the target temperature for stream 2. Stream 20 is used to supplement stream 21 in case the flow rate of 21 is not sufficient by itself for the level of cooling required. If the flow rate required for stream 21 is greater than the flow rate available from stream 15, then the flow rates of both stream 16 and 17 will be zero. For Configuration 1, the cooling water flow rate to the slag-water cooler is controlled to maintain the slag-water exit temperature.

The discharge pressure of the Discflo pump is one of the key design variables for this process. It determines the amount of energy that must be extracted by the pump which, in turn, is related to the size of the electromagnetic brake that will be required. It also determines the amount of dissolved gas flashing that occurs within the pump. The cooled slurry is depressurized from about 600 psig to 50 psig as it passes through slag-water letdown turbine PT-400. As the depressurizing slurry turns the discs within the turbine, the extracted energy produces a torque on the turbine shaft that is resisted by an eddy current brake. The eddy current brake is a frictionless, non-contact device that can be electronically adjusted in order to vary the shaft resistance and, in this way, the flow rate of slag-water slurry can be controlled. Depressurized slag-water slurry is passed through a ceramic-lined (SiC) hydrocyclone (V-400) in order to achieve an initial separation of slag and water. The majority of the slag exits the bottom of the hydrocyclone where the slag-water slurry is concentrated from about 40 wt.% solids to about 50 wt.% solids. A small quantity of fine particulate solids exits with the overhead water flow and passes through a flow control valve into the gas-water separator.

As the hydrocyclone overhead water stream passes through the flow control valve, the stream is further depressured and dissolved gases come out of solution. They are separated from the water stream in gas separator vessel V-410. The separated gases are passed through a backpressure control valve and then directed to the vacuum flash section of the BWF system in the gasification plant. V-410 is maintained at a constant liquid level by a flow control valve in the bottom discharge line. The gas stream is at a low pressure that is just enough to push the vapor into either the vacuum flash overhead of a single-stage vacuum flash or into the second vacuum flash overhead of a two-stage vacuum flash in the BWF system. There the gases combine with other gases released in the BWF system and are routed elsewhere for further processing.

The approximately 50 wt.% slag-water slurry stream from the bottom of the hydrocyclone is filtered in a vacuum belt filter package. The filtered slag (80% solids) is transported off site for sale or disposal. The filtrate is collected and transferred via filtrate pump P-402 to slag-water sump T-400. There, the filtrate combines with the hydrocyclone overflow water. The combined stream is shipped via P-403 to the gasification plant vacuum flash drum in the BWF system for further processing. With the exception of the slag-water letdown turbine, the CSRP uses equipment commonly found in many industrial, chemical and power plant processes.

6.4 Analysis and Discussion of the CSRP

6.4.1 Heat and Material Balance (HMB) Simulation and Configuration Optimization

An Aspen Plus® simulation of the continuous slag removal process (CSRP) was developed and used to improve the CSRP configuration as well as to improve integration of the CSRP with the rest of the IGCC plant. This resulted in additional cost savings due to elimination of some major equipment in the CSRP process and also due to reduction in size of some of the equipment in the black water flash (BWF) system. An Aspen Plus® simulation of GE's conventional lockhopper system was also developed for comparison.

The following were the assumptions for the base case CSRP IGCC simulation:

- Of the coarse slag and the slag fines that collect in the gasifier quench chamber, 40% of the slag fines and 100% of the coarse slag pass through the CSRP system. The rest passes directly to the BWF system via the black water blowdown line from the quench chamber.
- Slag-water slurry inlet stream solids concentration = 40 wt.%.
- Slag-water letdown turbine is operationally capable of depressurizing from 600 psig down to 10 psig.
- Hydrocyclone: 99.85 wt.% of the incoming solids go to the underflow and 71 wt.% of the incoming water goes to the underflow.
- Filtered slag final solids concentration = 70 wt.%.

The following list summarizes changes that were made to our initial CSRP concept in order to improve the process and to improve integration with the IGCC plant. Refer to the PFD shown in Figure 130.

- As described in a previous section, the CSRP configuration was evaluated in terms of two separate configurations based on the method for cooling the slag-water slurry stream entering the system. Upon integration with the rest of the IGCC plant, it was identified that the NH_3 stripper bottoms that was being cooled and used to fill the lockhopper flush drum in GE's conventional lockhopper system could now be utilized as the cooling medium for the inlet slag-water slurry stream in Configuration 2. Therefore the NH_3 bottoms stream now functions as cooling medium and is combined with the inlet slag-water slurry stream. This also eliminates the recycle water pump on stream 21 in Figure 126 and Figure 127). However, the NH_3 stripper bottoms stream is at a low pressure (37.45 psia) and, therefore, requires a positive displacement pump in order to pressurize the stream so that it can be injected into the slag-water slurry stream.

- According to the Discflo® pump vendor, the slag-water letdown turbine can handle up to 40% vapor within the pump head without operational issues. It was found in the simulation that cooling with the NH_3 bottoms stream resulted in a combined stream temperature of approximately 212°F (100°C) and the vapor fraction upon expansion came out to be < 1%. This allowed elimination of Configuration 1 with the double-pipe slag-water slurry cooler. Thus, the analysis that follows considers only Configuration 2 using direct injection of process water to cool the slag-water stream.

- The original idea was to let down the slag-water slurry from about 600 psig to roughly 50 psig, to operate the hydrocyclone at that pressure and to have a pressure letdown valve upstream of V-410 with a ΔP of 50 psi. However, in order to eliminate a heavy duty pressure letdown valve, it was decided to let down the slag-water slurry to 10 psig (this is expected to be within the capability of the Discflo pump). The hydrocyclone V-400 therefore operates at close to atmospheric pressure and the gas-water separator V-410 operates at a vacuum of 8 psia. The 8 psia vacuum pressure comes from connecting the overhead of V-410 to the vacuum pump in the gasification plant's BWF system. Ultimately the vapors from V-410 are sent to the sulfur recovery unit (SRU) as part of the sour gas. The bottoms stream from V-410 is sent to the slag sump and recycled back into the system via the slag sump pump.

- The vacuum belt filter was replaced with a slag drag conveyor and slag sump to facilitate fines recycle to gasifier for improved carbon conversion. As shown in Figure 130, the slag sump overhead water is split downstream of pump P-403 into stream 413, which goes to the coal-water slurry preparation unit, and stream 415, which goes to the gasification plant's BWF system. The stream 413 flow rate is calculated based on coal slurry water requirements. The remainder of the slag sump overhead water (stream 415) is sent to the vacuum flash drum in the black water flash system for use elsewhere in the gasification plant.

Table 61 shows the results of material balance calculations for all of the streams in the CSRP configuration shown in Figure 130. The stream numbers shown in the PFD correspond to the column headings in the table.

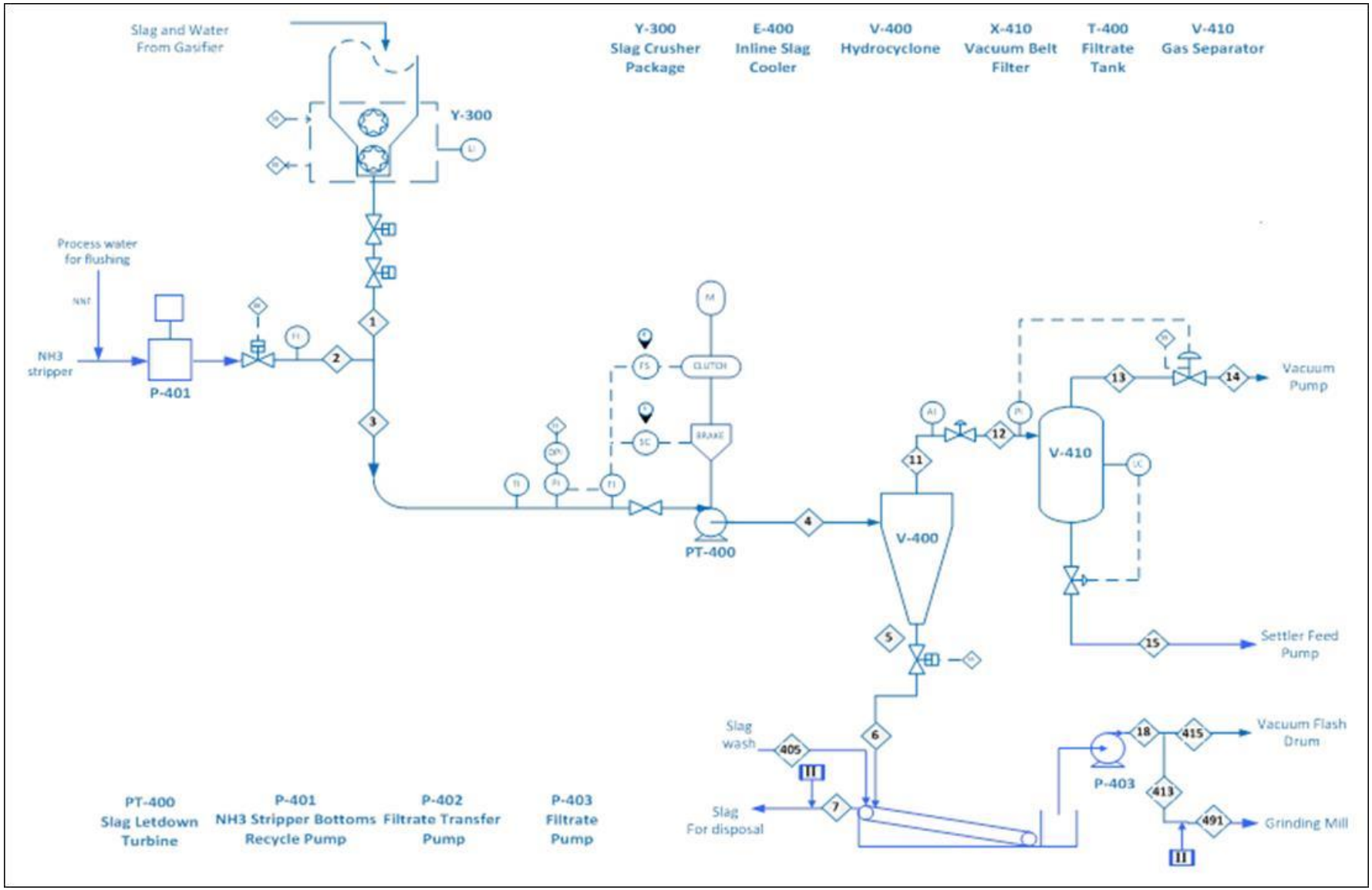

Figure 130. Improved CSRP Configuration

Table 61. Material Balance for Improved CSRP Configuration

	1	2	3	4	5	6	7	11	12	13	14	15	18	405	413	415	491
Temperature F	428.0	105.9	212.4	212.3	212.1	210.2	150.5	212.1	181.3	181.3	181.3	181.3	148.1	100.0	148.1	148.1	148.1
Pressure psia	610.5	610.5	610.5	24.7	21.7	14.7	14.7	21.7	8.0	8.0	8.0	8.0	49.7	114.5	49.7	49.7	49.7
Fluids Mole Flow lbmol/hr																	
CO	0.68	0.00	0.68	0.68	0.01	0.01	0.00	0.68	0.68	0.68	0.68	0.00	0.01	0.00	0.00	0.01	0.00
H2	0.78	0.00	0.78	0.78	0.01	0.01	0.00	0.78	0.78	0.78	0.78	0.00	0.01	0.00	0.00	0.01	0.00
CO2	1.78	0.01	1.79	1.79	0.33	0.33	0.02	1.46	1.46	1.45	1.45	0.00	0.31	0.00	0.02	0.29	0.05
H2O	2685.2	6616.3	9301.5	9301.5	6600.8	6600.8	605.7	2700.7	2700.7	94.5	94.5	2606.3	11432.4	2831.1	834.3	10598.1	1668.5
CH4	1.31E-04	2.62E-09	1.31E-04	1.31E-04	4.22E-08	4.22E-08	2.71E-09	1.31E-04	1.31E-04	1.31E-04	1.31E-04	2.08E-10	3.97E-08	0.00	2.90E-09	3.68E-08	5.79E-09
AR	9.99E-03	6.73E-07	9.99E-03	9.99E-03	1.34E-05	1.34E-05	8.60E-07	9.98E-03	9.98E-03	9.98E-03	9.98E-03	7.69E-08	1.26E-05	0.00	9.20E-07	1.17E-05	1.84E-06
N2	0.011	0.000	0.011	0.011	0.000	0.000	0.000	0.011	0.011	0.011	0.011	0.000	0.000	0.00	0.000	0.000	0.000
H2S	0.48	0.01	0.48	0.48	0.19	0.19	0.01	0.29	0.29	0.29	0.29	0.00	0.18	0.00	0.01	0.17	0.03
COS	0.017	0.000	0.017	0.017	0.002	0.002	0.000	0.014	0.014	0.014	0.014	0.000	0.002	0.00	0.000	0.002	0.000
NH3	1.08	2.03	3.11	3.11	2.19	2.19	0.14	0.92	0.92	0.34	0.34	0.58	2.63	0.00	0.19	2.44	0.38
O2	4.79E-12	8.36E-06	8.36E-06	8.36E-06	1.57E-07	1.57E-07	1.01E-08	8.20E-06	8.20E-06	8.20E-06	8.20E-06	1.18E-09	1.48E-07	0.00	1.08E-08	1.37E-07	2.16E-08
NACL	7.36	6.82	14.18	14.18	10.07	10.07	0.65	4.11	4.11	0.00	0.00	4.11	13.54	0.00	0.99	12.55	1.98
Total Fluids Flow lbmol/hr	2697.4	6625.2	9322.6	9322.6	6613.6	6613.6	606.6	2709.0	2709.0	98.0	98.0	2611.0	11449.1	2831.1	835.5	10613.6	1671.0
Total Fluids Flow lb/hr	48940	119628	168568	168568	119562	119562	10954.18	49005.86	49005.86	1803.371	1803.371	47202.49	206812	51002	15091.93	191720	30183.86
Vapor Frac	0.00	0.00	0.00	0.00	0.00	0.00	0.00	0.00	0.04	1.00	1.00	0.00	0.00	0.00	0.00	0.00	0.00
Liquid Frac	1.00	1.00	1.00	1.00	1.00	1.00	1.00	1.00	0.96	0.00	0.00	1.00	1.00	1.00	1.00	1.00	1.00
Solids Mass Flow lb/hr																	
CHAR	7164.9	0	7164.9	7164.9	7154.2	7154.2	0.0	10.7	10.7	0	0	10.7	7164.9	0	522.9	6642.1	1045.7
SLAG	25501	0	25501	25501	25462.75	25462.75	25462.75	38.2515	38.2515	0	0	38.2515	38.2515	0	2.791367	35.46013	5.582733
Total Solids Flow lb/hr	32666	0	32666	32666	32617	32617	25463	49	49	0	0	49	7203	0	526	6678	1051

6.4.2 Cost Estimate

6.4.2.1 Cost Comparison between Conventional Lockhopper System and CSRP

GE's internal cost database, a vendor quote for the slag-water letdown turbine and Aspen ICARUS KBase were used to perform cost estimates for the conventional lockhopper system base case and the CSRP using the sized equipment lists developed for each case. Table 62 provides a breakdown of the Total Installed Costs (TIC) that were calculated for both cases. Figure 131 shows a graphical representation of the Total Direct Field Cost (TDFC) component of the TIC. These costs are for equipment that is sized for a single IGCC train producing roughly 300 MWe.

Table 62. Comparison of TIC Estimates for Lockhopper System Base Case vs. CSRP

	Cost, $		Savings, $	% Savings
Category	**L/H System**	**CSRP**	**(L-C)**	**(L-C)/L**
Equipment	4,311,059	3,004,002	1,307,057	30%
Piping	739,053	466,910	272,144	37%
Civil	116,646	139,535	-22,889	-20%
Steel	10,417,048	139,404	10,277,644	99%
Instruments	1,019,597	709,705	309,892	30%
Electrical	865,073	433,356	431,717	50%
Insulation	102,455	84,535	17,921	17%
Paint	62,762	31,114	31,648	50%
Total Direct Field Cost (TDFC)	**17,633,694**	**5,008,560**	**12,625,133**	**72%**
Indirect Field Cost (IFC)	1,230,000	828,000	402,000	33%
Freight	388,200	222,700	165,500	43%
Engineering and Home Office	1,813,300	1,309,400	503,900	28%
Other Project Costs	1,599,810	1,021,554	578,256	36%
Contingency	1,358,587	1,006,825	351,762	26%
Total Non-Field Cost (TNFC)	5,159,897	3,560,479	1,599,418	31%
Total Installed Cost (TIC)	**25,039,150**	**9,397,039**	**15,642,111**	**62%**

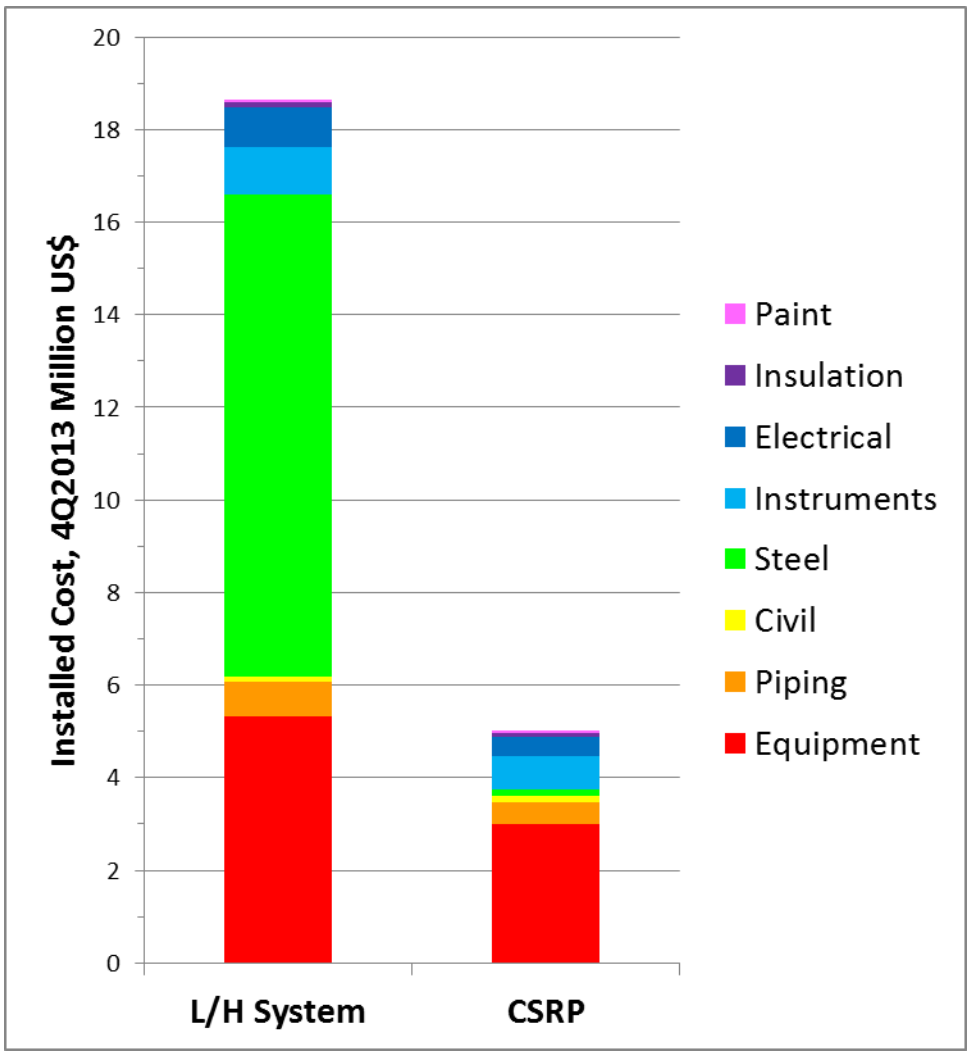

Figure 131. Lockhopper System vs. CSRP Total Direct Field Cost

The last line in Table 62 shows that the TIC of the lockhopper system is 25.0 M$, whereas the TIC of the CSRP is only 9.4 M$. This represents a single train cost savings of 15.6 M$, which corresponds to a reduction in cost for slag handling of 62%. As can be readily seen in Figure 131, the two major cost items driving this large difference in overall cost are the cost of the steel (green bars) and the cost of the major equipment (red bars).

There are two reasons for the huge difference in steel cost. First, the CSRP is inherently more compact than the lockhopper system. The major equipment is smaller and there is less of it. Second, the CSRP major equipment does not need to be stacked vertically one upon the other in order to take advantage of unobstructed gravity flow to move material through the system as is the case with the lockhopper system. This means that there is less height required in the gasifier support structure to hold all of the equipment. In fact, it may be possible to eliminate as much as 50 feet (i.e. three decks) of structure height by substituting a well-designed CSRP for the lockhopper system. Figure 132 and Figure 133 illustrate how these savings in structural steel occur.

Figure 132. Gasifier Support Structure Required for Lockhopper System

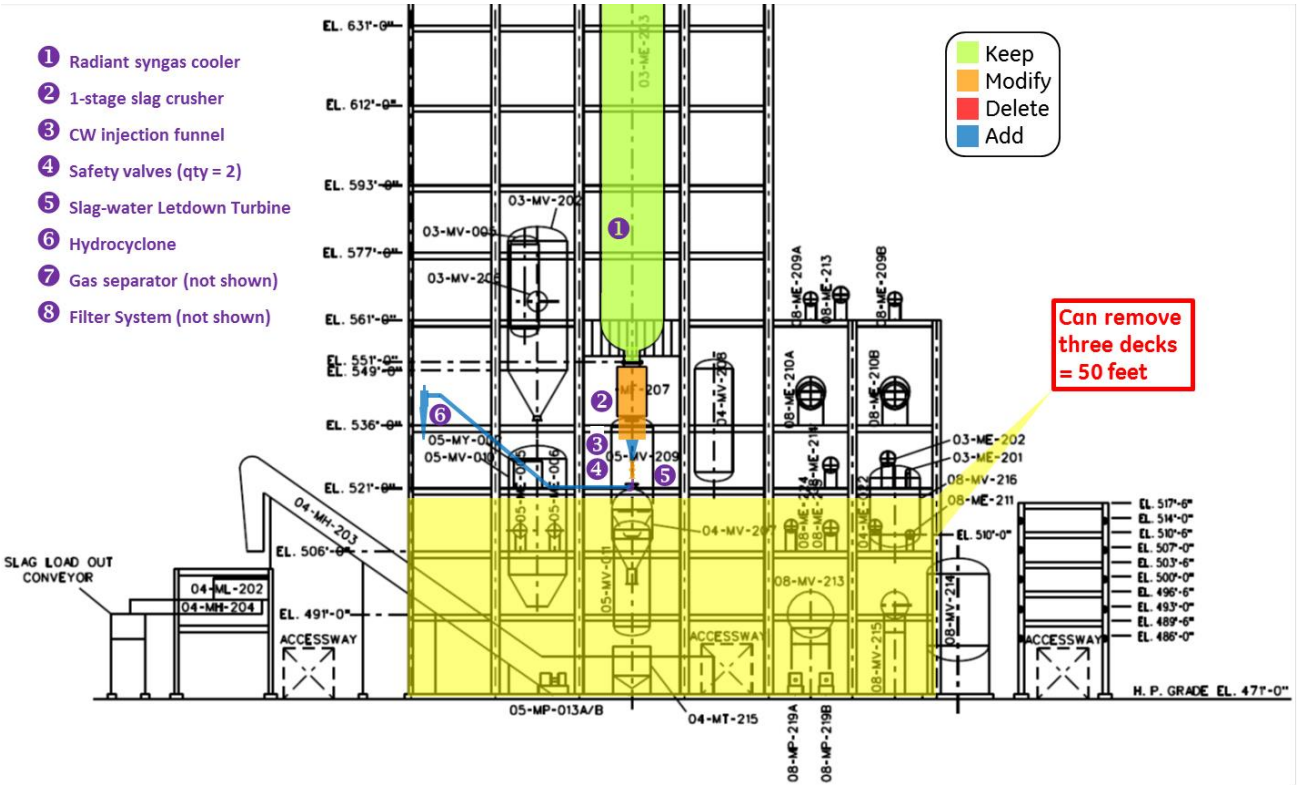

Figure 133. Gasifier Support Structure Required for CSRP

Figure 132 shows the major equipment for a lockhopper system installed underneath a Radiant Syngas Cooler (RSC) attached to a gasifier (not shown). With the exception of the lockhopper flush drum, which supplies a deluge of water to the lockhopper during dump mode, all of the large pieces of equipment are stacked one upon the other in order to provide an unobstructed, straight, downwards path for the gravitationally-driven flow of slag and water through the system. This stacking of equipment puts the bottom of the RSC five decks (80 ft.) above grade. The equipment colored in red indicates lockhopper system equipment that gets eliminated when a CSRP is used instead. Equipment in orange gets modified and equipment in green remains unchanged.

Figure 133 shows the major equipment for a CSRP installed underneath the RSC in place of the lockhopper system. Equipment colored in blue is new CSRP equipment that gets added in place of the lockhopper equipment colored in red in Figure 132. Equipment in orange represents CSRP equipment that is similar to the lockhopper equipment but is modified in some way in order to function as needed in the CSRP. For example, the slag crusher in the CSRP is a two-stage crusher (therefore larger) rather than a one-stage crusher as in the lockhopper system. And the two CSRP safety valves are nominally four- or six-inch valves compared with the 18-inch valves used in the lockhopper system and are, therefore, much smaller. Because all of the red-colored lockhopper system equipment gets removed when switching to a CSRP, it can be seen that up to three decks (50 ft.) of the gasifier support structure are no longer needed and can be removed. This is shown by the three bottom decks highlighted by the yellow box in Figure 133. The top of the yellow box represents the new grade, or ground level, for the gasifier structure in a plant using a CSRP. Note also that, because the CSRP controls the drop in pressure through the entire system, an appropriate amount of pressure may be left in the slag-water line connecting the discharge of the

letdown turbine to the inlet of the hydrocyclone. This residual pressure can be used to drive slag-water slurry upwards to a hydrocyclone that is elevated above the letdown turbine. Moreover, the residual pressure can also be used to drive slag-water laterally so that the gas separator vessel and the vacuum belt filter can be located a substantial distance from the gasifier structure, if needed. Consequently, the CSRP is much more flexible with respect to equipment layout.

Referring again to Table 62, the 10.3 M$ difference in steel cost between the lockhopper system and the CSRP represents the cost of the three decks that are not needed for the CSRP minus the difference in steel support costs for the major equipment of the lockhopper system and the CSRP. The savings in steel cost represents 81% of the savings in TDFC, while the savings of 1.3 M$ in major equipment cost represents 10% of the savings in TDFC. The CSRP equipment is inherently smaller than the lockhopper system equipment and, therefore, tends to be less expensive. The cost of civil work is the only category where the CSRP is more expensive than the lockhopper system. The reason for this is that the CSRP puts a lot more major equipment down at ground level rather than up in the gasifier structure. Therefore more concrete foundations for major equipment at ground level are required.

6.4.2.2 Black Water Flash System Equipment Size Reduction

The foregoing comparison of the costs of the lockhopper system and the CSRP treated those systems as though they were standalone systems. And, of course, they are not. In the case of the lockhopper system, in addition to receiving slag and water from the RSC sump, it also receives water from the bottom of the ammonia (NH3) stripper in order to refill the flush drum after a lockhopper dump. At the same time, it sends water containing slag fines to the black water flash system for degassing/deaeration and slag fines removal. In the case of the CSRP, the fact that it receives a continuous stream of slag-water from the RSC sump means that a certain amount of black water from the RSC sump that would normally be blown down through the black water flash system instead gets diverted through the CSRP. With that said, it is important to understand the integration of the lockhopper system and the CSRP with the rest of the gasification plant and, in particular, with the black water flash system, in order to understand the cost impact on the black water system that may arise from the use of a CSRP instead of a lockhopper system.

Referring to Figure 134, there are two major streams that feed the black water flash (BWF) system. The first is the continuous black water blow-down stream from the RSC sump to the LP flash drum. The second is the semi-continuous black water stream from the slag sump in the slag handling system (stream 415) that gets routed to the vacuum flash drum in the BWF system. When the lockhopper system is replaced with a CSRP, the continuous flow of slag-water slurry to the CSRP from the RSC sump causes the flow rate of the RSC sump black water blow-down stream to the BWF system to be reduced. As a result, the BWF system flash drum sizes can be reduced, which results in additional equipment cost savings beyond what is shown in Table 62. In Figure 134, 05-MV-109 is the LP flash drum, 05-MV-010 is the vacuum flash drum, 05-MV-011 is the vacuum flash overhead KO drum and 05-MV-021 is the vacuum pump KO drum. Pump 05-MP-012 is the vacuum flash bottoms pump, which is also known as the settler feed pump. For the CSRP case, there is a slight increase in the vacuum flash bottoms stream because the amount of water entering the BWF system from the slag sump is higher compared to the conventional lockhopper case. Since that stream is colder, less water vaporizes in the vacuum flash and the vacuum flash bottoms stream flow rate is higher. As a result, 05-MP-013 underneath the vacuum flash overhead knockout pot 05-MV-511 has a slightly lower flow rate. However, the difference in cost due to the flow difference through these two pumps is minor. As for the heat exchangers, 05-ME-005 has a lower flow rate since the RSC sump blowdown to the LP flash drum is reduced. Heat exchanger 05-ME-006 also

has lower flow rate because, as explained above, the vacuum flash overhead is reduced as a result of the colder water entering the vacuum flash drum from the slag sump. Note that the abbreviation GW in the figure stands for “Grey Water”.

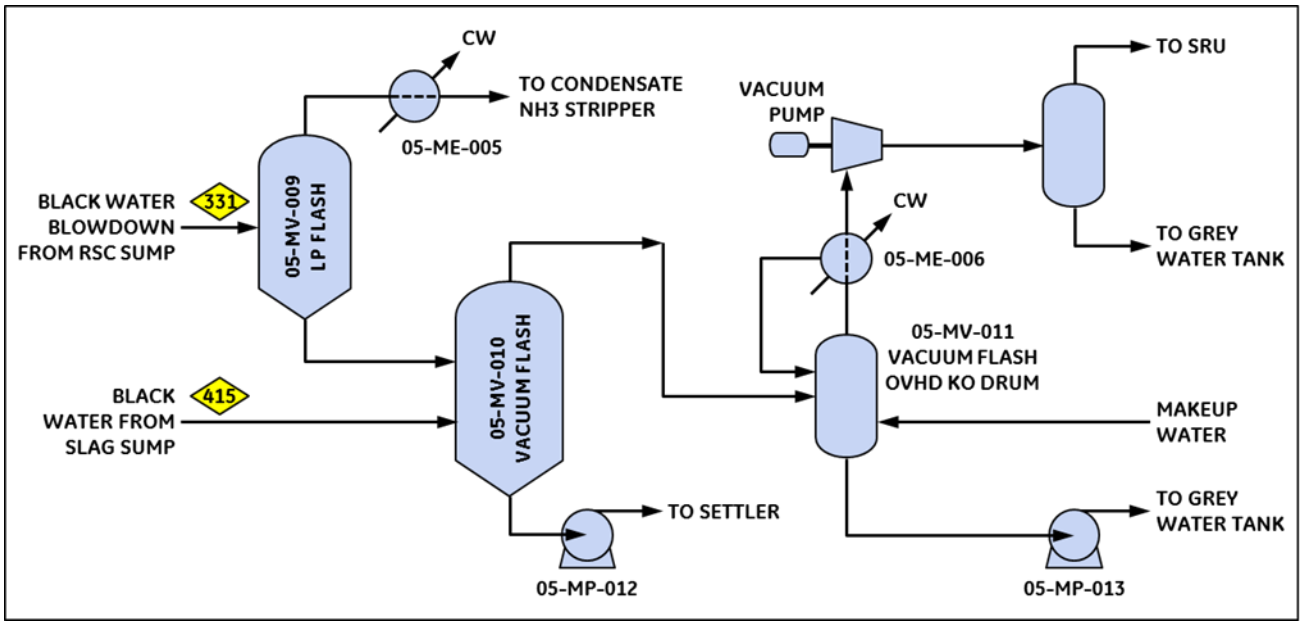

Figure 134. Schematic of BWF System

Table 63 shows the difference in flow rates to the BWF system between the conventional lockhopper and CSRP cases. Stream 331 carries the black water blowdown stream from the RSC sump to the BWF system LP flash drum. Stream 415 transfers black water from the slag sump to the vacuum flash drum.

Table 63. Inlet Stream Comparison for BWF system

	RSC Sump Blowdown to BWF LP Flash Drum		Slag Sump Black Water to BWF LP Flash Drum	
Fluids Flow lbmol/hr	Lockhopper	CSRP	Lockhopper	CSRP
CO	2.89	2.03	0.000	0.005
H2	3.46	2.32	0.000	0.007
CO2	7.61	5.28	0.006	0.291
H2O	11635.1	7975.1	7362.2	10598.1
CH4	0.000	0.000	0.00	0.00
AR	0.036	0.030	0.00	0.00
N2	0.055	0.033	0.00	0.00
H2S	1.98	1.41	0.006	0.168
COS	0.071	0.049	0.000	0.002
NH3	5.35	3.21	1.13	2.44
O2	6.64E-07	1.42E-11	4.31E-06	1.37E-07
NACL	30.2	21.9	5.1	12.5
Total Flow lbmol/hr	11686.7	8011.3	7368.4	10613.6
Total Flow lb/hr	211959	145352	132950	191720
Solids Flow lb/hr				
CHAR	10747.4	10747.4	5828.3	6642.1
SLAG	0	0	0.0	35.5
Total Flow lb/hr	10747.4	10747.4	5828.3	6677.5
Temperature F	396.9	413.6	121.0	155.5
Pressure psia	610.5	610.5	54.7	49.7

In comparing the lockhopper system to the CRSP, the main component to focus on is water, since the quantities of dissolved gases are small enough that they do not cause any significant impact on the sizing. As is evident in the table, the RSC sump blowdown to LP flash is reduced by about 30% in the CSRP configuration. The black water from the slag sump to the vacuum flash drum is increased by an equivalent amount, so one would intuitively expect this to cancel out the reduction in the LP drum size. However, this is not the case because another inlet to the vacuum flash drum is the bottoms stream from the LP flash drum, which is reduced by the same amount and hence compensates for this increase. Therefore, the net result is a decrease in the LP flash drum sizing and no change in the vacuum flash drum size. Another piece of equipment that would reduce in size is the LP flash let down valve. However that has not been included in this evaluation. Table 64 and Table 65 show sizing and total installed cost (TIC) information obtained using the Aspen economic evaluation tool.

Table 64. Sizing comparison for BWF System Equipment between CSRP and Lockhopper Cases

	Equipment #	05-MV-011	05-MV-109/209	05-MV-021	05-MV-010
Drums	**Lockhopper**				
	Vessel diameter [FEET]	5	6	3	8.5
	Vessel tangent to tangent height [FEET]	15	18.5	12	25
	CSRP				
	Vessel diameter [FEET]	5	5.5	3	8.5
	Vessel tangent to tangent height [FEET]	15	17	12	25.5
	Equipment #	05-MP-013	05-MP-112		
Pumps	**Lockhopper**				
	Liquid flow rate [GPM]	204.3	714.4		
	CSRP				
	Liquid flow rate [GPM]	187.8	757.9		
	Equipment #	05-ME-005	05-ME-006		
HX	**Lockhopper**				
	Heat transfer area [SF]	2909.0	1589.9		
	CSRP				
	Heat transfer area [SF]	2608.8	1092.8		

Table 65 shows a comparison of the TIC breakdown estimate between the CSRP and lockhopper cases. The TIC savings from reductions in the BWF system in the CSRP case come out to about $200,000 mainly due to the reduction in sizes of the LP flash drum and the two heat exchangers. This number can be added to the 15.6 M$ in TIC savings listed in Table 62, bringing the overall single train TIC savings of the CSRP to 15.8 M$ when compared with the cost of the conventional lockhopper system.

Table 65. TIC Cost Breakdown Comparison for BWF System Equipment

	Lockhopper	CSRP
Account	Total Cost ($)	
Equipment	1,380,715	1,256,614
AG Pipe	2,799,222	2,785,435
Piling	31,602	28,743
Concrete	113,849	108,498
Grout	6,620	6,694
Steel	80,686	79,012
Instrumentation	1,830,484	1,830,309
UG Electrical	44,265	44,252
AG Electrical	506,389	506,262
Pipe Insulation	244,553	255,351
Equip Insulation	68,554	68,397
Paint	49,075	43,332
Direct Totals	7,156,014	7,012,899
Const Equip & Indirects	1,518,100	1,511,700
Const Mgt, Staff, Supv	490,900	489,700
Freight	311,600	303,500
Engineering	1,222,300	1,221,900
Other Project Costs	1,298,001	1,280,106
Contingency	1,199,691	1,181,980
Indirect Totals	6,040,592	5,988,886
Project Totals:	13,196,606	13,001,785

6.4.3 Sensitivity Analysis

The amount of water in the inlet slag-water slurry stream was expected to have a noticeable impact on the sizing and cost of equipment in the CSRP. However, it was apparent that changes in slag-water flow rate to the CSRP produced countervailing changes in black water flow rate to the BWF system that had the potential to cause offsetting changes in equipment sizing and cost within the BWF system. Additionally, the slag-water letdown turbine is the key piece of equipment in the CSRP design, and vapor flashing in the turbine (driven by inlet temperature and outlet pressure) is a major concern due to issues surrounding potential cavitation and damage to this expensive piece of equipment. To that end, a sensitivity analysis was performed on three critical variables in order to evaluate the impact of variation in these parameters on equipment sizing and cost within the CSRP and the BWF system. The evaluated variables include:

1. Inlet slag-water slurry stream concentration that impacts water flow through the system
2. Slag-water slurry cooling temperature that impacts the vapor flashing in the slag-water letdown turbine
3. Slag-water letdown turbine discharge pressure that also impacts the vapor flashing in the turbine

6.4.3.1 Inlet Slag-Water Slurry Stream Solids Concentration

The following table (Table 66) shows the stream properties for the inlet slag-water slurry stream for 30 wt.%, 40 wt.% and 50 wt.% solids cases respectively.

Table 66. Inlet Slag-Water Slurry Stream Properties for 30 wt.%, 40 wt.% and 50 wt.% Solids Cases

Inlet stream 1			
Slag - water slurry conc.	30 wt %	40 wt %	50 wt %
CO	1.06	0.68	0.46
H2	1.22	0.78	0.52
CO2	2.77	1.78	1.19
H2O	4177.2	2685.2	1790.6
CH4	0.00020	0.00013	0.00009
AR	0.016	0.010	0.007
N2	0.017	0.011	0.007
H2S	0.74	0.48	0.32
COS	0.026	0.017	0.011
NH3	1.69	1.08	0.72
O2	0.00	0.00	0.00
NACL	11.70	7.36	4.86
Fluid Flow lbmol/hr	4196.42	2697.42	1798.69
Fluid Flow lb/hr	76146.95	48940.00	32631.96
Temperature F	422.64	427.96	434.66
Pressure psia	610.45	610.45	610.45
CHAR	7164.9	7164.9	7164.9
SLAG	25501.0	25501.0	25501.0
Solids Flow lb/hr	32665.9	32665.9	32665.9
Total flow lb/hr	108812.89	81605.94	65297.90

As is evident, the slag-water flow rate from the gasifier quench chamber reduces by about 57% going from 30 wt.% to 50 wt.% slurry concentration. However, this stream is mixed with all of the returning NH_3 stripper bottoms stream for cooling and, as seen in Table 67, this stream is highest for the 50 wt.% case and lowest for the 30 wt.% case. For the 50 wt.% case, the water to the CSRP is the lowest and therefore the quench blowdown to the BWF system is the highest. So the LP flash overhead to the ammonia stripper is also the highest. That is the reason why the NH_3 stripper bottoms recycle increases with increasing slag concentration entering the CSRP. Due to the stream mixing, the flowrate difference in stream 3 of Figure 130 (the turbine inlet stream) is largely evened out.

Table 67. NH_3 Stripper Bottoms Recycle Flowrate for the Three Cases

NH3 stripper water return		
Slag - water slurry conc.	lb/hr	Temp. (°F)
30 wt%	114,849	105
40 wt%	119,628	105
50 wt%	122,484	105

The following table (Table 68) shows the combined stream temperature to the slag-water letdown turbine for the three cases:

Table 68. Slag-Water Letdown Turbine Inlet Temperature for the Three Cases

Slag Letdown Turbine Inlet Temperature	
Slag - water slurry conc.	°F
30 wt%	243.7
40 wt%	212.4
50 wt%	189.3

The temperature of the combined stream is lowest for the 50 wt.% case since it has the highest recycle NH_3 stripper bottoms cooling flow and vice-versa for the 30 wt.% case.

The following table (Table 69) shows the vapor flashing upon expansion from 600 psig to 10 psig in the slag-water letdown turbine outlet for the three cases. The vapor flashing is negligible for all three cases. The amount of vapor that flashes in the turbine is highest for the 30% case, as expected, since the inlet is at the highest temperature compared to the other two cases.

Table 69. Volume Fraction of Vapor in Turbine Outlet for the Three Cases

Vapor flash in turbine discharge (stream 4)		
Slag - water slurry conc.	Vol. Fraction of vapor in Turbine outlet	Flow (lb/hr)
30 wt%	0.980%	1874.3
40 wt%	0.082%	138.1
50 wt%	0.031%	47.4

The following table (Table 70) shows the equipment sizing and cost comparison for the three cases.

Table 70. Equipment and Cost Sizing for Slag-Water Solids Concentration Sensitivity

Cost estimate							
Pumps							
	PT-400 (Slag Turbine)		P-401 (Pump for NH3 stripper bottoms)		P403 (CSRP Slag sump pump)		
	Fluid flowrate (gpm)	TIC ($)	Fluid flowrate (gpm)	TIC ($)	Fluid flowrate (gpm	TIC ($)	Total
30%	477.88	61800	252.18	108500	503.72	57600	227900
40%	418.90	57700	261.70	108700	460.93	57300	223700
50%	383.62	51100	267.73	108900	431.23	54400	214400

Drums							
	V-410						
	Flowrate (lb/hr)	Temp	Vap frac	Liq. Frac	Diameter (ft)	Tangent to tangent height (ft)	TIC ($)
30%	55465	225.52	0.0513	0.949	4.5	13.5	134100
40%	48874	213.35	0.0036	0.996	4.5	13.5	134100
50%	44922	191.05	0.0010	0.999	4.5	13	133400

Heat Exchangers		
	04ME004 (NH3 stripper bottoms cooler)	
	HX area ft2	TIC ($)
30%	3227.0	174600
40%	3412.5	177500
50%	3430.2	177700

The slag water letdown turbine (PT-400) is the only major equipment that sees all of the flow before it is split in the hydrocyclone and, as seen in the table, there is an approximately $100,000 cost difference between the 30 wt.% and 50 wt.% cases. However, this cost difference will get evened out in the BWF system sizing due to the reduced flow to the LP flash drum for the 30% case. The slag sump pump also follows the same trend due to the flow rate difference. As for the vacuum flash drum (V-410), being at the overhead of the hydrocyclone, the flowrate difference is too small to see any major difference in sizing. The same goes for the NH_3 stripper bottoms cooler. Overall, considering the major equipment in the CSRP, the 50 wt.% case comes to be about $100,000 lower. However, as mentioned before, this small cost savings will be counterbalanced elsewhere in the gasification plant, since the quench blowdown to the BWF system is higher and equipment in that system will need to be slightly upsized.

6.4.3.2 Slag-Water Slurry Cooling Temperature

The slag-water slurry cooling temperature variable is another critical variable due to its impact on vapor flashing in the slag-water letdown turbine, which is critical equipment. The following table (Table 71) shows the different slag-water slurry cooling temperatures and the resultant flashing volume fraction and the flow rate of vapor at the turbine outlet. The slag-water slurry stream is let down from 600 psig to 10 psig. 212°F (100°C) is the normal temperature of the mixed stream with the NH_3 stripper bottoms as the cooling medium and 140°F (60°C) was the proposed slag cooling temperature in the original two configurations. In the temperature range that was analyzed, the vapor flashing is negligible and going by the 40% vapor flashing limit that the vendor specified, it suggests there is a considerable cushion as far as the slag temperature cooling is concerned in case there are any upsets in the NH_3 stripper system (Figure 135).

Table 71. Vapor Flashing in Slag-Water Letdown Turbine Sensitivity to Slag-Water Slurry Cooling Temperature

Slag cool temp °F	Volume Fraction in Turbine discharge stream	Flow (lb/hr)
140	0.027%	46.3
160	0.032%	53.9
180	0.040%	67.4
195	0.051%	86.6
212	0.082%	138.1

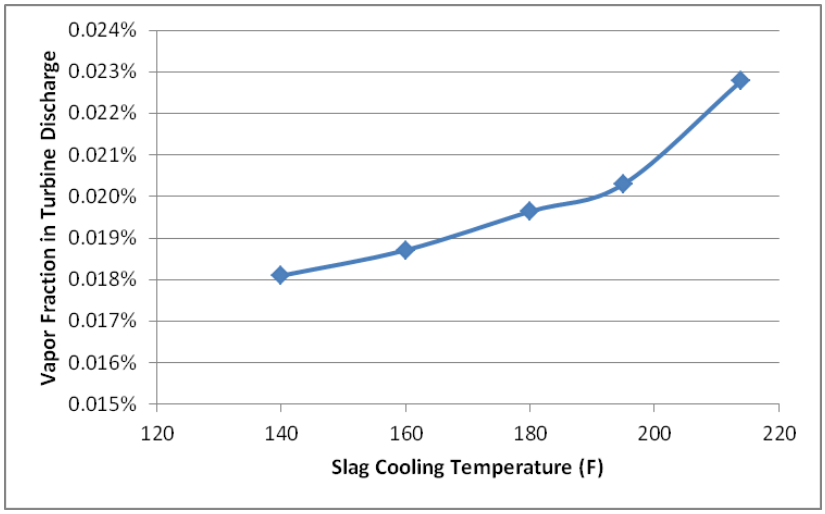

Figure 135. Vapor Flash Volume Fraction at Slag-Water Letdown Turbine Discharge

6.4.3.3 Slag-Water Letdown Turbine Discharge Pressure

The slag-water letdown turbine discharge pressure variable is another critical design variable due to its impact on vapor flashing in the turbine, which is a key piece of equipment. The turbine discharge pressure also has an effect on the design of downstream equipment. The following table (Table 72) shows the effect of different slag-water letdown turbine discharge pressures on the vapor flashing as well as the turbine energy extracted. These values are with the slag-water slurry cooling temperature of 212°F (100°C). As seen in Figure 136, the extracted energy reduces linearly with increasing discharge pressure and, for the range of interest; the turbine energy is between 52 to 58 KW. The vapor fraction is well within the limit set by the vendor for vapor flash fraction.

Table 72. Vapor Flashing and Turbine Extracted Energy with Different Discharge Pressures

Discharge pressure	Vapor flash	Flashed Vapor Flowrate at turbine discharge	Extracted Energy
psig	Vol. Fraction	Flow (lb/hr)	KW
10	0.082%	138.12	58.16
15	0.060%	100.95	57.66
25	0.041%	69.41	56.65
35	0.033%	55.08	55.65
45	0.028%	46.78	54.65
55	0.024%	41.29	53.65
65	0.022%	37.32	52.65

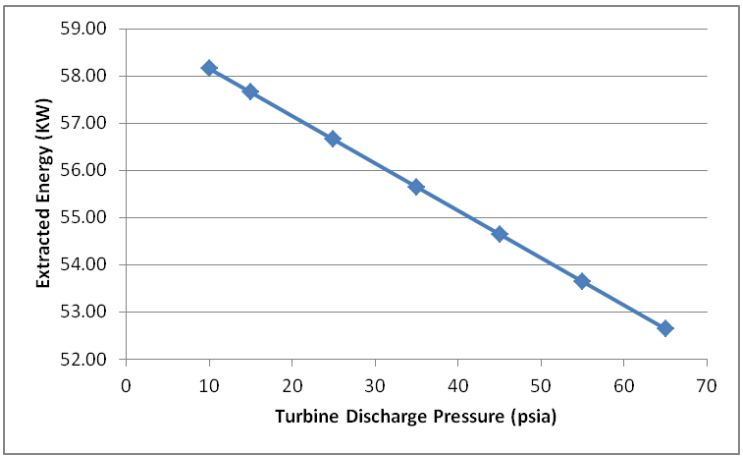

Figure 136. Turbine Extracted Energy with Different Discharge Pressures

6.4 RAM Analysis

A Reliability/Availability/Maintainability (RAM) analysis of the Continuous Slag Removal Process (CSRP) was performed and compared to the base case with lockhopper. The following three cases were compared:

a) Base Case with Lockhopper
b) Configuration 1 - CSRP with Slag-Water Slurry Cooler
c) Configuration 2 - CSRP with Direct Injection of Cooling Water

In all three cases, the slag handling systems were configured for an IGCC plant based on two 1800 cubic foot gasifier trains and producing roughly 600 MW of power.

Base Case: The conventional lockhopper based slag handling system is used to depressure and process the slag from the gasifier. Two cross-ties are used to connect portions of the slag handling systems of both gasifier trains in order to improve reliability. In the event that there is an equipment malfunction in Train 1 downstream of its lockhopper, the first cross-tie allows slag and water from the Train 1 lockhopper to be dumped into the slag sump of Train 2. And in the event that there is an

equipment malfunction in Train 2 downstream of its lockhopper, the second cross-tie allows slag and water from the Train 2 lockhopper to be dumped into the Train 1 slag sump. In order to accommodate the use of these two cross-ties, the equipment downstream of the lockhopper on both trains is sized to handle the combined slag and water from both trains.

Configuration 1: Cross-ties downstream of the hydrocyclones allow depressured slag-water slurry from one train to be handled in the vacuum belt filter of the second train in the event of an equipment malfunction. As in the Lockhopper Base Case, the vacuum belt filter systems are sized to accommodate the total flow from both trains. In addition, piping connections are provided to allow the use of an installed common spare slag-water letdown turbine in the event of a failure of the primary slag-water letdown turbine in either of the two trains.

Configuration 2: As with Configuration 1, cross-ties are used to allow depressured slag-water slurry from one train to be handled in the vacuum belt filter of the second train in the event of an equipment malfunction. And likewise, piping connections are provided to allow the use of an installed common spare slag-water letdown turbine in the event of a failure of the primary slag-water letdown turbine in either of the two trains.

In order to conduct a RAM analysis of a process, mean time between failure (MTBF) and mean time to repair (MTTR) data are needed for each piece of equipment in the process. For these three cases, the required data were obtained from a combination of equipment vendor data, an industry database and GE's in-house database acquired through experience at several commercial IGCC plants. The actual reliability, availability and maintainability (RAM) calculations were performed using the Visual SPAR 3.0 software package. Table 73 below shows a summary of the key results of the completed RAM analysis. The unreliability of 0.20% of Configuration 1, which has the slag-water cooler, is higher than the unreliability of the lockhopper system in the Base Case. And this contributes to a lower overall plant availability for Configuration 1 compared to the Base Case. In contrast, the unreliability of Configuration 2 (direct injection of cooling water) is lower than the Base Case. And this contributes to a slightly higher overall plant availability of 85.17% compared with the Base Case overall plant availability of 85.15. Based on these results, the Configuration 2 involving the recycle of water for direct quenching of the slag-water slurry is the preferred configuration for the CSRP. Through this analysis, it was demonstrated that the CSRP has a reliability that is comparable to GE's commercially available lockhopper-based Slag Handling System.

Table 73. Results of RAM Analysis of CSRP Cases 1 and 2 vs Base Case with Lockhopper

		Base case	CSRP - Case 1	CSRP - Case 2
Unit Unreliability	%	0.15	0.2	0.13
Overall Plant Availability	%	85.15	85.08	85.17

6.4.5 Testing and Development Plan

Having demonstrated 1) that the CSRP has comparable availability to GE's conventional lockhopper system and 2) that the CSRP is able to provide approximately 13.1 million dollars in total installed cost savings compared with the lockhopper system for a single IGCC train sized for a GE 7F turbine, the next question is: what will it take to progress the CSRP concept to commercial reality. The following is an outline of a five-phase testing and development plan that begins with proof-of-concept testing of the slag-water letdown turbine based on a Discflo pump head configured

to operate in reverse. Each phase builds on the success of the previous one by testing additional features of the CSRP. Progress from one phase to the next is driven by the achievement of key technical milestones by the end of each phase. The last phase involves a commercial-scale test of the complete CSRP at an operating gasification plant. The test plan includes the following five phases.

- Phase 1 – Proof of concept in pump manufacturer's facility
- Phase 2 – Process development in GE facility
- Phase 3 – Process extension to higher pressure (P), ΔP
- Phase 4 – Process extension to higher P, ΔP, and temperature (T) (at commercial gasification plant)
- Phase 5 – Full-scale hot demonstration at commercial gasification plant

In the following subsections, each of the five phases is described in more detail. The description for each phase includes a short introductory paragraph, a figure, a list of important test rig design and/or operating parameters, the location of the test rig, a list of tests to be performed using the test rig and a list of deliverables that must be achieved in order to proceed to the next phase.

6.4.5.1 Phase 1 - Proof of Concept

The purpose of Phase 1 is to quickly determine if a custom-modified head of a Discflo pump operated in the reverse direction can be made to work as a slag-water letdown turbine. The letdown turbine unit, which consists of the head of a Discflo pump, an eddy-current brake, an emergency friction brake, a clutch and a variable speed motor, will need to be assembled using compatible components from several vendors and made to work together as a single unit on a single shaft. By locating initial testing at the Discflo Corp. manufacturing site, the vendor of the most critical piece of equipment will be able to quickly make changes to the design of the pump head and the rotating discpac in order to ensure that the unit works properly as a letdown turbine. To simulate the stream of pressurized slag-water slurry that enters the letdown turbine from the gasifier quench chamber, a second Discflo pump will be used to pump model slurries of sand and pebbles from a reservoir into the inlet of the slag-water letdown turbine unit. This avoids the use of a large, high pressure vessel with a pressurized gas cap to simulate the quench chamber. Also, by establishing a continuously circulating flow loop, it allows tests to be run for much longer periods of time compared with a pressurized quench vessel that has been loaded with a fixed volume of model slag material. Thus, the use of a second Discflo pump to simulate the quench chamber is safer, more flexible and more cost effective.

1) Phase 1 test rig (Figure 137)
    a. Assemble a complete, single-shaft slag-water letdown turbine unit from components available from various vendors, including a custom-modified pump head from the Discflo Corporation.
    b. Use a second Discflo pump in normal operation mode to simulate the flow of high pressure slag-water slurry from a gasifier quench chamber.
    c. Low level of automation (mostly manual controls) to keep costs low.
    d. Test skid built for future expansion.
    e. 600-650 psig/dpsi, 70°F (21°C), 2-5 gpm.
2) Site: Discflo Corp. HQ (Santee, CA).
3) Tests
    a. Demonstrate reliable circulation w/ water and then w/ one model slurry (e.g. sand slurry) at minimum and maximum of ranges for P, ΔP and T.

b. Explore effect of manually added solids chunks to simulate the occasional large slag chunk or piece of refractory brick that may come out of the gasifier.
c. Demonstrate startup (S/U), shutdown (S/D) and emergency response.
d. Demonstrate effectiveness of brakes and clutch in controlling the speed and ΔP of the turbine.
e. Discflo Corp. determine optimal diameter, spacing, rpm, ribbing and discharge orifice size for discpac for the range of process parameters specified by GE.

4) Deliverables
   a. Proof-of-concept slag-water letdown turbine unit demonstrated at P, ΔP and T.
   b. Finalized pump head and discpac design from Discflo Corp.
   c. Functioning test rig ready for transport to GE facility for Phase 2.

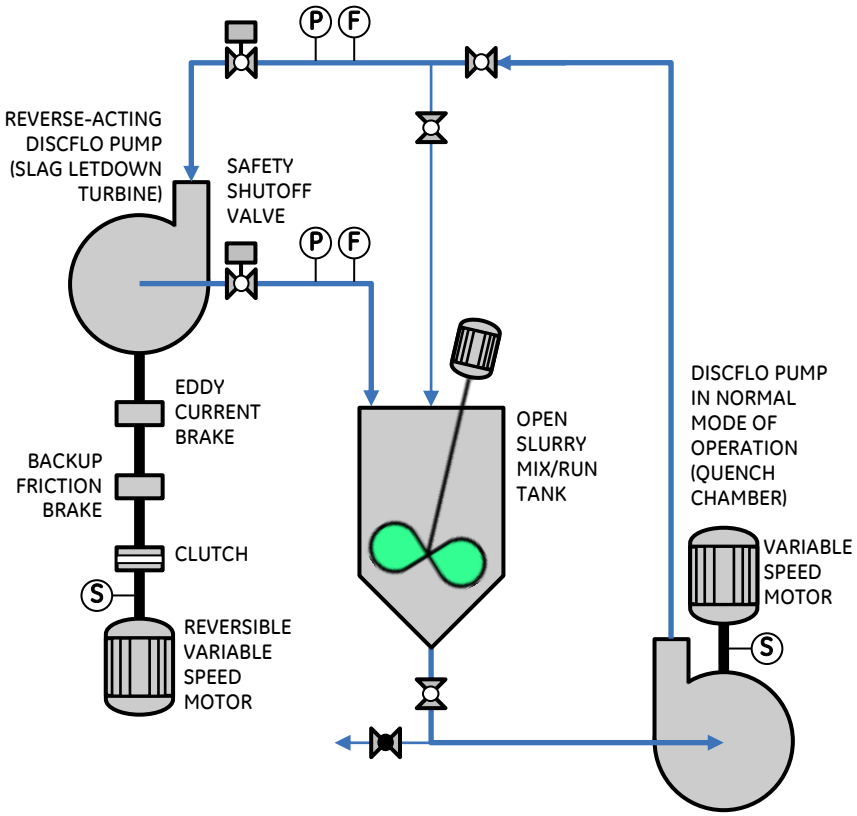

Figure 137. Test Rig Configuration for Phase 1

6.4.5.2 Phase 2 - Process Development

For Phase 2, the working test rig that was used to prove the basic operation of the slag-water letdown turbine unit at the vendor site will be moved to a GE test facility to continue testing and process development of the CSRP. The Key equipment of the test rig will remain the same, but extra instrumentation and an automatic control system will be added to facilitate making many test runs and to demonstrate GE's control system for the process. Phase 2 is when the basic operating map of the slag-water letdown turbine will be explored.

1) Phase 2 test rig (Figure 138)
   a. Use Phase 1 test rig.

b. Add additional instrumentation and automation to demonstrate proprietary GE control system.
c. 600-650 psig/dpsi, 70°F (21°C), 2-5 gpm.

2) Site: GE test facility
3) Tests
   a. Develop system performance map including:
      i. Several model solids, (sand, glass beads, ceramic beads, BBQ lava rock, slag from U.S. coal licensee)
      ii. Several particle size distributions (PSD) (fine, medium, coarse),
      iii. Several slurry concentrations (5, 10, 20, 40, 60 wt.%),
      iv. Test the above at several values of P and ΔP.
   b. Test system response to transients, e.g. oversize solids upsets and sudden changes in slurry concentration
   c. Demonstrate automated S/U, S/D, transient and emergency response.
4) Deliverables
   a. System performance map(s) up to 650 psig @ 70°F (21°C), with refined set of operating limits.
   b. Transient response map.
   c. Validated automation & control algorithms.

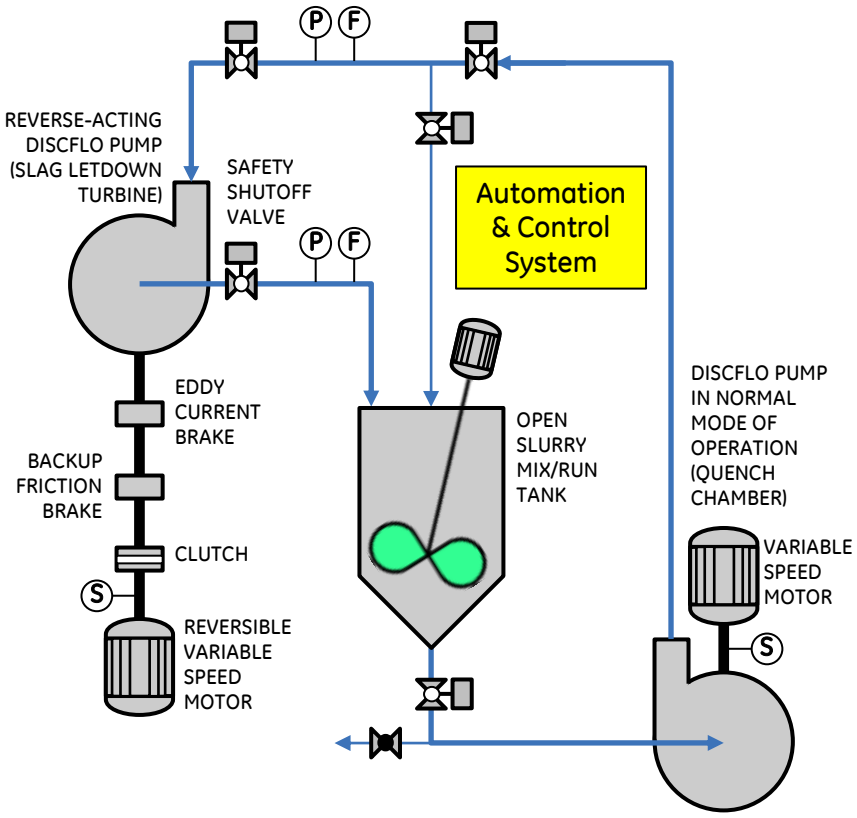

Figure 138. Test Rig Configuration for Phase 2

6.4.5.3 Phase 3 - Extend Pressure and ΔP Operating Ranges

A high pressure version of the Discflo pump currently available from the Discflo Corporation appears to be suitable for use as a slag-water letdown turbine for gasifiers operating at pressures

as high as 600 to 650 psig. However, for gasifiers operating at higher pressures, it may be necessary to put two letdown turbines in series in order to develop the pressure drop needed to fully depressurize the slag-water slurry stream. The test rig for this phase takes advantage of the capability for expansion built into the Phase 1 test rig to allow the addition of a second slag-water letdown turbine unit in series with the first, proof-of-concept unit as well as a second Discflo pump operated in the normal pumping mode to provide the simulated stream of slag-water slurry coming from a gasifier operating at pressures above 650 psig. The instrumentation and control system will be expanded in order to accommodate the additional equipment and the higher pressure operation of the entire system.

1) Phase 3 test rig (See Figure 139)
    a. Add second slag-water letdown turbine and second normally-acting pump to test rig used in Phase 2 in order to boost both total P and ΔP capability. Upgrade controls as needed.
    b. 1000-1250 psig/dpsi, 70°F (21°C), 2-5 gpm
2) Site – GE test facility
3) Tests
    a. Select several key test conditions from the operating map developed in Phase 2 and rerun those conditions to verify that the process operates the same at 1250 psig as it did at 650 psig. Expand system operating map at higher pressure as needed, depending on differences detected from operating map at lower pressure.
    b. Test response to several transients to see if system responds same as at lower pressure.
    c. Test various emergency response scenarios, e.g. failure of letdown turbine #1, letdown turbine #2 or failure of both.
4) Deliverables
    a. Validated automation and control algorithms.
    b. System performance map up to 1250 psig at 70°F (21°C), with refined set of operating limits.
    c. Transient response map at 1250 psig.
    d. Adequate emergency responses developed.

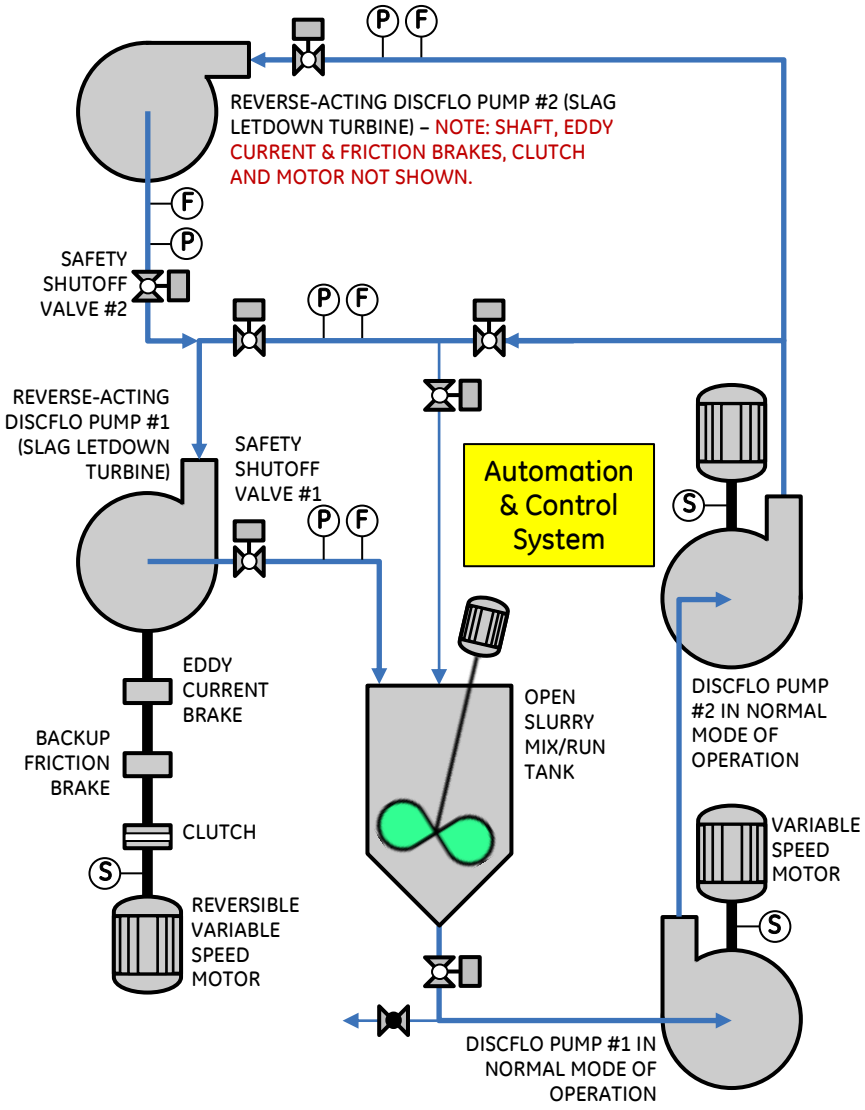

Figure 139. Test Rig Configuration for Phase 3

6.4.5.4 Phase 4 - Extend Temperature Operating Range

Testing done in Phases 1 through 3 will all be conducted at room temperature in order to avoid the complication and expense of adding equipment that could heat the model slag-water slurry stream to temperatures normally found in gasifier quench chambers. However, Phase 4 testing is designed to allow the introduction of higher temperatures into the test rig in order to explore the ability of the slag-water letdown turbine unit(s) to operate at both the temperatures and pressures normally found in commercial gasifier quench chambers. Testing during Phase 4 will confirm the results of material and energy balance calculations that indicated that the flashing of dissolved gases within the letdown turbine during operation would not be a problem that interfered with the operation of the turbine.

In order to avoid having to add heating and cooling equipment to the test rig for this phase, Phase 4 will be conducted as a slipstream test at a commercial gasification facility. The commercial plant lockhopper vessel will be modified to allow connection of the CSRP test skid to the lockhopper so

that a continuous slipstream of slag-water slurry may be obtained during normal operation of the commercial gasifier. One of the existing flanged nozzles on the lockhopper may be used for the connection so that the slipstream may be obtained without interfering with normal lockhopper operation. In order to move the test rig to a commercial facility for Phase 4, the test rig built for Phases 1 and 2 will need to be fabricated in modules that facilitate easy disassembly, transport and shipping as well as easy installation in an existing facility in which the gasifier support structure may already be crowded with existing equipment.

1) Phase 4 test rig (See Figure 140)
    a. Connect mobile test skid to commercial gasifier lockhopper to tap into source of high temperature slag and slag water with dissolved gases.
    b. Modify skid and plant controls as needed.
    c. 600-1250 psig/dpsi, 250-450°F (121-232°C), 2-5 gpm
2) Site – commercial coal gasification facility
3) Tests
    a. Confirm proper operation of test rig, including controls and safety system.
    b. Successfully operate the test rig during gasifier S/U, long-term ops, system transients and S/D. Target run times as long as gasifier run times.
    c. Test effect of cold water injection in controlling system temperatures and dissolved gas evolution.
    d. Collect and analyze slag, water and gas operating samples under different conditions.
    e. Capture operating, erosion and corrosion data.
4) Deliverables
    a. Successful long-term operation of test rig at host gasifier operating conditions.
    b. Successful system response to plant transients.
    c. Successful control of system temperatures and rate of dissolved gas evolution.
    d. Database of heat and material balance (HMB) data around the test rig plus erosion and corrosion rates.

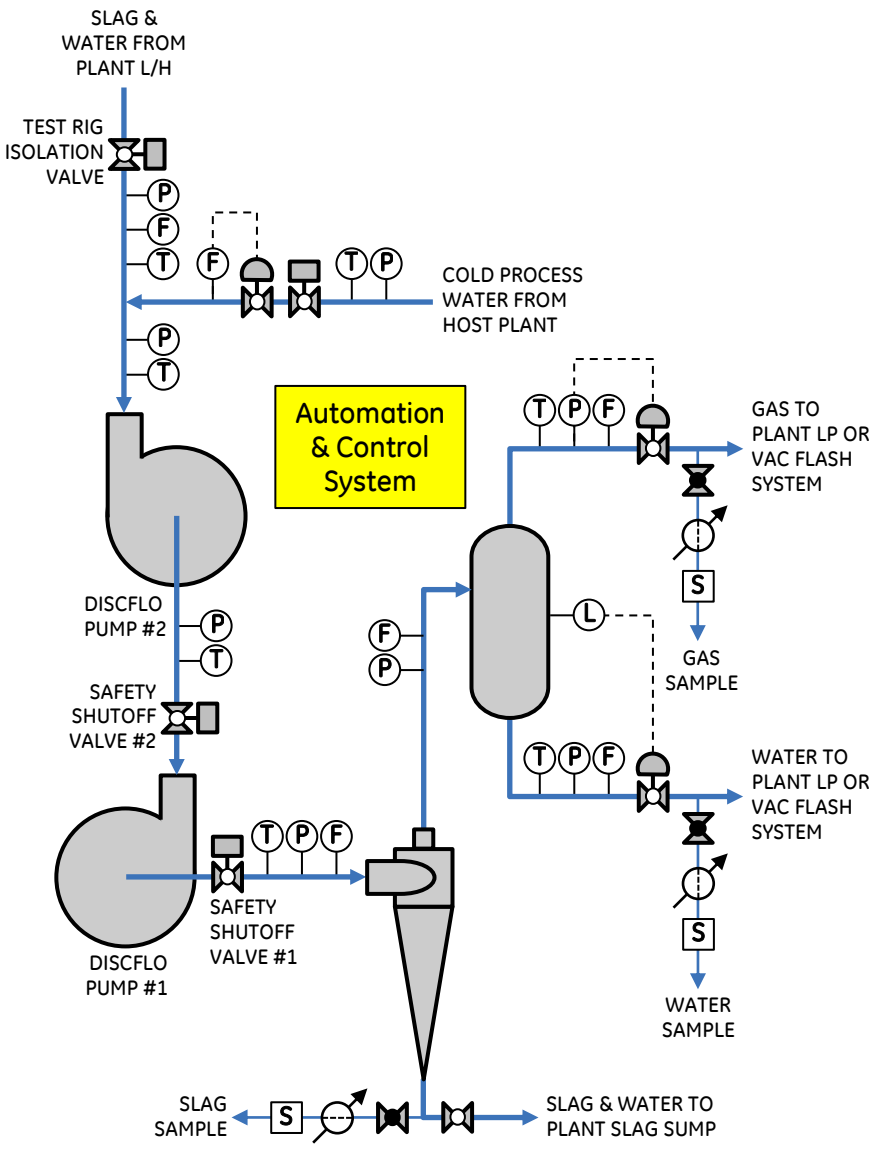

Figure 140. Test Rig Configuration for Phase 4

6.4.5.5 Phase 5 - Full-scale Hot Demo at a Launch Site

Phase 5 will involve a full-scale demonstration of a commercial size CSRP at an operating gasification facility. In order to minimize scale-up risk, it will be advantageous to select a host site with one of the smaller gasifiers in commercial operation today. Most likely, the demonstration unit will need to be installed in parallel with the host plant's existing lockhopper system in order to mitigate risk to existing plant operations. Note that Figure 138 shows two slag-water letdown turbines installed in parallel. If the host gasifier's normal operating pressure is low enough, only one letdown turbine unit will be required.

1) Phase 5 commercial demonstration unit (See Figure 141)
    a. Design and procure equipment sized to handle full slag-water slurry flow from commercial host.

   b. Connect commercial demo unit to bottom discharge of host plant's slag crusher using a large, inverted Y-connection to allow the demo equipment to be installed in parallel with the existing lockhopper system.
   c. 600-1250 psig/dpsi, 250-450°F (121-232°C), flow to be determined
2) Site – Commercial coal gasification plant
3) Tests
   a. Confirm proper operation of demo unit, including controls and safety system, using water only during preheat.
   b. Successfully operate the demo unit during gasifier S/U, long-term ops, system transients and S/D. Target run times as long as gasifier run times.
   c. Collect and analyze slag, water and gas operating samples under different conditions.
   d. Capture operating, erosion and corrosion data.
4) Deliverables
   a. Successful long-term operation of demo unit (all aspects) at host plant operating conditions.
   b. Successful system response to plant transients.
   c. Database of HMB data around the demo unit plus erosion and corrosion rates.

Once this five-phase testing and development plan has been successfully completed, the CSRP will be ready for commercial deployment in greenfield plants. Risk to the plant or plants that are constructed for the first time without lockhopper systems can be mitigated by the use of spare slag-water letdown turbine units, which can be shared between adjacent gasifier trains. Likewise, the installation of cross-tie piping that allows the equipment downstream of the letdown turbines to be shared between trains in an emergency can also mitigate risk.

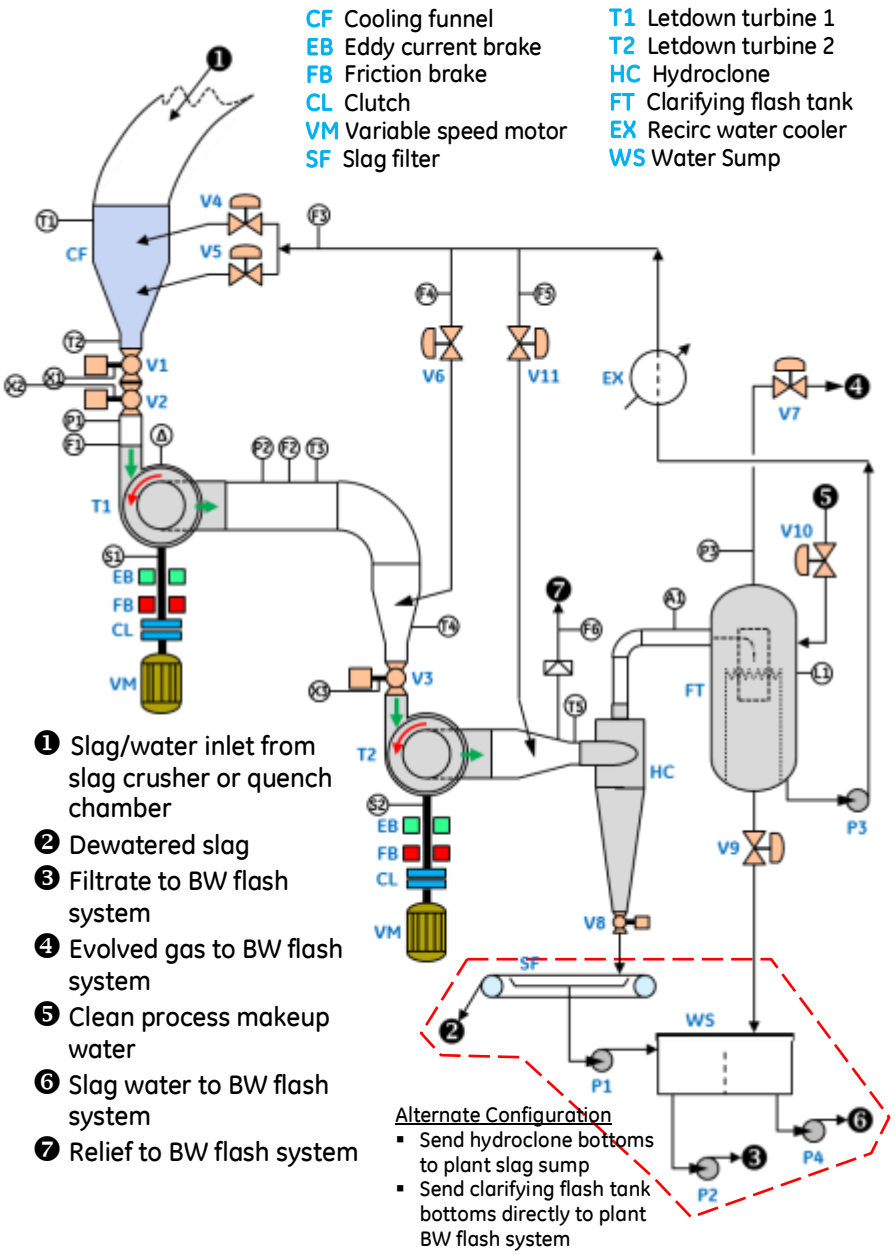

Figure 141. Commercial Demonstration Unit Configuration for Phase 5

Combination of CSRP and Black Water Flash System

In response to a suggestion from the DOE peer review session that took place in May 2014, a consolidation of the CSRP and the black water flash (BWF) system was investigated in an attempt to generate even more capital cost savings compared with what had already been demonstrated by the replacement of the lockhopper system with the CSRP. (This was not part of the original statement of performance objectives (SOPO).) The aim of this exercise was to eliminate a significant chunk of IGCC plant capital cost. The BWF system normally handles the finer fraction of slag plus any unconverted carbon, or char, that exits the gasifier quench chamber via the black water blow down line. The BWF system removes the fine slag and the char as well as dissolved

gases from the black water so that the water can be recycled to the gasifier quench chamber as grey water.

In order to combine the CSRP and the BWF system into a hybrid CSRP-BWF system, it was first necessary to insert an LP flash drum (V-420) between the letdown turbine and the hydrocyclone. In the standalone CSRP configuration, the amount of dissolved gases coming out of solution is negligible and it does not affect the operation of the hydrocyclone. But with the addition of the black water and all its dissolved gases, the amount of gas that would come out of solution inside the hydrocyclone would have overwhelmed the hydrocyclone. The hydrocyclone vendor warned us that evolved gas and water vapor would have filled the rotating core of the hydrocyclone to the point where the concentrated slag-water stream would not be able to pass through the bottom exit. But this problem is mitigated by removing most of the gas before the hydrocyclone.

The major function of the vacuum flash drum in the BWF system is to deaerate the slag sump water that is recycled back into the system to avoid corrosion issues. The elimination of this drum is compensated for by using a sealed slag drag conveyor/slag sump system with a nitrogen blanket. This removes the possibility of ambient O2 dissolving in the slag sump water.

The overhead gas stream from the relocated LP flash vessel is sent to the NH3 stripper, and the bottoms stream goes to the hydrocyclone. The water in the hydrocyclone underflow goes to the slag drag conveyor/slag sump from where it is recycled back into the system. As mentioned above, since the deaerating function of the BWF system vacuum flash drum was eliminated, the slag drag conveyor/slag sump needs to be sealed with a nitrogen blanket in order to avoid aeration of the slag sump recycle water. Stream 415is sent to the settler for final removal of fine particles instead of being sent to the vacuum flash drum. The slag wash make up, stream 405, is increased in the hybrid case in order to replace other make-up water streams that were lost with the elimination of the standalone BWF system.

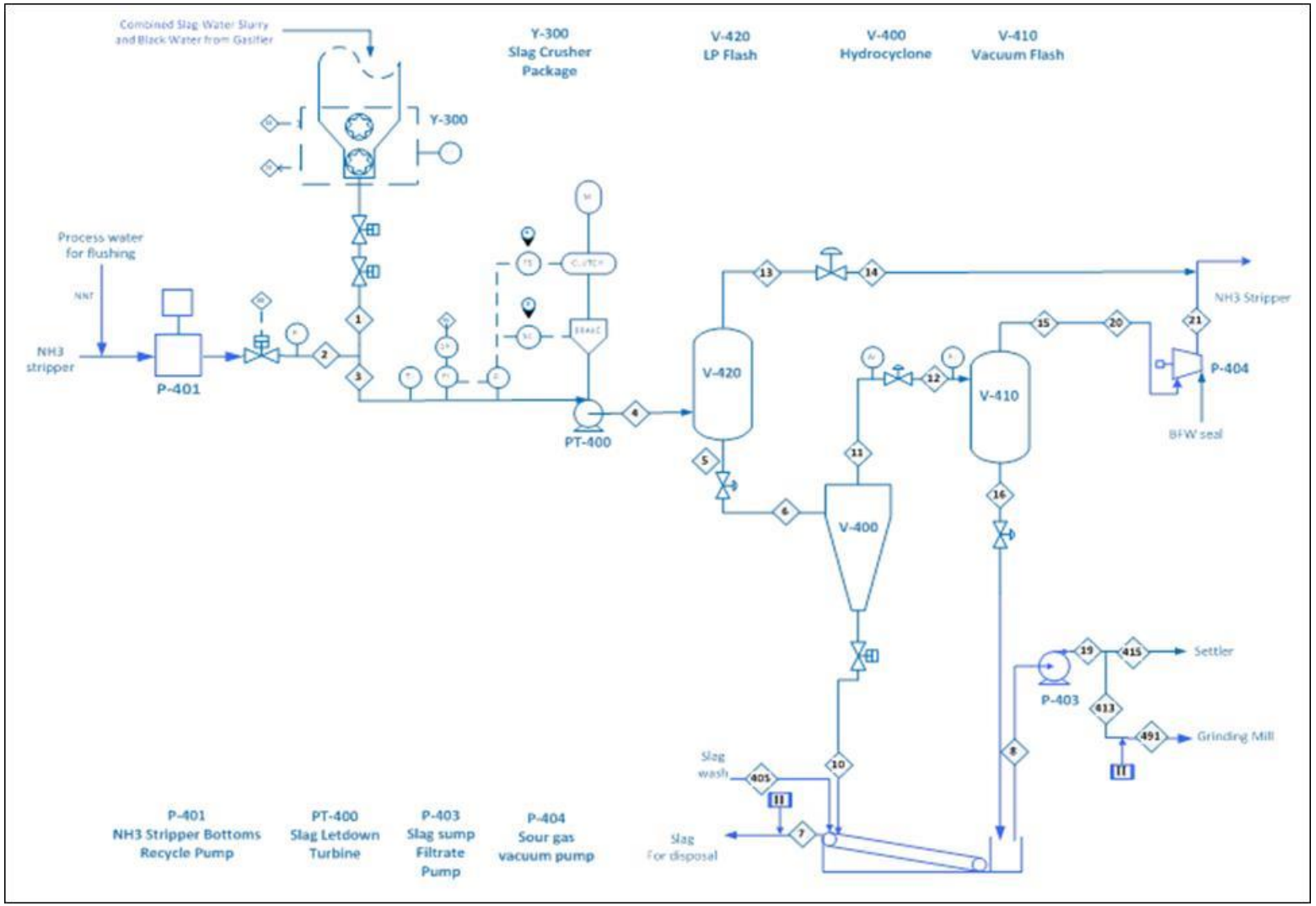

Figure 142. Schematic of Hybrid CSRP-BWF System

A new Aspen Plus® heat and material balance simulation was generated for the hybrid CSRP-BWF system. All of the water normally blown down through the black water system was routed along with the coarser slag-water slurry through a larger CSRP with the configuration shown in Figure 142. The following table (Table 74) shows the HMB streams for the hybrid CSRP-BWF system.

Table 74. HMB results for Hybrid CSRP-BWF System

	1	2	3	4	5	7	8	10	11	12	13	14	15	16	19	20	21	405	413	415	491	BFWSEAL
Substream: MIXED																						
Temperature F	419.2	105.9	291.0	238.6	238.6	155.3	148.1	232.2	232.2	232.2	238.6	238.6	182.9	182.9	148.2	182.9	239.2	100.0	148.2	148.2	148.2	105.0
Pressure psia	610.5	610.5	610.5	24.7	24.7	14.7	8.0	21.7	21.7	21.7	24.7	24.7	8.0	8.0	49.7	8.0	24.7	114.5	49.7	49.7	49.7	254.3
Mole Flow lbmol/hr																						
CO	2.12	0.00	2.12	2.12	0.00	0.00	0.00	0.00	0.00	0.00	2.12	2.12	0.00	0.00	0.00	0.00	0.00	0.00	0.00	0.00	0.00	0.00
H2	2.43	0.00	2.43	2.43	0.00	0.00	0.00	0.00	0.00	0.00	2.43	2.43	0.00	0.00	0.00	0.00	0.00	0.00	0.00	0.00	0.00	0.00
CO2	5.53	0.01	5.54	5.54	0.02	0.00	0.02	0.02	0.01	0.01	5.52	5.52	0.01	0.00	0.02	0.01	0.01	0.00	0.00	0.01	0.00	0.00
H2O	8354.3	6677.2	15031.5	15031.5	14115.0	605.7	18067.3	10021.7	4093.4	4093.4	916.5	916.5	243.6	3849.8	18067.3	243.6	326.8	4801.6	920.9	17146.4	1841.8	83.3
CH4	4.09E-04	2.75E-09	4.09E-04	4.09E-04	4.10E-09	1.19E-10	2.79E-09	2.91E-09	1.19E-09	1.19E-09	4.09E-04	4.09E-04	1.19E-09	1.19E-15	2.79E-09	1.19E-09	1.19E-09	0.00E+00	1.42E-10	2.65E-09	2.84E-10	0.00E+00
AR	3.12E-02	7.18E-07	3.12E-02	3.12E-02	1.15E-06	3.33E-08	7.82E-07	8.15E-07	3.33E-07	3.33E-07	3.12E-02	3.12E-02	3.33E-07	1.59E-12	7.82E-07	3.33E-07	3.33E-07	0.00E+00	3.99E-08	7.42E-07	7.97E-08	0.00E+00
N2	0.035	0.000	0.035	0.035	0.000	0.000	0.000	0.000	0.000	0.000	0.035	0.035	0.000	0.000	0.000	0.000	0.000	0.000	0.000	0.000	0.000	0.000
H2S	1.48	0.01	1.49	1.49	0.02	0.00	0.01	0.01	0.01	0.01	1.47	1.47	0.01	0.00	0.01	0.01	0.01	0.00	0.00	0.01	0.00	0.00
COS	0.052	0.000	0.052	0.052	0.000	0.000	0.000	0.000	0.000	0.000	0.052	0.052	0.000	0.000	0.000	0.000	0.000	0.000	0.000	0.000	0.000	0.000
NH3	3.31	1.81	5.12	5.12	2.88	0.08	2.37	2.05	0.84	0.84	2.24	2.24	0.43	0.41	2.37	0.43	0.43	0.00	0.12	2.25	0.24	0.00
O2	0.00	0.00	0.00	0.00	0.00	0.00	0.00	0.00	0.00	0.00	0.00	0.00	0.00	0.00	0.00	0.00	0.00	0.00	0.00	0.00	0.00	0.00
NACL	29.00	6.58	35.58	35.58	35.58	1.03	34.54	25.26	10.32	10.32	0.00	0.00	0.00	10.32	34.54	0.00	0.00	0.00	1.76	32.78	3.52	0.00
Total Flow lbmol/hr	8398.3	6685.6	15083.9	15083.9	14153.5	606.9	18104.3	10049.0	4104.5	4104.5	930.4	930.4	244.0	3860.5	18104.3	244.0	327.3	4801.6	922.8	17181.5	1845.6	83.3
Total Flow lb/hr	152619	120706	273325	273325	256413	10974.41	327545	182053	74359.84	74359.84	16912.06	16912.06	4395.379	69964.46	327545	4395.379	5895.379	86502	16695.42	310850	33390.83	1500
Vapor Frac	0.00	0.00	0.00	0.06	0.00	0.00	0.00	0.01	0.01	0.01	1.00	1.00	1.00	0.00	0.00	1.00	0.77	0.00	0.00	0.00	0.00	0.00
Liquid Frac	1.00	1.00	1.00	0.94	1.00	1.00	1.00	0.99	0.99	0.99	0.00	0.00	0.00	1.00	1.00	0.00	0.23	1.00	1.00	1.00	1.00	1.00
Mass Flow lb/hr																						
CHAR	17912.4	0.0	17912.4	17912.4	17912.4	0.0	17912.4	17885.5	26.9	26.9	0.0	0.0	0.0	26.9	17912.4	0.0	0.0	0.0	913.0	16999.3	1826.0	0.0
SLAG	25501	0	25501	25501	25501	25462.75	38.2515	25462.75	38.2515	38.2515	0	0	0	38.2515	38.2515	0	0	0	1.949729	36.30177	3.899457	0
Total Flow lb/hr	43413	0	43413	43413	43413	25463	17951	43348	65	65	0	0	0	65	17951	0	0	0	915	17036	1830	0

Comparing the fluid flow rate in stream 3 for the standalone CSRP (Table 61) and the hybrid CSRP-BWF system (Table 74), the fluid flow rate in the hybrid case is almost double. The following table (Table 75) shows the preliminary sizing comparison between the hybrid CSRP-BFW and the standalone CSRP configurations.

Table 75. Preliminary Sizing Comparison between Standalone and Hybrid CSRP Equipment

Cylinder	Hybrid	Standalone
Equipment number	V-410 (Vacuum Flash Drum)	
Vessel diameter [FEET]	5	4.5
Vessel tangent to tangent height [FEET]	14.5	13.5

Pump	Hybrid	Standalone	Hybrid	Standalone	Hybrid	Standalone
Equipment number	PT-400 (Slag Turbine)		P-401 (NH3 stripper bottoms recycle pump)		P-403 (Slag sump pump)	
Liquid flow rate [GPM]	697.1	418.9	266.1	261.7	751.7	460.9

The flash vessel V-410 on the hydrocyclone overflow line is smaller for the standalone case, but the sizing is not that much different because it is at the overhead of the hydrocyclone and most of the flow goes to the underflow. The slag-water letdown turbine (PT-400) and slag sump pump (P-403) for the hybrid case receive more than 150% of the flow compared with the standalone CSRP case.

The following table (Table 76) shows a comparison of the sizes of the key vessels between the hybrid CSRP-BWF system and the standalone BWF system configurations.

Table 76. Preliminary Sizing Comparison between Standalone BWF and Hybrid CSRP Vessels

Cylinder	Hybrid	Standalone
	LP Flash drum	
Equipment	V-420	05-MV-109
Vessel diameter [FEET]	6.5	5.5
Vessel tangent to tangent height [FEET]	20	17

V-420, the LP flash drum upstream of the hydrocyclone, receives all of the flow of hybrid system. Therefore, it is larger than the standalone BWF LP flash drums (05-MV-109). The elimination of the vacuum flash drum (05-MV-010) that is in the BWF system, but which is not required in the hybrid system, results in a TIC savings of about $155,000.

Combining the sizing results from Table 75 and Table 76, no significant cost savings are apparent with the hybrid CSRP-BFW system compared with the separate CSRP and BFW systems. This is due to the fact that the combination of the two systems essentially just transfers the flow of black water from the BWF system to the hybrid CSRP-BWF system. Even though we eliminated all of the BWF equipment, that gain is offset by 1) the addition of equipment in the CSRP for removing dissolved gases and 2) the increase in size of CSRP equipment (letdown turbine, hydrocyclone, slag drag conveyor/slag sump) needed to accommodate the increased flow rate of water through the hybrid system. The money that was saved by eliminating equipment from the black water blow down system (most importantly, the vacuum flash drum, 05-MV-010) was counterbalanced by the increased cost of the larger equipment that was required in the CSRP. These results do not warrant the effort or money that would need to be

spent in redesigning the gasification plant to accommodate the elimination of the BWF system and the substitution of the hybrid CSRP-BWF system for the standalone CSRP. Moreover, combining the CSRP and the BWF system compromises the ability to recycle unconverted carbon to the gasifier. Any unconverted carbon (char) exiting the gasifier tends to exit through the BWF system where it can be concentrated to the point that it makes economic sense to recycle it to the gasifier to boost overall carbon conversion. However, once the black water is combined with the slag water, the char gets diluted in a much larger combined stream. Separating that char from the larger, combined stream will be difficult, and more equipment will be required. This is a serious drawback for the combined scheme that, for all intents and purposes, cancels out the small capital cost savings that is realized by the elimination of BWF system equipment. Based on the above results, it does not appear as though it makes economic sense to combine the black water blow down system with the CSRP.

6.5 Conclusions

- Continuous slag letdown is a viable replacement for the lockhopper-based batch system because:
  - ✓ The modified IGCC layout, i.e. placing the gasifier closer to grade, simplifies access for operations and maintenance personnel and saves millions of dollars in gasifier structure costs.
  - ✓ With the elimination of the batch sequence of operations that cycle the vessel contents between high pressure and low pressure, the isolation valve service is less severe leading to a longer lasting and less costly design.
  - ✓ Reduced operating cost by reducing the flushing water demand
  - ✓ The continuous process does not require the tight sequence of controls operations that governs the batch operation.
- Based on a detailed technology evaluation, a slag-water letdown turbine, which is based on running a rotating parallel disc pump in reverse, was identified as the best option. The slag-water letdown turbine assembly will consist of a Discflo® pump head, an eddy current brake, a friction brake, a clutch and a variable speed electric motor - all connected via a common rotating shaft.
- The CSRP is 62% less expensive than the lockhopper system on a total installed cost basis. The total installed cost for the lockhopper system is 25.0 M$, whereas the total installed cost for the CSRP is 9.4 M$. Thus, 15.6 M$ in total installed cost is saved by using the CSRP rather than a lockhopper system. 81% of the savings in total direct field costs is attributable to the fact that the CSRP is a much more compact system that allows three decks (50 ft.) to be removed from the gasifier support structure. 10% of the cost savings in total direct field costs is attributable to the lower cost of the CSRP major equipment compared with the cost of the lockhopper system major equipment.
- In optimizing the CSRP configuration, it was found that the slag-water slurry cooler could be eliminated. That effectively removed one major point of unreliability in the system and also provided additional cost savings.
- Consolidation of the CSRP and the black water flash system showed no apparent savings due to the fact that the money that was saved by eliminating equipment from the black water flash system was largely counterbalanced by the increased cost of the larger equipment that was required in the CSRP. Additionally, once the black water is combined with the slag water, the char gets diluted in a much larger combined stream. Separating that char from the larger, combined stream will be difficult, and more

equipment will be required. Based on these conclusions, the hybrid design does not make economic sense.

6.6 Recommendations

- Future development of the CSRP based on the slag-water letdown turbine, must also engage a company with high pressure slag crushing capability. Since this piece of equipment delivers a key requirement for the reliable operation of the downstream equipment, the availability metrics for the CSRP will depend on the slag crusher for a successful design.
- A rigorous and detailed cost estimate to get a more accurate breakdown of total installed cost (TIC), structural and BWF cost savings is recommended before proceeding forward.
- The detailed testing and development plan outlined in a previous section should be carried out.

7.0 Overall Program Conclusions/Recommendations

GE sees opportunity in the global trend for cleaner power production using its IGCC technology. GE believes that power can be economically and cleanly produced from coal through the use of its technologies, and desires to utilize its coal gasification and power generation technology expertise to meet this goal. The objective of this 3-year project was to evaluate potential improvement in total installed cost and availability through deployment of a multi-faceted approach in the following categories: 1) Technology Evaluation, 2) Constructability, and 3) Design Methodology. Over the course of the project the teams embarked on vastly different paths all aiming towards the reduction of plant costs and the increase of plant availability. The execution of the project resulted in numerous brainstorming sessions and collaborations within GE Power & Water, within the General Electric Company (with other GE businesses), with contractors, vendors and universities and receiving input and feedback from the panel at the 2013 Peer Review (held by DOE) all working towards the common goal of improving the techno-economic position of IGCC in the US and around the world.

Table 77, below, shows the estimated benefits for each of the tasks pursued.

Table 77. Summary of Savings from Project by Task

Task	Item	Cost Savings	Availability Impact	Schedule Impact
Task 2 - Integrated Operations Philosophy	Summary of 48 assessed ideas	$4.9M for 2 trains	+0.25 pts in RAM	Increased gasifier run time
Task 3/4 - Slip Forming (SF) - Modularization (Mod)	Gasifier (SF & Mod)	<1% improvement ($2M)	None	6.5% shorter (3 months)
	Pipe Rack (Mod)	None*	None	None*
	Coal Silo (SF)	$1.5M cost increase	None	3 months shorter
Task 5 - Fouling Removal	Active fouling removal	Improve steam production, increase plant efficiency, lower COE	Possible improvement	None*
Task 6 - Improved Slag Handling	Continuous slag letdown equipment + Gasification structure + BWF equipment	$15.6M	Comparable to current equipment	Not Calculated

*Pipe rack modularization may show improvements in other geographical areas but did not show improvements for Gulf Coast region.

Task 2 looked at the cost/availability issue from an integration of operations point of view. In this case the team started with a plant design in which GE had already invested a considerably large amount of time and resources to enhance using lessons learned from past experiences in the power and chemical plant operations. From that point a cross-functional team of GE subject matter experts gathered together to brainstorm on further ideas to enhance the plant for cost reduction and availability improvements. The team generated 100 improvement ideas of which 48 went on for detailed exploration and analysis in the areas of sparing philosophies, maintainability in terms of spare usages, and others. The monetary results of the activities may be found in Table 77.

More than just those specific results came an overall question on how best to use these methods of maintainability came the question of how to best integrate the aspects of operations and maintenance, together, to produce even better outcomes. This activity began with the relatively simple perspective of “nipping here and tucking there” items that could be improved based on further lessons learned and stories that emerge from the operation of actual plants. Overall, the task illuminated that one could improve the overall operational and maintenance expenses and timing by spending more resources in the front end with the customer end-users

and technology provider engineers experienced in real-world applications to enhance the process of detailing the design to better meet the end-user's needs. Also the team found that the use of an experienced team focused on integrated operations philosophy meeting periodically throughout the construction of new plants could work some of these items and result in a lower cost, more available plant in the end.

Some of the tasks produced somewhat expected results while others produced results that surprised the teams working on them. The team working on the slip forming and modularization tasks were greatly surprised that the new construction techniques chosen for study did not show the significant cost reductions that were expected at the beginning of the program. One reason is the choice of perform all the comparisons and analyses for a US Gulf Coast region where access to ports and skilled labor is not a problem. The following situations could lead to clear improvements in cost and schedule when considering "stick built" vs. slip forming or modularization constructions methods:

- Improvements in the Gasification Island design to better take advantage of the non-stick built methodologies
- Site geological and geographical conditions
- Site labor rates
- Site labor availability and skills
- Steel and concrete costs
- Production revenue (increase of initial revenue by being able to start the plant earlier)

Task 5 followed a very robust methodology to research state of the art and existing technologies, understanding the physics behind the fouling morphology, determining the best means of removing the fouling via detailed analysis, simulating fouling phenomena on specimens, and finally testing the feasibility of an active fouling removal system during the course of the program. A pulse detonation engine was determined to be the most favorable way of removing fouling in the RSC in this task. The team demonstrated, via subscale testing at the University of Texas at Arlington, that it is feasible to remove fouling from the RSC using PDE using repeated detonations. Ash removal during these tests ran from a typical range of 40% to 60% removal of flyash after 60 shots to as much as 95%. It follows that removing flyash from the platens of the RSC would increase the steam produces from the system, thereby increasing plant efficiency and reducing the overall cost of electricity (COE). While the tests demonstrated the feasibility of the system the following is recommended to continue development of the technology to commercialization:

- Examine the feasibility of partial filling for fouling removal
- Further validate the scaling law through a larger and higher pressure facility
- Develop surrogate fouling coupons with well-defined properties to allow for a systematic quantification of material removal
- Perform systematic repeated detonations on surrogate fouling coupons to quantify the removal rate of both coupons mounted in front and at the back of the platen versus the number of detonation pulses

Task 6 showed that continuous slag letdown is a less expensive and viable replacement for the lockhopper-based batch system that is currently used in IGCC plants. The benefits of this replacement may be found in Table 77. Recommendations for taking this system to commercialization are:

- Future development of the CSRP based on the slag-water letdown turbine, must also engage a company with high pressure slag crushing capability. Since this piece of equipment delivers a key requirement for the reliable operation of the downstream equipment, the availability metrics for the CSRP will depend on the slag crusher for a successful design.
- A rigorous and detailed cost estimate to get a more accurate breakdown of total installed cost (TIC), structural and BWF cost savings is recommended before proceeding forward.
- Sensitivity analysis showed a wide range of potential operating points for the slag-water slurry concentration, slag-water slurry cooling temperature and slag-water letdown turbine discharge pressure. Further analysis needs to be performed to finalize the optimal NOC operating points
- The CSRP configuration optimization was done post-RAM analysis. Therefore the RAM analysis does not include some major changes like the elimination of slag-water cooler which is source of unreliability. Therefore, an updated RAM analysis is recommended to identify the final RAM improvements.
- Executing simulations at different load conditions would identify pinch points in the system and might also help identify additional optimization/integration areas.

Overall, this project produced results on many fronts. Some of the ideas could be utilized immediately by those seeking to build an IGCC plant in the near future. These include the considerations from the Integrated Operations Philosophy task and the different construction techniques of Slip Forming and Modularization (especially if the proposed site is in a remote location or has a lack of a skilled workforce). Other results include ideas for promising technologies that require further development and testing to realize their full potential and be available for commercial operation. In both areas GE considers this project to be a success in identifying areas outside the core IGCC plant systems that are ripe for cost reduction and availability improvement opportunities.

Acknowledgment

The authors thank Cervante Sudduth of Kiewit Engineering, Steven Benson of Microbeam Technologies, Inc., and Dr. Frank Lu and team from the University of Texas at Arlington for their contributions to the designs, testing and analysis presented in this paper.

APPENDIX A

GRAPHICAL MATERIALS LISTS

List of Figures

Figure 1. Isometric of Stick-Built Structure 28
Figure 2. Concrete Slip form for Gasification Island Structure 29
Figure 3. Example of Kiewit project using modularization for a pipe rack type structure 30
Figure 4. Schematic illustration of coal gasifier and RSC with ash deposits of an IGCC Power Plant....33
Figure 5. Ash deposition process in coal gasification 35
Figure 6. Major physical transformations of ash components during gasification (modified based on Benson and Laumb, 2007) 36
Figure 7. Major mass transport mechanisms of ash components to heat transfer surfaces (Benson and Laumb, 2007)....37
Figure 8. Inertial impaction for ash deposition. (a) Inertial impaction with sticking and rebounding particles; (b) Deposit is coarse grained, with max thickness occurring at stagnation point tapering to zero beyond 50°. (modified based on Baxter, 2000) 37
Figure 9. Thermophoresis impaction for ash deposition. (a) Thermophoretic deposition on a tube in a cross flow; (b) Deposit is finer grained with an evenly distributed buildup around the tube. (modified based on Baxter, 2000)....38
Figure 10. Iron sulfide phase coating the surface of particles produced in an entrained flow gasifier (Brooker and Oh, 1995). 40
Figure 11. Transport and bonding mechanisms of ash components to heat transfer surfaces in syngas cooling systems....43
Figure 12. Temperature impacts on bonding phase formation.....43
Figure 13. Soot blowers at TECO (Tampa Electric Company 2002).....46
Figure 14. A typical PDE for fouling removal (McCormick, 2006). (a) Basic shape and size of PDE; (b) Installed PDE device.....47
Figure 15. Application of PDE wave for fouling removal (McCormick, 2006). (a) PDE nozzle with tube bundles; (b) CFD analysis of PDE wave interaction with tube bundles. 48
Figure 16. Water lance penetrates through heat exchanger wall.....49
Figure 17. Typical rapper device. 49
Figure 18. Relationship between slag thermal conductivity (k) and porosity. (Wain, 1992) 52
Figure 19. Thermal conductivity and porosity based on work conducted by Rezaei and others (2000)....53
Figure 20. Relationship between shock parameters (R and R') and slag porosity (Wain and others, 1992).....54
Figure 21. PIP as a function of distance from nozzle exit (Jameel and others, 1994). 56
Figure 22. PIP as a function distance from the nozzle for air and steam (Jameel and others, 1994).....56
Figure 23. PIP as a function distance from nozzle exit for various lance pressures (Jameel and others, 1994).....57
Figure 24. PIP profiles for a free jet and between platens (Kermani and others, 2001). 57

Figure 25. PIP versus tensile strength required to break simulated deposit (Kaliazine and others, 1997).....58
Figure 26. PIP required to remove the deposit versus tensile strength for different attack angles (Kaliazine and others, 1997).....59
Figure 27. Drag force as a function of distance between nozzle and deposits of different heights (Kermani and others, 2001).....59
Figure 28. Comparison of pressure profile between acoustic horn and PDE. (a) acoustic horn; (b) PDE (McCormick, 2007).....62
Figure 29. Fouling Removal Mechanisms Pareto Chart. 63
Figure 30. Stages in a PDE cycle.....65
Figure 31. Preliminary PFD for PDE fouling removal system for RSC Applications. 66
Figure 32. Diagram of RSC heat transfer surface, and CFD model. (a) RSC platen orientation and attached PDE; (b) CFD model for PDE regions, species present, and interfaces.....67
Figure 33. CFD model geometry. 68
Figure 34. Gas species mass fractions vs. time for Case D.....70
Figure 35. Platen load variation with time from a single PDE pulse wave for Case D. (a) Bulk force; (b) Max pressure. 70
Figure 36. Snapshot of PDE wave pressure contour for Case D. 71
Figure 37. Snapshot of PDE wave pressure distribution on platen for Case D. (a) total pressure force and force components in PDE direction and vertical direction; (b-i) evolution of pressure distribution on platen surface induced by a single PDE pulse wave. 72
Figure 38. Simplified PDE/RSC layout for analytical model. 74
Figure 39. Top view of 3D CFD model geometry.....75
Figure 40. Diagram of 3D CFD model top view showing regions, species present, and interfaces.....75
Figure 41. Graph of predicted PDE load on platen vs time and table of maximum platen load values.....77
Figure 42. Platen pressure load induced by a single PDE pulse wave at 1ms time. (a) Normal operating condition; (b) 50% oxygen reduction condition; (c) PDE failure condition. 78
Figure 43. Propagation of PDE pressure wave contours around RSC platens from the top-down view in normal operating conditions (baseline). 79
Figure 44. Propagation of PDE pressure wave contours between RSC platens from the PDE centerline side view in normal operating conditions (baseline).....79
Figure 45. Evolution of platen pressure load induced by a single PDE pulse wave in the normal operating condition. 80
Figure 46. Propagation of PDE pressure wave contours around RSC platens from the top-down view in the low oxygen case. 81
Figure 47. Propagation of PDE pressure wave contours between RSC platens from the PDE centerline side view in low oxygen case. 81
Figure 48. Evolution of platen pressure load induced by a single PDE pulse wave, in the low oxygen case. 82
Figure 49. Propagation of PDE pressure wave contours around RSC platens from the top-down view in the PDE failure case. 83
Figure 50. Propagation of PDE pressure wave contours between RSC platens from the PDE centerline side view in the PDE failure case. 83
Figure 51. Evolution of platen pressure load induced by a single PDE pulse wave, in the PDE failure case. 84
Figure 52. A typical RSC platen geometry.....86

Figure 53. Mesh density of the cantilevered plate with fixed Constraint. 87
Figure 54. First 7 Mode Shapes. 88
Figure 55. Deflection (UY) vs. time (to t = 1.3 seconds) [Front]. 88
Figure 56. Deflection (UY) vs. time (Left: deflection at the center of the plate, Right: deflection at the free end). 89
Figure 57. Result of fouling removal over time. 89
Figure 58. Percent shear stress above allowable vs. time. 90
Figure 59. Simplifies PID for PDE fouling removal subscale testing. 92
Figure 60. Pressure transducer with water cooled jacket. 96
Figure 61. Ion detector diagram. 97
Figure 62. Side cutaway CAD rendition of the testing rig. 99
Figure 63. Schematic diagram of PDE 100
Figure 64. Schematic diagram of platens installed in the receiver tank. 101
Figure 65. CAD drawings of Platen #1 - fly-ash platen. (a) External view; (b) Cutaway view showing ring heater locations. 101
Figure 66. CAD drawing of Platen #2 - instrumented platen. (a) External view; (b) External view for other surface. 102
Figure 67. Photographs of test facility. (a) View downstream; (b) PDE. 102
Figure 68. Signal from an accelerometer mounted on a platen. 104
Figure 69. Spectral content of the acceleration. 104
Figure 70. AFS solenoid valve assembly. 107
Figure 71. Phases of a PDE operation cycle. 108
Figure 72. Simplified diagram of syngas fouling simulator (SFS) reactor system including water injection/steam. 110
Figure 73. Schematic diagram of syngas fouling simulator (SFS) reactor system including water injection/steam. 111
Figure 74. SFS reactor system ash deposition testing. 111
Figure 75. Ash accumulation on a simulated heat transfer surface produced in the SFS. 112
Figure 76. Ash/Slag Adhesion Test System. 112
Figure 77. Example of ash adhesion testing for a selected ash material for three metals (temperature is the steel temperature). 113
Figure 78. Backscattered scanning electron image of TECO ash MTI 14-219. 115
Figure 79. Viscosity-temperature relationships of the Knight Hawk, Galatia, Duke, and TECO coal ash. 117
Figure 80. Viscosity-temperature relationships of the first Wabash fly ash compared to that of the TECO and Duke ash materials. 118
Figure 81. Viscosity-temperature relationships of the second Wabash fly ash compared to that of the TECO and Duke ash materials. 118
Figure 82. Overview of ash behavior indices for gasification systems. 122
Figure 83. Coupon dimensions (inches). 123
Figure 84. New probe constructed to accommodate coupons in both upstream and downstream orientations. (a): Overall view; (b): Probe tip showing slots for the coupons. 125
Figure 85. Pre-treated coupons produced at 600 ºF. 127
Figure 86. Backscattered electron image of coupon cross-section (MTI 14-268) showing analysis points 1-11. 134
Figure 87. Backscattered electron image of coupon cross-section (MTI 14-268) showing analysis points 1-7. 134

Figure 88. Backscattered electron image of coupon cross-section (MTI 14-274) showing analysis points 1-15. 136
Figure 89. Backscattered electron image of coupon cross-section (MTI 14-274) showing analysis points 1-7. 136
Figure 90. Backscattered electron image of coupon cross-section (MTI 14-288) showing analysis points 1-5. 138
Figure 91. Backscattered electron image of coupon cross-section (MTI 14-288) showing analysis points 1-7. 138
Figure 92. Backscattered electron image of coupon cross-section (MTI 14-290) showing analysis points 1-6. 140
Figure 93. Backscattered electron image of coupon cross-section (MTI 14-290) showing analysis points 1-5. 140
Figure 94. Backscattered electron image of coupon cross-section (MTI 14-292) showing analysis points 1-6. 142
Figure 95. Backscattered electron image of coupon cross-section (MTI 14-292) showing analysis points 1-6. 142
Figure 96. Backscattered electron image of coupon cross-section (MTI 14-296) showing analysis points 1-6. 144
Figure 97. Backscattered electron image of coupon cross-section (MTI 14-296) showing analysis points 1-6. 144
Figure 98. Thickness of the layer retained on coupon where most of the ash materials flaked off. 145
Figure 99. Backscattered electron image of coupon cross-section (MTI 14-248) showing analysis points 1-9. 148
Figure 100. Backscattered electron image of coupon cross-section (MTI 14-248) showing analysis points 1-9. 148
Figure 101. Backscattered electron image of coupon cross-section (MTI 14-248) showing analysis points 1-9. 150
Figure 102. Backscattered electron image of coupon cross-section (MTI 14-248) showing analysis points 1-9. 150
Figure 103. Backscattered electron image of coupon surface (MTI 14-246). 152
Figure 104. Backscattered electron image of coupon surface (MTI 14-246) showing analysis areas 1 - 3. 152
Figure 105. Backscattered electron image of coupon surface (MTI 14-246) showing analysis areas 1 - 2. 153
Figure 106. Backscattered electron image of coupon surface (MTI 14-246) showing analysis areas 1 - 3. 153
Figure 107. Sticking test apparatus. 154
Figure 108. Adhesive strength of ash layer on extreme composition coupons exposed in the syngas cooler simulator as a function of temperature. 156
Figure 109. Pressure at the platen center base length PDE. 157
Figure 110. Pressure at platen center for extended length PDE. 158
Figure 111. Instrumented blunt nose cone pitot used for total pressure measurement. 158
Figure 112. Pitot probe arrangement in the tank. 159
Figure 113. Pressure decay of the blast wave. 160
Figure 114. Wave Characterization at the PIV Plane (17in from PDE exit). 161
Figure 115. A single-shot image of the exhaust jet approaching the left platen. 162

Figure 116. Images of the exhaust jet from an overfilled PDE; sequence from left to right and top to bottom. 163
Figure 117. Lockhopper System Schematic 174
Figure 118. Continuous Solids Transport by Successive Batching of Parallel Vessels Taken from Streat, M., “Lockhoppers and Pipe Feeders” in *Slurry Handling, Design of Solid-Liquid Systems.* 176
Figure 119. Continuous Solids Transport by Successive Batching of Parallel Piping Taken from Szivak, A., Illes, K. and L. Varga, “Up-to-Date Hydraulic Transport Systems for the Delivery of Industrial Wastes”. *Fifth International Conference on the Hydraulic Transport of Solids in Pipes.* May, 1978. 176
Figure 120. Kamyr Chamber Feeder for Continuous Solids Transport Taken from Streat, M., “Lockhoppers and Pipe Feeders” in *Slurry Handling, Design of Solid-Liquid Systems.* 177
Figure 121. Continuous Solids Transport by Lockhopper Pump Taken from Abulnaga, B. E., *Slurry Systems Handbook.* McGraw-Hill, 2002. 178
Figure 122. Restriction Elements – Option 1 182
Figure 123. Lipstick Valve PFD – Option 2 186
Figure 124. Coal Slurry Letdown Valve (a.k.a. “Lipstick” Valve) 187
Figure 125. Slag-Water Letdown Turbine PFD – Option 3 191
Figure 126. Slag-Water Slurry Cooler (Configuration 1) 197
Figure 127. Direct Injection of Cooling Water (Configuration 2) 199
Figure 128. Slag letdown turbine equipment assembly 200
Figure 129. Discflo pump – Normal configuration 201
Figure 130. Improved CSRP Configuration 205
Figure 131. Lockhopper System vs. CSRP Total Direct Field Cost 208
Figure 132. Gasifier Support Structure Required for Lockhopper System 209
Figure 133. Gasifier Support Structure Required for CSRP 210
Figure 134. Schematic of BWF System 212
Figure 135. Vapor Flash Volume Fraction at Slag-Water Letdown Turbine Discharge 219
Figure 136. Turbine Extracted Energy with Different Discharge Pressures 220
Figure 137. Test Rig Configuration for Phase 1 223
Figure 138. Test Rig Configuration for Phase 2 224
Figure 139. Test Rig Configuration for Phase 3 226
Figure 140. Test Rig Configuration for Phase 4 228
Figure 141. Commercial Demonstration Unit Configuration for Phase 5 230
Figure 142. Schematic of Hybrid CSRP-BWF System 232

List of Tables

Table 1. Summary of Ideas and Estimated Savings 14
Table 2. Gasifier Island cost and schedule for traditional vs. slip form/modularization 29
Table 3. Coal Silo cost and schedule for slip form vs. jump form 31
Table 4. Analysis of deposits, slags, and coal ash from Cool-Water syngas cooler (elemental wt. %). 41
Table 5. RSC deposit analysis (elemental wt. %) 41
Table 6. RSC deposit analysis on a carbon-free equivalent oxide basis, normalized to 100%...41
Table 7. Results for Fouling Removal Patent Search 44
Table 8. Relative flow velocity and dwell time of flue gas, gas accelerated by SHOCKSystem blast wave, and the conventional soot blower jet (Parish, 2006) 61
Table 9. Key attributes for RSC fouling removal system. 62
Table 10. Qualitative differences between detonations and deflagrations in gases. 64
Table 11. Platen maximum loads for each configuration. 72
Table 12. Results of modal analysis on platen vibrations 105
Table 13. Proximate and ultimate analysis of TECO ash (MTI 14-219). 114
Table 14. SEM morphological analysis of TECO ash sample (MTI 14-219), results expressed as equivalent oxide, normalized to 100%. 114
Table 15. Analysis summary of Knight Hawk and Galatia coal samples 115
Table 16. Ash composition summary comparing Knight Hawk and Galatia coal ash to that of TECO and Duke fine ash. 116
Table 17. Ash fusion temperature (F) analysis for Knight Hawk and Galatia coals. 117
Table 18. Comparison of the Wabash Fly Ash samples to the Duke and TECO ash. 117
Table 19. Ash fusion temperature (F) analysis of Wabash fly ash. 119
Table 20. CCSEM Results for Galatia coal. 119
Table 21. CCSEM Results for Knight Hawk coal. 120
Table 22. Calculated performance indices for Galatia and Knight Hawk coals. 122
Table 23. Syngas composition used in the study. 124
Table 24. Pre-treatment of coupons at 600 °F (316° C) for 8 hours. 125
Table 25. Pre-treatment of coupons at 700 °F for 8 hours. 125
Table 26. Pre-treatment of coupons at 850 °F for 8 hours. 126
Table 27. SEM analysis of pre-treatment layer of coupon (elemental wt. %). 127
Table 28. Test matrix for fouling deposit coupon preparation. 128
Table 29. Tests Results for fouling coupon preparation. 128
Table 30. Coupon preparation tests results indicating which ash stuck or flaked off. 129
Table 31. Pictures for fouling coupons prepared in syngas fouling simulator. 131
Table 32. Morphology analysis results of Coupon CU-3 (MTI 14-268), with elemental results expressed as weight percent, normalized to 100%. 133
Table 33. Morphology analysis results of Coupon CU-6 (MTI 14-274), with elemental results expressed as weight percent, normalized to 100%. 135
Table 34. Morphology analysis results of Coupon CU-13 (MTI 14-288), with elemental results expressed as weight percent, normalized to 100%. 137
Table 35. Morphology analysis results of Coupon CU-14 (MTI 14-290), with elemental results expressed as weight percent, normalized to 100%. 139
Table 36. Morphology analysis results of Coupon CU-15 (MTI 14-292), with elemental results expressed as weight percent, normalized to 100%. 141

Table 37. Morphology analysis results of Coupon CU-17 (MTI 14-296), with elemental results expressed as weight percent, normalized to 100%. 143
Table 38. Extreme condition testing. 146
Table 39. Extreme condition testing in syngas cooler simulator. 146
Table 40. Morphological analysis of coupon cross-section 14-248 produced with extreme deposit compositions. 147
Table 41. Morphological analysis of coupon cross-section 14-248 produced under the extreme conditions. 149
Table 42. SEM surface analysis of Coupon 14-246. 151
Table 43. Adhesive strength of ash layer on extreme composition coupon 14-247 exposed in a muffle furnace. 155
Table 44. Adhesive strength of ash layer on extreme composition coupons exposed in the syngas cooler simulator. 155
Table 45. Photographic comparison of coupons before and after fouling removal testing. 164
Table 46. Photographic comparison of coupons before and after fouling removal testing for extreme condition cases. 167
Table 47. Photographic comparison of coupons for before, after, and after retesting of fouling removal testing. 168
Table 48. Fouling coupon removal testing results 169
Table 49. Summary of slag handling experience at gasification plants with lockhopper systems 178
Table 50. Design Basis for Continuous Slag Removal Process Development 180
Table 51. Material Balance – Restriction Element – Option 1 183
Table 52. Sized Equipment List – Restriction Element – Option 1 183
Table 53. Operating conditions for Option 1 184
Table 54. Material Balance – Lipstick Valve – Option 2 188
Table 55. Sized Equipment List – Lipstick Valve – Option 2 188
Table 56. Operating Conditions for Option 2 189
Table 57. Material Balance - Slag-Water Letdown Turbine – Option 3 192
Table 58. Sized Equipment List – Slag-Water Letdown Turbine – Option 3 192
Table 59. Operating Conditions – Slag-Water Letdown Turbine – Option 3 193
Table 60. Comparison of Total Installed Cost for Options 1, 2 and 3 194
Table 61. Material Balance for Improved CSRP Configuration 206
Table 62. Comparison of TIC Estimates for Lockhopper System Base Case vs. CSRP 207
Table 63. Inlet Stream Comparison for BWF system 213
Table 64. Sizing comparison for BWF System Equipment between CSRP and Lockhopper Cases 214
Table 65. TIC Cost Breakdown Comparison for BWF System Equipment 215
Table 66. Inlet Slag-Water Slurry Stream Properties for 30 wt.%, 40 wt.% and 50 wt.% Solids Cases 216
Table 67. NH_3 Stripper Bottoms Recycle Flowrate for the Three Cases 216
Table 68. Slag-Water Letdown Turbine Inlet Temperature for the Three Cases 217
Table 69. Volume Fraction of Vapor in Turbine Outlet for the Three Cases 217
Table 70. Equipment and Cost Sizing for Slag-Water Solids Concentration Sensitivity 218
Table 71. Vapor Flashing in Slag-Water Letdown Turbine Sensitivity to Slag-Water Slurry Cooling Temperature 219
Table 72. Vapor Flashing and Turbine Extracted Energy with Different Discharge Pressures 219
Table 73. Results of RAM Analysis of CSRP Cases 1 and 2 vs Base Case with Lockhopper 221

Table 74. HMB results for Hybrid CSRP-BWF System.....233
Table 75. Preliminary Sizing Comparison between Standalone and Hybrid CSRP Equipment 234
Table 76. Preliminary Sizing Comparison between Standalone BWF and Hybrid CSRP Vessels 234
Table 77. Summary of Savings from Project by Task.....237

REFERENCES

Abbott, M.F.; Austin, L.G. Studies on Slag Deposit Formation in Pulverized-Coal Combustors: 4. Comparison of Sticking Behaviour of Minerals and Low-Temperature and ASTM High-Temperature Coal Ash on Medium Carbon Steel Substrates. Fuel 1982, pp. 765–770.

Abbott, M.F.; Conn, R.E.; Austin, L.G. Studies on Slag Deposit Formation in Pulverized-Coal Combustors: 5. Effect of Flame Temperature, Thermal Cycling of the Steel Substrate and Time on the Adhesion of Slag Drops to Oxidized Boiler Steels. Fuel 1985 6, pp. 827–831.

Abbott, M.F.; Austin, L.G. Slag Deposit Initiation Using a Drop Tube Furnace. In *Mineral Matter and Ash in Coal*; Vorres, K.S., Ed., ACS Symposium Series 301, Washington, DC, 1986.

Abulnaga, B. E., Slurry Systems Handbook. McGraw-Hill, 2002.

Austin, L.G., (1984), Ash Deposition in Syngas Coolers of Slagging Gasifiers, Pennsylvania State University, University Park, Pennsylvania, 16802, EPRI AP-3806 Report 1654-11

Bakker, W., High Temperature Corrosion in Gasifiers, Materials Research, Vol. 7, No.1, 53-59, 2004

Baxter, L.L., (2000), Ash Deposit Formation and Deposit Properties: A Review, Brigham Young University, Provo, UT 84602

Baxter, L.L., (2007), Thermal Transport to a Reactor Wall with a Time Varying Ash Layer, Brigham Young University, Provo, UT 84602

Benson, S.A., “Laboratory Studies of Ash Deposit Formation During the Combustion of Western U.S. Coals”, Ph.D. Thesis, The Pennsylvania State University, 1987.

Benson, S.A. and Laumb, M.A., The Path to Higher Availability through Reduced Syngas Cooler Fouling, Gasification Technologies Conference, October 14-17, 2007, San Francisco, CA.

Benson, S.A.; Laumb, M.L. *Minimizing Ash Impacts on Power System Performance through Advanced Coal and Ash Analysis Methods*, Pre-Conference Session presented at the 2007 Energy Generation Conference, Bismarck, ND, January 2007.

Black & Veatch, (2006), Holcomb Generation Expansion Project, Coal Technology Selection Study, Final report August 2006, Project 144102

Brooker, D. D., (1992), Chemistry of Deposit Formation in a Coal Gasification Syngas Cooler, Texaco R & D, Beacon, NY 12508

Clyde-Bergemann, 2008 (www.clydebergemann.com)

Coal Conversion Systems Technical Data Book. Prepared for the DOE under Contract No. AC01-81 FEO5157 by Institute of Gas Technology, 2/1978. P 8a.

CoalTech Pty Ltd. (2007), Consultancy in Coal Utilization Technology, http://www.coaltech.com.au/Slagging&Fouling.html

Conversations between Ray Steele and engineers at Knighthawk Engineering (www.knighthawk.com), April 2, 2012.

Hanjalić, K.; Smajević, I. *Device of Detonational Impulse Cleaning of Inner Surfaces of High-Pressure Charcoal Gasification Reactor*, Patent No. YU175688, 1990.

Hanijalić, K; Smajević, I. *Laboratory Investigation and Full-Scale Experience on Detonation-Wave Technique for On-Load Cleaning of Gas-Side Boiler Heating Surfaces*, Proc. 2nd European Conference on Industrial Furnaces and Boilers, Vilamoura, Portugal, 1991.

Hanijalić, K; Smajević, I. *Further Experience in Using Detonation Waves for Cleaning Boiler Heating Surfaces,* International Journal of Energy Research, 17, 1993, pp. 583-595.

Hanijalić, K; Smajević, I. *Detonation-Wave Technique for On-Load Deposit Removal From Surfaces Exposed to Fouling: Part I-Experimental Investigation and Development of the Method*, Journal of Engineering for Gas Turbines and Power, 116, Jan. 1994a, pp. 223-230.

Hanijalić, K; Smajević, I. *Detonation-Wave Technique for On-Load Deposit Removal From Surfaces Exposed to Fouling: Part II-Full-Scale Application*, Journal of Engineering for Gas Turbines and Power, 116, Jan. 1994b, pp. 231-236.

Harris Products Group, (2012), *Flashback Arrestors*, Web. 09 Oct 2012. ‹http://www.harrisproductsgroup.com/en/Expert-Advice/Articles/Flashback-Arrestors.aspx›.

Haselbeck, John L. et al., “Cost and Performance Baseline for Fossil Energy Plants Volume 1: Bituminous Coal and Natural Gas to Electricity”. DOE/2010/1397, Nov. 2010.

Heinz P. Block and Burdis, Allan R., “Pump User’s Handbook – Life Extension (3rd Edition). Fairmont Press, 2010.

Hunter, 1997 (Hunter, 1997), patent number 5,672,184, for the use of a pulse detonation device to remove particle build up on candle filter system in coal gasifiers to dislodge particulate build up on the candles.

Huque, Z.; Mei, D.; Biney, P.O.; Zhou, J. *Slag Characterization and Removal Using Pulse Detonation Technology during Coal Gasification*, Final Report, U.S. Department of Energy, DE-FG22-95MT95010—10, July 30, 1998

Hutchism, F.H., (2009), IGCC Electric Power, About Gasification, http://www.clean-energy.us/facts/gasification.htm

Jameel, M.I.; Cormack, D.E.; Tran, H.; Moskal, T.E. *Sootblower Optimization Part 1: Fundamental Hydrodynamics of Sootblower Nozzle and Jet*, Tappi Journal, 77(5), May 1994, pp. 135-142.

Kaliazine, A.; Cormack, D.E.; Ebrahimi-Sabet, A.; Tran, H. The Mechanics of Deposit Removal in Kraft Recovery Boilers, Journal of Pulp and Paper Science, 25(12), Dec. 1999, pp. 418-424.

Kaliazine,A.L.; Piroozmand,F.; Cormack, D.E.; Tran, H.N. *Sootblower Optimization II: Deposit and Sootblower Interaction*, Tappi Journal, 80(11), Nov 1997, pp. 201-207.

Karassik, Igor J.; Messina, Joseph P.; Cooper, Paul; Heald, Charles C, "Pump Handbook, 3rd Edition". McGraw-Hill, 2001.

Kaliazine, A.; Cormack, D.E.; Ebrahimi-Sabet, A.; Tran, H. *The Mechanics of Deposit Removal in Kraft Recovery Boilers*, Journal of Pulp and Paper Science, 25(12), Dec. 1999, pp. 418-424.

Kermani, K.; Cormack, D.E.; Tran, H.; Kaliazine, A.; Tandra, D.S., *Numerical Modeling of Sootblower Jet Flow*, International Chemical Recovery Conference 2001, Whistler, BC Canada, pp. 101-104.

Krishnan, R. P., "Assessment of Slurry Pressure Letdown Valve and Slurry Block Valve Technology for Direct Coal Liquefaction Demonstration and Pioneer Commercial Plants." DOE/1984/Contract Number DE-AC05-840R21400.

McCormick, A. T., (2006), *DTE's Experience with Pratt & Whitney's SHOCKSystem™ an Online Detonation Cleaning™ Slag and Ash Removal Product*, <www.prbcoals.com/pdf/paper_archives/58808.pdf>.

McCormick, A. T., (2007), A Comparison of Online Cleaning Technologies: Detonation, Acoustic and Conventional Steam or Air Sootblowing, http://www.energypulse.net/centers/article/article_display.cfm?a_id=1513

Meyers, R. A., (1981), Coal Handbook, M. Dekker, University of Michigan

Moza, A.K., (1978), A new test for Characterizing the Slag Deposition Properties of a Coal Ash

Moza, A.K.; Austin, L.G.; Tressler, R.E. *Some Results of the Wetting and Adherence of Synthetic Coal Ash Droplets on Steel*. Journal of Engineering for Power 1980, pp. 679–683.

Moza, A.K.; Austin, L.G. *Studies on Slag Deposit Formation in Pulverized Coal Combustors. 1. Results on the Wetting and Adherence of Synthetic Coal Ash Drops on Steel*. Fuel 1981, pp. 1057–1064.

Moza, A.K.; Austin, L.G. *Studies on Slag Deposit Formation in Pulverized-Coal Combustors: 3. Preliminary Hypothesis for the Sticking Behaviour of Slag Drops on Steels*. Fuel 1982, pp. 161–165.

National Instruments, (2013), *Data Acquisition*, Web. 22 Mar 2013. < http://www.ni.com/data-acquisition/>.

Panicker, Philip K., (2008), *The Development and Testing of Pulsed Detonation Engine Ground Demonstrators*, University of Texas at Arlington

Parish, M., (2006), Boiler Tube Erosion Reduction using the SHOCKSystem™ Online Detonation Cleaning™ Product, Pratt & Whitney, 3633 – 136th Place SE, Suite 310, Bellevue, WA 98006

Podimov, V. N., 1979, *On the Mechanism of Impulse Cleaning*, Kazan University.

Raask, E. *Mineral Impurities in Coal Combustion*; Hemisphere Publishing Company: Washington, 1985.

Rahimi, M.; Owen, J.; Mistry,J. *Thermal stresses in boiler tubes arising from high-speed cleaning jets*, International Journal of Mechanical Sciences 45 (2003) pp. 995–1009.

Rezaei, H.R.; Gupta, R.P.; Bryant, G.W.; Hart, J.T.; Liua, G.S.; Bailey, C.W.; Wall, T.F.; Miyamae, S.; Makino, K.; Endo, Y. *Thermal conductivity of coal ash and slags and models used*, Fuel 79 (2000) pp. 1697-1710.

Smajevic, I. and Hanjalic, K. www.smajevic.co.ba/IJPGC03-abstract.doc. 16-19 June 2003. Electronic. 27 April 2012.

Smajević, I.; Hanjalić, K. *Device for Reliable Detonation–Impulse Cleaning of Heating Surfaces of Power and Other Boilers While They're Working*, Patent No. YU172888, 1991.

Speight, J.G., (2005), Handbook of Coal Analysis, Wiley, Hoboken, NY

Streat, M., "Lockhoppers and Pipe Feeders" in Slurry Handling, Design of Solid-Liquid Systems

Szivak, A., Illes, K. and L. Varga, "Up-to-Date Hydraulic Transport Systems for the Delivery of Industrial Wastes". Fifth International Conference on the Hydraulic Transport of Solids in Pipes. May, 1978.

Tampa Electric Company, (2002), Tampa Electric Polk Power Station, Integrated Gasification Combined Cycle Project, Final Technical Report, Tampa Electric Company, Polk Power Station, Tampa, FL 33601, DE-FC-21-91MC27363

Tampa Electric Company, (2002), Tampa Electric Polk Power Station, Integrated Gasification Combined Cycle Project, Final Technical Report, Tampa Electric Company, Polk Power Station, Tampa, FL 33601, DE-FC-21-91MC2736

Tangsathitkulchai, M.; Austin, L.G. *Nature of the Surface Involved in Fly Ash Adhesion on Boiler Steel*. Fuel 1985, pp. 1764–1765.

Tangsathitkulchai, M., and Austin, L.G., Fundamental Studies of the Mechanisms of Slag Deposit Formation, Topical Technical Report Prepared for the U.S. Department of Energy, DOE/PC/70770-T9, March 1986.

Texaco, (1987), Crossover Duct Plugging, Port Arther Research Laboratories, Port Arther, TX

Topacio, A., “Proposal No. 1A: Based on Standard Product.” Presentation to GE Gasification Brainstorming Session, Feb. 15, 2012.

U.S. Energy Information Administration, September 10 2012, “Revenue from Retail Sales of Electricity”, http://www.eia.gov/beta/enerdat/#/topic/6?agg=0,1&geo=g&freq=A.

U.S. Energy Information Administration, September 10 2012, “Net Generation for All Sectors”, http://www.eia.gov/beta/enerdat/#/topic/0?agg=0,1&geo=g&freq=A.

Wabash River Coal Gasification Repowering Project Final Technical Report, 8/2000. Work performed under Cooperative Agreement DE-FC21-92M C29310, USDOE/NETL Office of Fossil Energy.

Wain, S.E.; Livingston, W.R.; Sanyal, A.; Williamson, J. Thermal and Mechanical Properties of Boiler Slags of Relevance to Sootblowing. In *Inorganic Transformations and Ash Deposition During Combustion*; Benson, S.A., Ed.; Engineering Foundation Conference, 1992.

LIST OF ACRONYMS AND ABBREVIATIONS

2D	2 Dimensional
3D	3 Dimensional
ARC	Aerodynamics Research Center
BWF	Black Water Flash
CAPEX	Capital Expenditures
CAD	Computer Aided Design
CBI	Chicago Bridge & Ironworks
CCSEM	Computer-Controlled Scanning Electron Microscopy
CFD	Computational Fluid Dynamics
CJ	Chapman-Jouquet
CO	Carbon Monoxide
CSRP	Continuous Slag Removal Process
DAQ	Digital Acquisition System
DDT	Deflagration-to-Detonation Transition
DOE	Department of Energy
EDS	Energy Dispersive Spectrometer
EPC	Engineering, Procurement and Construction
FEA	Finite Element Analysis
FOA	Funding Opportunity Announcement
GE	General Electric Company
GW	Grey Water
H_2	Hydrogen
H_2S	Hydrogen Sulfide
HE	High Energy
HMB	Heat and Material Balance
HTD	High Temperature Deposition
ID	Inner Diameter
IGCC	Integrated Gasification Combined Cycle
LE	Low Energy
LP	Low Pressure
LTD	Low Temperature Deposition
MTBF	Mean Time between Failures
MTD	Moderate Temperature Deposition
MTTR	Mean Time to Repair
OPEX	Operating Expenditures
P	Pressure
PDE	Pulse Detonation Engine
PFD	Process Flow Diagram
PID	Piping and Instrumentation Diagram
PIP	Peak Impact Pressure
PIV	Particle Image Velocimetry
PSD	Particle Size Distribution
RAM	Reliability, Availability, Maintainability
RBD	Reliability Block Diagram
RCM	Reliability Centered Maintenance
RSC	Radiant Syngas Cooler

S/D	Shutdown
S/U	Startup
SEM	Scanning Electron Microscopy
SFS	Syngas Fouling Simulator
SME	Subject Matter Expert
SOP	Standard Operating Procedure
SOPO	Statement of Performance Objectives
SPIV	Stereo Particle Image Velocimetry
SRU	Sulfur Recovery Unit
T	Temperature
TECO	Tampa Electric Company
TIC	Total Installed Cost
TTL	Transistor-Transistor Logic
UTA	University of Texas at Arlington

APPENDIX B

Copy of Kiewit Final Report

Title Sheet

FEASIBILITY STUDIES TO IMPROVE PLANT AVAILABILITY AND REDUCE TOTAL INSTALLED COST IN IGCC PLANTS

Final Report - August 2014

DOE Cooperative Agreement No. DE-FE0007859

Period of Performance: Through June 2014

For
Affordability IGCC Project, Texas, USA
Integrated Gasification Combined Cycle (IGCC)
Slip form and Modularization

For GE Energy (USA)
And United States Department of Energy

Submitted To:
GE Energy (USA), LLC
1333 West Loop South
Houston, TX 77027
DUNS – 167528368

Submitted By:
Kiewit Power Engineers
9401 Renner Blvd.
Lenexa, Ks. 66219

Co-Authors:
Thomas Heausler
913-689-3972
Thomas.Heausler@kiewit.com

Steve Frankosky
612-501-8058
Steve.Frankosky@ibberson.com

Cervente Sudduth
913-953-5796
Cervente.Sudduth@kiewit.com

Table of Contents:

Title Sheet
Table of Contents
Executive Summary
Introduction
Gasifier Structure
Gasifier Stick-built Construction
Slip form/Modularization
Conclusion – Stick-Built and Slip Form/Modularization Options
Recommendations

Pipe Rack Modularization

Coal Silo – Slip Form Compared to Traditional Jump Form

Appendix A – Structural Design Criteria
Appendix B – General Arrangement
Appendix C – Isometric of Stick-Built Structure
Appendix D – Stick-Built Plans and Elevations
Appendix E – Stick-Built Erection/Assembly Sequence
Appendix F – Slip Form Plans and Elevations
Appendix G – Slip Form Erection/Assembly Sequence
Appendix H – Coal Silos
Appendix I – Cost Estimate Spreadsheet
Appendix J – Schedule
Appendix K – Assumptions Log
Appendix L – Position Paper October 2013
Appendix M – AACE – Cost Estimate Classification System

Executive Summary

For the Gasification Structure, a General Arrangement of equipment was selected and was based primarily upon data provided to Kiewit and reportedly similar to the Edwardsport, Indiana IGCC plant. A Structural Steel structure (Stick-Built) was designed and optimized. A concrete Slip form structure was also designed and optimized. The Stick-Built structure is estimated to cost $321,000,000. The Slip-Form structure is estimated to cost $319,000,000. The construction duration of the Stick-Built Structure is 46 months and the construction duration of the Slip form structure is 43 months.

A study of Pipe Rack Modularization was performed. The pipe rack study analyzed the potential benefits of fabricating pipe racks in a series of modules at an offsite facility. This would allow the pipe rack modules to be fabricated in a controlled environment that can reduce onsite labor risk and decrease the pipe rack installation schedule. Modularization is frequently used on large scale industrial projects in challenging or remote regions and areas with unskilled labor. It was concluded that for a Gulf Coast location, the benefits of pipe rack modularization are minimal.

A study of Coal Silo construction was performed. Two methods of construction were explored: Traditional "Jump Form" method and the "Slip form" method. Cost for the Jump Form is estimated to be $3,000,000 over a 5 1/2 month duration; and cost for the Slip form is estimated to be $4,500,000 over a 4 1/2 month duration. However, both methods should be considered on a project specific basis due to project specific variations which could significantly affect cost and schedule.

It is recommended that schedule, cost, safety, environmental, and geographical issues be reviewed on a specific project basis when considering the options mentioned herein.

Introduction

The United States Department of Energy has contracted GE Energy to study the affordability of an Integrated Gasification Combined Cycle (IGCC) plant. GE Energy has contracted Kiewit to provide this report. Kiewit has shown expertise and success in the design and construction of large industrial facilities for many years.
In October 2013, Kiewit submitted a Position Paper to GE Energy (See Appendix H). The Position Paper concluded that it would be beneficial to explore potential cost and schedule savings in the following areas:

Gasification Island: Consideration of a Slip form concrete walled structure with floor modules in lieu of the traditional Stick-Built construction.

Pipe Rack Modularization: Consideration of assembly of steel components into a module prior to lifting into final position.

Coal Silos: Consideration of a slip form construction in lieu of a traditional "jump-form" wall silo construction.

Gasifier Structure

For the Gasification Structure, a General Arrangement of equipment was selected and was based primarily upon data provided to Kiewit and reportedly similar to the Edwardsport, Indiana IGCC plant. The structure is approximately 22 stories tall (292' tall) and has plan dimensions of 135' x 150' at the base and 65' x 150' for the upper 13 floors. Details of the Structural Design Criteria and major Equipment are included in Appendix A. Drawings of the General Arrangement are shown in Appendix B. The General Arrangement drawings of Appendix B apply to both the Stick-Built and Slip form designs.

Assumptions have been made and form the basis of the General Arrangement. It was proposed that the Radiant Syngas Cooler (RSC) will be delivered to site in three cylindrical sections. Wall thickness will be 4 to 7 inches thick. The three sections will be welded together in their horizontal position and adjacent to structure; and then lifted to their vertical location within the structure. Internals (e.g. heat exchanger type piping and refractory brick and related items) will be assembled in the vertical RSC vessel. The top, or dome, of RSC will be field welded in its final location. The Gasifier vessel will similarly be field welded/attached in its final position. See Appendix E and G for graphical depictions.

A Structural Steel structure (Stick-Built) was designed and optimized. A concrete Slip form structure was also designed and optimized.

Gasifier Stick-Built Construction

The term "Stick built" is used herein to describe the method of assembly and erection for the steel framed structure. Individual Structural Steel pieces/elements will be shop fabricated and shipped to the site. A crane will erect the elements one piece at a time. Column elements will be up to 60' long. Beam elements will be up to 30' long. Elements will generally be field bolted into their final location. Diagonal bracing will be installed in the outer bays, but not in front of the RSC bay initially. The structure will be stable and safe to resist winds and seismic forces expected during the construction phase. After the RSC is installed, diagonal bracing will be installed in the bay in front of the RSC and this configuration will be resistant to the maximum wind and seismic forces expected over the life of the structure.

A three dimensional computer model was created (see Appendix C). Gravity Wind and Seismic loads were calculated and applied to the model. Columns, Beams, Vertical Bracing, and Horizontal Bracing were optimized based upon iterative computer analysis. Final member sizes are as shown on drawings in Appendix D.

All Columns, Beams, Vertical Bracing, and Horizontal Bracing were accommodated in a Quantity Take Off (see Appendix I). These quantities and configurations form the basis of the Construction Cost estimate and Schedule as described below.

See Appendix E for Stick-Built Erection/Assembly Sequence

Slip form/Modularization

In addition to designing the Gasification Structure using the traditional stick-built method described above, the Gasification Structure was also to be designed as a Slip form concrete option. The purpose of the two methods is to compare and contrast the two construction methods to determine if any savings can be identified in material costs, labor and/ or construction schedule. As with the stick-built option, the Slip form concrete option was designed in accordance with the Design Criteria described above.

The floors of the Slip form option were laid out to match those of the stick-built option in both plan and elevation. Drawings of the Slip form concrete structure are shown in Appendix F. Slip Form Erection and Assembly Drawings are shown in Appendix G. During the design of an actual Gasification Structure, the floor layouts could be optimized to reduce the number of floors which, although might be required for bracing the Stick-built structural steel, would not be required for the bracing of the concrete Slip form structure. Specifically identified are up to five floors in the tower above elevation 124'-0" which contain no major equipment. The elimination of these floors could further

reduce the weight of steel required to complete the structure and (further) reduce the construction schedule.

The Slip form was designed with two bays open to allow the Gasifier and Radiant Syngas Cooler (RSC) to be installed at the convenience of their schedules. To allow these openings, additional interior walls were added to brace the openings. The interior walls are also used as shear walls to resist horizontal loads, e.g. wind and seismic loads. The remainder of the structure, including all areas of flooring, with the exception of the area bounded by Gridlines E and G and 2 and 3 or 6 and 7, can be installed as the equipment for the individual floors becomes available.

The floors of the Slip form structure are intended to be installed as floor modules. The size of each floor module is limited by the size of the concrete cell in which it is located. The floor modules would be partially built either elsewhere onsite or offsite, they would then be positioned in the base of the Gasification structure, the final connections would be made between the partial modules, the equipment for that floor module would be installed while still located at grade level, and then the entire module would be hoisted into its final location using a strand jack system supported by the roof which lifts at a maximum rate of 7.8 inches per minute.

Unlike the Stick-built, the floors for the Slip form option would be installed starting from the top floors down. A benefit of using this method is that most of the heavy lifting is supported off the Slip form structure and the largest, most expensive cranes would need to spend less time on site during construction. Additionally, the presence of the interior walls provides multiple areas for work to progress safely at different stages. When a module is being lifted, work cannot proceed under the floor, however, in the cell adjacent, with the concrete wall between, work could be progressing on the next module. With multiple cells, multiple crews could be at work, e.g. in one cell a crew could be lifting a module; in the next cell, the equipment could be installed on the module; and in the next cell, a crew could be making the final connections joining a floor module. Additionally, with the number of internal cells, multiple crews for each process could be working at the same time.

Additional savings to the schedule may be obtained by locating pipes and conduit on each floor module prior to lifting the modules. The pipefitters and electricians could then install their materials using chainfalls, etc. without interfering with the work below them. These workers would also not have heavy loads being lifted over their heads requiring work stoppages for safety reasons.

Schedule

The schedule for the construction of the Slip form Gasification structure for this study starts once the foundation has been cast and attains its required 28-day concrete compressive strength. This is the same starting point for both the Stick-built and Slip form options. The design and construction of the foundation is not included in this study since both foundations will be relatively the same.

Construction of the Slip form option begins with erecting the slip on the foundation. This process will take approximately 10 to 12 weeks. The slip will consist of three levels, an upper level for the installation of reinforcement and embed plates, the main level to complete installation of the reinforcement and embed plates and pour and vibrate concrete, and the finishing scaffold hung below the main deck to finish the concrete surface as it exits the slip. The slip will be supported by (59) 22-ton jack rods and the roof beams for the completed structure will be used as part of the slip.

The walls of the slip will be 16 inches thick for the full height of the slip. The time required to slip the Gasification Structure to 292' feet is approximately 32 days, with the slip breaking in two parts at 124'. After slipping the concrete, six to eight weeks are required to disassemble the slip. At the completion of the slip disassembly, load may be applied to the structure immediately.

Internal floors in the Gasification structure are intended to be hoisted into their final position using a strand jack system supported by the roof. The individual floor modules are to be partially assembled offsite or elsewhere onsite. The partially assembled floors will be positioned at grade in the structure and final connections will be made creating a single floor unit. Any equipment located on that floor will be installed and the module will be hoisted into final position at a maximum rate of 7.8 inches per minute. Prior to hoisting, piping and electrical skids can also be positioned on the floor allowing the pipefitters and electricians to install these items with work proceeds on floors below them. As mentioned above, because of the multiple cells, crews can perform work at multiple levels throughout the structure. It is estimated that the process of installing the floor modules will take 16 months.

While work on the Gasification Slip proceeds, the Radiant Syngas Cooler (RSC) can be assembled elsewhere on site. A strand jack system consisting of (4) 150-ton strand jacks will be located on the roof. Cranes will be used to locate the top of the RSC inside the structure, where the strand jacks will connect to the RSC. The floor members which support the RSC will be attached to the base of the vessel. With a crane controlling the base of the RSC, the strand jacks will lift the vessel into its final location and floor members will be connected. A crane will be used to install the refractory and the internals into the RSC and place the head on top of the RSC. The Gasifier will then be installed on top of the head of the RSC. When work is complete on the RSC and Gasifier, the remaining floors around and below them can be installed, the roof closed up, and the louvers around the Gasifier installed. The process will be repeated for the second Gasifier train.

Refer to Appendix H for a detailed Cost Estimate; Appendix J for Construction Schedule; and Appendix K for a Project Assumptions Log.

Safety

As with all construction projects, safety is a significant concern. With large projects, it is not always possible for one trade to complete their work prior to other trades beginning their work, because of the need to maintain an optimum schedule. For example, prior to completion of the final erection of a structure, the pipefitters may need to start work in the lower floors of the structure. This creates a dangerous situation where heavy structural members are being lifted over the heads of the workers below. Likewise, the tools and materials that these trades require are being lifted over the heads of the ironworkers.

The Slip form option eliminates some of these safety issues. By virtue of the multi-cell design that is required for resistance of lateral loads, isolated work areas are created throughout the structure. Multiple crews can be working throughout the structure with a level of safety provided by the concrete wall between them and what is happening in the next cell. In one cell, a floor module can be hoisted into place with no one working under it. In the adjacent cell equipment can be installed on a floor module to prepare for final hoisting. In the cell next to that, a crew can be performing the final connections of a floor module. With the number of internal cells, multiple crews can be completing each of these tasks in multiple cells enabling quicker assembly of the structure.

The Slip form option also eliminates the issue of other trades working under the ironworkers. Since the floor modules are installed from the top of the structure down, the pipefitters and electricians will be working above the ironworkers so no heavy structural members will be lifted over their heads. Additionally, tools and materials required by the pipefitters and electricians could be staged on the floor modules prior to hoisting them into place thereby eliminating heavy loads being lifted over the heads of the ironworkers below and a solid floor will exist between the two crews.

Modularization

Modularization typically results in increased labor productivity. This savings can be substantial based on the location and type of work being performed. Kiewit's cost estimate is based on taking advantage of modularization to perform a portion of the work at grade. The portions of work being pre-fabricated are the floor modules. These floor modules will be assembled in a controlled environment and will be outfitted with grating, handrail, small equipment, piping, skids and cable tray prior to being hoisted into place.

By installing piping and small equipment at grade, labor productivity can be increased. Based on experience and project specific challenges, Kiewit has assumed this productivity increase to be 7%. This increase was included for the mechanical and electrical operations on the slipform option.

The more substantial savings by pre-assembling the floor modules are the schedule savings. For the base stick-built option, the piping and electrical operations cannot begin until the structure is essentially complete. This creates a start to finish scenario where the critical path of the schedule will go through the structural steel operation. By assembling the floor modules at grade, this work can begin well before the structure is

complete. Therefore, a large portion of the mechanical work will be driven by procurement/design rather than the structural operation. This should result in an overall reduced construction schedule for the slipform option.

Estimate Accuracy

The accuracy class of the estimate was determined using the AACE report titled Cost Estimate Classification System – As Applied in Engineering, Procurement, and Construction for the Process Industries dated November 29, 2011. Per table 1 – Cost Estimate Classification Matrix for Process Industries (See Appendix M) the overall estimate accuracy is a combination of a Class 4 and Class 3 estimate. The estimate accuracy is based on the information provided and maturity of the design deliverables. Below is the expected accuracy:

Estimate Section	Class	Expected Accuracy
Site Work	4	-15% to +30%
Foundation Concrete / Piling	3	-10% to +30%
Structural Steel	3	-10% to +20%
Slipform Operation	3	-10% to +20%
Piping / Equipment	4	-20% to +50%
Electrical / Instrumentation	4	-20% to +50%
Building / Painting	4	-20% to +50%
Construction Equipment	4	-15% to +30%
Overhead / Indirects	4	-15% to +30%

Conclusions – Stick-Built and Slip Form/Modularization Option

The Stick-Built structure is estimated to cost $320,860,104.00. The Slip-Form structure is estimated to cost $318,876,950.00; resulting in a potential savings of $1,983,154.00 versus the Stick-Built structure. The construction duration of the Stick-Built Structure is 46 months and the construction duration of the Slip form structure is 43 months.

There are many benefits in choosing the Slip form concrete option over the stick-built option. First, when erecting a structure the height of the Gasifier with the weights of equipment involved in the erection, very large, expensive cranes are required to make the required lifts. In the Slip form concrete option, much of the heavy lifting is accomplished by the structure itself. Although large cranes will be needed on site during some stages of construction, this will allow the larger cranes to remain on site for shorter length of time, saving overall construction costs.

In the Stick-built option, the vertical spacing of the floors is partially controlled by the requirements of bracing the columns. In the Slip form concrete option, the allowable vertical clear span of the concrete pilaster is greater than that required by steel columns.

In the upper portions of the Gasifier structure (at elevations above 124') as many as 10 floors have been identified that do not contain any major equipment. Another benefit is that it may be possible to eliminate as many as five of these levels in the Slip form option of the Gasification Structure and other levels may not require full floors.

Eliminating these same floors in the stick-built option may not be possible without increasing the size of the columns because the strength of the columns is controlled by the length between bracing points. Although the stick-built option would benefit from the reduced weight of the floors not being present, it may require much larger structural steel columns. The greater benefit for removing floors would occur in the slip form option. Additionally, the greatest amount of time for the slip form option is in the hoisting of the floors using the strand jack process. If these floors could be eliminated, it would reduce the construction schedule by as much as 4 months. For this study, since all of the nuances of non-structural items, such as equipment and required access, are not defined in copious detail, the floors for both options were assumed to be the same for both the stick-built and slip form options.

As indicated above, by virtue of the internal cell structure of the Slip form option, the safety of the workers is greatly increased. Floor modules at various levels of construction can be in process in multiple cells. Multiple crews working to install floors may shorten work schedule. While these crews are working, they will not be working under suspended loads, except when they attach the floor modules after being hoisted into position.

On many construction projects, pipefitters and electricians are asked to begin their work prior to the structure being fully assembled. This practice leads to unsafe conditions because heavy materials and equipment are often suspended above their heads during lifting operations. In the Slip form option, the floor modules are installed from the top down so the safety of pipefitters and electricians is increased because they are working above suspended loads, instead of below them. Additionally, their work may be able to start sooner, thereby saving schedule. The safety of the ironworkers is not decreased by the other trades working above them because there is a solid floor between them and the work above. Any tools and materials needed by these other trades can also be located on the floor prior to hoisting it into location, eliminating the need to lift heavy loads above the heads of the ironworkers below.

The Slip form concrete option also provides some unique challenges over the stick-built option. First among these challenges is that the concrete structure may retain too much heat during operations. The stick-built option is a very open structure allowing heat to dissipate by air moving through the structure. This problem has been at least partially accounted for by providing operable louvers on all faces at the level of the gasifier and leaving the front of the structure open as well as other small openings not yet identified. If needed, vent fans could also be provided on the roof to force air movement through the structure. Any cost for roof fans is not included in this report.

Since the floor modules in the Slip form option are erected from the top down and the walls of the slip are solid, if a floor module is delayed during its installation, it delays every floor module below it in that cell. Not included in the schedule provided with this report is the availability of the equipment to be installed on each floor. If that equipment is not available when the floor module is ready, it delays every floor below it in that cell. Since the Slip form Gasifier option is a solid structure, once the major equipment is installed on the floor module and lifted into place it is locked into the structure. In the stick-built option, portions of the vertical bracing and perhaps even some floors could be removed temporarily to change out larger equipment, if needed. Smaller equipment in the Slip form option would not be locked in the structure since hoistways would be provided through the floors either by providing a permanent opening, or removable grating. The gasifier and RSC would also not be locked in since the beams and floors locking it into the structure could be removed similar to when these pieces were originally installed.

In an effort to minimize the number of penetrations through the concrete walls of the Slip form option, piping and conduits coming into the structure will be centrally located with branches coming off the vertical and horizontal main lines. This process will cause an increase in piping and conduit materials. To accommodate the centrally located utilities, a vertical pipe chase is provided at the intersections of Grid Lines 8 and E. From this vertical section, horizontal lines will branch off at selected intervals parallel to Grid Line E. From the main horizontal lines, smaller and smaller lines will branch off to minimize penetrations through the vertical walls. Some of the additional cost of piping and conduit will be offset by savings in guardrail since the structure is no longer open on the sides.

Recommendations

It is recommended that schedule, cost, safety, environmental, and geographical issues be reviewed on a specific project basis when considering the options mentioned herein. A project specific analysis of the Stick-built option as well as the Slip form option would quantify the above issues and result in selection of the better option for the particular site.

Pipe Rack Modularization

A study of Pipe Rack Modularization was performed. The pipe rack study analyzed the potential benefits of fabricating pipe racks in a series of modules at an offsite facility. This would allow the pipe rack modules to be fabricated in a controlled environment that can reduce onsite labor risk and decrease the pipe rack installation schedule. Modularization is frequently used on large scale industrial projects in challenging or remote regions and areas with unskilled labor. It was concluded that for a Gulf Coast location, the benefits of pipe rack modularization are minimal.

The pipe rack analysis assumed the fabrication yard location to be in the Gulf Coast Region. The modularization of the pipe racks presents several advantages and

disadvantages over the traditional Stick-built construction method. Below are listed out the findings:

Advantages

- Reduce/minimize on-site labor
- Labor cost reduction based on fabrication location. The labor cost decrease can be substantial based on union vs. non-union and remote site construction
- Reduction of on-site safety risk by moving work to an offsite fabrication yard
- Reduction of construction schedule through parallel activities (i.e. foundation concrete and module fabrication occurring concurrently)
- Majority of steel/mechanical installation occurs in a controlled yard environment. This can increase productivity and reduce weather related delays
- Typically reduces quality risks due to fabrication controlled environment

Dis-advantages

- Increased cost for transportation. Marine deliveries require roll-on/roll-off capable bulkheads that can accept a deep draft barge. Delivery by roads requires permits and planned route has to accept over-sized loads. A completed module can weigh in excess of 100 tons
- Additional bracing is typically required for transportation loads (i.e. wave action). The transportation loading can be in excess of 30% of the module dead load
- All piping and equipment must be secure prior to transportation which can add additional labor and materials
- On-site module installation generally requires larger equipment, lift and set pipe racks modules.

Conclusions

Due to the location of the job, we do not anticipate any substantial cost savings through the use of modular pipe racks. The use of pipe rack modules would be more beneficial in a remote site location with high labor risk. The labor risk may be characterized by the high cost of labor (upwards of 300% more than the gulf coast) or by the lack of skilled labor.

Coal Silo – Slip Form Compared to Traditional Jump Form

A study of Coal Silo construction was performed. Two methods of construction were explored: Traditional "Jump Form" method and the "Slip form" method. Cost for the Jump Form is estimated to be $3,000,000 over a 5 1/2 month duration; and cost for the Slip form is estimated to be $4,500,000 over a 4 1/2 month duration. However, both methods should be considered on a project specific basis due to project specific variations which could significantly affect cost and schedule.

Coal silos have traditionally been built using the jump form method. This method consists of installing the reinforcing of a silo in place, placing the forms that vary in height from 4 to 6 feet, and installing and vibrating the concrete, and letting it set for a period of time. The following day, the forms are jacked to the top of the wall, and the process is completed again until the full height of the structure is completed. This method contrasts with the Slip form method where the slip is constantly in motion and pouring operations continue 24 hours a day until the structure is completed.

The purpose of this study is to determine if there is any material savings or schedule savings between the two methods of construction.

As with the Gasification structure, the location of the Coal silo is assumed to occur in the Gulf Coast Region of the United States. Structural loadings will comply with the International Building Code, 2012 which references ASCE 7-10. For the design of a silo, the most significant load used for design is the unit weight of the material stored. As provided, the unit weight of coal was assumed to be 46 pounds per cubic foot, with an angle of repose assumed at 38 degrees from horizontal, and an internal angle of friction of 27 degrees. In addition, wind loads of 150 mph (Hurricane Region) with an importance factor of 1.0 were used to verify the design. Structural design is in compliance with the American Concrete Institute (ACI) Building Code and Commentary 318-11 and the Standard Practice for Design and Construction of Concrete Silos and Stacking Tubes for Storing Granular Materials 313-97.

Since information regarding the soils was not available, the design of foundations was not included in this study. It was assumed for the sake of the study that the foundations were similar. This assumption is not completely accurate. For the jump form option, the two coal silos cannot be cast together like the Slip form option. This will result in the foundations for the jump form being slightly larger.

Since the design of the ring beam supporting the hopper and the supporting columns are similar, their design is also not included in this study. Again, this assumption is not exactly correct. Although the design of the columns is the same, the construction can be somewhat different. For the jump form option, after the silo is cast, crews return to form up and cast the columns. For the Slip form option, columns can be cast similar to the jump form method, but they can also be cast monolithically with the slip. Although this option does not save materials, it can save construction schedule.

In addition to the above, the following items were also assumed to be the same for either the jump form or Slip form option and were not included in the estimate: temporary roads an laydown areas; temporary electrical; surveying and site layout; trash removal; hot weather concreting; testing; employee welfare facilities; and concrete washout facilities.

Upon completion of the foundation, work on the silos will commence. Similar to the Gasification Structure, the construction of the Slip form coal silos is completed in three major phases; build the slip deck, slip the silos, and disassemble the deck. The process of assembling the deck is estimated to take 6 weeks, slipping the silos is a 24 hour a day process which is estimated at 7 days, and disassembling the slip is estimated to last 8 weeks. Building the roof and finishing will take an additional 4 weeks. This results in a total construction schedule of 4 1/2 months for the coal silo walls, pilasters and roof using the Slip form option.

The process of building the coal silo walls and roof using the jump form option is estimated at 5 1/2 months to 6 months. The cost of building the coal silo walls and pilasters using the Slip form option is estimated at $4,500,000. Using the jump form option, this cost is estimated in the range of $3,000,000.

Conclusions

Based on the information above, a month of schedule can be saved, however the Slip forming process is more expensive (for this hypothetical silo arrangement). However, the budgets and schedule of both options are similar enough that each project should be evaluated on individual basis to determine the most cost effective option.

For reference and context purposes, a copy of the Position Paper written by Kiewit in October of 2013 is included as Appendix L.

Appendix A Structural Design Criteria

Structural Design Criteria:

For
Affordability IGCC Project, Texas, USA
Integrated Gasification Combined Cycle (IGCC)
Slip forming and Modularization

For GE Energy (USA)
And United States Department of Energy

The following forms the Basis of Design for the Study of Structural Steel (Stick-Built) and Concrete Slip form/Modular structural designs.

Location:
Gulf Coast Region of United States

Loading:
Codes and Standards:
ASCE 7-10 (IBC 2012)

Dead Load: Self Weight of structure and permanent non-structural elements
Operating Load: Equipment and Tanks (empty and full) See Equipment list below

Live Load: 300 psf for each floor level. Note: 65'x150' (300 psf) = 2925 kips
For Columns and Global structural Analysis, use 75 psf live load per floor. Note: 65'x150' (75 psf) = 731 kips
Piping: Included in floor live load value.

Rick Category IV (failure could pose hazard to community; hazardous fuel and waste could pose threat to public)

Wind: 150 mph (Hurricane Region) 20 miles inshore from coastline of Texas/Gulf of Mexico, (3% probability of exceedance in 50 years = 1700 year Mean Return Period);
Importance Factor 1w = 1.0
Seismic: Ss = 0.07; S1 = .04; Importance Factor Ie = 1.5, Ip = 1.5, Site Class D
Snow: Ground Snow Loads: Zero
Ice: Zero

Materials:
(The version/edition of Standards shall match those referenced in Loading Standards above)
AISC 360
ACI 318

ACI 313

Foundation Basis:

Mat Foundation with allowable net bearing pressure of 2000 psf for dead and live loads, with 1 1/3 allowable increase for load combinations which include wind or seismic. Stability of mat shall be verified using service level loads with a minimum factor of safety of 1.5 or alternatively analyzing stability with 0.6 dead load as per ASCE 7 Allowable Stress Design Load Combinations. Alternatively, deep foundations (piles) may be required for this type of structure. Cost of deep foundations are expected to be essentially the same for Stick-built and Slip form structures. Deep foundations are included in cost comparisons. Soil improvement or other significant remediation is not considered in this Study.

Fireproofing: At Edwardsport, IN, the lowest 7 stories have fireproofing applied to the primary structural steel beams and columns. The diagonal braces and floor beams do not appear to have fireproofing. Fireproofing for this study shall include:
Structural Steel Stick-built : None
Concrete Slip form walls and steel floors: None

Roof and Floors:
All floors are to consist of bra grating. If a solid floor surface is required, a PL1/4" checker plate may be added over the bar grating. An allowance for this shall dead load shall be included in floor framing design. Roof enclosure, if required, will be of same checker plate material.

Equipment at roof:
Exhaust ducts and exhaust silencers exist at the roof level. These items are accommodated within the live loads specified for floors/roof. Their weights and support steel are relatively small and likely very similar support schemes will be used for both the stick-built and Slip form structures. Therefore, no additional detail or information is required for this item.

Stair Tower:
Not included in Study.

Construction Sequence and Assembly:
RSC will likely be delivered to site in three cylindrical sections. Wall thickness will be 4 to 7 inches thick. The three sections will be welded together in their horizontal position and adjacent to structure; and then lifted to their vertical location within the structure. Internals (e.g. heat exchanger type piping and refractory brick and related items) will be assembled in the vertical RSC vessel. The top, or dome, of RSC will be field welded in its final location. The Gasifier vessel will similarly be field welded/attached in its final position.

Minor Equipment and Piping:
For the purposes of this study, minor pieces of equipment and piping are defined as those of smaller weight that can generally be structurally accommodated by the floor live load allowance. Such approach is deemed to not adversely affect the comparison of stick-built to Slip form structures.

Major Equipment List:

Gasifier:
172 kips erection; 68 kips refractory; Internals: - ; Operating Weight = 240 kips
22' long, 12.5' diameter

RSC:
1032 Kips (Shipping), 551 kips internals; 416 kips refractory; Operating Weight 2,529 kips (approximately 530 kips dirty water)
144' long, 15.6' diameter

Steam Drum:
338 kips shipping; operating weight = 419 kips
55' long 8' diameter

HPO N2 Buffer:
33.6 kips; operating weight = 94 kips
13'-6" (t/t) long, 5' diameter

Syngas Scrubber:
355.7 kips; operating weight = 406 kips
36' long (t/t), 14' diameter

Slag Crusher:
47 kips; operating weight = 100 kips

Lockhopper:
190 kips; operating weight = 320 kips (cycles from 320 kips to 190 kips)
7'-6" long (t/t), 10'-6" diameter

Vacuum Flash:
84.4 kips, operating weight = 146 kips (62 kips dirty water)
22' long (t/t), 13' diameter

LH Flush Drum:
46.6 kips, operating weight = 90 kips (44 kips water, cycles from 46.6 kips to 90 kips)
24'-6" long, 10'6" diameter

HG Guard Drum:
546 kips, operating weight = 546 kips (internals included)
17’ long (t/t), 10’ diameter

COS Shift Reactor:
546 kips, operating weight = 546 kips (internals included)
19’-3” long (t/t), 17’ diameter

(t/t) = indicates length measured tangent to tangent of cylindrical portion of tank.

Appendix B – General Arangement

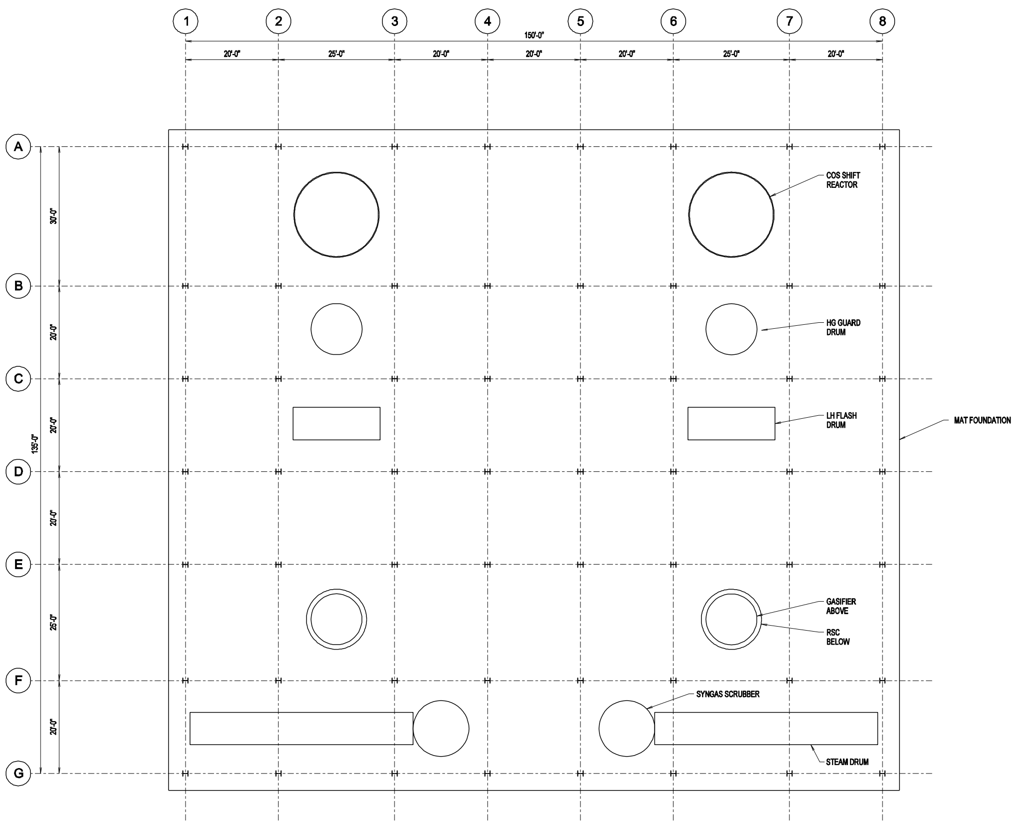

FOUNDATION PLAN

GENERAL ARRANGEMENT

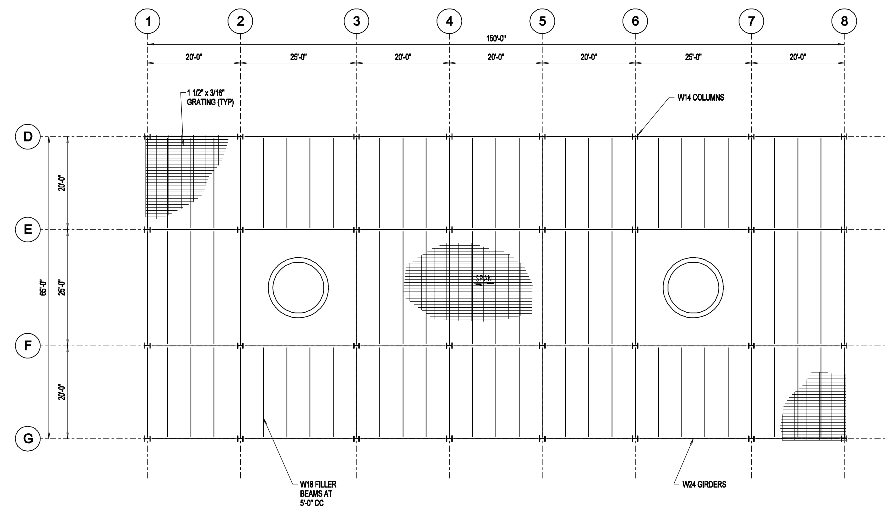

TYPICAL FLOOR FRAMING PLAN

GENERAL ARRANGEMENT

SCALE IN FEET

SCALE: 3/32" = 1'-0"

PLANT NORTH

- PRELIMINARY -
NOT FOR CONSTRUCTION

REV		DESIGN BY	DRAWN BY	CHECKED BY	DATE
A	ISSUED FOR REPORT	T.HEAUSLER	J.BIELAK	C.SUDDUTH	06-18-14

AFFORDABILITY IGCC PROJECT, TEXAS, USA

INTEGRATED GASIFICATION COMBINED CYCLE (IGCC)
SLIP FORMING AND MODULARIZATION

Kiewit

Kiewit Power Engineers Co.
- North Carolina (KPE-NC)
9401 Renner Boulevard
Lenexa, Kansas 66219

GENERAL ARRANGEMENT

ENGINEER/DESIGN ORIGINATOR: T.HEAUSLER
LEAD ENG: -
ENG MGR: -
PROJ MGR: C.SUDDUTH

DRAWING NUMBER: 2013-070-ST-001

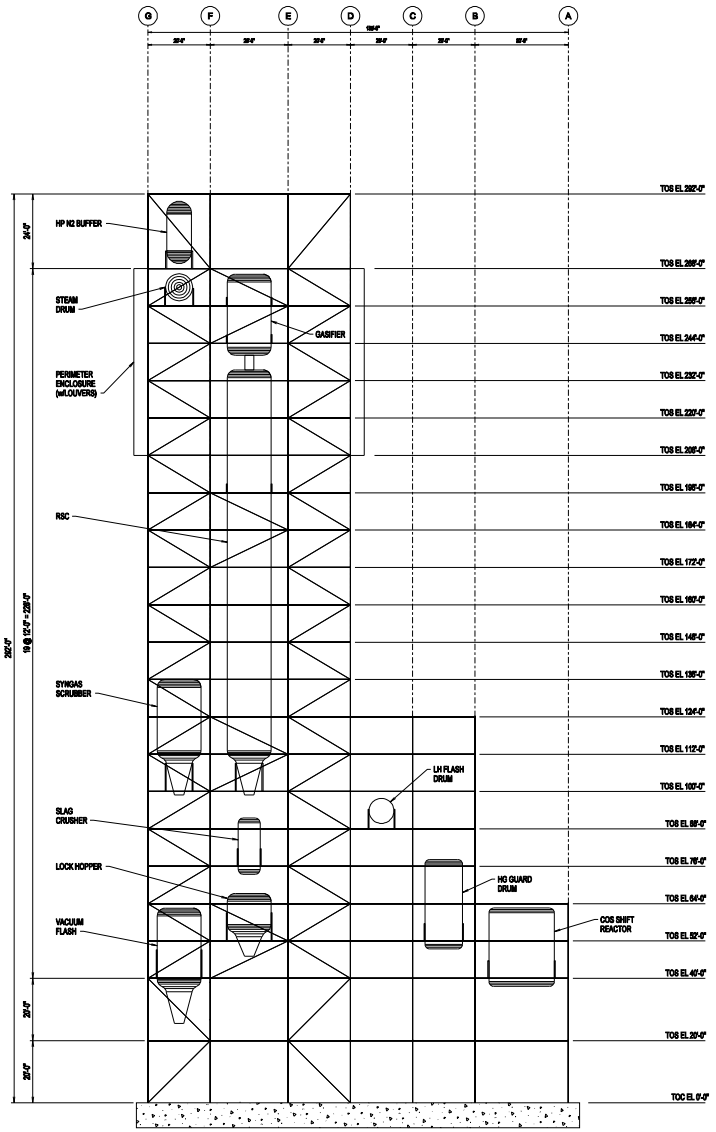

SIDE ELEVATION

GENERAL ARRANGEMENT

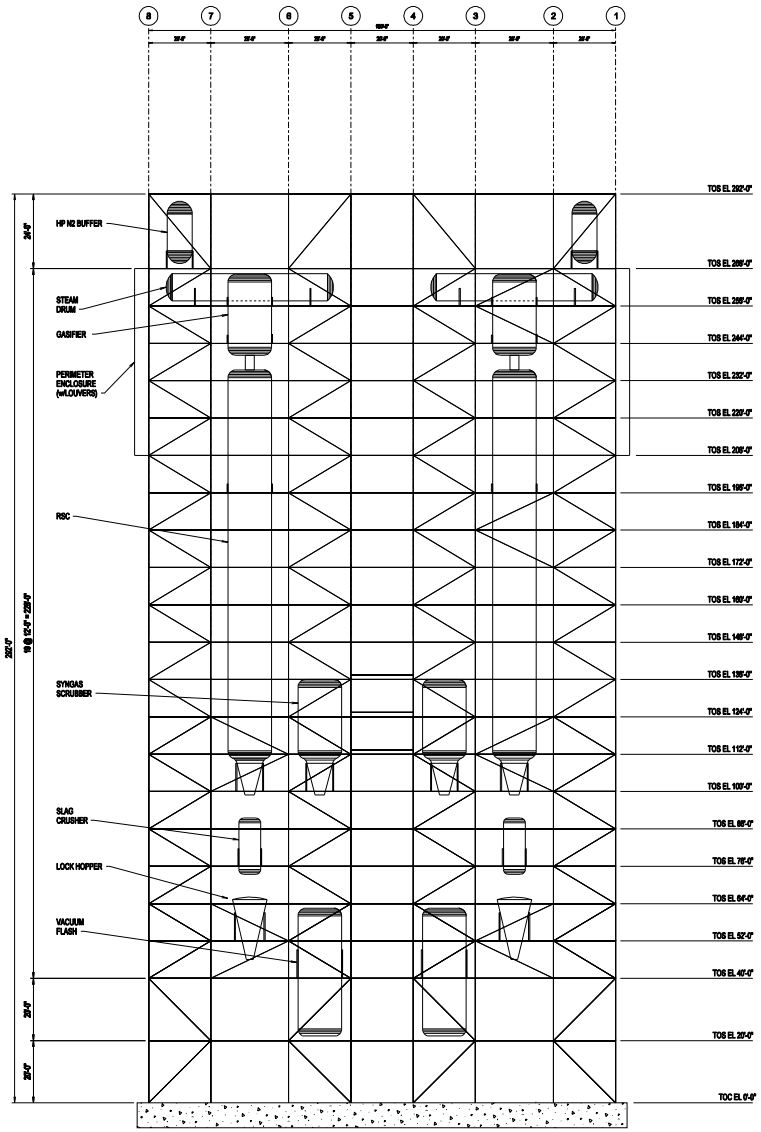

FRONT ELEVATION

GENERAL ARRANGEMENT

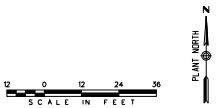

SCALE: 1/16" = 1'-0"

- PRELIMINARY -
NOT FOR CONSTRUCTION

REV	DESIGN BY	DRAWN BY	CHECKED BY	DATE
A	ISSUED FOR REPORT			
	T.HEAUSLER	J.BIELAK	C.SUDDUTH	06-18-14

AFFORDABILITY IGCC PROJECT, TEXAS, USA

INTEGRATED GASIFICATION COMBINED CYCLE (IGCC)
SLIP FORMING AND MODULARIZATION

Kiewit

Kiewit Power Engineers, Co.
- North Carolina (KPE-NC)
9401 Renner Boulevard
Lenexa, Kansas 66219

GENERAL ARRANGEMENT

ENGINEER/DESIGN ORIGINATOR	T.HEAUSLER
LEAD ENG	-
ENG MGR	-
PROJ MGR	C.SUDDUTH

DRAWING NUMBER

2013-070-ST-003

Appendix C – Isometric of Stick-Built Structure

Isometric of Stick- Built Structure

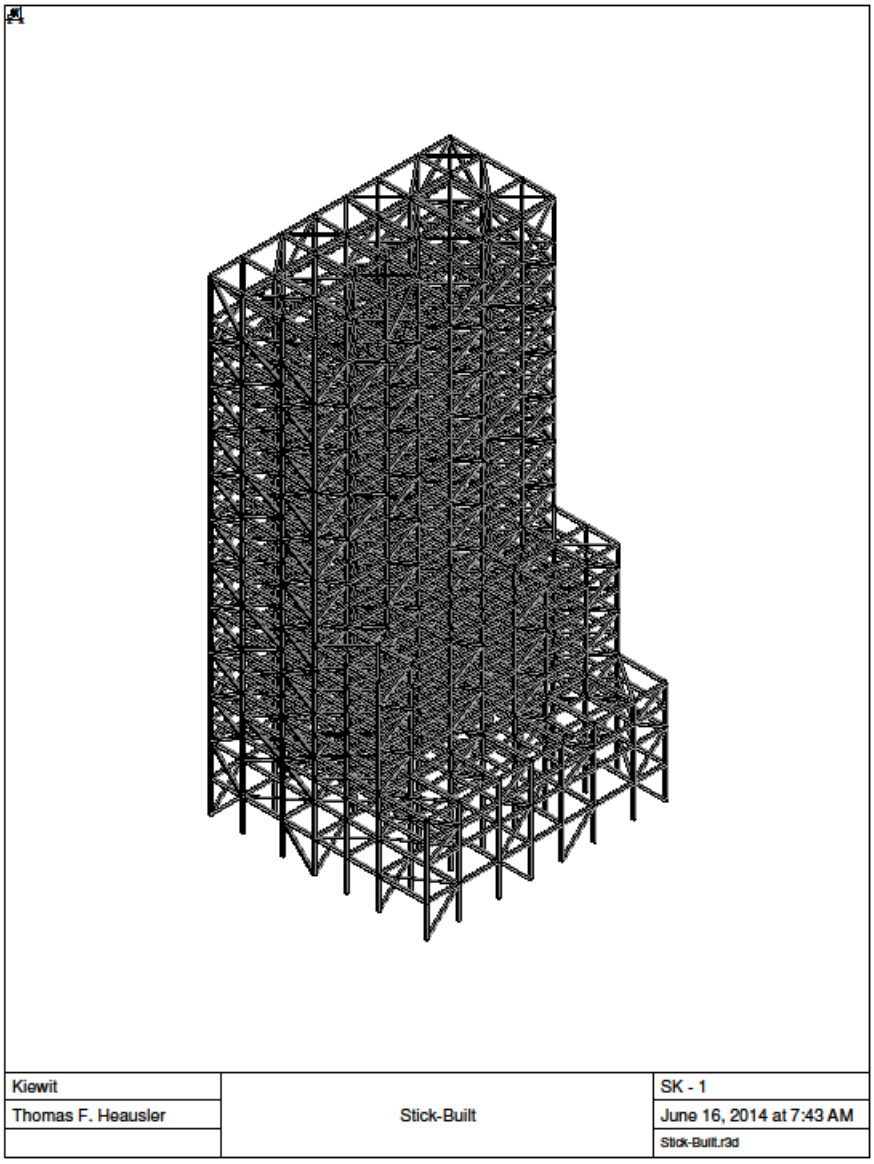

Kiewit	Stick-Built	SK - 1
Thomas F. Heausler		June 16, 2014 at 7:43 AM
		Stick-Built.r3d

Appendix D – Stick-Built Plans and Elevations

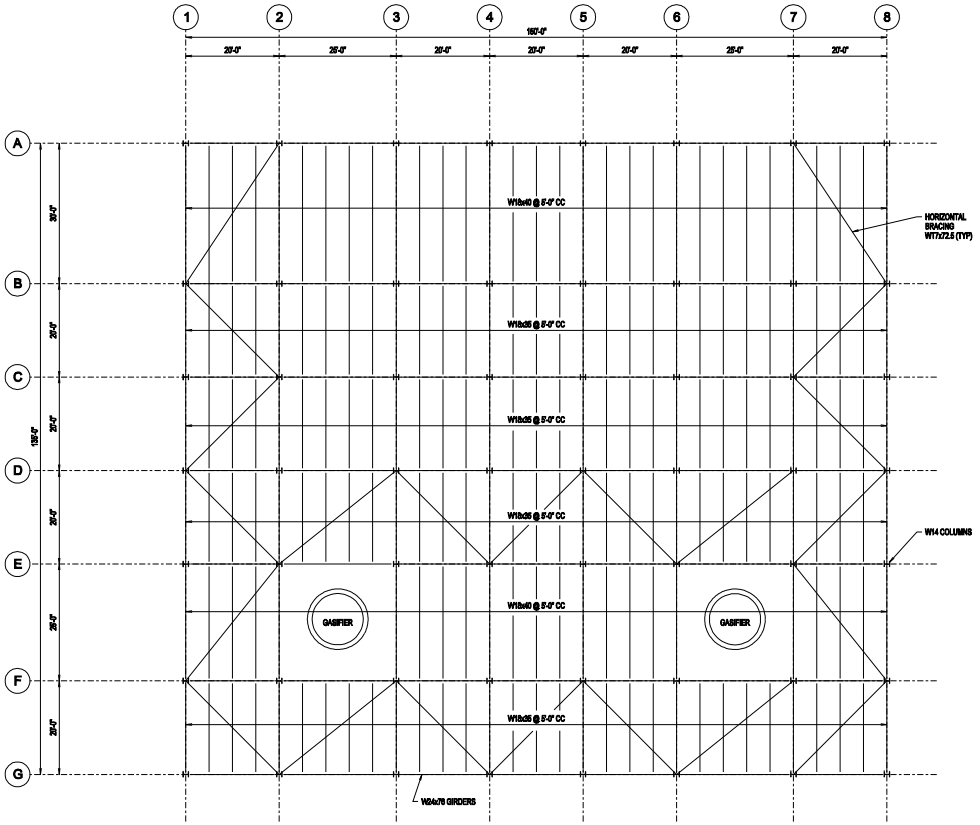

LOWER LEVEL FRAMING PLAN

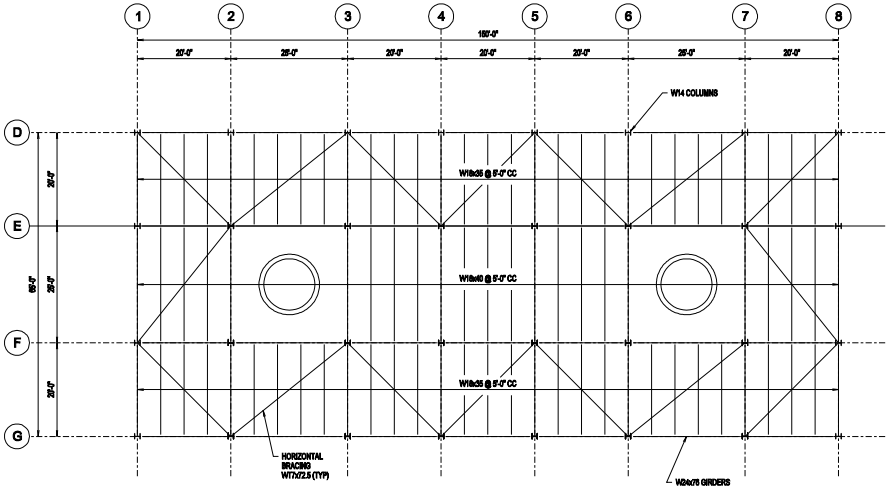

UPPER LEVEL FRAMING PLAN

- PRELIMINARY -
NOT FOR CONSTRUCTION

REV	DESIGN BY	DRAWN BY	CHECKED BY	DATE
A	T.HEAUSLER	J.BIELAK	C.SUDDUTH	06-18-14
	ISSUED FOR REPORT			

AFFORDABILITY IGCC PROJECT, TEXAS, USA

INTEGRATED GASIFICATION COMBINED CYCLE (IGCC)
SLIP FORMING AND MODULARIZATION

Kiewit
Kiewit Power Engineers Co.
North Carolina (KPE-NC)
9401 Renner Boulevard
Lenexa, Kansas 66219

GENERAL ARRANGEMENT

ENGINEER/DESIGN ORIGINATOR	T.HEAUSLER
LEAD ENG	-
ENG MGR	-
PROJ MGR	C.SUDDUTH

DRAWING NUMBER
2013-070-ST-002

8 0 8 16 24
SCALE IN FEET
SCALE: 1/32" = 1'-0"

PLANT NORTH

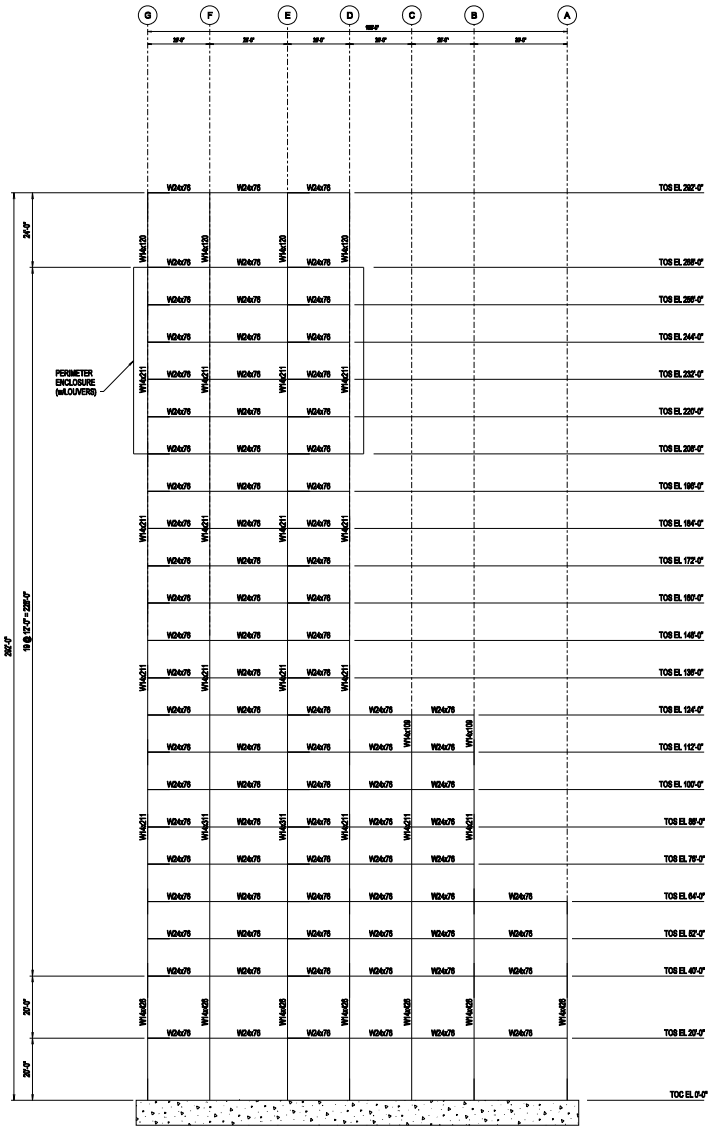

TYPICAL INTERIOR ROW ELEVATION

STEEL FRAMING

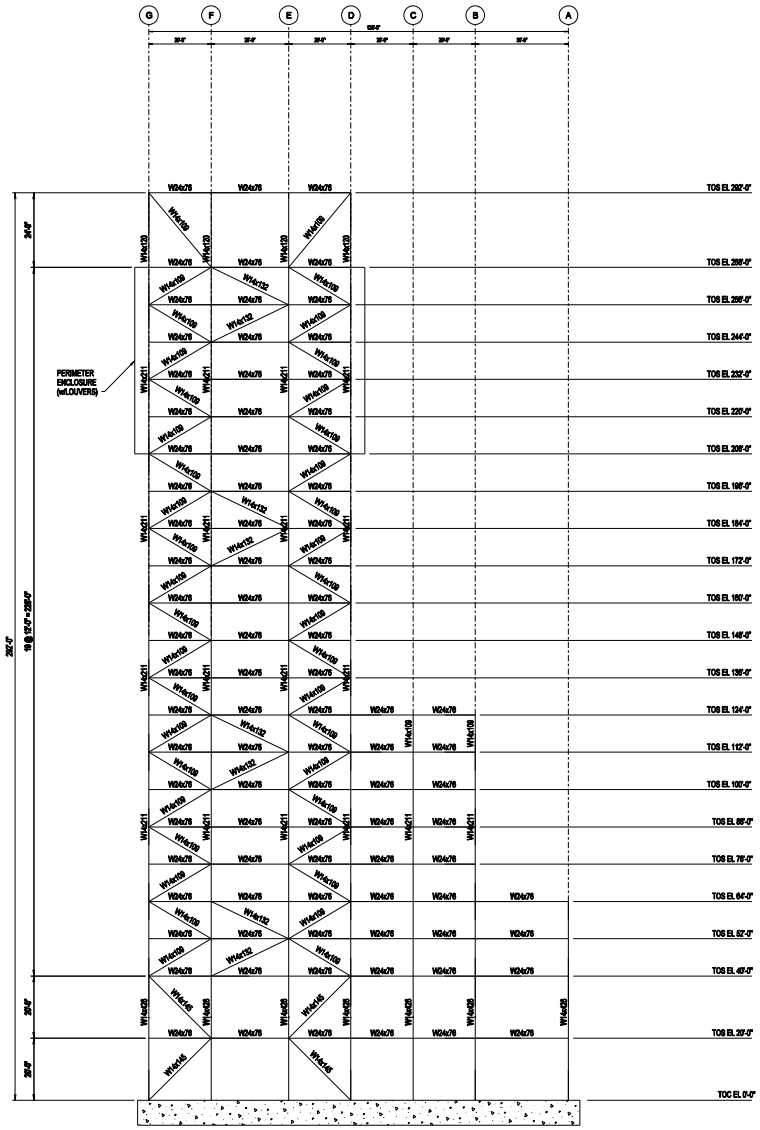

TYPICAL EXTERIOR ROW ELEVATION

STEEL FRAMING

12 0 12 24 36
SCALE IN FEET
SCALE: 1/16" = 1'-0"

- PRELIMINARY -
NOT FOR CONSTRUCTION

REV	DESIGN BY	DRAWN BY	CHECKED BY	DATE
A	ISSUED FOR REPORT	T.HEAUSLER	J.BIELAK	C.SUDDUTH	06-18-14

AFFORDABILITY IGCC PROJECT, TEXAS, USA

INTEGRATED GASIFICATION COMBINED CYCLE (IGCC)
SLIP FORMING AND MODULARIZATION

Kiewit

Kiewit Power Engineers Co.
- North Carolina (KPE-NC)
9401 Renner Boulevard
Lenexa, Kansas 66219

STEEL FRAMING
EXTERIOR AND INTERIOR ELEVATIONS

ENGINEER/DESIGN ORIGINATOR	T.HEAUSLER
LEAD ENG	-
ENG MGR	-
PROJ MGR	C.SUDDUTH

DRAWING NUMBER
2013-070-ST-004

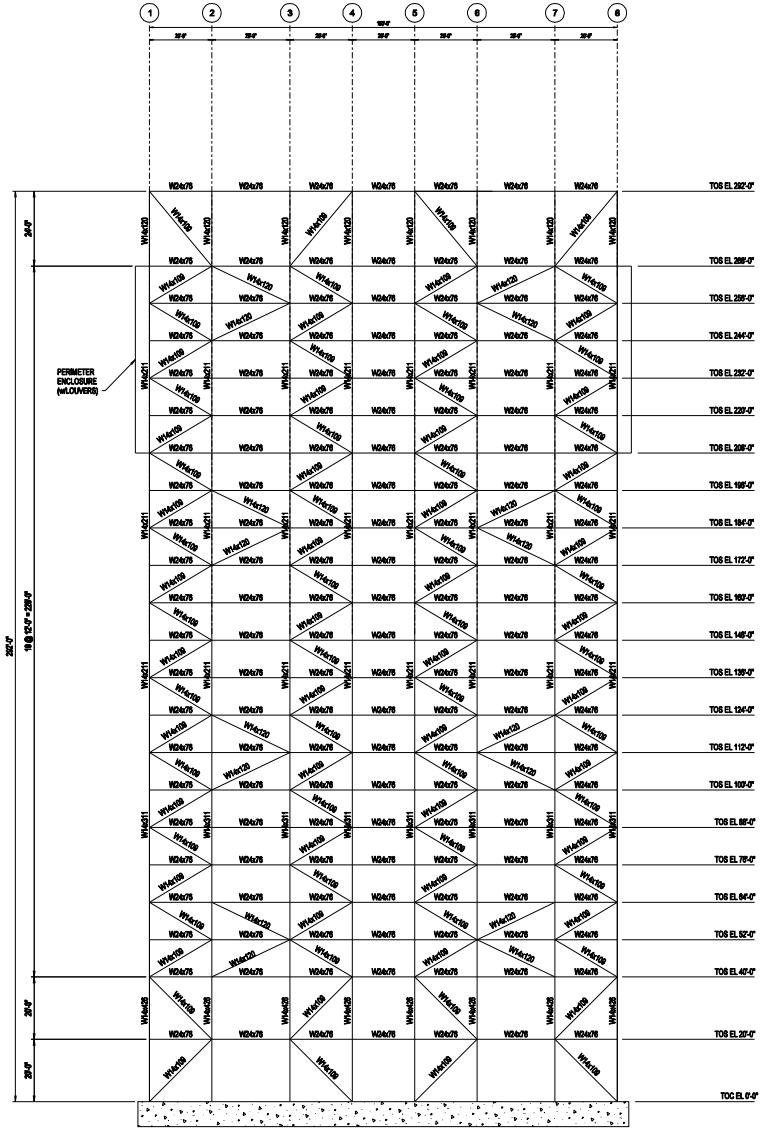

TYPICAL EXTERIOR FRAME ELEVATION

12 0 12 24 36
SCALE IN FEET
SCALE: 1/8" = 1'-0"

- PRELIMINARY -
NOT FOR CONSTRUCTION

REV	DESIGN BY	DRAWN BY	CHECKED BY	DATE
A	ISSUED FOR REPORT			
	T. HEASLER	J. BIELAK	C. SUDDUTH	06-18-14

AFFORDABILITY IGCC PROJECT, TEXAS, USA

INTEGRATED GASIFICATION COMBINED CYCLE (IGCC)
SLIP FORMING AND MODULARIZATION

Kiewit

Kiewit Power Engineers Co.
- North Carolina (KPE-NC)
9401 Renner Boulevard
Lenexa, Kansas 66219

STEEL FRAMING
EXTERIOR AND INTERIOR ELEVATIONS

ENGINEER/DESIGN ORIGINATOR	T. HEASLER
LEAD ENG	-
ENG MGR	-
PROJ MGR	C. SUDDUTH

DRAWING NUMBER
2013-070-ST-005

Appendix E – Stick-Built Erection/Assembly Sequence

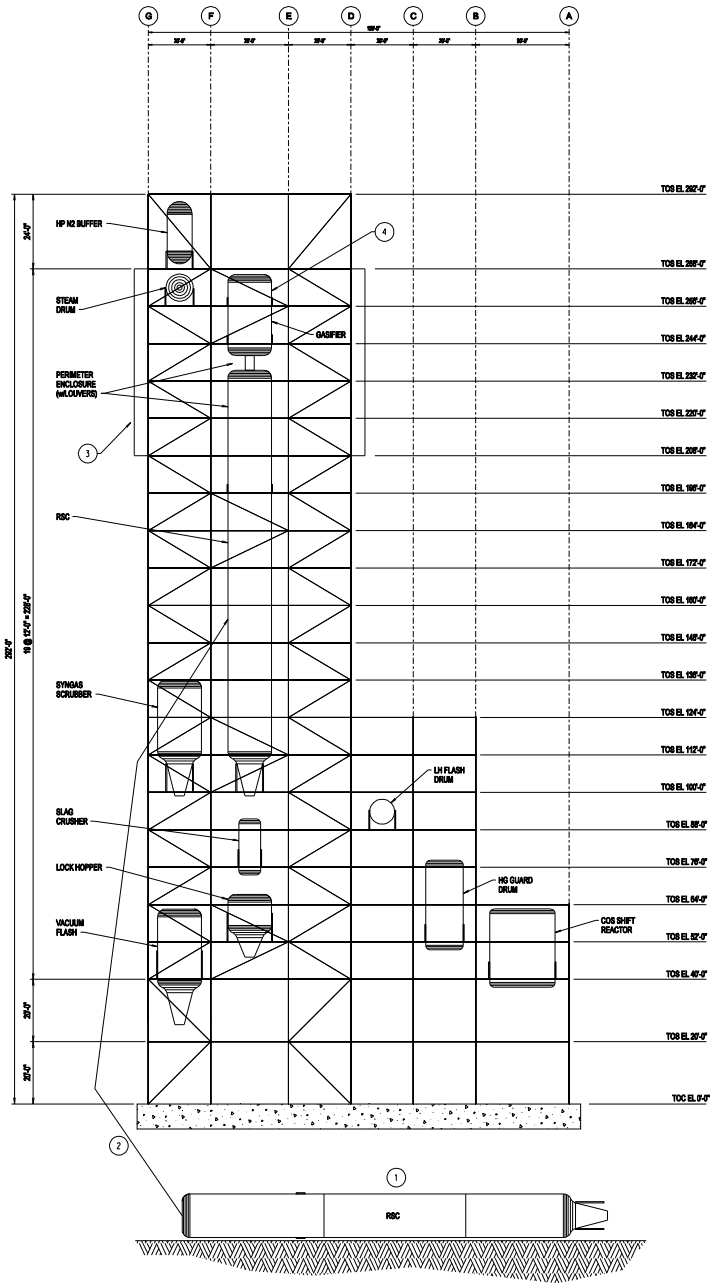

SIDE ELEVATION
ASSEMBLY SEQUENCE

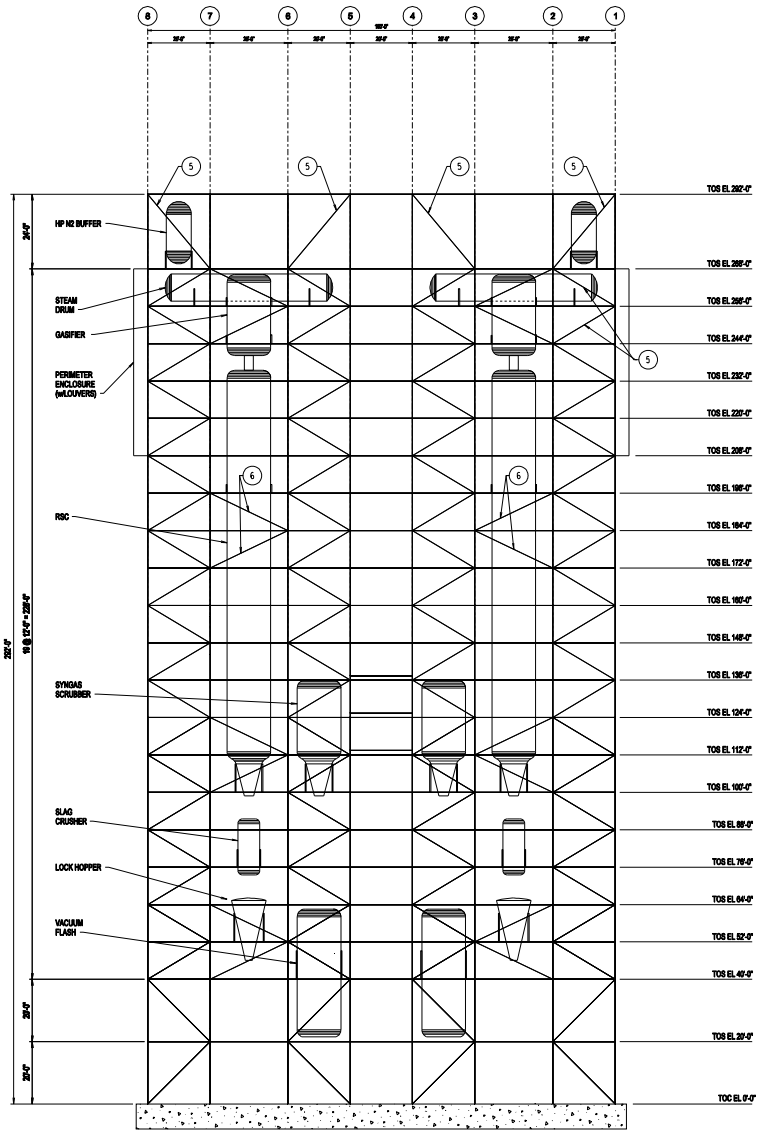

FRONT ELEVATION
ASSEMBLY SEQUENCE

SCALE IN FEET
12 0 12 24 36
SCALE: 1/16" = 1'-0"

PLANT NORTH

NOTES:

SIDE ELEVATION

1. RSC IS DELIVERED TO SITE IN 3 CYLINDRICAL PIECES AND WELDED TOGETHER IN HORIZONTAL POSITION.
2. THEN LIFTED TO VERTICAL POSITION WITHIN STRUCTURE WITH CRANE.
3. RSC INTERNAL PIPES AND REFACTORY BRICK ARE INSERTED BY CRANE.
4. RSC DOME AND GASIFIER ARE LIFTED AND WELDED.

FRONT ELEVATION

5. DIAGONAL BRACES IN THESE BAYS ARE INSTALLED FIRST.
6. DIAGONALS IN THESE BAYS ARE INSTALLED AFTER RSC IS INSTALLED.

- PRELIMINARY -
NOT FOR CONSTRUCTION

REV	DESIGN BY	DRAWN BY	CHECKED BY	DATE
A	ISSUED FOR REPORT			
	T.HEAUSLER	J.BIELAK	C.SUDDUTH	06-18-14

AFFORDABILITY IGCC PROJECT, TEXAS, USA

INTEGRATED GASIFICATION COMBINED CYCLE (IGCC)
SLIP FORMING AND MODULARIZATION

Kiewit

Kiewit Power Engineers Co.
- North Carolina (KPE-NC)
9401 Renner Boulevard
Lenexa, Kansas 66219

GENERAL ARRANGEMENT
ASSEMBLY SEQUENCE

ENGINEER/DESIGN ORIGINATOR	T.HEAUSLER
LEAD ENG	-
ENG MGR	-
PROJ MGR	C.SUDDUTH

DRAWING NUMBER
2013-070-ST-006

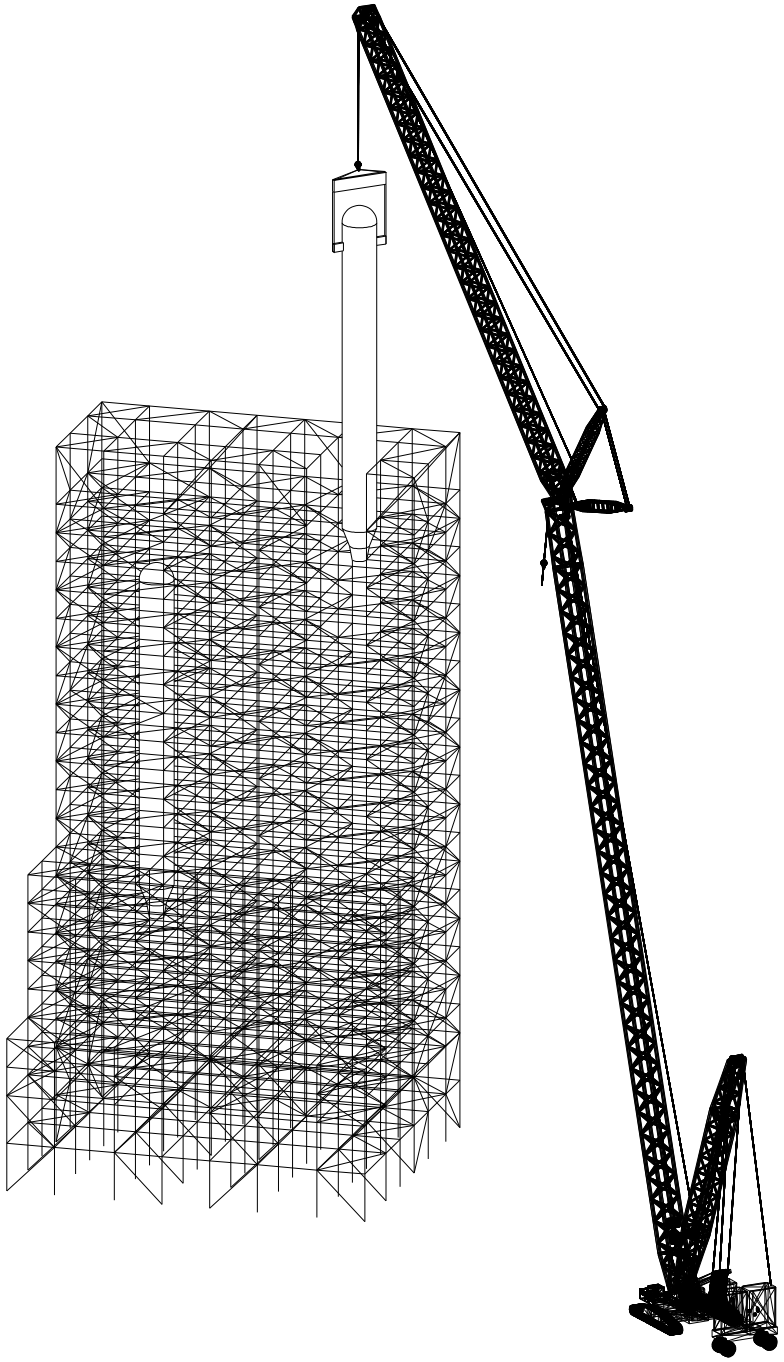

– PRELIMINARY –
NOT FOR CONSTRUCTION

REV	DESIGN BY	DRAWN BY	CHECKED BY	DATE
A	ISSUED FOR REPORT	T.HEASULER	J.BIELAK	C.SUDDUTH	06-18-14

AFFORDABILITY IGCC PROJECT, TEXAS, USA

INTEGRATED GASIFICATION COMBINED CYCLE (IGCC)
SLIP FORMING AND MODULARIZATION

Kiewit

Kiewit Power Engineers, Co.
- North Carolina (KPE-NC)
9401 Renner Boulevard
Lenexa, Kansas 66219

GENERAL ARRANGEMENT
LIFTING ASSEMBLY

ENGINEER/DESIGN ORIGINATOR	T.HEAUSLER
LEAD ENG	–
ENG MGR	–
PROJ MGR	C.SUDDUTH

DRAWING NUMBER

2013-070-ST-007

Appendix F – Slip Form Plans and Elevations

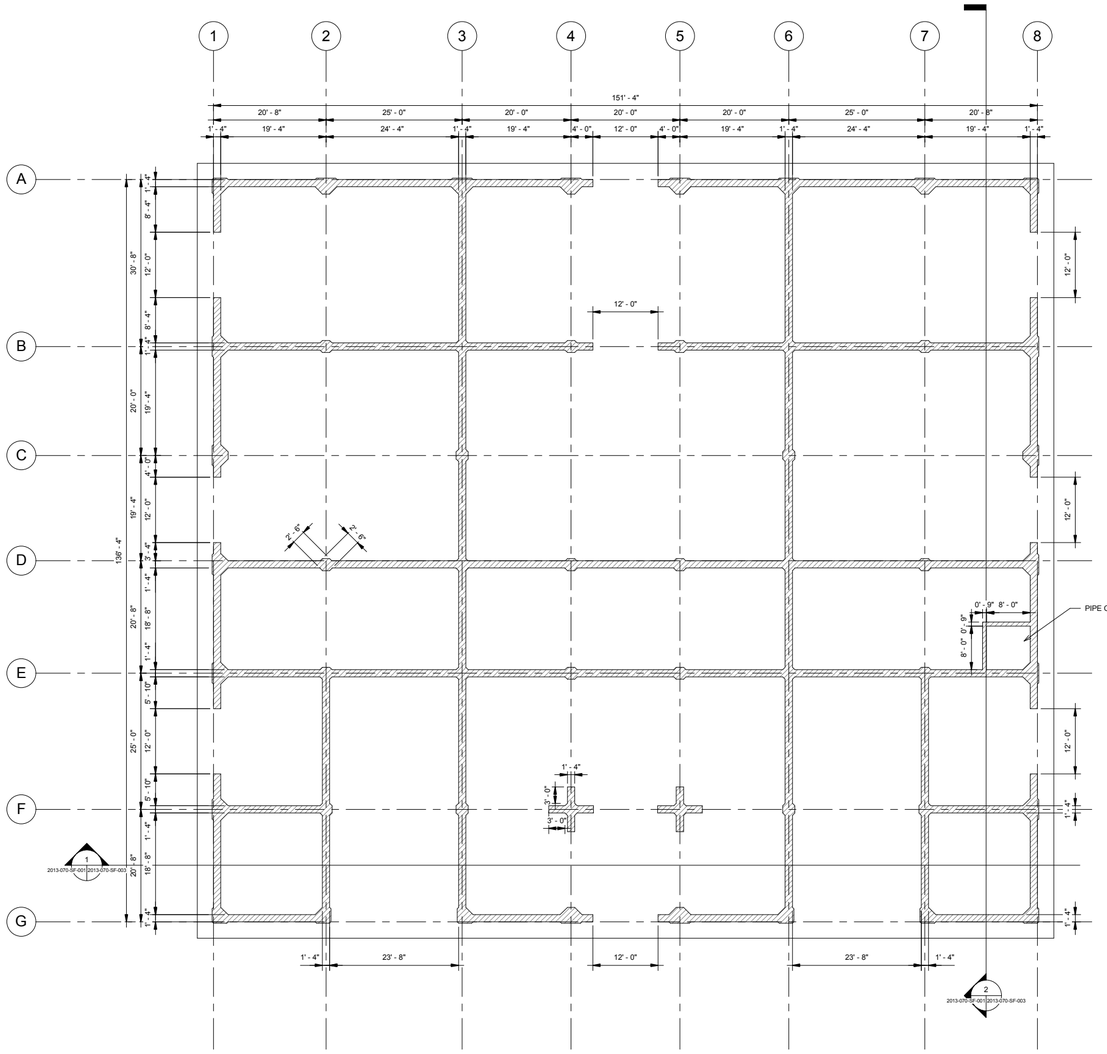

PLAN - GASIFICATION SLIP AT GRADE

3/32" = 1' - 0"

PLAN - GASIFICATION SLIP AT 124' - 0"

3/32" = 1' - 0"

-PRELIMINARY-
NOT FOR CONSTRUCTION

REV	DESIGN BY	DRAWN BY	CHECKED BY	DATE
A	ISSUED FOR APPROVAL			
	S. DRAKE	M. KELLY	-	06/04/14

AFFORDABILITY IGCC PROJECT, TEXAS, USA

INTEGRATED GASIFICATION COMBINED CYCLE
(IGCC)
SLIP FORMING AND MODULARIZATION

Kiewit

xKiewit Power Engineers, Co.
- North Carolina (KPE-NC)
9401 Renner Boulevard
Lenexa, Kansas 66219

GENERAL ARRANGEMENT

8 0 8 16 24
SCALE IN FEET
SCALE: 3/32" = 1'-0"

PLANT NORTH

ENGINEER/DESIGN ORIGINATOR	S. DRAKE
LEAD ENG	-
ENG MGR	-
PROJ MGR	S. SUDDUTH

DRAWING NUMBER

2013-070-SF-001

C:\Users\matt.r.kelly\Documents\GE GASIFICATION_MattR.Kelly.rvt

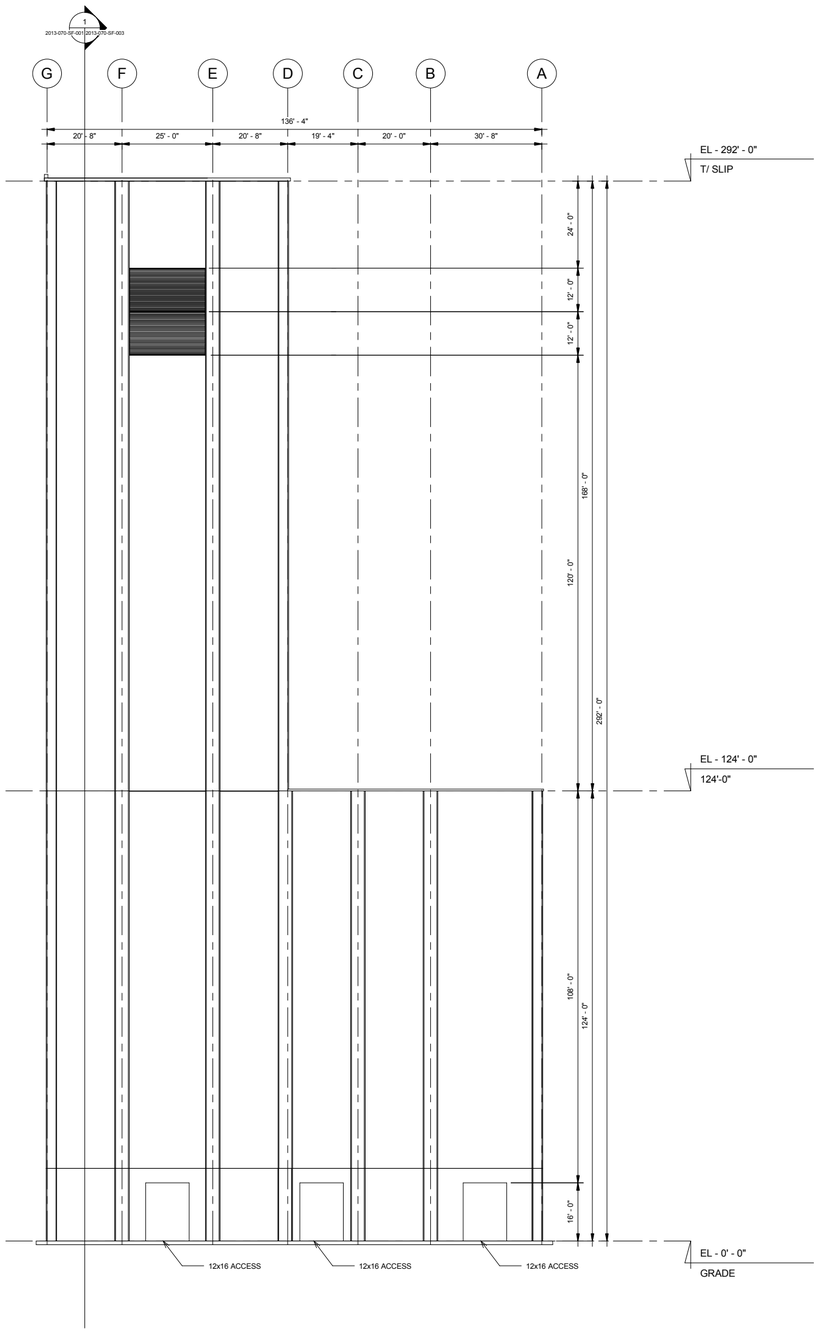

ELEVATION - EAST AT GRID 8

1/16" = 1' - 0"

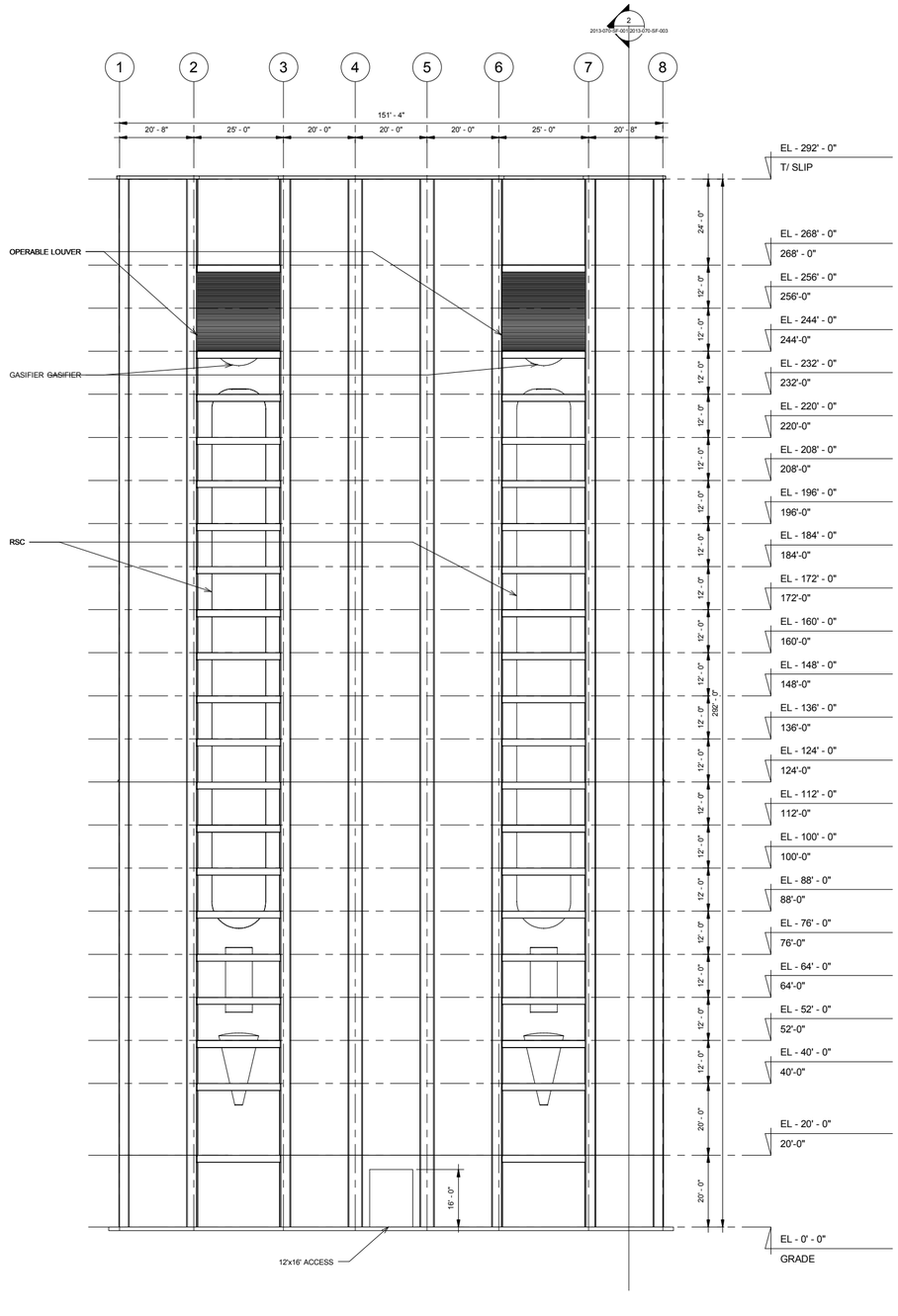

ELEVATION - SOUTH AT GRID G

1/16" = 1' - 0"

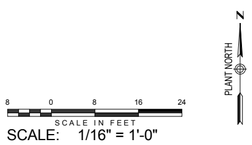

SCALE: 1/16" = 1'-0"

-PRELIMINARY-
NOT FOR CONSTRUCTION

REV	DESIGN BY	DRAWN BY	CHECKED BY	DATE
A	ISSUED FOR APPROVAL			
	S. DRAKE	M. KELLY	-	06/04/14

AFFORDABILITY IGCC PROJECT, TEXAS, USA

INTEGRATED GASIFICATION COMBINED CYCLE
(IGCC)
SLIP FORMING AND MODULARIZATION

Kiewit

xKiewit Power Engineers, Co.
- North Carolina (KPE-NC)
9401 Renner Boulevard
Lenexa, Kansas 66219

GENERAL ARRANGEMENT

ENGINEER/DESIGN ORIGINATOR	S. DRAKE
LEAD ENG	-
ENG MGR	-
PROJ MGR	S. SUDDUTH

DRAWING NUMBER

2013-070-SF-002

C:\Users\mattr.kelly\Documents\GE GASIFICATION_MattR.Kelly.rvt

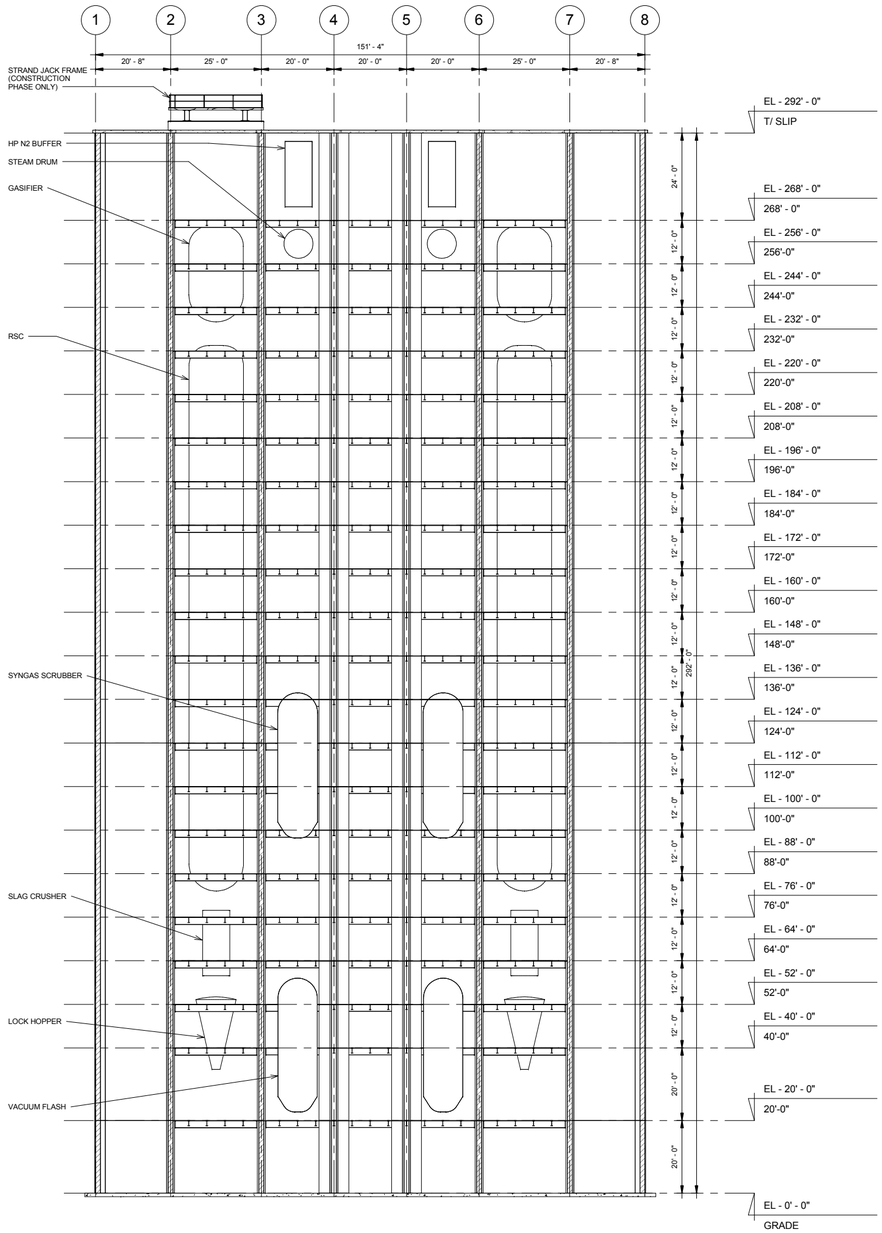

SECTION - GASIFICATION SLIP LOOKING NORTH

1/16" = 1' - 0"

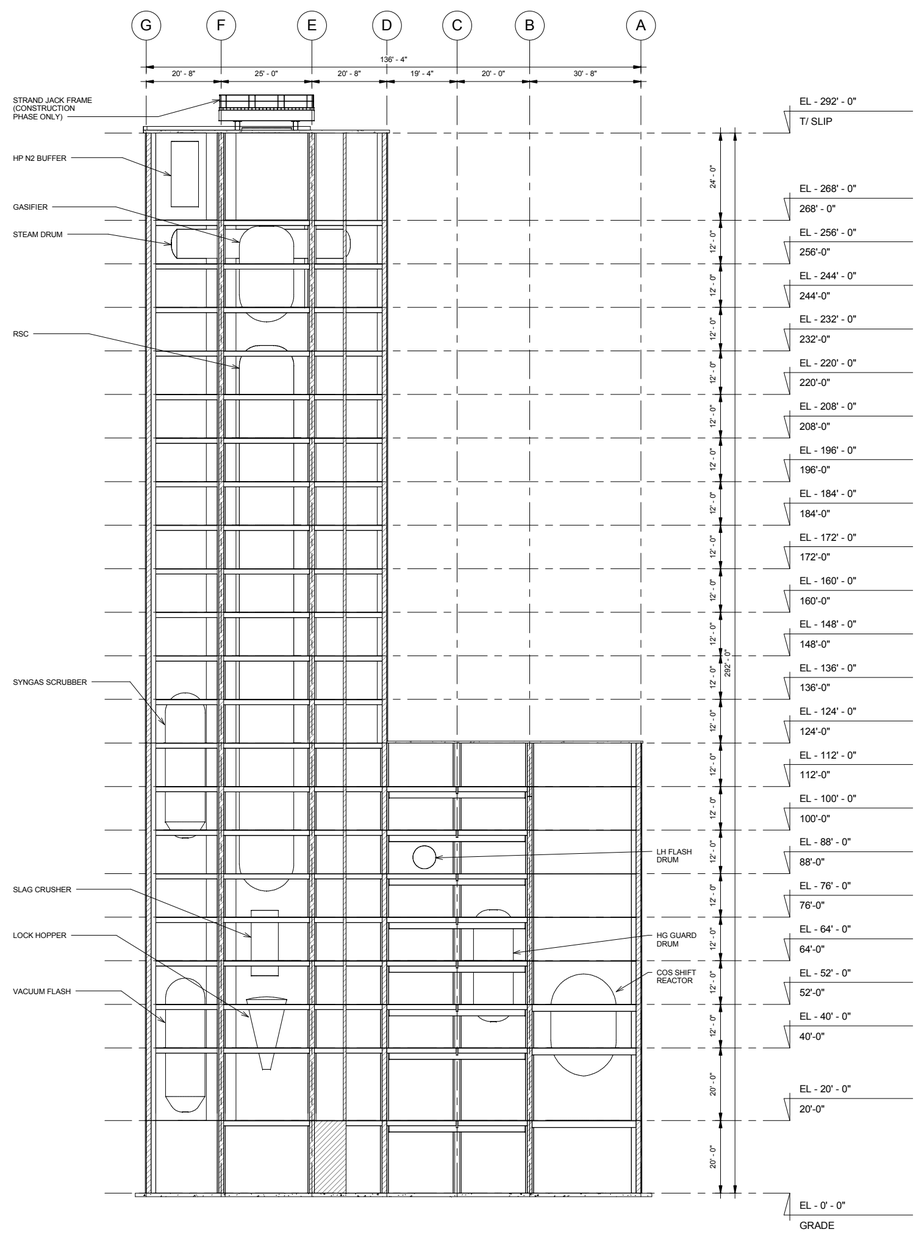

SECTION - GASIFICATION SLIP LOOKING WEST

1/16" = 1' - 0"

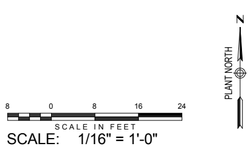

SCALE: 1/16" = 1'-0"

-PRELIMINARY-
NOT FOR CONSTRUCTION

REV	DESIGN BY	DRAWN BY	CHECKED BY	DATE
A	ISSUED FOR APPROVAL			
	S. DRAKE	M. KELLY	-	06/04/14

AFFORDABILITY IGCC PROJECT, TEXAS, USA

INTEGRATED GASIFICATION COMBINED CYCLE
(IGCC)
SLIP FORMING AND MODULARIZATION

Kiewit

x:Kiewit Power Engineers, Co.
- North Carolina (KPE-NC)
9401 Renner Boulevard
Lenexa, Kansas 66219

GENERAL ARRANGEMENT

ENGINEER/DESIGN ORIGINATOR	S. DRAKE
LEAD ENG	-
ENG MGR	-
PROJ MGR	S. SUDDUTH

DRAWING NUMBER

2013-070-SF-003

C:\Users\matt.r.kelly\Documents\GE GASIFICATION_MattR.Kelly.rvt

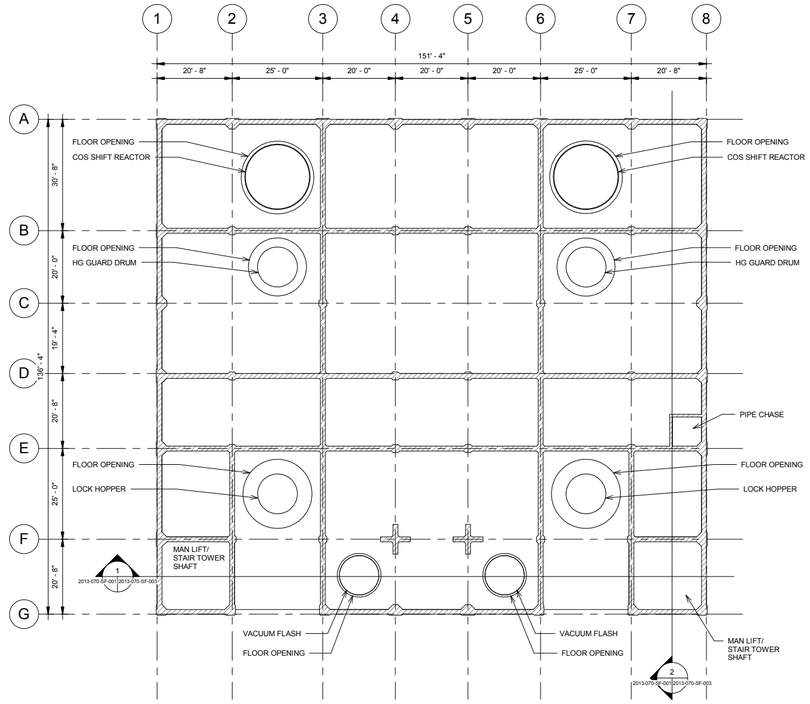

PLAN - GASIFICATION SLIP AT 52' - 0"

1/16" = 1' - 0"

NOTE: STRUCTURAL STEEL NOT SHOWN FOR CLARITY, SEE GA6 FOR STRUCTURAL STEEL INFORMATION

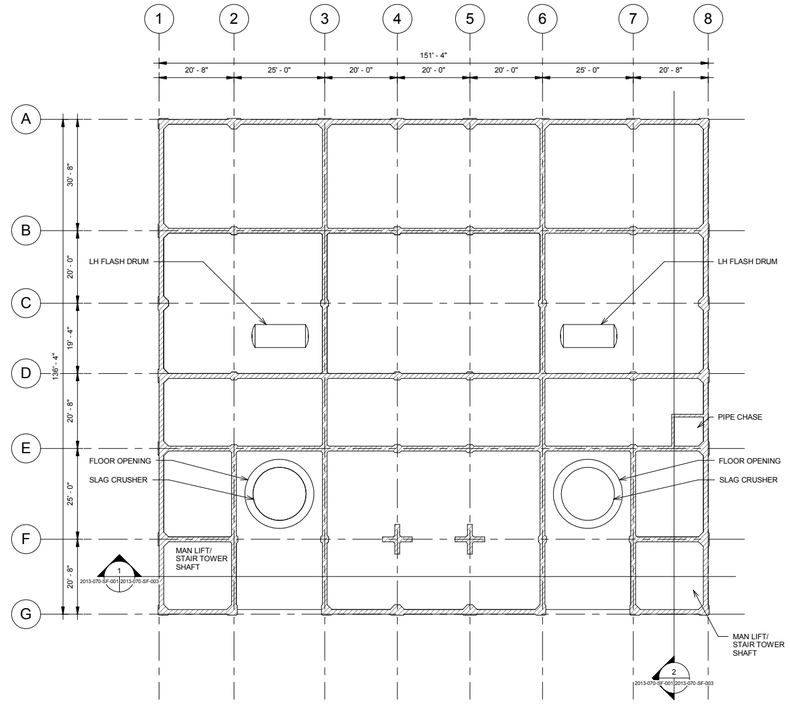

PLAN - GASIFICATION SLIP AT 88' - 0"

1/16" = 1' - 0"

NOTE: STRUCTURAL STEEL NOT SHOWN FOR CLARITY, SEE GA6 FOR STRUCTURAL STEEL INFORMATION

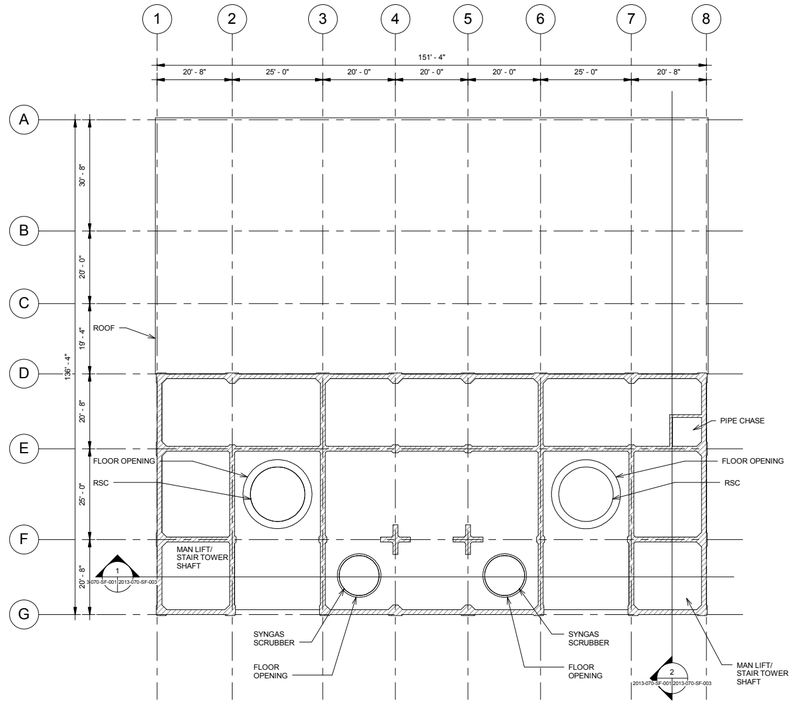

PLAN - GASIFICATION SLIP AT 124' - 0"

1/16" = 1' - 0"

NOTE: STRUCTURAL STEEL NOT SHOWN FOR CLARITY, SEE GA6 FOR STRUCTURAL STEEL INFORMATION

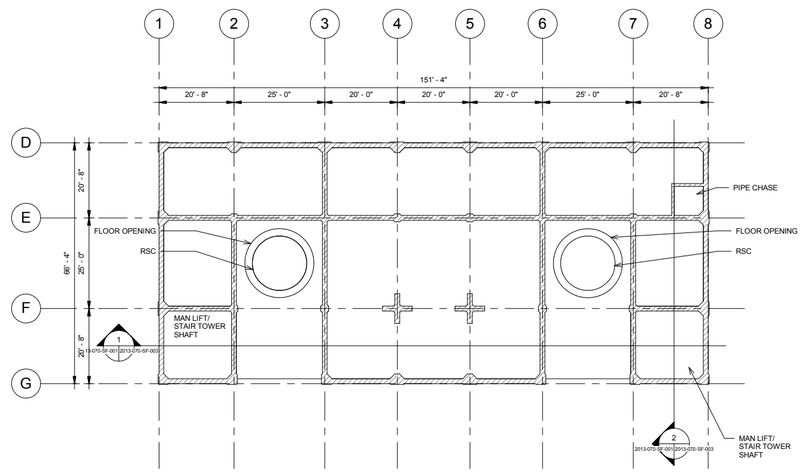

PLAN - GASIFICATION SLIP AT 196' - 0"

1/16" = 1' - 0"

NOTE: STRUCTURAL STEEL NOT SHOWN FOR CLARITY, SEE GA6 FOR STRUCTURAL STEEL INFORMATION

8 0 8 16 24

SCALE IN FEET

SCALE: 1/16" = 1'-0"

PLANT NORTH

-PRELIMINARY-
NOT FOR CONSTRUCTION

REV	DESIGN BY	DRAWN BY	CHECKED BY	DATE
A	S. DRAKE	M. KELLY	-	06/04/14

ISSUED FOR APPROVAL

AFFORDABILITY IGCC PROJECT, TEXAS, USA

INTEGRATED GASIFICATION COMBINED CYCLE (IGCC)
SLIP FORMING AND MODULARIZATION

x:Kiewit Power Engineers, Co.
- North Carolina (KPE-NC)
9401 Renner Boulevard
Lenexa, Kansas 66219

GENERAL ARRANGEMENT

ENGINEER/DESIGN ORIGINATOR	S. DRAKE
LEAD ENG	-
ENG MGR	-
PROJ MGR	S. SUDDUTH

DRAWING NUMBER

2013-070-SF-004

C:\Users\matt.kelly\Documents\GE GASIFICATION_MattR.Kelly.rvt

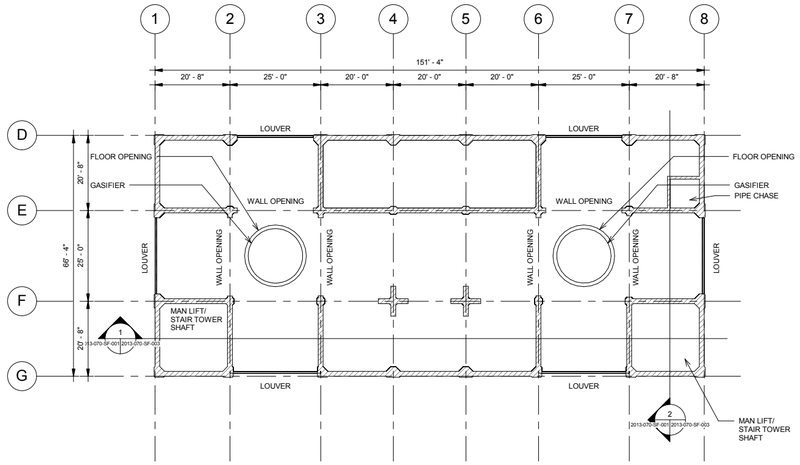

PLAN - GASIFICATION SLIP AT 244' - 0"

1/16" = 1' - 0"

NOTE: STRUCTURAL STEEL NOT SHOWN FOR CLARITY, SEE GA6 FOR STRUCTURAL STEEL INFORMATION

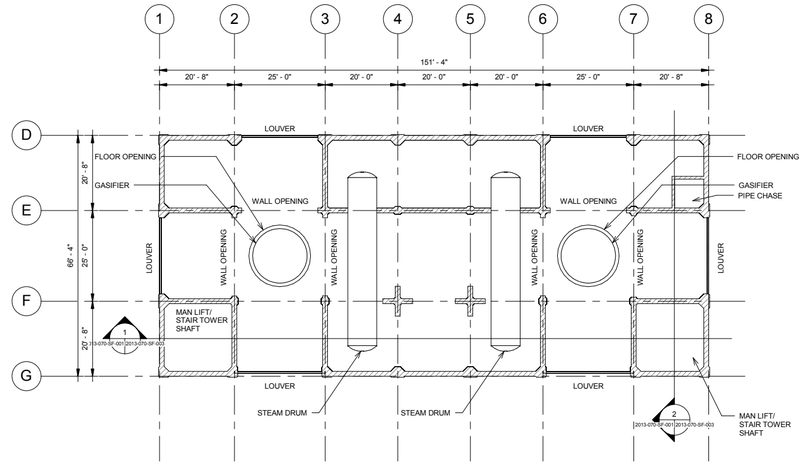

PLAN - GASIFICATION SLIP AT 256' - 0"

1/16" = 1' - 0"

NOTE: STRUCTURAL STEEL NOT SHOWN FOR CLARITY, SEE GA6 FOR STRUCTURAL STEEL INFORMATION

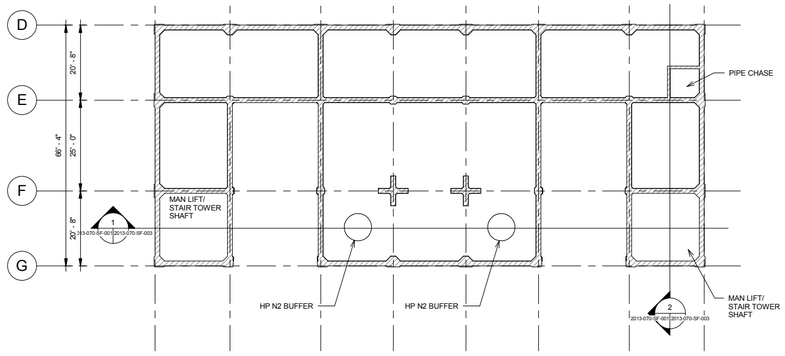

PLAN - GASIFICATION SLIP AT 268' - 0"

1/16" = 1' - 0"

NOTE: STRUCTURAL STEEL NOT SHOWN FOR CLARITY, SEE GA6 FOR STRUCTURAL STEEL INFORMATION

8 0 8 16 24

SCALE IN FEET

SCALE: 1/16" = 1'-0"

PLANT NORTH

N

-PRELIMINARY-
NOT FOR CONSTRUCTION

REV	DESIGN BY	DRAWN BY	CHECKED BY	DATE
A	S. DRAKE	M. KELLY	-	06/04/14

ISSUED FOR APPROVAL

AFFORDABILITY IGCC PROJECT, TEXAS, USA

INTEGRATED GASIFICATION COMBINED CYCLE
(IGCC)
SLIP FORMING AND MODULARIZATION

x:Kiewit Power Engineers, Co.
- North Carolina (KPE-NC)
9401 Renner Boulevard
Lenexa, Kansas 66219

GENERAL ARRANGEMENT

ENGINEER/DESIGN ORIGINATOR	S. DRAKE
LEAD ENG	-
ENG MGR	-
PROJ MGR	S. SUDDUTH

DRAWING NUMBER

2013-070-SF-005

C:\Users\matt.kelly\Documents\GE GASIFICATION_MattR.Kelly.rvt

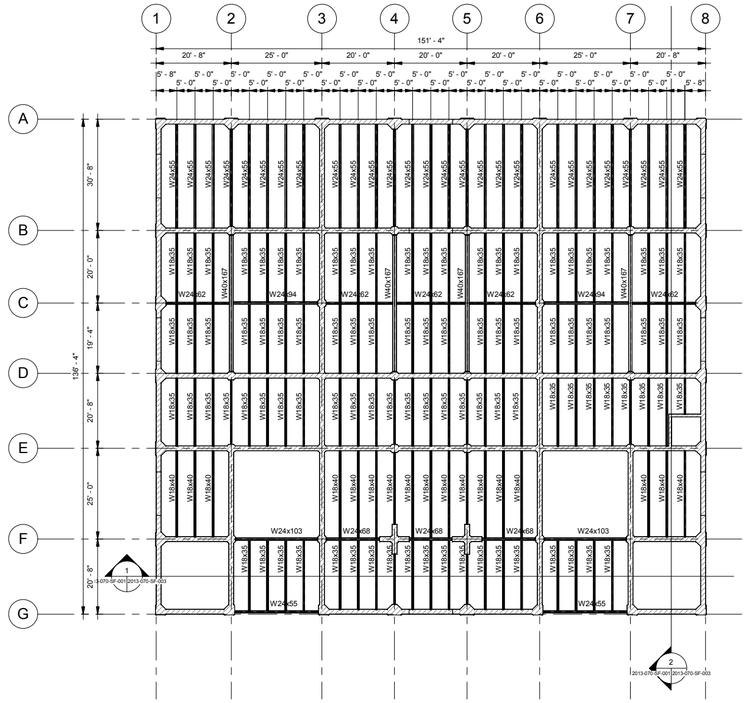

PLAN - STRUCTURAL STEEL

1/16" = 1' - 0" AT 20'-0"
40'-0"
52'-0"

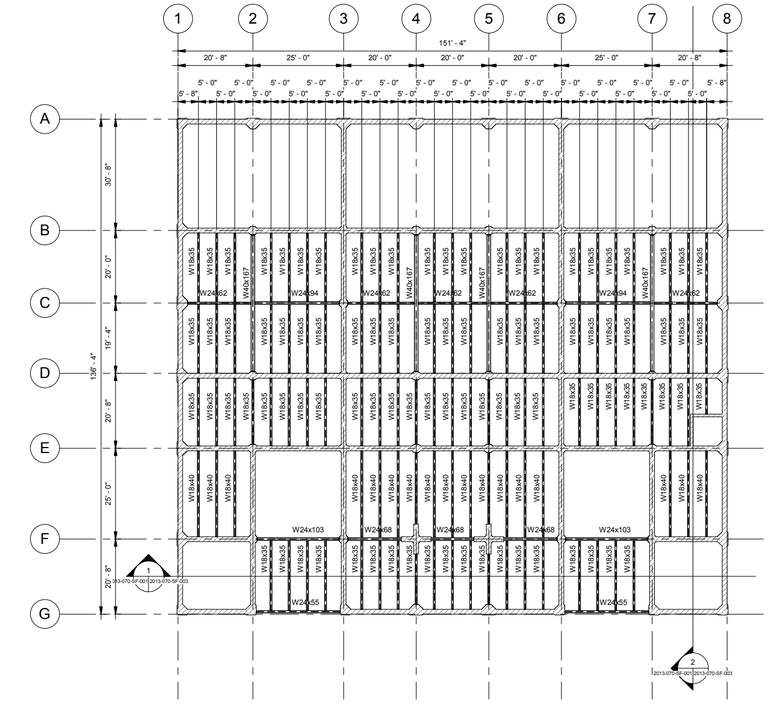

PLAN - STRUCTURAL STEEL

1/16" = 1' - 0" AT 64'-0"
76'-0"
88'-0"
100'-0"
112'-0"

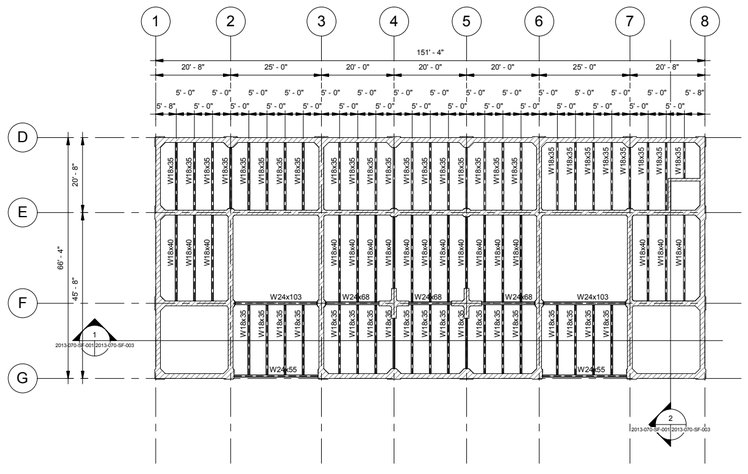

PLAN - STRUCTURAL STEEL

1/16" = 1' - 0" AT 124'-0"
136'-0"
148'-0"
160'-0"
172'-0"
184'-0"
196'-0"
208'-0"
220'-0"
232'-0"
244'-0"
256'-0"
268'-0"

8 0 8 16 24
SCALE IN FEET
SCALE: 1/16" = 1'-0"

PLANT NORTH

-PRELIMINARY-
NOT FOR CONSTRUCTION

REV	DESIGN BY	DRAWN BY	CHECKED BY	DATE
A	S. DRAKE	M. KELLY	-	06/04/14

ISSUED FOR APPROVAL

AFFORDABILITY IGCC PROJECT, TEXAS, USA

INTEGRATED GASIFICATION COMBINED CYCLE
(IGCC)
SLIP FORMING AND MODULARIZATION

x:Kiewit Power Engineers, Co.
- North Carolina (KPE-NC)
9401 Renner Boulevard
Lenexa, Kansas 66219

GENERAL ARRANGEMENT

ENGINEER/DESIGN ORIGINATOR	S. DRAKE
LEAD ENG	-
ENG MGR	-
PROJ MGR	S. SUDDUTH

DRAWING NUMBER

2013-070-SF-06

C:\Users\matt.r.kelly\Documents\GE GASIFICATION_MattR.Kelly.rvt

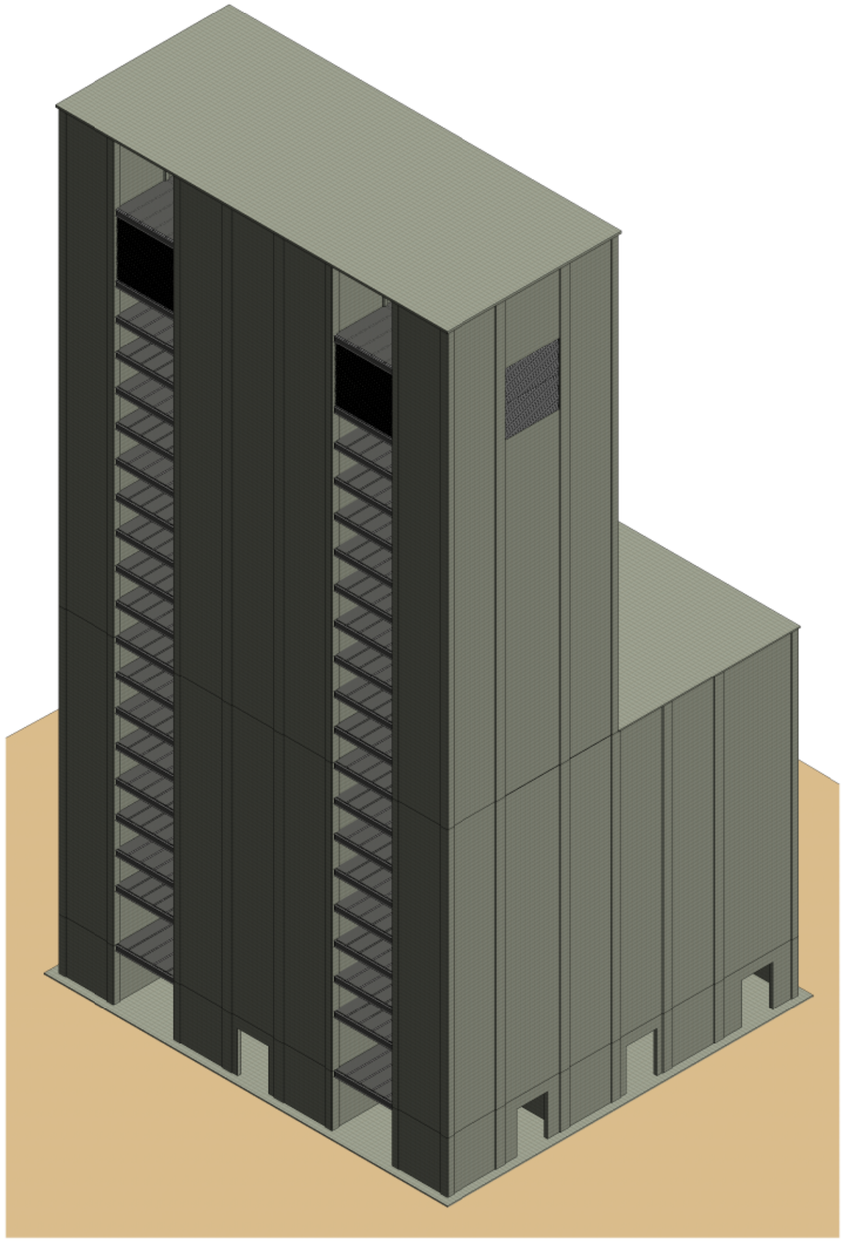

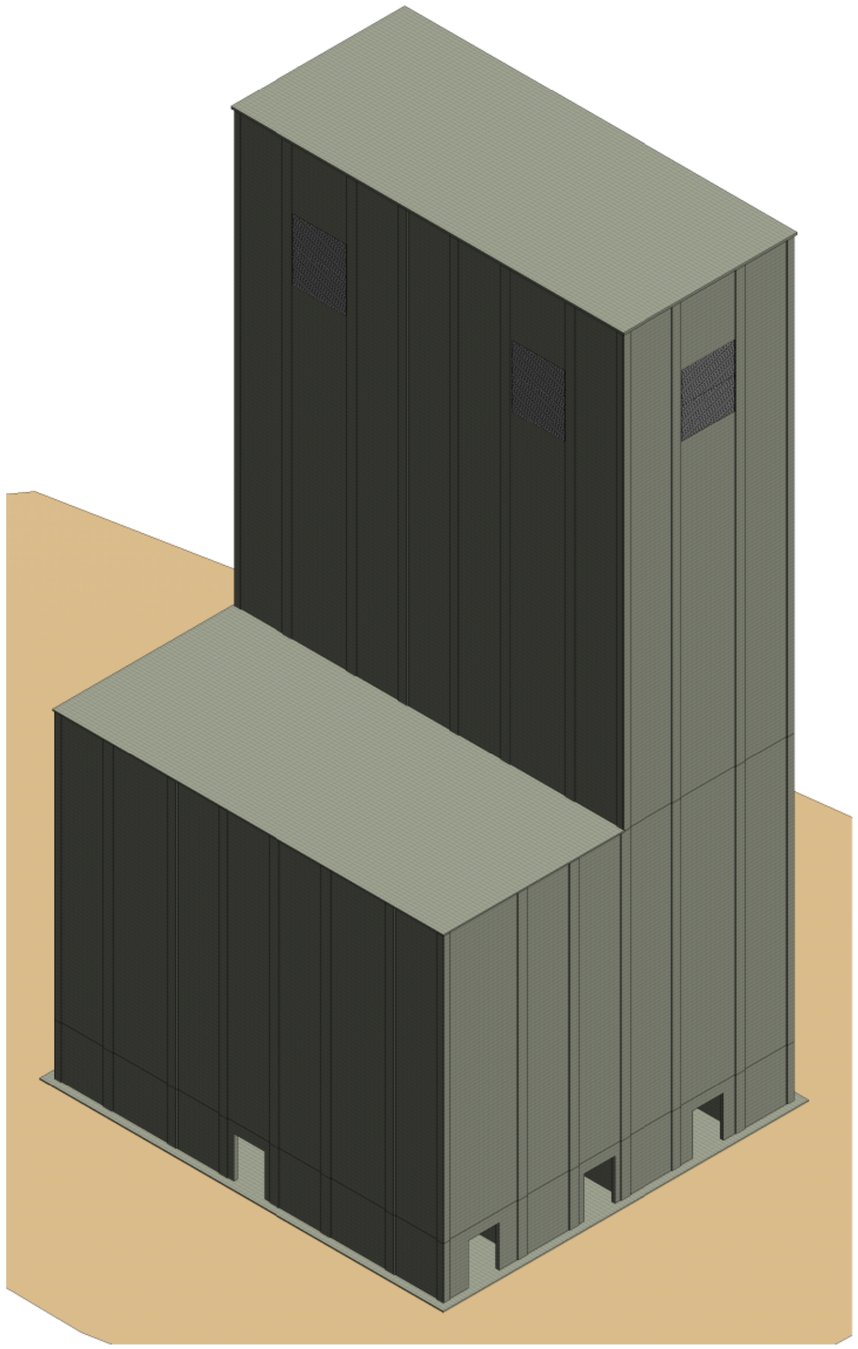

8 0 8 16 24

SCALE IN FEET

SCALE:

PLANT NORTH

N

-PRELIMINARY-
NOT FOR CONSTRUCTION

REV	DESIGN BY	DRAWN BY	CHECKED BY	DATE
A	S. DRAKE	M. KELLY	-	06/04/14
	ISSUED FOR APPROVAL			

AFFORDABILITY IGCC PROJECT, TEXAS, USA

INTEGRATED GASIFICATION COMBINED CYCLE
(IGCC)
SLIP FORMING AND MODULARIZATION

Kiewit

x:Kiewit Power Engineers, Co.
- North Carolina (KPE-NC)
9401 Renner Boulevard
Lenexa, Kansas 66219

GENERAL ARRANGEMENT

ENGINEER/DESIGN ORIGINATOR	S. DRAKE
LEAD ENG	-
ENG MGR	-
PROJ MGR	S. SUDDUTH

DRAWING NUMBER

2013-070-SF-008

C:\Users\matt.kelly\Documents\GE GASIFICATION_MattR.Kelly.rvt

Appendix G – Slip Form Erection/Assembly Sequence

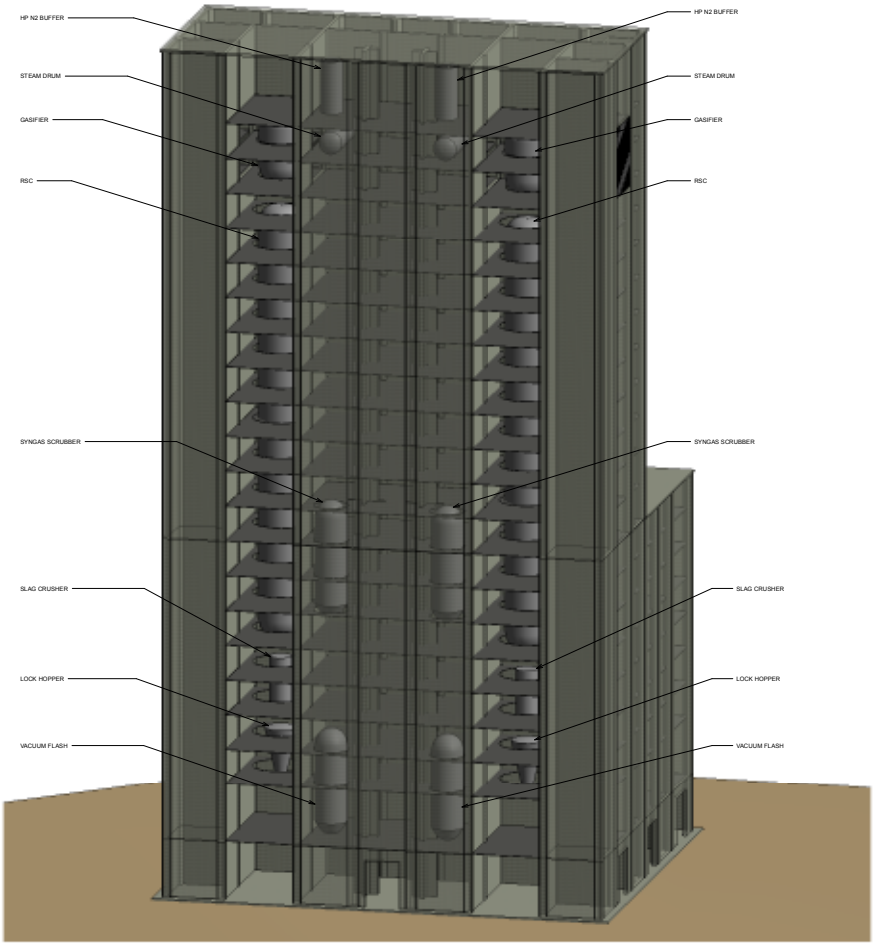

SLIP FORM WITH EQUIPMENT SHOWN

SCALE:

8 0 8 16 24
SCALE IN FEET

PLANT NORTH

-PRELIMINARY-
NOT FOR CONSTRUCTION

REV	DESIGN BY	DRAWN BY	CHECKED BY	DATE
A	ISSUED FOR APPROVAL			
	S. DRAKE	M. KELLY		06/04/14

AFFORDABILITY IGCC PROJECT, TEXAS, USA

INTEGRATED GASIFICATION COMBINED CYCLE
(IGCC)
SLIP FORMING AND MODULARIZATION

Kiewit

xKiewit Power Engineers, Co.
- North Carolina (KPE-NC)
9401 Renner Boulevard
Lenexa, Kansas 66219

GENERAL ARRANGEMENT

ENGINEER/DESIGN ORIGINATOR	S. DRAKE
LEAD ENG	
ENG MGR	
PROJ MGR	S. SUDDUTH

DRAWING NUMBER

2013-070-SF-009

C:\Users\mattr.kelly\Documents\GE GASIFICATION_MattR.Kelly\.rvt

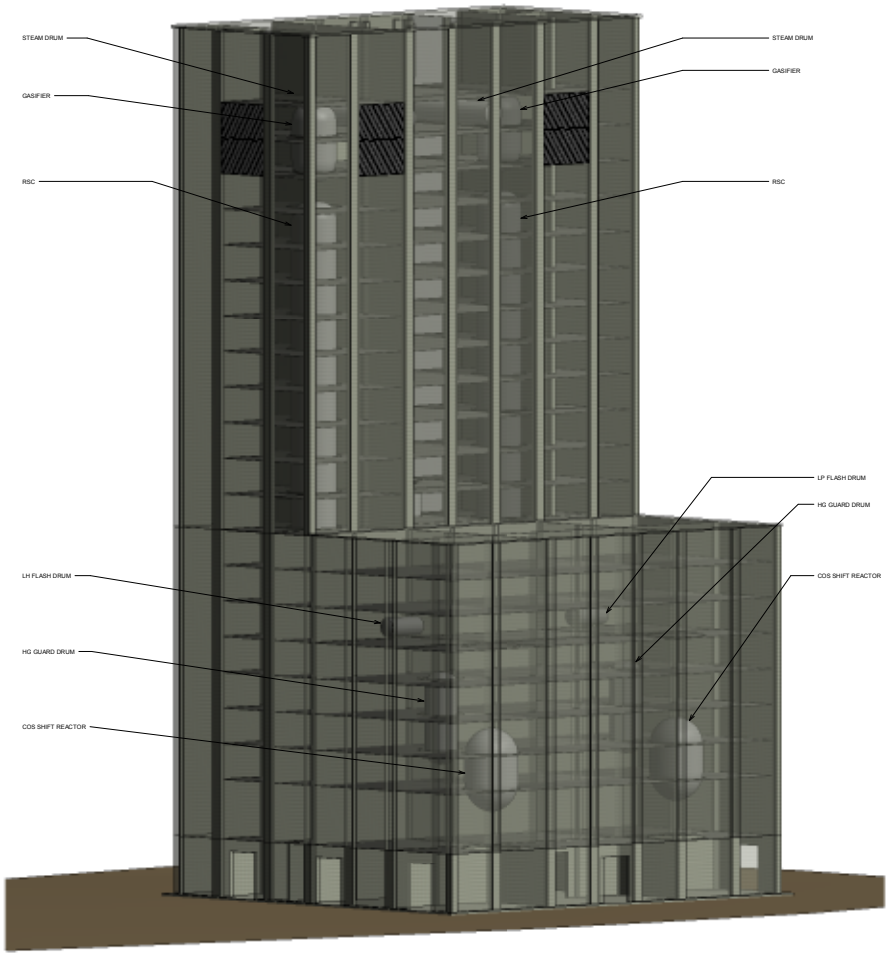

SLIP FORM WITH EQUIPMENT SHOWN

8 0 8 16 24
SCALE IN FEET

SCALE:

PLANT NORTH

-PRELIMINARY-
NOT FOR CONSTRUCTION

REV	DESIGN BY	DRAWN BY	CHECKED BY	DATE
A	ISSUED FOR APPROVAL			
	S. DRAKE	M. KELLY		06/04/14

AFFORDABILITY IGCC PROJECT, TEXAS, USA

INTEGRATED GASIFICATION COMBINED CYCLE
(IGCC)
SLIP FORMING AND MODULARIZATION

Kiewit

xKiewit Power Engineers, Co.
- North Carolina (KPE-NC)
9401 Renner Boulevard
Lenexa, Kansas 66219

GENERAL ARRANGEMENT

ENGINEER/DESIGN ORIGINATOR	S. DRAKE
LEAD ENG	
ENG MGR	
PROJ MGR	S. SUDDUTH

DRAWING NUMBER
2013-070-SF-010

C:\Users\mattr.kelly\Documents\GE GASIFICATION_MattR.Kelly.rvt

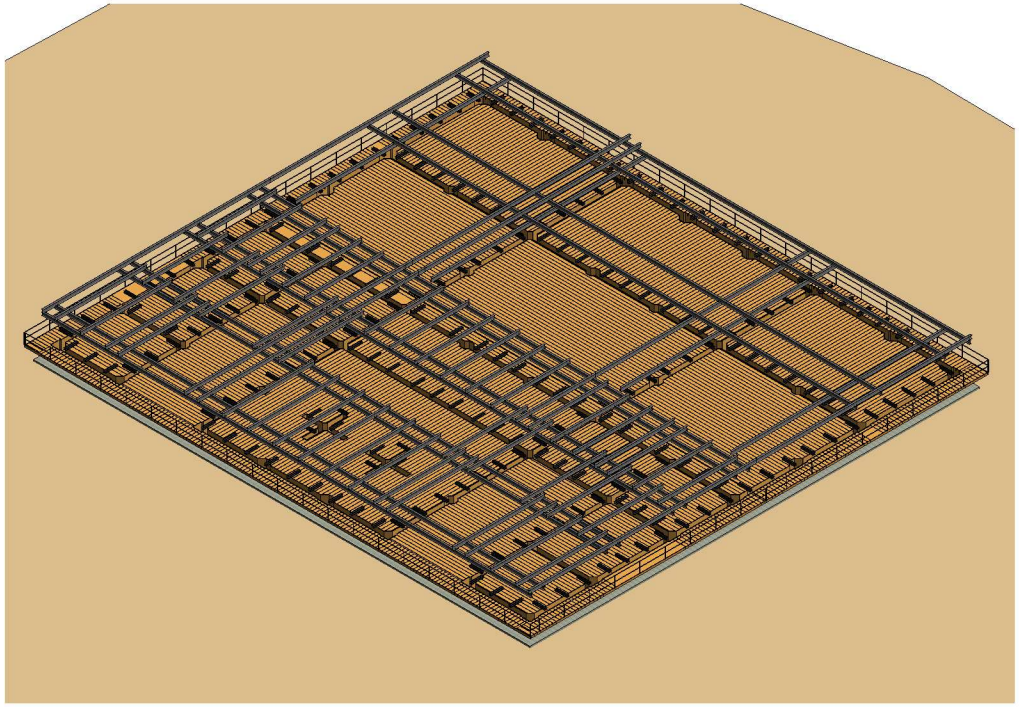

SLIP DECK AT GRADE/FOUNDATION

-PRELIMINARY-
NOT FOR CONSTRUCTION

REV	DESIGN BY	DRAWN BY	CHECKED BY	DATE
A	ISSUED FOR APPROVAL			
	S. DRAKE	M. KELLY		06/04/14

AFFORDABILITY IGCC PROJECT, TEXAS, USA

INTEGRATED GASIFICATION COMBINED CYCLE
(IGCC)
SLIP FORMING AND MODULARIZATION

Kiewit

xKiewit Power Engineers, Co.
- North Carolina (KPE-NC)
9401 Renner Boulevard
Lenexa, Kansas 66219

GENERAL ARRANGEMENT

ENGINEER/DESIGN	
ORIGINATOR	S. DRAKE
LEAD ENG	
ENG MGR	
PROJ MGR	S. SUDDUTH

DRAWING NUMBER

2013-070-SF-011

8 0 8 16 24
SCALE IN FEET
SCALE:

PLANT NORTH

N

C:\Users\mattr.kelly\Documents\GE GASIFICATION_MattR.Kelly.rvt

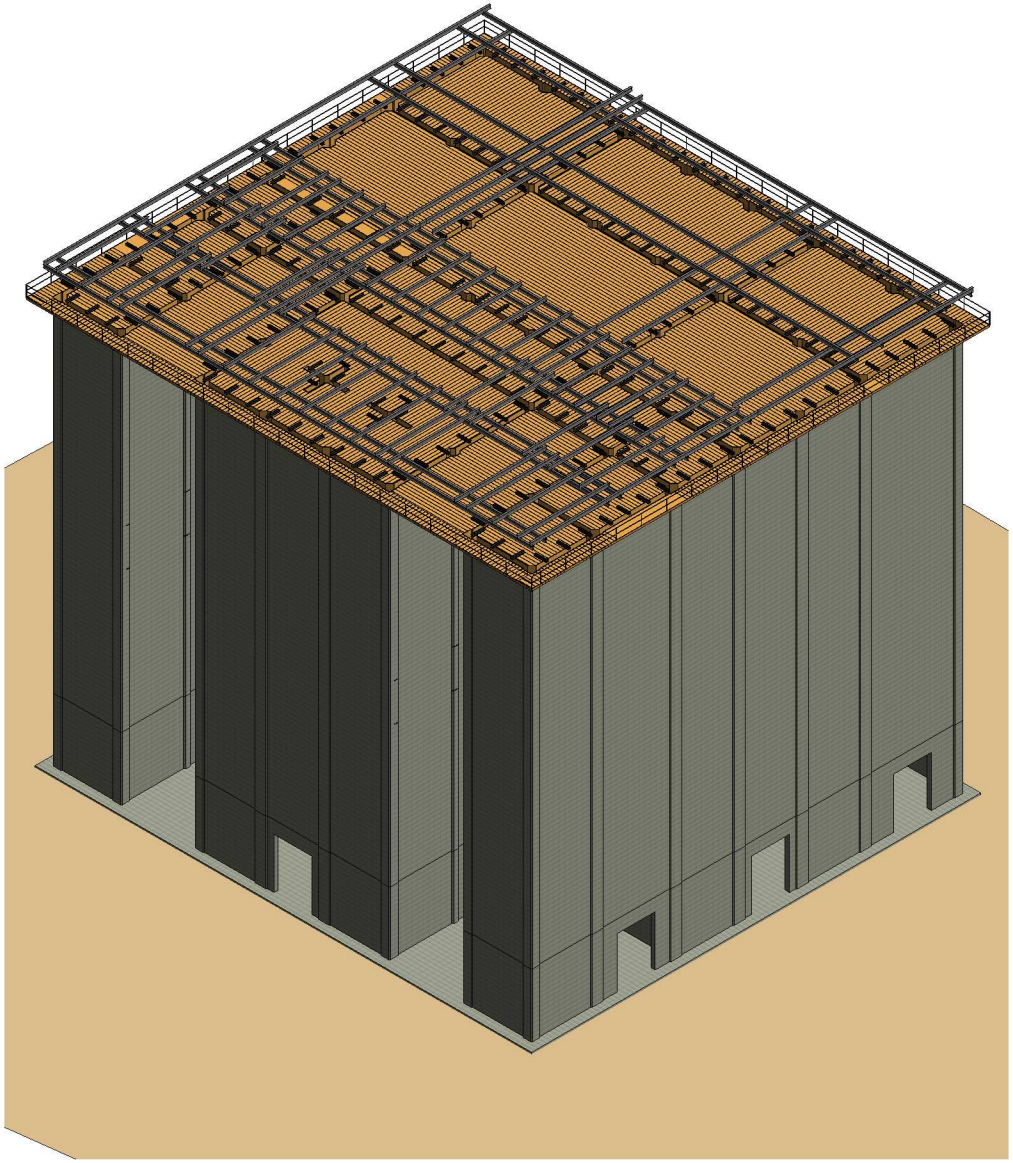

SLIP DECK AT ELEVATION 124'-0"

SCALE:

8 0 8 16 24
SCALE IN FEET

PLANT NORTH

-PRELIMINARY-
NOT FOR CONSTRUCTION

REV	DESIGN BY	DRAWN BY	CHECKED BY	DATE
A	ISSUED FOR APPROVAL			
	S. DRAKE	M. KELLY		06/04/14

AFFORDABILITY IGCC PROJECT, TEXAS, USA

INTEGRATED GASIFICATION COMBINED CYCLE
(IGCC)
SLIP FORMING AND MODULARIZATION

Kiewit

xKiewit Power Engineers, Co.
- North Carolina (KPE-NC)
9401 Renner Boulevard
Lenexa, Kansas 66219

GENERAL ARRANGEMENT

ENGINEER/DESIGN	
ORIGINATOR	S. DRAKE
LEAD ENG	
ENG MGR	
PROJ MGR	S. SUDDUTH

DRAWING NUMBER

2013-070-SF-012

C:\Users\matt.kelly\Documents\GE GASIFICATION_MattK (Kelly).rvt

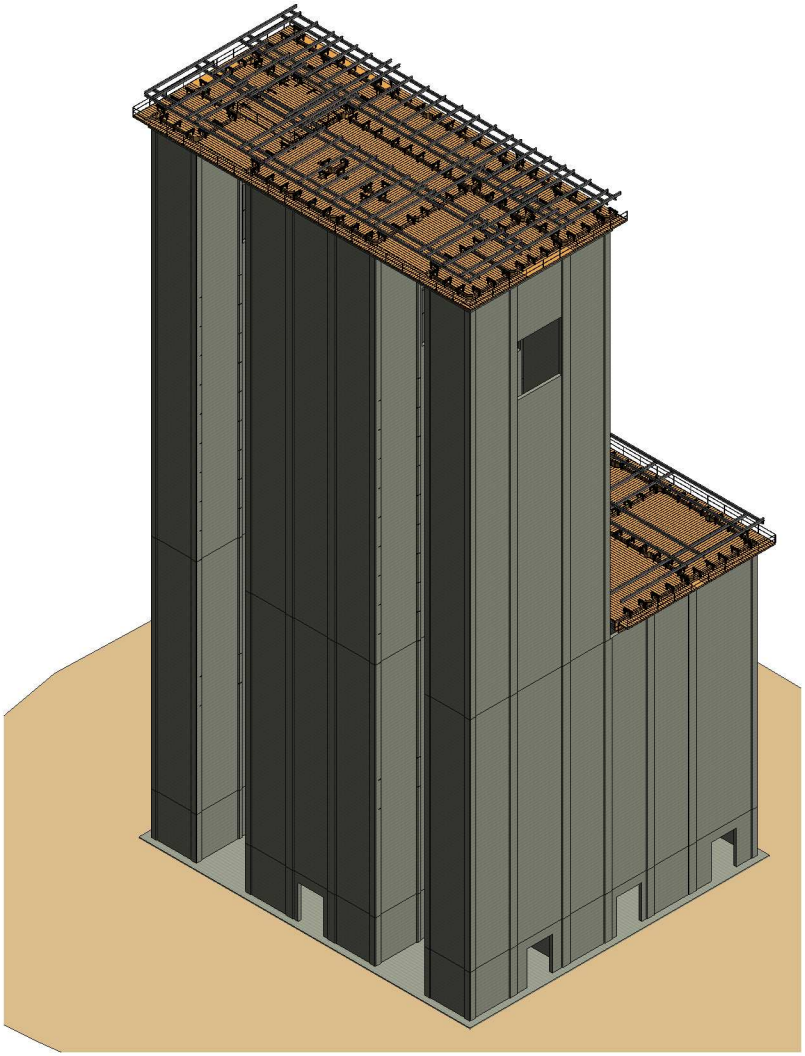

SLIP DECK AT ELEVATION 292'-0" PRIOR TO DISASSEMBLY OF DECK

-PRELIMINARY-
NOT FOR CONSTRUCTION

REV	DESIGN BY	DRAWN BY	CHECKED BY	DATE
A	ISSUED FOR APPROVAL			
	S. DRAKE	M. KELLY		06/04/14

AFFORDABILITY IGCC PROJECT, TEXAS, USA

INTEGRATED GASIFICATION COMBINED CYCLE
(IGCC)
SLIP FORMING AND MODULARIZATION

Kiewit

xKiewit Power Engineers, Co.
- North Carolina (KPE-NC)
9401 Renner Boulevard
Lenexa, Kansas 66219

GENERAL ARRANGEMENT

ENGINEER/DESIGN ORIGINATOR	S. DRAKE
LEAD ENG	
ENG MGR	
PROJ MGR	S. SUDDUTH

DRAWING NUMBER
2013-070-SF-013

8 0 8 16 24
SCALE IN FEET
SCALE:

PLANT NORTH

C:\Users\mattr.kelly\Documents\GE GASIFICATION_MattR.Kelly.rvt

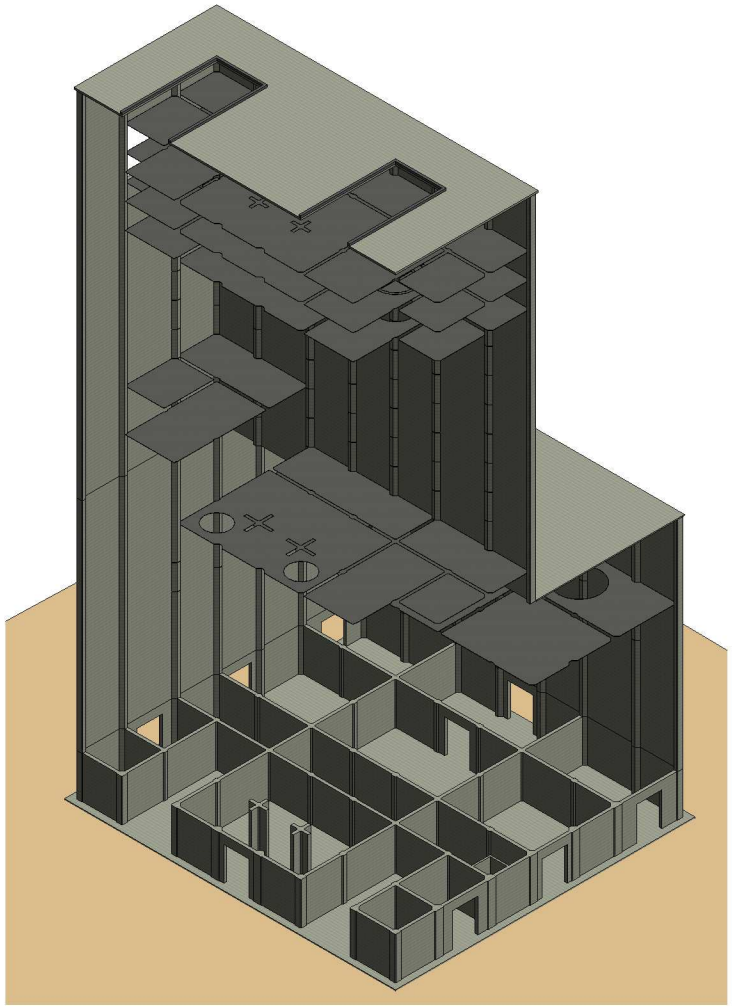

LIFTING FLOOR MODULES WITH STRAND JACKS

SCALE:

8 0 8 16 24
SCALE IN FEET

PLANT NORTH

-PRELIMINARY-
NOT FOR CONSTRUCTION

REV	DESIGN BY	DRAWN BY	CHECKED BY	DATE
A	ISSUED FOR APPROVAL			
	S. DRAKE	M. KELLY		06/04/14

AFFORDABILITY IGCC PROJECT, TEXAS, USA

INTEGRATED GASIFICATION COMBINED CYCLE
(IGCC)
SLIP FORMING AND MODULARIZATION

Kiewit

xKiewit Power Engineers, Co.
- North Carolina (KPE-NC)
9401 Renner Boulevard
Lenexa, Kansas 66219

GENERAL ARRANGEMENT

ENGINEER/DESIGN ORIGINATOR	S. DRAKE
LEAD ENG	
ENG MGR	
PROJ MGR	S. SUDDUTH

DRAWING NUMBER

2013-070-SF-014

C:\Users\matt.kelly\Documents\GE GASIFICATION_MattK.kdy.r.4

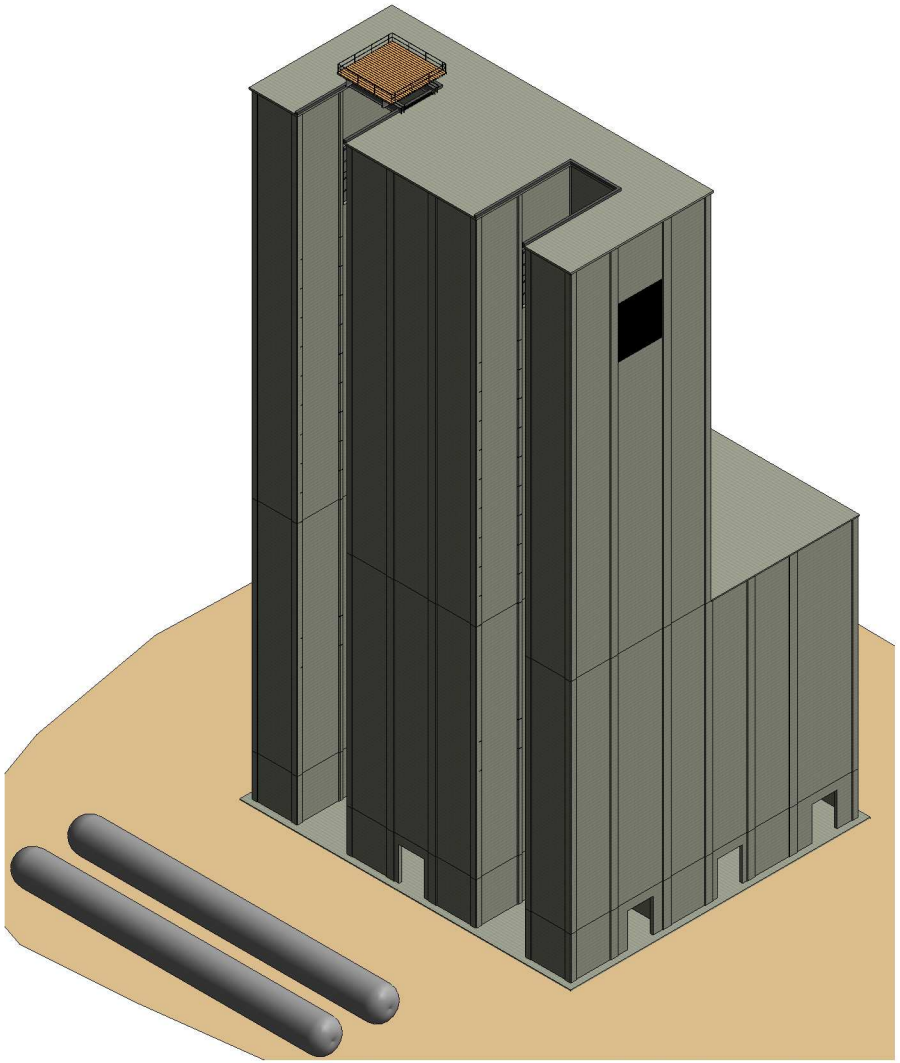

RSC ASSEMBLED ON GROUND

SCALE:

8 0 8 16 24
SCALE IN FEET

PLANT NORTH

-PRELIMINARY-
NOT FOR CONSTRUCTION

REV	DESIGN BY	DRAWN BY	CHECKED BY	DATE
A	ISSUED FOR APPROVAL			
	S. DRAKE	M. KELLY		06/04/14

AFFORDABILITY IGCC PROJECT, TEXAS, USA

INTEGRATED GASIFICATION COMBINED CYCLE
(IGCC)
SLIP FORMING AND MODULARIZATION

Kiewit

xKiewit Power Engineers, Co.
- North Carolina (KPE-NC)
9401 Renner Boulevard
Lenexa, Kansas 66219

GENERAL ARRANGEMENT

ENGINEER/DESIGN ORIGINATOR	S. DRAKE
LEAD ENG	
ENG MGR	
PROJ MGR	S. SUDDUTH

DRAWING NUMBER

2013-070-SF-015

C:\Users\mattr.kelly\Documents\GE GASIFICATION_MattR.Kelly.rvt

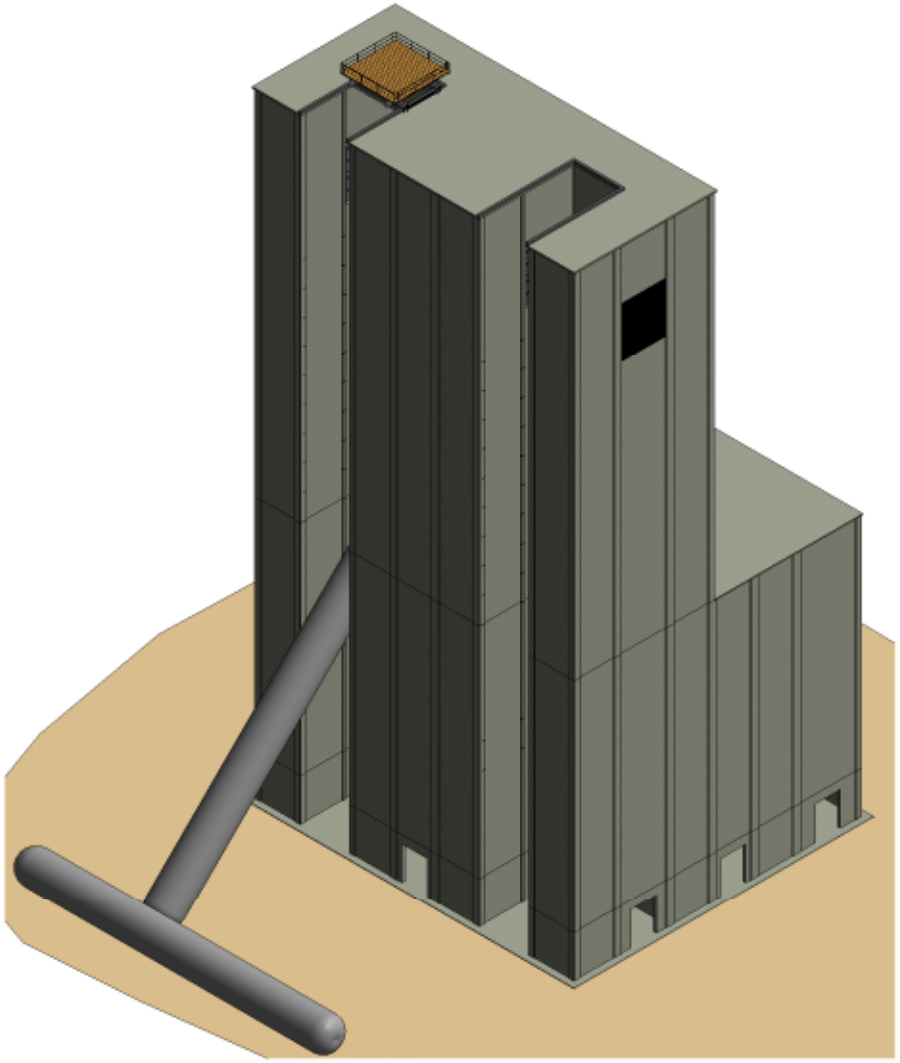

RSC TILTED/LIFTED TO VERTICAL POSITION

SCALE:

8 0 8 16 24
SCALE IN FEET

PLANT NORTH

-PRELIMINARY-
NOT FOR CONSTRUCTION

REV	DESIGN BY	DRAWN BY	CHECKED BY	DATE
A	ISSUED FOR APPROVAL			
	S. DRAKE	M. KELLY		06/04/14

AFFORDABILITY IGCC PROJECT, TEXAS, USA

INTEGRATED GASIFICATION COMBINED CYCLE
(IGCC)
SLIP FORMING AND MODULARIZATION

Kiewit

xKiewit Power Engineers, Co.
- North Carolina (KPE-NC)
9401 Renner Boulevard
Lenexa, Kansas 66219

GENERAL ARRANGEMENT

ENGINEER/DESIGN ORIGINATOR	S. DRAKE
LEAD ENG	
ENG MGR	
PROJ MGR	S. SUDDUTH

DRAWING NUMBER

2013-070-SF-016

C:\Users\mattr.kelly\Documents\GE GASIFICATION_MattR.Kelly.rvt

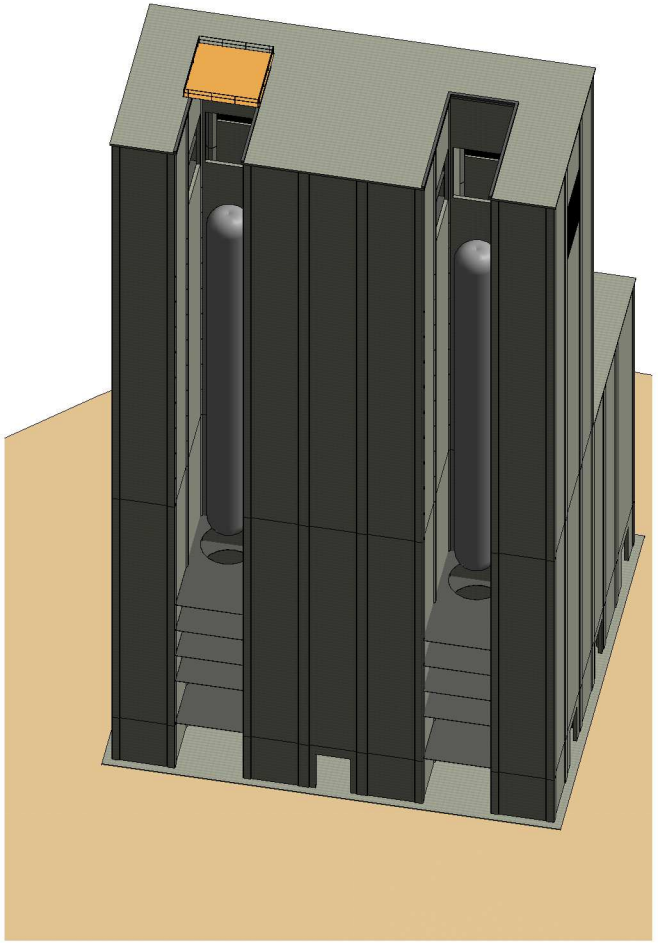

RSC IN FINAL POSITION

SCALE:

8 0 8 16 24
SCALE IN FEET

PLANT NORTH

-PRELIMINARY-
NOT FOR CONSTRUCTION

REV	DESIGN BY	DRAWN BY	CHECKED BY	DATE
A	ISSUED FOR APPROVAL			
	S. DRAKE	M. KELLY		06/04/14

AFFORDABILITY IGCC PROJECT, TEXAS, USA

INTEGRATED GASIFICATION COMBINED CYCLE
(IGCC)
SLIP FORMING AND MODULARIZATION

Kiewit

xKiewit Power Engineers, Co.
- North Carolina (KPE-NC)
9401 Renner Boulevard
Lenexa, Kansas 66219

GENERAL ARRANGEMENT

ENGINEER/DESIGN ORIGINATOR	S. DRAKE
LEAD ENG	
ENG MGR	
PROJ MGR	S. SUDDUTH

DRAWING NUMBER

2013-070-SF-017

C:\Users\mattr.kelly\Documents\GE GASIFICATION_MattR.Kelly.rvt

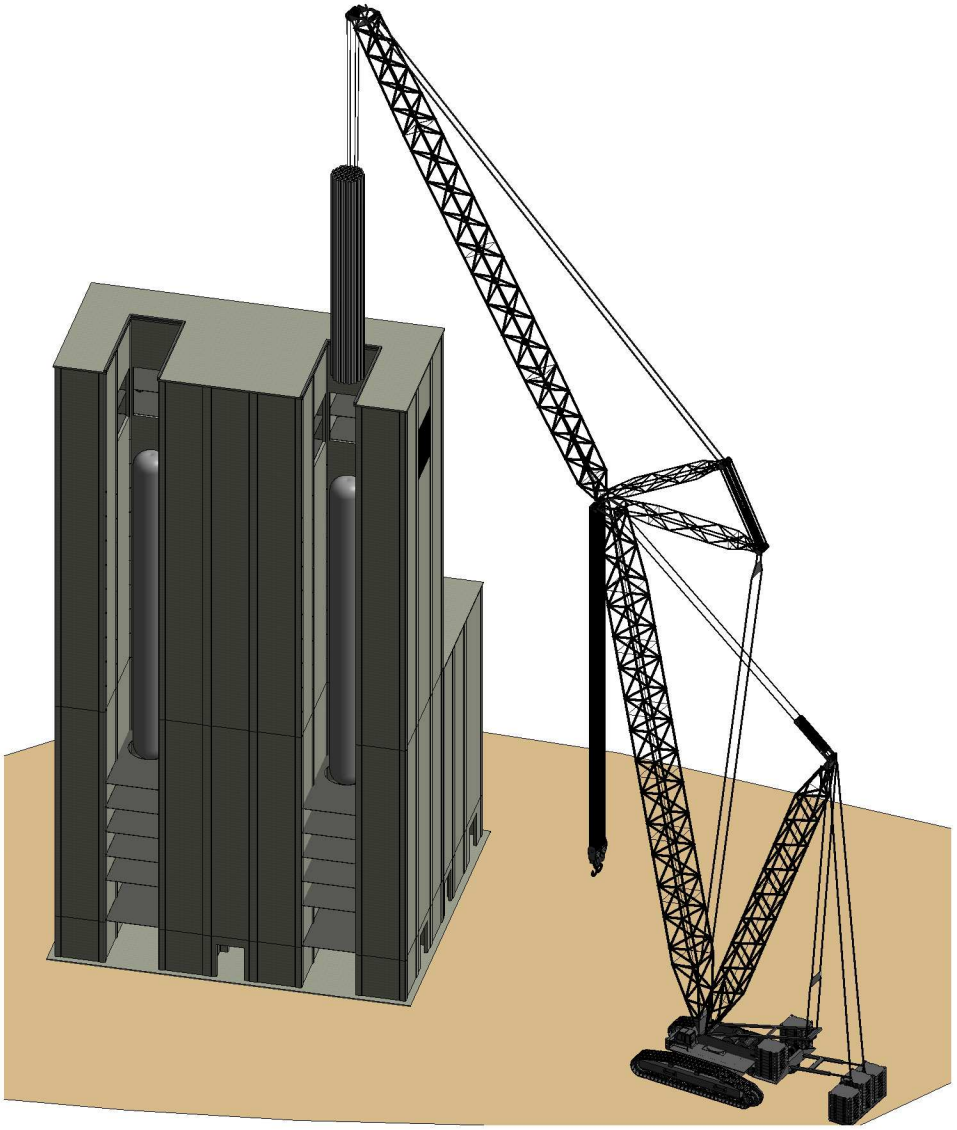

INSTALLATION OF RSC INTERNALS

SCALE:

8 0 8 16 24
SCALE IN FEET

PLANT NORTH

-PRELIMINARY-
NOT FOR CONSTRUCTION

REV	DESIGN BY	DRAWN BY	CHECKED BY	DATE
A	ISSUED FOR APPROVAL			
	S. DRAKE	M. KELLY		06/04/14

AFFORDABILITY IGCC PROJECT, TEXAS, USA

INTEGRATED GASIFICATION COMBINED CYCLE
(IGCC)
SLIP FORMING AND MODULARIZATION

Kiewit

xKiewit Power Engineers, Co.
- North Carolina (KPE-NC)
9401 Renner Boulevard
Lenexa, Kansas 66219

GENERAL ARRANGEMENT

ENGINEER/DESIGN ORIGINATOR	S. DRAKE
LEAD ENG	
ENG MGR	
PROJ MGR	S. SUDDUTH

DRAWING NUMBER

2013-070-SF-018

C:\Users\matt.kelly\Documents\GE GASIFICATION_MattK (Kelly).rvt

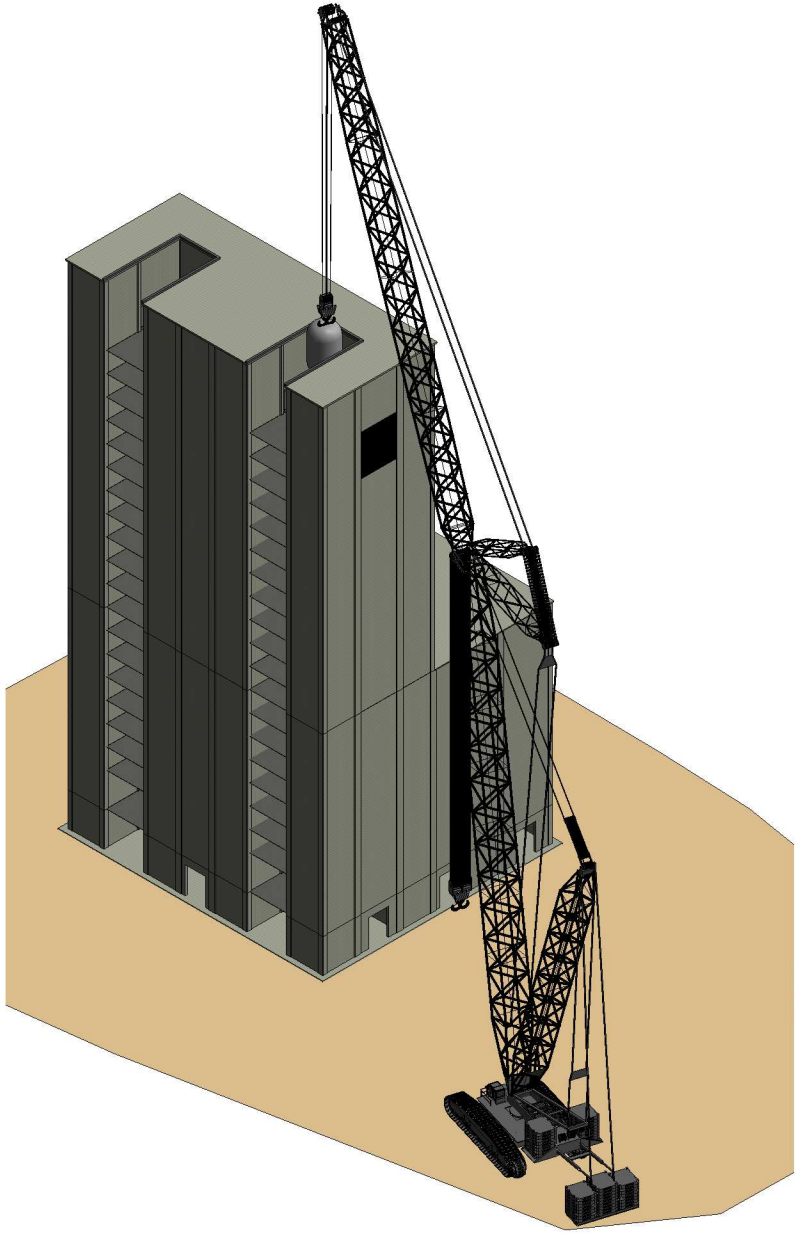

INSTALLATION OF GASIFIER

SCALE:

8 0 8 16 24
SCALE IN FEET

PLANT NORTH

-PRELIMINARY-
NOT FOR CONSTRUCTION

REV	DESIGN BY	DRAWN BY	CHECKED BY	DATE
A	ISSUED FOR APPROVAL			
	S. DRAKE	M. KELLY		06/04/14

AFFORDABILITY IGCC PROJECT, TEXAS, USA

INTEGRATED GASIFICATION COMBINED CYCLE
(IGCC)
SLIP FORMING AND MODULARIZATION

Kiewit

xKiewit Power Engineers, Co.
- North Carolina (KPE-NC)
9401 Renner Boulevard
Lenexa, Kansas 66219

GENERAL ARRANGEMENT

ENGINEER/DESIGN ORIGINATOR	S. DRAKE
LEAD ENG	
ENG MGR	
PROJ MGR	S. SUDDUTH

DRAWING NUMBER

2013-070-SF-019

C:\Users\mattr.kelly\Documents\GE GASIFICATION_MattR.Kelly.rvt

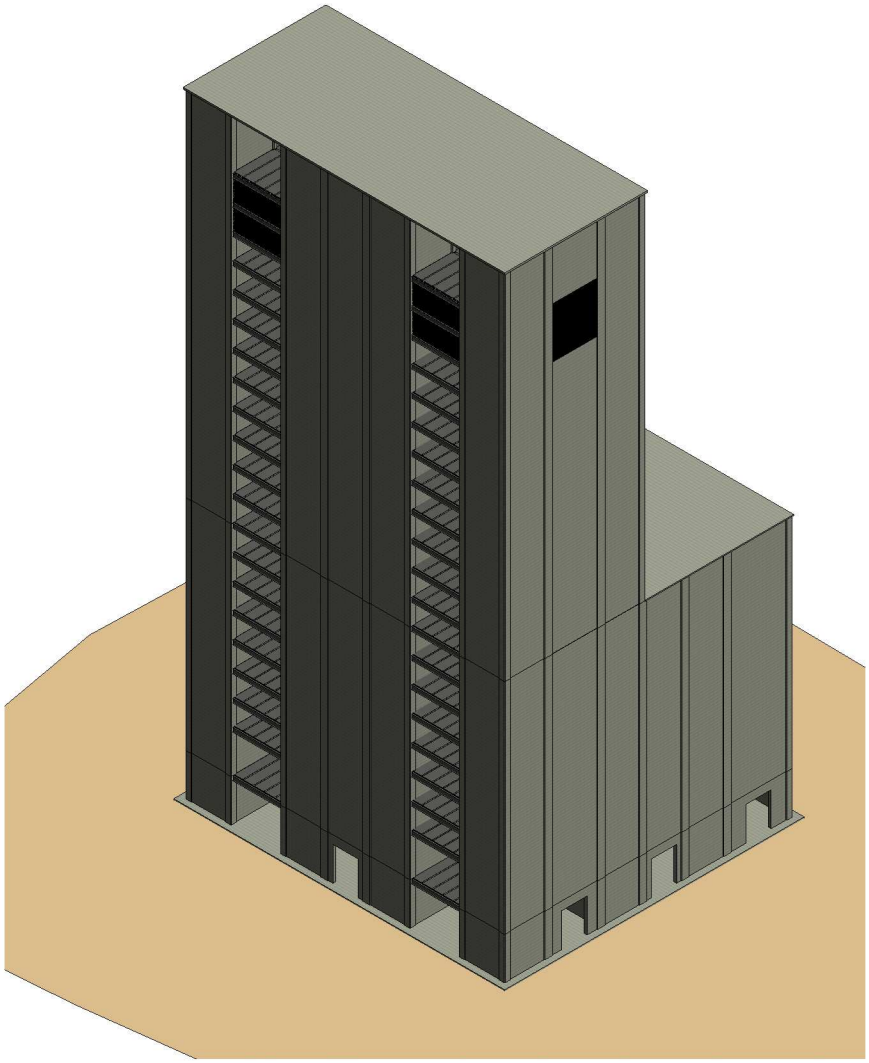

SLIP FORM STRUCTURE IN FINAL CONDITION

SCALE: 8 0 8 16 24 SCALE IN FEET

PLANT NORTH

-PRELIMINARY-
NOT FOR CONSTRUCTION

REV	DESIGN BY	DRAWN BY	CHECKED BY	DATE
A	ISSUED FOR APPROVAL			
	S. DRAKE	M. KELLY		06/04/14

AFFORDABILITY IGCC PROJECT, TEXAS, USA

INTEGRATED GASIFICATION COMBINED CYCLE
(IGCC)
SLIP FORMING AND MODULARIZATION

Kiewit

xKiewit Power Engineers, Co.
- North Carolina (KPE-NC)
9401 Renner Boulevard
Lenexa, Kansas 66219

GENERAL ARRANGEMENT

ENGINEER/DESIGN ORIGINATOR	S. DRAKE
LEAD ENG	
ENG MGR	
PROJ MGR	S. SUDDUTH

DRAWING NUMBER

2013-070-SF-020

C:\Users\matt.kelly\Documents\GE GASIFICATION_MattK.kelly.rvt

Appendix H – Coal Silos

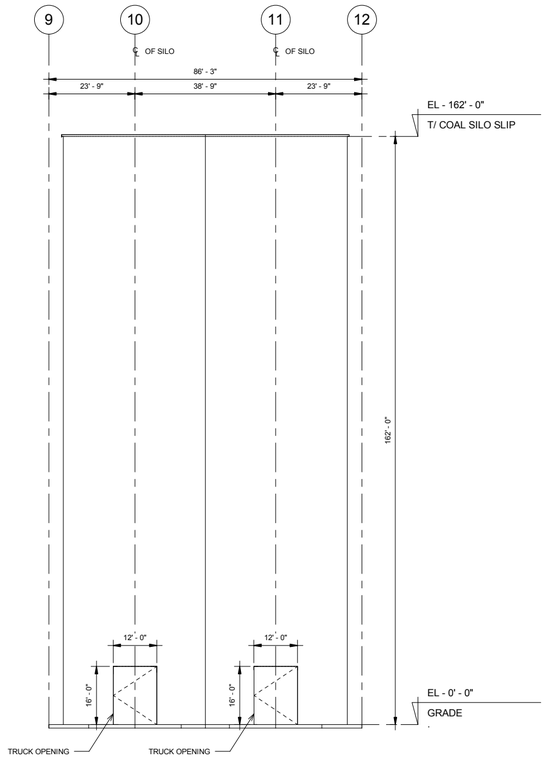

ELEVATION - COAL SILOS

1/16" = 1' - 0"

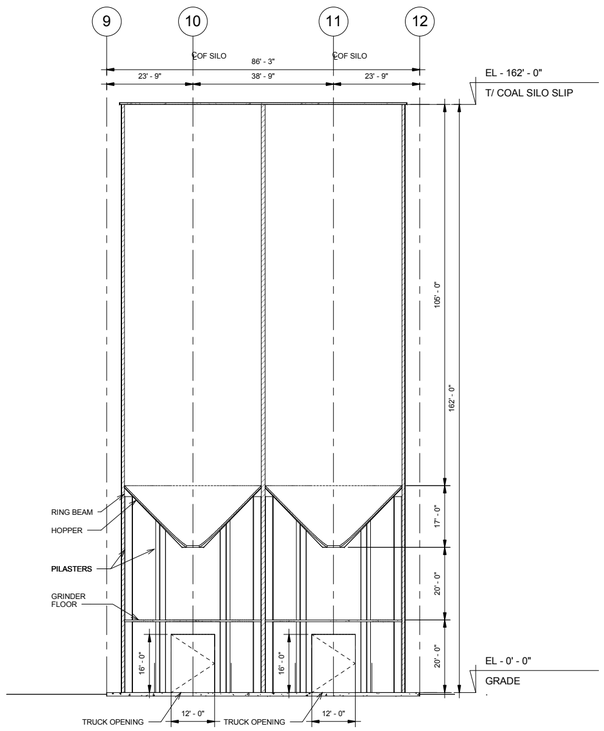

SECTION - COAL SILOS

1/16" = 1' - 0"

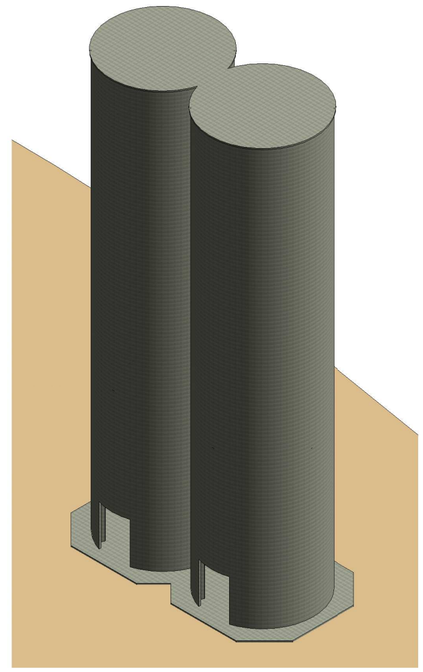

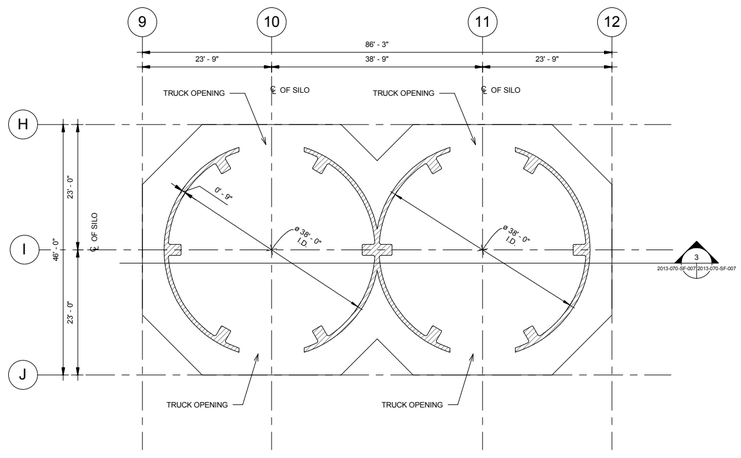

PLAN - COAL SILOS AT GRADE

1/16" = 1' - 0"

-PRELIMINARY-
NOT FOR CONSTRUCTION

REV	DESIGN BY	DRAWN BY	CHECKED BY	DATE
A	ISSUED FOR APPROVAL			
	S. DRAKE	M. KELLY	-	06/04/14

AFFORDABILITY IGCC PROJECT, TEXAS, USA

INTEGRATED GASIFICATION COMBINED CYCLE
(IGCC)
SLIP FORMING AND MODULARIZATION

Kiewit

x:Kiewit Power Engineers, Co.
- North Carolina (KPE-NC)
9401 Renner Boulevard
Lenexa, Kansas 66219

GENERAL ARRANGEMENT

ENGINEER/DESIGN ORIGINATOR	S. DRAKE
LEAD ENG	-
ENG MGR	-
PROJ MGR	S. SUDDUTH

DRAWING NUMBER

2013-070-SF-007

8 0 8 16 24
SCALE IN FEET

SCALE: As indicated

PLANT NORTH

C:\Users\matt.kelly\Documents\GE GASIFICATION_MattRKelly.rvt

Appendix I – Cost Estimate Spreadsheet

		Owner	Stick-Built Option	Slipform Option	
		Project	GE Feasibility Study	GE Feasibility Study	
		Location	Gulf Coast, TX	Gulf Coast, TX	
		Technology	GE IGCC	GE IGCC	
		Estimate Typ			Notes
Project Information			*Indicative Estimate*	*Indicative Estimate*	
		COD			
		Total Direct ManHours	1,423,902	1,344,818	
		Mech/Elec ManHours	1,005,497	937,550	
		Indirect Manhours	436,321	418,776	
		Labor Type	Non-Union	Non-Union	
Structural Exc./Backfill (Direct)		Labor $	$ 329,056	$ 329,056	
		STS & Const. Equip $	$ 578,579	$ 578,580	
		PM & Sub $	$ 120,330	$ 120,324	
		Subtotal $	**$ 1,027,965**	**$ 1,027,960**	
		ManHours	**7,859**	**7,859**	
		Exc. & BF (CY)	27,100	27,100	
		Total $/CY Ex & BF	$ 37.93	$ 37.93	
Mech/Elec Support (Direct)		Labor $	$ 91,067	$ 91,067	
		STS & Const. Equip. $	$ 160,124	$ 160,124	
		PM & Sub $	$ 33,300	$ 33,300	
		Subtotal $	**$ 284,491**	**$ 284,491**	
		ManHours	**2,175**	**2,175**	
		Exc. & BF (CY)	7,500	7,500	
		Total $/CY	$ 37.93	$ 37.93	
Sitework (Direct)		Labor $	$ 55,478	$ 55,478	
		STS & Const. Equip. $	$ 97,547	$ 97,547	
		PM & Sub $	$ 23,532	$ 23,532	
		Subtotal $	**$ 176,556**	**$ 176,556**	
		ManHours	**1,325**	**1,325**	
		Mass Exc. & BF (CY)	5,300	5,300	
		Total $/CY	$ 33.31	$ 33.31	
Summary Section Sitework Mech/Elec Structural -Exc./Backfill		Labor $	$ 475,601	$ 475,601	
		STS & Const. Equip. $	$ 836,249	$ 836,250	
		PM & Sub $	$ 177,162	$ 177,156	
		Item Subtotal $	**$ 1,489,012**	**$ 1,489,007**	
		ManHours	**11,359**	**11,359**	
		Mass Exc. & BF (CY)	39,900	39,900	
		Total $/CY	$ 37.32	$ 37.32	
Deep Foundations - Piling (Direct)		Labor $	$ 42,813	$ 42,813	
		STS & Const. Equip. $	$ 5,120	$ 5,120	
		PM & Sub $	$ 3,584,000	$ 3,584,000	
		Item Subtotal $	**$ 3,631,933**	**$ 3,631,933**	
		ManHours	**1,024**	**1,024**	
		Qty. Piles (EA)	1,024	1,024	
		Total $/Pile	$ 3,547	$ 3,547	
Foundation Concrete (Direct)		Labor $	$ 828,446	$ 828,446	
		STS $	$ 243,840	$ 243,840	
		PM & Sub $	$ 2,001,300	$ 2,001,300	
		Item Subtotal $	**$ 3,073,586**	**$ 3,073,586**	
		ManHours	**20,320**	**20,320**	
		Concrete (CY)	5,700	5,700	
		Total $/CY	$ 539.23	$ 539.23	
Slipform Concrete (Direct)		Labor $		$ 4,480,827	
		STS $		$ 3,526,476	
		PM & Sub $		$ 28,054,787	
		Item Subtotal $		**$ 36,062,090**	
		ManHours		**109,905**	
		Concrete (CY)		18,211	
		Total $/CY		$ 1,980.24	
Strucutural Steel/Misc. Metals (Direct)		Labor $	$ 8,031,717	$ 3,009,685	
		STS $	$ 967,908	$ 362,702	
		PM & Sub $	$ 29,734,443	$ 9,722,625	
		Item Subtotal $	**$ 38,734,068**	**$ 13,095,012**	
		ManHours	**193,582**	**72,540**	
		Tons	8,384	3,733	
		Total $/Ton	$ 4,620.00	$ 3,507.91	

		Owner	Stick-Built Option	Slipform Option	
		Project	GE Feasibility Study	GE Feasibility Study	
		Location	Gulf Coast, TX	Gulf Coast, TX	
		Technology	GE IGCC	GE IGCC	
		Estimate Typ			Notes
Project Information			*Indicative Estimate*	*Indicative Estimate*	
		COD			
		Total Direct ManHours	1,423,902	1,344,818	
		Mech/Elec ManHours	1,005,497	937,550	
		Indirect Manhours	436,321	418,776	
		Labor Type	Non-Union	Non-Union	
Piping & Insulation * (Direct)		Labor $	$ 23,978,034	$ 22,299,571	
		STS $	$ 3,838,240	$ 3,569,563	
		PM & Sub $	$ 37,250,000	$ 37,250,000	
		Item Subtotal $	**$ 65,066,274**	**$ 63,119,134**	
		ManHours	**548,320**	**509,938**	
		LF Pipe	149,000	149,000	
		Total $/LF	$ 436.69	$ 423.62	
Mechanical Equipment * (Direct)		Labor $	$ 6,472,500	$ 6,019,425	
		STS $	$ 1,800,000	$ 1,800,000	
		PM & Sub $	$ 6,000,000	$ 6,000,000	
		Item Subtotal $	**$ 14,272,500**	**$ 13,819,425**	
		ManHours	**150,000**	**139,500**	
		Qty	300	300	
		STS $/MHr	$ 12.00	$ 12.90	
Startup & Performance Testing * (Direct)		Craft Labor $	$ 1,016,972	$ 1,016,972	
		STS $	$ 772,535	$ 772,535	
		PM & Sub $	$ 7,732,851	$ 7,732,851	
		Staff Labor $			
		Item Subtotal $	**$ 9,522,358**	**$ 9,522,358**	
		Staff & Craft ManHours	**24,877**	**24,877**	
		Craft Support ManHours Only	**24,877**	**24,877**	
Electrical * (Direct)		Labor $	$ 10,644,975	$ 9,899,827	
		STS $	$ 1,485,000	$ 1,381,050	
		PM & Sub $	$ 10,725,000	$ 10,725,000	
		Item Subtotal $	**$ 22,854,975**	**$ 22,005,877**	
		ManHours	**247,500**	**230,175**	
		LF Cable	1,650,000	1,650,000	
		LF UG Conduit			
Instrumentation * (Direct)		Labor $	$ 1,659,612	$ 1,576,631	
		STS $	$ 208,800	$ 208,800	
		PM & Sub $	$ 377,000	$ 377,000	
		Item Subtotal $	**$ 2,245,412**	**$ 2,162,431**	
		ManHours	**34,800**	**33,060**	
		Qty Instr. (EA)	2,900	2,900	
		Total $/Qty	$ 774.28	$ 745.67	
Building Subcontracts (Direct)		Labor $	$ -	$ -	
		STS $			
		PM & Sub $	$ 1,200,000		
		Item Subtotal $	**$ 1,200,000**	**$ -**	
		ManHours			
Painting * (Direct)		Labor $	$ -	$ -	
		STS $			
		PM & Sub $	$ 3,500,000	$ 2,000,000	
		Item Subtotal $	**$ 3,500,000**	**$ 2,000,000**	
		ManHours			
Construction Equipment (Direct)		Labor $			
		STS & Const. Equip. $	$ 27,903,345	$ 21,163,123	
		PM & Sub $			
		Item Subtotal $	**$ 27,903,345**	**$ 21,163,123**	
		Job Total Mhrs	1,860,223	1,763,594	
		Const. Equip $/Job Total MHrs	$ 15.00	$ 12.00	

		Owner	Stick-Built Option	Slipform Option	
		Project	GE Feasibility Study	GE Feasibility Study	
		Location	Gulf Coast, TX	Gulf Coast, TX	
		Technology	GE IGCC	GE IGCC	
		Estimate Typ			Notes
Project Information			*Indicative Estimate*	*Indicative Estimate*	
		COD			
		Total Direct ManHours	1,423,902	1,344,818	
		Mech/Elec ManHours	1,005,497	937,550	
		Indirect Manhours	436,321	418,776	
		Labor Type	Non-Union	Non-Union	
Job Related Overhead (Indirect)		Labor $	$ 21,860,865	$ 20,720,440	
		Co. Rent & STS $	$ 11,550,000	$ 11,550,000	
		PM & Sub $			
		Item Subtotal $	**$ 33,410,865**	**$ 32,270,440**	
		JRO ManHours	**336,321**	**318,776**	
		Total Direct MHr	1,423,902	1,344,818	
Laydown * (Direct)		Labor $	$ -	$ -	
		STS $			
		PM & Sub $	$ 1,000,000	$ 1,000,000	
		Item Subtotal $	**$ 1,000,000**	**$ 1,000,000**	
		ManHours			
Temp Power (Direct)		Labor $	$ 1,215,893	$ 1,215,893	
		STS $	$ 1,200,000	$ 1,200,000	
		PM & Sub $			
		Item Subtotal $	**$ 2,415,893**	**$ 2,415,893**	
		ManHours	**28,270**	**28,270**	
Scaffold (Direct)		Labor $	$ 5,288,460	$ 5,288,460	
		STS $	$ 835,020	$ 835,020	
		PM & Sub $			
		Item Subtotal $	**$ 6,123,480**	**$ 6,123,480**	
		ManHours	**139,170**	**139,170**	
Operational Support (Indirect)		Labor $	$ 8,790,000	$ 8,790,000	
		Co. Rent & STS $	$ 19,165,721	$ 18,101,245	
		PM & Sub $	$ 2,847,804	$ 2,689,635	
		Item Subtotal $	**$ 30,803,525**	**$ 29,580,880**	
		Overhead Staff ManHours	**100,000**	**100,000**	
		Overhead Craft ManHours	**45,000**	**45,000**	
		Total Direct MHr	1,423,902	1,344,818	
Summary Section		Labor $	$ 15,294,353	$ 15,294,353	
		Co. Rent & STS $	$ 21,200,741	$ 20,136,265	
Laydown		PM & Sub $	$ 3,847,804	$ 3,689,635	
Temp Power		**Item Subtotal $**	**$ 40,342,898**	**$ 39,120,253**	
Scaffold		**Overhead Staff ManHours**	**100,000**	**100,000**	
Escalation		**Overhead Craft ManHours**	**212,440**	**212,440**	
Op Support		Total Direct MHr	1,423,902	1,344,818	
Commercial Cost		STS $	$ 1,000,000	$ 1,000,000	
		Item Subtotal $	**$ 1,000,000**	**$ 1,000,000**	
Speadsheet Check	Subtotal Direct Labor $		$ 58,826,577	$ 56,154,151	
	Subtotal Equipment/STS $		$ 39,852,217	$ 35,904,479	
OK	Subtotal Direct PM/Subs $		$ 101,280,456	$ 108,624,719	
	Subtotal Direct $		$ 199,959,250	$ 200,683,349	
	Subtotal Direct MHr		1,423,902	1,344,818	

		Owner	Stick-Built Option	Slipform Option	
		Project	GE Feasibility Study	GE Feasibility Study	
		Location	Gulf Coast, TX	Gulf Coast, TX	
		Technology	GE IGCC	GE IGCC	
		Estimate Typ			Notes
Project Information			*Indicative Estimate*	*Indicative Estimate*	
		COD			
		Total Direct ManHours	1,423,902	1,344,818	
		Mech/Elec ManHours	1,005,497	937,550	
		Indirect Manhours	436,321	418,776	
		Labor Type	Non-Union	Non-Union	
Estimate Summary Margin/Risk Analysis	Subtotal Indirect $		$ 65,214,390	$ 62,851,320	
	Subtotal Indirect $ w/ Overhead		$ 91,731,754	$ 89,204,787	
	Subtotal Indirect MHr		436,321	418,776	
	Subtotal Indirect Labor $		$ 30,650,865	$ 29,510,440	
	Grand Total Cost $		**$ 265,173,640**	**$ 263,534,670**	
	Grand Total MH		**1,860,223**	**1,763,594**	
	Grand Total Comparable Cost		$ 265,173,640	$ 263,534,670	
	Grand Total Comparable MHr		1,860,223	1,763,594	
	Corporate Overhead / Contingency (%)		10.000%	10.000%	
	Corporate Overhead / Contingency		$ 26,517,364	$ 26,353,467	
	Grand Total Cost		**$ 291,691,004**	**$ 289,888,137**	
	Project Margin		10.00%	10.00%	
	Total Margin $		$ 29,169,100	$ 28,988,814	
	Grand Total Contract Value		**$ 320,860,104**	**$ 318,876,950**	

*** Indicates a plug quantity based on historical design & experience**

Estimate Legend	
Item	**Description**
STS	Small tools & services
Const. Equip.	Construction equipment
PM	Permanent Materials
Sub	Subcontract
Ex	Excavation
BF	Backfill
Mech/Elec	Mechanical/Electrical excavation & backfill
MHr	Manhour
UG	Underground
Instr.	Instrumentation
OSR	Outside rent (equipment)
JRO	Job related overhead

Appendix J - Schedule

Kiewit

Schedule Comparison

Area	Discipline / Item	Qty	Unit	Start (Mo)	Finish (Mo)	Hrs
	NTP			1.0		
	Start-up			37.0	48.0	
	Mechanical Completion				43.0	
	Substantial Completion				48.0	
	Completetion - Schedule				48.0	
	ENGINEERING / PROCURMENT					
	Engineering / Detialing					
	Procurment					
	GASIFICATION - STICK BUILT OPTION					1,172,141
	Site Mobilization			7.0	10.0	
	Gasification Civil	39,900	CY	10.0	19.0	11,395
	Gasification Piling	1,024	EA	10.0	12.0	1,024
	Gasification Foundation Concrete	5,700	CY	12.0	18.0	20,320
	Gasification Structural Steel	8,384	Ton	17.0	39.0	193,582
	Gasification Equipment	1	LS	20.0	40.0	150,000
	Gasification Piping	149,000	LF	19.0	44.0	548,320
	Gasification Electrical	1,650,000	LF	19.0	46.0	247,500
	GASIFICATION - SLIPFORM OPTION					1,105,297
	Site Mobilization			7.0	10.0	
	Gasification Civil	39,900	CY	10.0	19.0	11,395
	Gasification Piling	1,024	EA	10.0	12.0	1,024
	Gasification Foundation Concrete	5,700	CY	12.0	18.0	20,320
	Pre-Assembly of Structural Steel Floor Modules	8,384	Ton	15.0	27.0	72,540
	Slipform Concrete	18,211	CY	17.0	23.0	69,822
	Floor Module Erection	1	LS	21.0	40.0	40,083
	Gasification Equipment	1	LS	19.0	40.0	150,000
	Gasification Piping	149,000	LF	18.0	41.0	509,938
	Gasification Electrical	1,650,000	LF	18.0	43.0	230,175
					Total	1,172,141
					Period Gain	
					To-Date Gain	

	YEAR 1												YEAR 2												YEAR 3											
	Jan	Feb	Mar	Apr	May	Jun	Jul	Aug	Sep	Oct	Nov	Dec	Jan	Feb	Mar	Apr	May	Jun	Jul	Aug	Sep	Oct	Nov	Dec	Jan	Feb	Mar	Apr	May	Jun	Jul	Aug	Sep	Oct	Nov	Dec
	1	2	3	4	5	6	7	8	9	10	11	12	13	14	15	16	17	18	19	20	21	22	23	24	25	26	27	28	29	30	31	32	33	34	35	36
	1.0	1.0	1.0	1.0	1.0	1.0	1.0	1.0	1.0	1.0	1.0	1.0	1.0	1.0	1.0	1.0	1.0	1.0	1.0	1.0	1.0	1.0	1.0	1.0	1.0											
		1.0	1.0	1.0	1.0	1.0	1.0	1.0	1.0	1.0	1.0	1.0	1.0	1.0	1.0	1.0	1.0	1.0	1.0	1.0	1.0	1.0	1.0	1.0	1.0	1.0	1.0	1.0	1.0	1.0						
							1.0	1.0	1.0																												
										5.0	5.0	6.0	7.0	7.0	6.0	6.0	5.0	5.0																			
										2.0	3.0																										
												15.0	16.0	16.0	17.0	17.0	14.0																				
																	30.0	30.0	30.0	35.0	38.0	38.0	40.0	40.0	40.0	40.0	40.0	40.0	40.0	40.0	40.0	40.0	40.0	40.0	40.0	20.0	20.0	20.0
																				10.0	10.0	10.0	20.0	20.0	20.0	20.0	20.0	30.0	30.0	30.0	30.0	30.0	30.0	30.0	20.0	20.0	
																			20.0	20.0	35.0	60.0	75.0	90.0	120.0	125.0	135.0	140.0	150.0	150.0	150.0	150.0	150.0	140.0	140.0	100.0	100.0	50.0	50.0	40.0	40.0	20.0	20.0				
																			5.0	5.0	5.0	5.0	10.0	10.0	15.0	20.0	25.0	35.0	30.0	40.0	50.0	60.0	60.0	65.0	65.0	65.0	65.0	65.0	55.0	20.0	65.0	55.0	20.0	20.0	20.0		
							1.0	1.0	1.0																												
										5.0	5.0	6.0	7.0	7.0	6.0	6.0	5.0	5.0																			
										2.0	3.0																										
												15.0	16.0	16.0	17.0	17.0	14.0																				
															30.0	30.0	30.0	35.0	35.0	35.0	35.0	35.0	35.0	20.0	20.0	15.0											
																	40.0	40.0	50.0	50.0	50.0	50.0	40.0														
																					5.0	10.0	10.0	10.0	10.0	10.0	10.0	10.0	10.0	10.0	10.0	10.0	10.0	10.0	10.0	10.0	10.0	10.0	10.0								
																			10.0	10.0	10.0	20.0	20.0	20.0	20.0	20.0	20.0	30.0	30.0	30.0	30.0	30.0	30.0	30.0	20.0	20.0	20.0	10.0							
																		10.0	20.0	80.0	80.0	80.0	90.0	120.0	125.0	135.0	140.0	150.0	150.0	150.0	150.0	150.0	140.0	140.0	100.0	100.0	80.0	80.0	50.0	40.0						
																		10.0	10.0	40.0	40.0	40.0	40.0	40.0	40.0	40.0	40.0	40.0	40.0	50.0	60.0	60.0	65.0	65.0	65.0	65.0	65.0	55.0	20.0	65.0	55.0	20.0				
Total	1	2	2	2	2	2	4	4	4	16	18	44	48	48	78	78	140	137	182	287	310	350	382	372	412	426	431	456	471	501	520	530	525	520	480	410	380	320	215	165	160	95	40	20	20	0	0	
Period Gain	0.0%	0.0%	0.0%	0.0%	0.0%	0.0%	0.0%	0.0%	0.0%	0.2%	0.2%	0.5%	0.5%	0.5%	0.8%	0.8%	1.5%	1.4%	1.9%	3.0%	3.2%	3.6%	4.0%	3.9%	4.3%	4.4%	4.5%	4.7%	4.9%	5.2%	5.4%	5.5%	5.5%	5.4%	5.0%	4.3%	4.0%	3.3%	2.2%	1.7%	1.7%	1.0%	0.4%	0.2%	0.2%	0.0%	0.0%	0%
To-Date Gain	0.0%	0.0%	0.1%	0.1%	0.1%	0.1%	0.2%	0.2%	0.2%	0.4%	0.6%	1.1%	1.6%	2.0%	2.9%	3.7%	5.1%	6.6%	8.4%	11.4%	14.7%	18.3%	22.3%	26.1%	30.4%	34.9%	39.4%	44.1%	49.0%	54.2%	59.6%	65.1%	70.6%	76.0%	81.0%	85.3%	89.2%	92.6%	94.8%	96.5%	98.2%	99.2%	99.6%	99.8%	100.0%	100.0%	100.0%	10

Labor Hour Summary

	Stick-Built	Slipform
Civil	11,395	11,395
Concrete	20,320	130,225
Structural Steel	193,582	72,540
Mechanical	150,000	150,000
Piping	548,320	509,938
Electrical & Instrumentation	282,300	230,175
Start-up	24,877	24,877
	1,230,794	1,129,150
Maintenance	0	0
Indirect Craft	212,440	212,440
Total CMH	**1,443,234**	**1,341,590**

Craft By Discipline	YEAR 1												YEAR 2												YEAR 3											
	Jan	Feb	Mar	Apr	May	Jun	Jul	Aug	Sep	Oct	Nov	Dec	Jan	Feb	Mar	Apr	May	Jun	Jul	Aug	Sep	Oct	Nov	Dec	Jan	Feb	Mar	Apr	May	Jun	Jul	Aug	Sep	Oct	Nov	Dec
	1	2	3	4	5	6	7	8	9	10	11	12	13	14	15	16	17	18	19	20	21	22	23	24	25	26	27	28	29	30	31	32	33	34	35	36
Craft																																				
Excavation	1	1	1	1	1	1	1	1	1	11	11	13	15	15	13	13	11	11	1	1	1	1	1	1	1											
Concrete												30	32	32	34	34	68	40	50	50	50	50	40													
Structural Steel															30	30	60	65	65	70	78	83	85	70	70	65	50	50	50	50	50	50	50	50	50	30	30	30	10
Scaffolding																																				
Mechanical																			10	20	20	30	40	40	40	40	40	40	50	60	60	60	60	60	60	50	40	40	30							
Piping																		10	40	100	115	140	165	210	245	260	275	290	300	300	300	300	290	280	240	200	180	130	100	80	40	20	20				
Electrical & Instrumentation																		10	15	45	45	45	50	50	55	60	65	75	70	90	110	120	125	130	130	130	130	120	75	85	120	75	20	20	20			
Start-up																																				
Total	1	1	1	1	1	1	1	1	1	11	11	43	47	47	77	77	139	136	181	286	309	349	381	371	411	425	430	455	470	500	520	530	525	520	480	410	380	320	215	165	160	95	40	20	20	0	0	0

Schedule Legend (Colors)

	Decription
	Egineering / Procurment
	Civil / Structural
	Mechanical Piping / Equipment
	Electrical Cable / Equipment

Appendix K – Assumptions Log

Anchor Bolts Up - Estimate Plugs

GE Power and Water Slip form/Modularization Study
Project Assumptions
Date: 4-Jun-14

	General Project Design Assumptions:	
Item	Assumption	Comment
1	We have made a rough estimation of the necessary duration-based construction equipment and have included a temporary personnel hoist for the construction of the gasification structure. The coal silos will be accessed via a personnel stair	
2	No stairs, emergency ladders, swing doors, louvers, windows, overhead or roll up doors, permanent handrails, hoist beams, and other permanently installed materials	
3	Labor rates assume non-union direct labor work force	
4	Work hours assumed to be 5 – 10 hour days with 24/7 slipform operations	
5	See Design Basis Document for additional details regarding project design assumptions.	
6	Foundations are excluded because they are the same for both the stick-built and slipform Gasifier options	
7	All floors shown in the stick-built option are also required in the slipform option	
8	For the purposes of this study, minor pieces of equipment are defined as those that can generally be supported by the floor live load allowance.	

	Gasifier Specific Assumptions (Stick Built):	
Item	Assumption	Comment
1	The term "stick-built" is used herein to describe a method of construction and erection for this steel framed structure.	
2	The components of the structure are shop fabricated columns, beams and braces. Columns up to 60' will be erected.	
3	Beams up to 30' long will be used.	
4	Columns and beams will be assembled/erected individually and bolted or welded into there final positions.	
5	Diagonal bracing will be installed at outer bays, RSC will be installed, and then additional diagonal bracing will be installed in front of the RSC.	
6	Floors will be bar grating. Where a solid floor is required, a 1/4" thick checker plate will be added. This applies to roof if required.	
7	Exhaust ducts and silencers exist at the roof level. These items are accomodated within the design floor/roof live load allowance.	
8	The same or similar silencer support schemes will be used for both slipform and stick built.	
9	The RSC will be shipped to site in 3 cylindrical sections. The three sections will be welded together in the horizontal position.	
10	The RSC will then be lifted to vertical position with crane (stick-built) or strand jacks from slip form structure.	
11	Internals (e.g. heat exchanger piping and refactory brick will be assembled into the vertical RSC vessel via crane.	
12	The top/dome of RSC will be welded and then the gasifier attached to top of RSC.	

	Gasifier Specific Assumptions (Slip form/Modularization):	

Anchor Bolts Up - Estimate Plugs

Item	Assumption	Comment
1	The following items have not been contemplated in our indicative/ROM estimating effort for the gasification structure:	
a	Surveying and site layout, including benchmarks and reference elevations	
b	Trash removal	
2	Gasification structure is estimated at a slip rate of 5" per hour and a 32 day slip schedule	
3	Equipment is outside the scope of this report. Issues involved with equipment lead times are assumed to not affect the installation of floor modules. When the floors are ready to be installed, it is assumed that the equipment will be on-site, ready to install on the floor.	
4	Since the final location of the project is not known, sales taxes are not included in the estimate.	
5	The same or similar silencer support schemes will be used for both slipform and stick built.	
6	The RSC will be shipped to site in 3 cylindrical sections. The three sections will be welded together in the horizontal position.	
7	The RSC will then be lifted to vertical position with crane (stick-built) or strand jacks from slip form structure.	
8	Internals (e.g. heat exchanger piping and refactory brick will be assembled into the vertical RSC vessel via crane.	
9	The top/dome of RSC will be welded and then the gasifier attached to top of RSC.	

	Coal Silo Assumptions:	
Item	Assumption	Comment
1	The following items have not been contemplated in our indicative/ROM estimating effort for the coal silos:	
a	All temporary roads and laydown areas constructed and maintained	
b	Temporary electrical	
c	Surveying and site layout, including benchmarks and reference elevations	
d	Trash removal	
e	Hot weather concrete costs	
f	All testing	
g	Employee welfare facilities – toilets, offices, office supplies, OneIM costs	
h	Concrete washout facilities	
2	The coal silo ROM pricing includes only the slipform walls, costs for the following items have not been contemplated:	
a	Foundation	
b	Roof	
c	Bin bottom	
3	In talking with two jump form subcontractors, they tell us a jump form silos of similar dimension, although not joined together with a common marriage section, would be approximately 4.5 to 5 months. Jump form costs run in the range of $3,000,000.	
4	Our Indicative/ROM is in the range of $4,500,000 and a schedule of 6 months.	
5	Coal silos are estimated at a slip rate of 12" per hour and a 7 day slip schedule	
6	Since the final location of the project is not known, sales taxes are not included in the estimate.	

Anchor Bolts Up - Estimate Plugs

7	The foundations for the coal silos are not included, even though they will be slightly different	
8	The ring beams for the two coal silo options are the same.	
9	The design of the pilasters/columns for the coal silo are excluded because the design will be the same, but the erection of them will be slightly	

	Pipe Rack Assumptions:	
Item	Assumption	Comment
1	See report text	

	General Estimating Assumptions:				
Item	Resource Type	Description	UOM	Rate	Notes
	Labor Rates				
1	Composite Crew	Civil Works Crew	Mhr	$41.81	Non-Union -- 50 Hrs/Wk
2	Composite Crew	Concrete Crew (Formwork & Place)	Mhr	$40.77	Non-Union -- 50 Hrs/Wk
3	Composite Crew	Steel Erection (Ironworkers & Operators)	Mhr	$41.49	Non-Union -- 50 Hrs/Wk
4	Composite Crew	Mechanical Equipment (Millwrights)	Mhr	$43.15	Non-Union -- 50 Hrs/Wk
5	Composite Crew	Mechanical Piping (Pipefitters)	Mhr	$43.73	Non-Union -- 50 Hrs/Wk
6	Composite Crew	Electrical	Mhr	$43.01	Non-Union -- 50 Hrs/Wk
7	Composite Crew	Instrumentation	Mhr	$47.69	Non-Union -- 50 Hrs/Wk
8	Composite Crew	Startup/Performance Testing	Mhr	$40.88	Non-Union -- 50 Hrs/Wk
9	Staff	Staff Mhr (Overhead)	Mhr	$65.00	Salary
	Equipment Rates - 50 Hr Week				
1	Equipment	150 Ton Crawler (Manitowoc 555 or Similar)	Wk	$5,000.00	
2	Equipment	300 Ton Crawler (Manitowoc 2250 or Similar)	Wk	$9,600.00	
3	Equipment	400-450 Ton Crawler (Manitowoc 16000 or Similar)	Wk	$20,800.00	

Anchor Bolts Up - Estimate Plugs

4	Equipment	>650 Ton Crawler (Liebherr LR1750 or Similar)	Wk	$34,000.00	
5	Equipment	Manitowoc MAXER or Liebherr Ballast Wagon Attachment	Wk	$9,600.00	
6	Equipment	OSR 1,000 Ton Crane	Wk	$52,540.00	
7	Equipment	Tower Crane (Liebherr 630 or Similar)	Wk	$7,000.00	
8	Equipment	Construction Site Truck	Wk	$3,150.00	Pickup/Flatbed
9	Equipment	Diesel Air Compressor	Wk	$1,900.00	
10	Equipment	400A Diesel Welder	Wk	$1,100.00	
11	Equipment	Loader/Forklift (CAT 930 or 10k)	Wk	$3,500.00	
12	Equipment	120' Manlift	Wk	$4,200.00	
13	Equipment	60' Manlift	Wk	$2,900.00	
14	Equipment	Construction Elevator	Wk	$4,600.00	
	Permanent Material				
1	Piling	18" Auger Cast Piling (80' Depth)	EA	$3,500.00	
2	Concrete	4000 PSI Concrete (Includes concrete, anchor bolts, ice, accessories, etc)	CY	$165.00	
3	Concrete	5000 PSI Concrete (Includes concrete, anchor bolts, ice, accessories, etc)	CY	$175.00	
4	Concrete	6000 PSI Concrete (Includes concrete, anchor bolts, ice, accessories, etc)	CY	$185.00	
5	Concrete	Anchor Bolts	EA	$150.00	
6	Concrete	Embeded Metals	LB	$6,000.00	
7	Steel/Metals	Galvanized Main Steel - 50ksi	TN	$2,650.00	Includes connections
8	Steel/Metals	1-1/4" Serrated Steel Bar Grating	SF	$11.00	Galvanized
9	Steel/Metals	2" Serrated Steel Bar Grating	SF	$14.00	Galvanized
10	Steel/Metals	Horizontal Handrail w/Toe Plate- Galvanzied	LF	$49.00	Galvanized
11	Steel/Metals	3/8" Checkered Plate	SF	$34.00	
12	Steel/Metals	Stair Stringer w/ Tread	TN	$4,600.00	
13	Steel/Metals	Safety Swing Gate	EA	$370.00	
14	Steel/Metals	Ladder w/Cage- Galvanized	VF	$150.00	
15	Steel/Metals	Ladder w/o Cage- Galvanized	VF	$75.00	
16	Mechanical	Bulk Pipe	LF	$250.00	
17	Electrical	Cable	LF	$6.50	
18	Instrumentation	Instrumentation	EA	$130.00	
	Subcontractors				
1	Concrete	Rebar Supply/Install - 60ksi Uncoated	TN	$2,500.00	
2	Concrete	Rebar Supply/Install - 60ksi Uncoated (With Vertical Ultimate Couplers)	TN	$3,000.00	
3	Concrete	Concrete Pumping	CY	$13.00	
4	Building	Steel Cladding	SF	$30.00	
5	Building	Wall Girts (6.5 Lbs/SF)	TN	$2,650.00	
6	Painting	Painting Plug	LS	$3,500,000.00	
	ST&S (Small Tools & Services				
1	Direct ST&S	Formwork/Concrete/Rebar STS	CY	$50.00	
2	Mhr ST&S	Structural Steel	Mhr	$5.00	
3	Mhr ST&S	Piping	Mhr	$7.00	
4	Mhr ST&S	Mechanical Equipmennt	Mhr	$12.00	
5	Mhr ST&S	Startup	Mhr	$31.05	
6	Mhr ST&S	Electrical	Mhr	$6.00	
7	Concrete	Instrumentaiton	Mhr	$6.00	

	Pipe Rack Estimate Assumptions:			

Anchor Bolts Up - Estimate Plugs

Item	Resource Type	Description	UOM	Rate	Notes
	Labor Rates				
1		See report text			

Appendix L – Position Paper October 2013

FEASIBILITY STUDIES TO IMPROVE PLANT AVAILABILITY AND REDUCE TOTAL INSTALLED COST IN IGCC PLANTS

Position Paper
Task 3.1 – Conceptual Design of Slip form
Task 4.2 – Module Identification for Modularization
(Including update on Tasks 3 – 6)
Reporting Period
Beginning October 31, 2013
Ending December 6, 2013

Submitted To:
GE Energy (USA), LLC
1333 West Loop South
Houston, TX 77027
DUNS - 167528368

Submitted By:
Kiewit Power Engineers
9401 Renner Blvd.
Lenexa, Ks. 66219

Co-Authors:
Thomas Heausler
913-689-3972
Thomas.Heausler@kiewit.com

Steve Frankosky
612-501-8058
Steve.Frankosky@ibberson.com

Cervente Sudduth
913-953-5796
Cervente.Sudduth@kiewit.com

November 22, 2013

DOE Cooperative Agreement No. DE-FE0007859
Period of Performance: October 1, 2011 – September 30, 2014

Position Paper

For
Affordability IGCC Project, Texas, USA
Integrated Gasification Combined Cycle (IGCC)
Slip forming and Modularization

For GE Energy (USA)
And United States Department of Energy

1. Executive Summary:

The United States Department of Energy has contracted GE Energy to study the affordability of an Integrated Gasification Combined Cycle (IGCC) plant. GE Energy has contracted Kiewit to provide input into this report. Kiewit has shown expertise and success in the design and construction of large industrial facilities for many years.

Representatives from GE Energy and Kiewit visited the Duke Energy IGCC plant in Edwardsport, Indiana and reviewed related documents. IGCC plants are composed of many parts, the most significant structures may be defined as: Air Separation, Coal Handling, Gasification Island, Pipe Racks, Combustion Turbine, Steam Turbine, Byproduct Removal, Water Treatment, Cooling Towers, and Electrical Substation. Of these structures, it was concluded that the Gasification Island structure has the greatest potential for optimization and gains in affordability.

Traditionally the Gasification Island structures have been "Stick-Built", i.e. the structure is composed of structural steel columns, beams and braces which are individually hoisted into final position by cranes one "stick" or piece at a time. Alternative concepts studied herein include: Concrete Slip form and Concrete Slip form with Floor Modules, and Large Module Steel Structures.

It was concluded that the best potential gain for savings and affordability is to pursue the development of a concrete slip formed gasification structure with floor modules. This method provides potential cost savings in construction materials, reduced schedule, and reduced mobilization cost for large cranes. Kiewit will pursue this approach further and provide cost, schedule and constructability comparisons during phase II task deliverables (3.2, 3.3, 4.1, 4.3, and 4.4).

As an added value feature, it is recommended that further study explore the use of Concrete Slip form for the coal silos, and modularization of selected pipe rack structures. While these IGCC plant components present additional opportunity to reduce total schedule time and construction cost, the gasification structure has the greatest potential for overall construction time and capital cost reduction.

Position Paper

For
Affordability IGCC Project, Texas, USA
Integrated Gasification Combined Cycle
(IGCC)
Slip forming and Modularization

Table of Contents:

1. Executive Summary
2. Methods
    a. Site Visit Observations
    b. Structures Considered
    c. Existing Construction
3. Results and Discussion
    a. Proposed Concepts
    b. Recommendation
4. Conclusion
5. Graphical Material
6. References
7. Appendices

2. Methods

The United States Department of Energy has contracted GE Energy to study the affordability of an Integrated Gasification Combined Cycle (IGCC) plant. GE Energy has contracted Kiewit to provide input into this report. Kiewit has shown expertise and success in the design and construction of large industrial facilities for many years.

a. Site Visit Observations

On August 8, 2013, Representatives from Kiewit (Kiewit Construction, Kiewit Power Engineers, Kiewit Offshore Services (Large Modular Structures), and T.E. Ibberson (Slip form) visited with GE Energy personnel at the GE Energy Houston, Texas office and discussed IGCC technology, and the Scope and options of this study. On October 2, 2013 representatives from Kiewit and GE Energy visited the Duke Energy Edwardsport, Indiana facility. The team discussed the plant and gasification structure with on-site personnel and reviewed related documents.

b. Structures Considered

IGCC plants are composed of many parts, the most significant structures may be defined as:

- Air Separation
- Coal Handling
- Gasification Island
- Pipe Racks
- Combustion Turbine
- Steam Turbine
- Byproduct Removal
- Water Treatment
- Cooling Towers
- Electrical Substation.

With the exception of the Gasifier Island, most of these structures are traditional structures and have been optimized over many years at numerous industrial and power plant facilities. Further study of optimization for these traditional structures was concluded to not likely yield fruitful results. However, a few smaller structures, such as the coal silos and certain pipe racks have potential to be made more affordable and are mentioned later in this report (See Section 4. Conclusion and Appendix A).

Of these structures, it was concluded that the Gasification Island structure has the greatest potential for optimization and gains in affordability. This is because of its large size, large relative cost and unique support demands from the large Gasifier elements.

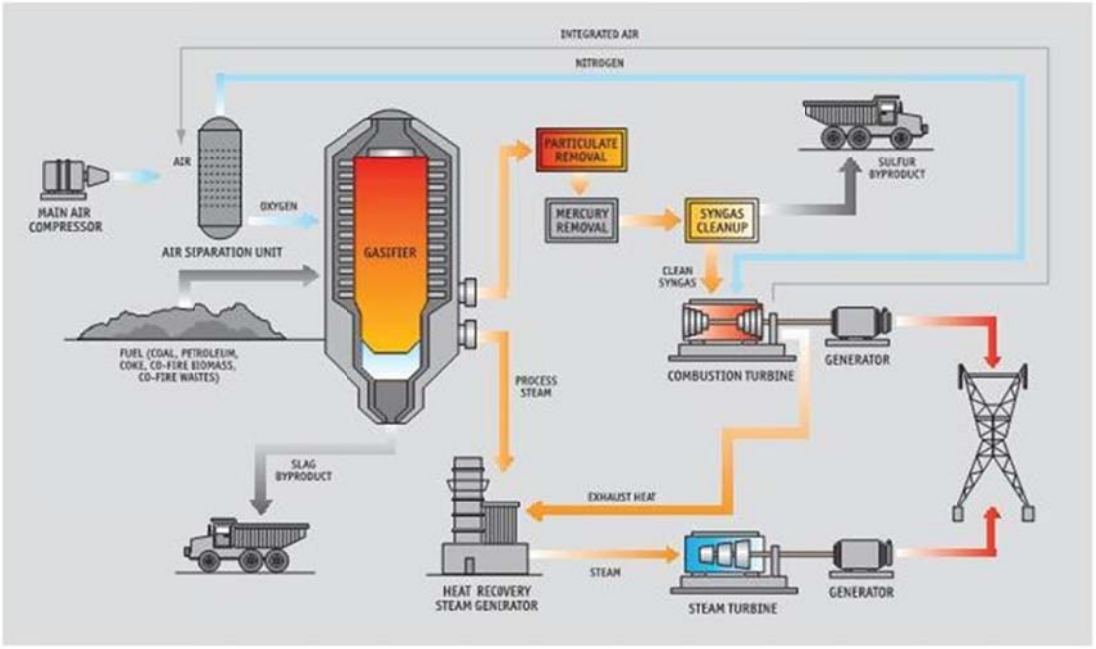

Figure 2.1: Edwardsport, IN; IGCC Process
From Duke Energy Fact Sheet Edwardsport, IN
http://www.duke-energy.com/pdfs/IGCC-Fact-sheet-12.10.pdf

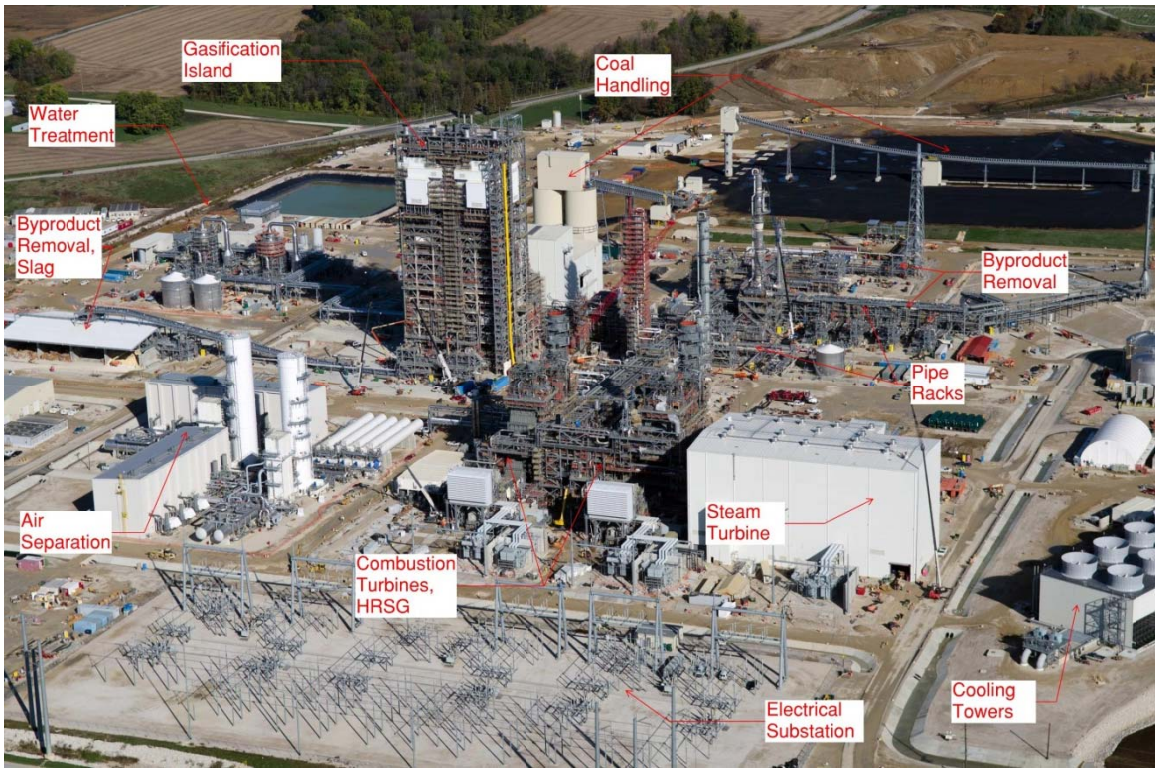

Figure 2.2: Edwardsport, IN; IGCC Aerial Photo of Plant
From Duke Energy, Edwardsport, IN IGCC website
http://www.duke-energy.com/about-us/edwardsport-overview.asp

c. Existing Construction

Traditionally, and as built at the Edwardsport Facility, Gasification Island structures have been "Stick-Built", i.e. the structure is composed of structural steel columns, beams and braces which are individually hoisted into final position by cranes one "stick" or piece at a time. The Edwardsport Gasification Structure is 312 feet tall. The Gasifier Vessel and Radiant Syngas Cooler (RSC) make up the largest and heaviest elements that need to be supported by the Structure. The top of the Gasifier Vessel is approximately 270 feet above grade. The stick built method required an extremely large crane to assemble the "sticks" at 312 feet and to lift the extremely heavy RSC and then lift the Gasifier to a location on top of the RSC. The cost and mobilization of such crane was reportedly significant. The cost and schedule required to assemble the "stick" was also significant.

Figure 2.3: Edwardsport, IN; IGCC Photo of Gasifier Island Structure
From Duke Energy, Edwardsport, IN IGCC website
http://www.duke-energy.com/about-us/edwardsport-overview.asp

Figure 2.4: Edwardsport, IN; IGCC Photo of Gasifier Island Structure
From Duke Energy, Edwardsport, IN IGCC website
http://www.duke-energy.com/about-us/edwardsport-overview.asp

3. Results and Discussion

In an effort to increase affordability, examination of the schedule, expense of large crane and cost of materials will be examined to produce a more detailed report based DOE approval to continue the Affordability study. Alternative concepts studied herein includes: Large module steel structures, concrete slip form, and concrete slip form with floor modules.

a. Proposed Concepts

"Stick-Built" Baseline

For the purposes of this study, Kiewit will develop a "Stick-Built" support structure. The purpose of this effort is to develop a simplified general arrangement of the major mechanical components, with a per floor live loading to account for smaller components and piping and operations. Foundations, structural steel columns, beams and bracing will be sized and then a schedule and cost estimate will be developed. The results will serve as a baseline for comparison to the other proposed options below.

The primary significant components considered will be:

- Gasifier
- Radiant Syngas Cooler (RSC)
- Slag Crusher
- Steam Drums
- Flash Drums
- Heat Exchangers
- Other Tanks and Vessels

A two – train process (two Gasifiers and RSC's) will be considered so as remain similar to the Edwardsport Facility.

Concrete Slip form

Concrete slip form construction is a construction method in which concrete is poured into a continuously moving form. Slip forming is well suited for tall structures with heavy gravity loading. Advantages over "Stick-Built" often include a shorter schedule and the ability to eliminate the need for large cranes. The resulting concrete slip formed structure is robust and can be used as the lifting apparatus for heavy equipment such as that required at a gasification island structure. The slip form structure can have openings in the exterior walls for equipment access, ventilation, and lifting platforms as required. See Figures 5.3 to 5.6 for additional information.

Concrete Slip form with Floor Modules.

The lifting capability of the slip formed shell may further be utilized to lift and cable jack floors into place. The floors may be steel or concrete and assembled on the ground safely and efficiently. Then the floor module may be lifted from the ground up to its final elevation in the structure. Addition of mechanical components and piping may also be

assembled on the floor at grade before lifting. See Figures 5.3 to 5.6 for additional information.

Large Module Steel Structures

Large Module Structure Construction was considered. This technique is popular for oil field and offshore oil platforms. The concept is similar to a mechanical skid whereby all structural, mechanical and electrical components are assembled off-site in a fabrication yard. For the Large Module concept the "skids" are multi-story and over 100' long in plan. The module is delivered to the jobsite and hoisted into place. Work in the more harsh conditions of the jobsite are minimized. The advantages are excellent quality control in an in-plant environment and minimal labor and schedule demands at the jobsite. The disadvantages include the need for access to water transport and/or rail as well as the need for extremely large cranes at the jobsite.

Large Module construction is common along the Gulf Coast of Texas. The use of this concept would require site selection to include water and rail access, as well as close proximity to urban labor and reasonable proximity to large fabrication yards. Such proximity to Gulf Coast water could trigger the need for the structure to resist hurricane force winds. This requirement would increase structural steel and foundation costs.

Based upon initial review of the Large Module Concept, it has been concluded that its limitations outweigh the benefits.

b. Recommendations

It is recommended that a baseline "Stick-Built" Structure be designed in adequate detail to determine a class 3 cost estimate and schedule for the gasifier structure. A similar design will be made for concrete slip form with floor modules. A class 3 cost estimate and schedule will then be created for the concrete slip form structure.

It is recommended that Kiewit proceed with the following sequence of tasks:

1. Develop a General Arrangement (GA) drawing defining the major equipment to be used as the baseline for all comparisons. The primary significant components considered will be: Gasifier, Radiant Syngas Cooler (RSC), Slag Crusher, Steam Drums, Flash Drums, Heat Exchangers and Other Tanks and Vessels.
2. The GA drawing will list the weight and overall dimensions of each component and define the height above grade for each.
3. To accomplish the above items, Kiewit will be reliant on GE Energy to provide the data defined.

After GE Energy provides Kiewit with the above data, Kiewit will then proceed as follows:

4. Develop design basis document for gasifier structure.
5. Develop preliminary structural calculations for design of "Stick-Built" structure, slip formed structure, and floor modules in slip formed structure.
6. Develop preliminary structural drawings for design of "Stick-Built" structure, slip formed structure, and floor modules in slip formed structure.

7. Develop a constructability and sequence of assembly for Slip form walls, Stick built structure, hoisting of gasifier and RSC, floor modules and any impact on assembly of equipment and piping.
8. Develop a Construction Schedule for each option.
9. Develop a class 3 cost estimate for each option.
10. Draft and complete final recommendation and report including conclusion of affordability, cost savings, schedule benefits.

4. Conclusion

It was concluded that the best potential gain for savings and affordability is to pursue development of a Concrete Slip form with Floor Modules. This method provides potential cost savings in construction materials, reduced schedule, and reduced mobilization cost for large cranes. Further detailed review of this conclusion will be made and a cost and schedule estimate will be performed. Results of the comparison will be presented and final conclusions will be made.

As an added value feature, it is recommended that further study explore the use of Concrete Slip form for the coal silos, and modularization of selected pipe rack structures. (See Appendix A for example photos of such structures). However, such further study is outside the scope of this report.

5. Graphical Material

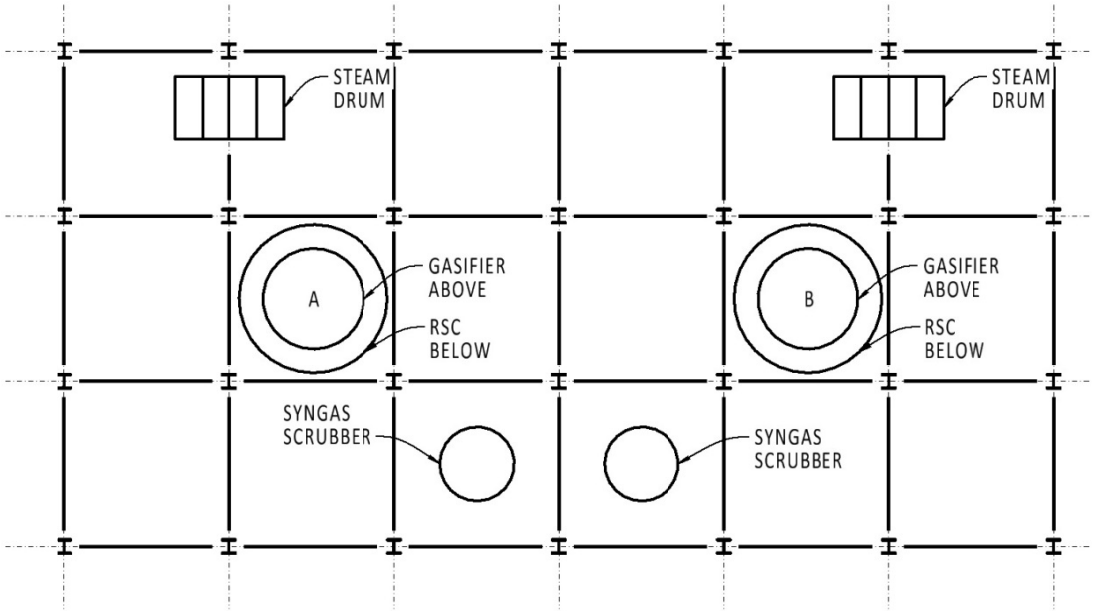

Figure 5.1: Edwardsport, IN; IGCC Gasifier Island Structure
Example of General Arrangement Plans

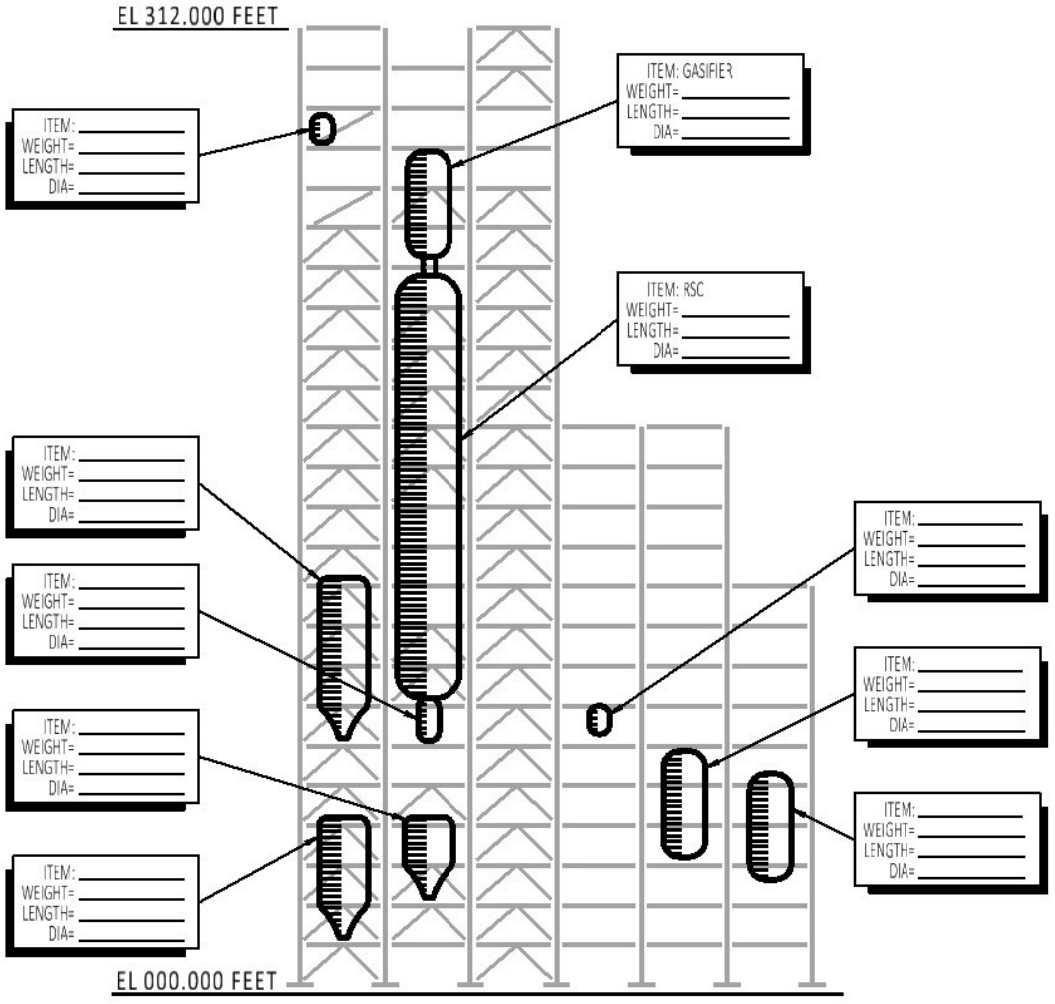

Figure 5.2: Edwardsport, IN; IGCC Gasifier Island Structure
Example of General Arrangement Elevation

6. References

Website: Duke Energy, Edwardsport, IN IGCC; http://www.duke-energy.com

7. Appendices

Appendix A

Figure A.1: Silo Storage Structures are excellent candidates for the Concrete Slip Form Method.
http://www.duke-energy.com/about-us/edwardsport-overview.asp

Figure A.2: Example of Pipe Rack with Gasifier Island in Background
http://www.duke-energy.com/about-us/edwardsport-overview.asp

Figure A.3: Example of Kiewit project using modularization for a pipe rack type structure.